

NOAA Technical Memorandum ERL ARL-229



**A STUDY TO CHARACTERIZE PERFORMANCE STATISTICS OF
VARIOUS GROUND-BASED REMOTE SENSORS**

Gennaro H Crescenti

Field Research Division
Idaho Falls, Idaho

Air Resources Laboratory
Silver Spring, Maryland
May 1999

NOAA Technical Memorandum ERL ARL-229

**A STUDY TO CHARACTERIZE PERFORMANCE STATISTICS OF
VARIOUS GROUND-BASED REMOTE SENSORS**

Gennaro H Crescenti

Field Research Division
Idaho Falls, Idaho

Air Resources Laboratory
Silver Spring, Maryland
May 1999



**UNITED STATES
DEPARTMENT OF COMMERCE**

**William M. Daley
Secretary**

**NATIONAL OCEANIC AND
ATMOSPHERIC ADMINISTRATION**

**D. JAMES BAKER
Under Secretary for Oceans
and Atmosphere/Administrator**

**Environmental Research
Laboratories**

**James L. Rasmussen
Director**

Notice

This document was prepared as an account of work sponsored by an agency of the United States Government. The views and opinions of the authors expressed herein do not necessarily state or reflect those of the United States Government. Neither the United States Government, nor any of their employees, makes any warranty, express or implied, or assumes any legal liability or responsibility for the accuracy, completeness, or usefulness of any information, product, or process disclosed, or represents that its use would not infringe privately owned rights. Mention of a commercial company or product does not constitute an endorsement by NOAA/ERL. Use of information from this publication concerning proprietary products or the tests of such products for publicity or advertising purposes is not authorized.

Table of Contents

	<u>Page</u>
Notice	ii
List of Figures	v
List of Tables	vi
List of Abbreviations and Acronyms	vii
List of Symbols	viii
Abstract	ix
1 Introduction	1
2 Data	2
2.1 Tower Sensors	2
2.2 Doppler Sodars	4
2.3 915-MHz Radar Wind Profiler and RASS	7
3 Performance Audits	8
3.1 Evaluation of Site Characteristics	8
3.2 Equipment Alignment	12
3.3 Simulated Wind Test	16
3.4 Independent Wind Measurement Comparison	17
3.5 Other Audit Procedures and Observations	18
4 Methodology	20
5 Analysis	24
5.1 Data Availability	24
5.2 Signal-to-Noise Ratio Screening	26
5.3 Wind Speed and Direction Statistics	29
5.4 Virtual Air Temperature Statistics	41
6 Conclusions	43
Acknowledgments	46
References	47

Appendix A: Data Availability Graphs	53
Appendix B: Wind Speed and Direction Scatter Plots with Statistics	63
Appendix C: Virtual Air Temperature Scatter Plots with Statistics	268

List of Figures

	<u>Page</u>
Figure 1. Photograph of the BAO tower.	2
Figure 2. Photograph of an R. M. Young wind monitor and ATI sonic anemometer.	3
Figure 3. Photograph of an AeroVironment 4000 phased-array mini-sodar.	5
Figure 4. Photograph of a Metek MODOS sodar.	5
Figure 5. Photograph of a Radian 600 sodar.	6
Figure 6. Photograph of a Radian 600PA sodar.	6
Figure 7. Photograph of a Radian LAP-3000 radar wind profiler and RASS.	7
Figure 8. Scatter plots of sodar versus tower wind speeds as a function of SNR.	28
Figure 9. Wind speed statistics for all cases and sensors.	30
Figure 10. Wind direction statistics for all cases and sensors.	31
Figure 11. Virtual air temperature statistics for all cases and sensors.	42

List of Tables

	<u>Page</u>
Table 1.	Manufacturer specified accuracies of tower-based <i>in situ</i> sensors. 3
Table 2.	Number of valid 15-min data records for tower sensors. 4
Table 3.	Doppler sodar specifications. 7
Table 4.	Vista table for AeroVironment 4000 sodar. 12
Table 5.	Vista table for Metek MODOS sodar. 13
Table 6.	Vista table for Radian 600 and 600PA sodars. 14
Table 7.	Vista table for Radian LAP 3000 radar wind profiler and RASS. 15
Table 8.	Performance audit results. 15
Table 9.	Variables used in scatter plots for audits. 18
Table 10.	Vector correlation coefficients for all cases. 32
Table 11.	Vector correlation coefficients as a function of relative humidity 33
Table 12.	Vector correlation coefficients as a function of Pasquill-Gifford stability 34
Table 13.	Vector correlation coefficients as a function of time of day 35
Table 14.	Vector correlation coefficients as a function of scalar wind speed 36
Table 15.	Vector correlation coefficients as a function of σ_θ 37
Table 16.	Vector correlation coefficients as a function of wind shear 38
Table 17.	Vector correlation coefficients as a function of Brunt-Vaisala frequency 39
Table 18.	Vector correlation coefficients as a function of bulk Richardson number 40
Table 19.	Total number cases for a particular stability classification. 53

List of Abbreviations and Acronyms

APT	Acoustic Pulse Transponder
BAO	Boulder Atmospheric Observatory
CDF	Common Data Format
EM	Electromagnetic
EPA	Environmental Protection Agency
ETL	Environmental Technology Laboratory
FAA	Federal Aviation Administration
INEEL	Idaho National Engineering and Environmental Laboratory
NOAA	National Oceanic and Atmospheric Administration
QA	Quality Assurance
QC	Quality Control
SNR	Signal-to-Noise Ratio

List of Symbols

α	Oblique Angle from the Zenith of a Sodar or Radar Beam
b	Y-intercept
B	Bias (Accuracy)
C	Comparability (Root-Mean-Square Difference)
g	Gravitational Acceleration Constant (9.81 m s^{-2})
m	Slope
N	Number of Observations
N_{BV}	Brunt-Vaisala Frequency (s^{-1})
Q_S	Incoming Solar Radiation (W m^{-2})
r	Correlation Coefficient
R_B	Bulk Richardson Number
RH	Relative Humidity (%)
r_v	Vector Correlation Coefficient
S	Precision (Standard Deviation)
SE	Standard Error of Linear Least-Squares Fit
S_h	Wind Shear (s^{-1})
SS	Horizontal Scalar Wind Speed (m s^{-1})
σ_θ	Standard Deviation of the Horizontal Vector Wind Direction (deg)
T	Air Temperature ($^\circ\text{C}$)
ΔT	Air Temperature Difference ($^\circ\text{C}$)
T_v	Virtual Air Temperature ($^\circ\text{C}$)
θ	Potential Temperature (K)
$\Delta\theta$	Potential Temperature Difference (K)
U	Eastward Wind Speed (m s^{-1})
Δu	Eastward Wind Speed Difference (m s^{-1})
V	Northward Wind Speed (m s^{-1})
Δv	Northward Wind Speed Difference (m s^{-1})
W	Vertical Wind Speed (m s^{-1})
WD	Horizontal Vector Wind Direction (deg)
WS	Horizontal Vector Wind Speed (m s^{-1})
X_i	i th Observation from Reference Instrument (BAO Tower)
Y_i	i th Observation from Test Instrument (Sodar, Radar, or RASS)
z	Height Above Ground Level (m)
Δz	Vertical Thickness of a Layer (m)

Abstract

A ground-based remote sensor characterization study was conducted for three weeks in April 1995 at the Boulder Atmospheric Observatory (BAO) in Erie, Colorado. An extensive data set was acquired from a suite of *in situ* sensors mounted at 10, 50, 100, 200, and 300 m on the BAO tower, four commercially available Doppler sodars (AeroVironment 4000, Metek MODOS, Radian 600, and Radian 600PA), a 915-MHz radar wind profiler (Radian LAP-3000), and a radio acoustic sounding system (Radian). The overall goal of the study was not to compare one ground-based remote sensor against another, but rather to document the performance of these sensors as a function of various atmospheric conditions. A secondary objective was to document quality assurance and quality control procedures that would lead to the acquisition of wind and temperature profiles of known quality.

Performance audits were conducted in accordance with the most current guidance available from the U. S. Environmental Protection Agency. The evaluation included an analysis of site characteristics, review of the operational configuration of the instruments, and testing the response of the sodars using an acoustic pulse transponder system.

Simple statistical parameters were used as a measure of the agreement between tower-based measurements and remote sensor data. These included linear least-squares regression fits, linear and vector correlation coefficient, bias (accuracy), comparability (root-mean-square difference), and precision (standard deviation). These statistics were derived as a function of eight different measures of atmospheric conditions and stability. These conditions and stability categories include relative humidity (RH), Pasquill-Gifford (PG) stability class, time of day (dawn, day, dusk, and night), scalar wind speed (SS), standard deviation of the horizontal wind direction (σ_θ), wind shear (S_h), the square of the Brunt-Vaisala frequency (N_{BV}^2), and the bulk Richardson number (R_B). This is the first time such a methodology has been used to examine wind and temperature data from these profiling systems.

Data availability from these ground-based remote sensors were examined as a function of the eight stability categories without regard to validity. Next, corrupted data were removed by increasing the signal-to-noise ratio (SNR) tolerance. Finally, these statistical parameters were examined to find common themes in remote sensor performance. Overall, excellent agreement was found between tower-based and remote sensor data. It was found that convective (unstable) conditions were conducive to more data capture with higher altitudes than for laminar (stable) conditions. Very low relative humidity also limits the range of sodars since the molecular attenuation dramatically increases under these conditions. However, more variance was observed in the statistics during convective and light wind conditions. Conversely, the scatter was quite small for stable conditions. The nonhomogeneous nature of the boundary layer may be responsible for the large scatter in data acquired by sensors separated on the order of several hundred meters for such conditions.

1 Introduction

There can be little doubt that Doppler sodars, radar wind profilers, and radio acoustic sounding systems (RASS) have led to significant advances in our understanding of the atmospheric boundary layer. These ground-based remote sensors have gained a reputation as effective and reliable tools for acquiring detailed information on atmospheric wind and temperature structure. A comprehensive review on the capabilities of these sensors and how they are used to investigate various atmospheric boundary layer problems is discussed by Clifford et al. (1994) and Neff (1998).

There has been a recent emphasis on the use of these technologies for various air quality programs (Crescenti, 1994). Many of these regulatory programs often require periods of long-term monitoring in order to develop an assessment of how various meteorological conditions affect pollution concentrations and distributions. Ultimately, data acquired by these ground-based remote sensors are used in various diagnostic and/or prognostic numerical air quality models. Reliable model results require, in part, reliable data input. Therefore, a quantitative assessment of the uncertainty in these measurements is needed to provide confidence in model results. Aggressive quality assurance (QA) and control (QC) procedures developed specifically for Doppler sodars, radar wind profilers, and RASS provide additional confidence in their data.

A basic requirement in the development of any measurement system is the verification of its data using quantitative comparisons against data from another sensor whose measurements are of known quality. For example, Doppler sodar data are frequently compared against measurements acquired by *in situ* sensors mounted on towers, balloons (tethered or released), kites, or aircraft (Crescenti, 1997). Several studies have also compared sodar data against measurements obtained by ground-based sensors such as lidars and other Doppler sodars. Similarly, wind and temperature profiles acquired by radar wind profilers and RASS, respectively, are often compared against data obtained by rawinsondes (May et al., 1989; Schroeder, 1990; Weber and Wuertz, 1990; Angevine and Ecklund, 1994). Simple statistical measures such as linear regression, correlation coefficient, bias, comparability, and precision are the most commonly used measures of uncertainty for these ground-based remote sensors.

A ground-based remote sensor characterization study was conducted for three weeks in April 1995 at the Boulder Atmospheric Observatory (BAO) in Erie, Colorado. An extensive data set was acquired from a suite of *in situ* sensors mounted on the BAO tower, four commercially available Doppler sodars, a 915-MHz radar wind profiler, and a RASS. The overall goal of the study was not to compare one ground-based remote sensor against another, but rather to document the performance of these sensors as a function of various atmospheric conditions. A secondary objective was to document QA and QC procedures that would lead to the acquisition of wind and temperature profiles of known quality. These data will aid in the further refinement of current regulatory guidance documents supplied by the U. S. Environmental Protection Agency (1987a; 1995). These documents provide regulatory agencies and users with a common and consistent set of guidelines for the collection, validation, and defense of data acquired by Doppler sodars, radar wind profilers, and radio acoustic sounding systems.

2 Data

The BAO is a research facility operated by the National Oceanic and Atmospheric Administration (NOAA) for the study of the planetary boundary layer and for the testing of various atmospheric sensors. This facility is located on gently rolling terrain 25 km east of the foothills of the Rocky Mountains in Erie, Colorado. The terrain is reasonably flat with gentle slopes to the north, east, and west. The steepest terrain gradient ($\sim 7\%$) is a small hill 2 km south. The center-piece of the BAO is the 300-m open lattice tower (Fig. 1). While the various meteorological sensors and data acquisition systems have evolved over the last two decades, the details on tower structure and geographical information described by Kaimal and Gaynor (1983) is still accurate.

The BAO was chosen as the study location for a number of reasons. There has been an established track record of successful sodar comparison studies conducted at the BAO over a number of years (Kaimal et al., 1980; Gaynor and Korrell, 1981; Finkelstein et al., 1986; Chintawongvanich et al., 1989; Gaynor et al., 1990). The nature of the boundary layer has also been well characterized (Schotz and Panofsky, 1980; Hahn, 1981; Soucy et al., 1982; Panofsky, 1984).

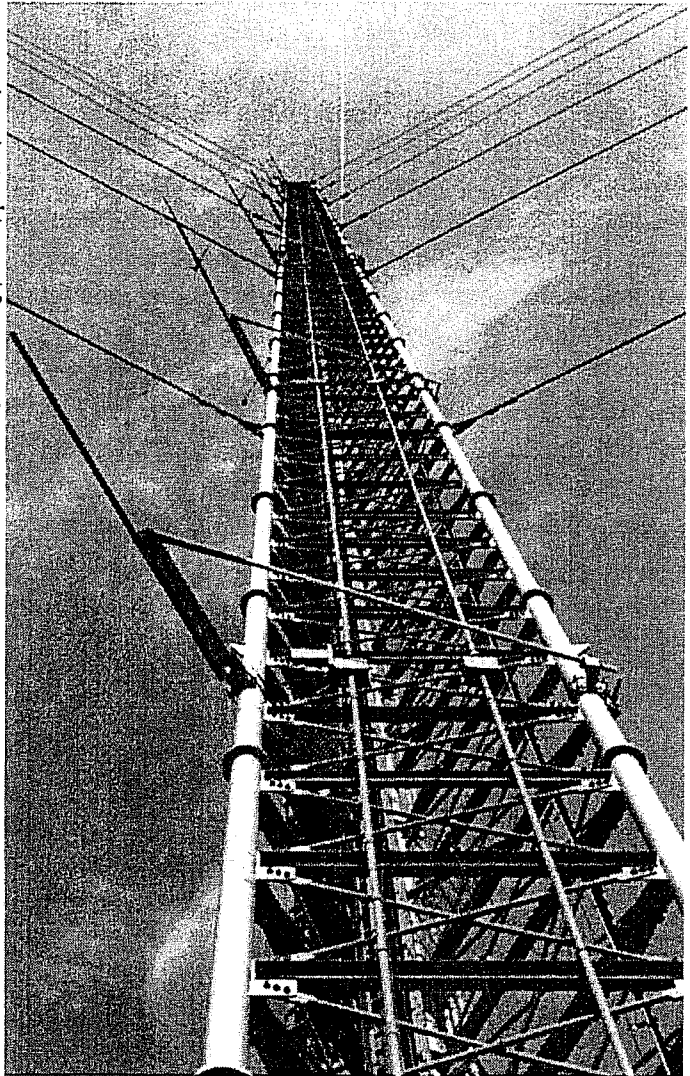


Figure 1. Photograph of BAO tower.

The study was conducted over a three-week period starting on 6 April 1995 and lasting through 27 April 1995. A suite of *in situ* sensors was mounted on the tower at five levels. Four Doppler sodars, a radar wind profiler, and RASS were situated around the perimeter of the tower.

2.1 Tower Sensors

The BAO tower was instrumented with a suite of *in situ* sensors at five levels. R. M. Young Company wind monitors (model 05701-RE) were used to measure the horizontal scalar (SS) and vector (WS) wind speed, horizontal vector wind direction (WD), and standard deviation of the horizontal vector wind direction (σ_θ) at 10, 50, 100, 200, and 300 m (Fig. 2). These anemometers were mounted approximately 2 m from the tower on retractable booms which were oriented towards

the south-southeast (154°). Vaisala HMP-35 sensors were used at the same levels to measure the ambient air temperature (T) and relative humidity (RH). These sensors were mounted inside R. M. Young Company Gill-aspirated radiation shields (model 43408) to minimize measurement errors associated with solar heating. The intakes of the radiations shields were at least 0.5 m away from the tower to minimize the effect of solar heating. Two R. M. Young Company 1000 ohm RTD platinum temperature probes (model 43347VC) were also placed inside Gill-aspirated radiation shields at 10 and 50 m to measure ambient air temperature. These two temperature probes were used to estimate the temperature difference (ΔT) between the two levels (i.e., temperature gradient). An Eppley Laboratory Inc. Precision Spectral Pyranometer (model PSP) located on the roof of the visitors center (approximately 4 m above ground level) was used to measure incoming solar radiation (Q_s). Manufacturer specified accuracies for these sensors are summarized in Table 1.

Five Campbell Scientific Inc. data loggers (model CR10) were placed at each instrument level. Each sensor was interrogated by its respective data logger at a frequency of 1 Hz. The data loggers were programed to record 15-minute block averages from the 1-Hz data of SS , WS , WD , σ_θ , T , RH , and ΔT . The five data loggers were networked into a personal computer located inside a trailer adjacent to the base of the tower. The averaged data were transmitted to and recorded by the computer once per hour. A separate computer was used to record 15-min averages of Q_s .

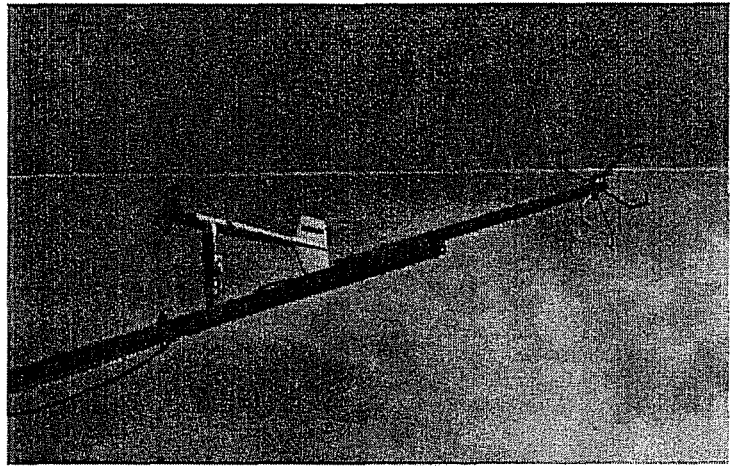


Figure 2. Photograph of an R. M. Young wind monitor and ATI sonic anemometer.

Table 1
Manufacturer specified accuracies of tower-based *in situ* sensors.

Sensor	Variable	Accuracy
R. M. Young Wind Monitor	SS, WS	$\pm 0.2 \text{ m s}^{-1}$
	WD	$\pm 3^\circ$
ATI Sonic Anemometer	U, V, W	$\pm 0.05 \text{ m s}^{-1}$
	T_v	$\pm 0.1 \text{ }^\circ\text{C}$
Vaisala HMP-35 Probe	RH	$\pm 2\% \text{ RH}$
	T	$\pm 0.3 \text{ }^\circ\text{C}$
R. M. Young RTD Probe	T	$\pm 0.1 \text{ }^\circ\text{C}$
Eppley PSP	Q_s	$\pm 1\% \text{ W m}^{-2}$

All bad data values were removed from the tower data set. These included outliers, spikes, and missing values due to power surges or outages. Data acquired from one level on the tower were compared against data from other levels to check for consistency. No attempt was made to replace those bad or missing values with interpolated data. Since the tower-based measurements are to be used as reference measurements, interpolated values could introduce added uncertainties in statistical comparisons. The number of valid data points for each variable at each level is given in Table 2. The maximum possible number of 15-min records during the study was 2052.

Table 2
Number of valid 15-min data records for tower sensors.

Variable	10 m	50 m	100 m	200 m	300 m
<i>SS, WS, WD, σ_θ</i>	1829	1687	2052	2049	2033
<i>T</i>	2052	1863	2052	2052	2051
<i>RH</i>	1849	1863	1993	2048	2052
ΔT	2052	1863			
Q_s	2052				
Sonic	850	1102	1260	895	156

Five Applied Technologies Inc. (ATI) sonic anemometers (model SWS-211/3K) were used to measure turbulent fluxes at 10, 50, 100, 200, and 300 m (Fig. 2). The Kaimal-type sonic heads were mounted approximately 3 m from the tower on the same booms as the wind monitors. The three-component wind speed (U, V, W) and virtual air temperature (T_v) were sampled and recorded to an optical disk at a rate of 10 Hz by a personal computer located in the same trailer as the previously mentioned computer. The computer was programmed to collect the raw sonic anemometer data, computed the 15-min mean and standard deviations of U, V, W , and T_v , horizontal wind speed and direction, as well as the covariances used to determine turbulent momentum and heat flux. The number of valid data points for each level is also given in Table 2. Unfortunately, a combination of many factors contributed to the relatively low availability of the sonic anemometer data. These included power outages, computer crashes, and failure of the sensor electronics.

2.2 Doppler Sodars

All known commercial manufacturers of Doppler sodars (in alphabetical order: AeroVironment, Metek, Radian, and Remtech) were invited to participate in the study. Three companies (in alphabetical order: AeroVironment, Metek, and Radian) accepted the invitation. A total of four Doppler sodars were deployed around the perimeter of the BAO tower by engineers and/or technicians of their respective companies. The distance of the outside guy wire anchor points to the base of the tower is approximately 275 m. The oblique angle beams of the sodars were oriented away from the tower so that reflections from the tower and its guy wires were avoided. In

addition, this strategy minimized any potential contamination of acoustic pulses from one sodar system to another. All four sodars recorded profiles of horizontal and vertical wind velocity as 15-min averages. Each sodar also recorded other parameters such as the signal-to-noise ratio (SNR), the number of return signals used in the average, and the amplitude. It should be noted that the sodar-generated data files differ from manufacturer to manufacturer. The manufacturers submitted their final data sets to NOAA's Environmental Technology Laboratory (ETL) at the conclusion of the study. Some basic sodar specifications are listed in Table 3.

An AeroVironment model 4000 phased-array mini-sodar (Fig. 3) was located near the south guy wire anchor point. Unlike other phased-array designs, the bank of transducers used for acoustic transmission and reception are mounted vertically rather than horizontally. This design avoids noise generated by rain drops impacting directly on the transducers. A "bounce board" is used to orient the acoustic pulse vertically and at oblique angles from the vertical. The AeroVironment mini-sodar was designed for high-resolution profiling of the first 100 to 200 m of the atmospheric boundary layer. Thus, the acoustic frequency and pulse length were much higher and shorter, respectively,

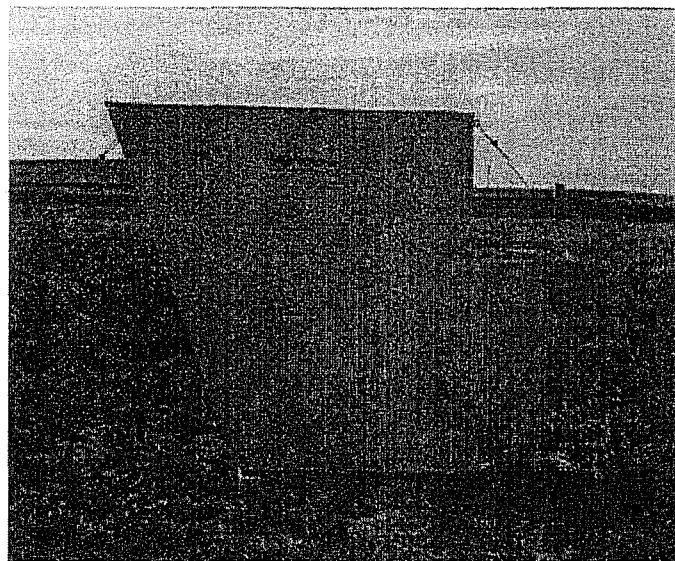


Figure 3. Photograph of an AeroVironment 4000 phased-array mini-sodar.

The acoustic frequency of this system was 4500 Hz with a pulse length of 50 ms. The maximum range was 200 m with a resolution of 5 m. The first reported height was 15 m above ground level. Daily ASCII data files contain horizontal wind speed and direction, horizontal wind speed along the oblique angle beams, and vertical wind speed.

The total number of received backscattered pulses for each of the three beams was also recorded. The maximum number of pulses per beam in a 15-min interval for this sodar was 229. In addition, the relative amplitude, SNR, and standard deviation for each beam was also documented at each level. In addition, a "reliability number" was included for each wind speed as a QC check

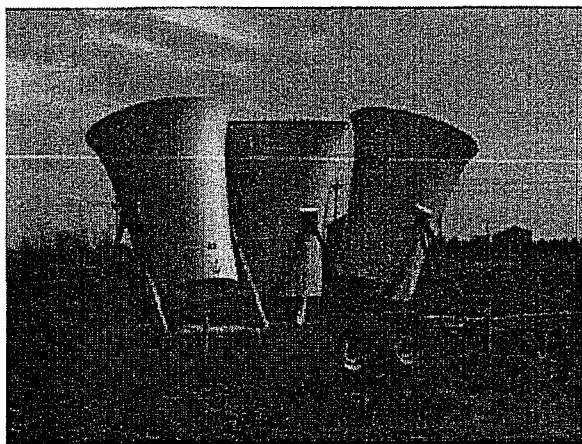


Figure 4. Photograph of a Metek MODOS sodar.

Ordinarily, most 3-beam configurations employ a A Metek model MODOS 3-beam sodar (Fig. 4) was located at the northeast guy wire anchor point. A cluster of seven upward facing transducers were located at the bottom of each antenna enclosure.

single transducer mounted on a tripod over a parabolic dish. The transducer emits the acoustic pulse downwards into the dish which acts as a focusing mechanism for the beam. In the case of the Metek sodar, the parabolic dish was eliminated and replaced by a small phased-array of seven transducers. Phasing of each beam was utilized to maintain a well-focused acoustic pulse. Another unique design feature was the tapered edges of the fiberglass acoustic enclosures. This was designed by Metek to minimize wind-generated noise and acoustic beam distortion. The frequency of this sodar was 2009 Hz with a pulse length of 150 ms. The resolution was 25 m with a range of 50 m to 650 m. The UNIX-based computer system used for sodar operation and data acquisition recorded various parameters (e.g., standard deviations, amplitudes, SNR) in large data files which would cover at least several days of information.

A Radian model 600 3-beam sodar (Fig. 5) was located at the northwest guy wire anchor point. The transmit frequency was 1850 Hz with a 150 ms pulse length. The operating range was 50 to 700 m with a resolution of 25 m. Daily ASCII data files were submitted by Radian to ETL in the so-called CDF (common data format). Wind speed, wind direction, and the three component winds were recorded. In

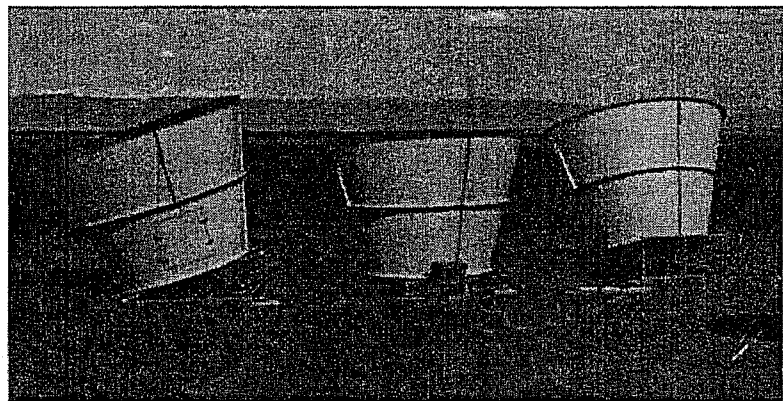


Figure 5. Photograph of a Radian 600 sodar.

addition, SNR and the number of received pulses in the 15-min sampling period (maximum of 47) were documented. A QC code was included as a measure of the reliability of each wind measurement.

A Radian model 600PA phased-array sodar (Fig. 6) was also located near its 3-beam counterpart near the northwest guy wire anchor point. The same pulse length of 150 ms was used for this sodar, however, the transmit frequency was much higher at 2125 Hz. The 275 Hz separation of frequencies between the two Radian sodars was sufficient to avoid any “cross-talk” interference. Range of the sodar was from 50 to 700 m with a 25-m resolution. Data were reported in the same CDF format. Both sodars utilized the same conical-shaped fiberglass enclosures.

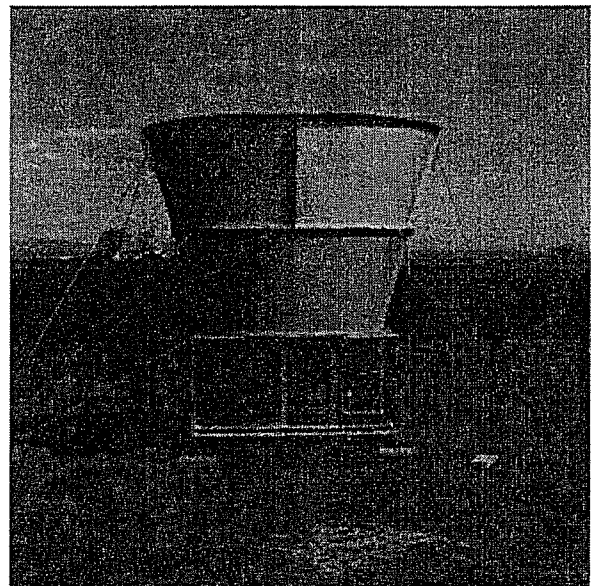


Figure 6. Photograph of a Radian 600PA sodar.

Table 3
Doppler sodar specifications.

	AeroVironment 4000	Metek MODOS	Radian 600	Radian 600PA
Type	phased-array	3-beam	3-beam	phased-array
Number of Transducers	32	7	1	120
Frequency (Hz)	4500	2009	1850	2125
Pulse Width (ms)	50	150	150	150
Pulse Interval (s)	1	4	4	4
Zenith Angle α (deg)	18	20	18	14.87
U-Axis Beam Direction (deg)	173	101	302	349
V-Axis Beam Direction (deg)	83	11	215	259
Minimum Reported Height (m)	15	50	50	50
Maximum Reported Height (m)	200	650	700	700
Resolution (m)	5	25	25	25

2.3 915-MHz Radar Wind Profiler and RASS

A Radian model LAP-3000 915-MHz radar wind profiler was included in the study (Fig. 7). This ground-based remote sensor was developed as a boundary layer profiler (Ecklund et al., 1988) and has been extensively used in many air quality studies (Neff, 1998). The radar was configured to operate in a dual mode. That is to say, two sets of wind profiles with different ranges and resolutions were obtained. Low transmit mode wind profiles were collected hourly from a range of 304

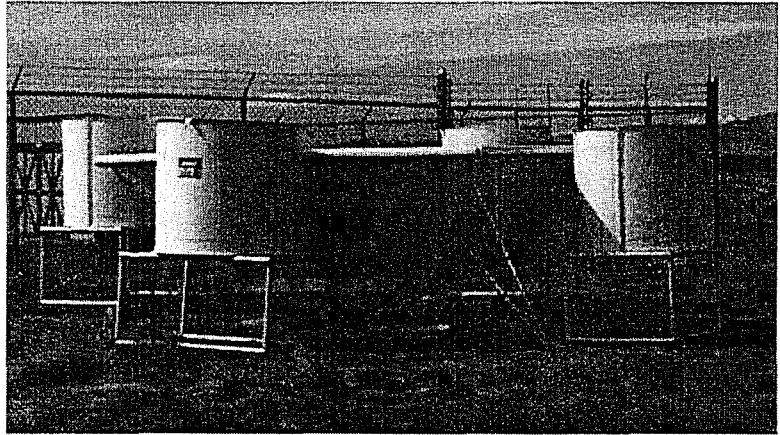


Figure 7. Photograph of a Radian LAP-3000 radar wind profiler and RASS.

to 3977 m with a resolution of about 193 m (20 measurement levels). High transmit mode wind profiles were acquired as 30-min averages from a range of 183 to 1740 m with a resolution of 55 m (30 levels). The radar was configured to transmit 3-beams (one vertical, two oblique angle beams oriented towards 335 and 245 degrees in azimuth). These data were delivered to ETL in CDF format. Virtual temperature profiles were acquired by the RASS twice per hour as 5-min averages. A total of 14 measurement levels were acquired from 112 to 1477 m with a resolution of 105 m.

3 Performance Audits

Detailed guidance or procedures on the auditing of Doppler sodars, radar wind profilers, and RASS have never been provided by regulatory agencies. The *On-Site Meteorological Program Guidance for Regulatory Modeling Applications* (U. S. EPA, 1987a) provides limited guidance, but only for sodars. A recent revision to the *Quality Assurance Handbook for Air Pollution Measurement Systems, Volume IV: Meteorological Measurements* (U. S. EPA, 1995) provides more current guidance but still falls short in detail. As a result, a variety of methods have evolved over the last several years.

Prior to the start of the study, Parsons Engineering Science was contracted to conduct performance audits on the Doppler sodars and radar wind profiler. The audits provided an independent assessment that the ground-based remote sensors were setup and operating in accordance with the manufacturers recommendations (Baxter, 1996). It should be pointed out that the procedures of this particular performance audit do not necessarily reflect the views or opinions of the manufacturers or other users of these ground-based remote sensors. Other techniques have been used in other monitoring studies. Those views, as well as the results from this particular performance audit are presented here in this paper.

The performance audits were conducted in accordance with the most current guidance available from the U. S. Environmental Protection Agency (EPA). The audit procedures were consistent with guidelines specified in the *Quality Assurance Handbook for Air Pollution Measurement Systems, Volume IV: Meteorological Measurements* (U. S. EPA, 1995) and the *On-Site Meteorological Program Guidance for Regulatory Modeling Applications* (U. S. EPA, 1987a). The evaluation included analysis of the site characteristics, review of the operational configuration of the instruments, and testing the response of the sodars using an Acoustic Pulse Transponder (APT) developed by Baxter (1994a; 1995). The audit of the radar only assessed the equipment setup. The audit procedures and results are described below.

3.1 Evaluation of Site Characteristics

A limiting factor in wind velocity determination for a Doppler sodar is usually the amount of environmental noise included with the backscattered signal (Neff and Coulter, 1986). Thus, a sodar must be able to differentiate the Doppler-shifted backscattered signal from all other ambient background noise. These external noise sources can be classified as active or passive and as broad-band (i.e., white noise or random frequency) or narrow-band (fixed-frequency). In general, a poor signal-to-noise ratio generally increases the variance of Doppler estimates and biases the Doppler-shifted frequency of the backscattered signal toward zero (Gaynor, 1977; Neff and Coulter, 1986). A full review on the degradation of Doppler sodar performance due to noise is given by Crescenti (1998). Part of the performance audit included the evaluation of site characteristics and identification of active and passive noise sources. It should be noted that the effects of active and passive noise may vary with atmospheric conditions. Thus, there are no definite pass/fail criteria.

Most ambient background noise is active broad-band. Examples include highway and road traffic, heavy machinery, industrial facilities, power plants, and airplanes. These noise sources produce a wide-band signal which can overlap the frequency bandwidth used by a sodar. Active broad-band noise effectively decreases the signal-to-noise ratio which results in a decrease in the maximum vertical range of the sodar since the backscattered signal can not be discerned from the active broad-band noise. Data from higher range gates are more susceptible to being lost to this kind of noise interference because of the exponential decrease in backscattered power with height. In general, the performance of a sodar will degrade as noise levels increase from these nearby sources. Some active broad-band noise sources such as highway traffic have a pronounced diurnal, weekly, and seasonal pattern.

Active fixed-frequency noise sources include the back-up beepers used on large trucks and forklifts, rotating fans, birds, and insects. These noise sources affect the performance of a sodar in different ways depending upon their type and proximity. If these noise sources possess frequencies close to that of a sodar's operating range, they may be misinterpreted by the sodar as valid backscattered data. That is to say, the algorithms used to determine the Doppler-shifted frequency of the backscattered signal are "fooled" by the active fixed-frequency noise. The result is an erroneous wind value that may be found in any number of the measurement heights that depend on the arrival time of the noise in relation to the initial transmit time of the sodar. Since a sodar expects only a very weak backscattered signal, strong active fixed-frequency noise sources may saturate the received signal. When this happens, the sodar is unable to determine any value for wind velocity. Some of these sources can be identified during the site selection process. One approach to reducing the problem of fixed-frequency noise sources is to use a coded pulse, i.e., a pulse has more than one peak frequency. A return pulse would not be identified as data unless peak frequencies were found in the return signal at the same frequency separation as the transmit frequencies. Pinkel and Smith (1992) introduced a repeat-sequence coding technique for Doppler sonars and sodars which was found to increase the precision of velocity estimates.

Passive noise sources are objects that reflect a transmitted acoustic pulse back to the sodar antenna. Examples of potential reflectors include buildings, trees, towers, and transmission lines. While most of the transmitted acoustic energy is focused in a narrow beam, side lobes do exist. In general, greater substantial side lobe energy exists for lower acoustic frequencies. Fixed-echoes are created when the side lobes reflect off of stationary objects and return the same acoustic frequency to the sodar receiver. A zero Doppler shift in the frequency would be interpreted by the sodar as a valid wind speed of 0 m s^{-1} . It is not always possible to predict which objects may be a problem. The antennas that are tilted at an oblique angle from the vertical, and that are used to determine the horizontal wind velocity, should be pointed in a direction away from those objects. Anything located in the same general direction in which the antenna is pointing and extending higher than several meters may be a potential reflector.

Algorithms have been developed which isolate and remove ambient background noise. Melling and List (1978) introduced a zero-crossing technique to extract wind velocities from the backscattered signal. Mastrantonio and Fiocco (1982) developed a technique to improve the

accuracy and precision of sodar wind measurements by isolating the backscattered signal from ambient noise by a spectral integration. Good results have been obtained with a noise reduction scheme developed by Gardiner and Hill (1986). The final few samples of each received backscattered signal are assumed to be due entirely to wind noise. This provides a baseline which is subtracted out of the next backscattered signal. Some commercially available sodars have algorithms which identify fixed-echoes. In general, the algorithms would identify backscattered frequencies with zero Doppler shift which remain constant in space and over time. That peak frequency would be eliminated and the next strongest backscattered frequency would be used in determining the wind velocity. It is not clear which methods, if any, are used by the manufacturers to minimize noise interference. Often, those algorithms are proprietary in nature, and thus not subject for release to the general public.

A qualitative assessment of active noise included identification of all artificially and naturally generated sources at the BAO. These included traffic from Interstate-25, air conditioners in equipment trailers, and birds. In addition, there were two sources of active noise common to all of the sodars. The first was the RASS that operated at the entrance to the BAO facility. The acoustic sources for the RASS were active twice per hour for 5 min at the start of each hour. The operating frequency of the RASS was outside the operating range of all the sodars except the Metek MODOS. Metek took precautions against interference by orienting their oblique angle antennas away from the RASS. The second active noise source was wind-generated noise from the tower and its guy wires. During very windy conditions ($> 10 \text{ m s}^{-1}$), a "whistling" effect was created. The frequency of the noise varied with changing wind speeds. However, audit capabilities at the time were unable to identify specific frequencies of tower-generated noise. It was noted (Baxter, 1996) that tower-generated noise due to high winds could potentially interfere with sodar operation by limiting the altitude range of the sodars as well as producing audible frequencies within the operating range of the sodars. Kaimal et al. (1980) discovered that BAO tower was a source of narrow-band noise in an earlier study. The closely spaced elements of the elevator/carriage support system on the tower generated noise with two spectral peaks when southwesterly winds exceeded 4 m s^{-1} . The first peak was located at 500 Hz and was of no consequence to any of the five sodars being evaluated. The second peak ranged between 1100 and 1300 Hz and affected the performance of at least one sodar. These frequencies are well below those used by the four sodars evaluated in this study.

Acoustic noise levels were measured on 4 April 1995 from 0930 to 1000 MDT using a Realistic 33-2055 digital sound level meter. The sound meter was placed on a tripod west of the tower in what is approximately the center of the BAO. This measurement was assumed to be representative of the overall facility. Noise levels were observed eight equally spaced directions. The maximum level was approximately 64 dB with average noise levels of less than 50 dB. Higher maximum values were due to nearby birds, traffic noise from Interstate-25, air conditioners for the electronics trailers, and the acoustic pulses emitted from the surrounding sodars. Unfortunately, due to time and budget constraints, only one noise survey was conducted. While it was shown from a single survey that the BAO facility is a quiet environment for the operation of Doppler sodars, it would have been useful if several more surveys were conducted at various times throughout the day to at least assess the levels of noise created by traffic from I-25, especially during rush hour.

The technology now exists to conduct a more quantitative noise survey with minimal cost and effort. A portable laptop computer, sound card and microphone are the only tools needed to identify the frequencies and relative intensities of background noise. While not in existence during this study, a recently available freeware program named Spectrogram (ver 3.1) was successfully used by Crescenti and Baxter (1998) to identify the frequencies of various noise sources in the vicinity of operating sodars during a subsequent air quality sodar study in southern California. The latest version of this program may be found at <http://www.monumental.com/rshorne/gram.html>. Both broad-band and narrow-band frequencies were generated by various mechanisms. Spectrogram allowed for easy identification of these noise sources. As a result, the output frequency of the sodar was changed to a bandwidth where there was no noise interference.

Ideally, a site should be relatively clear of obstacles that could act as potential fixed-echo reflectors for Doppler sodars. This is also true for objects that may act as ground-clutter in the operation of a radar wind profiler. However, ideal sites for either a sodar and/or radar are rare. Therefore, it is important to construct an obstacle vista table that contains information about the site (Baxter, 1994b; 1996). This includes identification of all natural and man-made objects surrounding the sensor, their azimuth, elevation angle above the horizon (i.e., height), and distance. The information provided in such a table can be used to assess potential interference in sodar or radar operations. Vista tables (Tables 4, 5 and 6) were constructed for the AeroVironment, Metek, and Radian sodars, respectively, during the performance audit. An indication of potential fixed-echo interference would be in the form of consistent depressions in the wind speed profile for an oblique angle beam oriented towards an object that may act as a reflector. A vista table was also constructed for the Radian LAP 3000 radar wind profiler and RASS (Table 7). Objects such as swaying power lines and trees are potential reflectors for the electromagnetic pulse transmitted by the radar.

The results of the site evaluations identified the locations of each sodar and radar as generally acceptable (Baxter, 1996). There were a number of reflective sources that could potentially contaminate the data, but each manufacturer oriented the oblique angle antenna beams away from those objects. In particular, the most significant reflective source was the 300-m tower and its guy wires. Minor sources included a variety of small buildings used to house electronics and data acquisition systems.

Another sodar system check performed as part of the audit was a so-called "listen only" test. That is to say, the sodar transmitters are turned off but the receivers remain on. This test can help determine if any background noise level produces a "measured" wind velocity. In practice, no valid wind values (i.e., -999 or blank) should be reported by a sodar. However, if any "valid" values are reported, then there may be an active noise source in the area generating frequencies in the operating range of the sodar. All sodars tested during the audit displayed only invalid data in the "listen only" test. Thus, additional confidence was gained that the BAO was a "quiet" site for the operation of a sodar.

Table 4
Vista table for AeroVironment 4000 sodar.

Mag. Azimuth (deg)	True Azimuth (deg)	Obstacle Elev. (deg)	Features/Distances/Other Notes
0	12	45	Guy wires going to top of tower
30	42	< 3	Flat terrain
60	72	< 3	Flat terrain, houses with trees ~ 1 km
90	102	< 3	Flat terrain, trees with no leaves ~ 1 km
120	132	< 3	Flat terrain
150	162	7	Tank and tower ~ 1 km
180	192	< 3	Flat terrain
195	207	< 3	Building ~ 75 m, start of guy wires
210	222	35	Guy wires ~ 25 m
240	252	66	Guy wires ~ 30 m
270	282	69	Guy wires ~ 40 m
310	322	65	Guy wires, trailer ~ 30 m
330	342	62	Guy wires close to top of BAO tower
340	352	59	BAO tower
354	6	50	Main compound buildings ~ 200 m

3.2 Equipment Alignment

The orientation of an antenna with respect to azimuth, whether it is an individual antenna of a 3-beam sodar system or a phased-array antenna of a sodar or radar, directly affects the accuracy of the sodar-derived or radar-derived wind direction. Similarly, the level of an antenna with respect to horizontal directly affects the calculation of the component wind velocities. Thus, another critical component of the performance audit was to verify antenna alignment and level.

A Brunton Pocket Transit (model F5007LM) was used to verify the orientation and level of the sodar and radar antennas for the two oblique angle antenna directions. The transit is tripod-mounted and can be read to an accuracy of approximately $\pm 0.5^\circ$.

Table 5
Vista table for Metek MODOS sodar.

Mag. Azimuth (deg)	True Azimuth (deg)	Obstacle Elev. (deg)	Features/Distances/Other Notes
0	12	< 3	Houses, trees, power lines ~ 500 m
30	42	< 3	Houses, trees, power lines ~ 400 m
60	72	< 3	Houses, trees, power lines ~ 800 m
90	102	< 3	Power lines ~ 400 m
120	132	< 3	Houses, trees, power lines ~ 1 km
150	162	< 3	Trees ~ 1 km, water tank ~ 2 km
165	177	6	Instrument trailers ~ 50 m
180	192	< 3	Instrument trailers ~ 60 m
210	222	25	Guy wires ~ 300 m
225	237	49	BAO Tower
240	252	37	Guy wires ~ 30 m
270	282	< 3	Power lines ~ 2 km
300	312	< 3	Houses ~ 1 km
330	342	< 3	Houses, trees ~ 1 km

The magnetic sitings were corrected with respect to true north with solar observations of the sun's azimuth angle in both directions (U. S. EPA, 1995). The corrected orientation was then compared to the values in the software settings of each sodar and radar. The audit results for the azimuths are given in Table 8. The audit found that all of these antennas were aligned to within 1° in azimuth. Antenna levels were checked using the inclinometer integral to the transit. All four sodars and the radar were found to be with $\pm 0.5^\circ$ from horizontal. For alignment, the criteria for acceptable orientation of the oblique angle beams is $\pm 2^\circ$. This is readily achievable and consistent with the wind vane orientation from U. S. EPA (1995) specified guidance while the criteria for the level of an antenna is $\pm 1^\circ$. It was noted that some of the systems did not lend themselves to straight-forward checks of the antenna level or zenith angle measurement. This is an important item during the setup and audit stages of a monitoring program. The level of the parabolic antennas of the RASS were not checked for leveling. However, a recent study by Coulter (1998) suggests that RASS acoustic antennas should be level to within $\pm 1^\circ$.

Table 6
Vista table for Radian 600 and 600PA sodars.

Mag. Azimuth (deg)	True Azimuth (deg)	Obstacle Elev. (deg)	Features/Distances/Other Notes
0	12	< 3	Houses, trees ~ 1 km
30	42	< 3	Houses, trees ~ 1 km
60	72	< 3	Houses, trees ~ 1 km
90	102	22	Guy wires ~ 400 m
105	117	46	BAO tower ~ 300 m, FM-CW radar ~ 40 m
120	132	31	Guy wires ~ 500 m
150	162	< 3	Flat terrain
180	192	< 3	Flat terrain
210	222	< 3	Flat terrain
240	252	< 3	Flat terrain
270	282	< 3	Tree with no leaves ~ 1 km
300	312	< 3	Flat terrain, high tension towers ~ 1.5 km
330	342	< 3	Houses, trees, and power lines ~ 1 km

The verification of the proper operation of each transducer in a phased-array sodar is critical for the acquisition of valid data. The failure of a transducer, a bank of transducers, or the driver switching electronics can degrade the focus of the acoustic beam and its steering. For this study, no audit procedures were performed on this particular aspect. However, this is a critical step to add confidence in the proper operation of a phased-array sodar. Some manufacturers have self diagnostic algorithms to test each individual transducer in a phased-array. These should be utilized every several (4 to 6) months since prolonged exposure of these transducers can lead to failure. One technique of evaluating the integrity of a phased-array antenna is to test the relative amplitude output of each transducer. The procedure involves sequentially placing a test element over each transducer of the array and measuring the voltage induced into the test element from each transmit pulse. The analog peak voltage of each pulse can be observed and compared to other elements in the array. The test element should have a foam insulation seal around the mating surface to minimize interference from adjacent phased-array transducers. The measurements are typically taken over multiple cycles of the beam transmit sequence.

Table 7
Vista table for Radian LAP 3000 radar wind profiler and RASS.

Mag. Azimuth (deg)	True Azimuth (deg)	Obstacle Elev. (deg)	Features/Distances/Other Notes
0	12	27	Guy wires ~ 500 m, power lines ~ 2 km
10	22	31	BAO tower ~ 500 m
30	42	< 3	Houses, power lines ~ 2 km
60	72	< 3	Trees with no leaves ~ 1.5 km
90	102	< 3	Flat terrain
120	132	8	Light pole ~ 30 m
150	162	11	Building
180	192	7	Power lines ~ 200 m
210	222	5	Power lines ~ 300 m
240	252	14	10-m tower ~ 20 m
270	282	< 3	Flat terrain
300	312	< 3	Trees with no leaves ~ 3 km
330	342	< 3	Trees, power lines ~ 3 km

Table 8
Performance audit results.

	AV 4000	Metek MODOS	Radian 600	Radian 600PA	Radian LAP 3000
Beam 1 Direction (°)	83.0	10.5	215.0	259.0	335.5
Beam 2 Direction (°)	173.0	101.0	302.0	349.0	245.5
APT Results (m s ⁻¹)					
Horizontal Avg. Diff.	0.04	-0.17	-0.2	0.01	
Horizontal Max. Diff.	-0.08	-0.21	-0.5	0.03	
Vertical Avg. Diff.	-0.09	0.05	-0.1	-0.05	
Vertical Max. Diff.	-0.21	0.07	-0.1	-0.11	
Clock Time Difference (s)	11	-4	-2	-1	4

3.3 Simulated Wind Test

An important aspect to any measurement program is the need to quantitatively verify the response of a sensor to known inputs. The output of conventional *in situ* sensors such as a cup anemometer can easily be confirmed by placing the sensor in a wind tunnel or by rotating the shaft at a known speed. Unfortunately, the verification of wind velocity data from a Doppler sodar is more problematic but not impossible.

Sodar-derived wind velocities are obtained by the measurement of the frequency shift and the time of arrival of a backscattered acoustic pulse. Thus, the only means of truly providing a known input into a sodar is the introduction of specific acoustic frequencies at known time intervals. The difference between the transmit frequency and a simulated backscattered frequency corresponds to a Doppler shift introduced by winds moving to or away from the antenna. The time of arrival of a simulated return with respect to the transmit pulse represents a specific altitude based on the speed of sound and the beam zenith angle. The Acoustic Pulse Transponder (APT) was developed by Baxter (1995) to input acoustic frequencies at predetermined times into a sodar for the verification of a simulated wind profile.

The APT is a microcomputer based system used for auditing Doppler sodars. This system first detects the transmitted acoustic pulse from the sodar antenna then transmits a preprogrammed pulse sequence back at the sodar. The pulse sequence consists of one or more sequential frequencies at specifically timed intervals that represent known frequency offsets from the sodar. The frequency offsets and time of the pulses simulate a wind profile along each of the sodar component axes. The APT can be programmed for the number of pulses, pulse duration, pulse frequency, and timing delays. The APT system consists of three modules: The pulse transponder, system interface, and portable laptop computer.

The pulse transponder is placed near the sodar antenna and serves two purposes. It acts as a receiver (microphone) that detects the transmit pulse from the sodar antenna. The pulse transponder also acts as a speaker that transmits the audio frequencies back into the sodar antenna.

The system interface provides the link between the pulse transponder and laptop computer. The interface converts the detected acoustic pulse received by the transponder into a digital signal that is transmitted to the computer via the RS-232 port. In addition, the interface amplifies and conditions the audio frequencies generated by the computer that are sent to the transponder.

The laptop computer detects the transmit pulse in the RS-232 port and initiates the pulse timing sequence. The computer software calculates the retransmission timing and frequency to be generated based on a preprogrammed configuration that is specific to the sodar being audited. The frequencies generated by the computer are transmitted to the system interface by means of an audio pickup. The system configuration as well as a record of each retransmitted pulse is recorded in a documentation file.

The APT has an accuracy of 1 Hz from 1390 to 4606 Hz. The accuracy of the pulse timing is 2 ms which corresponds to an altitude resolution of better than 1 m. A more complete description of the APT is given by Baxter (1994a; 1995)

A simple wind profile simulation was applied to each sodar. The APT was programmed to simulate wind velocities about 3 to 4 m s⁻¹ in the lower portion of the sodar operating range. The upper portion of the profile was programmed to smoothly increase wind velocities to 7 to 8 m s⁻¹ in the opposite direction. The results of the APT tests (Table 8) show agreement within ±0.2 m s⁻¹. Thus, the APT tests provided additional confidence that all of the sodars properly received the generated acoustic pulse and computed the proper wind profiles based on known frequency inputs.

3.4 Independent Wind Measurement Comparison

An operational check using independent wind measurements can help establish the “reasonableness” of the sodar or radar-derived winds. This procedure can help identify any major problem with the system such as improper sensor alignment or defective beam steering. It is important to note that this is a necessary procedure even if an APT test is included in a sodar audit.

The comparison to independent wind measurements depends on the actual instrument used for data collection (e.g., tower, tetheredsonde, rawinsonde, kite, or another ground-based remote sensor). Prior to the comparison, it is important to assure the independent data are processed using similar methods as the sodar or radar data, i.e., calculated vector averages. A typical acceptance criteria may be ±20° for wind direction and ±2 m s⁻¹ for speed. For two sodar systems measuring the same volume this criteria may be much tighter while comparisons of data collected from a radar and kite measurements may be much broader. Exceedance of the criteria does not necessarily mean either system is malfunctioning but instead alerts the user that further evaluations may be needed to determine the reason for the differences. Militana et al. (1991), Virag et al. (1992) and Wilkerson et al. (1994) have outlined sodar audit procedures using tetheredsondes. Similarly, West and Ferullo (1990) present a sodar audit procedure using tower measurements.

U. S. EPA (1987a) had proposed one form of performance auditing using instruments such as a tetheredsondes to collect at least 120 sample intervals for comparison of sodar data. This large number of samples reflected a lack of trust of the sodar technology with the need to reprove the operation through expensive multi-day tests every six months. A permit must be issued by the Federal Aviation Administration (FAA) for tetheredsonde deployments. This can be logistically difficult, especially in areas near airports. Another limitation with tetheredsonde deployment is the difficulty of using them in high wind conditions (> 10 m s⁻¹). However, with better guidance and the improvement of sodar technology (Crescenti, 1997), such aggressive comparisons have become unnecessary.

Regardless of the platform used for comparison, West and Ferullo (1990) compiled several different types of scatter plots as part of their audit procedure. This plots are especially helpful with displaying discrepancies that are not obvious in statistical measures of scatter (e.g., bias,

comparability, precision, correlation coefficient). A summary of the variables used in those plots is given in Table 9. For example, plotting ΔWD (sodar wind speed minus tower wind speed) as the dependent variable (y-axis) as a function of the independent variable (x-axis) WS (tower) usually shows large scatter of wind directions for light wind conditions and smaller differences for more moderate wind speeds. Of course, the independent variables are data acquired by so-called “standard sensors” (i.e., tower, tethersonde). West and Ferullo (1990) also point out that constructing multiple scatter plots is helpful for finding discrepancies in the sodar data as well as discrepancies in the standard measurements. In their case of comparing sodar wind directions against tower wind directions, they discovered that the tower-based vane was misaligned by 24° . Virag et al. (1992) point out that uncertainty in tethersonde height can lead to scatter in comparisons against sodar derived winds, especially in zones of significant wind shear. Thus, the lesson learned is that even standard measurements used in audits can contain errors.

Table 9
Variables used in scatter plots for audits
(based on West and Ferullo, 1990).

Dependent Variable	vs	Independent Variable
WS	vs	WS
WD	vs	WD
ΔWS	vs	time
ΔWS	vs	WS
ΔWS	vs	WD
ΔWS	vs	ΔWD
ΔWD	vs	time
ΔWD	vs	WS
ΔWD	vs	WD

Due to the nature of the study, an independent wind measurement comparison was not performed as part of the audit. Data acquired by the tower-based *in situ* sensor are used to evaluate the performance of these ground-based remote sensors.

3.5 Other Audit Procedures and Observations

Since computer clocks can drift in time, each was checked to assure all data were collected in an appropriate time synchronization. This is especially important if there are interferences created between instruments such as the RASS and one or more sodars. The time becomes crucial if there

is an overlap and more than one sample interval may become contaminated. At the outset of the program all of the instrument clocks were synchronized with a WWV clock at the tower. The drift in sodar/radar clock time varied from -1 to +11 s over the course of several days.

Finally, attention was focused on the manufacturer's definition of wind component values. In some instances, the horizontal wind components obtained from the oblique angle beams were rotated to align with 90° (east) and 0° (north) to form the commonly accepted meteorological values of U and V . Other manufacturers simply reported the component velocities with respect to the oblique angle antennas but still labeled these velocities as U and V . There are advantages and drawbacks of each definition, however, it is incumbent on the user to understand the reporting convention for proper data validation and interpretation.

4 Methodology

Most evaluation studies have utilized simple statistical techniques to assess the overall reliability of Doppler sodar, radar wind profiler and RASS measurements. For example, many investigators use linear least-squares regressions of the form

$$y = mx + b \quad (1)$$

where m is the slope and b is the y-intercept describing the fit of the remote sensor data (y) as a function of the reference data (x). The amount of scatter (root-mean-square difference) about a linear fit is often reported as the standard error (SE). For example, regression fits of sodar wind speed as a function of tower wind speed can be easily determined. Similarly, fits can be determined for wind direction values from a remote sensor as a function of tower-based wind direction data.

Another simple statistical measure of remote sensor reliability is the linear correlation coefficient r which is defined as the ratio of the covariance between two variables x and y to the square root of the product of the variance of x and the variance of y . The equation is defined as

$$r = \frac{\sigma_{xy}}{\sqrt{\sigma_x^2 \sigma_y^2}} \quad (2)$$

By definition, r ranges from -1 to +1. Two variables (e.g., sodar wind speed and tower wind speed) are perfectly correlated (i.e., vary together) when $r = 1$. Conversely, those two same variables are perfectly negatively correlated (i.e., vary oppositely) when $r = -1$. Variables with no net variation yield $r = 0$. However, when using a linear correlation to assess the reliability of both wind speed and wind direction from a sodar or radar against tower-based values, two separate values of r must be determined.

Crosby et al. (1993) proposed a definition for a vector correlation coefficient r_v in which the effects of both magnitude and direction are included in a simple scalar value that is a measure of the degree of association between the vectors of interest. The following definition for r_v consists of matrix multiplications of variances and covariances of the wind velocity components:

$$r_v = \frac{f}{g} \quad (3)$$

where

$$\begin{aligned} f = & \sigma_{u_1 u_1} [\sigma_{u_2 u_2} \sigma_{v_1 v_2} \sigma_{v_1 v_2} + \sigma_{v_2 v_2} \sigma_{v_1 u_2} \sigma_{v_1 u_2}] + \sigma_{v_1 v_1} [\sigma_{u_2 u_2} \sigma_{u_1 v_2} \sigma_{u_1 v_2} + \sigma_{v_2 v_2} \sigma_{u_1 u_2} \sigma_{u_1 u_2}] \\ & + 2[\sigma_{u_1 v_1} \sigma_{u_1 v_2} \sigma_{v_1 u_2} \sigma_{u_2 v_2}] + 2[\sigma_{u_1 v_1} \sigma_{u_1 u_2} \sigma_{v_1 v_2} \sigma_{u_2 v_2}] - 2[\sigma_{u_1 u_1} \sigma_{v_1 u_2} \sigma_{v_1 v_2} \sigma_{u_2 v_2}] \\ & - 2[\sigma_{v_1 v_1} \sigma_{u_1 u_2} \sigma_{u_1 v_2} \sigma_{u_2 v_2}] - 2[\sigma_{u_2 u_2} \sigma_{u_1 v_1} \sigma_{u_1 v_2} \sigma_{v_1 v_2}] - 2[\sigma_{v_2 v_2} \sigma_{u_1 v_1} \sigma_{u_1 u_2} \sigma_{v_1 u_2}] \end{aligned} \quad (4)$$

and

$$g = [\sigma_{u_1 u_1} \sigma_{v_1 v_1} - \sigma_{u_1 v_1} \sigma_{u_1 v_1}] [\sigma_{u_2 u_2} \sigma_{v_2 v_2} - \sigma_{u_2 v_2} \sigma_{u_2 v_2}] \quad (5)$$

By definition, a perfect correlation between two sets of vectors yields a value of $r_v = 2$. Zero correlation exists when $r_v = 0$.

Other statistics of comparison that have been used are the bias (accuracy) B and the comparability (root-mean-square difference) C . They are defined (Hoehne, 1971) as

$$B = \frac{1}{N} \sum_{i=1}^N (Y_i - X_i) \quad (6)$$

$$C = \left[\frac{1}{N} \sum_{i=1}^N (Y_i - X_i)^2 \right]^{1/2} \quad (7)$$

where N is the number of observations, X_i is the i th observation from the reference instrument (in this case, the BAO tower), and Y_i is the i th observation from the sensor in question (i.e., Doppler sodar, radar wind profiler, or RASS). The bias is simply a measure of a systematic error. The comparability is a useful statistic since it combines both bias and random errors. The precision (standard deviation) S is defined as

$$S = (C^2 - B^2)^{1/2} \quad (8)$$

As noted by Crescenti (1997) who reviewed a compilation of sodar comparison studies, many investigators often compute these statistics for an entire data set regardless of atmospheric conditions or stability. When the data sets were subdivided, it was often day versus night so that Doppler sodars could be evaluated for convective (unstable) versus laminar (stable) conditions, respectively. Unfortunately, these simple statistics were not generated as a function of various measures of atmospheric conditions or stability.

Eight different measures of atmospheric conditions and stability are used in this study to measure the statistical characteristics of these ground-based remote sensors. They include: relative humidity (RH), Pasquill-Gifford (PG) stability class, time of day, scalar wind speed (SS), standard deviation of the horizontal wind direction (σ_θ), wind shear (S_h), the square of the Brunt-Vaisala frequency (N_{BV}^2), and the bulk Richardson number (R_B). These parameters were chosen since they are easily derived from tower-based measurements.

Molecular attenuation of acoustic signals from Doppler sodars significantly increases with decreasing relative humidity (Neff, 1975; Crescenti, 1998), especially for relative humidity less than 40%. In addition, radar wind profilers also demonstrate much better performance at higher humidities. Thus, statistical estimates were derived for five classes of surface (10-m) relative humidity. The statistics were generated for relative humidities between 0 - 20%, 20 -40%, 40 - 60%, 60-80%, and 80-100%.

Pasquill-Gifford (PG) stability class was determined using by the solar radiation/delta-T method (Coulter, 1994). One of six stability classes (A, B, C, D, E, or F) was determined from 10-m tower wind speed, the incoming solar radiation, and the tower-based temperature difference between 10 and 50 m. These stability classes are useful in characterizing an unstable (A, B, C), neutral (D), or stable (E, F) boundary layer.

Time of day was divided into four categories: dawn, day, dusk, and night. The transitional times of dawn and dusk were included to examine those instances when the boundary layer was making the transition from stable to unstable and from unstable to stable, respectively. For this study, dawn is defined as the time in the early morning when the Sun is between 10° below the horizon to 20° above the horizon. Dusk is defined as the time in the late afternoon when the Sun is between 10° above the horizon to 20° below the horizon. Of course, day is the time between dawn and dusk when the Sun is above the horizon while night is between dusk and dawn when the Sun is below the horizon.

Strong winds can generate localized noise that can potentially interfere with Doppler sodar operations (Crescenti, 1998). In addition, strong winds can effectively push the acoustic signal generated by a RASS source away from the vertically pointing radar beam, thereby degrading temperature measurements. The surface (10-m) scalar wind speed was subdivided into four categories: near calm (< 2 m s⁻¹), light wind (2 - 5 m s⁻¹), moderate wind (5 - 10 m s⁻¹), and strong wind (> 10 m s⁻¹).

The standard deviation of the horizontal wind direction σ_θ acquired by the 10-m wind monitor was used to measure the horizontal homogeneity of the wind field. Four categories were created: very homogenous (< 10 deg), moderately homogeneous (10 - 20 deg), moderately nonhomogeneous (20 - 30 deg), and very nonhomogeneous (> 30 deg).

A simple measure of mechanical mixing can be estimated by computing the wind shear. For this study, S_h is defined as:

$$S_h = \left[\left(\frac{\Delta u}{\Delta z} \right)^2 + \left(\frac{\Delta v}{\Delta z} \right)^2 \right]^{1/2} \quad (9)$$

where Δu and Δv are differences in the wind velocity components over the vertical thickness Δz (10

and 50 m). Four categories were created: no wind shear ($< 0.02 \text{ s}^{-1}$), light wind shear ($0.02 - 0.04 \text{ s}^{-1}$), moderate wind shear ($0.04 - 0.06 \text{ s}^{-1}$), and strong wind shear ($> 0.06 \text{ s}^{-1}$).

Conversely, a simple measure of the thermal mixing (i.e., buoyancy) can be estimated by computing the Brunt-Vaisala frequency N_{BV} which is defined (e.g., Stull, 1988) as:

$$N_{BV} = \left(\frac{g}{\theta} \frac{\Delta\theta}{\Delta z} \right)^{1/2} \quad (10)$$

where g is the acceleration due to gravity (9.81 m s^{-2}), θ and $\Delta\theta$ are the mean and difference of potential temperature, respectively, over the vertical thickness Δz (10 and 50 m). In this application, four categories of the square of the Brunt-Vaisala frequency (N_{BV}^2) were created: unstable ($< 0 \text{ s}^{-2}$), slightly stable ($0 - 0.001 \text{ s}^{-2}$), moderately stable ($0.001 - 0.002 \text{ s}^{-2}$), and strongly stable ($> 0.002 \text{ s}^{-2}$).

Finally, the bulk Richardson number R_B is a simple measure of the ratio of thermal mixing to mechanical mixing and is defined (e.g., Stull, 1988) as:

$$R_B = \frac{g}{\theta} \frac{\Delta\theta \Delta z}{(\Delta u)^2 + (\Delta v)^2} \quad (11)$$

R_B is computed from temperature and wind velocities at 10 and 50 m. Four categories for R_B were created: strongly unstable (< -0.5), moderately unstable ($-0.5 - 0.25$), moderately stable ($0.25 - 1$), and strongly stable (> 1).

Some data were eliminated in order to avoid an artificial bias or scatter in these statistical parameters. Data were not considered when the tower-based vector wind speed was less than 0.5 m s^{-1} (i.e., below the starting threshold of the wind monitor). In addition, data were not considered when the wind direction was between 302° clockwise to 32° . This was done to avoid tower-generated turbulence and is consistent with the methodology developed by Kaimal (1986).

5 Analysis

The first step in the evaluation and performance of these ground-based remote sensors is an analysis of data availability as a function of atmospheric conditions and stability. Next, those data acquired by a particular remote sensor are screened by their respective signal-to-noise ratios in order to remove obvious outliers when the SNR is low. After those bad data have been removed, the performance statistics of the wind speed and direction data have been computed and analyzed as a function of atmospheric conditions and stability. Finally, the same methodology is applied to the virtual air temperature data acquired by the RASS.

5.1 Data Availability

Many regulatory monitoring programs usually have a criteria requiring a minimum amount of data to be collected over a particular time frame (e.g., U. S. EPA, 1987b). If a sensor can not meet that criteria, then its use may be problematic. The amount of wind velocity data collected by Doppler sodars or radar wind profilers over a particular vertical range can vary from hour-to-hour, day-to-day. This can be attributed to attenuation of transmitted acoustic or electromagnetic (EM) signals of the previously mentioned sensors by various atmospheric conditions.

Plots of data availability as a function with height are shown in Appendix A. These plots include data acquired by the AeroVironment sodar, both Radian sodars, the radar wind profiler (both the high resolution/low range mode and low resolution/high range mode), and the RASS. Unlike most sodars, the Metek sodar reported data at all range gates. The first set of the graphs show the percentage of "valid" data reported by each remote sensor for the entire experiment. The parabolic decrease of wind velocity data with height reported by the sodars is consistent with the findings from other studies (Santovasi, 1986; Piringer, 1994). Data availability profiles reported by the radar profiler compare with those found by other investigators (Ecklund et al., 1990; Martner et al., 1993; Whiteman and Bian, 1996). The data availability profile of RASS temperature data also conforms to findings from previous studies (Bonino et al., 1986; Schroeder, 1990; Martner et al., 1993).

More than 90% of the data reported by the AeroVironment sodar was available to a height of 75 m and 50% were available to a height of about 150 m. The Radian 600 sodar reported a data capture of 90 and 50% to heights of 200 and 450 m, respectively, while the Radian 600PA reported data availability of 90 and 50% to heights of 125 and 325 m, respectively. As expected, data availability at higher altitudes for the sodar is limited by the molecular attenuation of the acoustic signal (Neff, 1975; Crescenti, 1998).

It should be noted that the data availability profiles for the radar and RASS are shifted to lower percentages because of several power outages. In most circumstances, the data availability is usually high in the first 1 km of the atmosphere. For example, a 915-MHz radar wind profiler and RASS located at the Idaho National Engineering and Environmental Laboratory (INEEL) reliably acquired wind and temperature profiles for more than three years. A data capture for the radar of more than 90% was found from the lowest range gate to a height of 1.3 km while 50% of the data

were available to a height of 2.7 km. Similarly, more than 90% of temperature data were available to a height of 600 m and 50% to a height of 1.2 km. It should be noted that out of a possible 17,520 profiles for 1998 (48 profiles per day times 365 days), a total of 100 (0.57%) wind profiles and 102 (0.58%) temperature profiles were lost due to a loss of electricity or disruption in remote communications with the radar and RASS.

Data availability shows a significant decrease in sodar-reported wind values when the relative humidity is less than 20%. As originally shown by Neff (1975) and later by Crescenti (1998), molecular attenuation for acoustic frequencies significantly increases as relative humidity decreases. Thus, it is reasonable to expect a substantial decrease in the total amount of available data in very arid environments. Ordinarily, the range for radar wind profilers is greater for higher humidities due to a greater humidity refractive index. However, no apparent relationship exists between surface relative humidity and data availability of the radar and RASS for this study.

Using PG classes, it can be seen in Appendix A that more data is reported to greater heights by the sodars during generally convective conditions (class A, B, C) while less data is reported for more neutral to stable conditions (class D, E, F). The data availability profiles are quite dramatic for the AeroVironment and Radian 600PA sodars. To some extent, the same is also true for the data availability profiles of the radar. In both cases, the turbulent nature of the convective boundary layer provides the necessary scattering mechanisms to return a portion of the transmitted acoustic or EM signals back towards the surface. Stable boundary layers tend to be more stratified and less turbulent and thus are not as conducive to scattering the transmitted signal back towards its point of origin. The RASS is somewhat unique. More data is returned under stable conditions at lower altitudes (< 500 m) while more data is returned for convective conditions at higher altitudes (> 500 m). Bonino et al. (1986) show data availability for RASS data based on PG classes. In their study, data availability profiles show similar decreases with height.

When the data are separated in accordance with the time of day, the AeroVironment sodar shows a much greater data capture for day time conditions than any other category. This, of course, can be attributed to generally convective conditions. The two Radian sodars, however, do not show any significant distinction between the various time of day categories. The radar and RASS data availability profiles suggests less data during night and dawn, i.e., those times when the atmosphere is most stable.

In general, the stronger the scalar wind speed, the less data reported by the sodars. Wind at and near the ground normally produces most of the ambient noise sensed by a sodar except in urban, industrial, and other populated areas where artificial noise often exceeds the natural ambient noise (Simmons et al., 1971). Several investigators (Parry et al., 1975; Hardesty et al., 1977; Finkelstein et al., 1986; Evers and Neisser, 1990; Dahlquist, 1993) have noted the loss or corruption of data due to wind-generated noise when horizontal wind velocities were greater than 10 m s^{-1} . This is because high surface winds generate localized dynamic and acoustic noise against the surfaces of the sodar antenna shields. Wind noise can be appreciable at exposed locations such as mountain tops and other terrain features with sharp relief (Asimakopoulou et al., 1980). In general, increased wind

speeds cause a reduction in sounding range (Bonino et al., 1986). Similar data availability profiles are also seen for the radar and RASS. Stronger winds lead to less available data. In the case of the RASS, strong winds “push” the acoustic signals away from the transmitted radar EM beam, thus reducing the effective Bragg scattering necessary to acquire temperature profiles (Peters and Kirtzel, 1994; May et al., 1996). Strong winds also usually typical of neutral conditions, thereby further decreasing the backscattered intensity.

All of the sodars exhibit high data capture when σ_θ is large. In general, large values of σ_θ are associated with generally light winds and unstable conditions (e.g., Lumley and Panofsky, 1964; Mitchell, 1982; U. S. EPA, 1987a). The same is also seen for the radar data availability profiles. However, the RASS profiles show just the opposite behavior. It is not clear why this happens since small values of σ_θ are associated with strong winds which consequently lead to a degradation in RASS data.

Both Radian sodars, the radar and the RASS exhibit a clear relationship with wind shear. In general, strong wind shear (i.e., strong winds) will create substantial wind-generated noise, and thus will reduce the effective range of a sodar (Crescenti, 1998). The same is true for the RASS since strong winds will generally displace the acoustic signal away from the radar’s EM beam. Thus, the best data capture is observed when wind shear is small (i.e., light winds and convective conditions).

The square Brunt-Vaisala frequency suggests the best data availability for all sensors under convective conditions is when $N_{BV}^2 < 0$. These profiles also suggest for large values of N_{BV}^2 (i.e., very stable conditions), data capture is worse.

Finally, the best data availability profiles for all of these sensors are found when $R_B < 0.25$ (i.e., convective conditions). For stable conditions when $R_B > 0.25$, the data availability was diminished.

While all of these stability parameters are not mutually exclusive, they suggest that Doppler sodars, radar wind profilers, and RASS are more effective in acquiring more data to higher altitudes under light winds and convective conditions. Their performance is degraded under strong winds and stable conditions.

5.2 Signal-to-Noise Ratio Screening

The previous section focused on the amount of data acquired by a ground-based remote sensor without any regard to the quality of the data. It is important to avoid the “more data is better syndrome” commonly encountered in various monitoring programs. Just because a sensor reports a value as valid does not necessarily mean it is correct. There are many ways data can be corrupted, both for tower-based *in situ* sensors and for ground-based remote sensors. A perfect example of this actually happened during this study. On one particular weekend, strong winds pushed the 10-m retractable boom on the BAO tower by 60 degrees counterclockwise. The data loggers continued

to record signals transmitted from the wind monitor and sonic anemometers. The boom was reoriented to its proper alignment on the following Monday morning. To make matters worse (or at least more confusing), the 50-m boom was pushed in by 60 degrees on the following weekend as the result of another strong wind episode. Once again, the boom was realigned to its proper configuration on the following Monday morning.

These problems were accidentally overlooked in the early stages of data analysis. There was fairly good agreement between tower and sodar wind speeds. However, wind direction data showed substantial variation. This problem with the tower data was flagged only after reexamination of the experiment log books. Without human intervention, a misaligned boom would go unchecked for a long period of time if such a monitoring station was located in a remote area. Thus, other checks are needed for QA.

Fortunately, these ground-based remote sensors do have some means to assure that bad data, or at least questionable data, are flagged and removed from good data. For example, the AeroVironment sodar records not only wind speed and direction at various heights, but also records information such as SNR, amplitude of the backscattered acoustic signal, and the number of valid signal returns for each sampling interval. The other sodars as well as the radar wind profiler and RASS have similar recorded data. This information is essential for the acquisition of sound and scientifically defensible database.

As an illustration of the importance of using the SNR as a QC check, six scatter plots are shown of the AeroVironment wind speed compared against the tower wind speed at 50 m (Fig. 8). The first scatter plot contains all data reported by the sodar with a SNR > 0 (note that the AeroVironment SNR value differs from other SNR reported by other sodars which scale those numbers differently). Because of the low SNR tolerance, bad data were reported by the sodar when high wind conditions ($> 10 \text{ m s}^{-1}$) existed. Wind-generated noise biased many of the sodar wind speed data towards low values. Five data points were eliminated by increasing the SNR tolerance level to 20. No improvement was observed in the statistics. However, by increasing the tolerance to include data with a SNR > 25 , significant improvement can be seen. The elimination of 17 data points resulted in an improvement from 1.97 to 1.57 m s^{-1} in the precision. Each succeeding scatter plot shows marked improvement by eliminating data points with low SNR values. The last in the series of plots shows the best overall statistics with a precision of 0.65 m s^{-1} . Only about 10% of the reported data were discarded by selecting a sufficiently high SNR tolerance level. While there may have been "good data" eliminated using this screening technique, most of the "bad" were eliminated. Of course, each site is unique. As stated earlier, the BAO is relatively quiet (in terms of acoustic noise). However, noise was generated when winds speeds were greater than 10 m s^{-1} as the air flowed through and around the tower, as well as its guy wires. Other locations may have greater potential of acoustic interference for Doppler sodars. Careful screening of data acquired by ground-based remote systems should be done with regard to the SNR, amplitude, and number of valid returns in a given time interval.

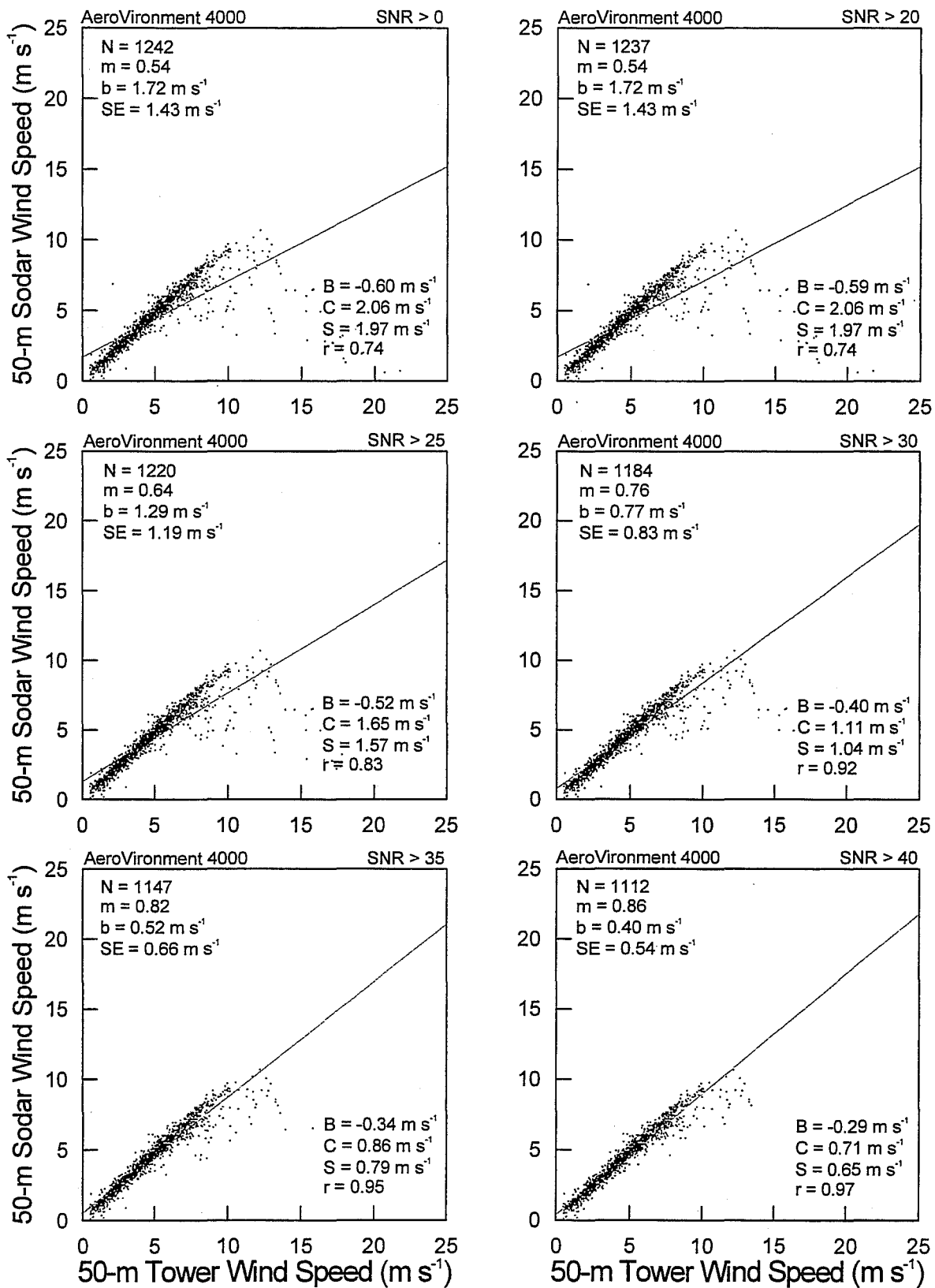


Figure 8. Scatter plots of sodar versus tower wind speeds as a function of SNR.

Many investigators have developed various objective techniques for the automatic screening of wind and temperature profiles acquired by radar wind profilers and radio acoustic sounding systems, respectively (Weber et al., 1993; Miller et al., 1994a, 1994b; Wilczak et al., 1995; Argentini et al., 1996; Jordan et al., 1997). Employment of these algorithms can dramatically improve the quality of an upper-air data set with relatively little effort. In addition, similar screening based on the SNR can also eliminate potentially erroneous data. Users of these ground-based remote sensors should consult with manufacturers on the availability of QC screening routines.

5.3 Wind Speed and Direction Statistics

The statistics discussed in Section 4 were computed for the winds of each sodar and radar wind profiler for their respective data sets. Scatter plots of sodar or radar wind speed against tower wind speed with statistics can be seen in Appendix B. In addition, similar plots for wind direction are also included for wind direction in Appendix B. The bias, comparability, precision, and correlation for the wind speed and wind direction are shown in Figures 9 and 10, respectively. The sensors are represented by following symbols: AeroVironment (○); Metek (□); Radian 600 (Δ); Radian 600PA (∇); and radar wind profiler (◇). The bias for wind speed and wind direction reported by the sodars and radar at all levels was between -0.5 to 1.0 m s⁻¹ and -5 to +10 deg, respectively. The scatter in the data, i.e., the comparability and precision, were quite good. In general, the precision for the sodar wind speeds ranged between 0.5 and 1.0 m s⁻¹. More scatter was observed in the radar values of S which ranged from 2.0 to 2.5 m s⁻¹. Values of S for wind direction for the sodars ranged between 10 and 30 deg while the radar values of S were between 35 and 45 deg. The correlation coefficients are also quite good for the sodar wind speed and directions with values of r in excess of 0.90, but not quite so good for the radar with values ranging between 0.75 and 0.85. These sodar statistics are comparable to the numerous comparison studies reported by Crescenti (1997). Ground clutter contamination is probably the main reason for the large scatter observed in the radar wind data. Birds, swaying trees, nearby vehicular traffic, and overflying aircraft can all contribute to an increased variance in the data. However, these values are still comparable to numerous comparison studies between radar wind profilers and other measurement platforms (Gage et al., 1988; Weber and Wuertz, 1990; May, 1993; Angevine and MacPherson, 1995; Dobos et al., 1995).

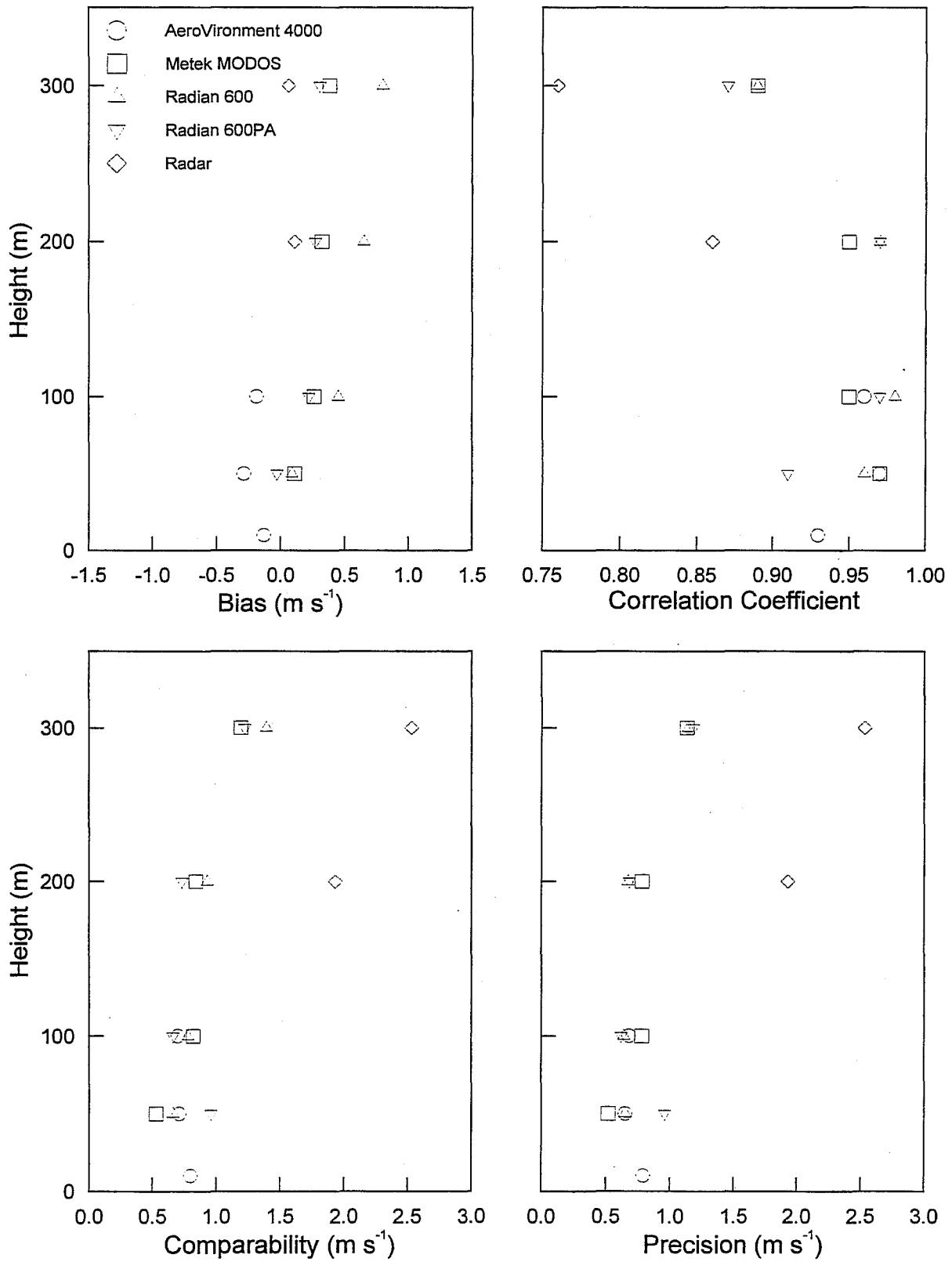


Figure 9. Wind speed statistics for all cases and sensors.

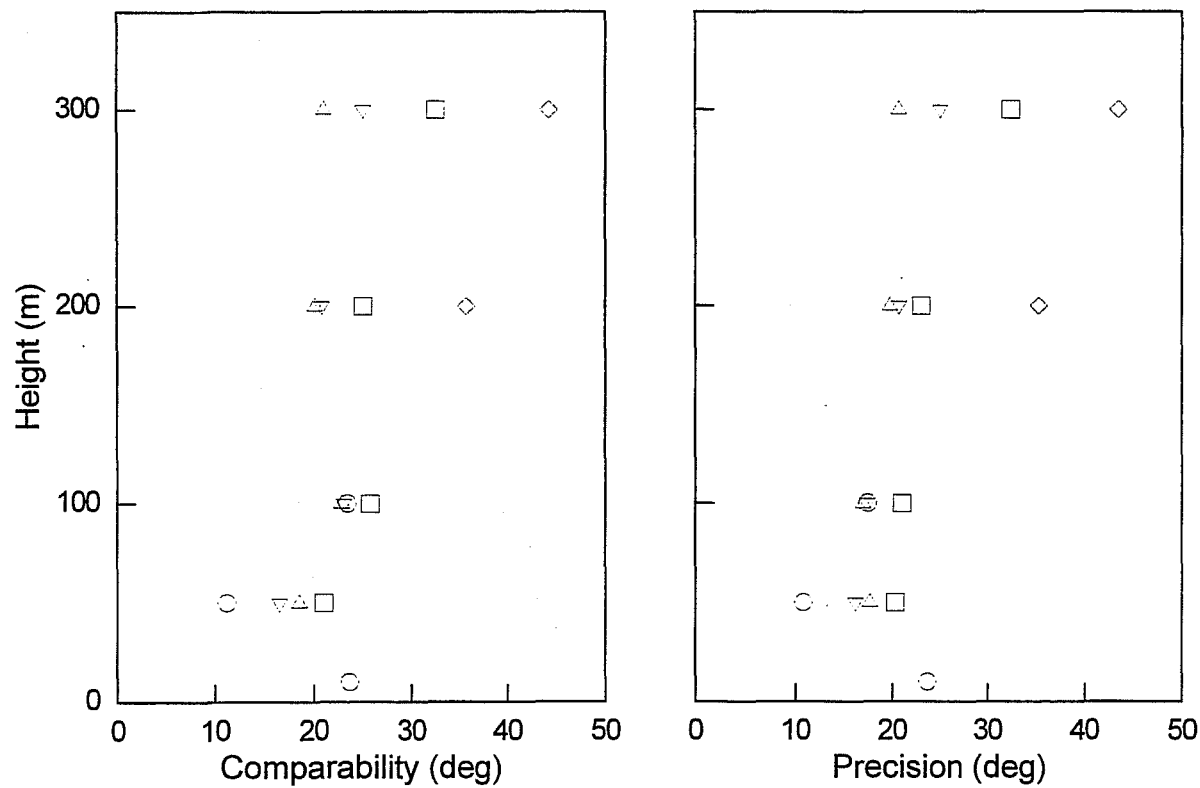
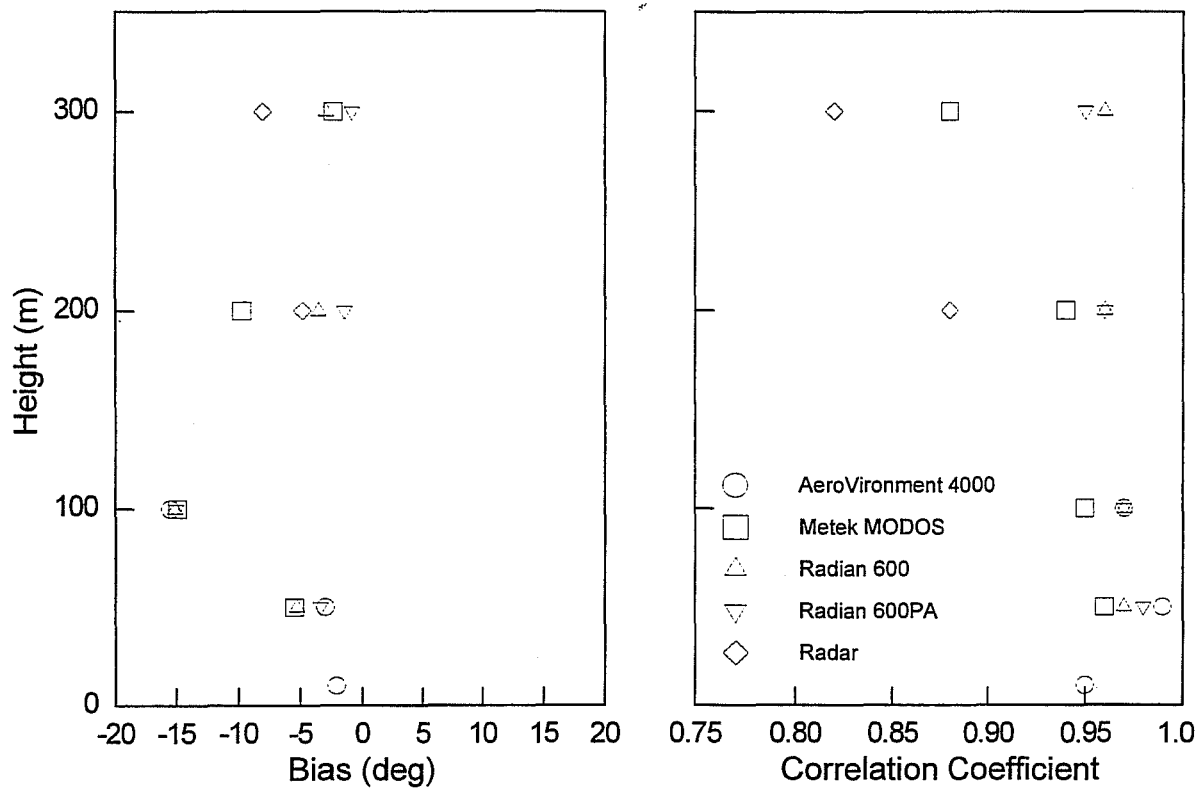


Figure 10. Wind direction statistics for all cases and sensors.

The vector correlation coefficient r_v for the sodars and the radar for all conditions at each level are listed in Table 10. Values of r_v are exceptionally good for the sodars with values exceeding 1.8 for all measurement levels. In general, r_v decreases with height. This may be due, in part, to spatial variability between the tower and the measurement volume of each respective sodar and radar. Recall that the oblique angle beams of each system were oriented away from the BAO tower. The distance between the tower and measurement volume increases as $z \tan \alpha$ where α is the oblique angle from the zenith of the sodar or radar beam.

Table 10
Vector correlation coefficients for all cases.

	r_v
AeroVironment 4000	
10 m	1.83
50 m	1.95
100 m	1.93
Metek MODOS	
50 m	1.90
100 m	1.89
200 m	1.84
300 m	1.49
Radian 600	
50 m	1.93
100 m	1.95
200 m	1.93
300 m	1.83
Radian 600PA	
50 m	1.86
100 m	1.93
200 m	1.92
300 m	1.79
LAP-3000	
200 m	1.69
300 m	1.50

It was shown that sodar range was limited under very dry conditions. However, no apparent relationship exists between the statistics as a function of the relative humidity. All sodars show similar values of S for each RH classification. Values of r_v as a function RH are listed in Table 11. Some values of r_v for very dry conditions ($RH < 20\%$) tend to suggest that there is more disagreement between tower wind vectors and sodar wind vectors. However, those are not statistically significant.

Table 11
Vector correlation coefficients as a function of relative humidity.

	0 - 20%	20 - 40%	40 - 60%	60 - 80%	80 - 100%
AeroVironment 4000					
10 m	1.96	1.94	1.87	1.82	1.72
50 m	1.90	1.95	1.94	1.97	1.97
100 m	1.89	1.92	1.92	1.93	1.94
Metek MODOS					
50 m	1.49	1.96	1.52	1.94	1.95
100 m	1.51	1.94	1.72	1.92	1.94
200 m	1.34	1.91	1.66	1.90	1.96
300 m	1.03	1.10	1.49	1.79	1.91
Radian 600					
50 m	1.85	1.94	1.88	1.93	1.96
100 m	1.82	1.95	1.92	1.94	1.97
200 m	1.90	1.95	1.88	1.92	1.96
300 m	1.90	1.91	1.84	1.87	1.72
Radian 600PA					
50 m	1.85	1.93	1.81	1.88	1.76
100 m	1.86	1.94	1.89	1.93	1.96
200 m	1.90	1.95	1.85	1.89	1.95
300 m		1.93	1.80	1.86	1.70
LAP-3000					
200 m	1.52	1.77	1.27	1.67	1.56
300 m	1.33	1.43	1.19	1.65	1.43

Significant scatter is observed in the sodar and radar data under very convective conditions (PG class A, B). Values of S range from 0.6 to 0.9 m s^{-1} for wind speed and 30 to 60 deg for wind direction. The amount of scatter significantly decreases with increasing stability. In general, the least amount of scatter is seen for classes E and F. Values of S range from 0.3 to 0.4 m s^{-1} and 5 to 15 deg for class E and F. Values of r_v (Table 12) are quite good for classes C and D (1.85 to 1.95) and exceptionally high (~ 1.95) under the most stable atmospheric conditions (class E and F).

Table 12
Vector correlation coefficients as a function of Pasquill-Gifford stability.

	A	B	C	D	E	F
AeroVironment 4000						
10 m	1.55	1.88	1.92	1.87	1.17	0.91
50 m	1.59	1.88	1.95	1.97	1.94	1.88
100 m	1.37	1.79	1.88	1.95	1.94	1.97
Metek MODOS						
50 m	1.13	1.52	1.75	1.95	1.96	1.62
100 m	0.82	1.31	1.82	1.95	1.95	
200 m	0.68	1.13	1.76	1.89	1.93	1.93
300 m	0.64	1.01	1.68	1.50	1.58	
Radian 600						
50 m	1.14	1.70	1.92	1.95	1.84	1.82
100 m	0.96	1.67	1.91	1.96	1.94	1.87
200 m	0.88	1.55	1.91	1.97	1.96	1.94
300 m	0.81	1.51	1.88	1.89	1.96	1.91
Radian 600PA						
50 m	0.80	1.65	1.83	1.88	1.57	1.53
100 m	1.14	1.58	1.90	1.96	1.94	1.91
200 m	0.92	1.64	1.87	1.96	1.93	1.96
300 m	1.08	1.65	1.80	1.85	1.77	
LAP-3000						
200 m	0.86	1.37	1.29	1.74	1.22	1.21
300 m	0.88	1.39	1.44	1.56	0.86	

Similar behavior is reflected in these statistics as a function of time of day. In general, the best agreement between tower and remote sensors occurs during dawn, dusk and night. Day time conditions usually show the most variability. Again, this is due to the convective nature of the boundary layer, especially under light wind conditions. While scatter in wind speed and wind direction is greater for day time conditions, overall agreement is still quite good. Values of r , listed in Table 13 reflect these agreements between sets of wind vectors.

Table 13
Vector correlation coefficients as a function of time of day.

	Dawn	Day	Dusk	Night
AeroVironment 4000				
10 m	1.71	1.93	1.70	1.76
50 m	1.98	1.92	1.97	1.98
100 m	1.93	1.89	1.97	1.96
Metek MODOS				
50 m	1.93	1.74	1.95	1.95
100 m	1.96	1.80	1.94	1.96
200 m	1.92	1.73	1.83	1.87
300 m	1.90	1.52	1.75	1.07
Radian 600				
50 m	1.92	1.90	1.96	1.94
100 m	1.96	1.91	1.97	1.96
200 m	1.96	1.86	1.98	1.96
300 m	1.59	1.82	1.95	1.90
Radian 600PA				
50 m	1.87	1.84	1.80	1.87
100 m	1.95	1.88	1.97	1.96
200 m	1.94	1.84	1.95	1.97
300 m	1.44	1.78	1.92	1.94
LAP-3000				
200 m	1.69	1.67	1.69	1.67
300 m	1.52	1.54	1.45	1.41

Not surprisingly, a lot of variance is observed between the tower and remote sensors for near calm wind conditions ($SS < 2 \text{ m s}^{-1}$). Under such conditions, large variations can be expected in the wind field and substantial disagreement can occur, even over relatively short distances of a few hundred meters. As expected, less scatter is found when the winds are light to moderate. Values of S for wind direction are quite good for moderate wind speeds. Unfortunately, very little data was acquired by the sodars under strong winds ($> 10 \text{ m s}^{-1}$). This is due to wind-generated noise which interferes with the operation of the sodar. This has been a recurring theme found by many other investigators (Parry et al., 1975; Hardesty et al., 1977; Finkelstein et al., 1986; Evers and Neisser, 1990; Dahlquist, 1993). The radar, on the other hand, is not susceptible to acoustic noise interference like the sodar and does much better during strong wind episodes. Values for r_v as a function of SS are listed in Table 14.

Table 14
Vector correlation coefficients as a function of scalar wind speed.

	< 2 m s ⁻¹	2 - 5 m s ⁻¹	5 - 10 m s ⁻¹	> 10 m s ⁻¹
AeroVironment 4000				
10 m	1.17	1.77	1.89	1.98
50 m	1.80	1.96	1.96	
100 m	1.78	1.94	1.91	
Metek MODOS				
50 m	1.68	1.86	1.91	
100 m	1.44	1.88	1.93	
200 m	1.35	1.83	1.88	
300 m	1.33	1.56	1.13	
Radian 600				
50 m	1.61	1.91	1.96	
100 m	1.65	1.93	1.96	
200 m	1.70	1.94	1.97	
300 m	1.69	1.87	1.65	
Radian 600PA				
50 m	1.47	1.83	1.88	
100 m	1.66	1.92	1.96	
200 m	1.69	1.92	1.95	
300 m	1.67	1.82	1.63	
LAP-3000				
200 m	1.20	1.54	1.66	1.90
300 m	1.04	1.36	1.42	

The most dramatic statistics are seen as a function of σ_θ . The correlation and vector correlation coefficients (Table 15) degrade substantially as σ_θ increases to larger values. Conversely, the best agreement is found when $\sigma_\theta < 10$ deg. Values of S range from 5 to 10 deg when $\sigma_\theta < 10$ deg and ~ 50 deg when $\sigma_\theta > 30$ deg. While S is generally larger for the radar than the sodars, data acquired by the radar shows similar behavior with σ_θ . Of course these results should not be surprising since small σ_θ are associated with large wind speeds while large σ_θ are often found with light winds. Large values of σ_θ are associated with a nonhomogeneous boundary layer (Lumley and Panofsky, 1964; Mitchell, 1982; U. S. EPA, 1987a). Spatial separations between the tower and sampling volumes of the remote sensors can lead to significant disagreement.

Table 15
Vector correlation coefficients as a function of σ_θ .

	< 10 deg	10 - 20 deg	20 - 30 deg	> 30 deg
AeroVironment 4000				
10 m	1.83	1.84	1.69	1.59
50 m	1.97	1.95	1.88	1.72
100 m	1.95	1.92	1.84	1.65
Metek MODOS				
50 m	1.96	1.83	1.52	1.08
100 m	1.96	1.86	1.30	0.94
200 m	1.95	1.65	1.14	0.64
300 m	1.56	1.54	0.86	0.68
Radian 600				
50 m	1.96	1.92	1.68	1.40
100 m	1.97	1.93	1.74	1.39
200 m	1.97	1.93	1.59	1.43
300 m	1.82	1.89	1.59	1.38
Radian 600PA				
50 m	1.87	1.86	1.73	1.38
100 m	1.97	1.92	1.70	1.40
200 m	1.96	1.92	1.71	1.40
300 m	1.76	1.86	1.64	1.45
LAP-3000				
200 m	1.79	1.54	1.26	0.76
300 m	1.56	1.50	0.85	0.81

The statistics are also very dramatic as a function of wind shear S_w . Values of S generally improve with larger wind shear for wind speed. However, the improvement is very dramatic for the wind direction comparisons. With little or no wind shear ($< 0.02 \text{ s}^{-1}$), S ranges from 30 to 40 deg. However, for strong wind shear ($> 0.06 \text{ s}^{-1}$), the precision is ~ 5 deg. When the wind speed and wind directions are combined and analyzed as vectors, values of r_v (Table 16) are very good to exceptional (> 1.9) when wind shear exists ($> 0.02 \text{ s}^{-1}$). A stronger wind shear regime provides stronger scatter given equal background potential temperature gradients (Gaynor, 1979). The turbulence continually creates and destroys microscale (0.01 - 10 m) temperature gradients, thereby enhancing acoustic backscatter.

Table 16
Vector correlation coefficients as a function of wind shear.

	$<$ 0.02 s^{-1}	$0.02 -$ 0.04 s^{-1}	$0.04 -$ 0.06 s^{-1}	$>$ 0.06 s^{-1}
AeroVironment 4000				
10 m	1.64	1.73	1.86	1.95
50 m	1.88	1.95	1.96	1.98
100 m	1.82	1.92	1.94	1.95
Metek MODOS				
50 m	1.67	1.89	1.94	1.98
100 m	1.51	1.94	1.93	1.96
200 m	1.37	1.83	1.87	1.97
300 m	1.24	1.74	1.55	1.10
Radian 600				
50 m	1.77	1.93	1.94	1.96
100 m	1.76	1.93	1.94	1.97
200 m	1.65	1.94	1.97	1.98
300 m	1.60	1.95	1.94	1.96
Radian 600PA				
50 m	1.66	1.80	1.85	1.96
100 m	1.71	1.92	1.95	1.96
200 m	1.66	1.93	1.96	1.98
300 m	1.57	1.90	1.93	1.96
LAP-3000				
200 m	1.19	1.41	1.70	1.75
300 m	1.15	1.49	1.63	1.37

Once again, the variance between tower and remote sensor measurements is largest for unstable conditions ($N_{BV}^2 < 0$) and smallest during stable conditions ($N_{BV}^2 > 0$). The most dramatic statistics are seen for the wind direction where values of S are ~ 5 deg for moderately to strongly stable conditions. Vector correlation coefficients are also good for a thermally stratified atmosphere (Table 17).

Table 17
Vector correlation coefficients as a function of Brunt-Vaisala frequency squared.

	< 0.000 s ⁻²	0.000 - 0.001 s ⁻²	0.001 - 0.002 s ⁻²	> 0.002 s ⁻²
AeroVironment 4000				
10 m	1.84	1.75	1.79	1.96
50 m	1.93	1.95	1.97	1.98
100 m	1.90	1.95	1.96	1.98
Metek MODOS				
50 m	1.77	1.92	1.85	1.96
100 m	1.82	1.92	1.89	1.96
200 m	1.79	1.84	1.70	1.95
300 m	1.65	1.66	1.44	0.97
Radian 600				
50 m	1.90	1.95	1.91	1.89
100 m	1.92	1.95	1.93	1.96
200 m	1.88	1.96	1.97	1.96
300 m	1.83	1.94	1.95	1.91
Radian 600PA				
50 m	1.77	1.83	1.89	1.93
100 m	1.89	1.94	1.93	1.97
200 m	1.87	1.96	1.96	1.93
300 m	1.81	1.92	1.95	1.88
LAP-3000				
200 m	1.68	1.63	1.54	1.46
300 m	1.51	1.48	1.28	0.83

Finally, the bulk Richardson number combines both mechanical the thermal mixing. Using these stability criteria, the best agreement was found for the moderately unstable (-0.5 to 0.25) and moderately stable (0.25 - 1) conditions. These are reflected by values of r_v listed in Table 18. For strongly stable conditions ($R_B > 1$), variance increases for both wind speed and wind direction measurements. For strongly unstable conditions ($R_B < -0.5$), the variance is largest.

Table 18
Vector correlation coefficients as a function of bulk Richardson number.

	< -0.50	-0.50 - 0.25	0.25 - 1.00	> 1.00
AeroVironment 4000				
10 m	1.75	1.82	1.84	1.75
50 m	1.89	1.95	1.98	1.97
100 m	1.83	1.93	1.97	1.95
Metek MODOS				
50 m	1.69	1.94	1.92	1.89
100 m	1.56	1.93	1.92	1.86
200 m	1.47	1.93	1.79	1.38
300 m	1.27	1.67	0.93	1.28
Radian 600				
50 m	1.76	1.95	1.92	1.88
100 m	1.75	1.96	1.94	1.92
200 m	1.66	1.96	1.96	1.88
300 m	1.60	1.95	1.93	1.90
Radian 600PA				
50 m	1.69	1.83	1.90	1.81
100 m	1.71	1.95	1.95	1.92
200 m	1.68	1.95	1.96	1.84
300 m	1.64	1.92	1.88	1.83
LAP-3000				
200 m	1.08	1.60	1.63	1.27
300 m	0.98	1.48	1.07	0.85

5.4 Virtual Air Temperature Statistics

The same statistics were computed for virtual air temperature. Scatter plots with statistics of RASS versus tower T_v can be seen in Appendix C. The agreement between tower and RASS T_v is exceptionally good with $r = 0.99$ at all three comparison levels. The bias ranges from -0.3 °C at 100 m increasing in a linear fashion to 0.6 °C at 300 m. The precision ranges from 0.85 to 1.04 °C. These values are comparable to those found in other comparison studies (May et al., 1989; Martner et al., 1993; Angevine and Ecklund, 1994; Angevine et al., 1994; Moran and Strauch, 1994).

There does not appear to be any dependence of the statistics as a function of RH . However, values of S are much greater than 1 °C for PG classes of A and B and decrease with increasing stability. The smallest value of S occurs for classes D and E (~ 0.4 to 0.7 °C). When examining T_v as a function of time of day, the categories of day, dusk and night produces the least amount of variability ($S \sim 0.5$ to 0.6 °C), increasing to $S \sim 0.7$ °C during dawn with a maximum of scatter ($S \sim 1.0$ to 1.3 °C) during the day. When considering scalar wind speed, the greatest variance ($S \sim 1$ to 1.5 °C) occurs for near calm conditions while the smallest variance is generally associated with moderate to strong winds. Like the wind speed and wind direction acquired by the sodars and radar, the precision shows a strong dependence on σ_θ . For $\sigma_\theta < 10$ deg, $S \sim 0.6$ °C. However, when $\sigma_\theta > 20$, S ranges from 1.2 to 1.7 °C. The horizontal inhomogeneity of the boundary layer is responsible for large variations over short distances. The precision also shows a strong dependence on S_h with values of 1 to 1.4 °C for little or no shear to a minimum of 0.5 to 0.6 °C when $S_h > 0.06$ s⁻¹. When considering the thermal mixing (i.e., Brunt-Vaisala frequency), the largest variance in T_v is observed for unstable conditions ($N_{BV}^2 < 0$) and smallest for large positive values of N_{BV}^2 . Similarly, R_B shows the same behavior. Values of $S \sim 1$ to 1.5 when $R_B < -0.5$. For moderately unstable ($-0.5 < R_B < 0.25$) to moderately stable ($0.25 - 1$) conditions, values of S range from 0.5 to 0.7 °C. The precision worsens for strongly stable ($R_B > 1$) conditions with values ranging from 0.7 to 1.1 °C.

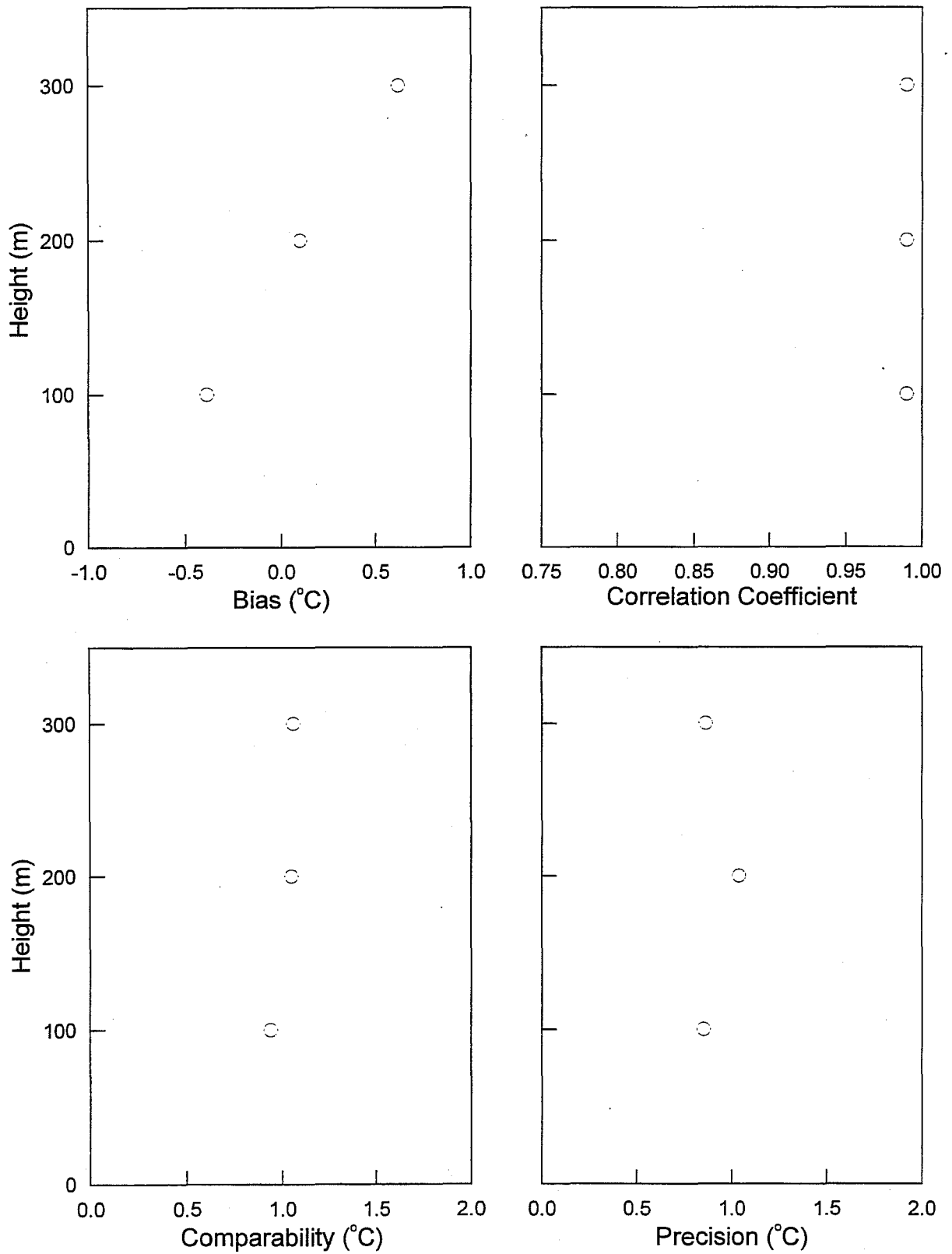


Figure 11. Virtual air temperature statistics for all cases and sensors.

6 Conclusions

A ground-based remote sensor characterization study was conducted for three weeks in April 1995 at the Boulder Atmospheric Observatory in Erie, Colorado. An extensive data set was acquired from a suite of *in situ* sensors mounted at 10, 50, 100, 200, and 300 m on the BAO tower, four commercially available Doppler sodars (AeroVironment 4000, Metek MODOS, Radian 600, and Radian 600PA), a 915-MHz radar wind profiler (Radian LAP-3000), and a RASS (also Radian). The overall goal of the study was not to compare one ground-based remote sensor against another, but rather to document the performance of these sensors as a function of various atmospheric conditions. A secondary objective was to document QA and QC procedures that would lead to the acquisition of wind and temperature profiles of known quality.

Prior to the start of the study, performance audits were conducted in accordance with the most current guidance available from the U. S. Environmental Protection Agency. The evaluation included analysis of the site characteristics which identified noise sources and types, background noise levels, a "listen only" test, and the construction of vista tables identifying obstacles that may be potential reflectors of acoustic and EM signals. A review of the operational configuration of the instruments included checks on equipment alignment and the verification of proper operation of these sensors. Simulated wind tests were also conducted which tested the response of the sodars using an Acoustic Pulse Transponder (APT) developed by Baxter (1995). Other audit procedures (not used in this study) are summarized as additional and/or alternate methods of verification.

Simple statistical parameters were used as a measure of the agreement between tower-based measurements and remote sensor data. These included linear least-squares regression fits which yielded the slope m , y-intercept b , and standard error SE about the fit. The linear correlation coefficient r and vector correlation coefficient r_v were also used as statistical measures. Other statistics of comparison that were used include the bias (accuracy) B , comparability (root-mean-square difference) C , and precision (standard deviation) S .

Eight different measures of atmospheric conditions and stability were used in this study to measure the statistical characteristics of these ground-based remote sensors. They include: relative humidity (RH), Pasquill-Gifford (PG) stability class, time of day (dawn, day, dusk, and night), scalar wind speed (SS), standard deviation of the horizontal wind direction (σ_θ), wind shear (S_h), the square of the Brunt-Vaisala frequency (N_{BV}^2), and the bulk Richardson number (R_B). These parameters were chosen since they are easily derived from tower-based measurements.

Data availability from these ground-based remote sensors were examined as a function of the eight stability categories. This was done without regard to the accuracy of the remote sensor data. In general, convective (unstable) conditions were conducive to more data capture at higher altitudes than for laminar (stable) conditions. Very low relative humidity also limits the range of sodars since the molecular attenuation dramatically increases under these conditions.

It is important to avoid the "more data is better syndrome" commonly encountered in various

monitoring programs. Just because a sensor reports a value as valid does not necessarily mean it is correct. There are many ways data can be corrupted, both for tower-based *in situ* sensors and for ground-based remote sensors. Thus, an example was shown that included all "valid" data. By increasing the SNR tolerance (i.e., eliminating data with low SNR values), corrupted data due to noise interference for the AeroVironment sodar were eliminated. This was also done for the other ground-based sensors.

Performance statistics of the wind speed, wind direction, and virtual air temperature data were computed for each entire data set and as a function of the eight categories. Overall, excellent agreement was found between tower-based and remote sensor data. Biases for wind speed and wind direction reported by the sodars and radar at all levels under all conditions ranged from -0.5 to 1.0 m s^{-1} and -5 to +10 deg, respectively. The precision for the sodar wind speeds ranged between 0.5 and 1.0 m s^{-1} . More scatter was observed in the radar values of precision which ranged between 2.0 to 2.5 m s^{-1} . Values of S for wind direction for the sodars ranged between 10 and 30 deg while the radar values of S were between 35 and 45 deg. The correlation coefficients are also quite good for the sodar wind speed and directions with values of r in excess of 0.90, but not quite so good for the radar with values ranging between 0.75 and 0.85. These sodar statistics are comparable to numerous comparison studies. Ground clutter contamination is probably the main reason for the large scatter observed in the radar wind data. Birds, swaying trees, nearby vehicular traffic, and overflying aircraft can all contribute to an increased variance in the data. However, these values are still comparable to numerous comparison studies between radar wind profilers and other measurement platforms.

In general, more variance was observed in the statistics (i.e., larger values S , SE) during convective conditions. Conversely, the scatter was quite small for stable conditions. In many instances, values of S were less than 0.5 m s^{-1} and 10 deg for wind speed and wind direction, respectively, during stable episodes. Considerable scatter was observed for very light wind conditions ($SS < 2 \text{ m s}^{-1}$, $\sigma_\theta > 30 \text{ deg}$). This is not to say that the sodars, radar and RASS acquired incorrect data. Rather, inhomogeneity of the boundary layer can produce conflicting numbers from sensors separated on the order of several hundred meters.

It should be pointed out that this is a limited data in the sense it was collected at a specific location during a specific time of year. Thus, a full cross section of possible conditions was not encountered. Nevertheless, a sufficient number of data points were collected to demonstrate the behavior of these sensors under various conditions. This information can be extremely useful to individuals conducting audits of sodars or radars. Under convective, light-wind conditions, large discrepancies may be found even though the remote sensor is working properly.

Finally, the time for comparison studies is over. There are a substantial number of research papers (see Crescenti, 1997) that have compared these remote sensors against a "reference" measurement system. It is quite evident from these previous studies and from this study, that the technology is mature and should be (and often are) used for routine monitoring applications. The greatest challenge is finding a suitable site to locate a remote sensor. Outside interferences such as

noise or birds can corrupt wind or temperature profiles. With an aggressive QA/QC plan, reliable data can be collected with a high amount of confidence. The only time a comparison study should be needed in the future is when the technology undergoes a significant change. This can be with new hardware (e.g., new antenna design) or with new software (e.g., new algorithms to determine spectral peak of backscattered signal).

Doppler sodars, radar wind profilers, and RASS have led to significant advances in our understanding of the atmospheric boundary layer. While the data availability of a remote sensor may be limited by specific atmospheric conditions, they are still effective and reliable tools for acquiring detailed information on atmospheric wind and temperature structure.

Acknowledgments

There are a number of people who I wish to express my most sincere thanks for successfully executing this field study. First and foremost, I wish to thank William Mitchell for funding this study. He has understood the importance of establishing quality assurance and quality control guidance so that reliable and accurate meteorological data can be acquired for regulatory monitoring. Without his foresight and leadership, this study would not have been possible. Next, but no less important, are the significant contributions by Brian Templeman for his extraordinary effort in preparing the BAO (usually during less than favorable conditions) and overseeing the data acquisition phase of the study. Special thanks are also extended to Catherine Russell for her help with countless logistical problems encountered before the study, during the study, and after the study. I would also like to express my appreciation to William Neff and John Gaynor for their patience each has extended to me with my many questions. I also wish to thank Julie Neal for assisting me in the early stages of data screening. Thanks are also extended to the commercial vendors for their cooperation and sharing their insights on the challenges of collecting upper-air data. They include Kenneth Underwood and Jeff Bradley of AeroVironment; Gerhard Peters of Metek; Paul Reveley and Scott McLoughlin (formerly) of Radian. I wish to extend my most sincere thanks Robert Baxter of Parsons-Engineering Science for conducting the audits on the ground-based remote sensors. His knowledge and experience with the many aspects on QA/QC issues are a critical component of this study. My gratitude is expressed to Kirk Clawson, John Gaynor, and Doug Soule for providing a critical review of this document.

References

- Angevine, W. M., and W. L. Ecklund, 1994: Errors in radio acoustic sounding of temperature. *J. Atmos. Oceanic Technol.*, **11**, 837-842.
- Angevine, W. M., and J. I. MacPherson, 1995: Comparison of wind profiler and aircraft wind measurements at Chebogue Point, Nova Scotia. *J. Atmos. Oceanic Technol.*, **12**, 421-426.
- Angevine, W. M., W. L. Ecklund, D. A. Carter, K. S. Gage, and K. P. Moran, 1994: Improved radio acoustic sounding techniques. *J. Atmos. Oceanic Technol.*, **11**, 42-49.
- Argentini, S., G. Mastrantonio, A. Viola, P. Pettre, and G. Dargaud, 1996: Sodar performance and preliminary results after one year of measurements at Adelie Land Coast, East Antarctica. *Bound.-Layer Meteor.*, **81**, 75-103.
- Asimakopoulos, D. N., D. G. Deligiorgi, and D. P. Lalas, 1980: Acoustic sounder observations of the atmospheric boundary layer from the top of a steep mountain. *J. Appl. Meteor.*, **19**, 109-112.
- Baxter, R. A., 1994a: Development of a universal acoustic pulse transponding system for performance auditing of sodars. Proc., *7th International Symposium on Acoustic Remote Sensing*, Boulder, CO, International Society for Acoustic Remote Sensing, 3.35-3.40.
- Baxter, R. A., 1994b: Performance of sodar audits under the new USEPA guidance. Proc., *7th International Symposium on Acoustic Remote Sensing*, Boulder, CO, International Society for Acoustic Remote Sensing, 8.13-8.18.
- Baxter, R. A., 1995: Performance auditing of sodars under the new USEPA guidance - applications of a new instrument to quantitatively assess sodar performance. Preprint, *Ninth Symposium on Meteorological Observations and Instrumentation*, Charlotte, NC, Amer. Meteor. Soc., 442-446.
- Baxter, R. A., 1996: Quality assurance of remote wind profilers during the 1995 EPA Sodar Characterization Study. Preprint, *Ninth Joint Conference on the Applications of Air Pollution Meteorology with the AWMA*, Atlanta, GA, Amer. Meteor. Soc., 556-560.
- Bonino, G., G. Elisei, A. Marzorati, and P. Trivero, 1986: Results on planetary boundary layer sounding by automatic RASS. *Atmos. Res.*, **20**, 309-316.
- Chintawongvanich, P., R. Olsen, and C. A. Biltoft, 1989: Intercomparison of wind measurements from two acoustic Doppler sodars, a laser Doppler lidar, and in situ sensors. *J. Atmos. Oceanic Technol.*, **6**, 785-797.

- Clifford, S. F., J. C. Kaimal, R. J. Latatits, and R. G. Strauch, 1994: Ground-based remote profiling in atmospheric studies: an overview. *Proc. IEEE*, **82**, 313-355.
- Coulter, C. T., 1994: An evaluation of a solar radiation/delta-T method for estimating Pasquill-Gifford (P-G) stability categories. Preprint, *Eighth Joint Conference on the Applications of Air Pollution Meteorology with the AWMA*, Nashville, TN, Amer. Meteor. Soc., 40-47.
- Coulter, R. L., 1998: A study of the effects of an additional sound source on RASS performance. Preprint, *Tenth Symposium on Meteorological Observations and Instrumentation*, Phoenix, AZ, Amer. Meteor. Soc., 223-227.
- Crescenti, G. H., 1994: Overview of PAMS meteorological monitoring requirements. Proc., *International Symposium on Measurement of Toxic and Related Air Pollutants*, Durham, NC, Air & Waste Management Association, 245-253.
- Crescenti, G. H., 1997: A look back on two decades of Doppler sodar comparison studies. *Bull. Amer. Meteor. Soc.*, **78**, 651-673.
- Crescenti, G. H., 1998: The degradation of Doppler sodar performance due to noise: a review. *Atmos. Environ.*, **32**, 1499-1509.
- Crescenti, G. H., and R. A. Baxter, 1998: Some examples of noise interference on Doppler sodar performance. Preprint, *Tenth Symposium on Meteorological Observations and Instrumentation*, Phoenix, AZ, Amer. Meteor. Soc., 228-232.
- Crosby, D. S., L. C. Breaker, and W. H. Gemmill, 1993: A proposed definition for vector correlation in geophysics: theory and application. *J. Atmos. Oceanic Technol.*, **10**, 355-367.
- Dahlquist, H., 1993: A one dimensional wind profile model with stability and eddy viscosity estimations from sodar data. *Bound.-Layer Meteor.*, **62**, 329-351.
- Dobos, P. H., R. J. Lind, and R. L. Elsberry, 1995: Surface wind comparisons with radar wind profiler observations near tropical cyclones. *Wea. Forecasting*, **10**, 564-575.
- Ecklund, W. L., D. A. Carter, and B. B. Balsley, 1988: A UHF wind profiler for the boundary layer: Brief description and initial results. *J. Atmos. Oceanic Technol.*, **5**, 432-441.
- Ecklund, W. L., D. A. Carter, B. B. Balsley, P. E. Currier, J. L. Green, B. L. Weber, and K. S. Gage, 1990: Field tests of a lower tropospheric wind profiler. *Radio Sci.*, **25**, 899-906.
- Evers K., and J. Neisser, 1990: Vertical sodar measurements at different sites in summer. *Atmos. Environ.*, **24A**, 2541-2545.

- Finkelstein, P. L., J. C. Kaimal, J. E. Gaynor, M. E. Graves, and T. J. Lockhart, 1986: Comparison of wind monitoring systems. Part II: Doppler sodars. *J. Atmos. Oceanic Technol.*, **3**, 594-604.
- Gage, K. S., J. R. McAfee, W. G. Collins, D. Söderman, H. Böttger, A. Radford, and B. Balsley, 1988: A comparison of winds observed at Christmas Island using a wind-profiling Doppler radar with NMC and ECMWF analyses. *Bull. Amer. Meteor. Soc.*, **69**, 1041-1046.
- Gardiner, B. A., and M. K. Hill, 1986: Acoustic sounder observations from an elevated location. *Bound.-Layer Meteor.*, **36**, 307-316.
- Gaynor, J. E., 1977: Acoustic Doppler measurement of atmospheric boundary layer velocity structure functions and energy dissipation rates. *J. Appl. Meteor.*, **16**, 148-155.
- Gaynor, J. E., 1979: The importance of moisture fluctuations and wind shear in acoustic backscatter in GATE. *J. Appl. Meteor.*, **18**, 1472-1480.
- Gaynor, J. E., and J. A. Korrell, 1981: Instrument intercomparisons at the Boulder Atmospheric Observatory during 1980. NOAA Tech. Memo. ERL WPL-69, 38 pp.
- Gaynor, J. E., C. B. Baker, and J. C. Kaimal, 1990: The International Sodar Intercomparison Experiment. Proceedings, *Fifth International Symposium on Acoustic Remote Sensing of the Atmosphere and Oceans*, S. P. Singal, ed., Tata McGraw-Hill Publishing, New Delhi, India, 67-74.
- Hahn, C. J., 1981: A study of the diurnal behavior of boundary-layer winds at the Boulder Atmospheric Observatory. *Bound.-Layer Meteor.*, **21**, 231-245.
- Hardesty R. M., P. A. Mandics, D. W. Beran, and R. G. Strauch, 1977: The Dulles Airport acoustic-microwave radar wind and wind shear measuring system. *Bull. Amer. Meteor. Soc.*, **58**, 910-918.
- Hoehne, W. E., 1971: Standardized functional tests. NOAA tech. memo. NWST&EL-12, U. S. Department of Commerce, 23 pp.
- Jordan, J. R., R. J. Latatits, and D. A. Carter, 1997: Removing ground and intermittent clutter contamination from wind profiler signals using wavelet transforms. *J. Atmos. Oceanic Technol.*, **14**, 1280-1297.
- Kaimal, J. C., 1986: Flux and profile measurements from towers in the boundary layer. *Probing the Atmospheric Boundary Layer*, D. H. Lenschow, Ed., Amer. Meteor. Soc., 19-28.
- Kaimal, J. C., and J. E. Gaynor, 1983: The Boulder Atmospheric Observatory. *J. Climate Appl.*

Meteor., **22**, 863-880.

Kaimal, J. C., H. N. Baynton, and J. E. Gaynor (eds.), 1980: The Boulder Low-Level Intercomparison Experiment. BAO Rep. No. 2, Wave Propagation Laboratory, NOAA/ERL, Boulder, CO, 189 p.

Lumley, J. L., and H. A. Panofsky, 1964: *The Structure of Atmospheric Turbulence*. Interscience, New York, 239 p.

Martner, B. E., D. B. Wuertz, B. B. Stankov, R. G. Strauch, E. R. Westwater, K. S. Gage, W. L. Ecklund, C. L. Martin, and W. F. Dabberdt, 1993: An evaluation of wind profiler, RASS, and microwave radiometer performance. *Bull. Amer. Meteor. Soc.*, **74**, 599-613.

Mastrantonio, G., and G. Fiocco, 1982: Accuracy of wind velocity determinations with Doppler sodars. *J. Appl. Meteor.*, **21**, 823-830.

May, P. T., 1993: Comparison of wind-profiler and radiosonde measurements in the tropics. *J. Atmos. Oceanic Technol.*, **10**, 122-127.

May, P. T., K. P. Moran, and R. G. Strauch, 1989: The accuracy of RASS temperature measurements. *J. Appl. Meteor.*, **28**, 1329-1335.

May, P. T., T. Adachi, T. Tsuda, and R. J. Latatits, 1996: The spatial structure of RASS echoes. *J. Atmos. Oceanic Technol.*, **13**, 1275-1284.

Melling, H., and R. List, 1978: Doppler velocity extraction from atmospheric acoustic echoes using a zero-crossing technique. *J. Appl. Meteor.*, **17**, 1274-1285.

Militana, L., P. E. Virag, and S. C. Mauch, 1991: Case studies of wind profiler performance auditing procedures. Proc., *84th Annual Meeting & Exhibition*, Vancouver, BC, Air & Waste Management Assoc., Paper 91-54.10.

Miller, P. A., T. W. Schlatter, D. W. van de Kamp, M. F. Barth, and B. L. Weber, 1994a: An unfolding algorithm for profiler winds. *J. Atmos. Oceanic Technol.*, **11**, 32-41.

Miller, P. A., M. F. Barth, D. W. van de Kamp, T. W. Schlatter, B. L. Weber, D. B. Wuertz, and K. A. Brewster, 1994b: An evaluation of two automated quality control methods designed for use with hourly wind profiler data. *Annales Geophysicae*, **12**, 711-724.

Mitchell, A. E., Jr., 1982: Comparison of short-term dispersion estimates resulting from various atmospheric stability classification methods. *Atmos. Environ.*, **16**, 765-773.

Moran, K. P., and R. G. Strauch, 1994: The accuracy of RASS temperature measurements corrected

- for vertical air motion. *J. Atmos. Oceanic Technol.*, **11**, 995-1001.
- Neff, W. D., 1975: Quantitative evaluation of acoustic echoes from the planetary boundary layer. NOAA Tech. Memo. ERL-322 WPL-38, Boulder, CO, 34 p.
- Neff, W. D., 1998: Advances in meteorological measurement methods for application to air quality research and monitoring. *Atmos. Environ.*, submitted.
- Neff, W. D., and R. L. Coulter, 1986: Acoustic remote sensing. *Probing the Atmospheric Boundary Layer*, D. H. Lenschow, Ed., Amer. Meteor. Soc., 201-239.
- Panofsky, H. A., 1984: Vertical variation of roughness length at the Boulder Atmospheric Observatory. *Bound.-Layer Meteor.*, **28**, 305-308.
- Parry H. D., M. J. Sanders, and H. P. Jensen, 1975: Operational applications of a pure acoustic sounding system. *J. Appl. Meteor.*, **14**, 67-77.
- Peters, G., and H. J. Kirtzel, 1994: Measurements of momentum flux in the boundary layer by RASS. *J. Atmos. Oceanic Technol.*, **11**, 63-75.
- Pinkel, R., and J. A. Smith, 1992: Repeat-sequence coding for improved precision of Doppler sonar and sodar. *J. Atmos. Oceanic Technol.*, **9**, 149-163.
- Piringer, M., 1994: Selected results of a sodar intercomparison experiment. *Meteor. Z.*, **3**, 132-137.
- Santovasi, J. A., 1986: Meteorological monitoring using sodar for electric utility air quality applications. *J. Air Pollut. Control Assoc.*, **36**, 1130-1137.
- Schotz, S., and H. A. Panofsky, 1980: Wind characteristics at the Boulder Atmospheric Observatory. *Bound.-Layer Meteor.*, **19**, 155-164.
- Schroeder, J. A., 1990: A comparison of temperature soundings obtained from simultaneous radiometric, radio-acoustic, and rawinsonde measurements. *J. Atmos. Oceanic Technol.*, **7**, 495-503.
- Simmons W. R., J. W. Wescott, and F. F. Hall, Jr., 1971: Acoustic echo sounding as related to air pollution in urban environments. NOAA Tech. Rep. ERL 216-WPL 17, Boulder, CO, 77 p.
- Soucy, R., R. Woodward, and H. A. Panofsky, 1982: Vertical cross-spectra of horizontal velocity components at the Boulder Atmospheric Observatory. *Bound.-Layer Meteor.*, **24**, 57-66.
- Stull, R. B., 1988: *An Introduction to Boundary Layer Meteorology*. Kluwer Academic Publishers, Dordrecht, 666 p.

- U. S. Environmental Protection Agency, 1987a: On-Site Program Guidance for Regulatory Modeling Applications. EPA-450/4-87-013, Office of Air Quality Planning and Standards, Research Triangle Park, NC.
- U. S. Environmental Protection Agency, 1987b: Ambient Monitoring Guidelines for Prevention of Significant Deterioration. EPA-450/4-87-007, Office of Air Quality Planning and Standards, Research Triangle Park, NC, 95 p.
- U. S. Environmental Protection Agency, 1995: Quality Assurance Handbook for Air Pollution Measurement Systems, Volume IV: Meteorological Measurements. EPA-600/R-94/038d, Office of Research and Development, Research Triangle Park, NC.
- Virag, P. E., S. C. Mauch, and L. M. Militana, 1992: A review of sodar audit procedures using a tethered sonde measurement system. Proc., *85th Annual Meeting & Exhibition*, Kansas City, MO, Air & Waste Management Assoc., Paper 92-101.03.
- Weber, B. L., and D. B. Wuertz, 1990: Comparison of rawinsonde and wind profiler radar measurements. *J. Atmos. Oceanic Technol.*, **7**, 157-174.
- Weber, B. L., D. B. Wuertz, D. C. Welsh, and R. McPeck, 1993: Quality controls for profiler measurements of winds and RASS temperatures. *J. Atmos. Oceanic Technol.*, **10**, 452-464.
- West, J. L., and A. F. Ferullo, 1990: Doppler acoustic sounder performance audit tower versus sounder. Proc., *83rd Annual Meeting & Exhibition*, Pittsburgh, PA, Air & Waste Management Assoc., Paper 90-86.2
- Whiteman, C. D., and X. Bian, 1996: Solar semidiurnal tides in the troposphere: detection by radar profilers. *Bull. Amer. Meteor. Soc.*, **77**, 529-542.
- Wilczak, J. M., R. G. Strauch, F. M. Ralph, B. L. Weber, D. A. Merritt, J. R. Jordan, D. E. Wolfe, L. K. Lewis, D. B. Wuertz, J. E. Gaynor, S. A. McLaughlin, R. R. Rogers, A. C. Riddle, and T. S. Dye, 1995: Contamination of wind profiler data by migrating birds: characteristics of corrupted data and potential solutions. *J. Atmos. Oceanic Technol.*, **12**, 449-467.
- Wilkerson, G. W., P. A. Catizone, and T. D. Coble, 1994: Use of a tethered sonde measurement system to conduct a Doppler sodar performance audit. Preprint, *Eighth Joint Conference of the Applications of Air Pollution Meteorology with the AWMA*, Nashville, TN, Amer. Meteor. Soc., 61-67.

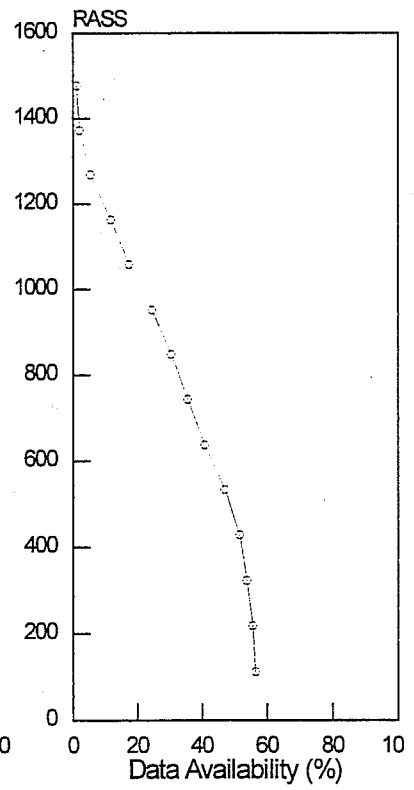
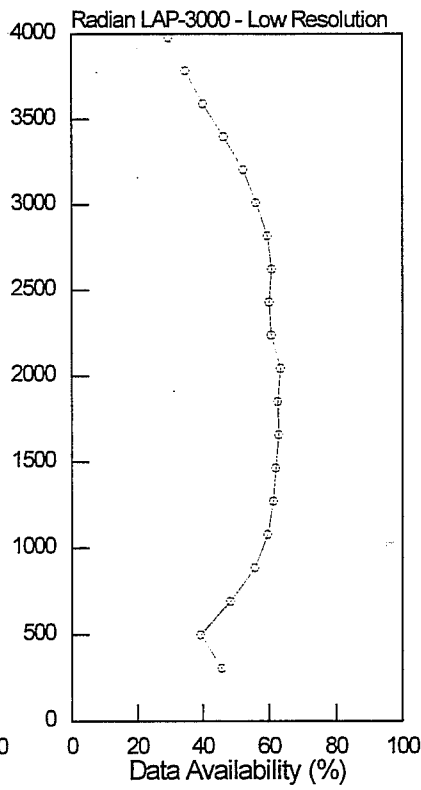
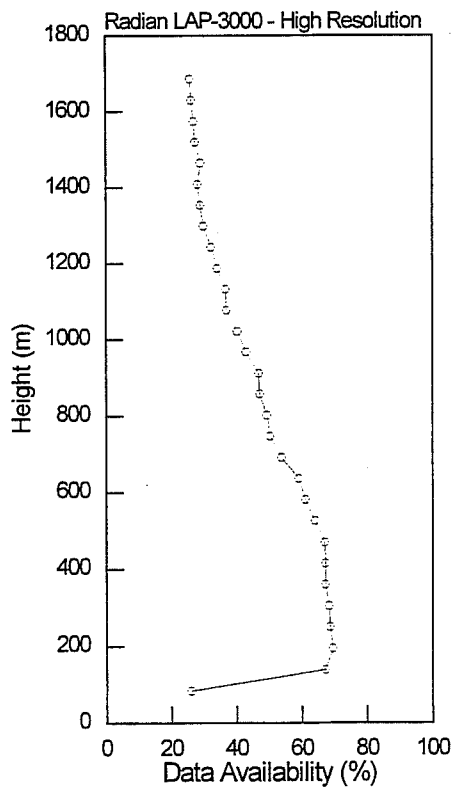
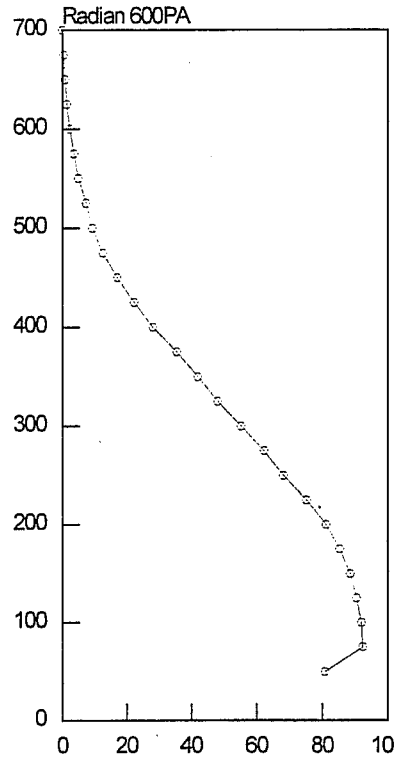
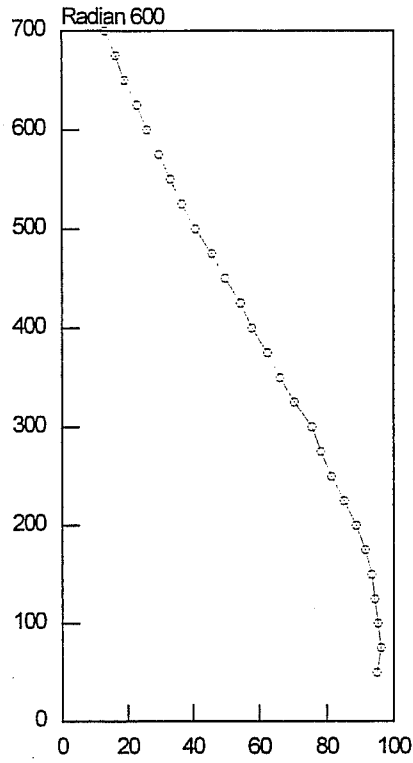
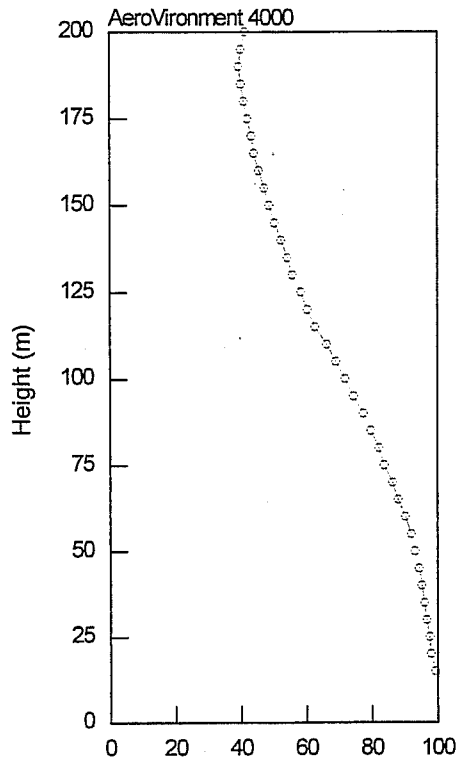
Appendix A: Data Availability Graphs

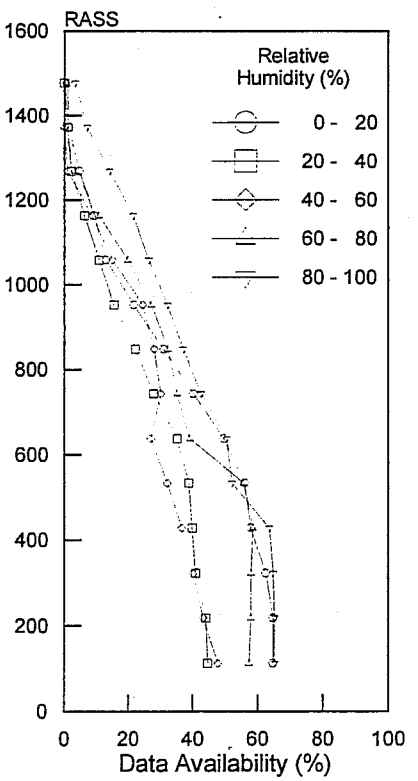
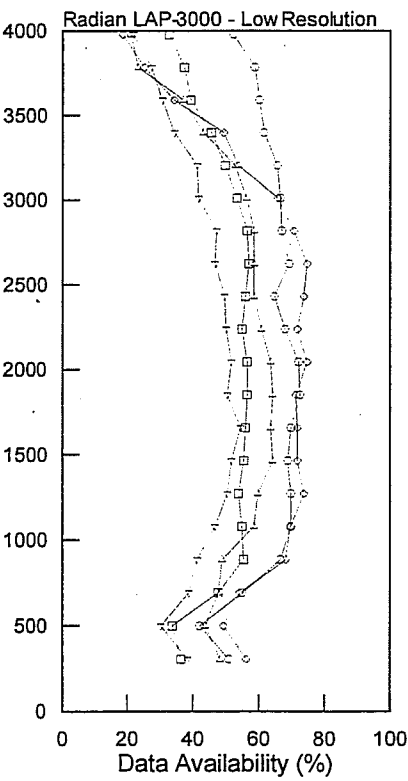
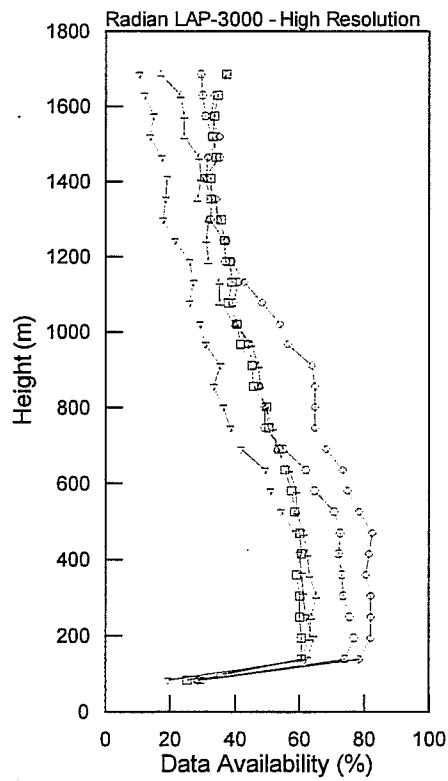
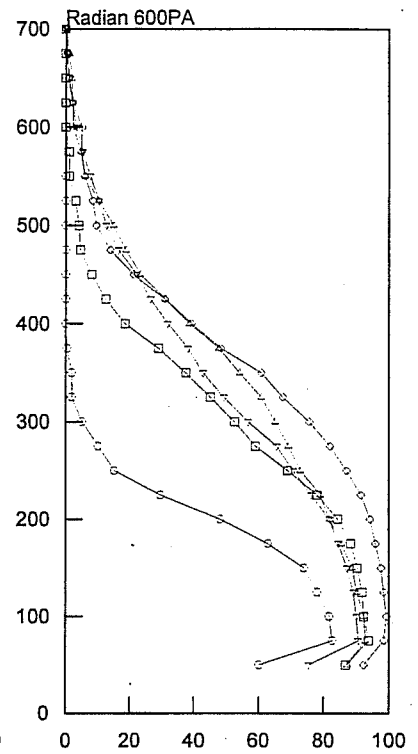
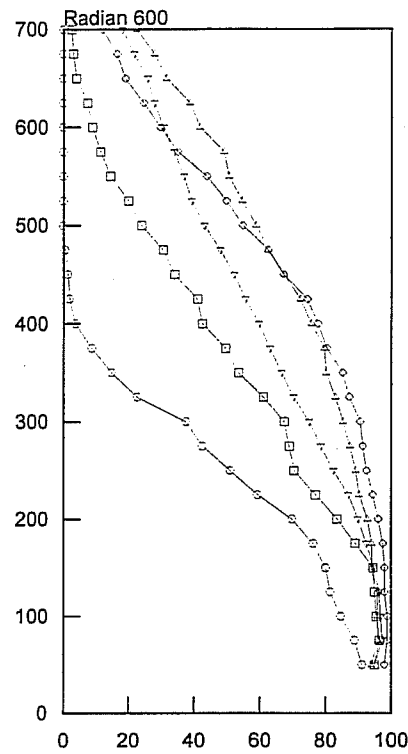
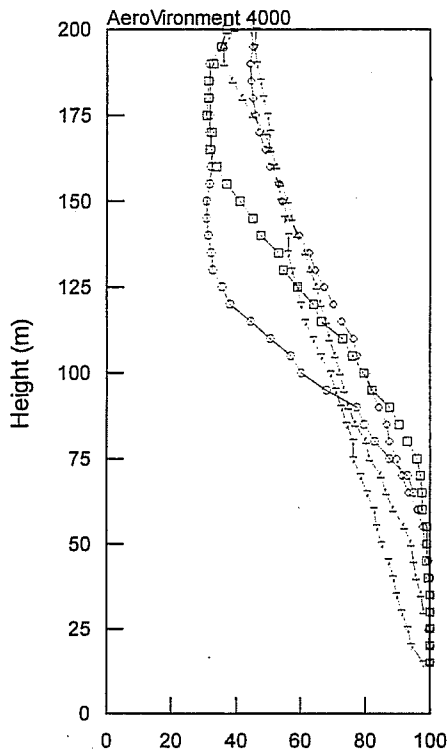
The next nine pages are graphs of data availability for the AeroVironment 4000 sodar, Radian 600 sodar, Radian 600PA sodar, Radian LAP-3000 radar wind profiler (high and low resolution modes, respectively), and the Radian RASS. The first two pages show data availability of each sensor for all conditions for the entire experiment. Thus, a 100% data capture for a particular range gate of a sodar would constitute 2052 valid data points (winds determined 4 times per hour over a time period of 21 days and 9 hours). In the case of the radar wind profiler and RASS, a complete set of data for a particular range gate would total 1026 points (winds and temperatures determined twice an hour).

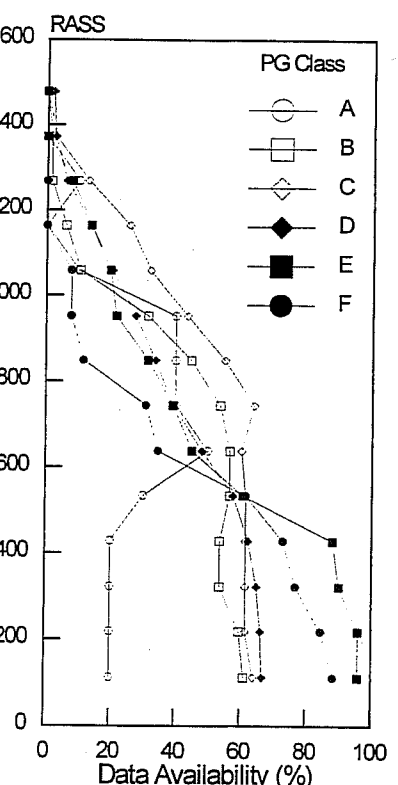
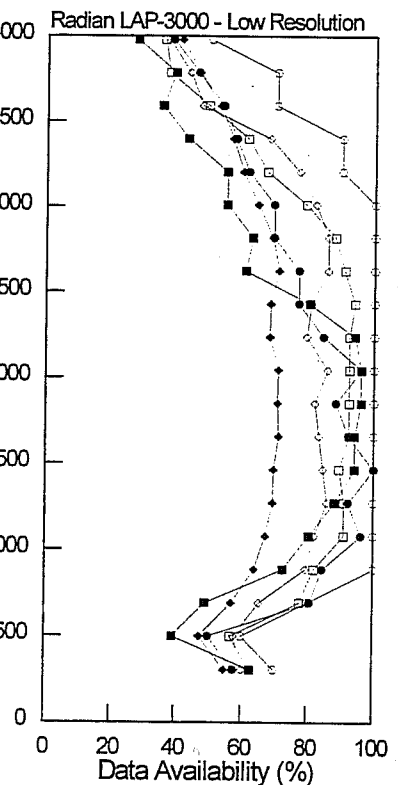
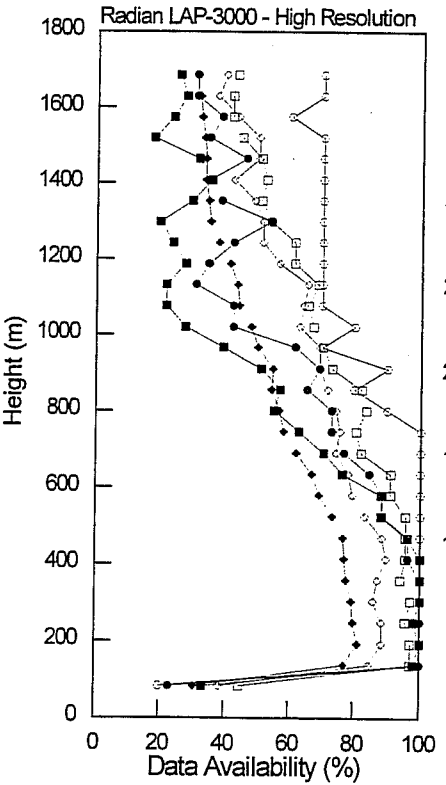
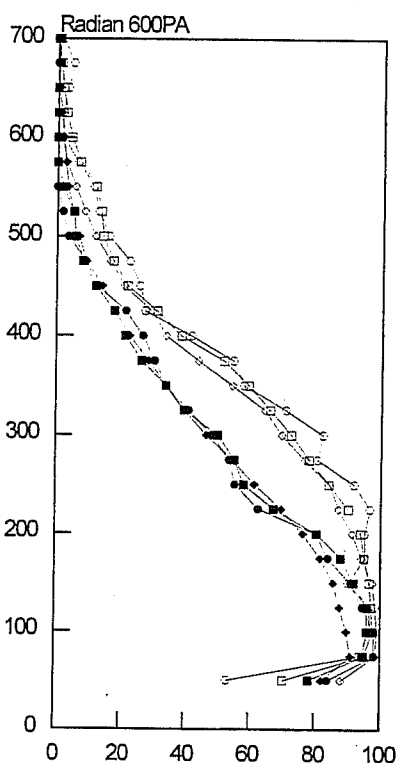
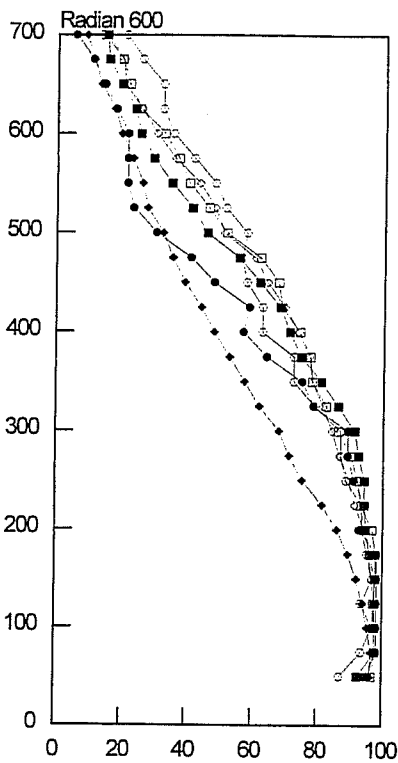
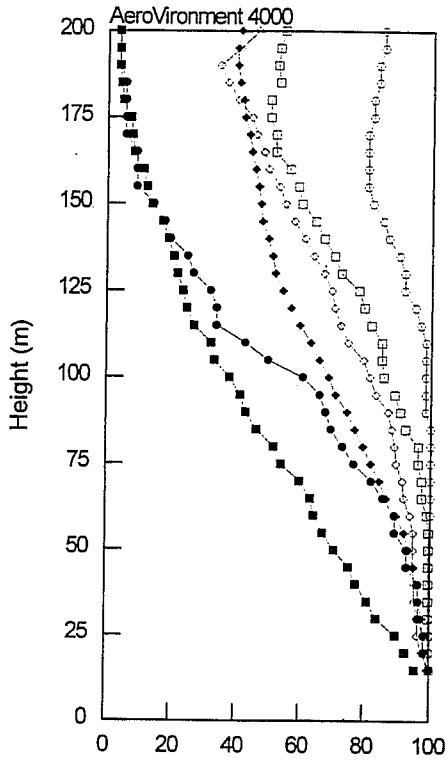
The graphs that follow are the data availabilities as a function of varying atmospheric conditions or stability. For these cases, each data availability profile is determined by the number of reported data values for a particular stability classification (e.g., when relative humidity was between 20 and 40%) divided by the total number of cases that occurred during the study for that particular stability classification which is listed in Table 19.

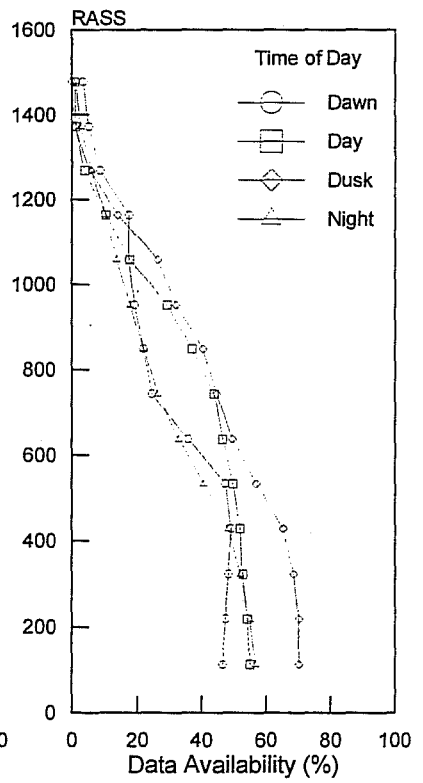
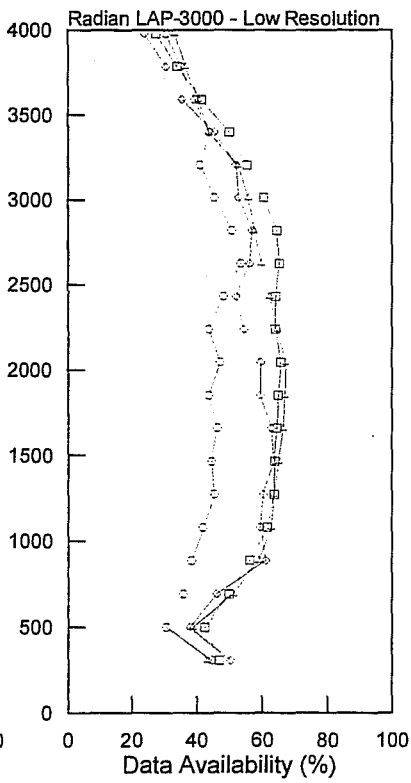
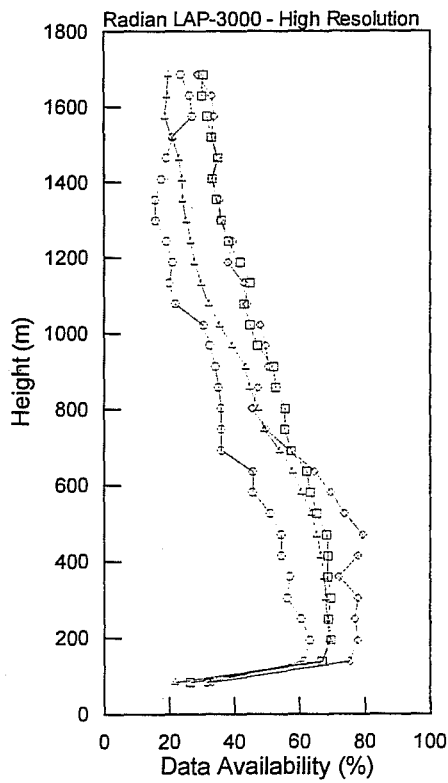
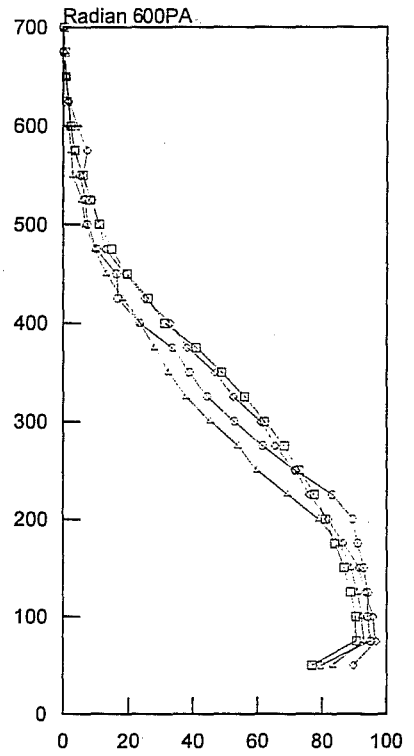
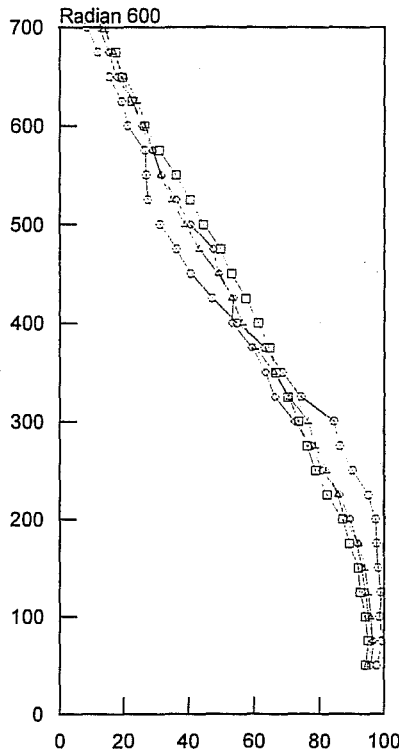
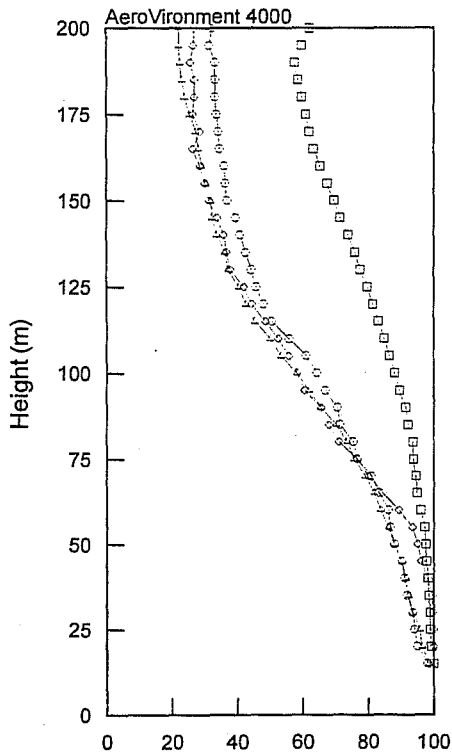
Table 19
Total number cases for a particular stability classification.

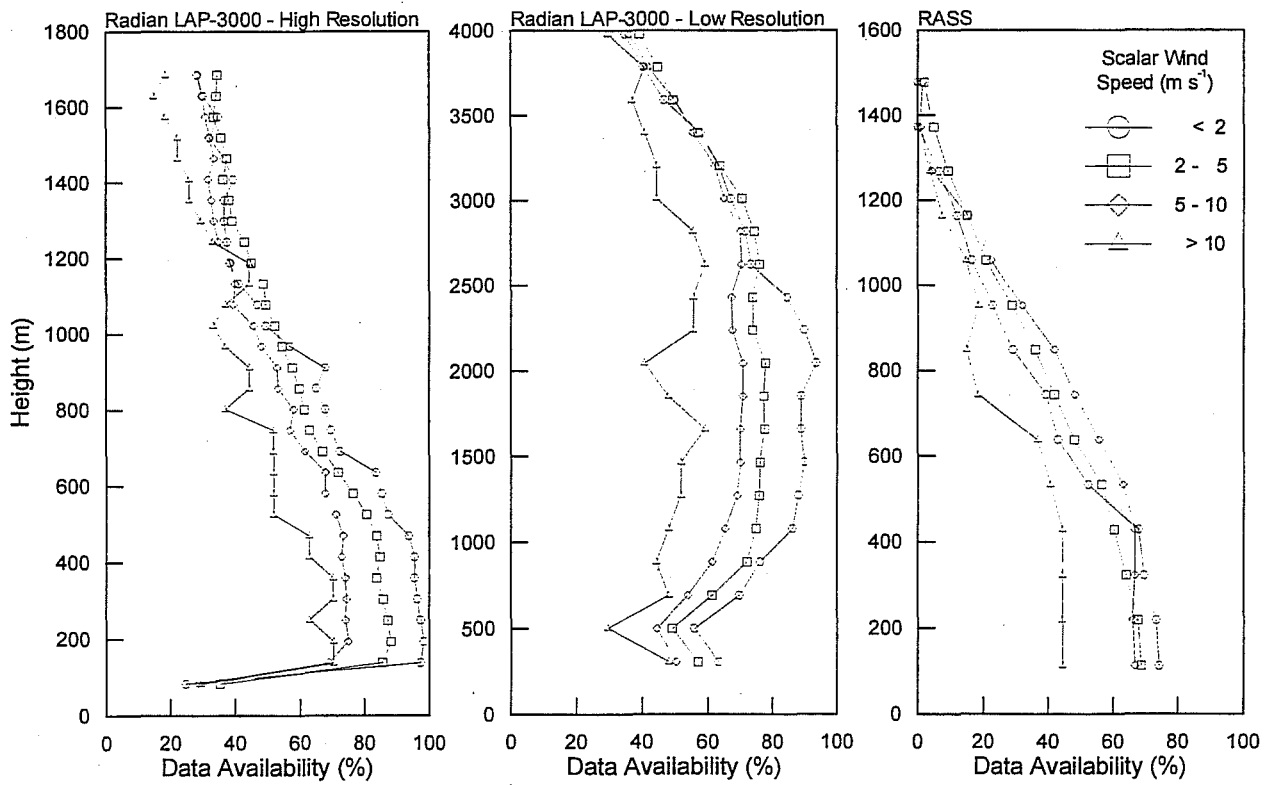
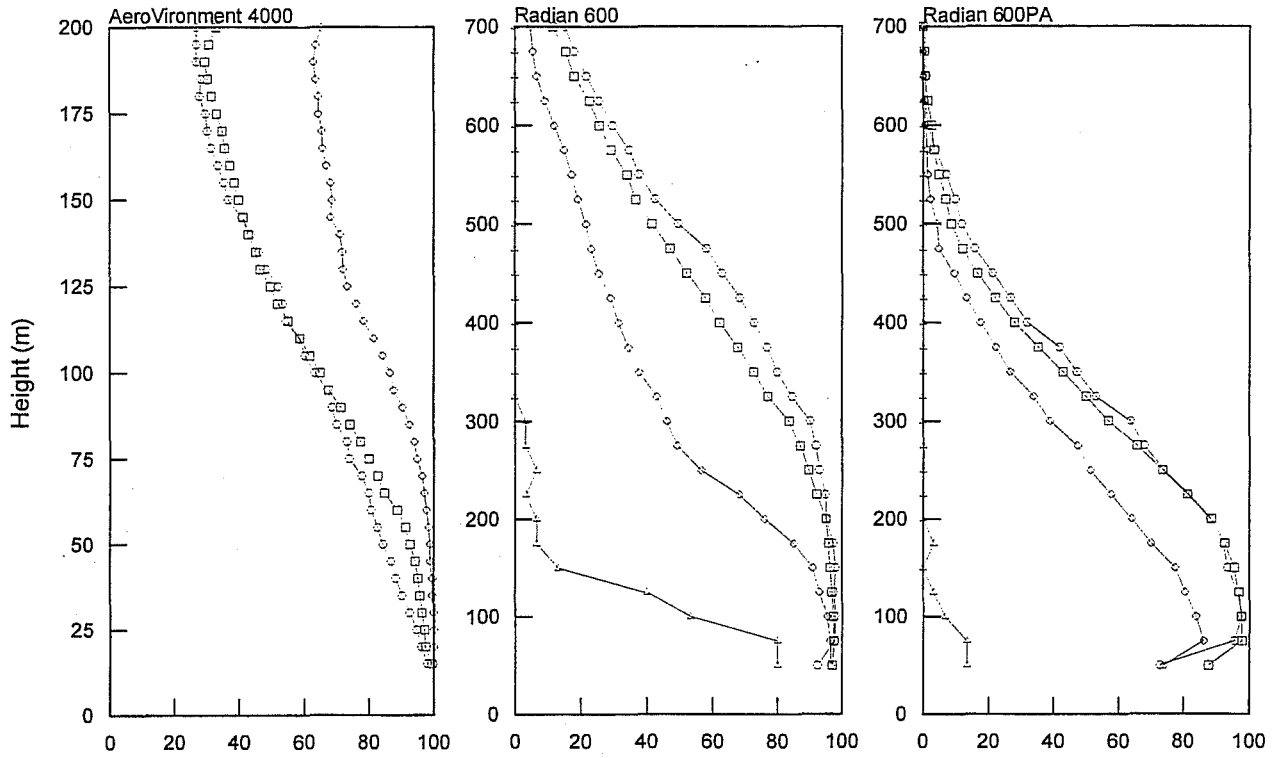
<i>RH</i> (%)	<i>N</i>	PG Class	<i>N</i>	Time of Day	<i>N</i>	<i>SS</i> (m s ⁻¹)	<i>N</i>
0 - 20	216	A	62	Dawn	226	< 2	409
20 - 40	200	B	183	Day	901	2 - 5	955
40 - 60	358	C	211	Dusk	246	5 - 10	435
60 - 80	388	D	1100	Night	679	> 10	30
80 - 100	687	E	174				
		F	56				
σ_θ (deg)	<i>N</i>	<i>S_h</i> (s ⁻¹)	<i>N</i>	<i>N</i> ² _{BV} (s ⁻²)	<i>N</i>	<i>R_B</i>	<i>N</i>
< 10	1032	< 0.02	519	< 0.000	941	< -0.5	442
10 - 20	489	0.02-0.04	516	0.000 - 0.001	558	-0.5 - 0.25	612
20 - 30	162	0.04-0.06	345	0.001 - 0.002	238	0.25 - 1	355
> 30	146	> 0.06	211	> 0.002	126	> 1	182

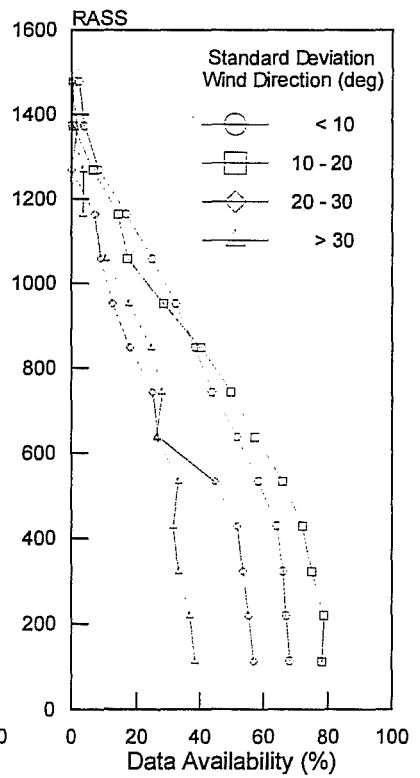
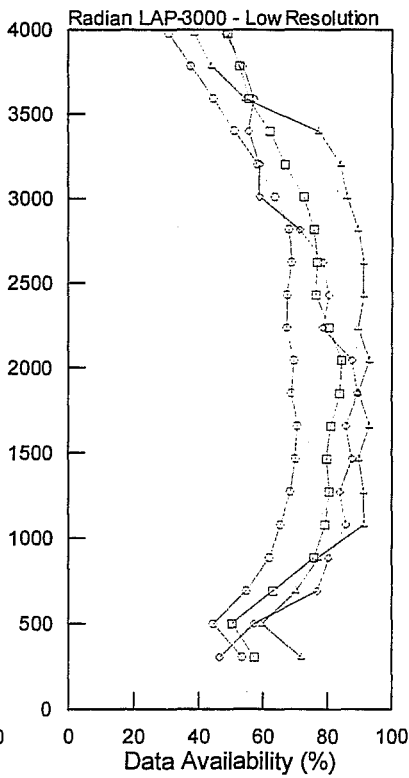
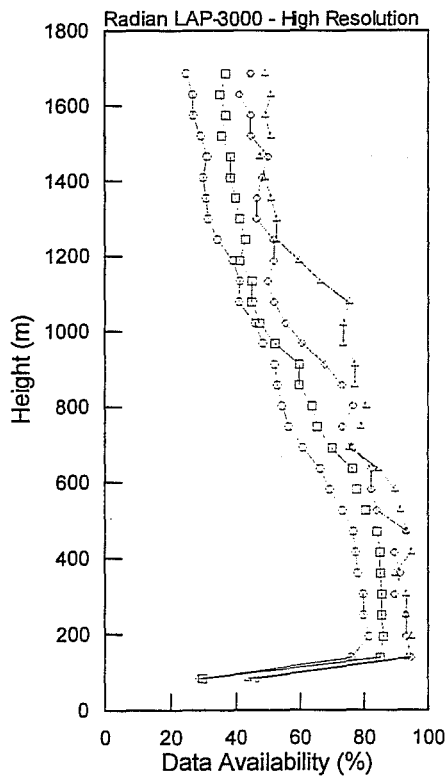
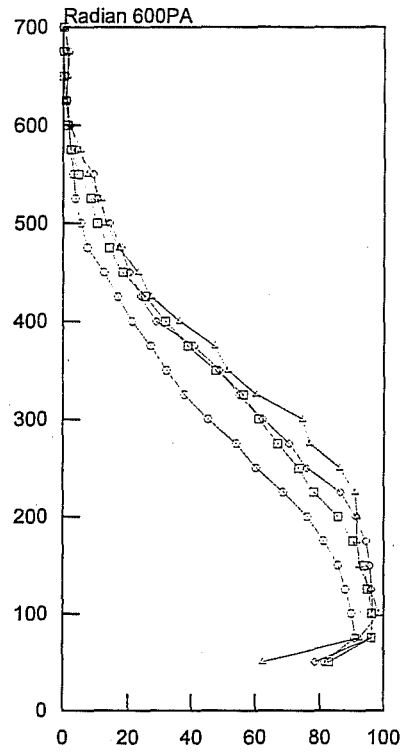
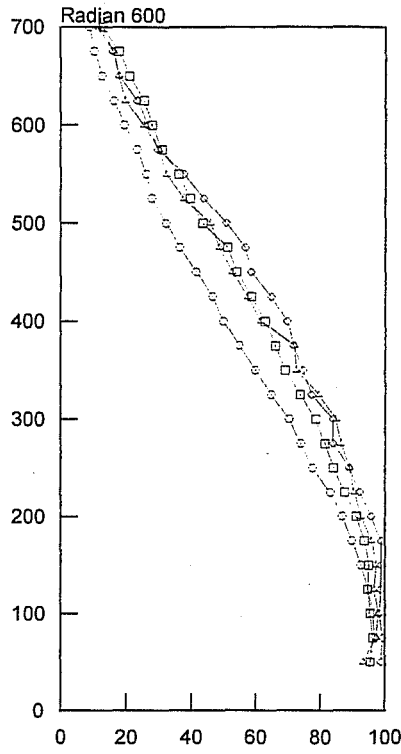
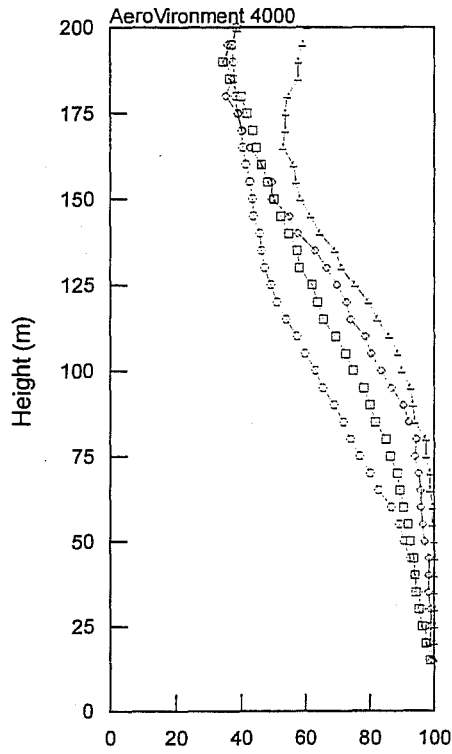


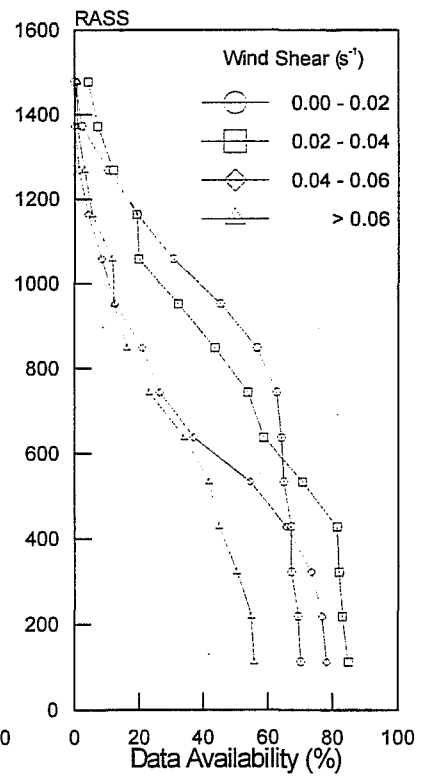
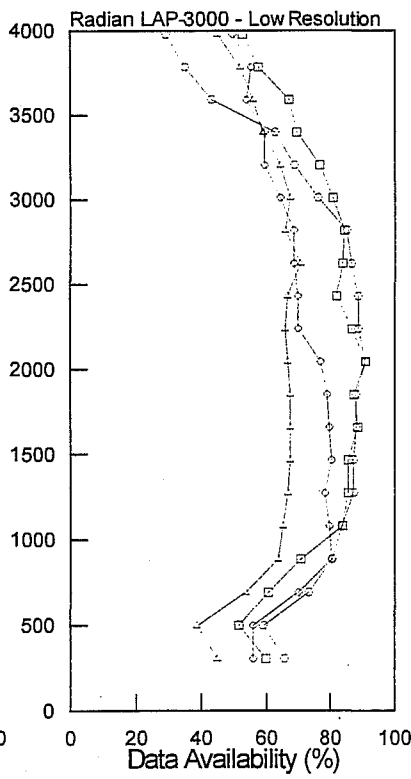
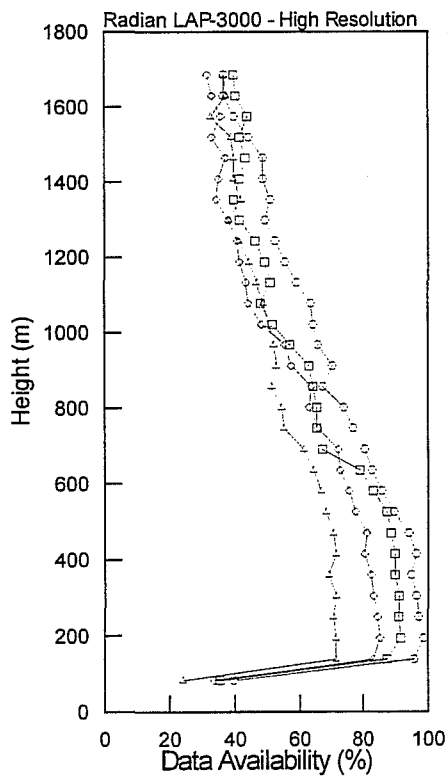
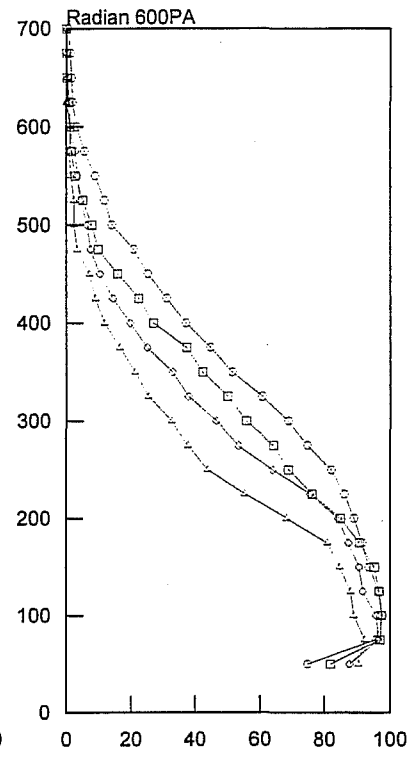
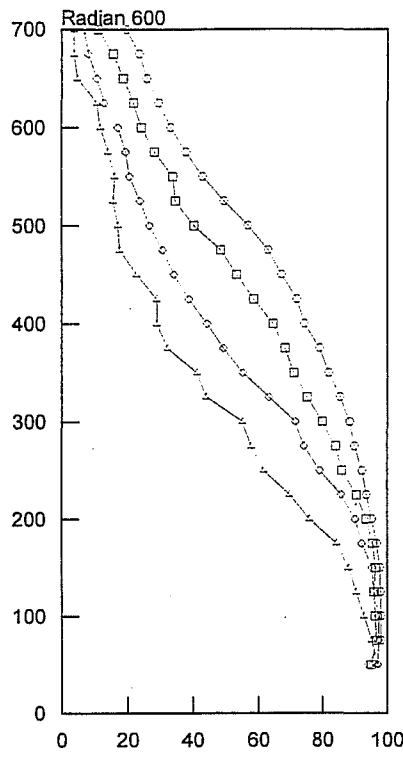
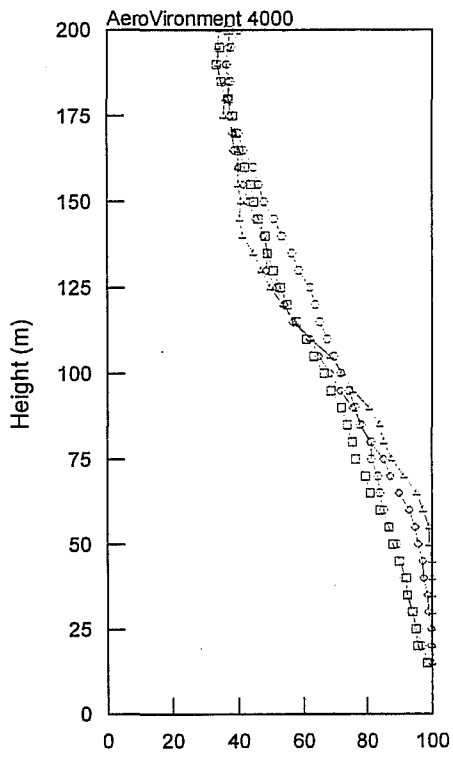


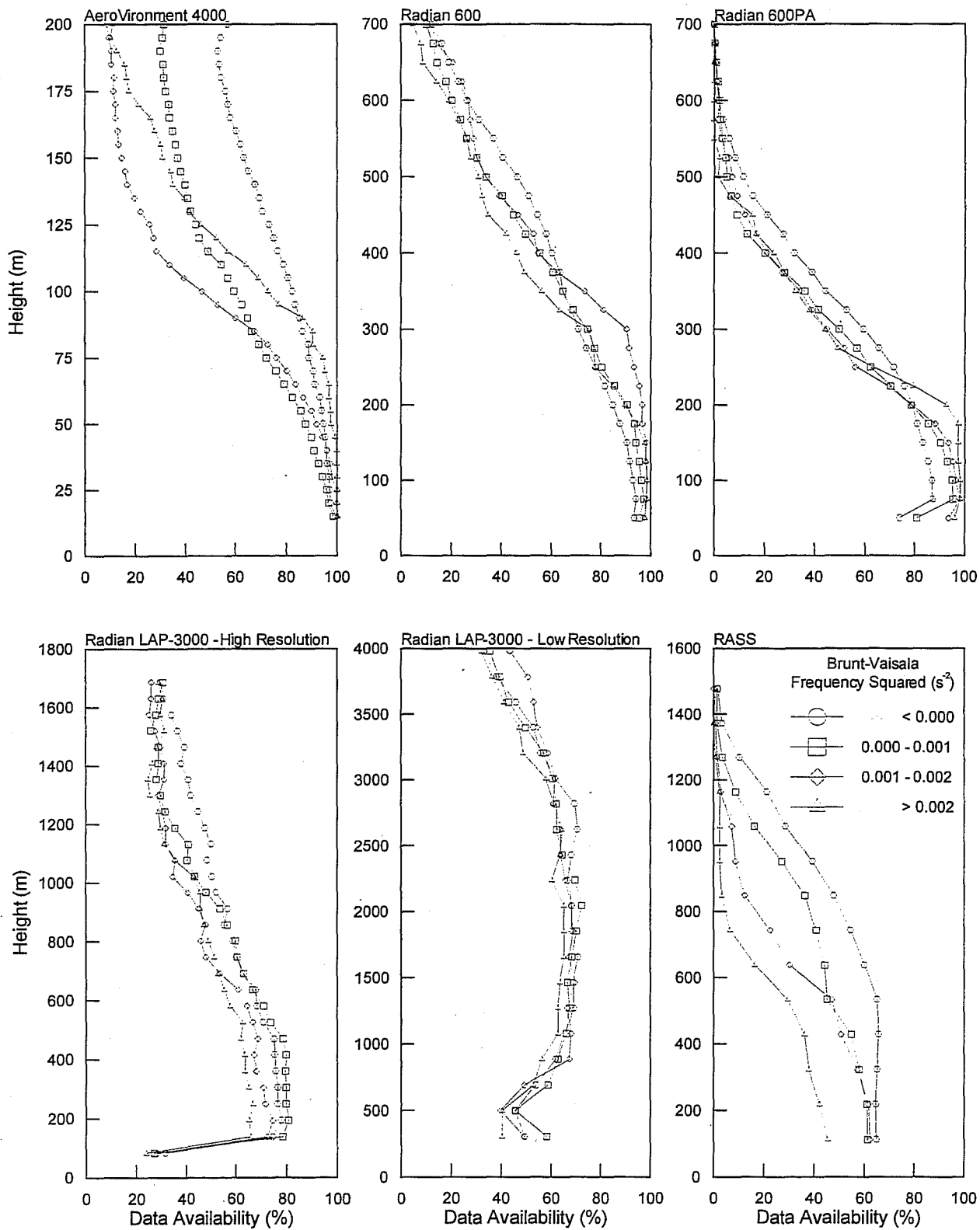


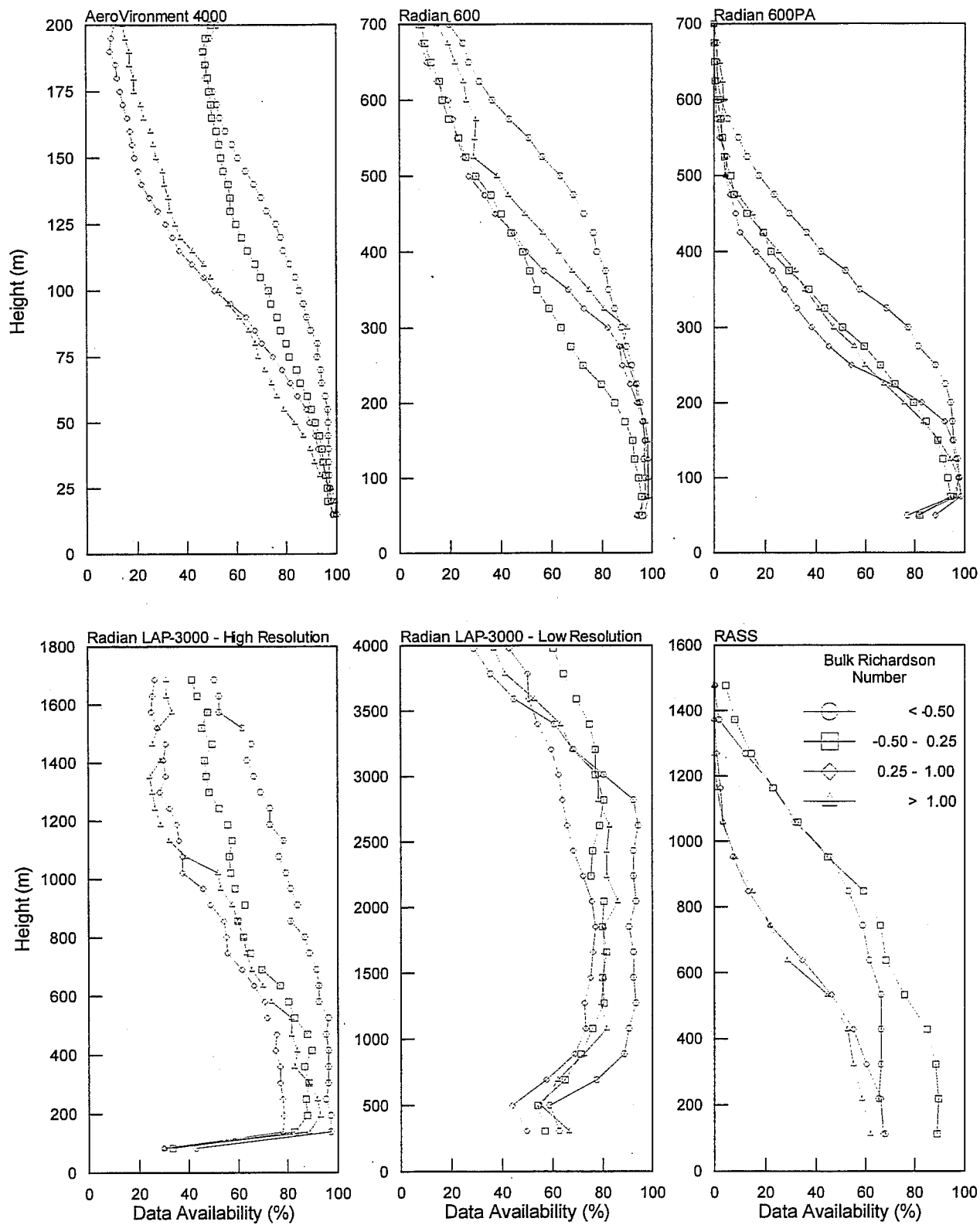












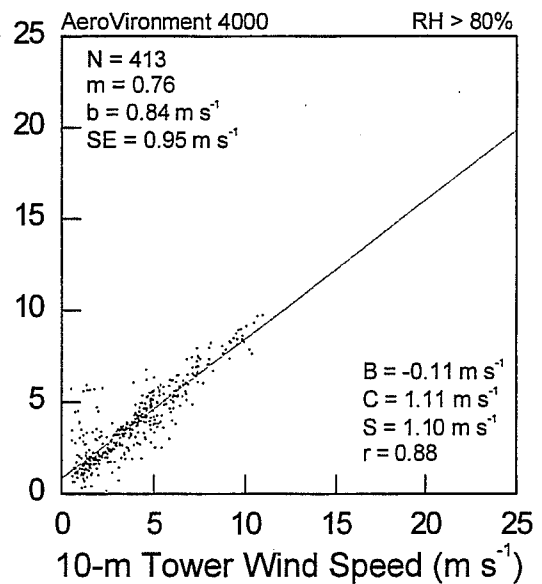
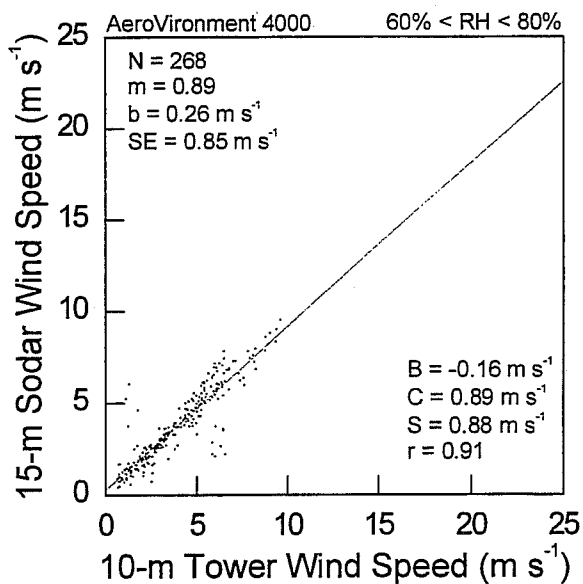
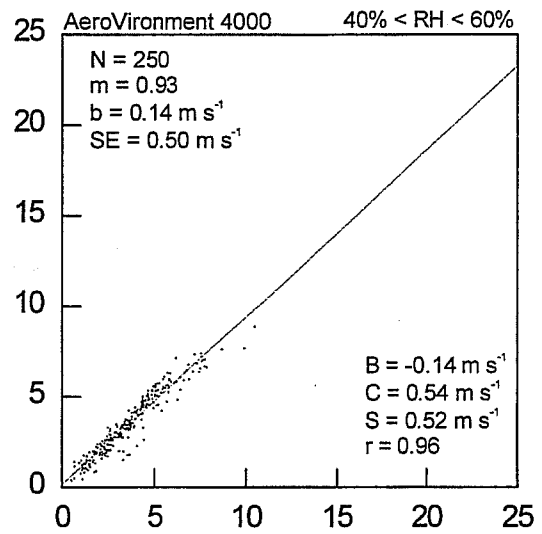
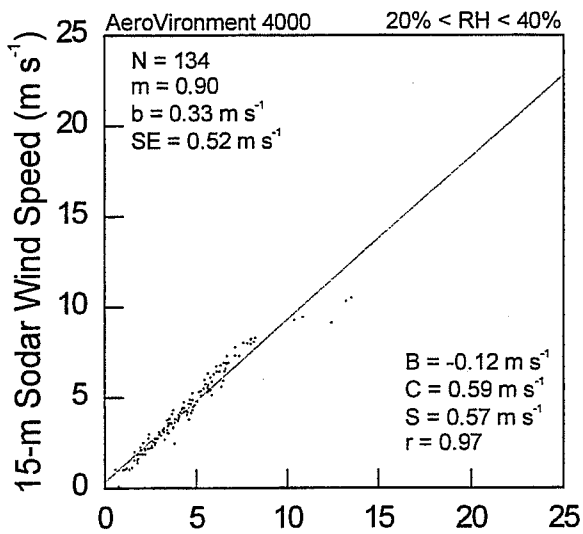
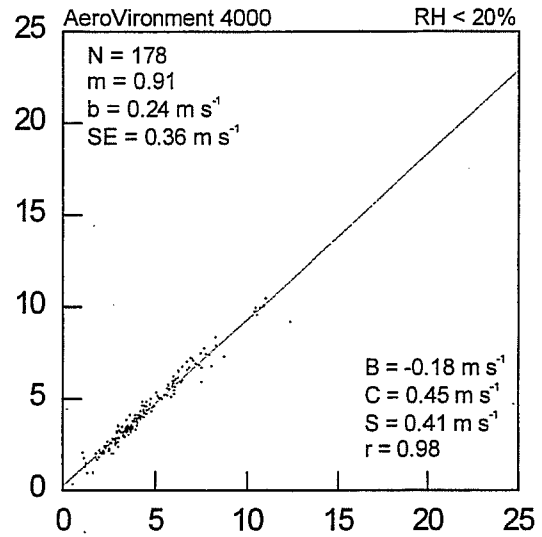
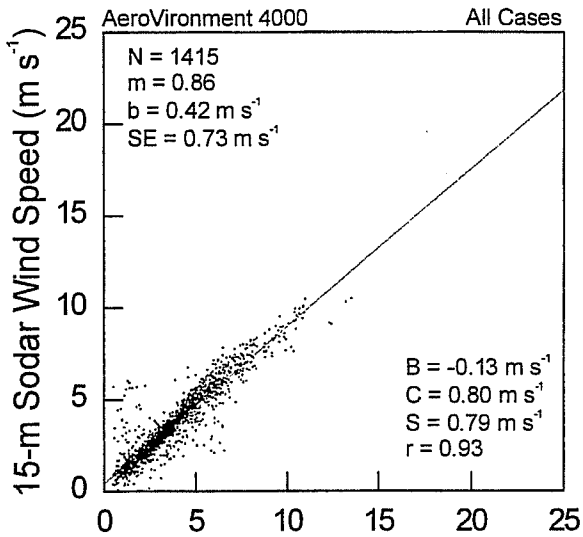
Appendix B: Wind Speed and Direction Scatter Plots with Statistics

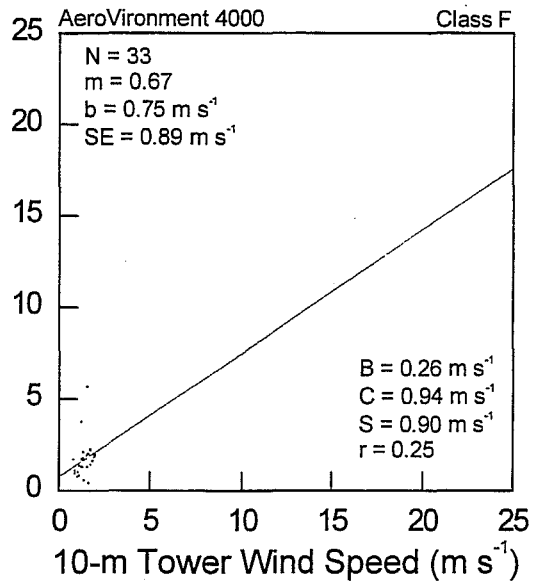
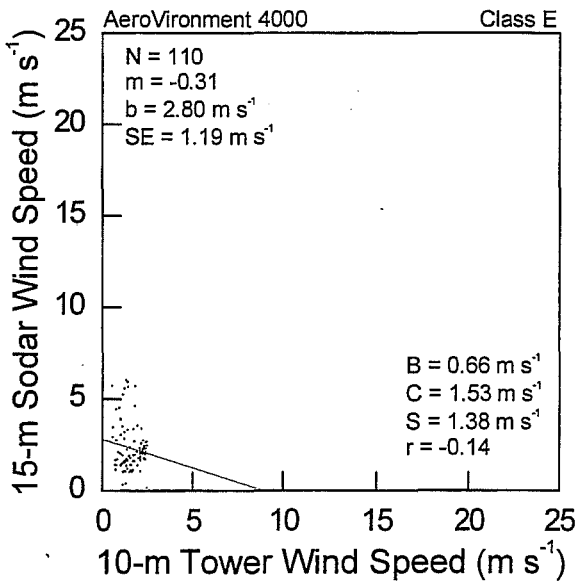
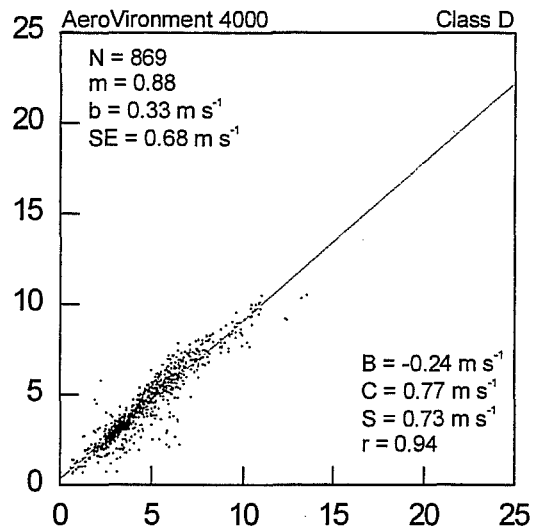
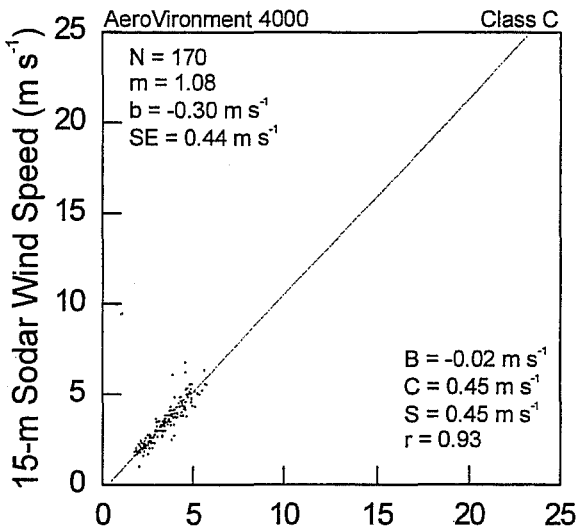
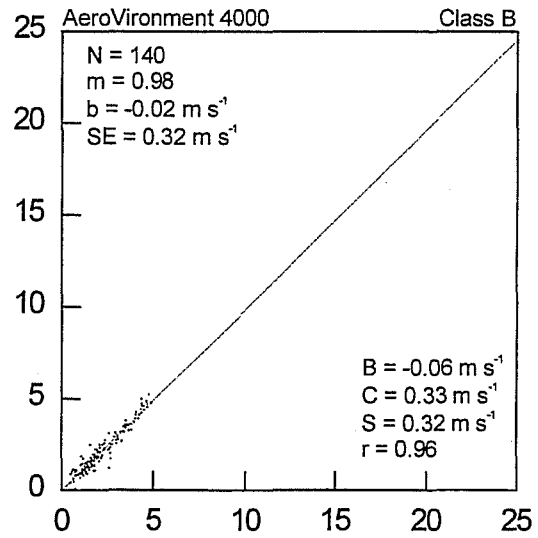
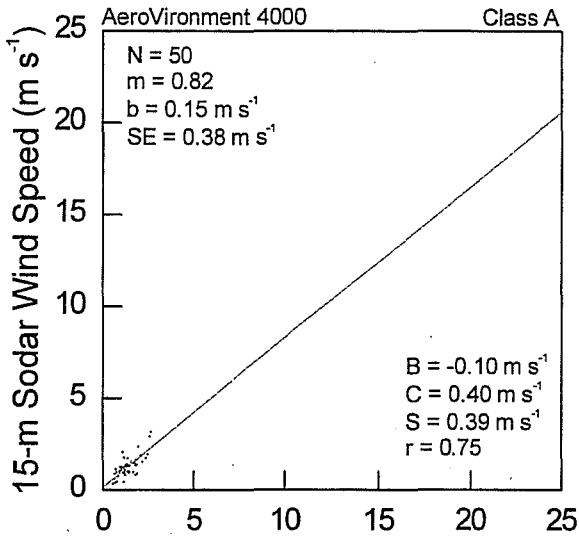
The next 204 pages are scatter plots of wind speed and wind direction of the AeroVironment 4000 sodar, Metek MODOS sodar, Radian 600 sodar, Radian 600PA sodar, and Radian LAP-3000 radar wind profiler (high resolution mode) plotted against tower-based wind speed and direction, respectively. The scatter plots are organized in groups of six pages each. Each group consists of a variable (e.g., wind speed) for a particular measurement height (e.g., 100 m) for the following atmospheric conditions or stabilities: all cases, relative humidity (RH), Pasquill-Gifford stability class (A, B, C, D, E, and F), time of day (dawn, day, dusk, and night), scalar wind speed (SS), standard deviation of the horizontal wind direction (σ_θ), wind shear (S_h), Brunt-Vaisala frequency squared (N^2_{BV}), and the bulk Richardson number (R_B).

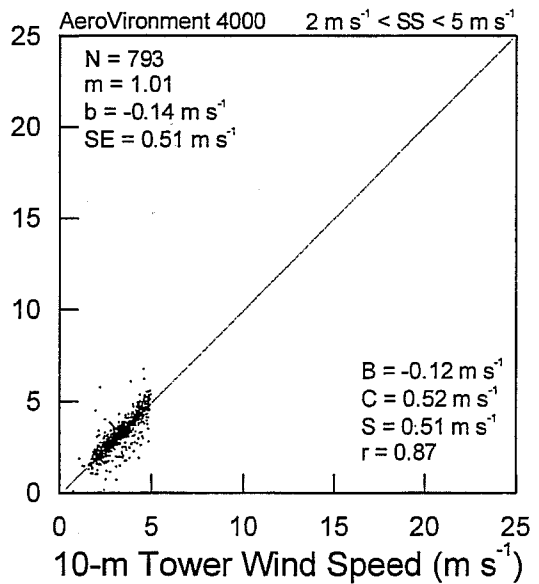
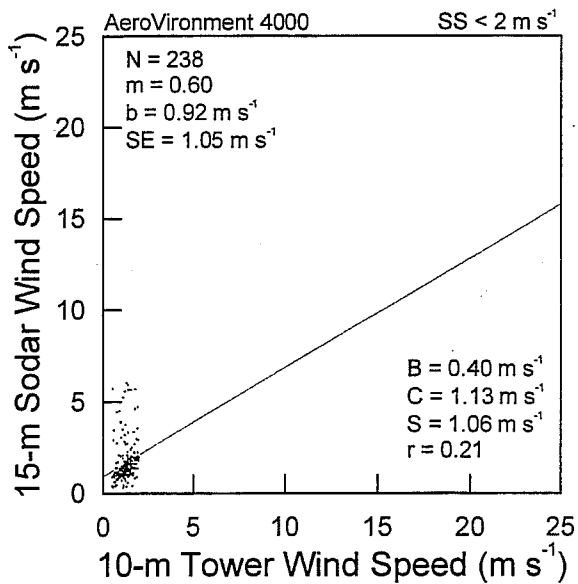
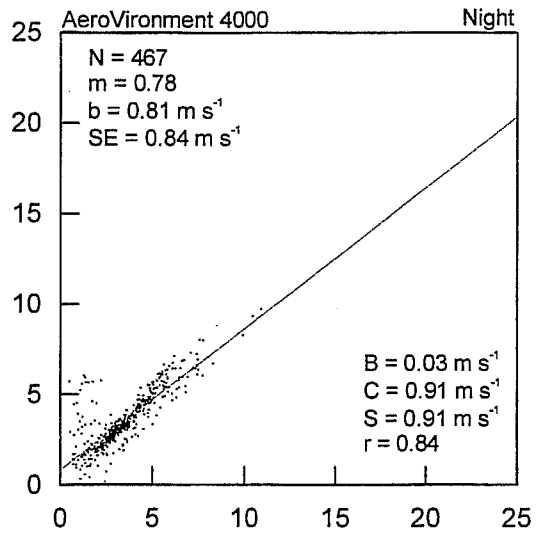
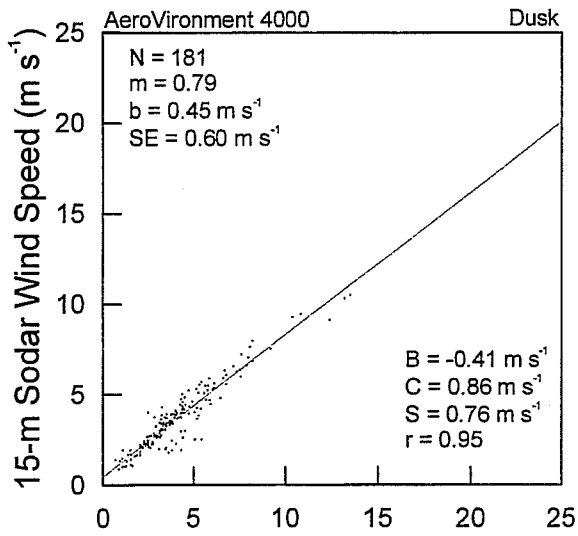
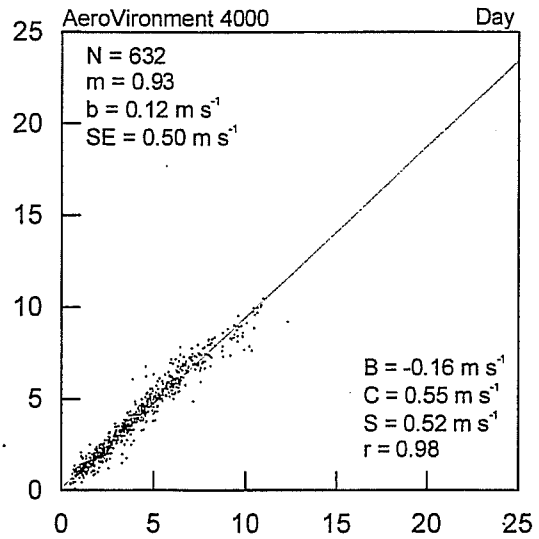
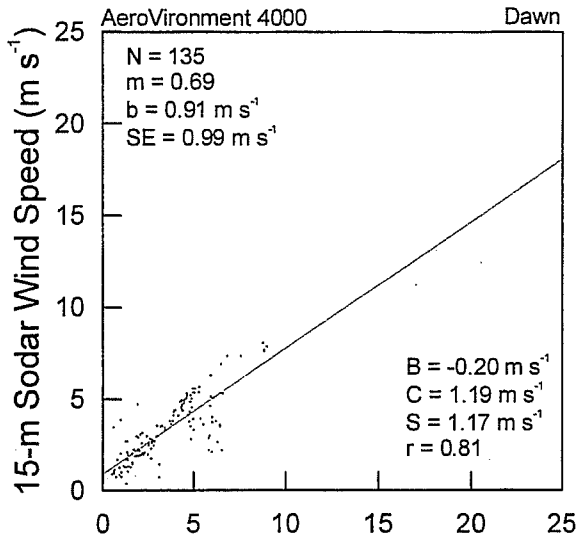
Each individual scatter plot contains the following statistical information:

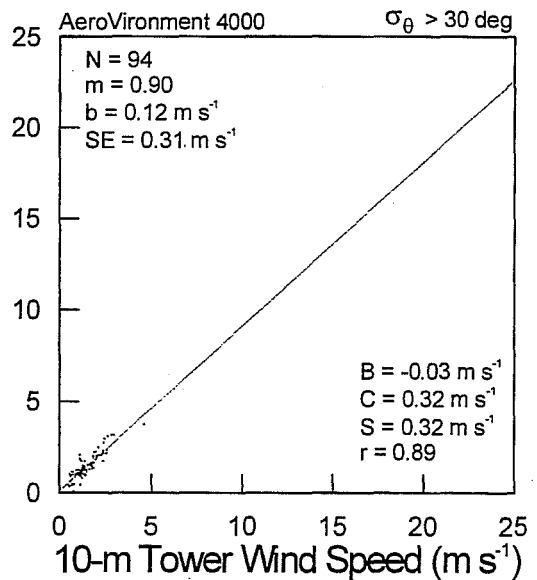
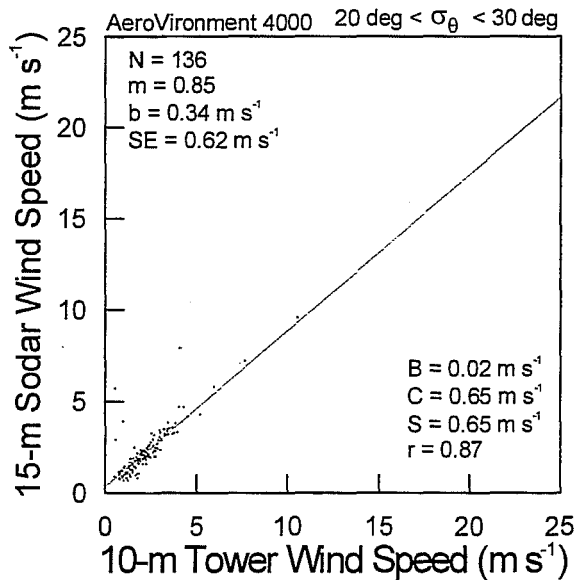
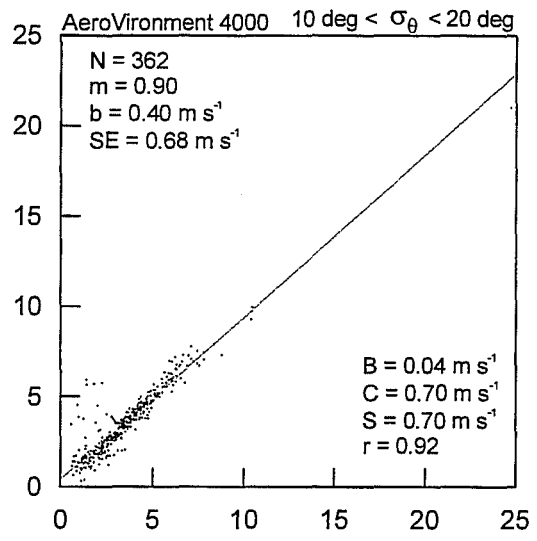
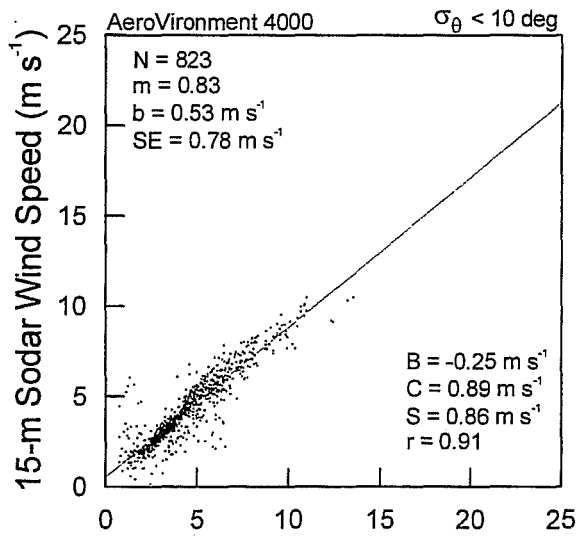
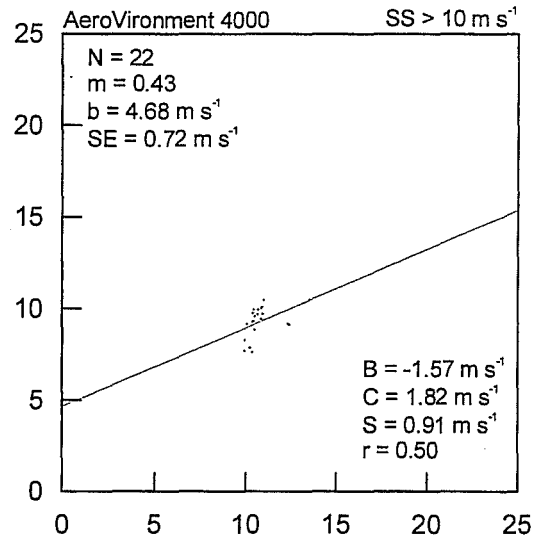
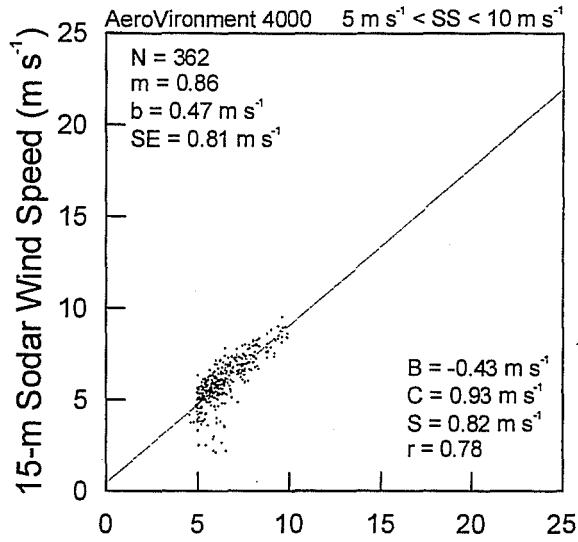
N	number of reported data points
m	slope of linear regression
b	y-intercept of linear regression
SE	standard error (rms difference) about the linear regression
B	bias
C	comparability
S	precision
r	correlation coefficient

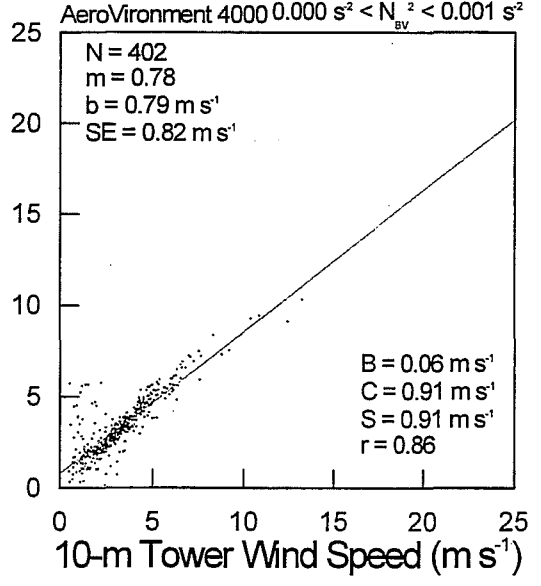
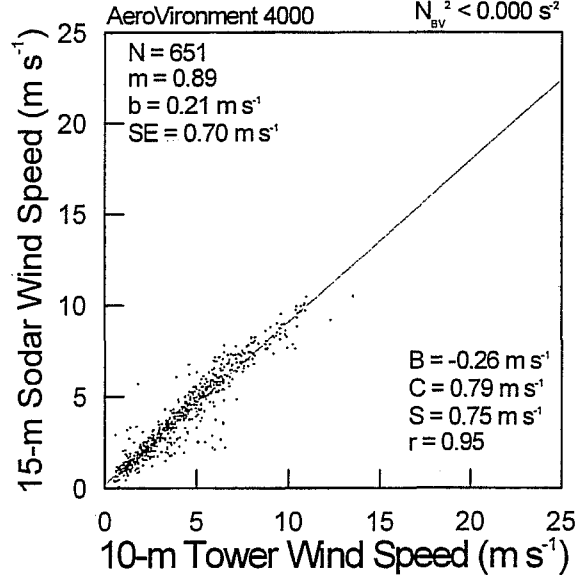
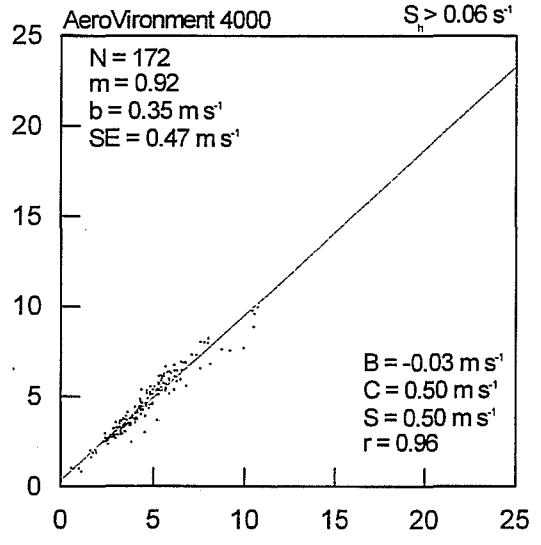
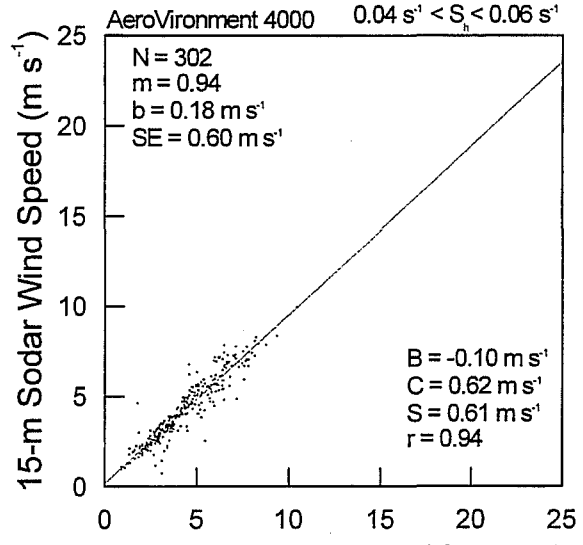
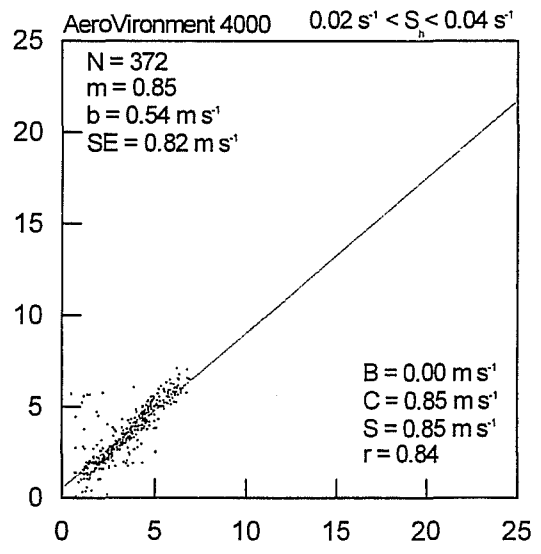
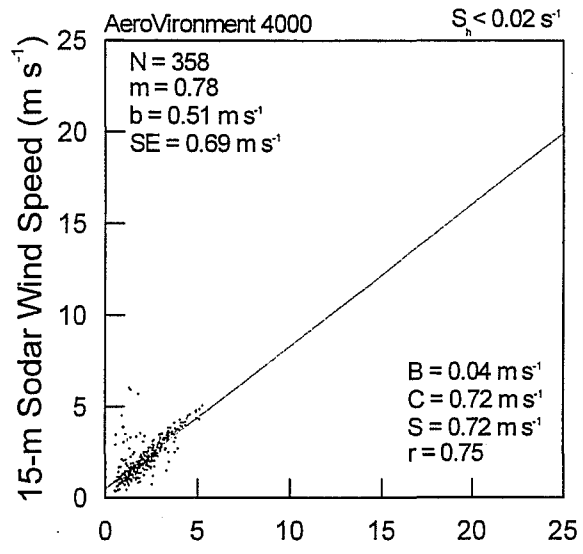
In the case where N was less than 10, no statistics are given for that particular case. Also note that straight lines representing the linear regressions are not shown for the wind direction cases. This is because of a limitation in the graphics program of the "wrap around" effect of reported wind direction values. For example, the graphics program interprets the difference between a tower wind direction value of 40 degrees and a sodar wind direction of 350 degrees as 310. In actuality, the difference is really only 50. However, this "wrap around" effect was eliminated for the above statistical parameters.

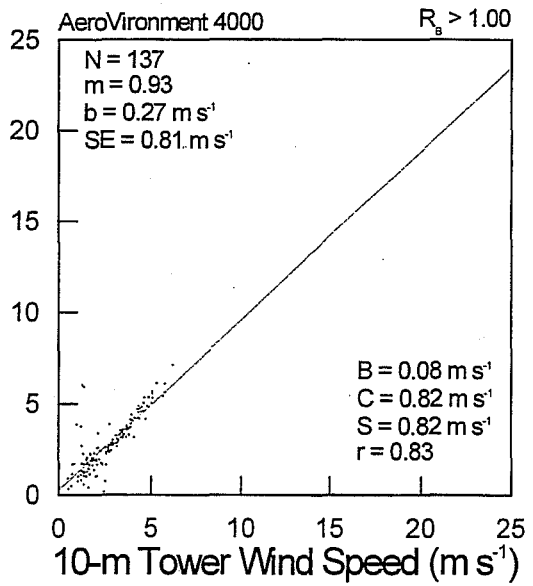
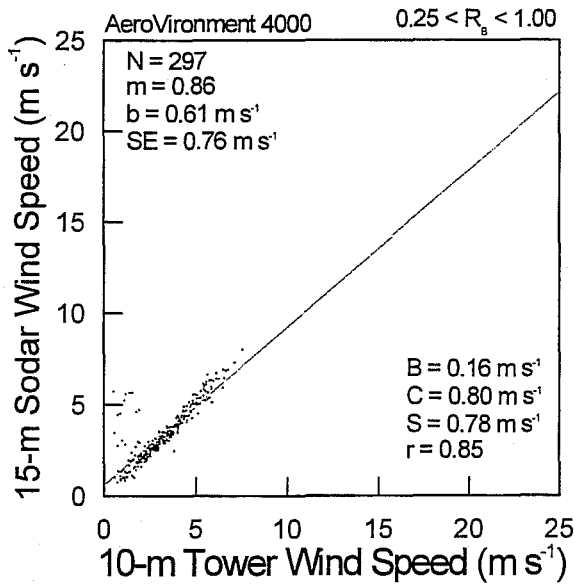
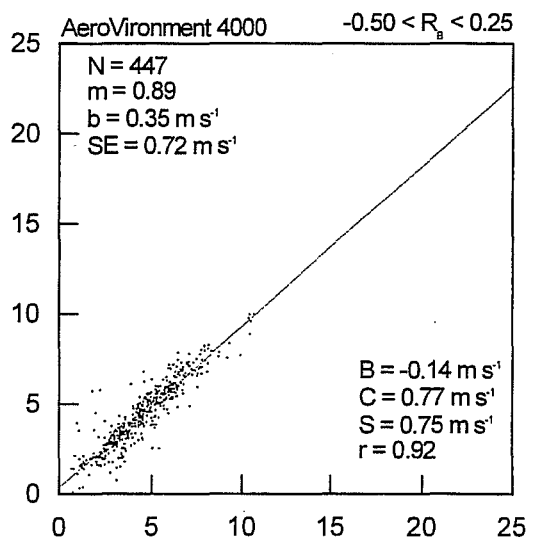
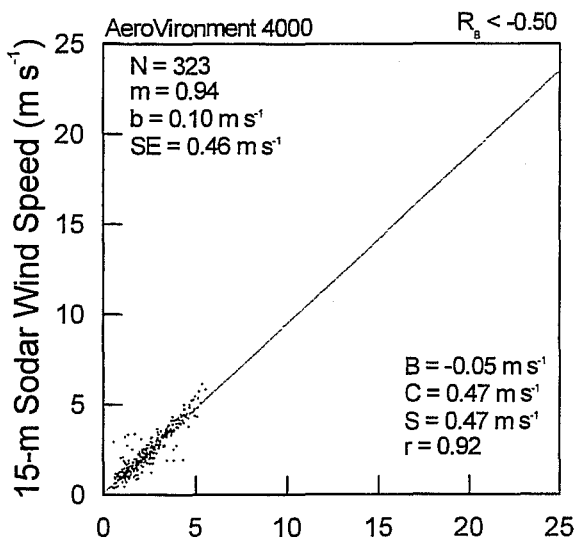
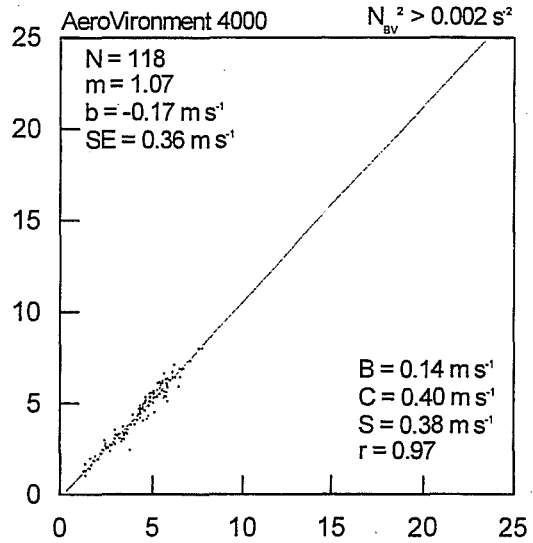
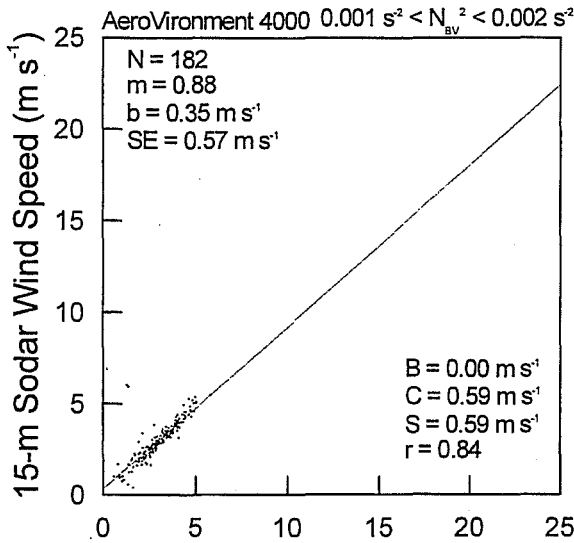


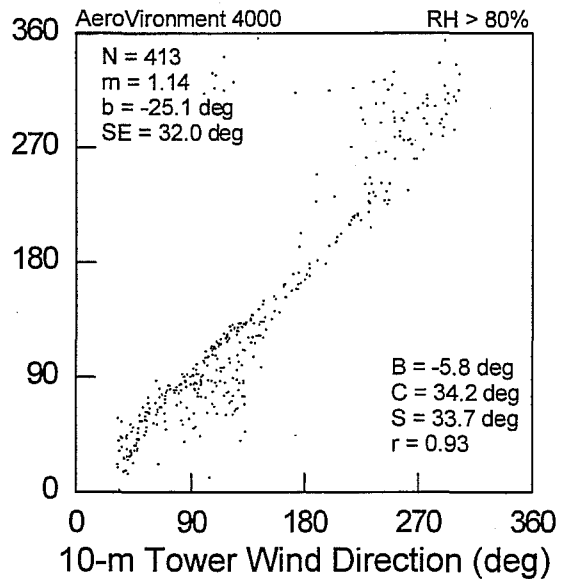
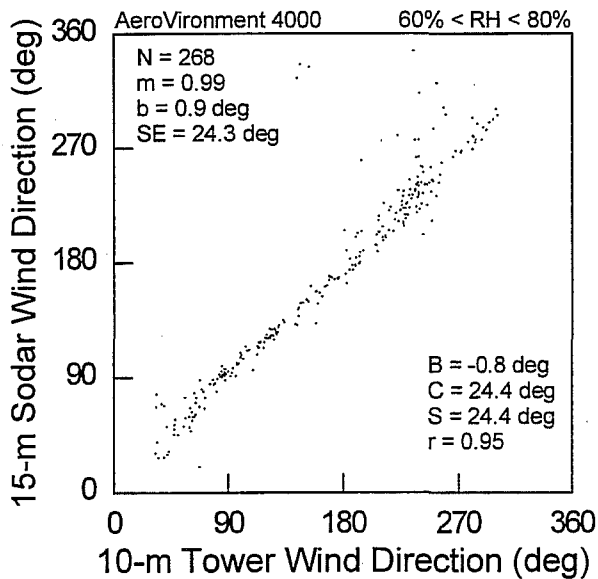
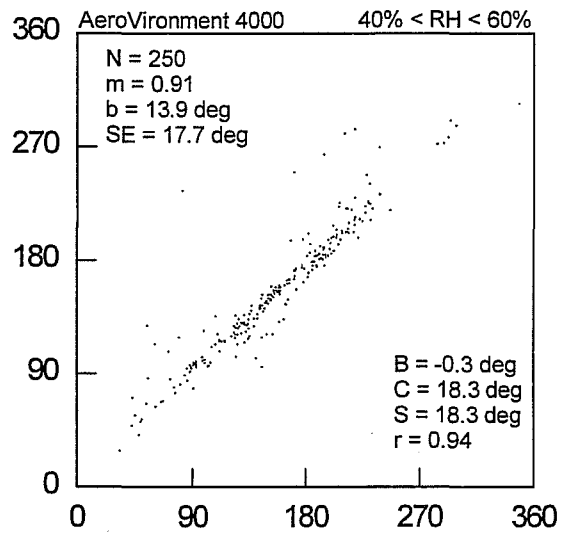
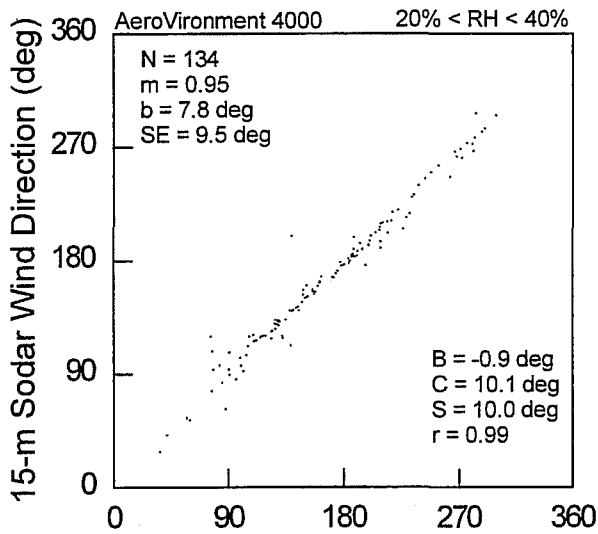
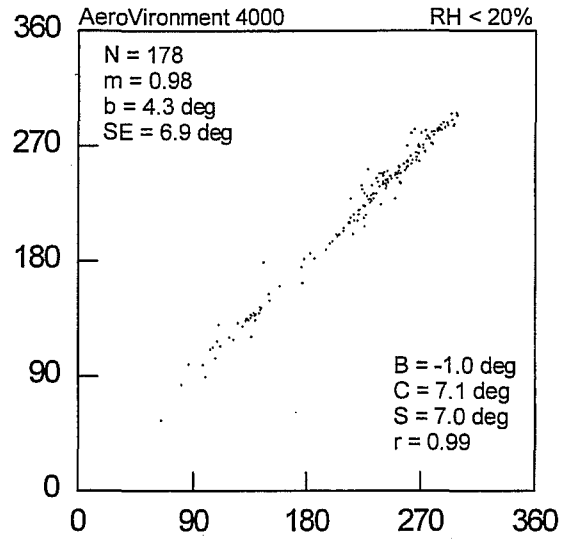
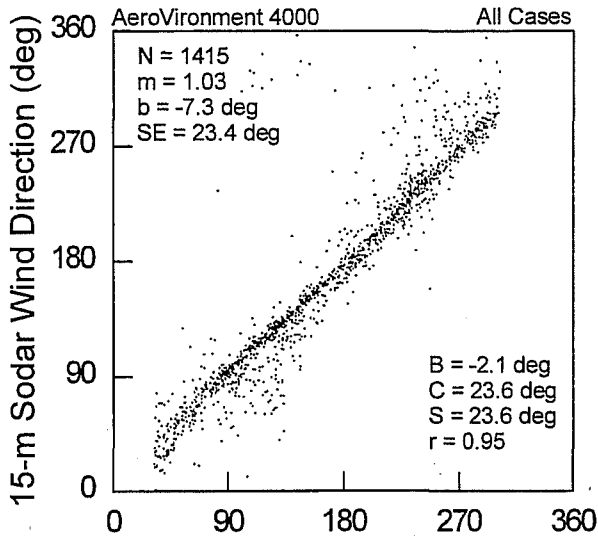


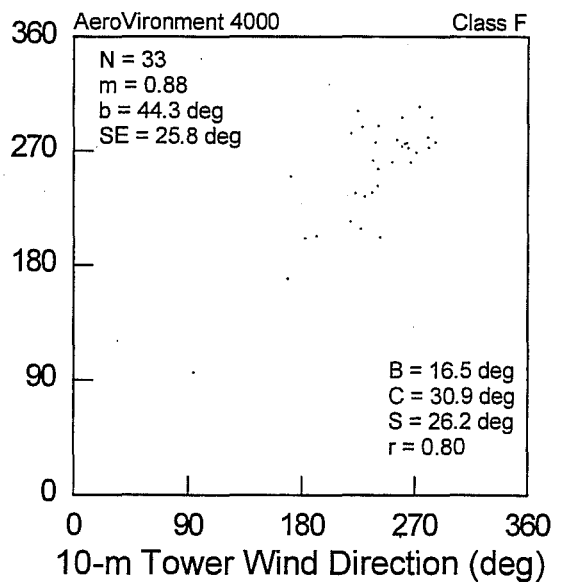
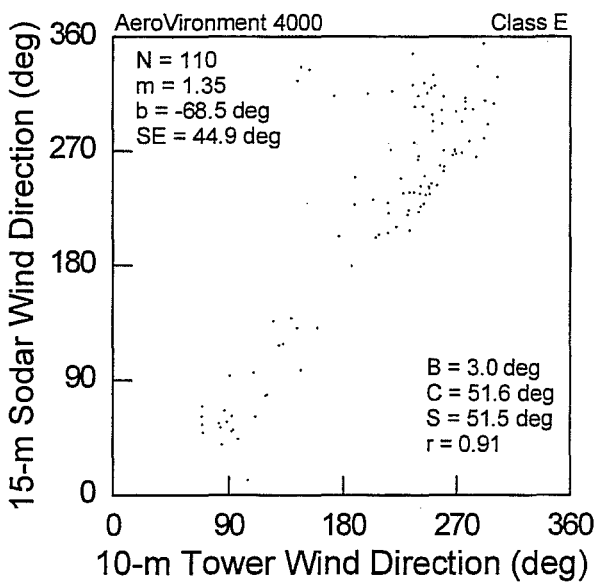
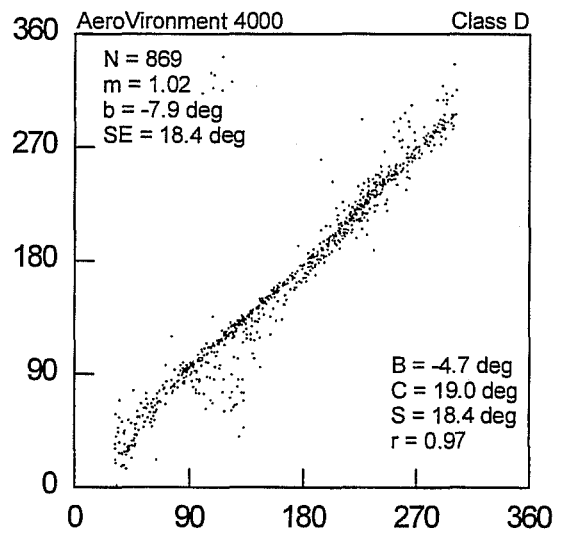
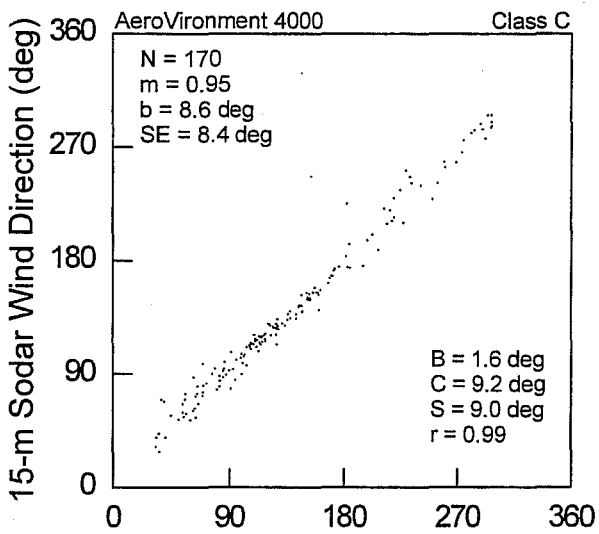
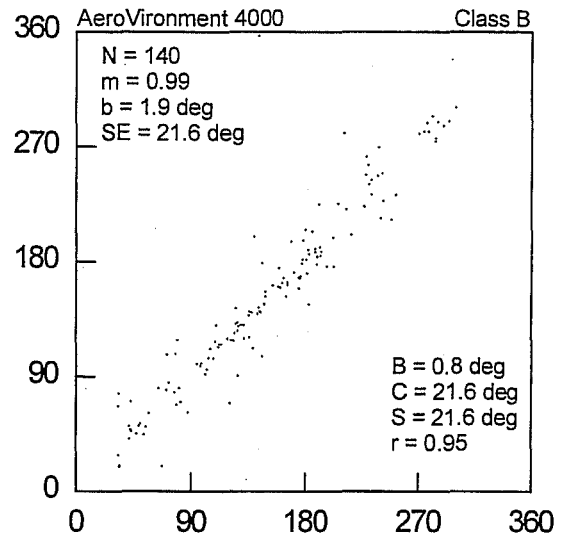
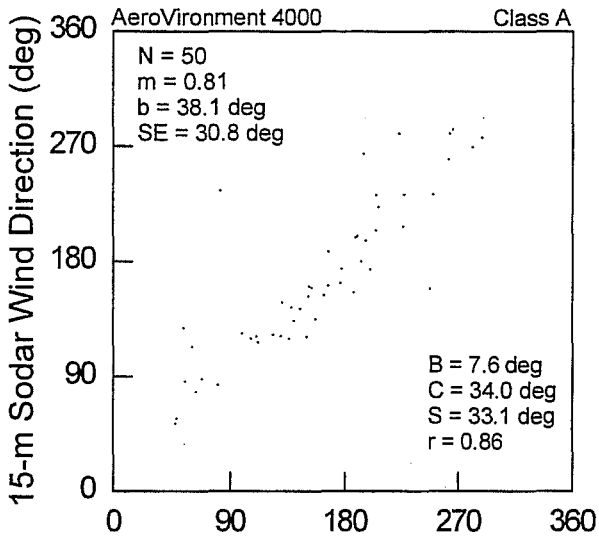


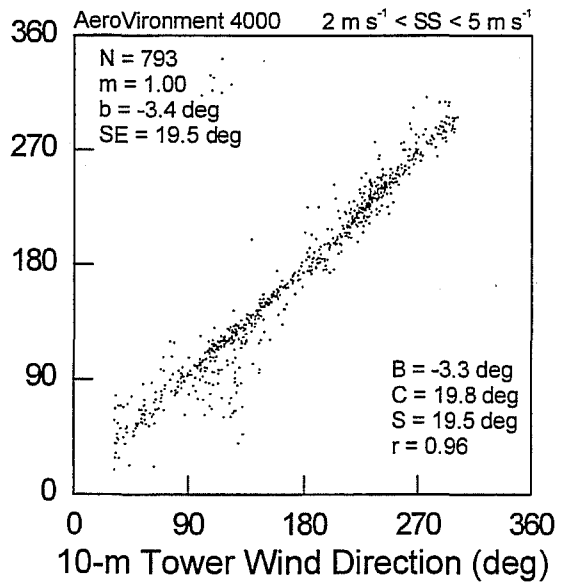
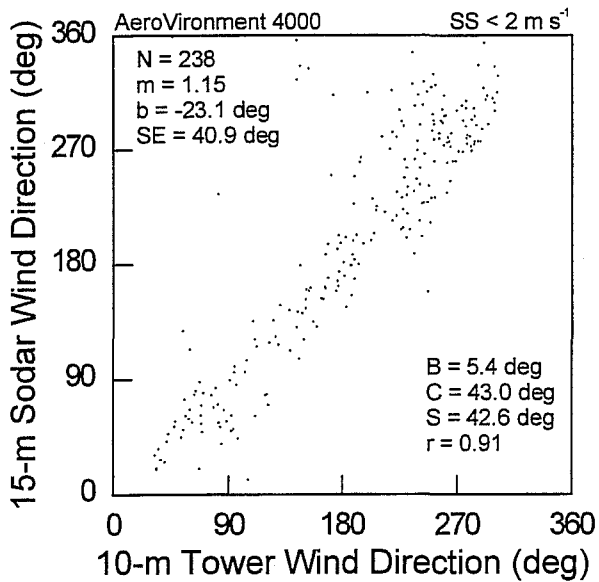
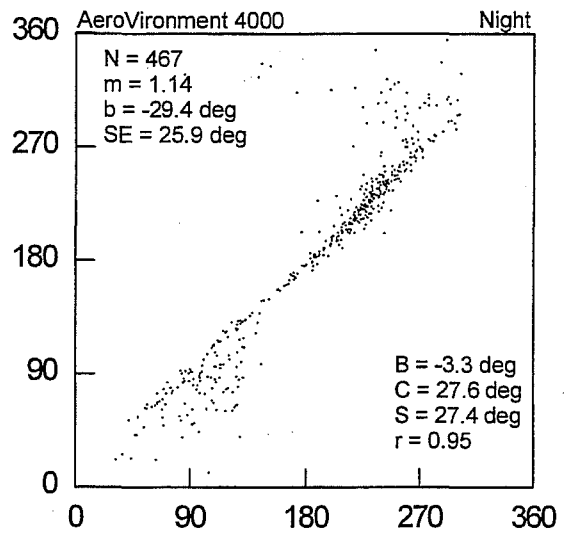
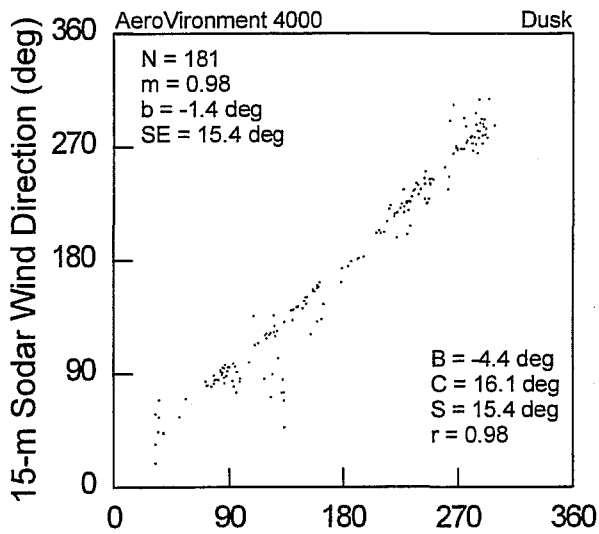
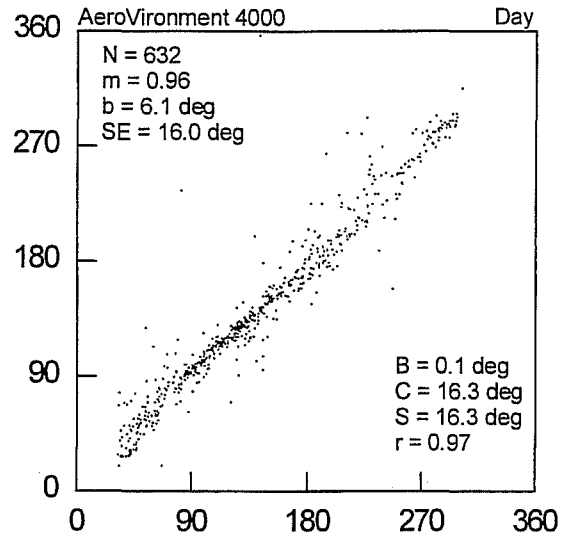
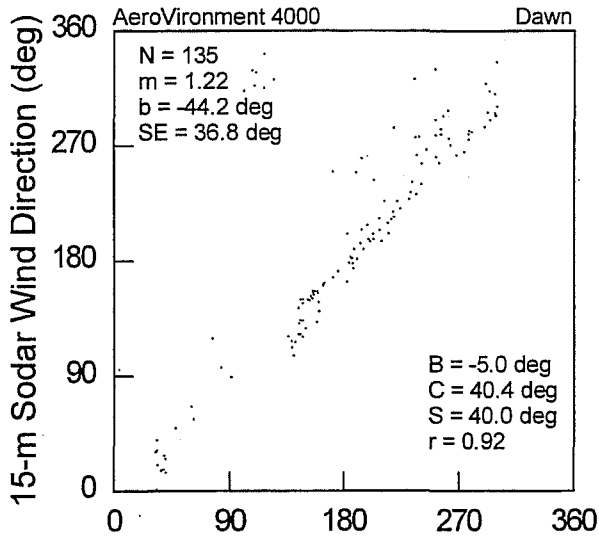


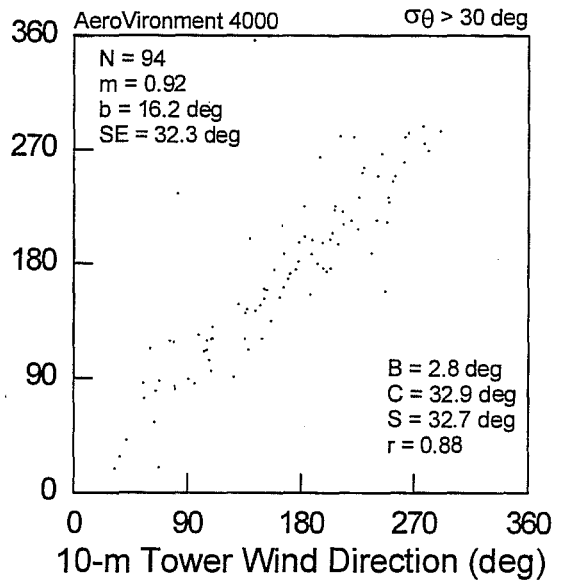
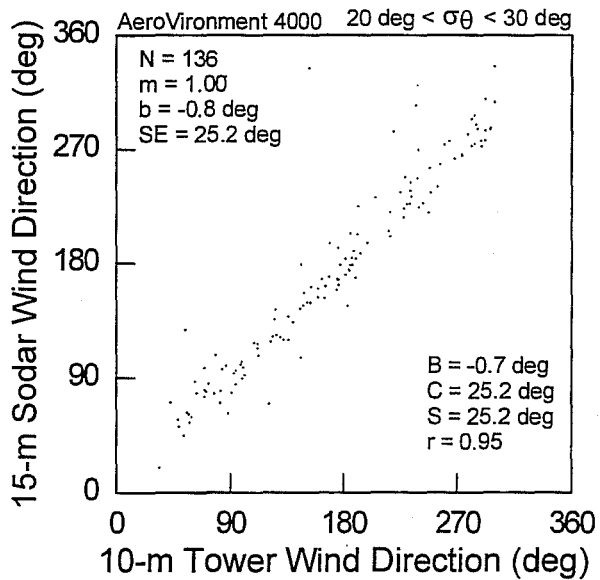
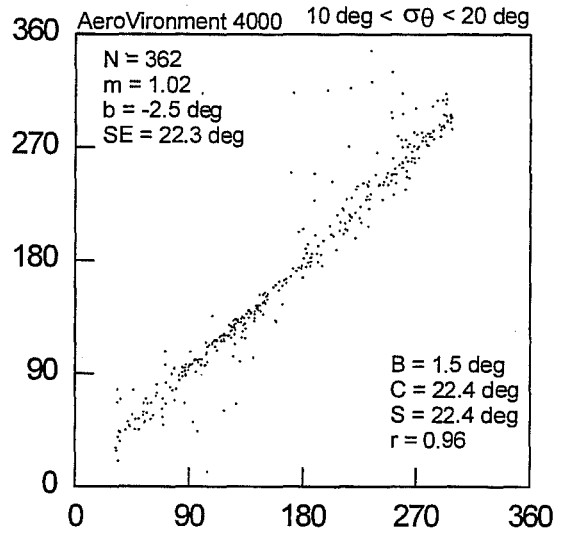
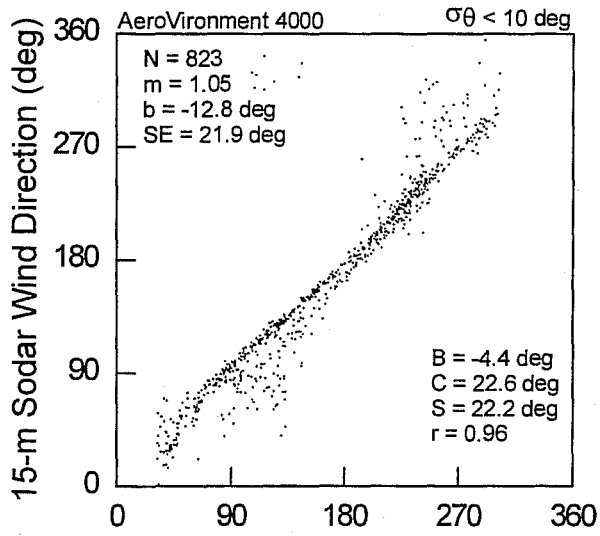
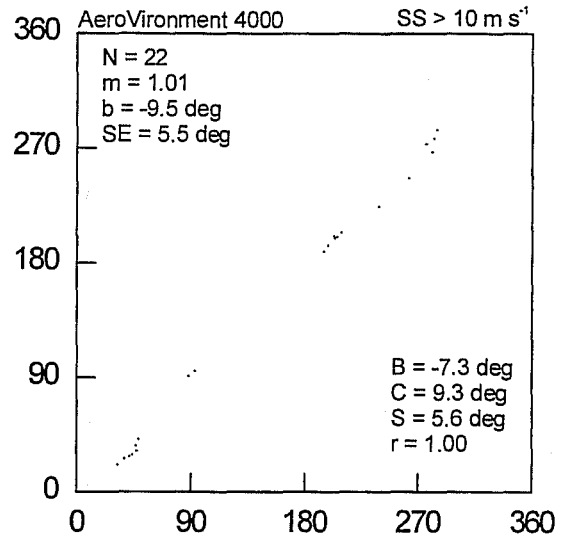
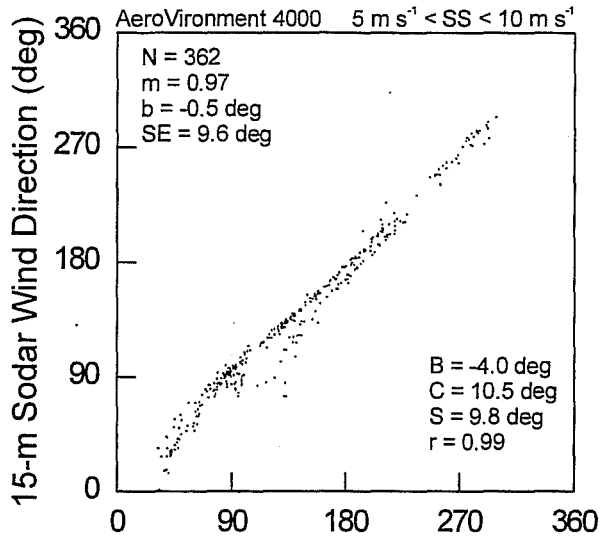


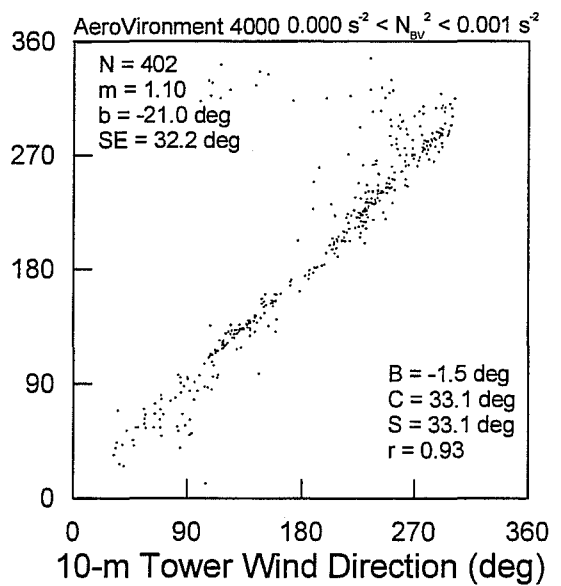
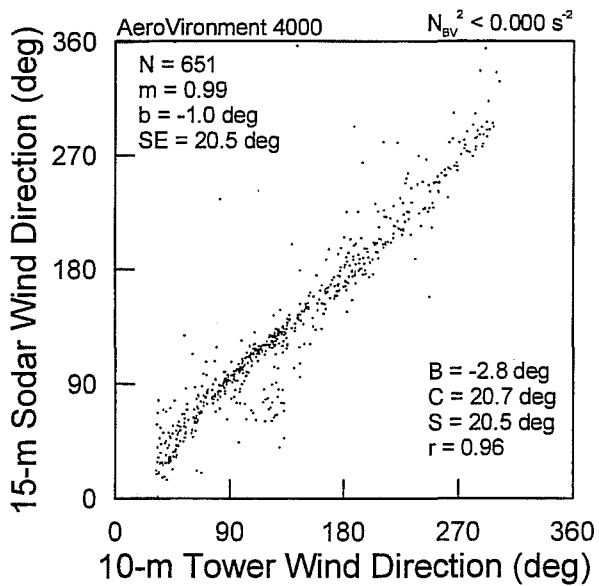
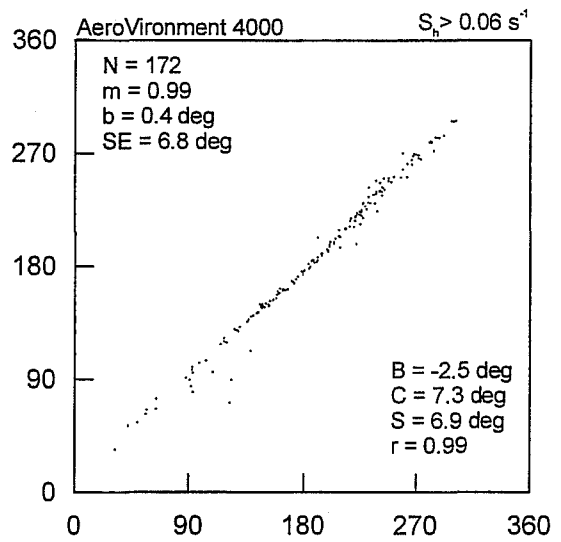
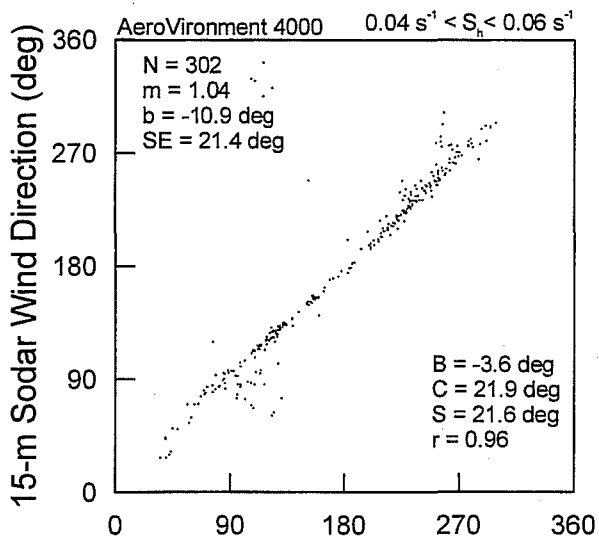
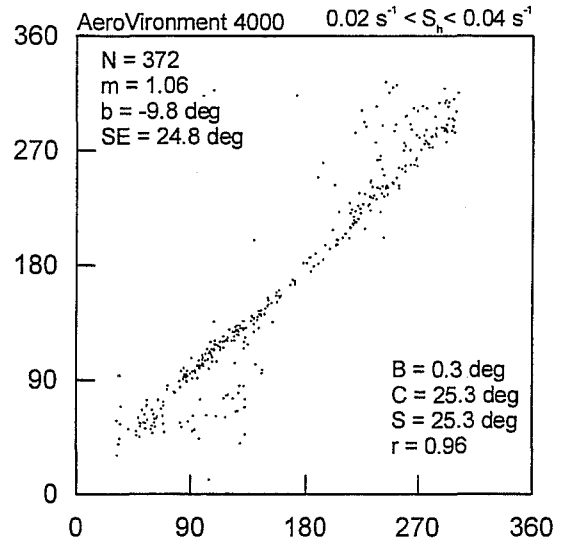
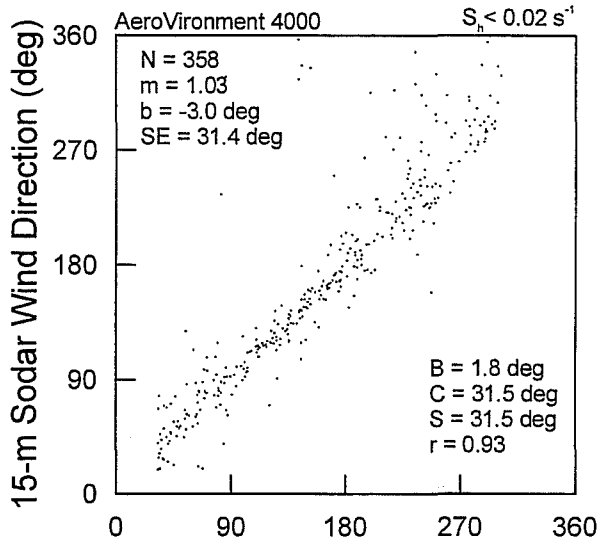


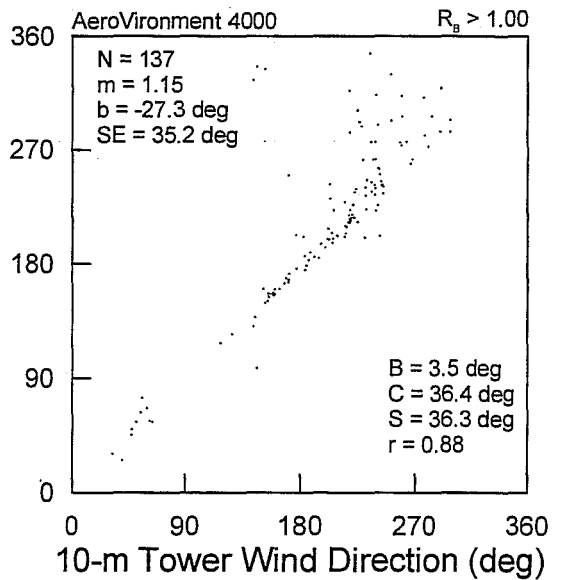
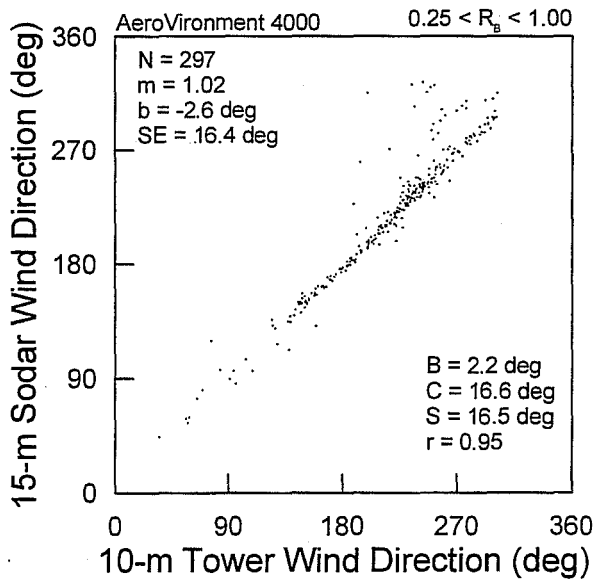
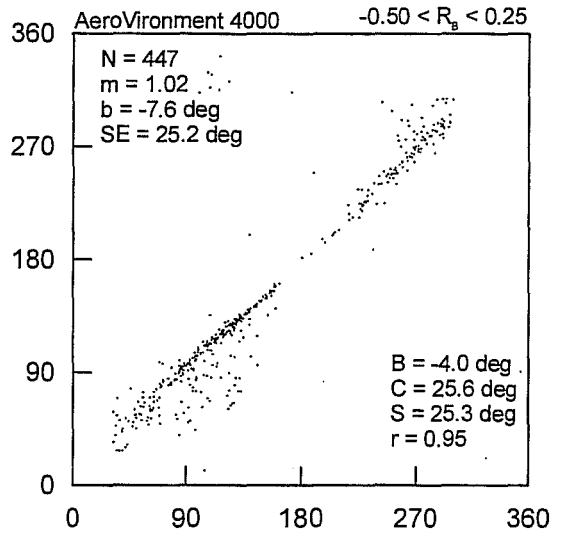
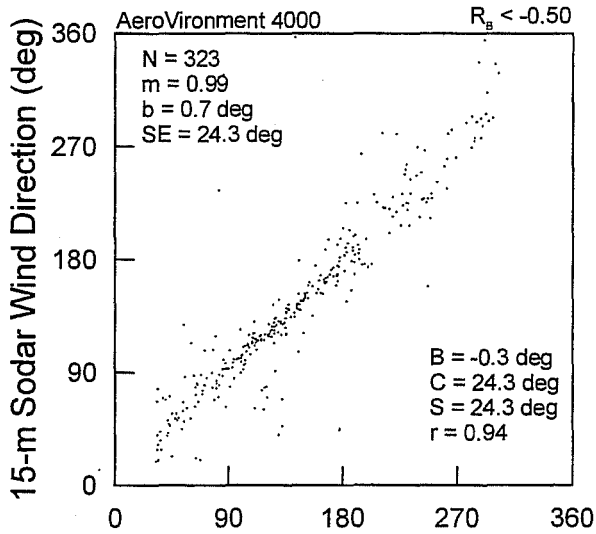
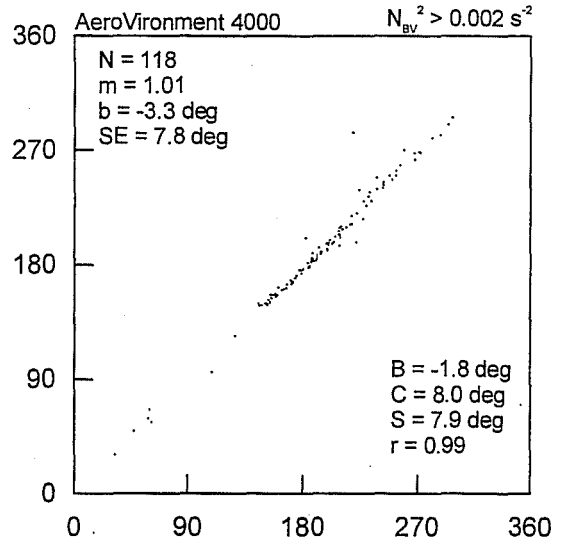
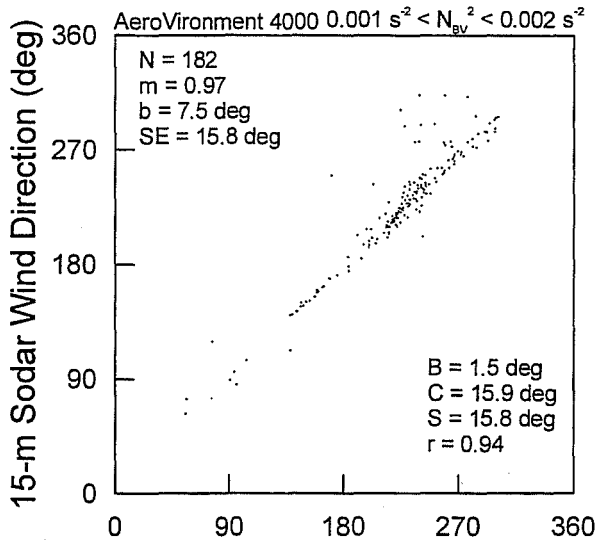


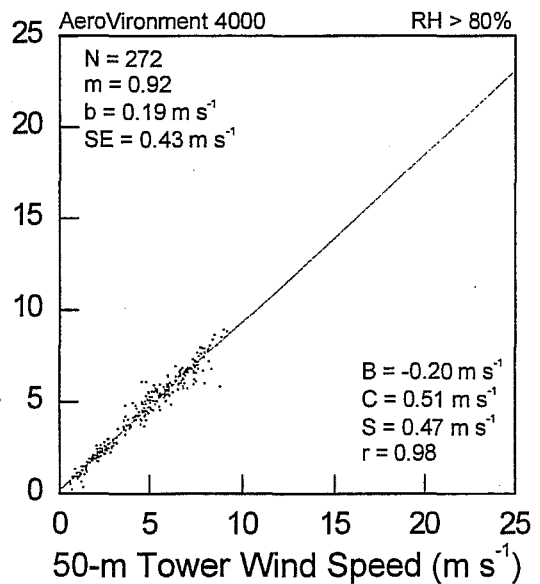
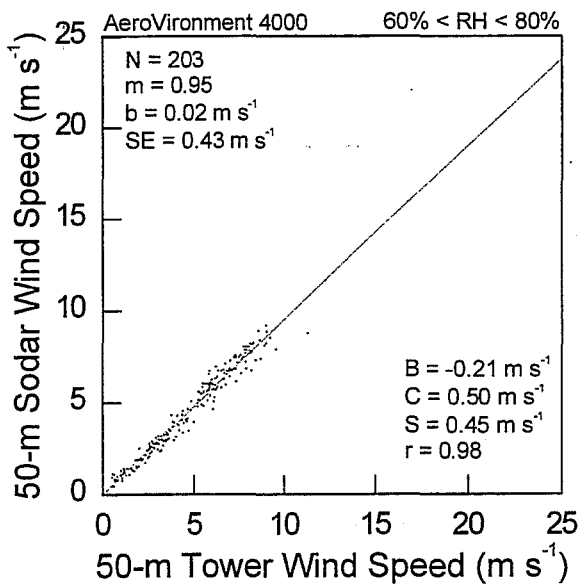
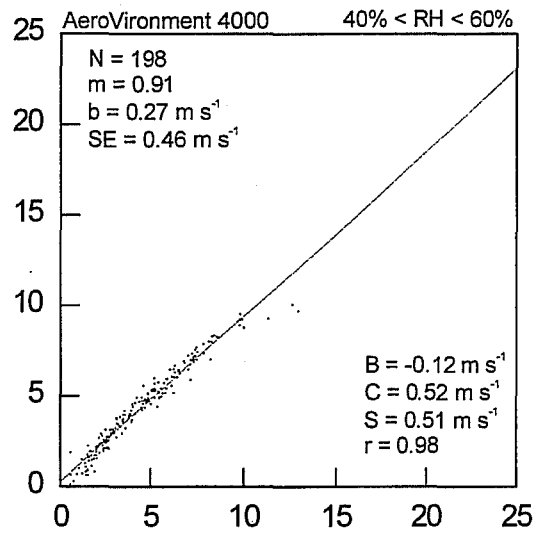
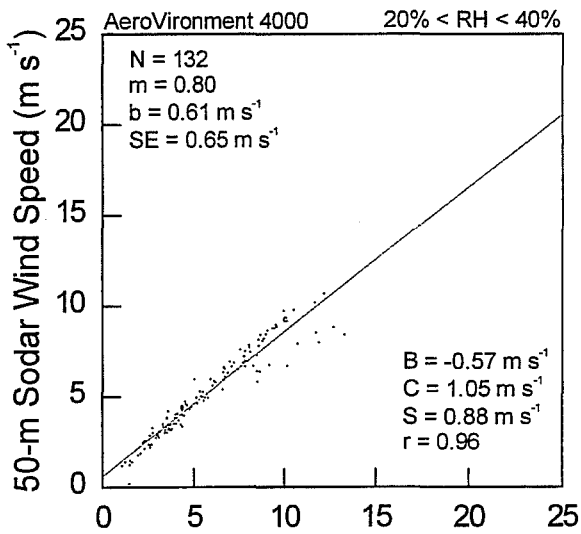
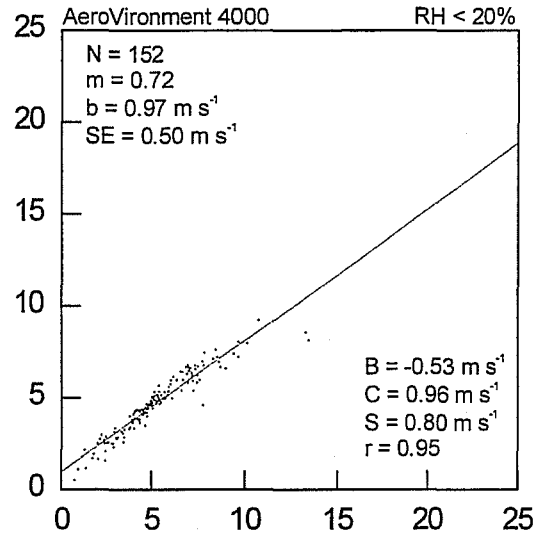
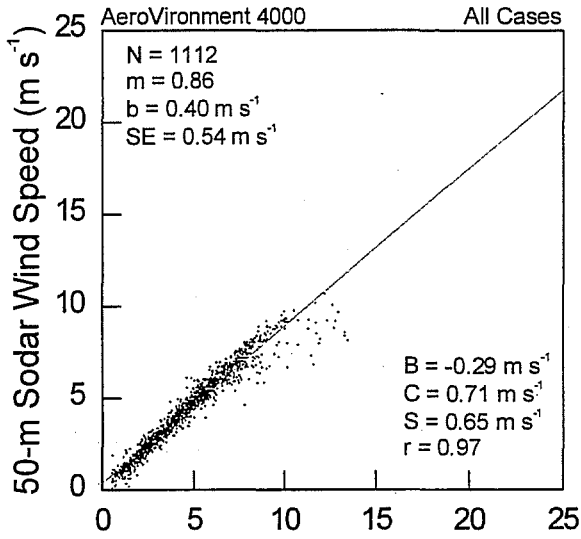


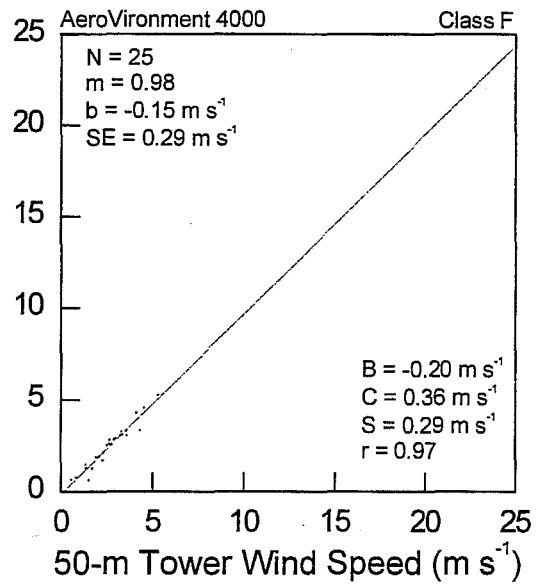
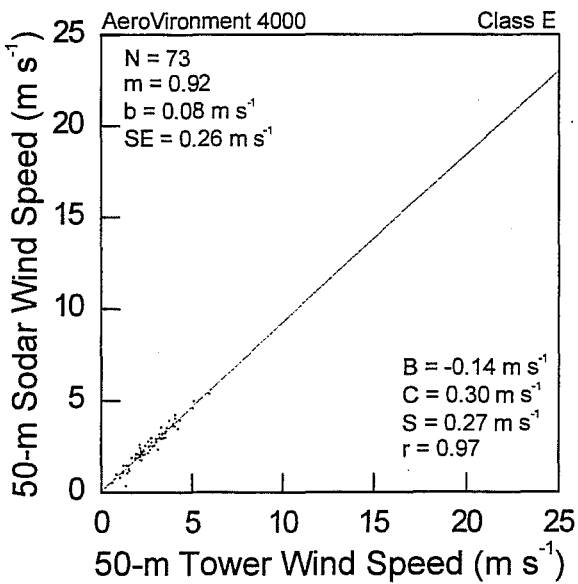
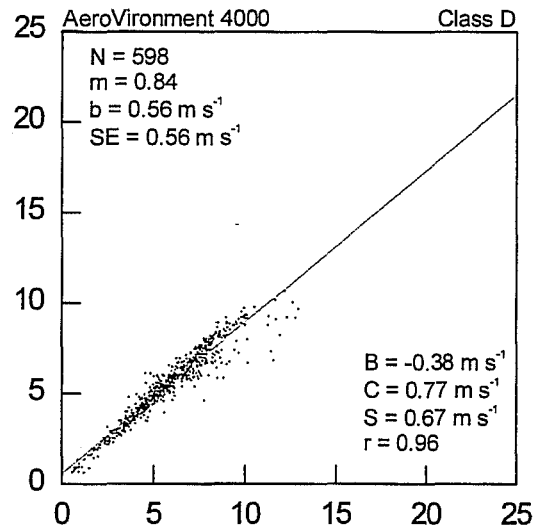
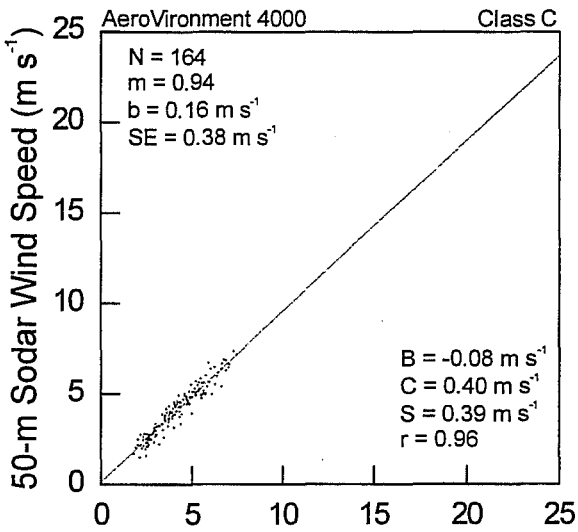
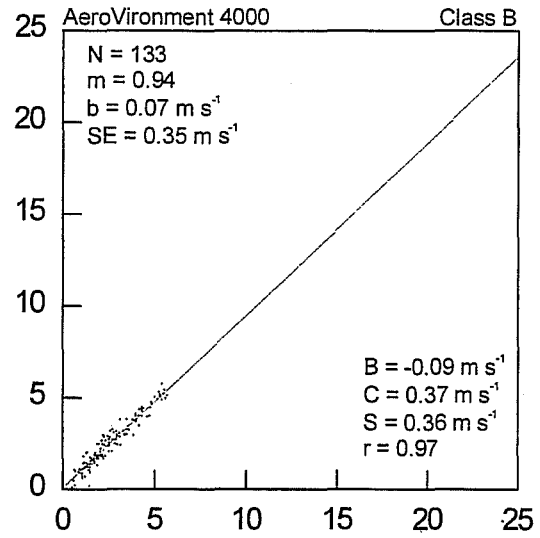
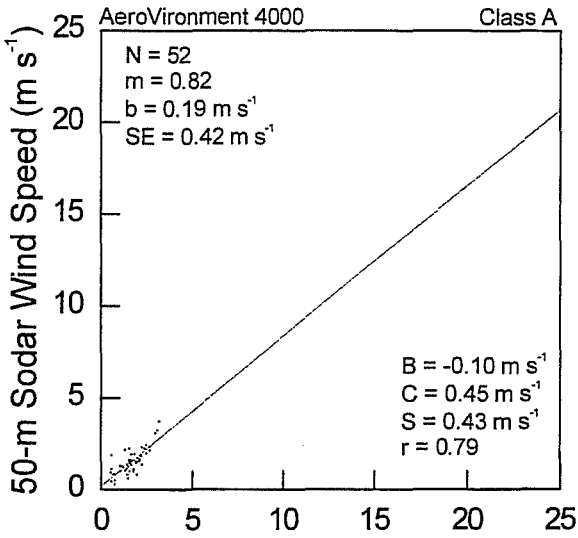


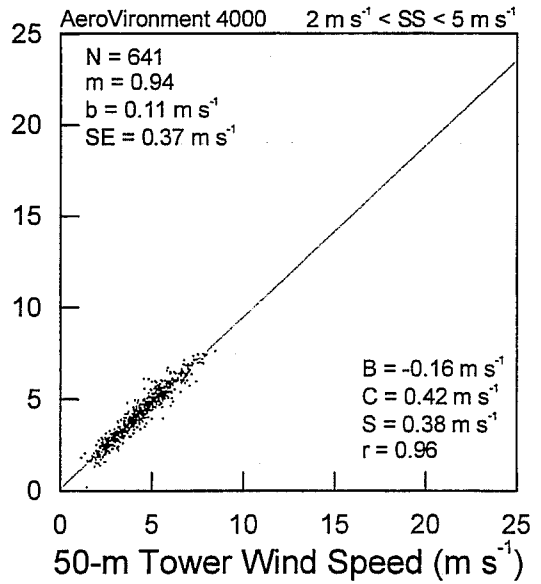
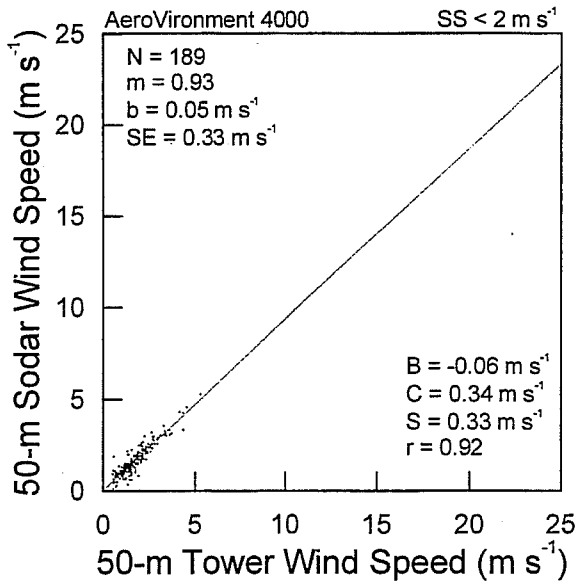
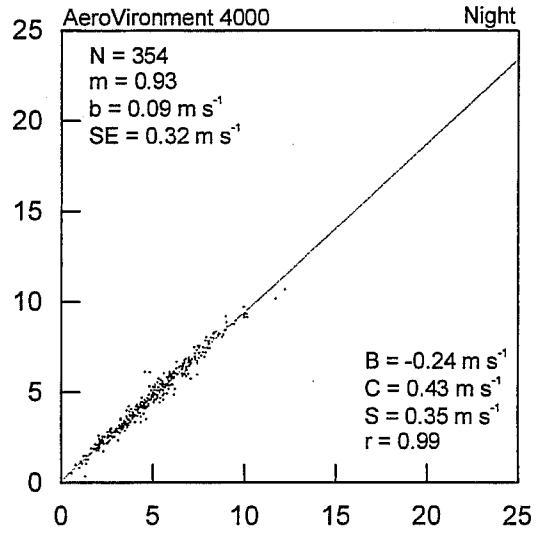
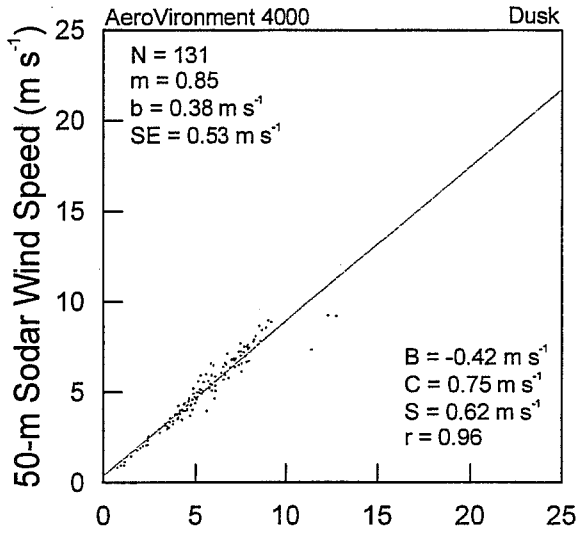
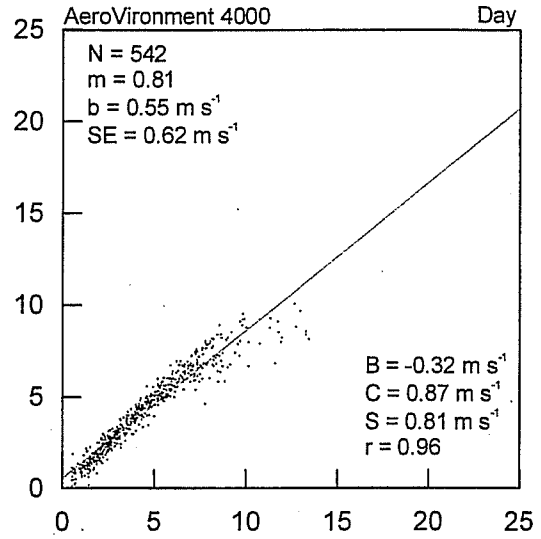
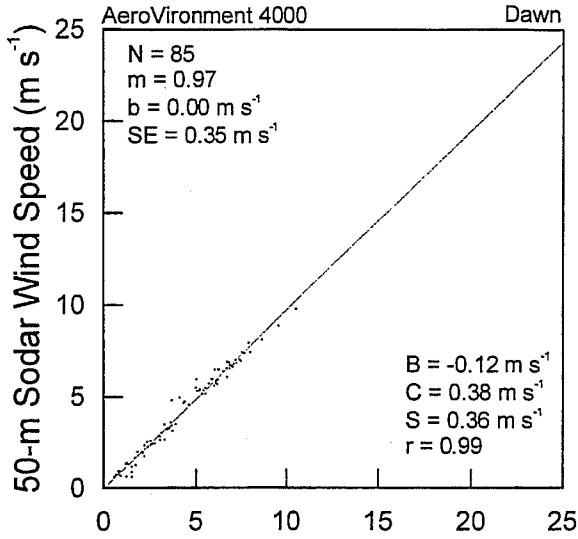


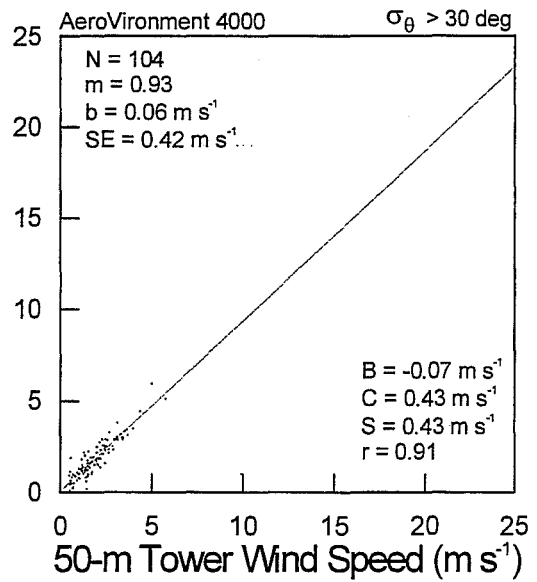
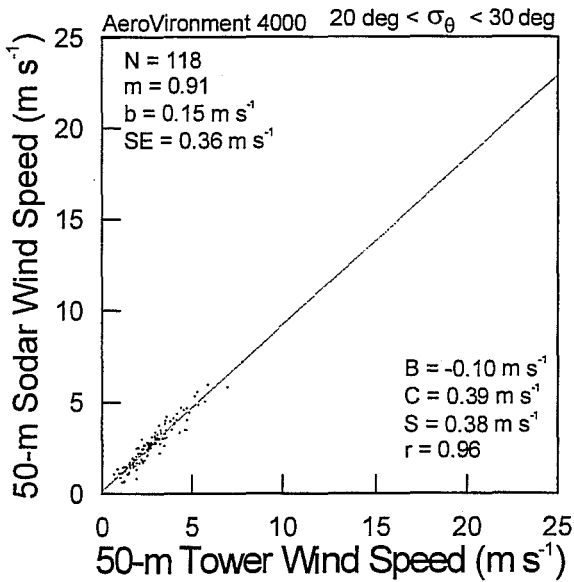
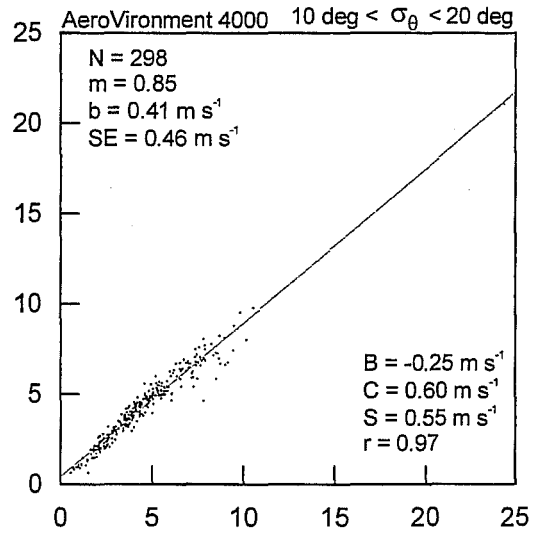
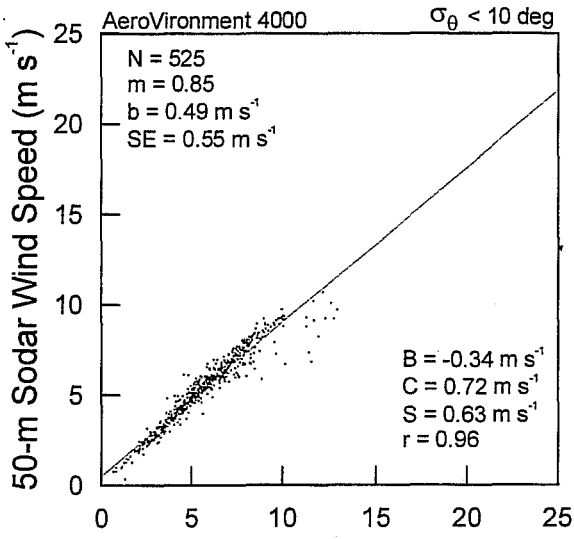
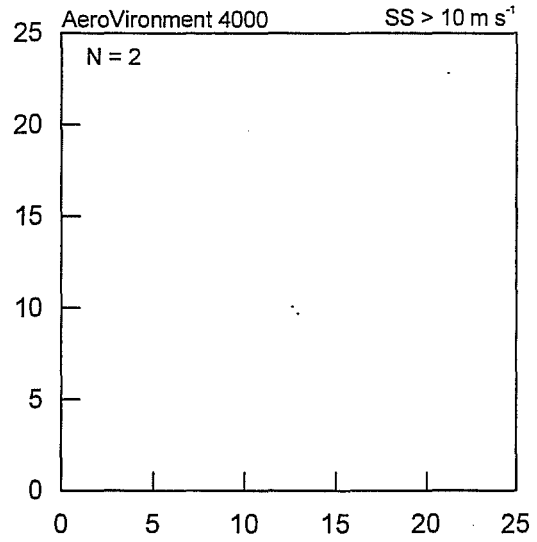
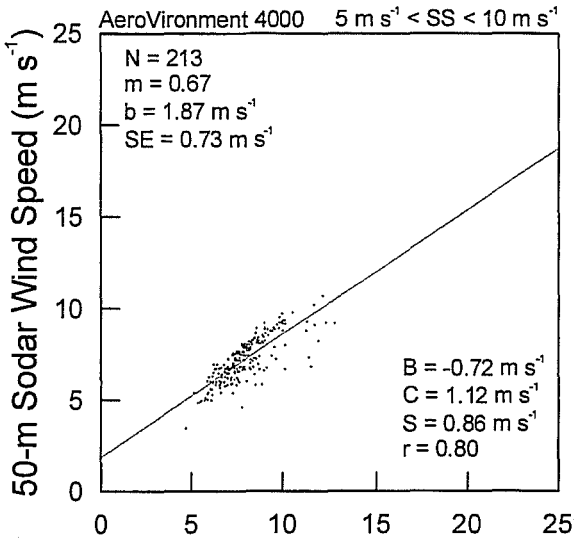


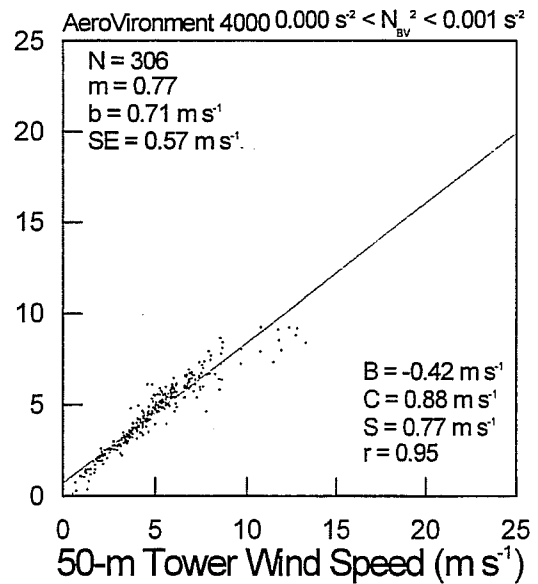
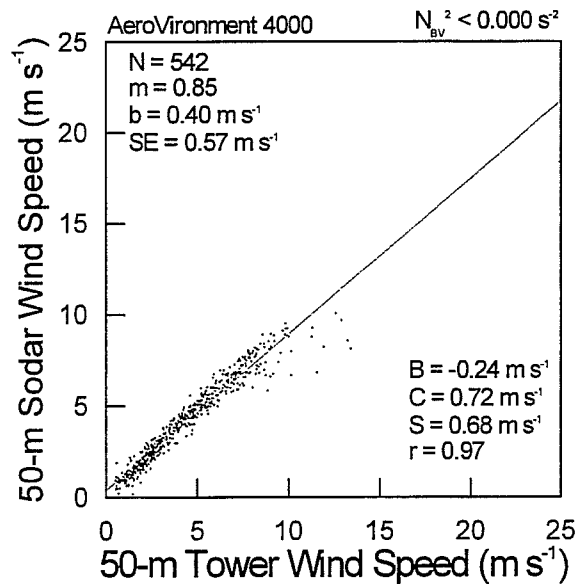
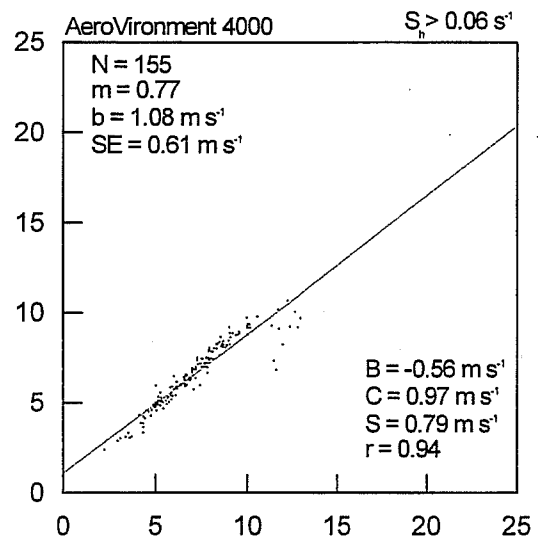
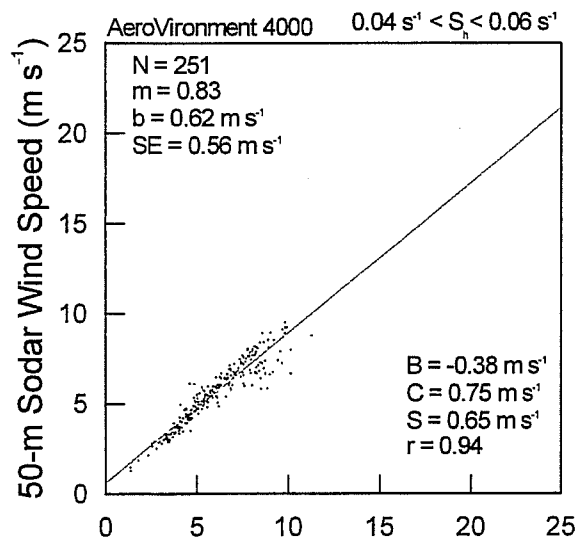
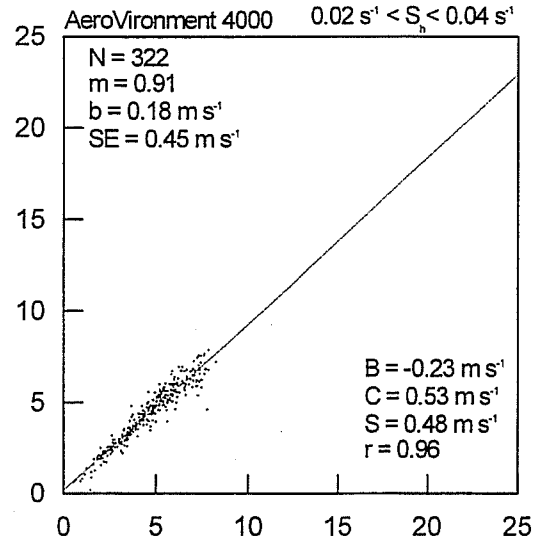
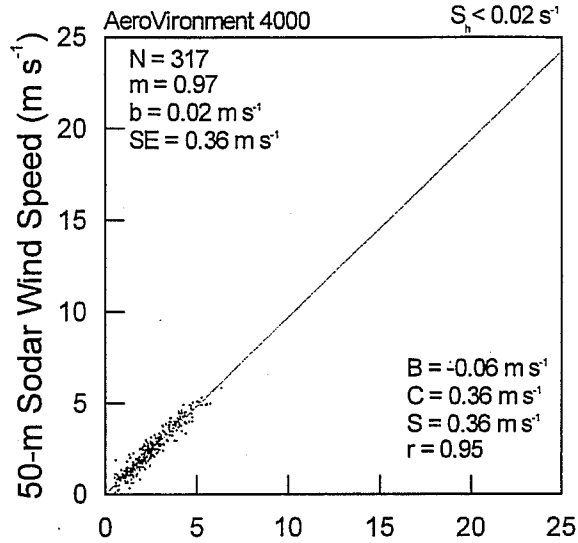


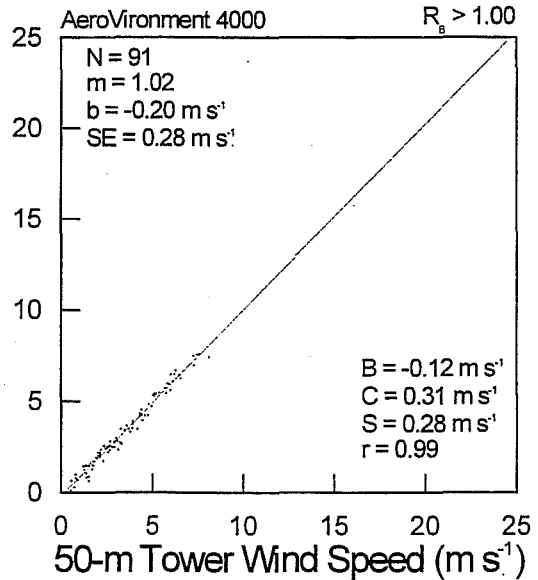
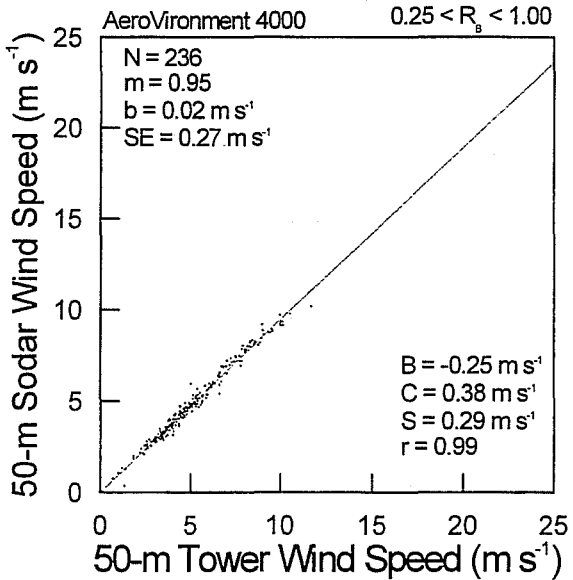
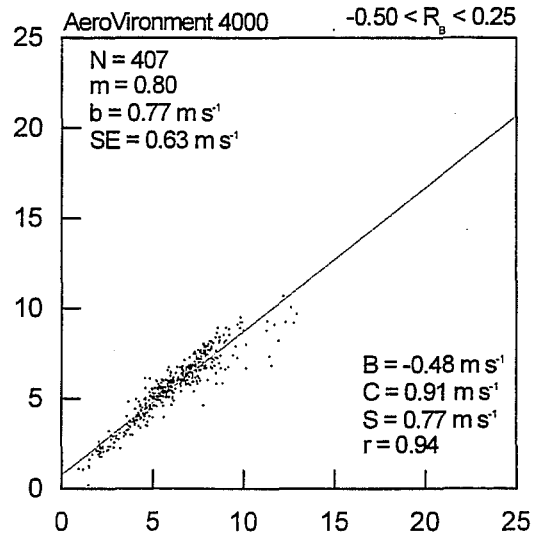
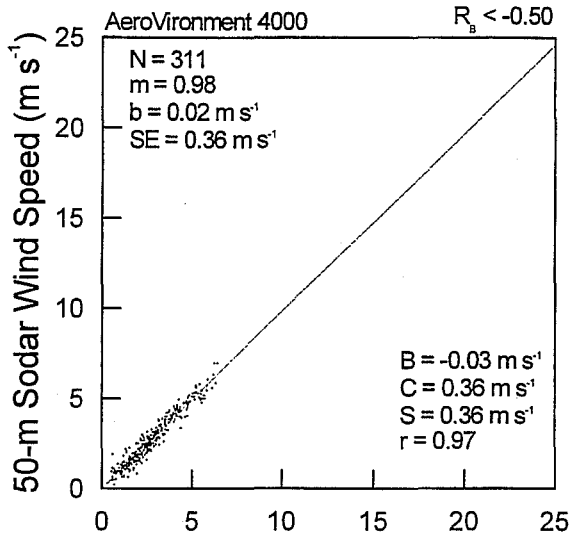
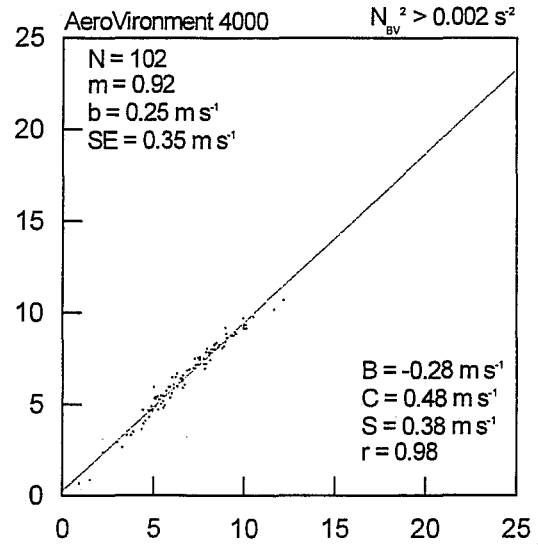
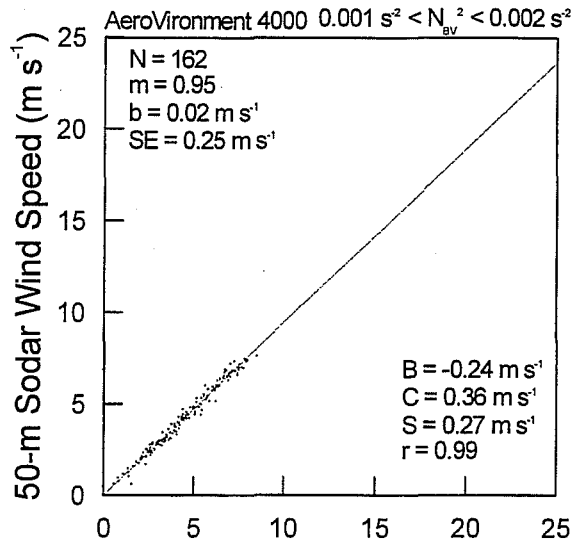


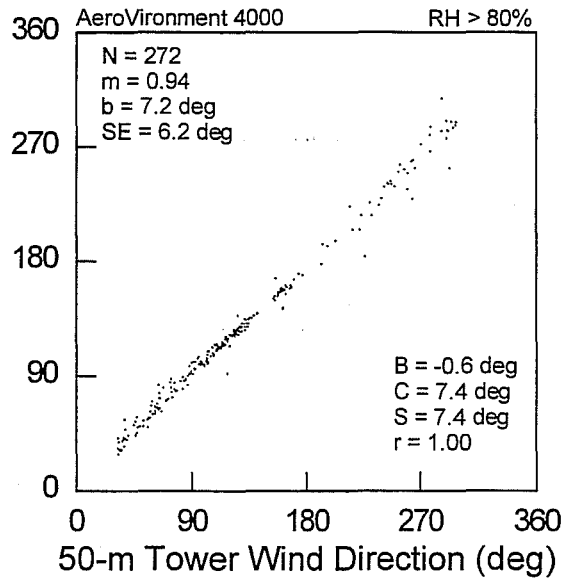
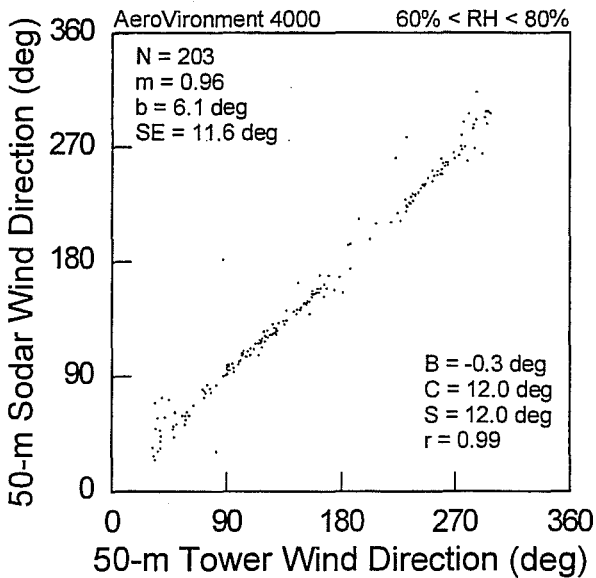
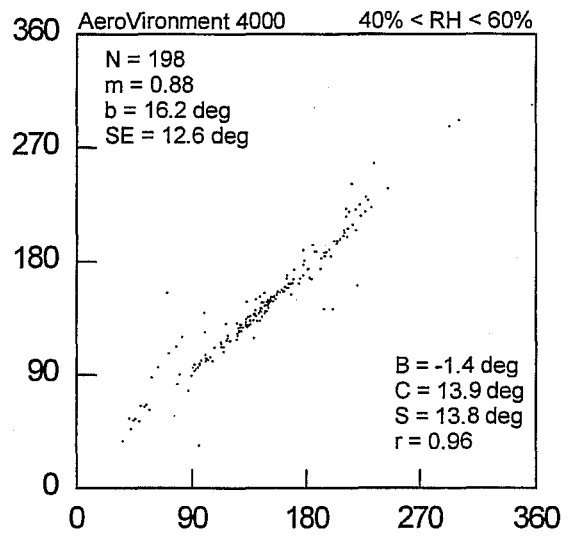
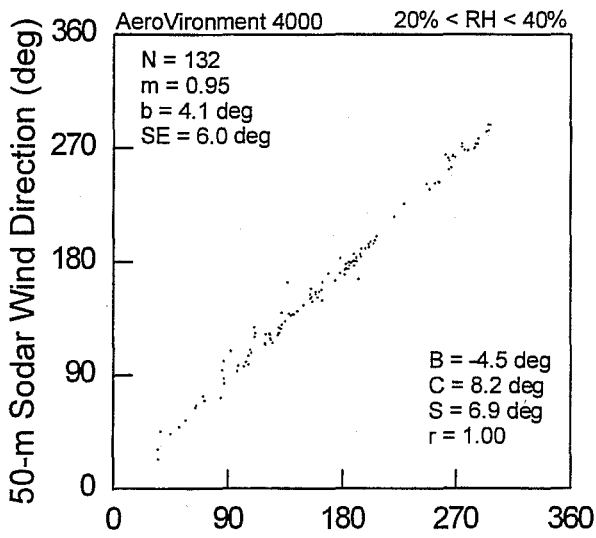
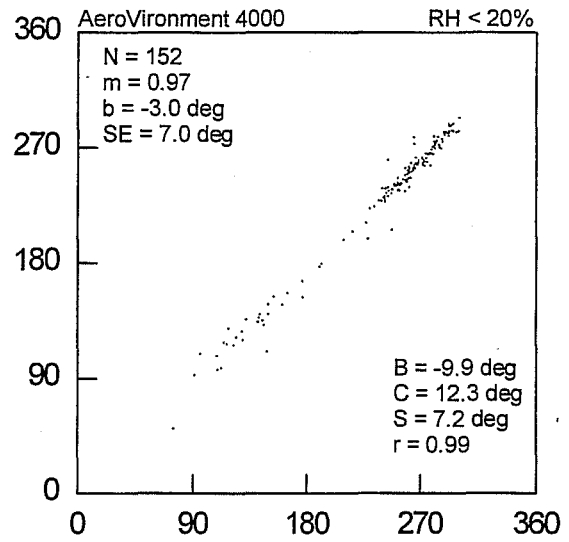
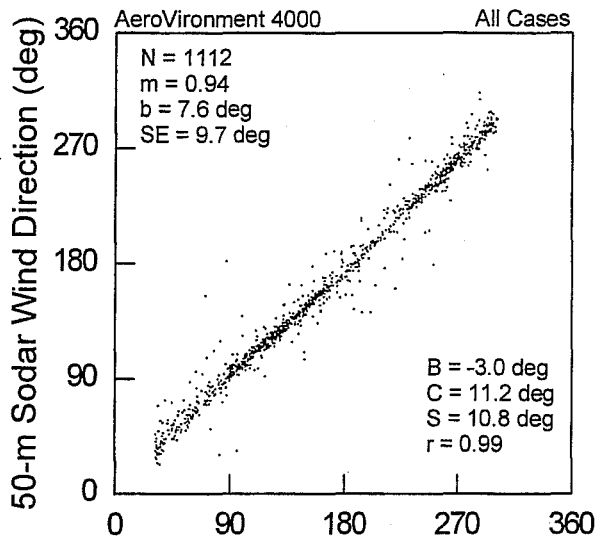


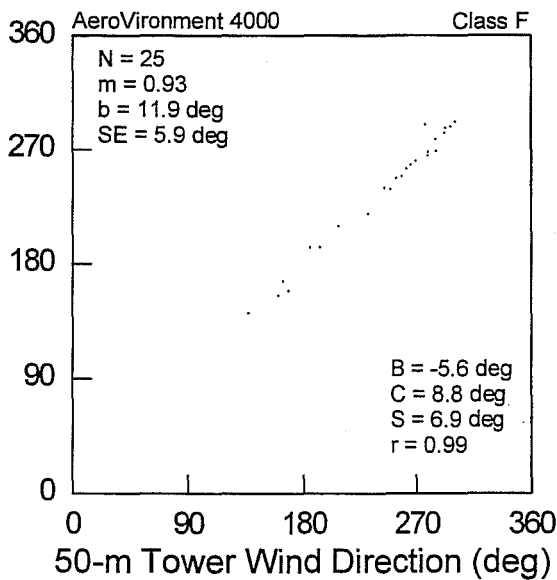
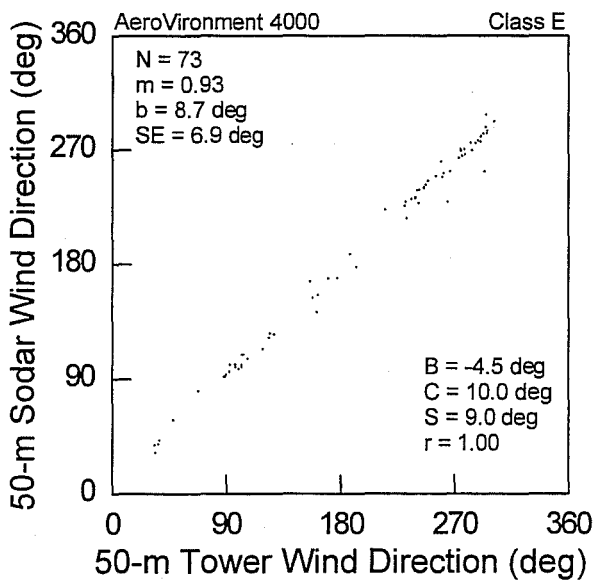
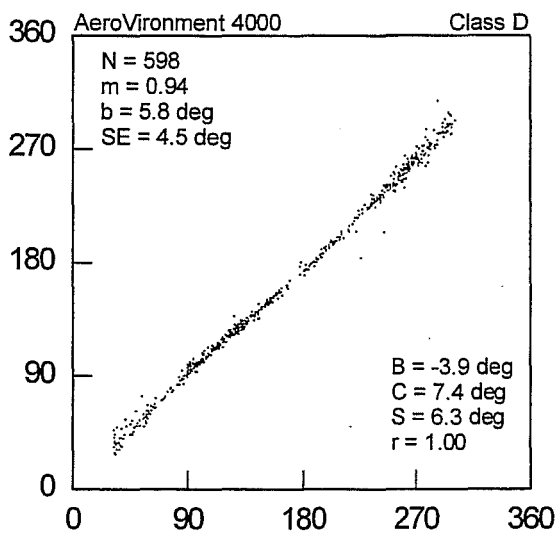
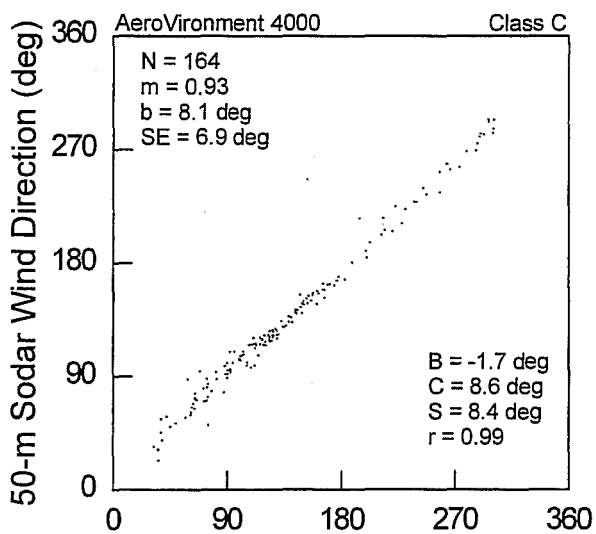
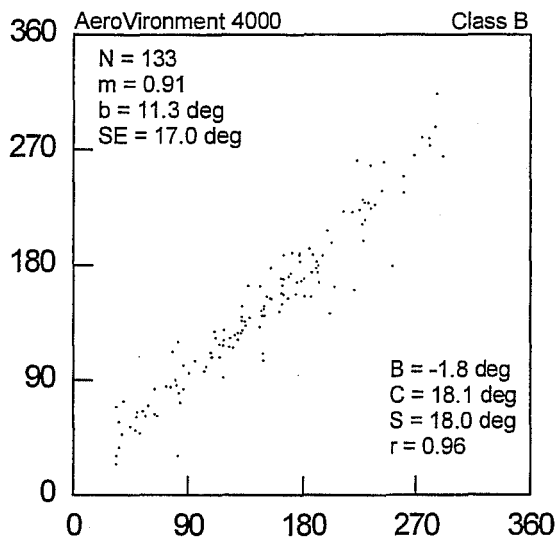
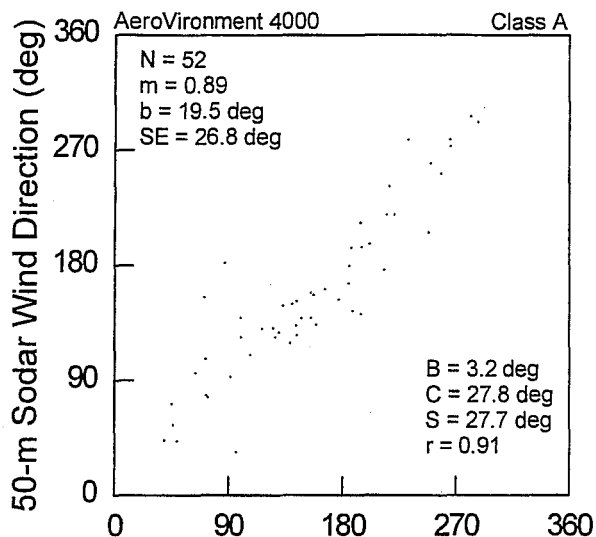


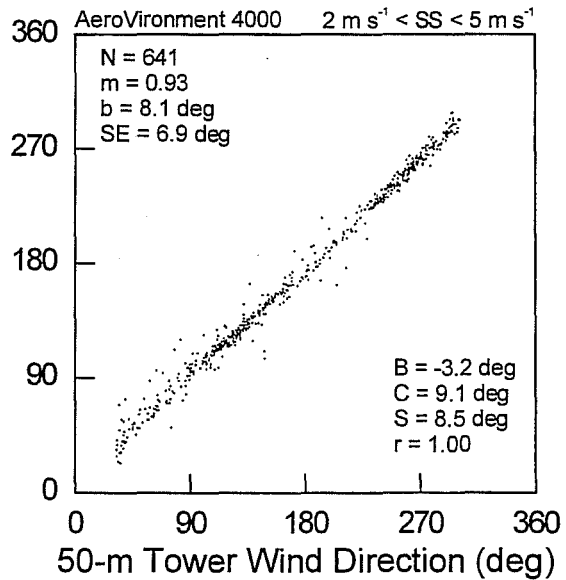
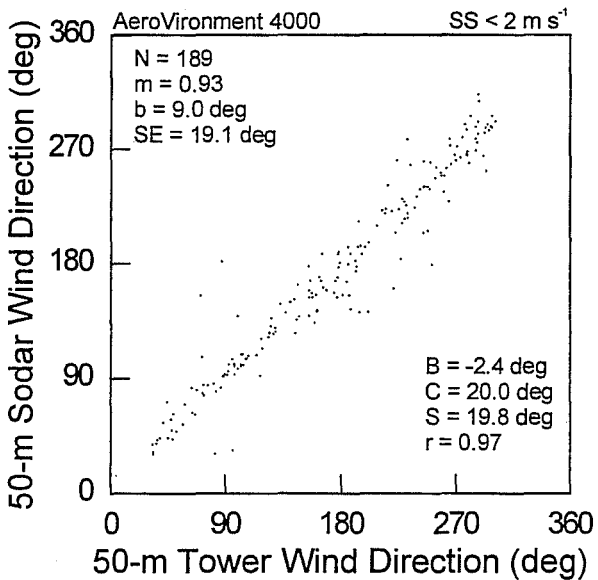
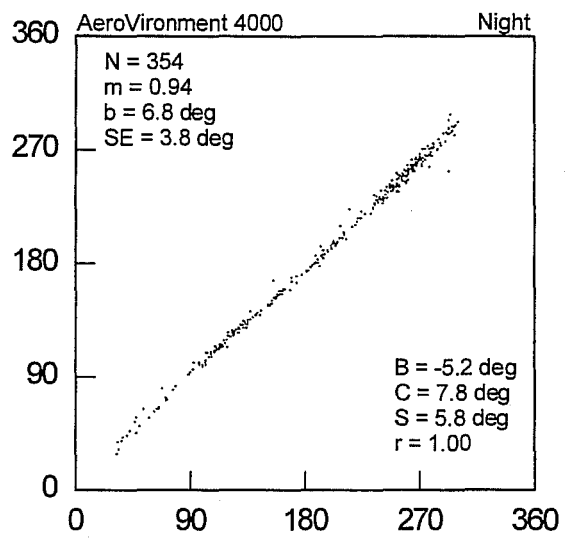
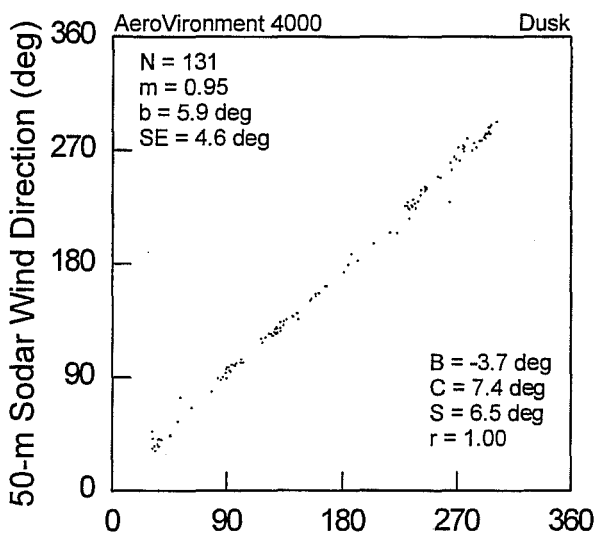
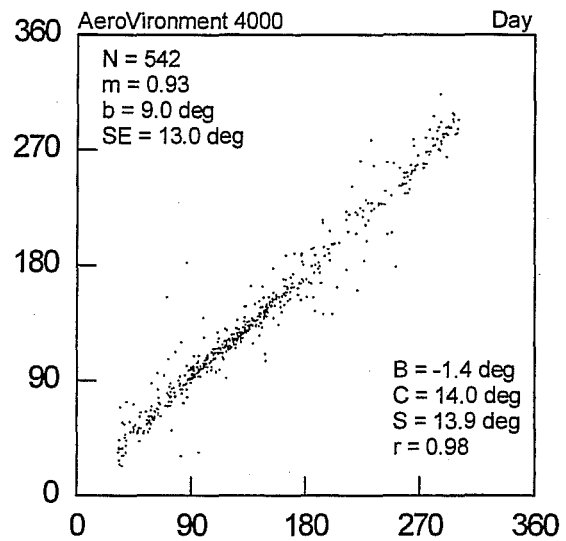
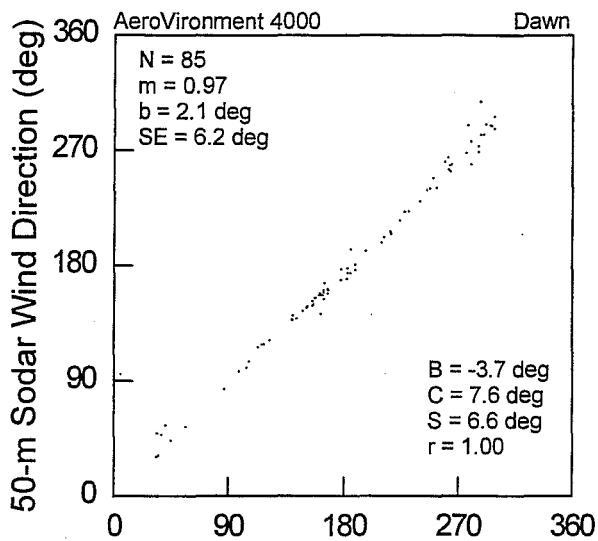


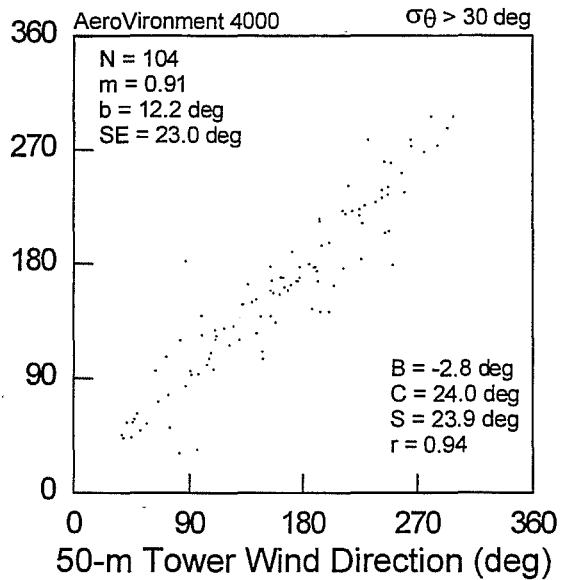
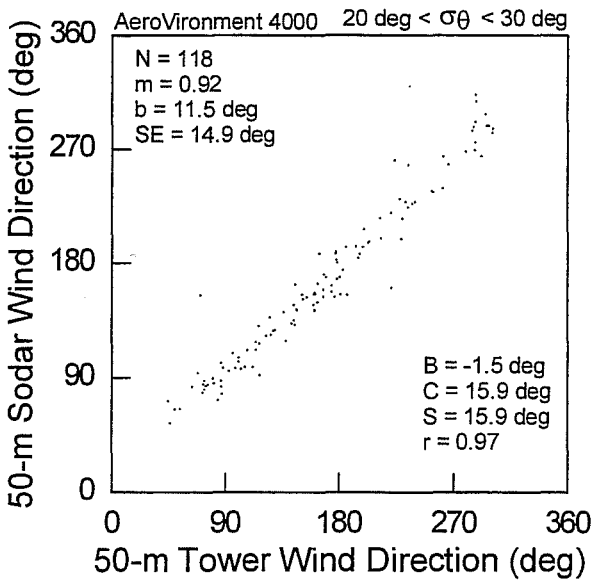
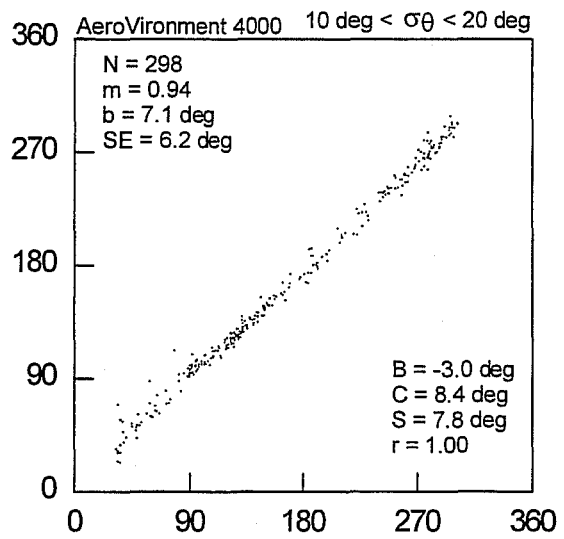
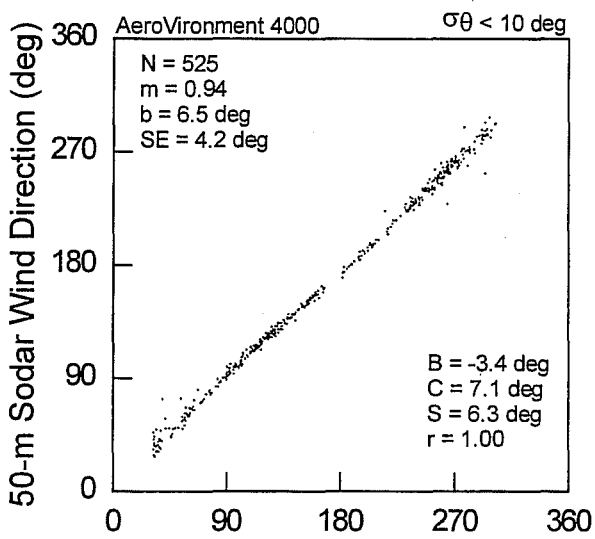
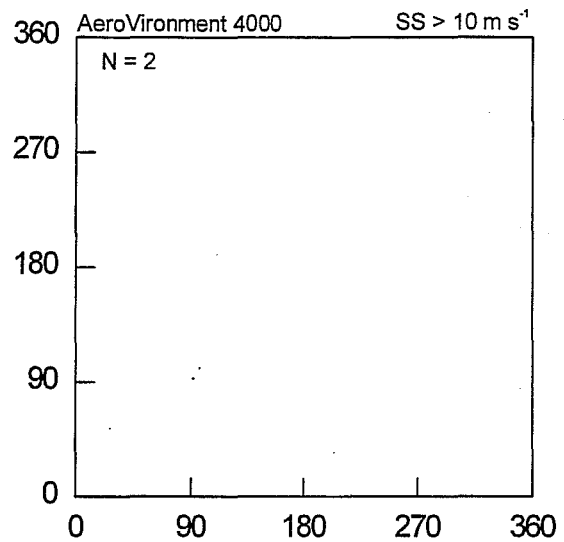
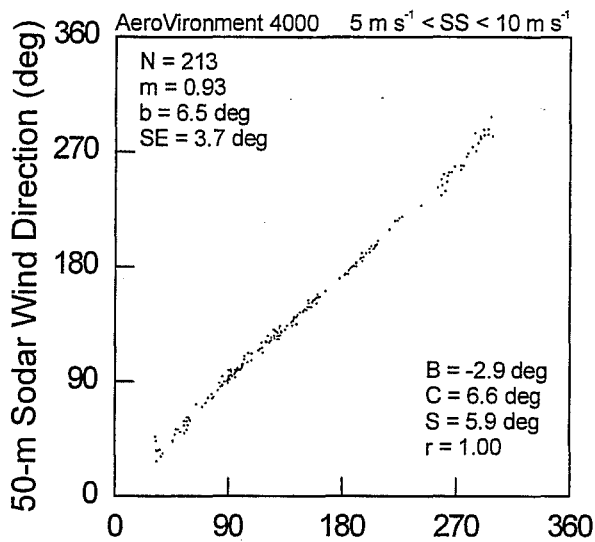


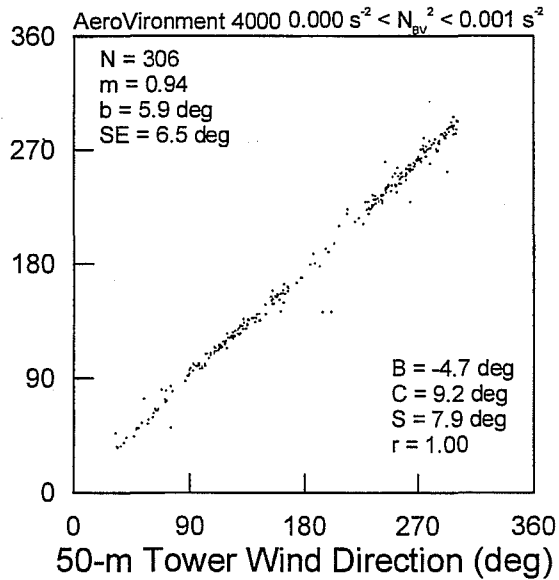
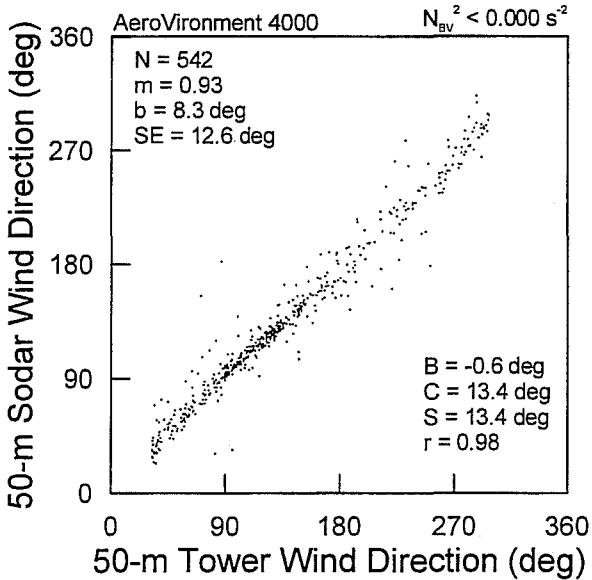
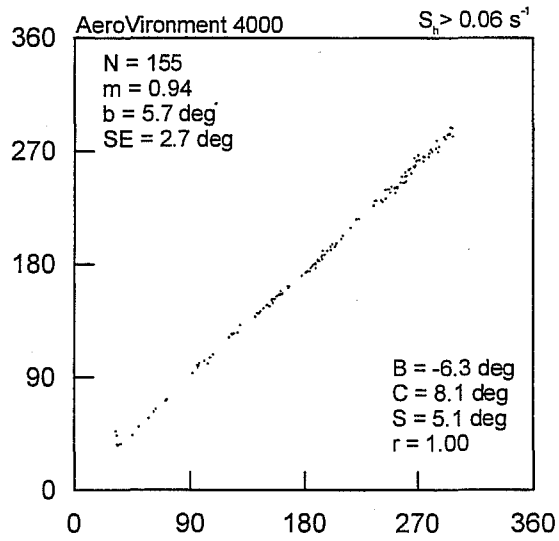
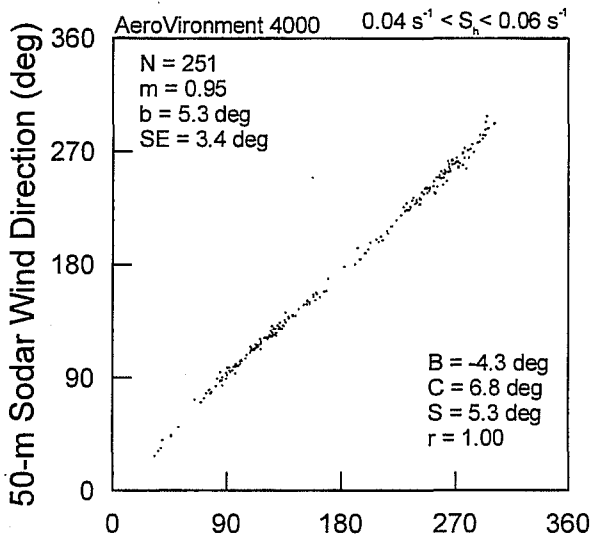
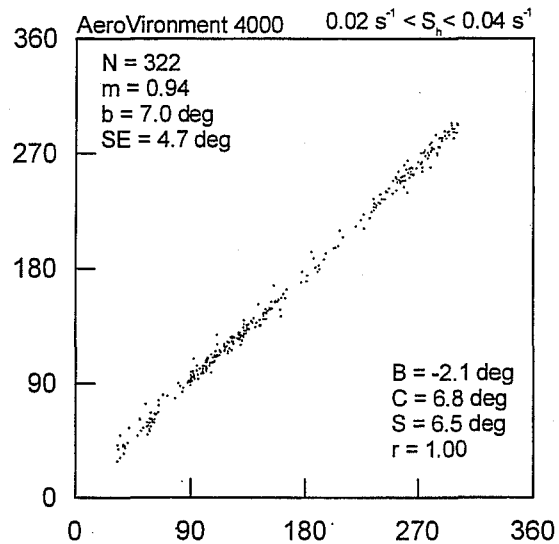
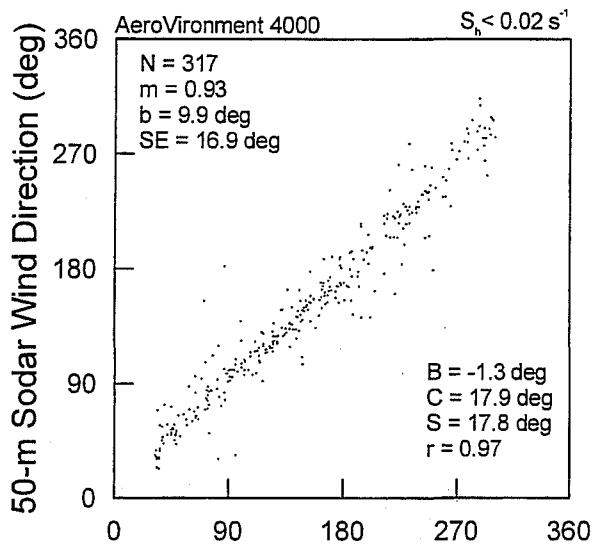


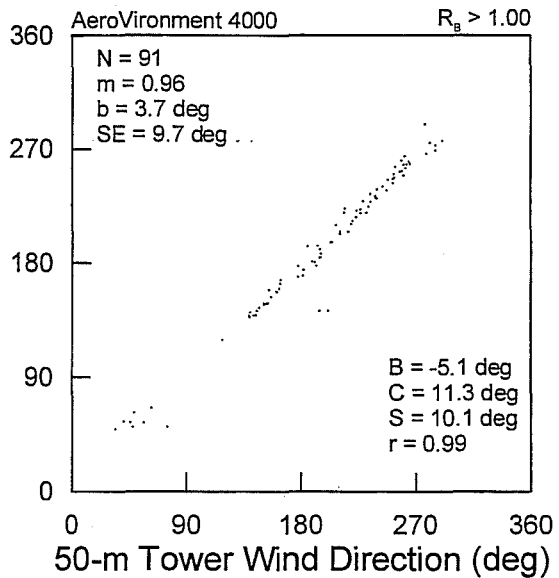
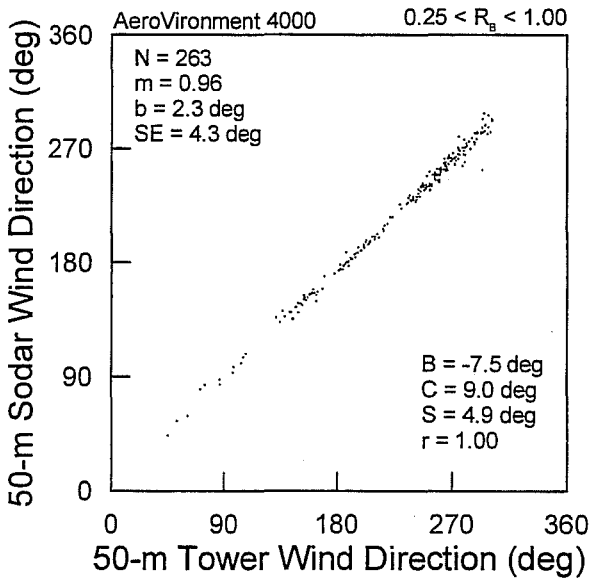
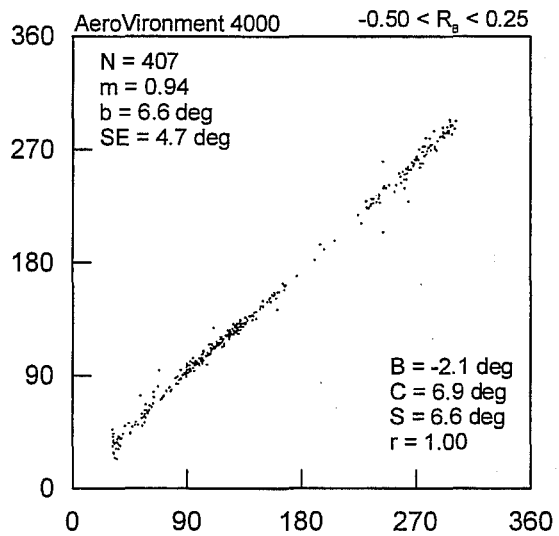
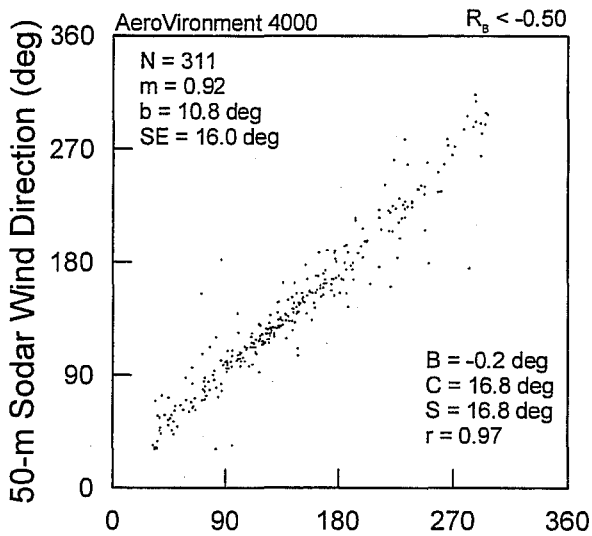
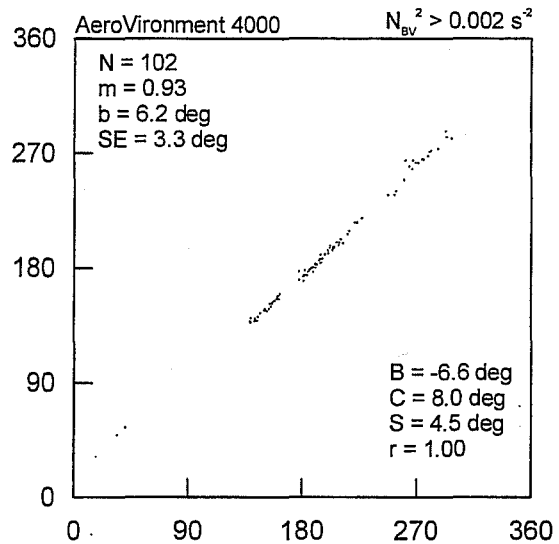
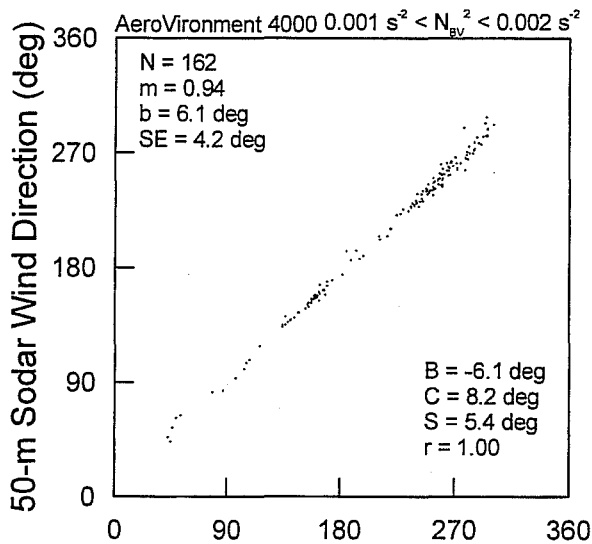


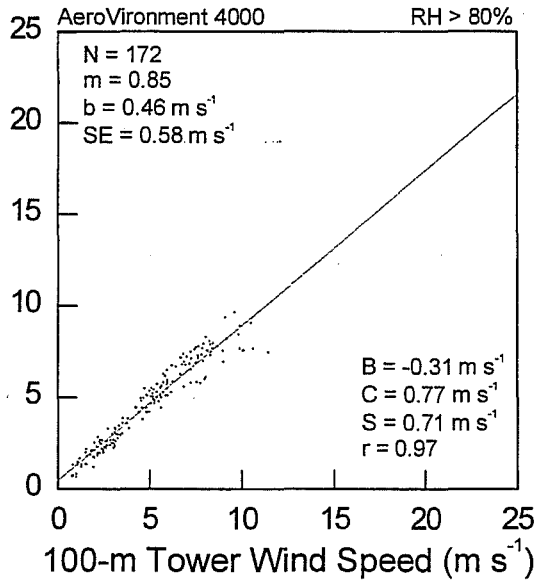
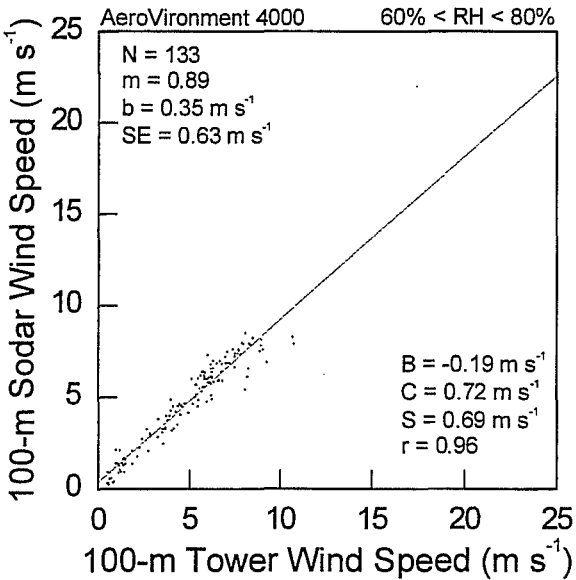
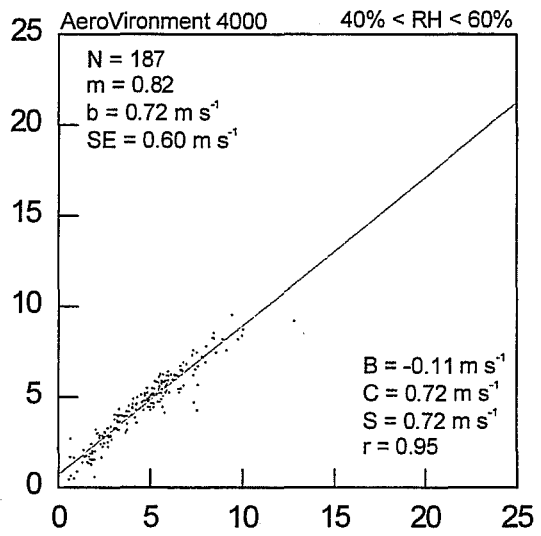
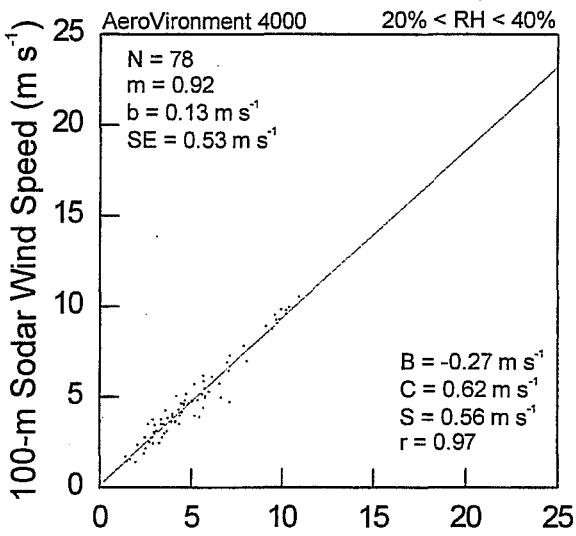
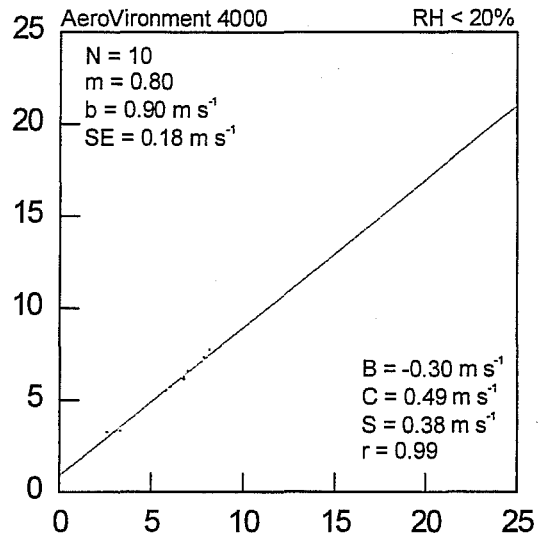
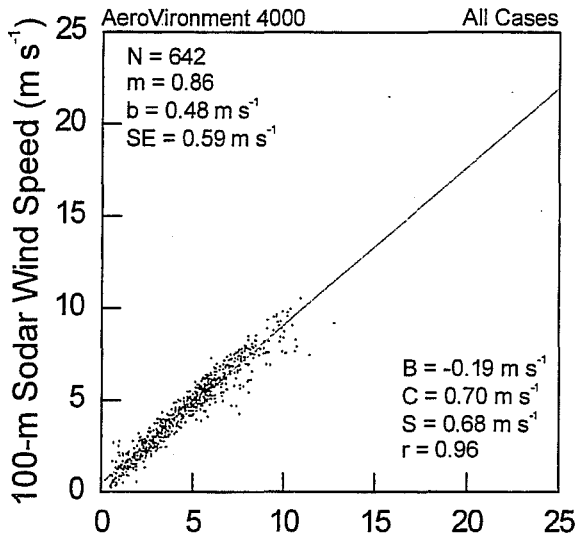


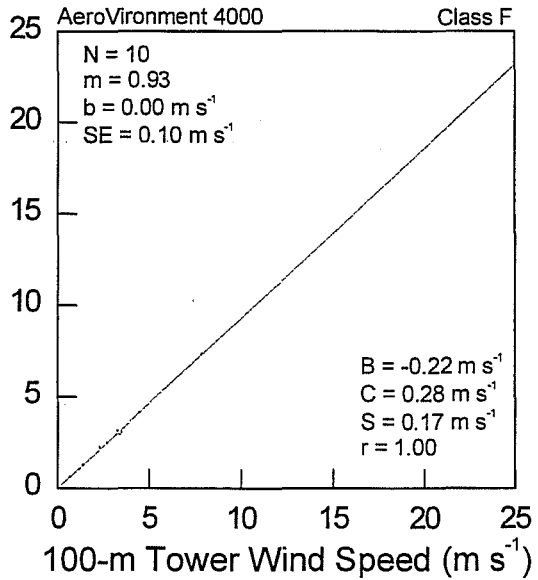
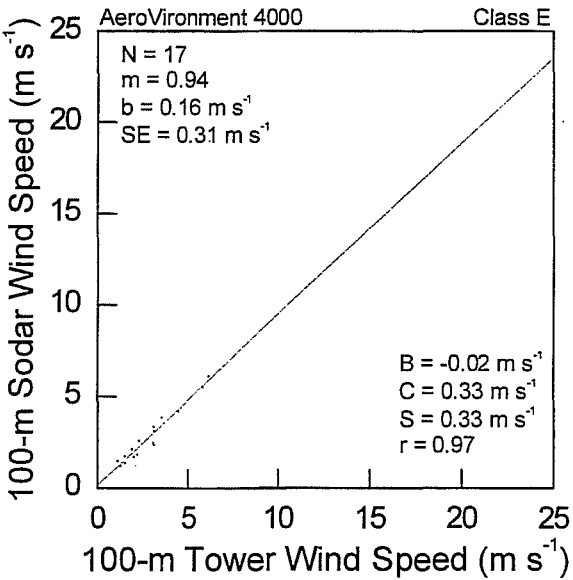
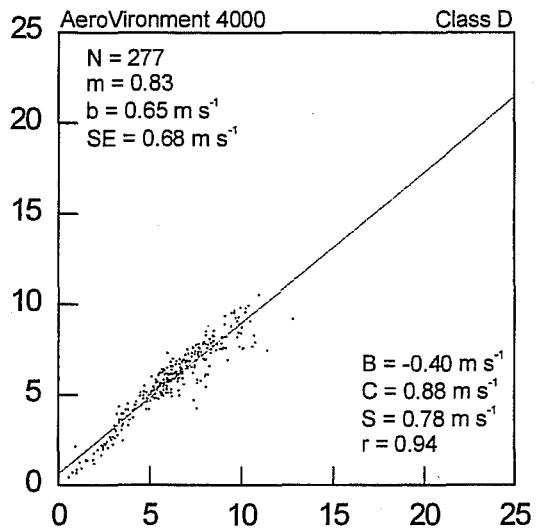
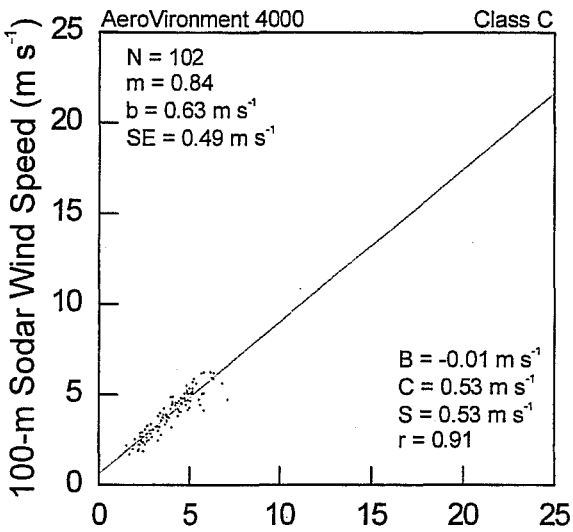
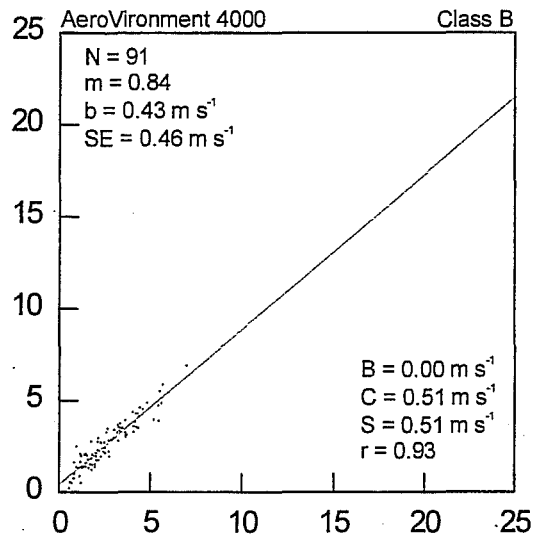
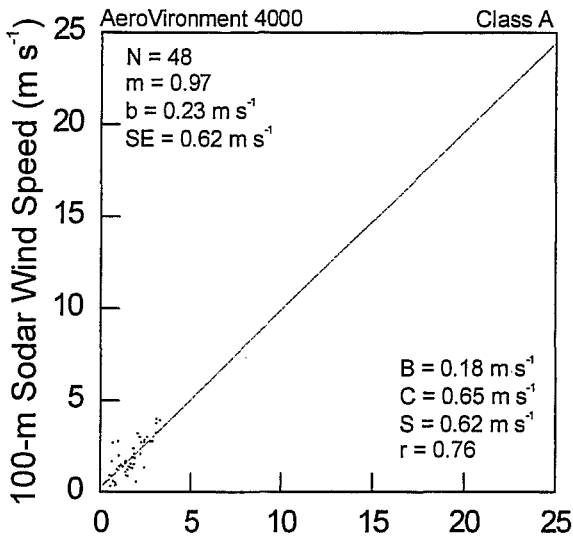


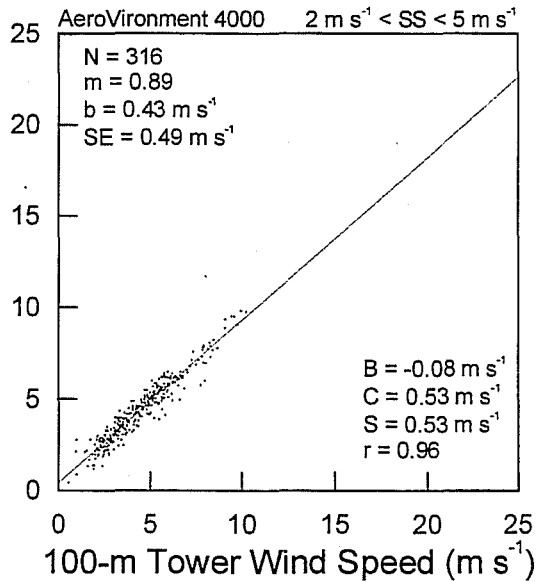
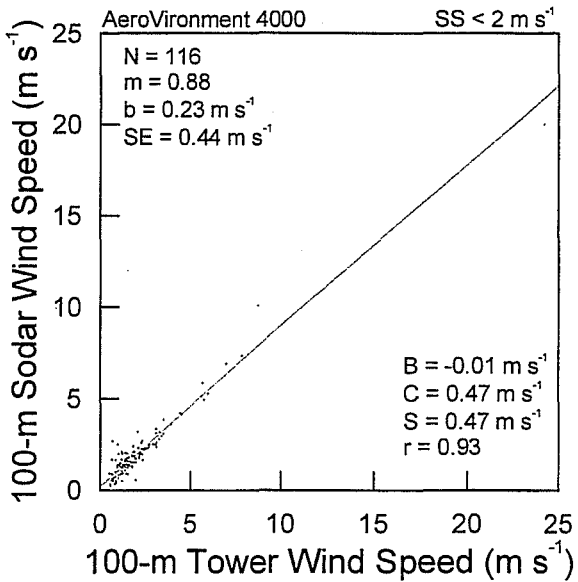
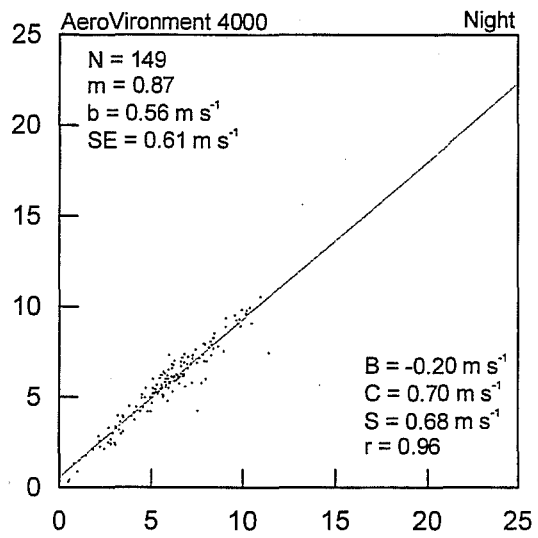
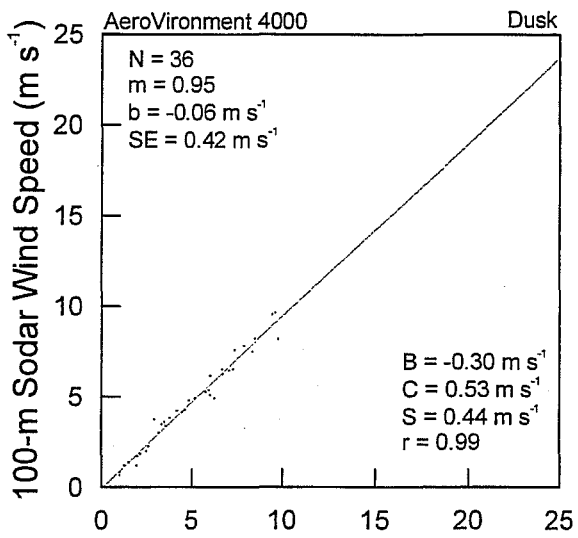
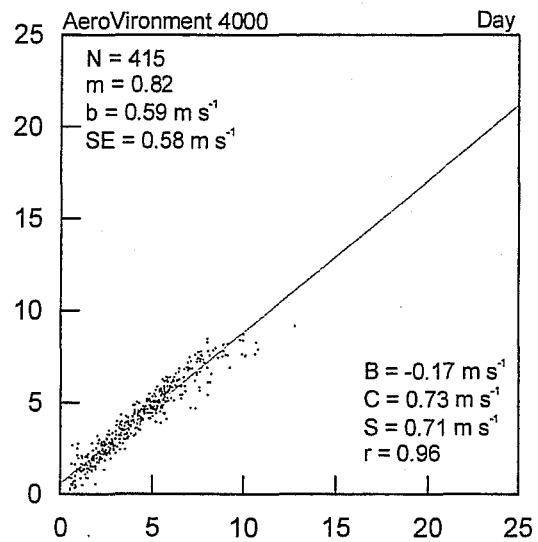
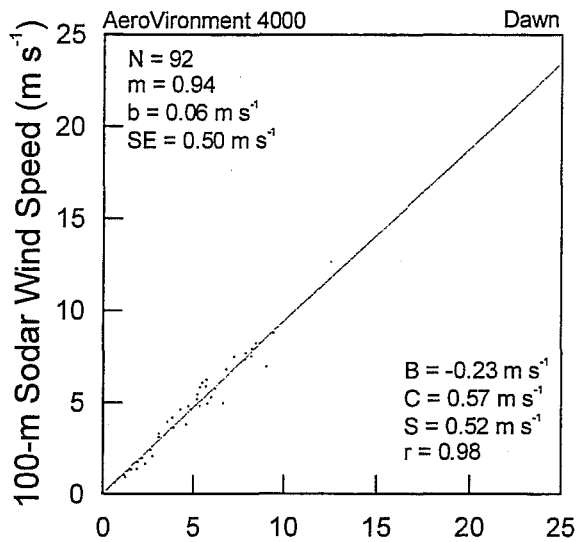


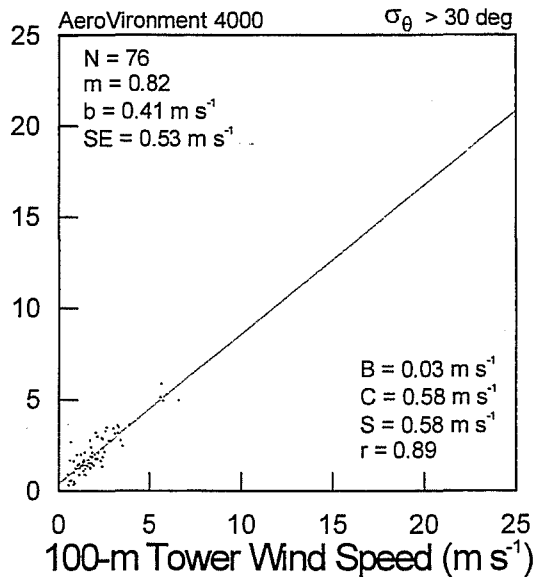
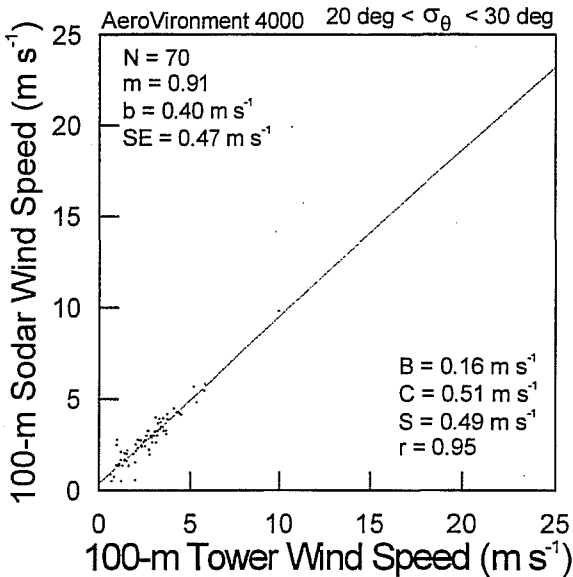
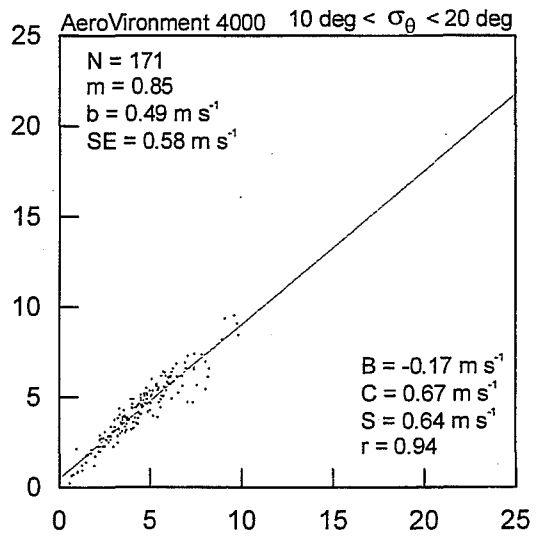
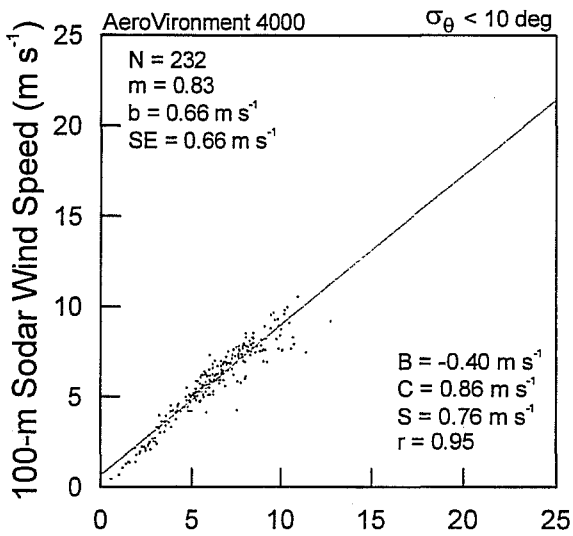
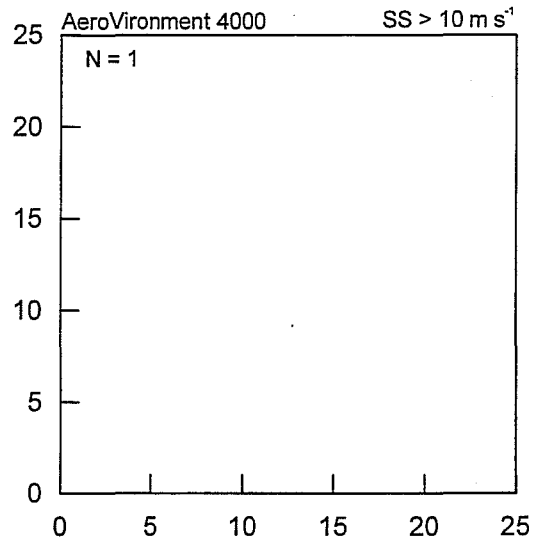
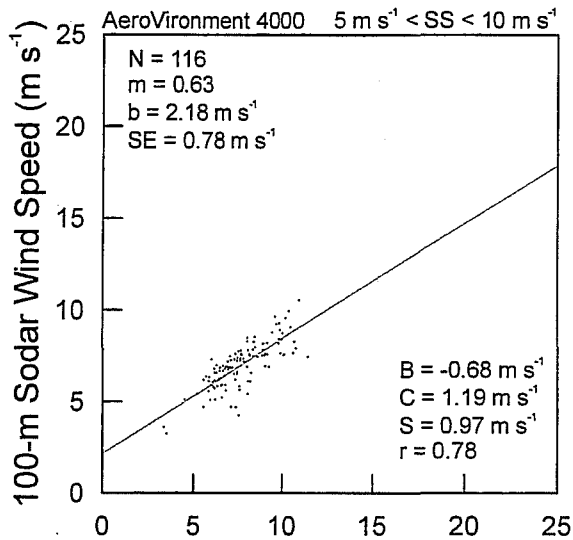


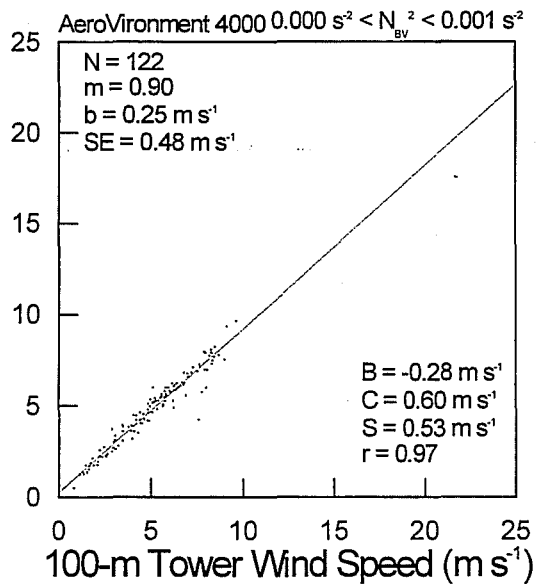
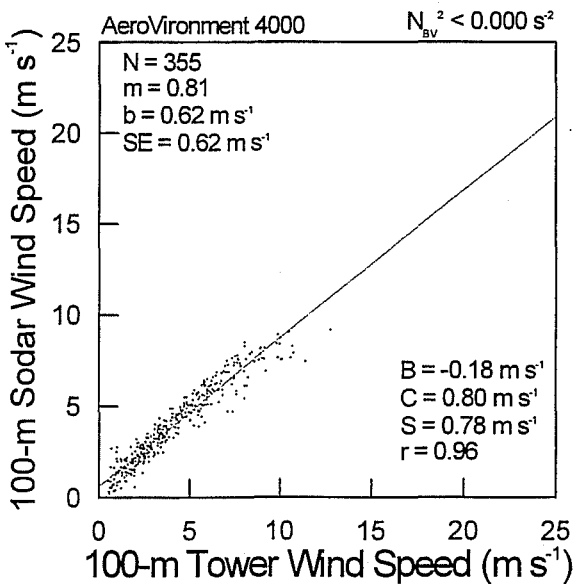
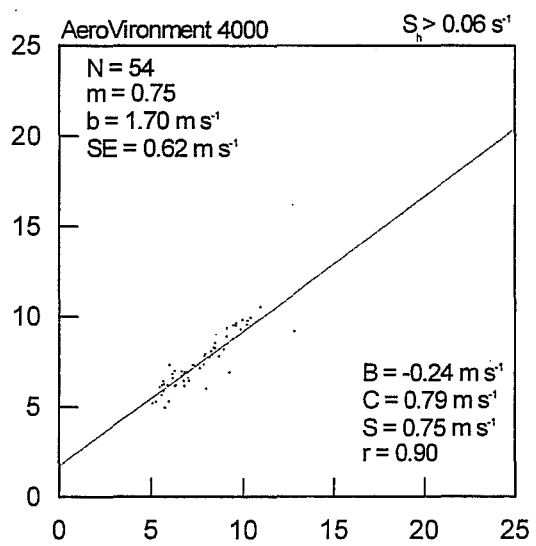
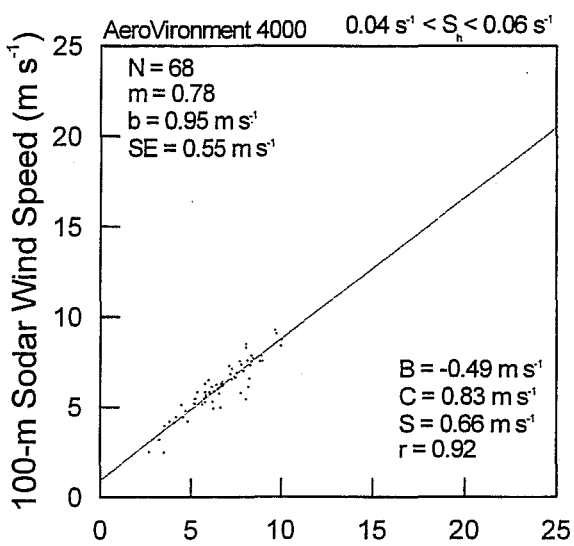
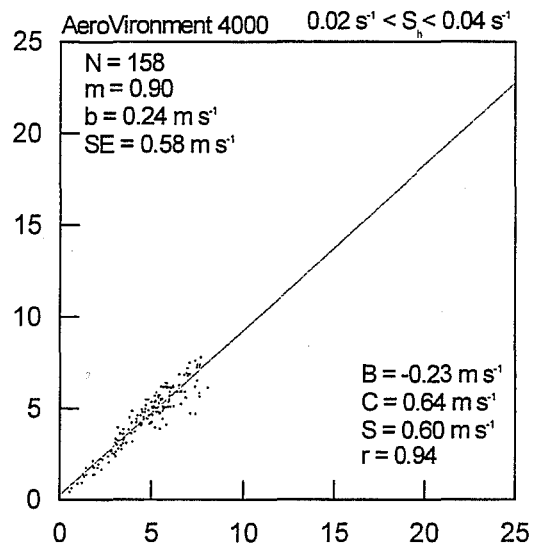
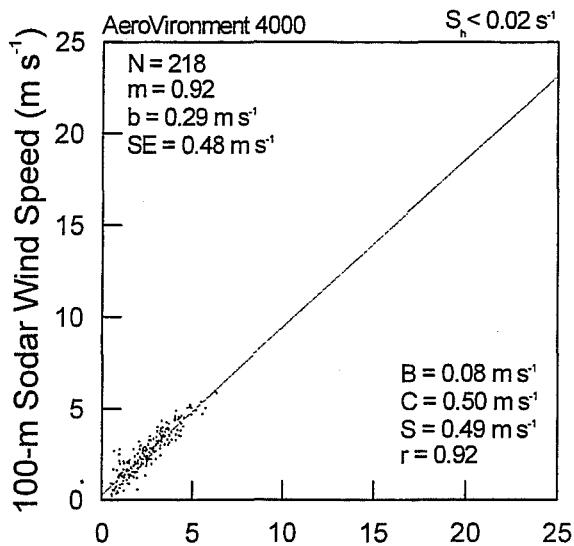


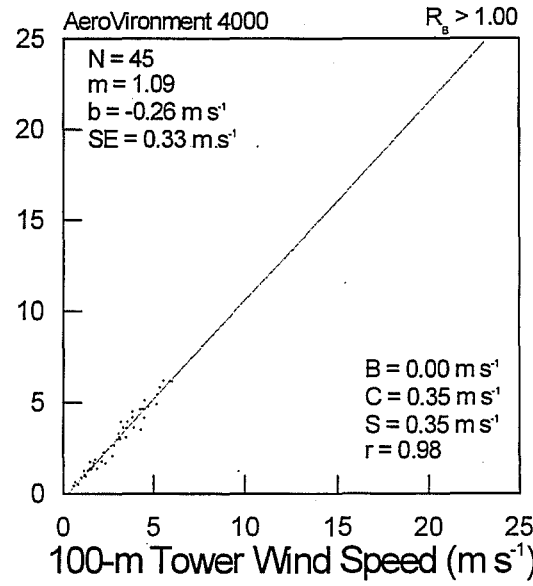
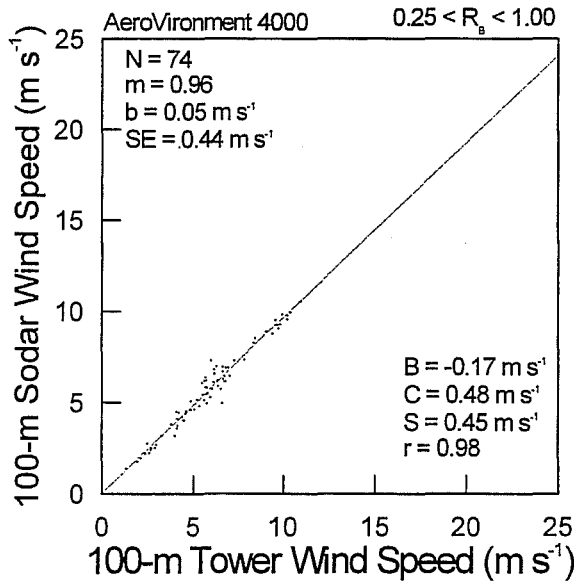
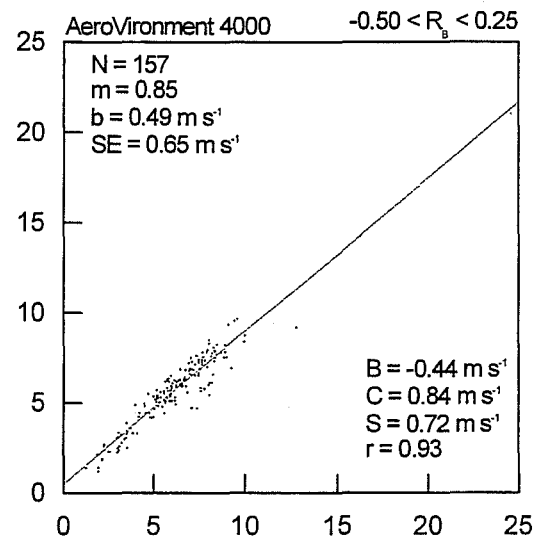
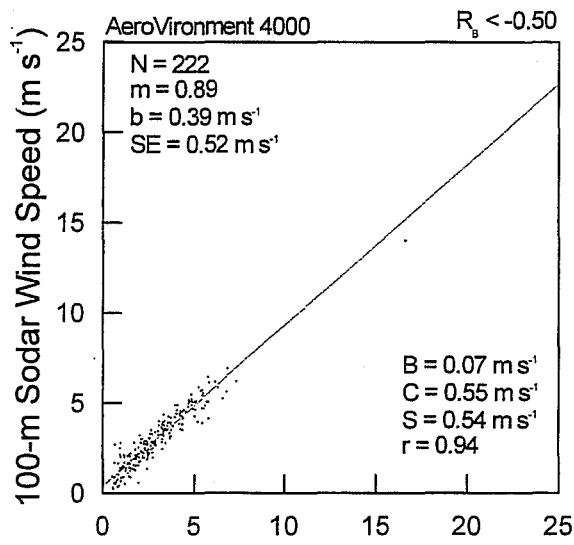
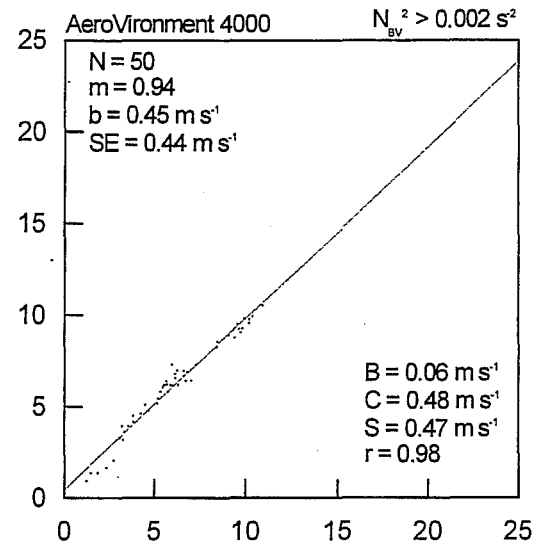
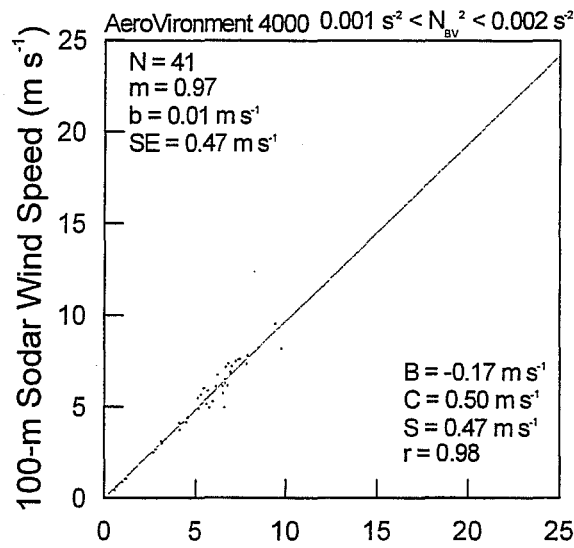


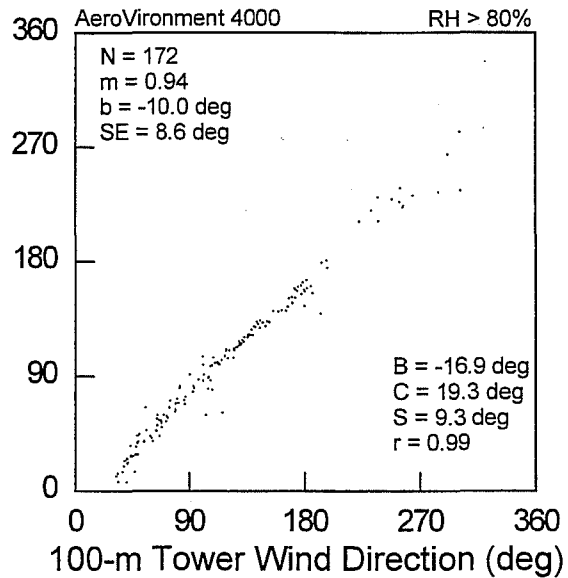
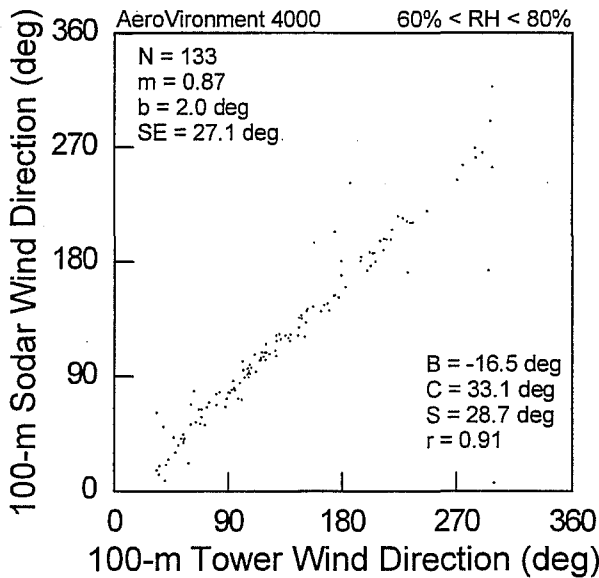
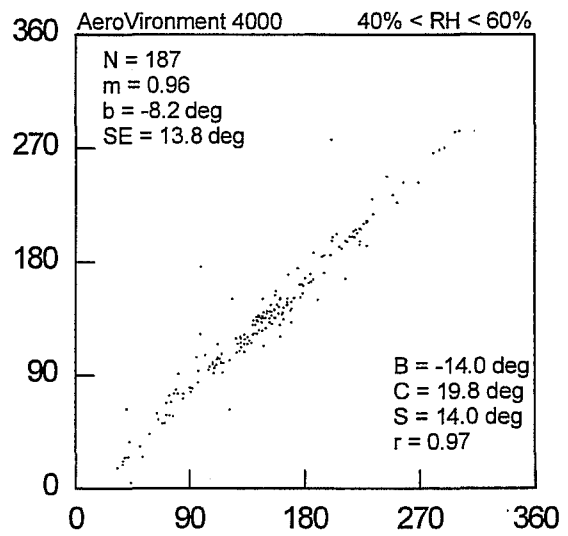
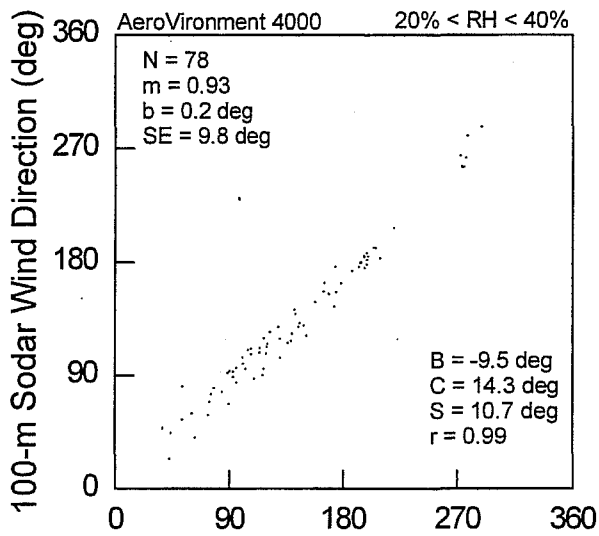
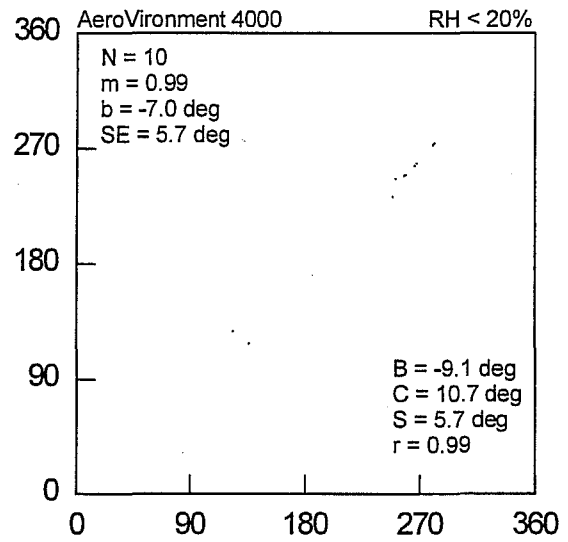
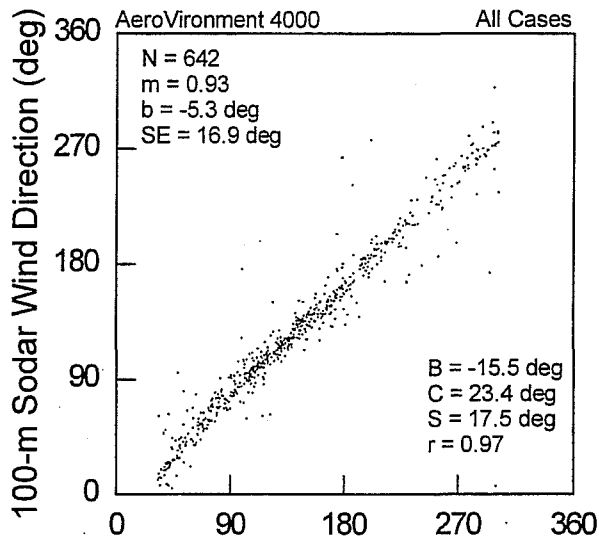


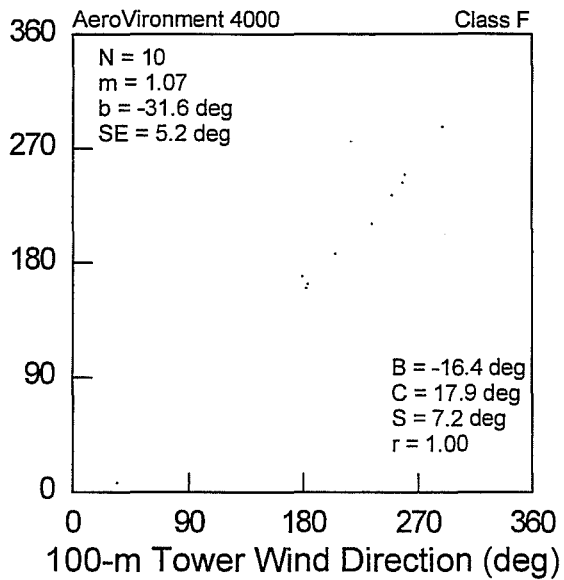
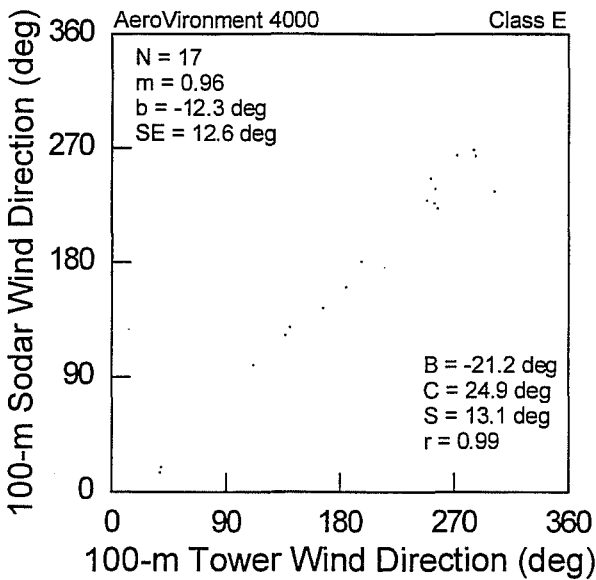
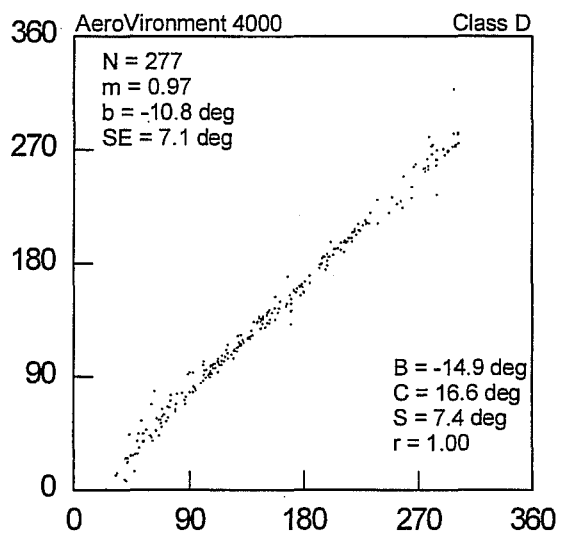
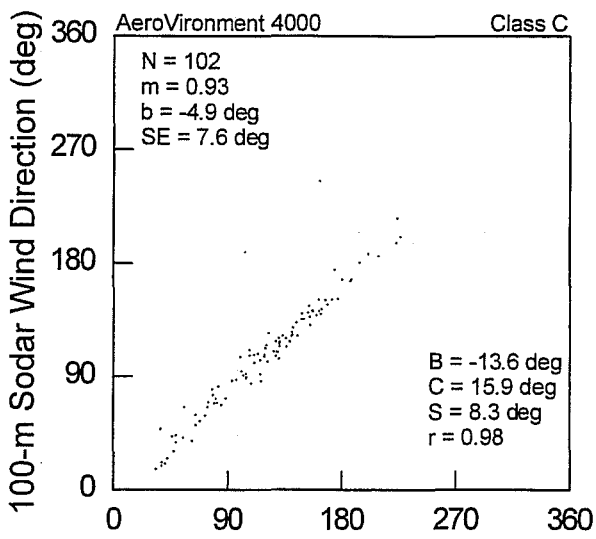
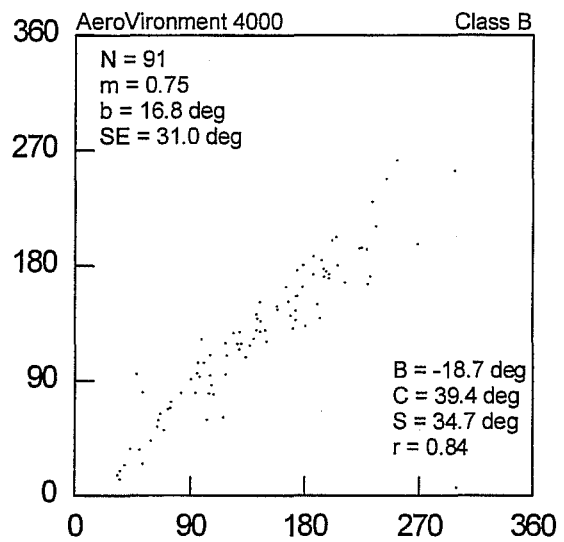
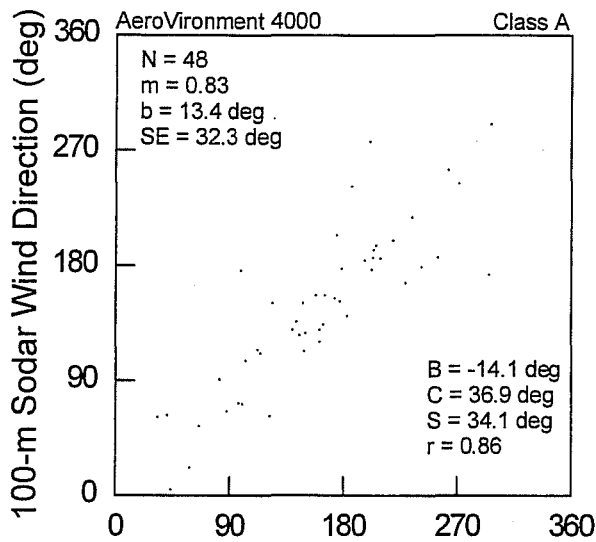


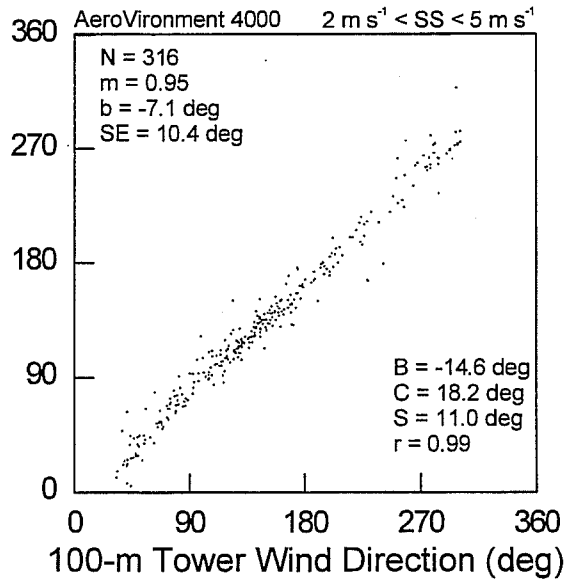
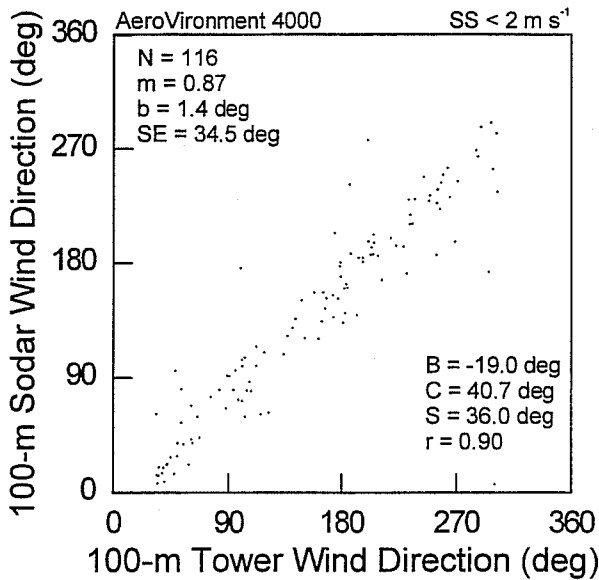
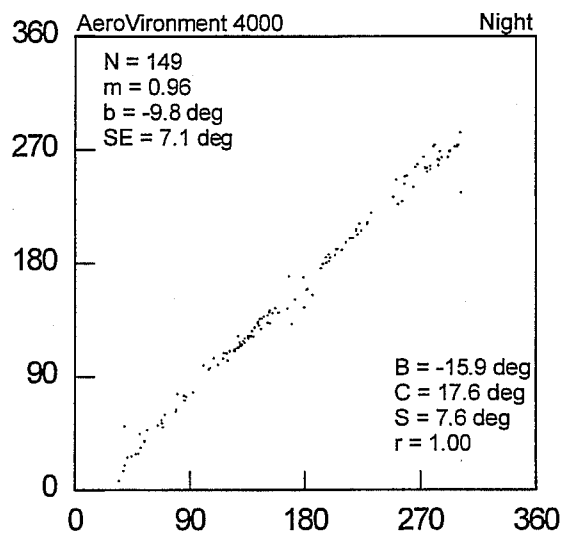
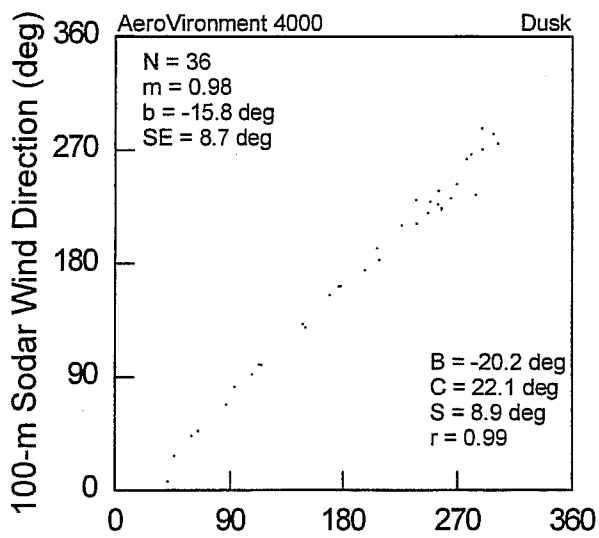
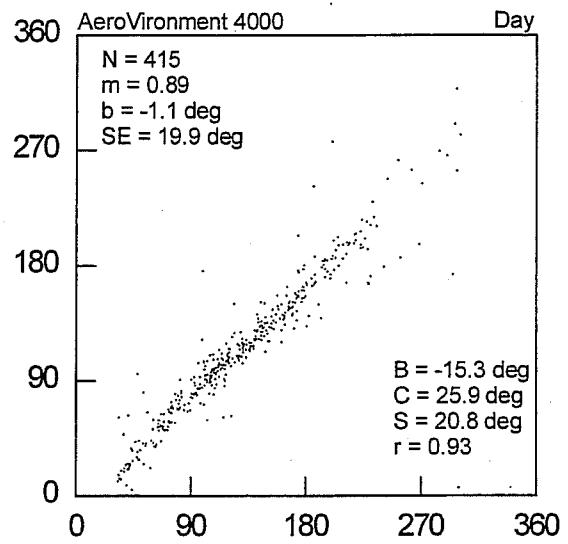
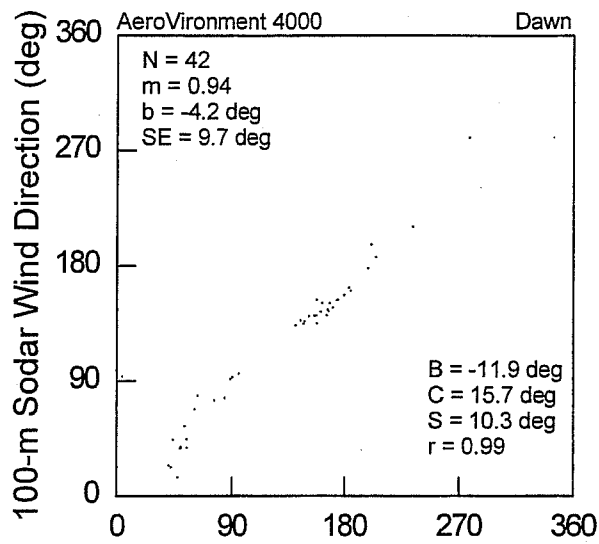


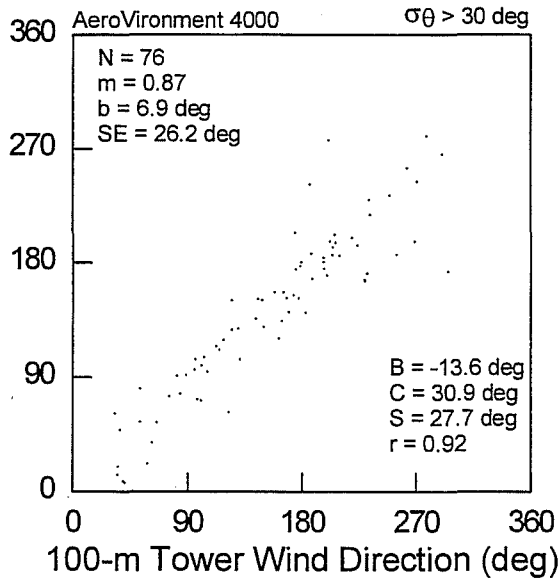
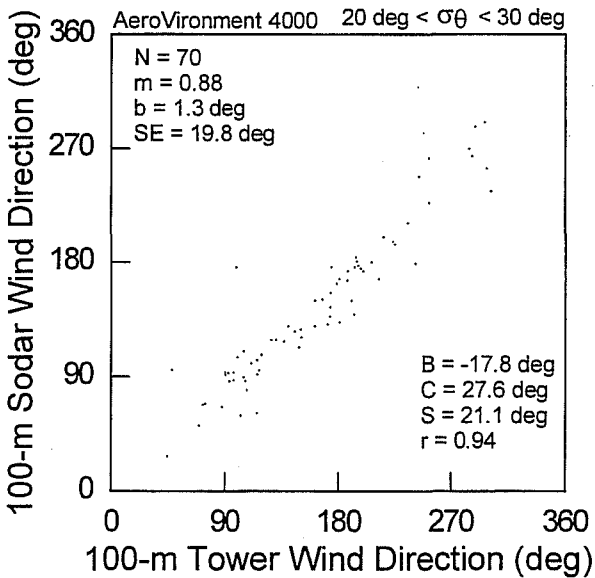
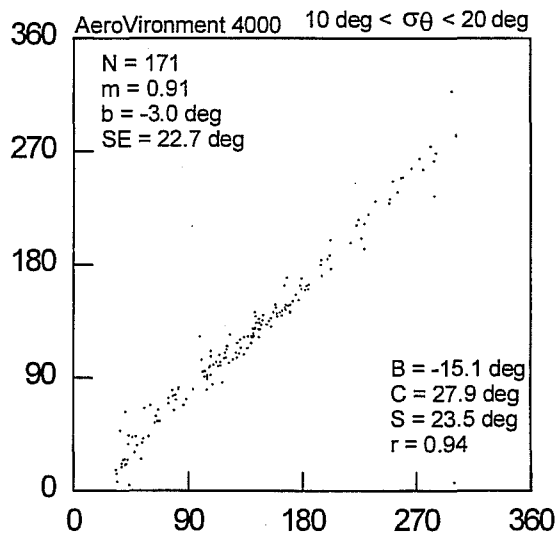
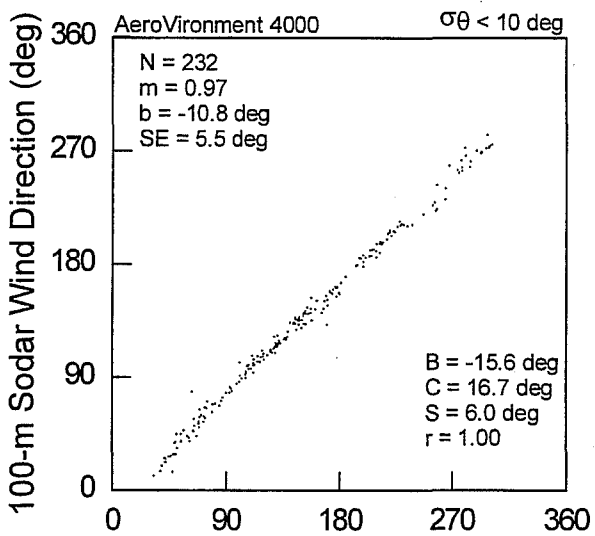
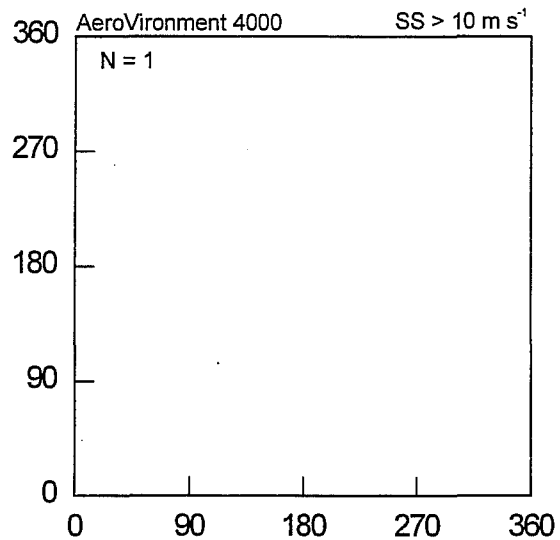
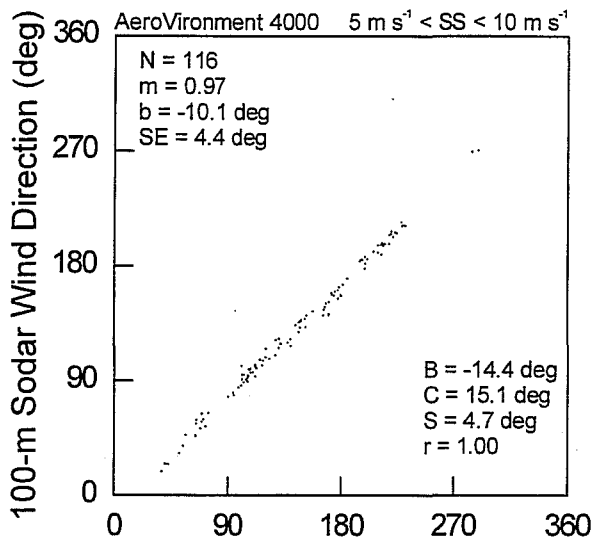


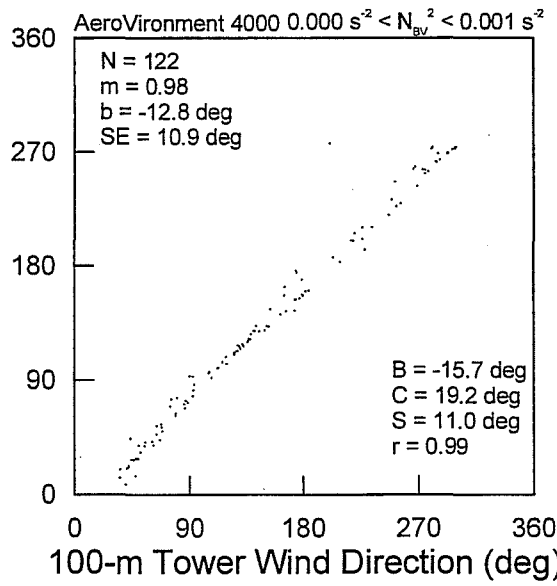
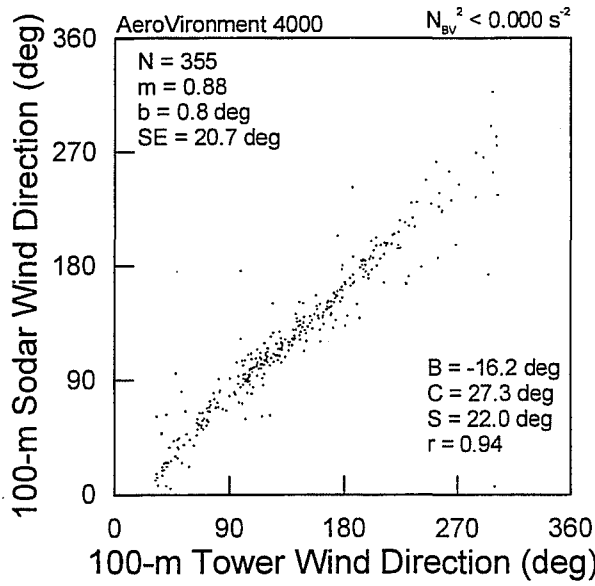
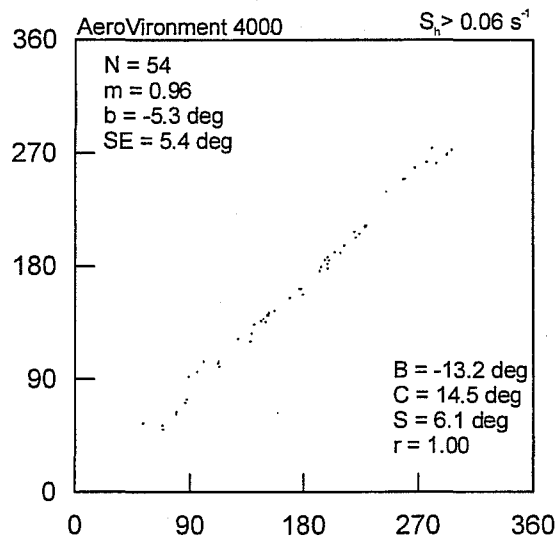
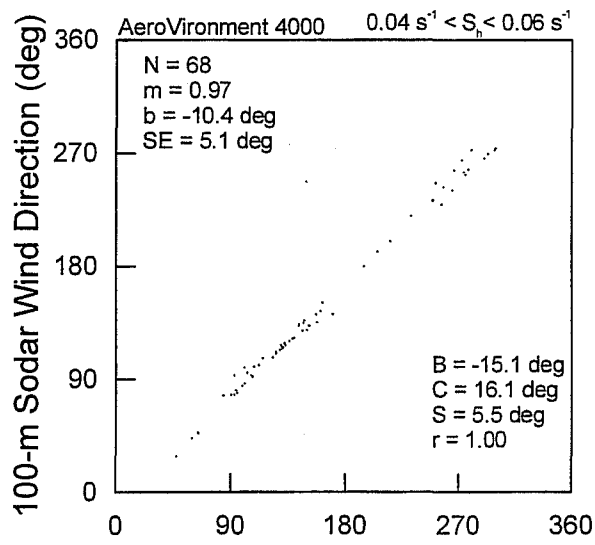
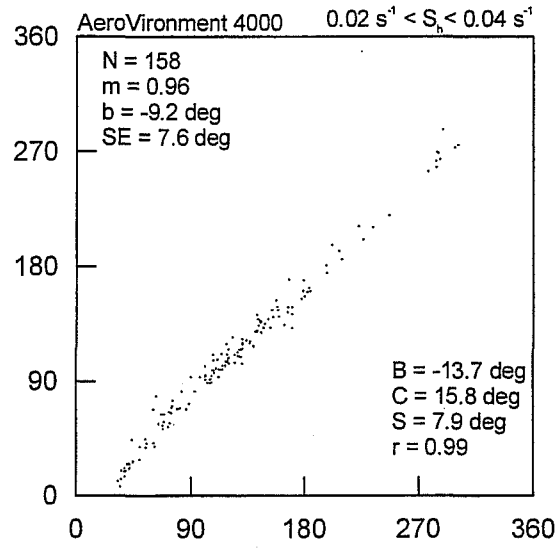
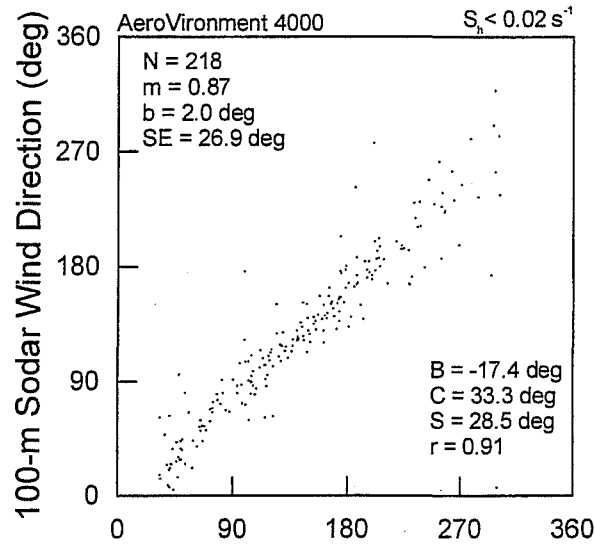


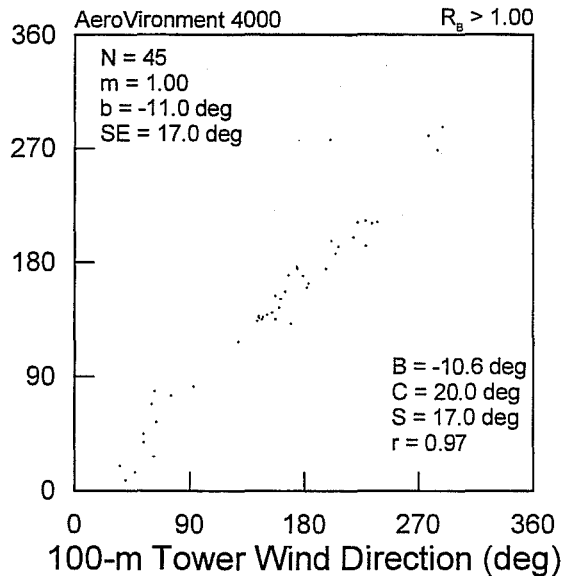
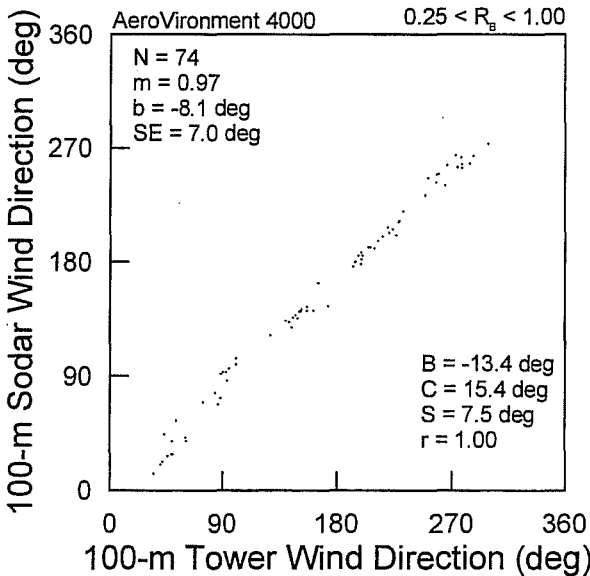
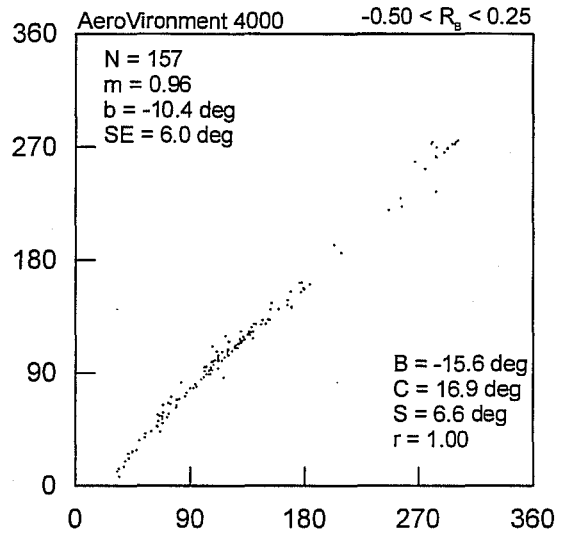
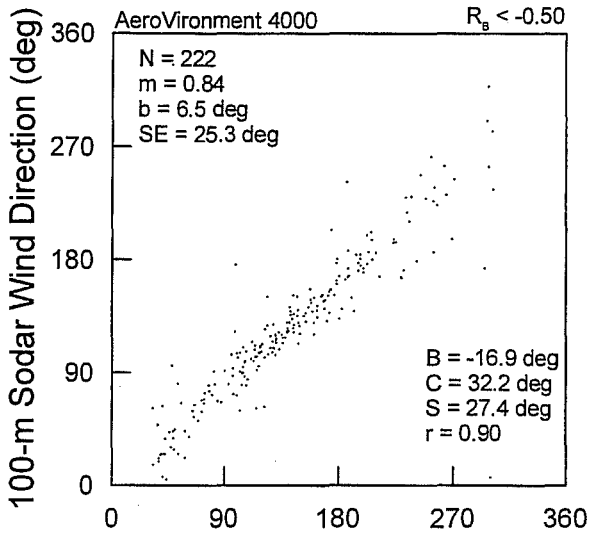
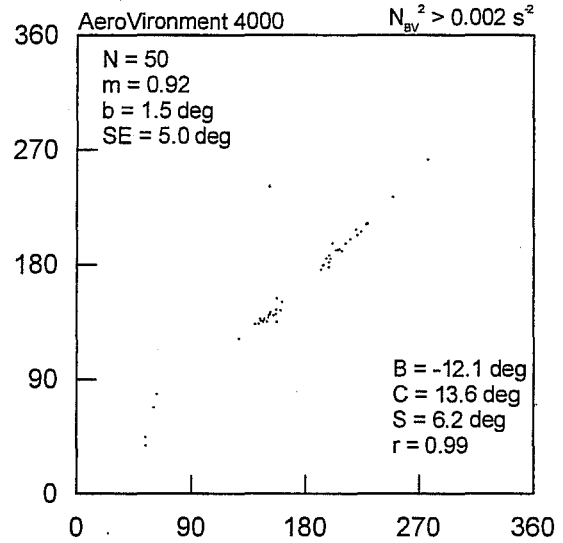
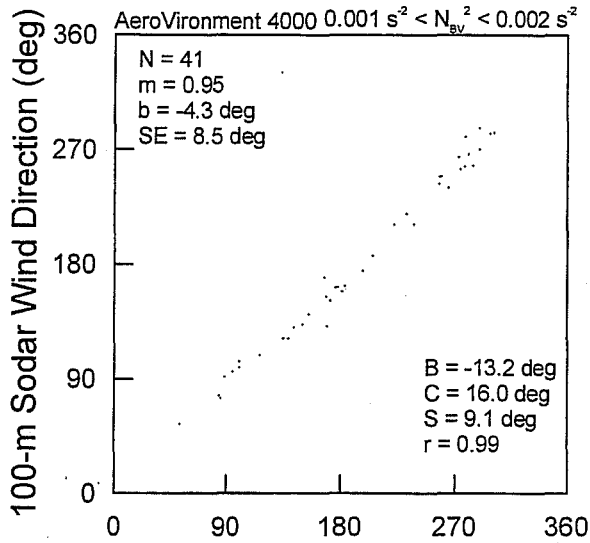


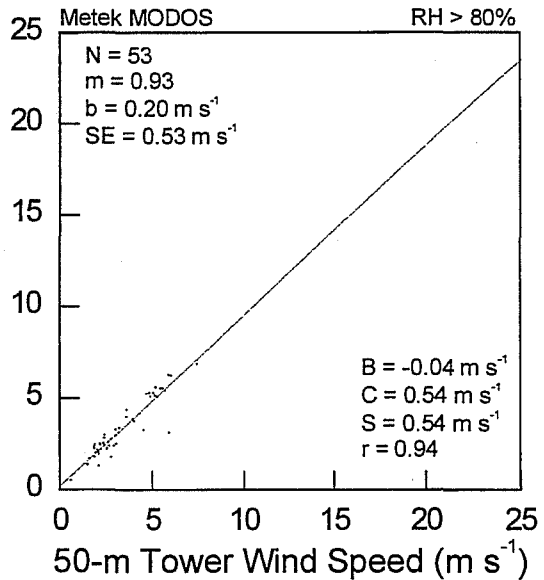
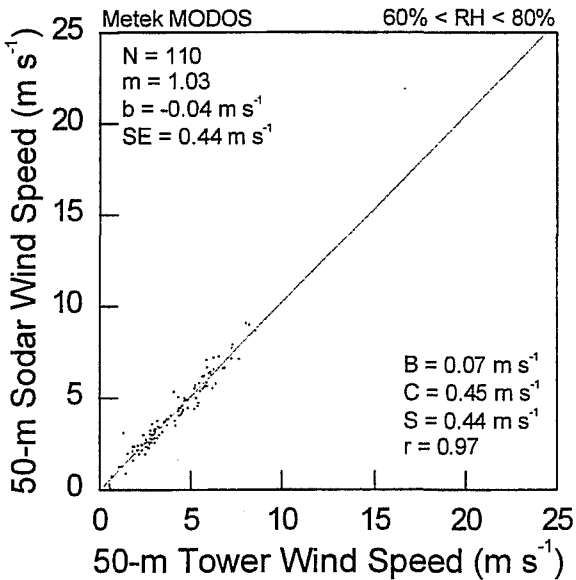
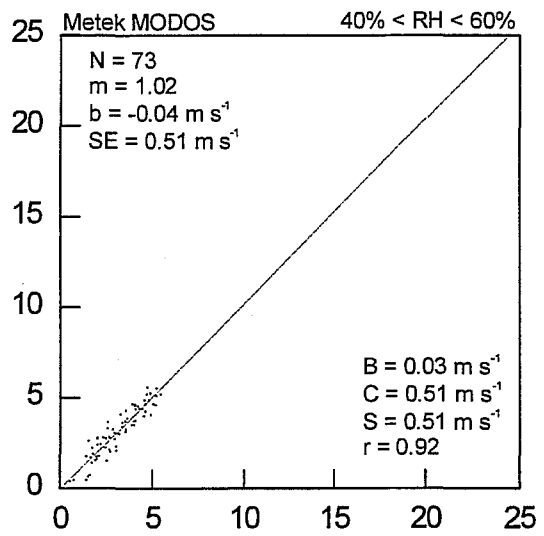
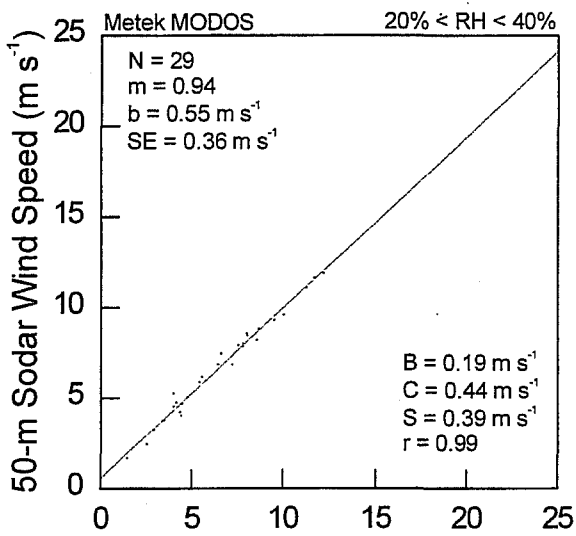
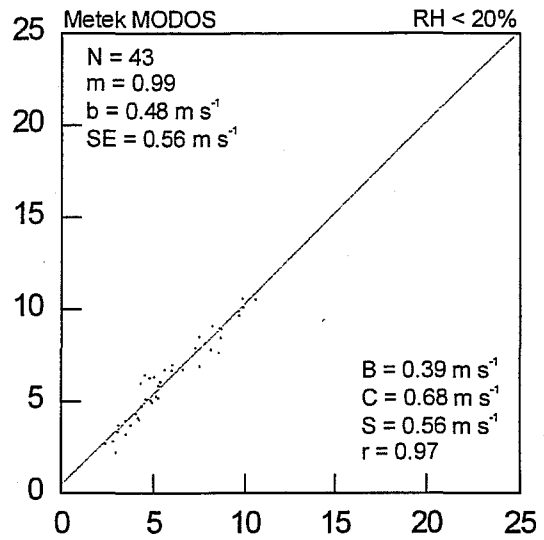
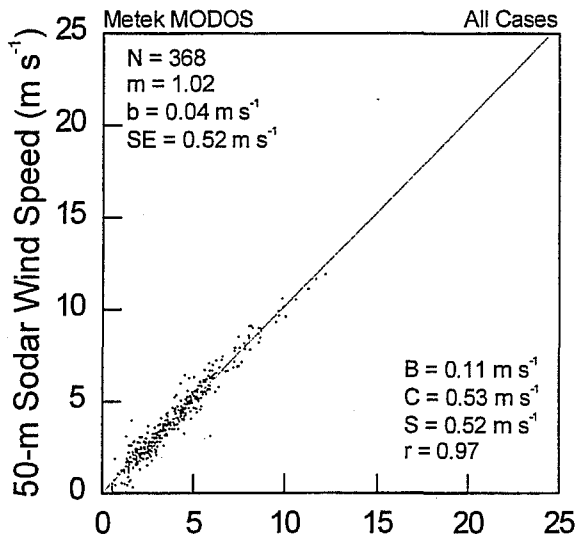


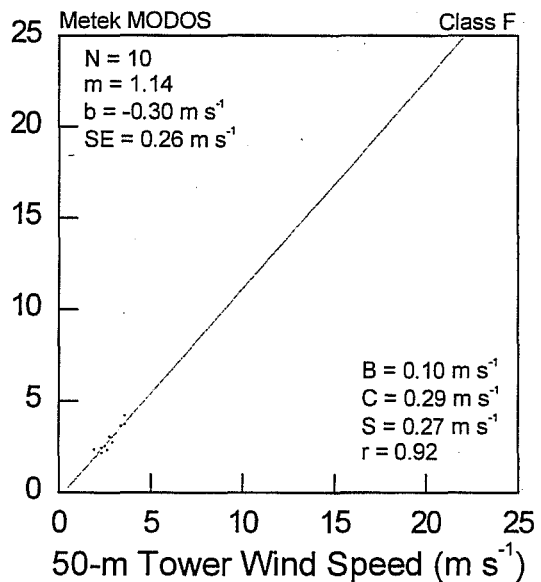
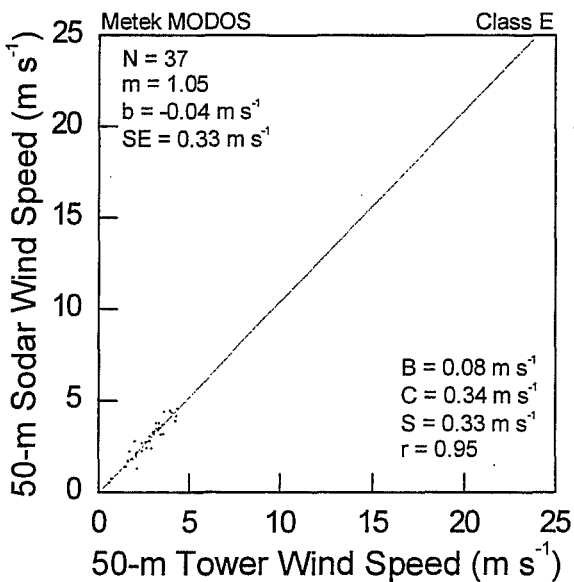
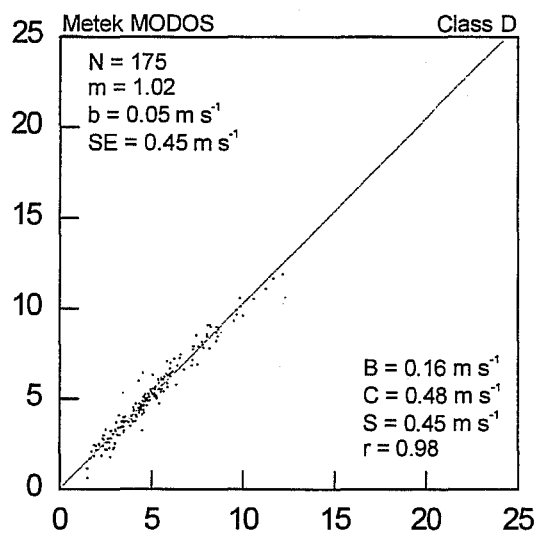
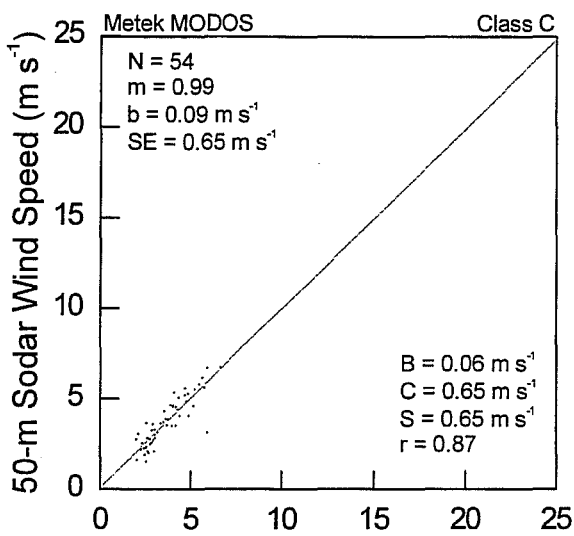
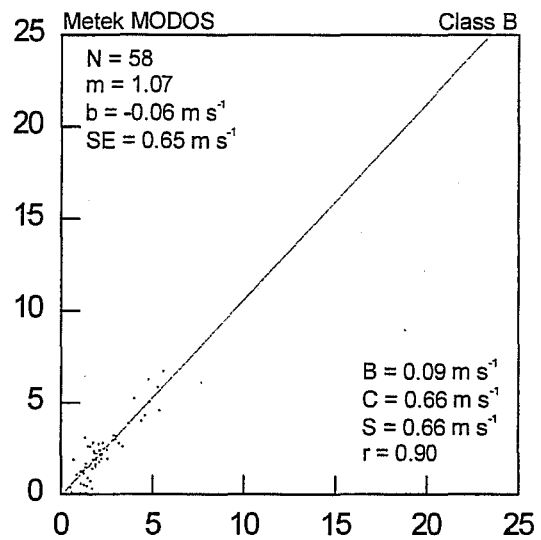
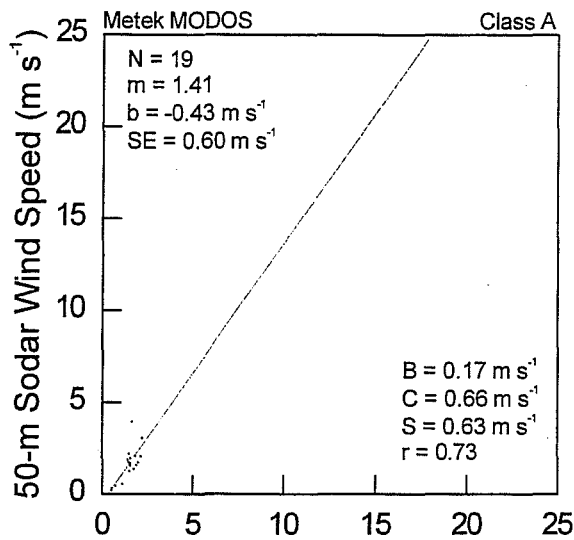


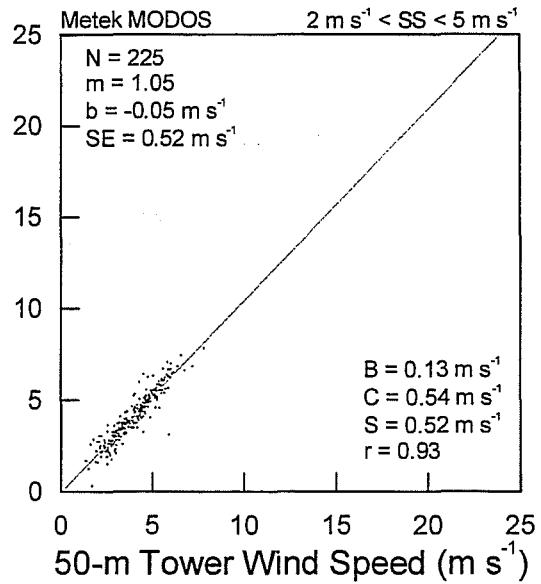
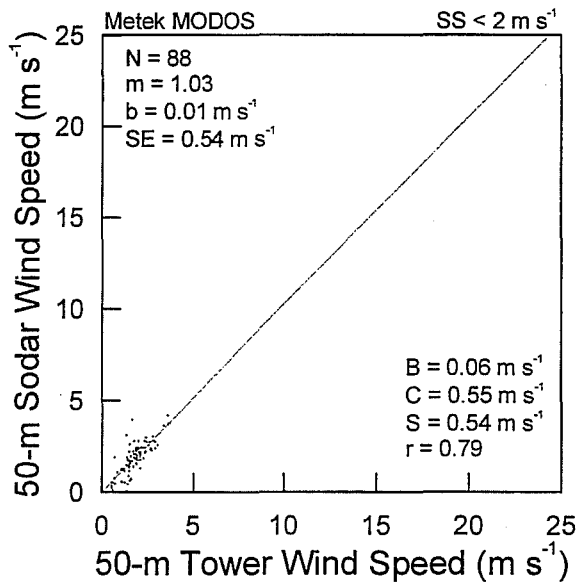
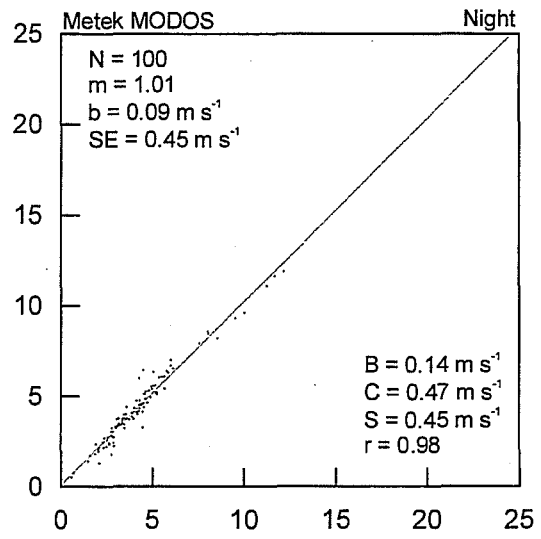
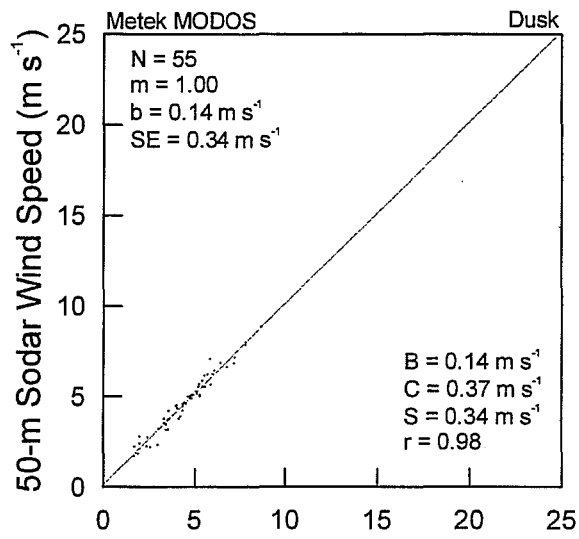
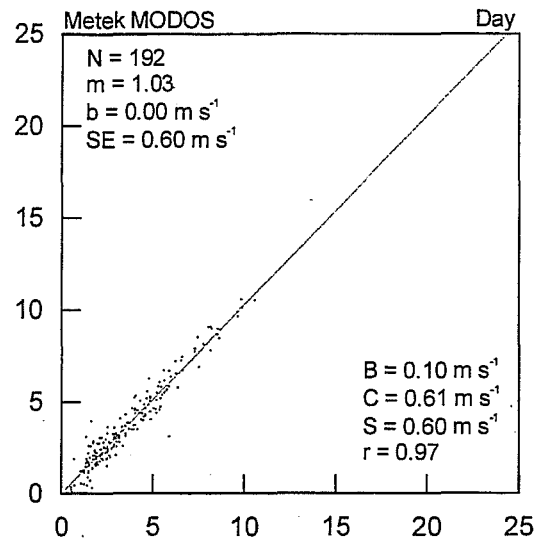
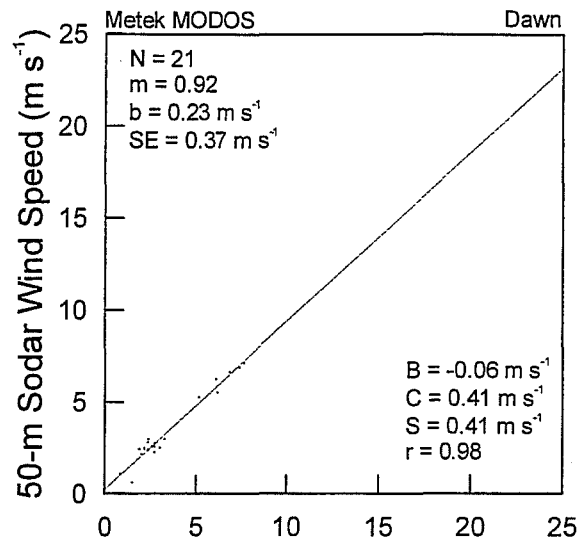


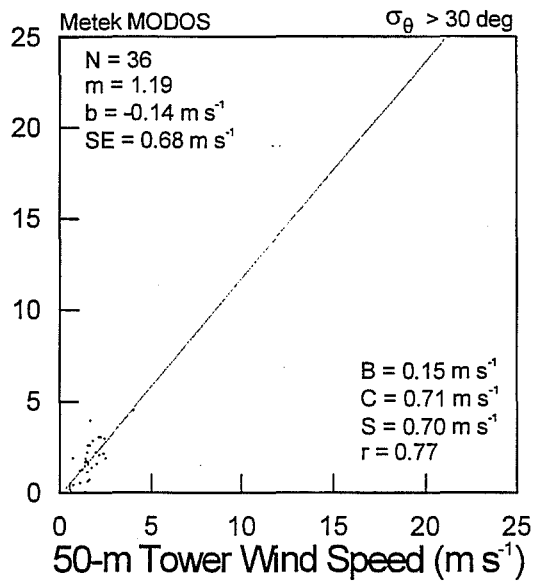
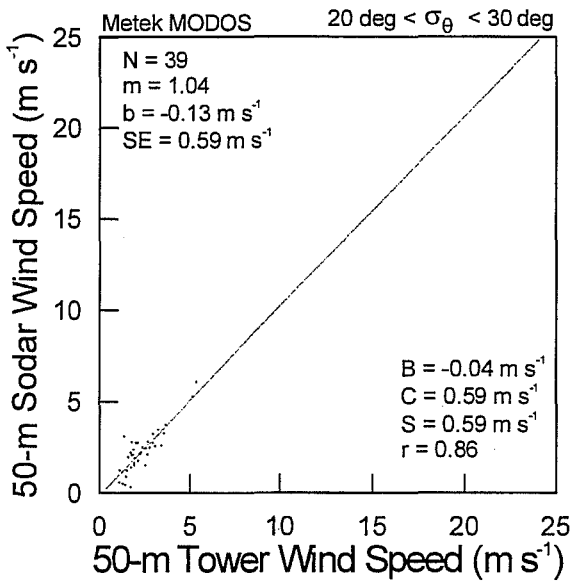
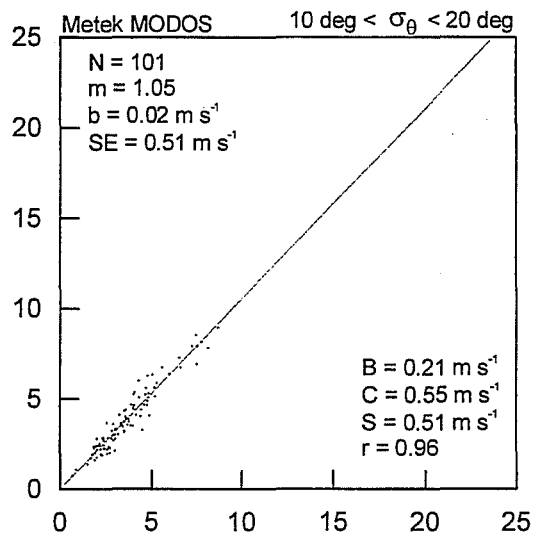
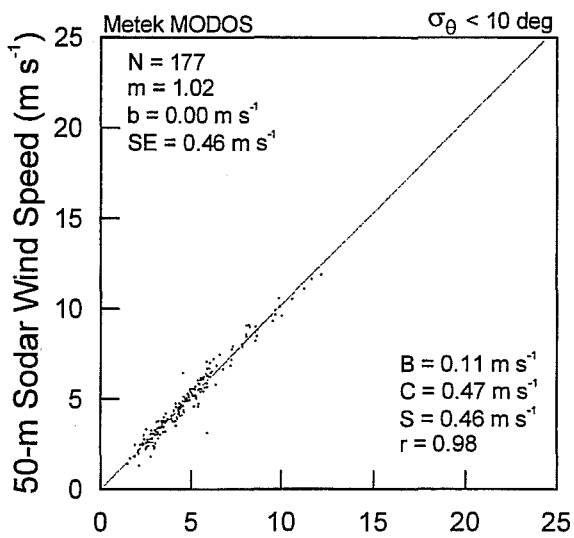
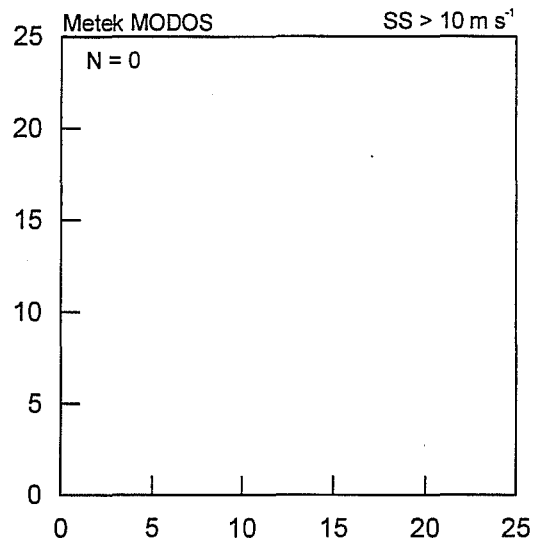
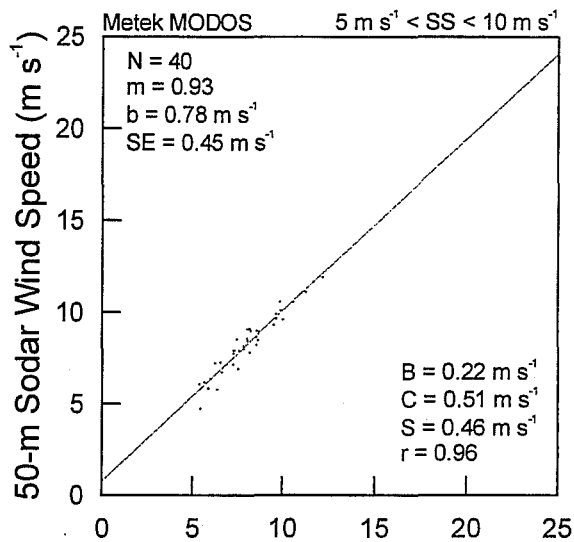


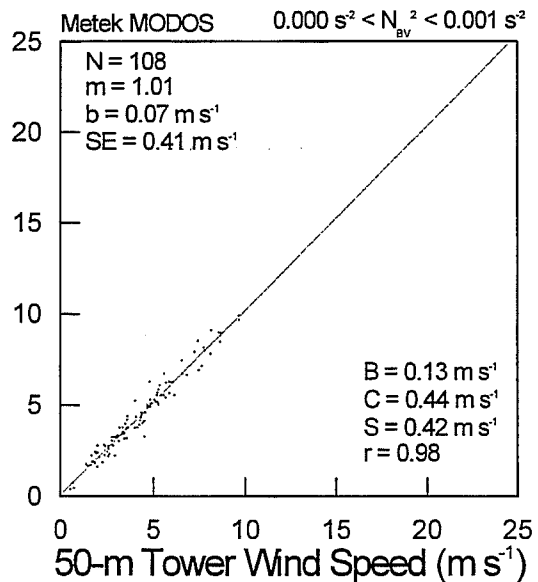
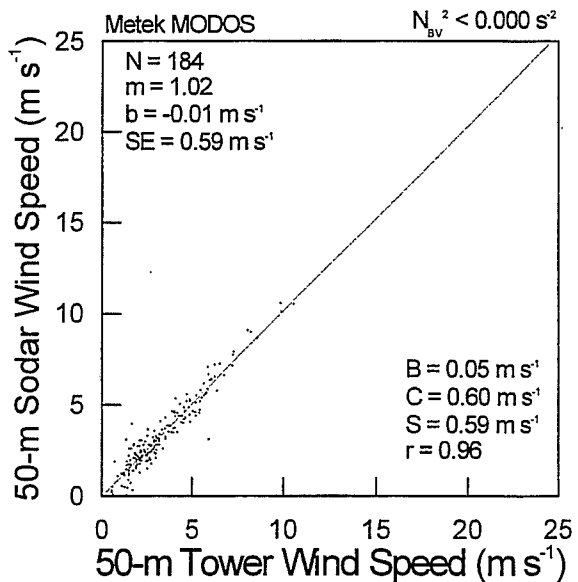
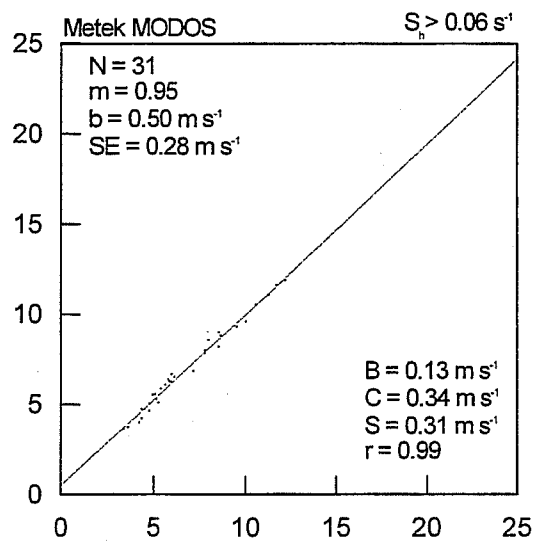
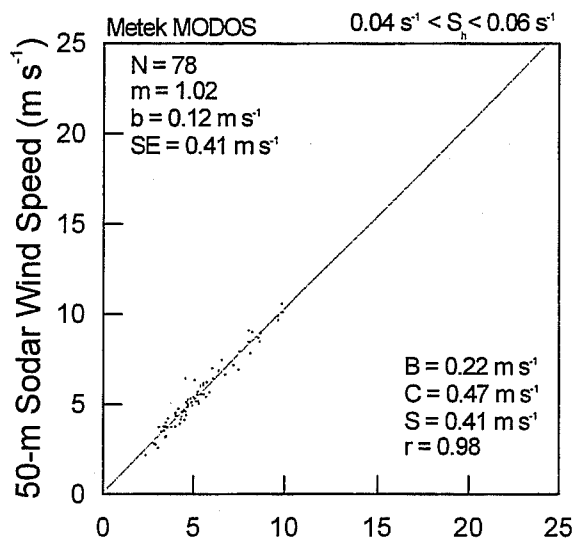
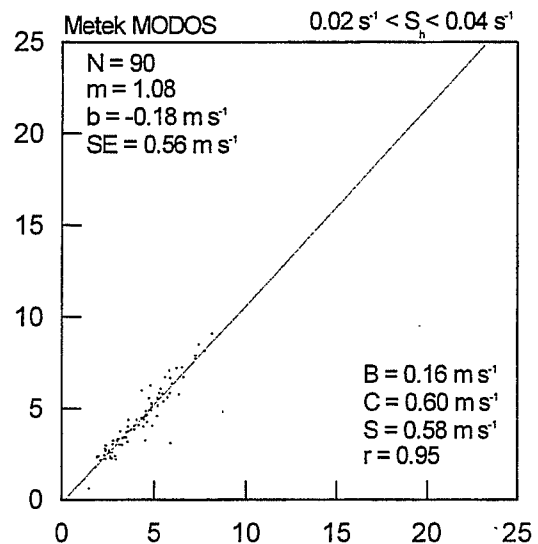
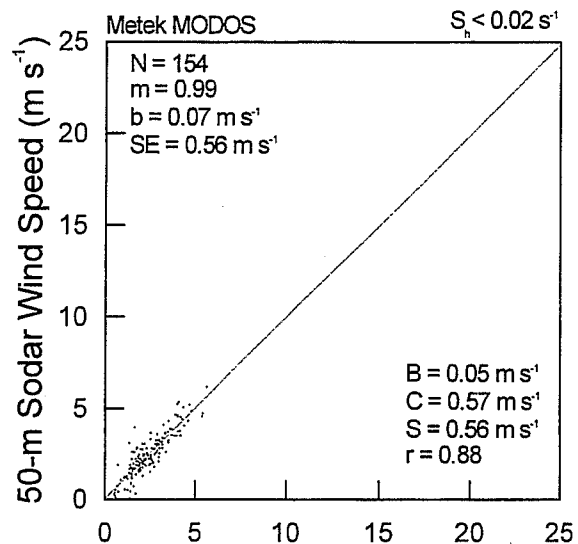


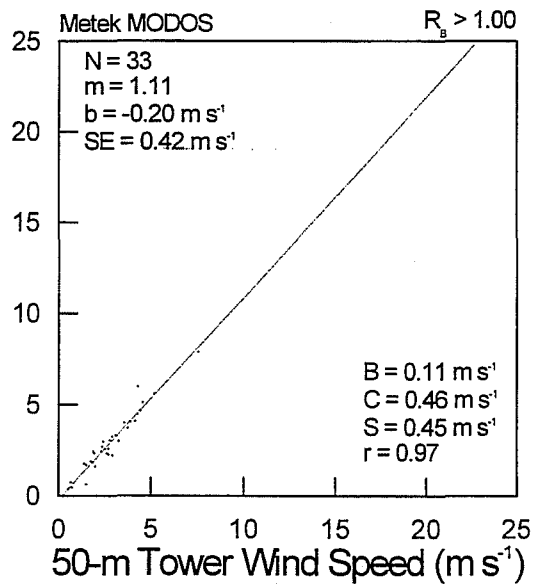
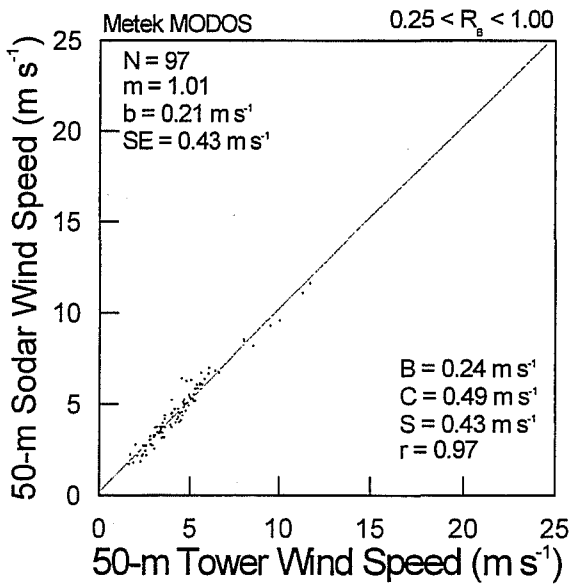
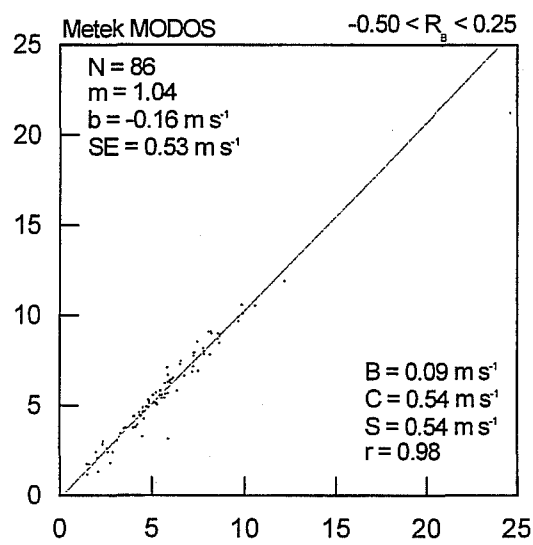
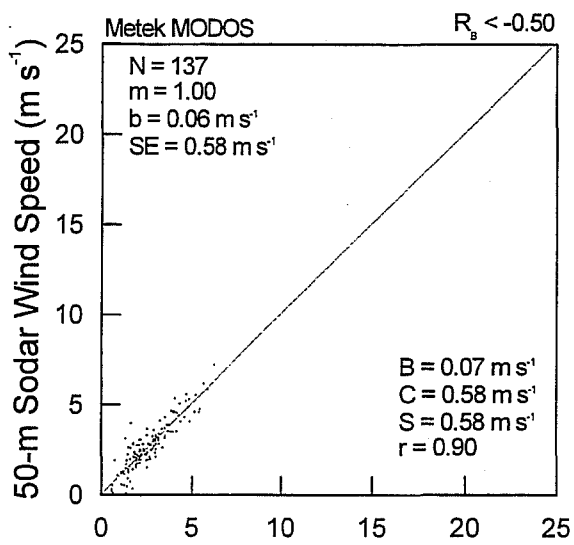
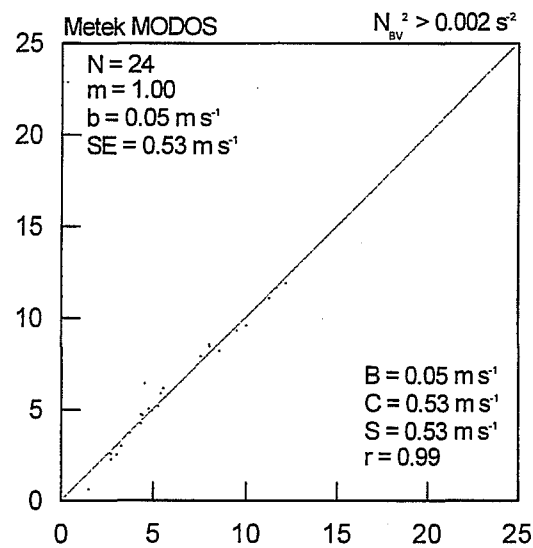
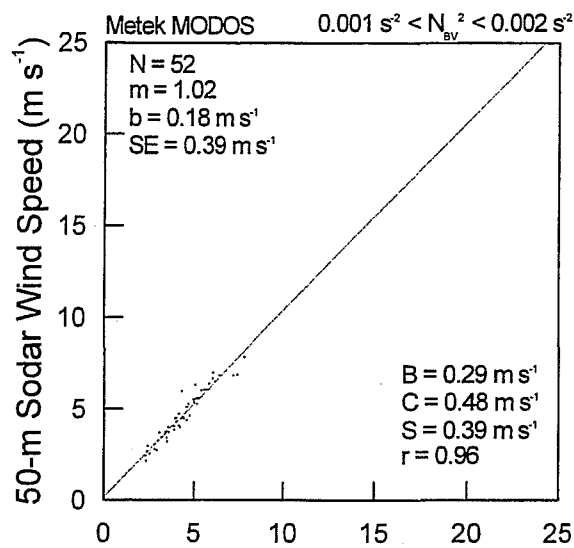


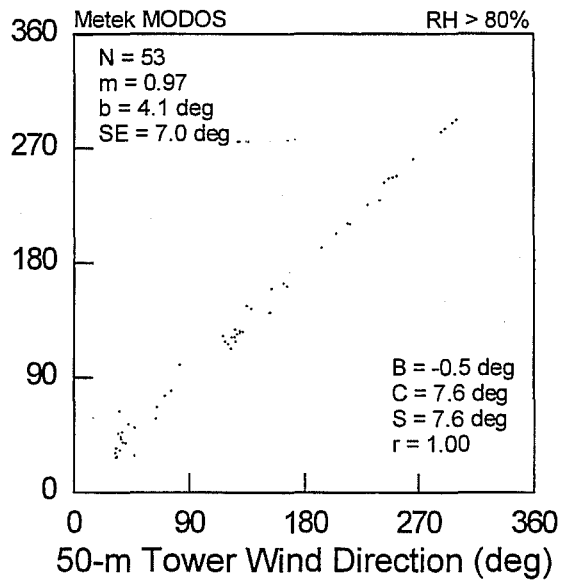
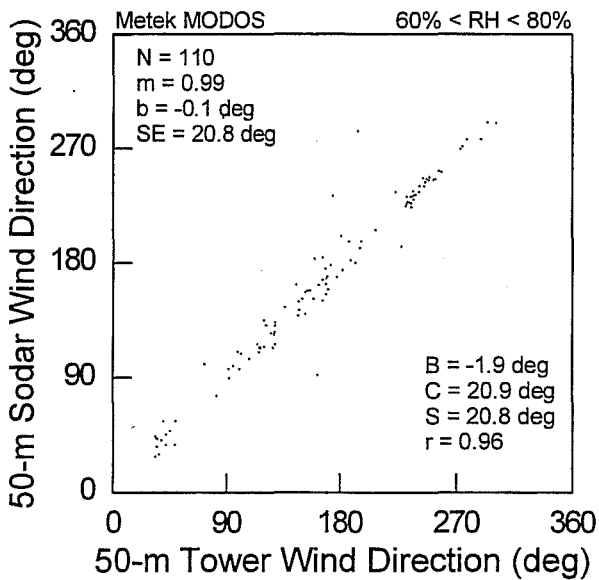
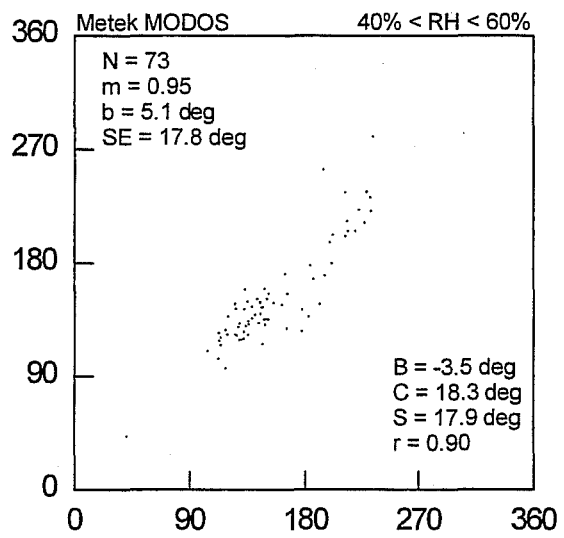
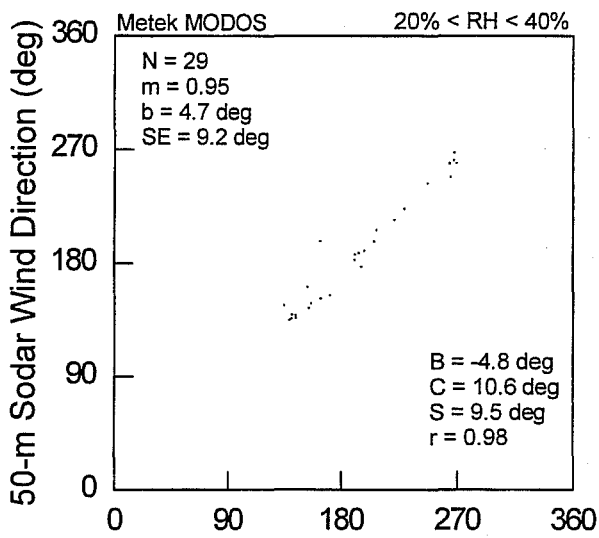
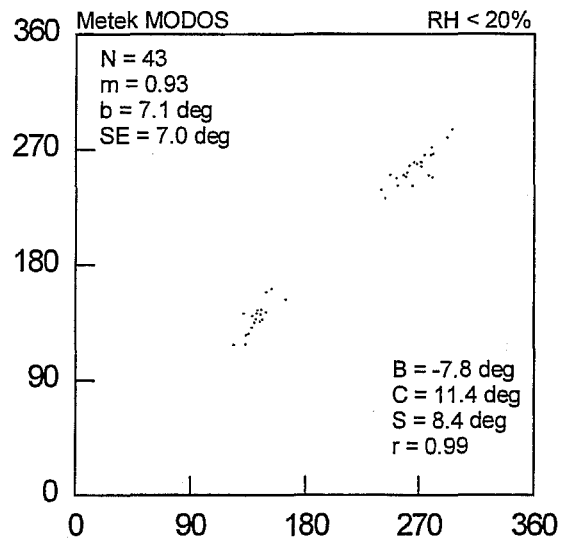
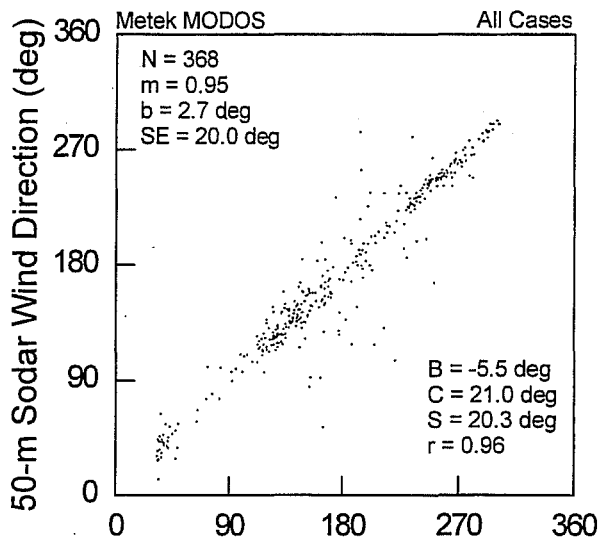


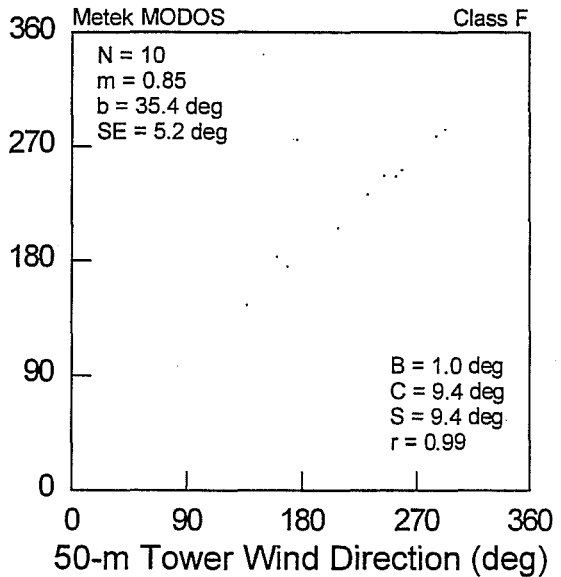
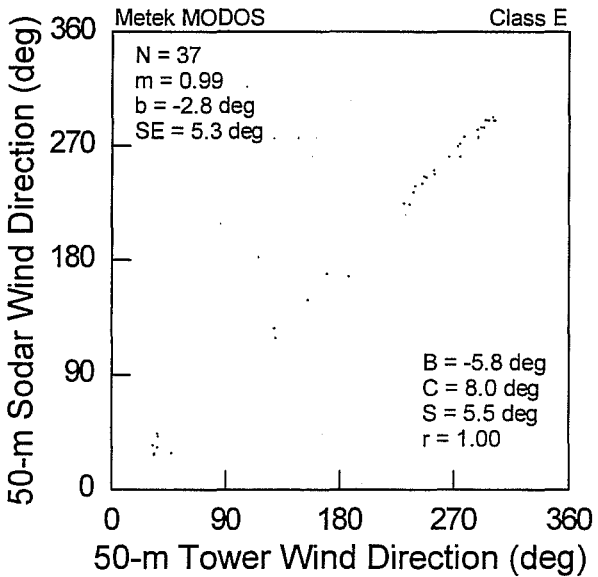
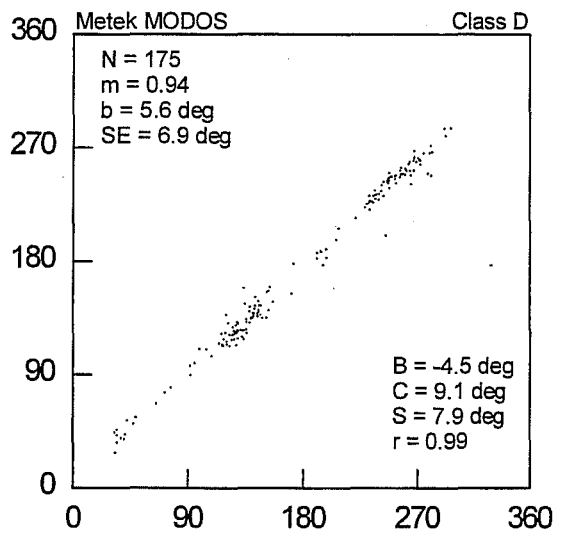
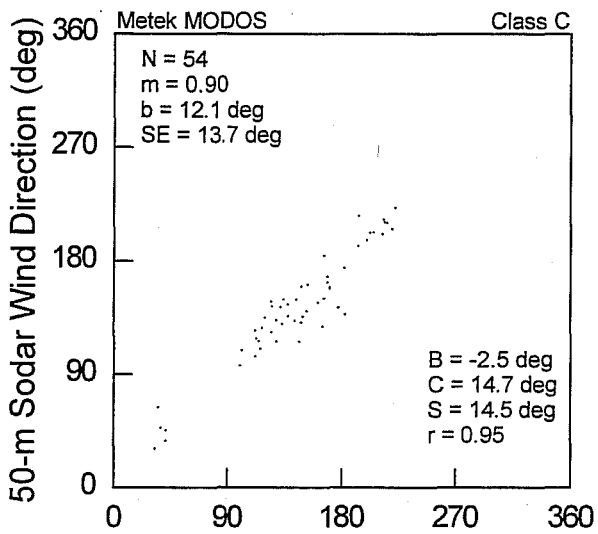
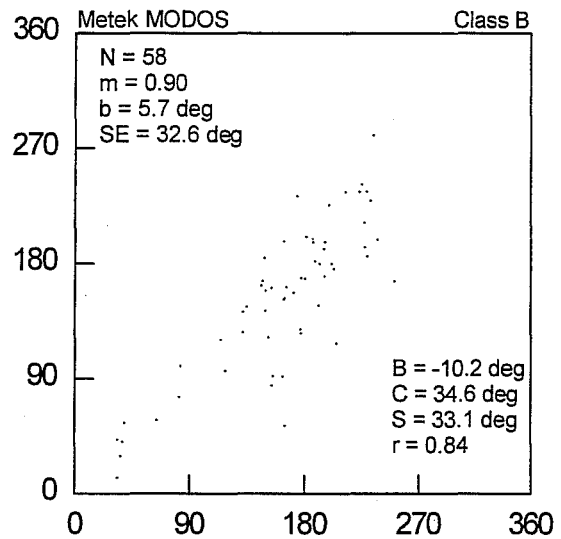
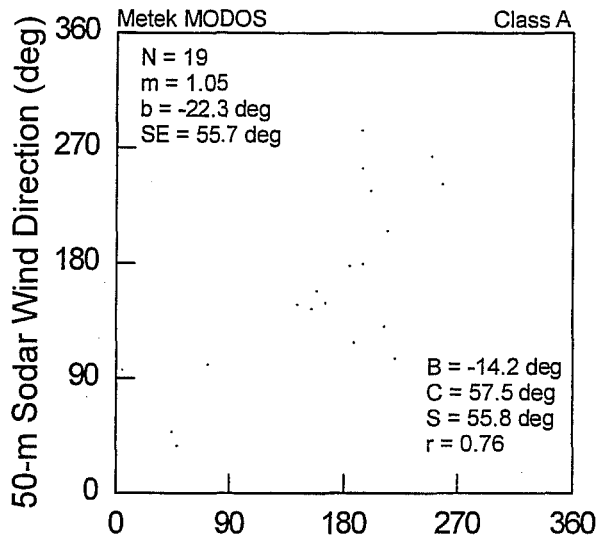


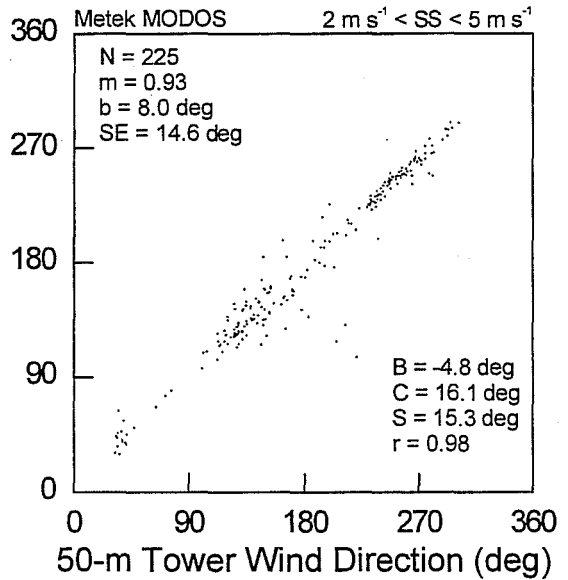
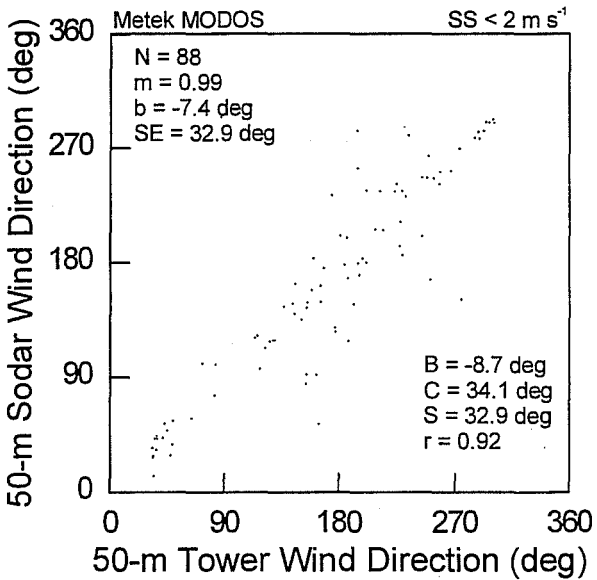
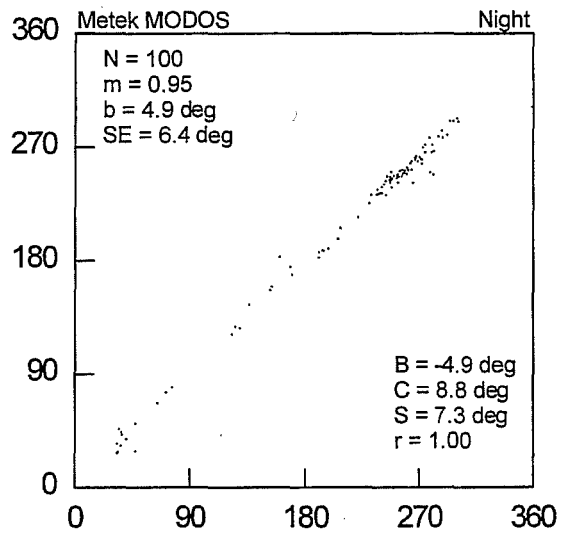
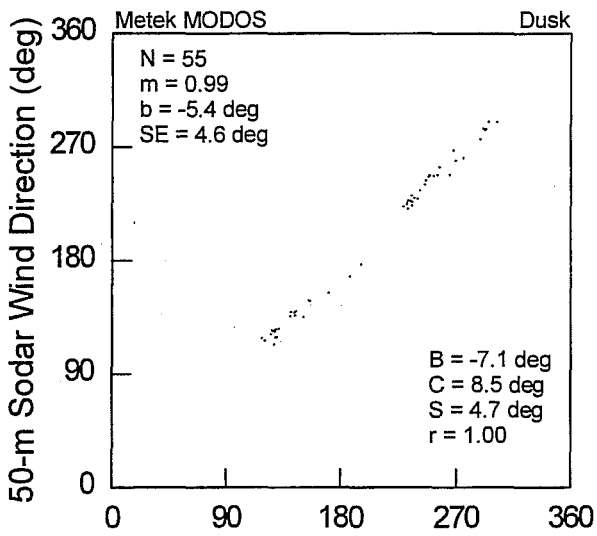
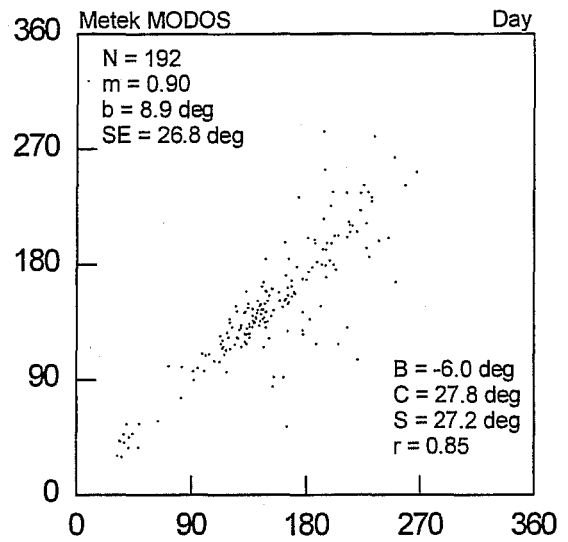
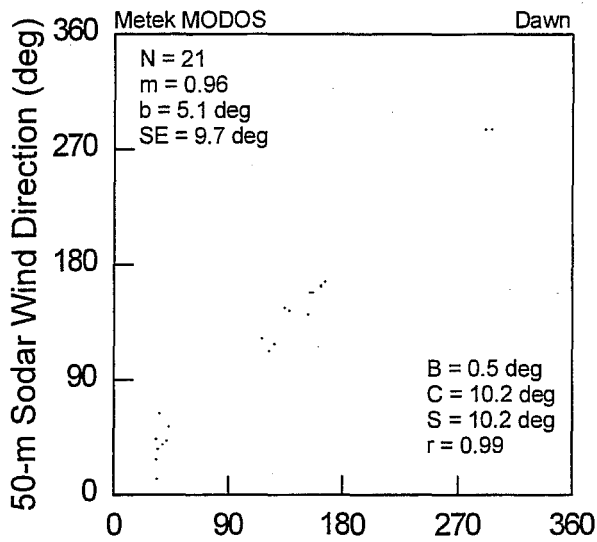


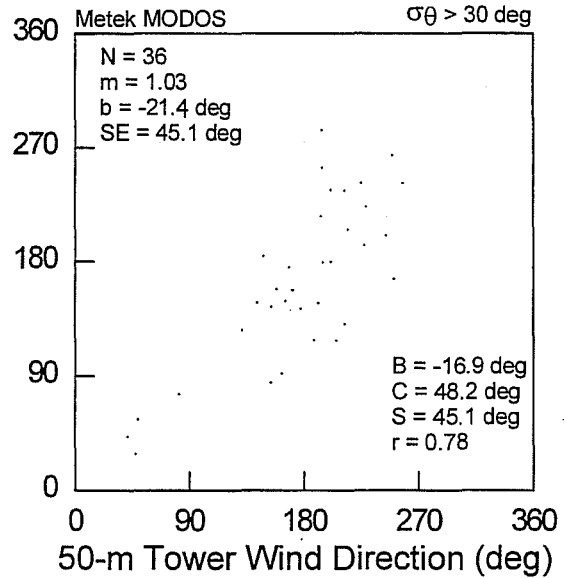
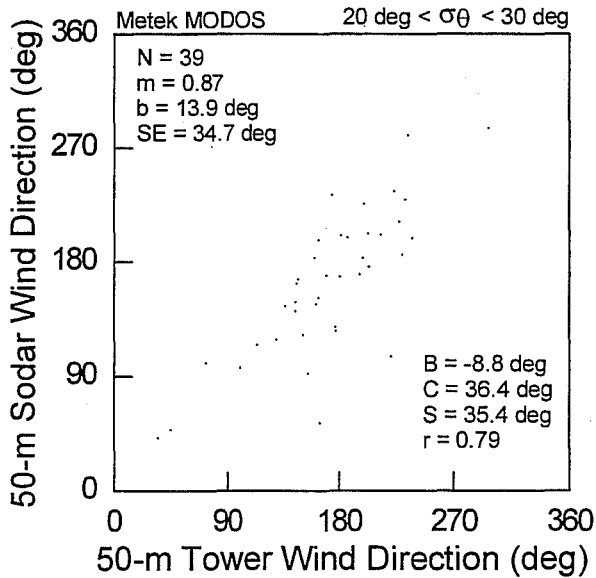
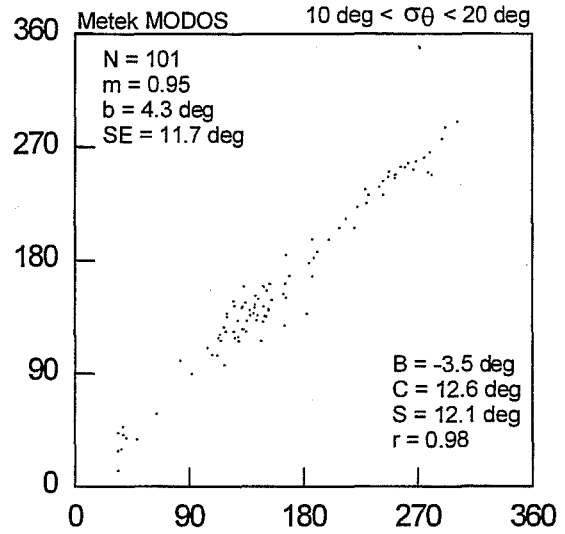
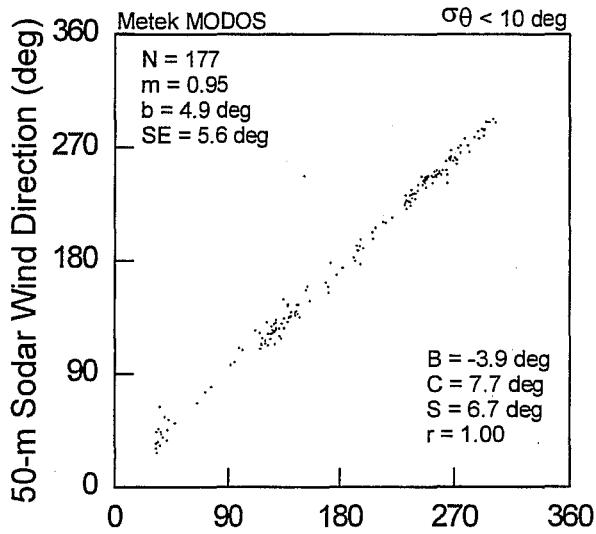
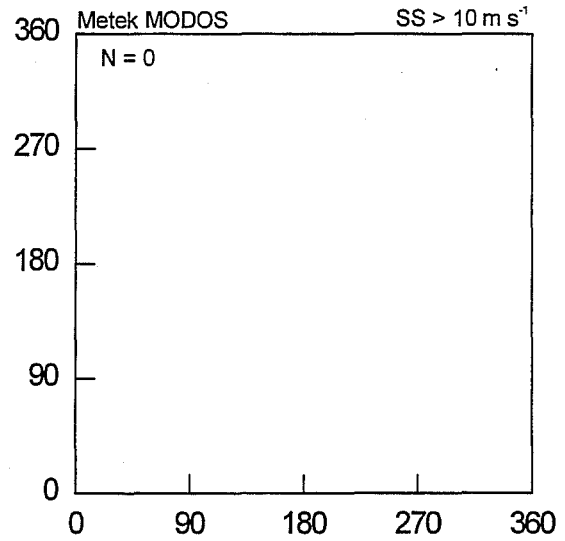
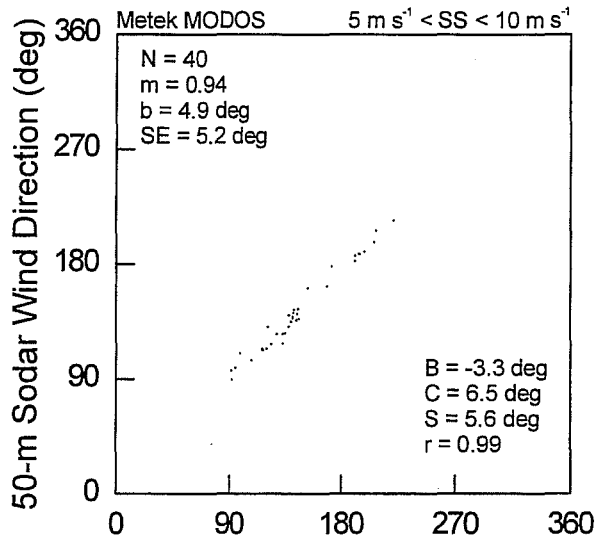


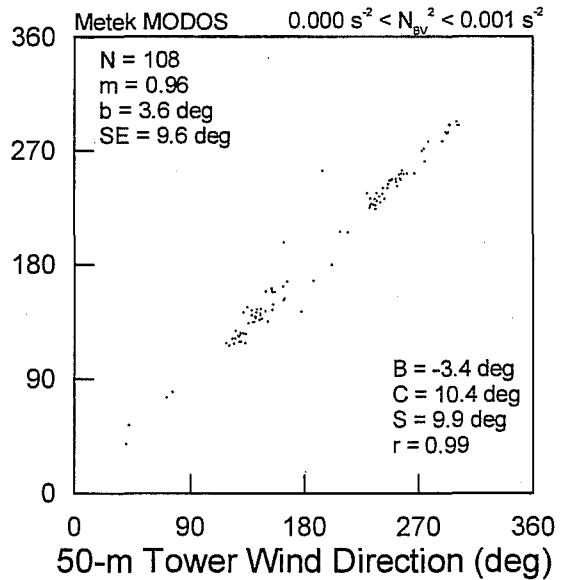
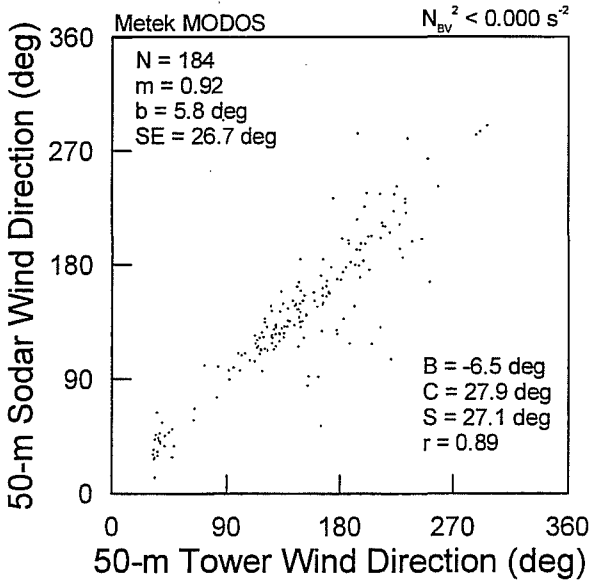
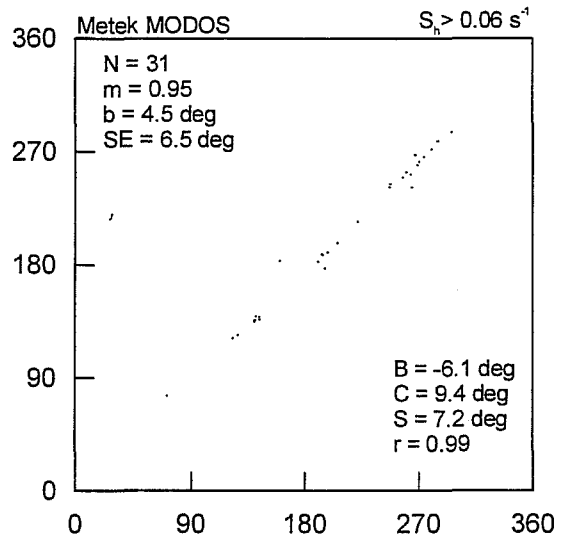
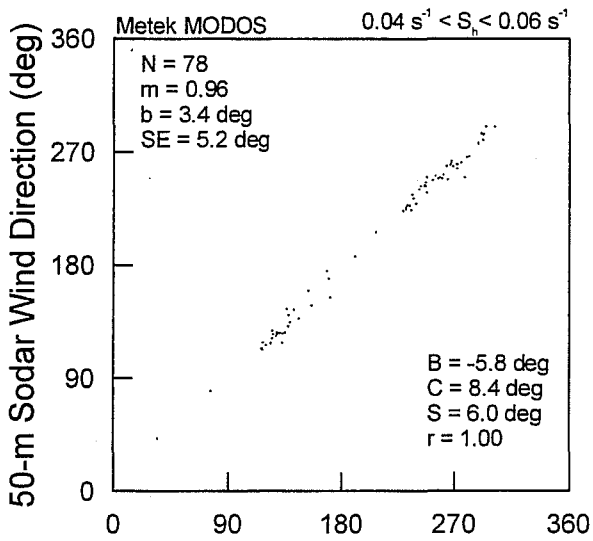
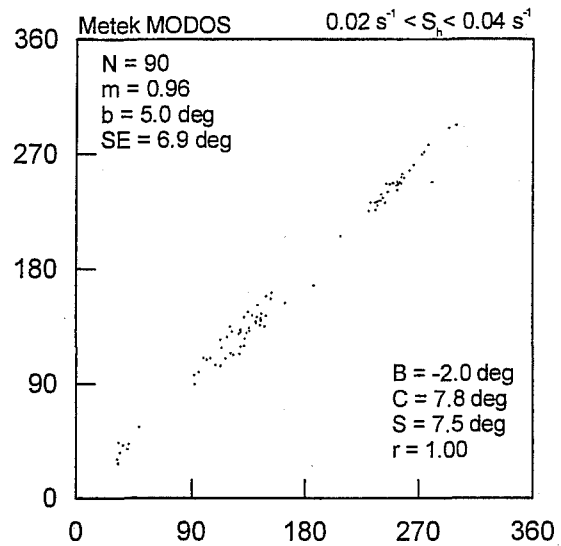
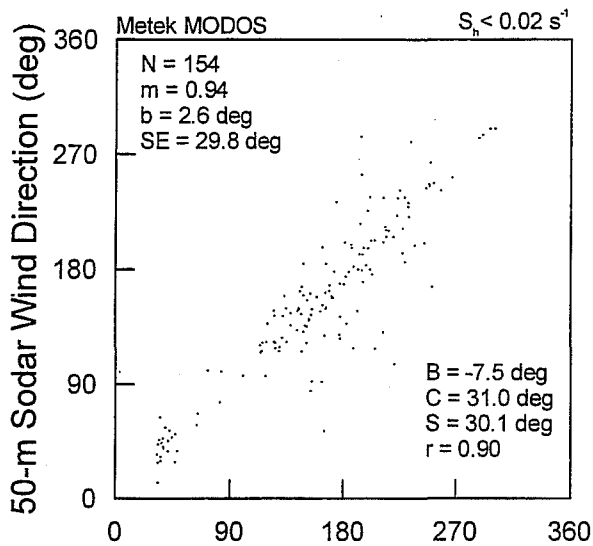


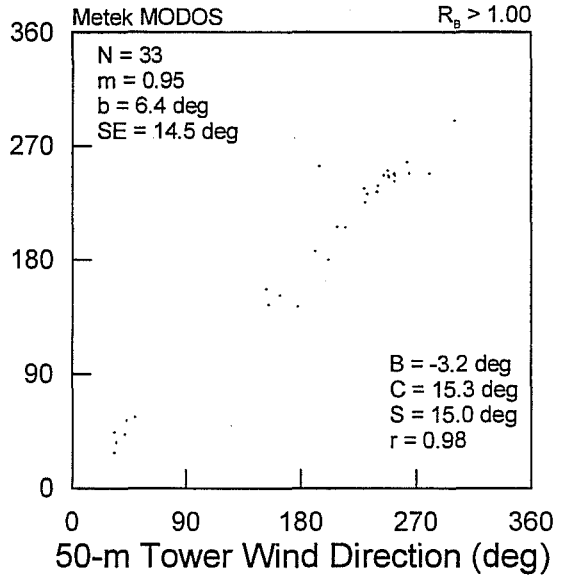
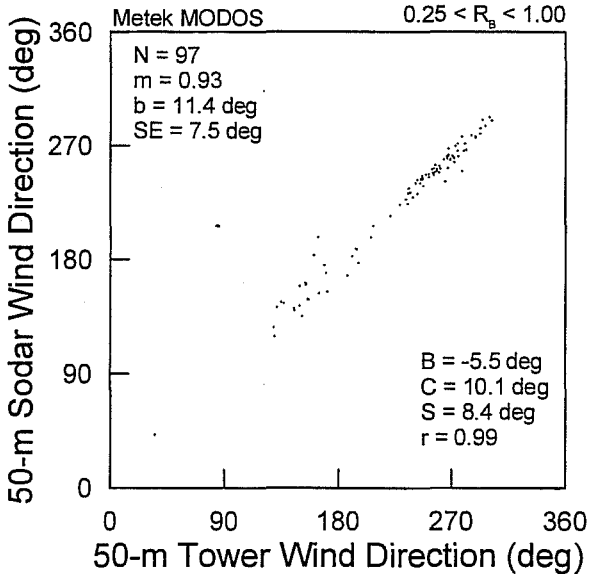
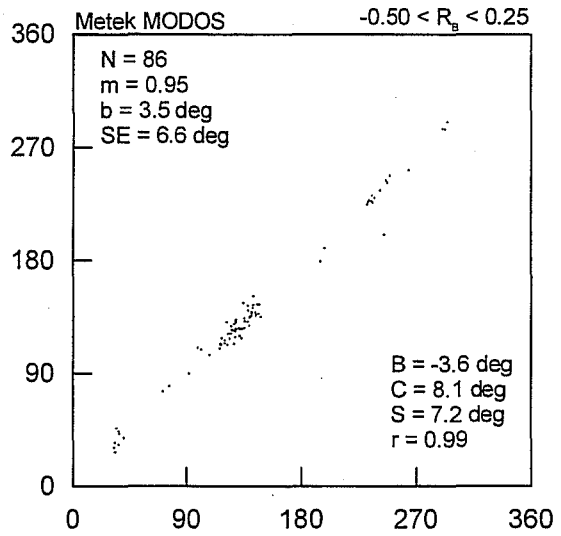
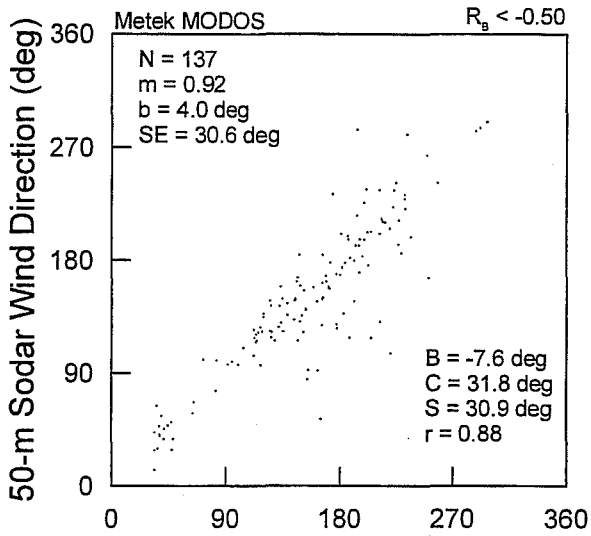
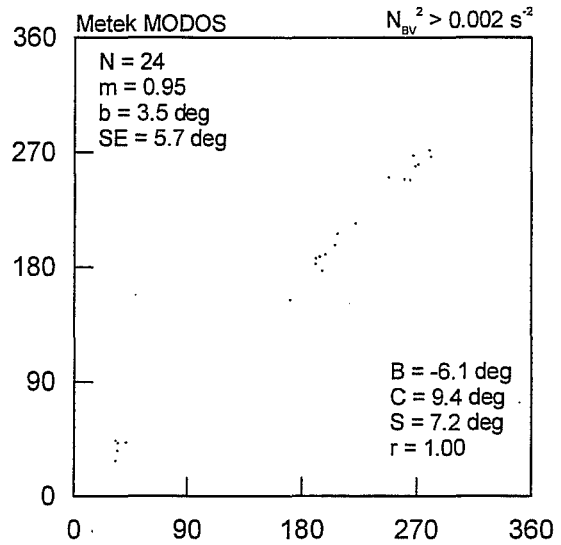
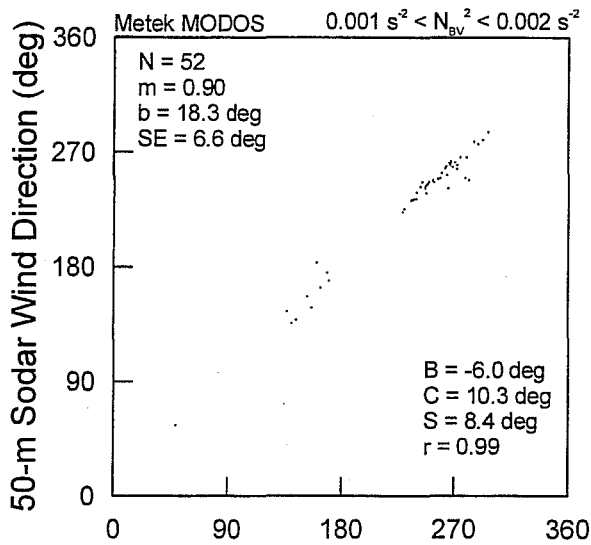


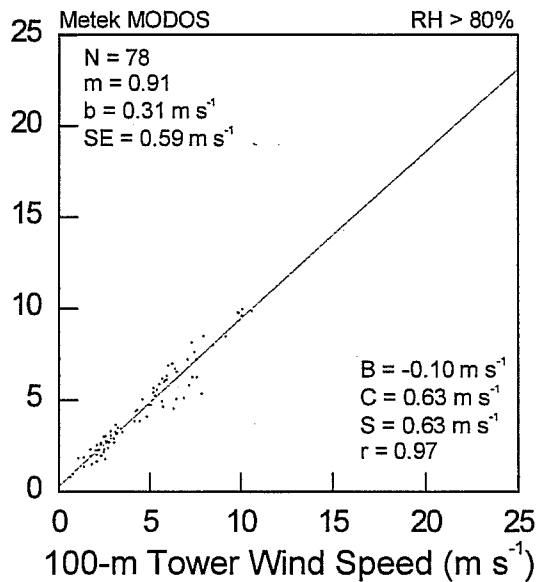
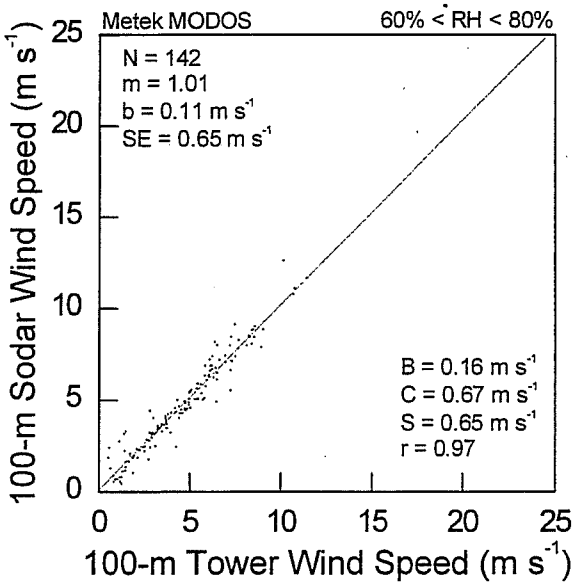
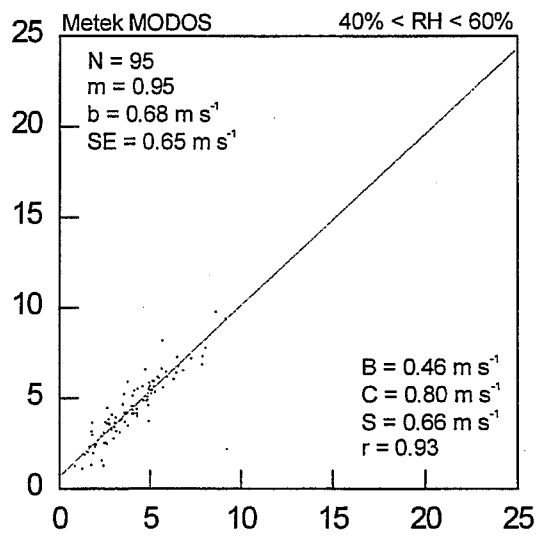
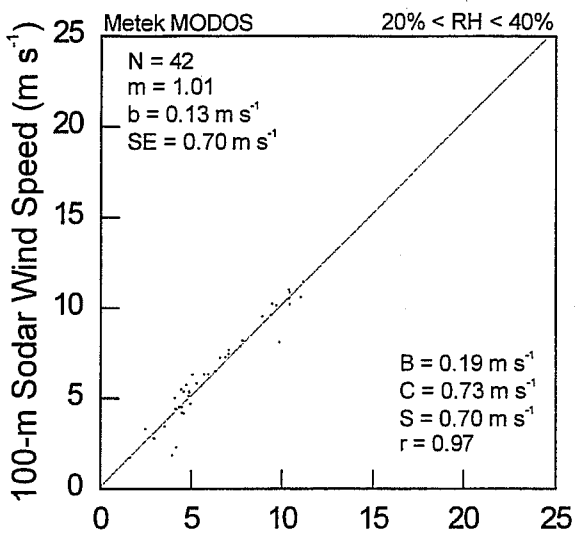
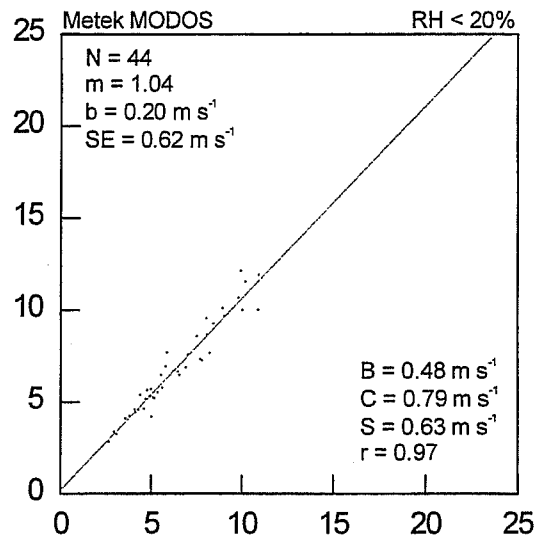
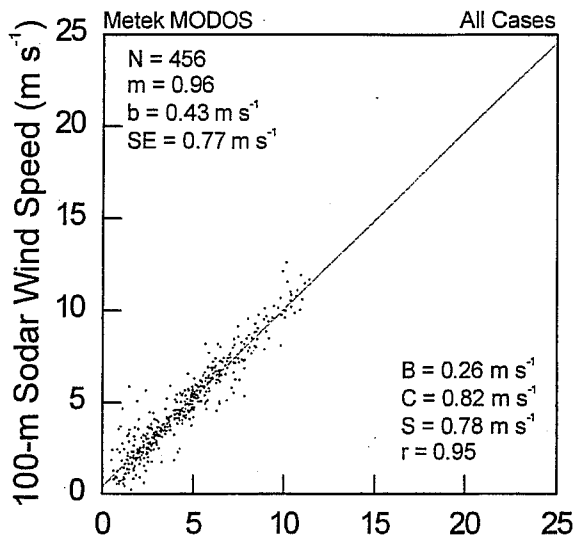


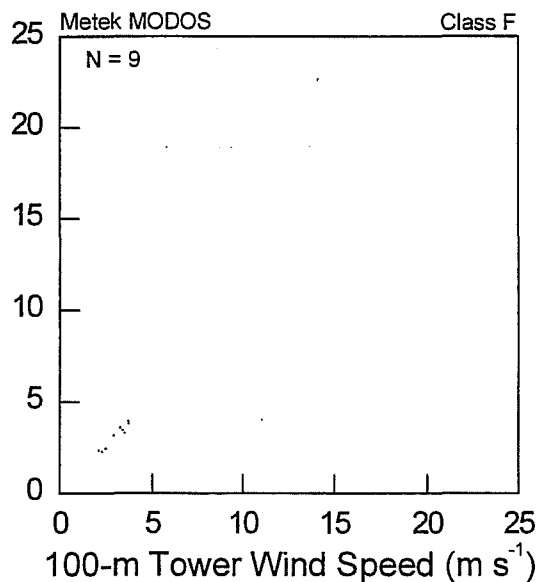
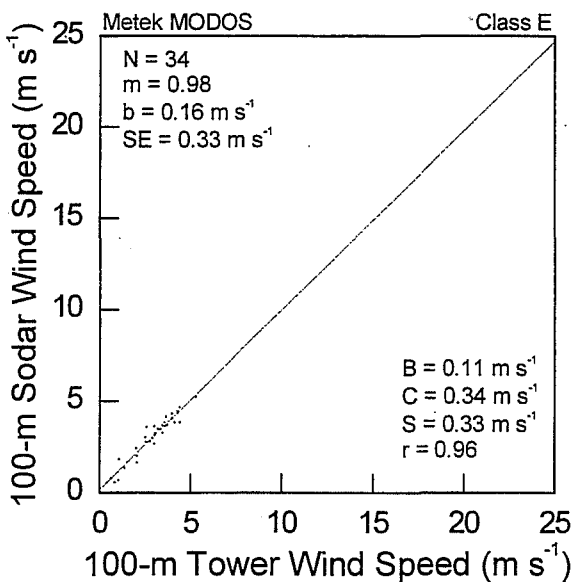
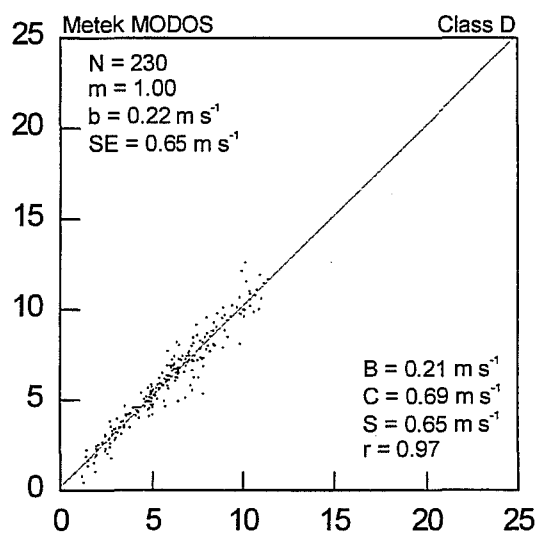
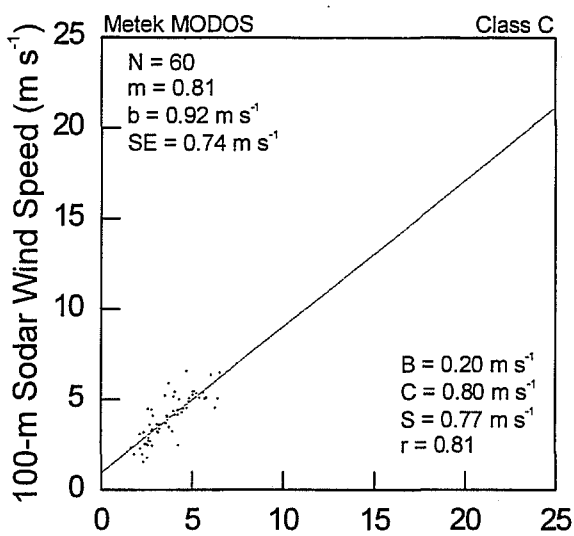
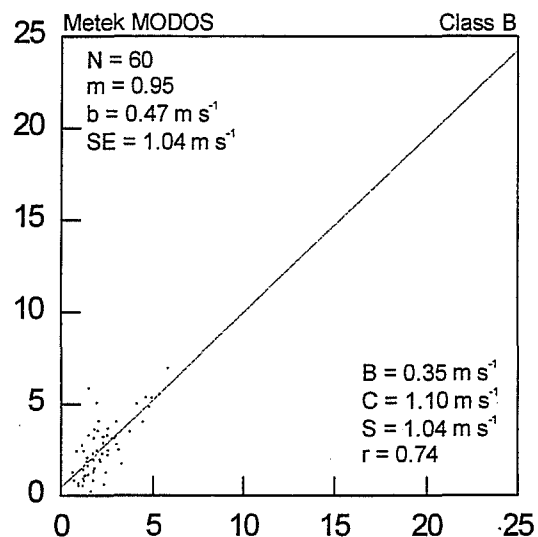
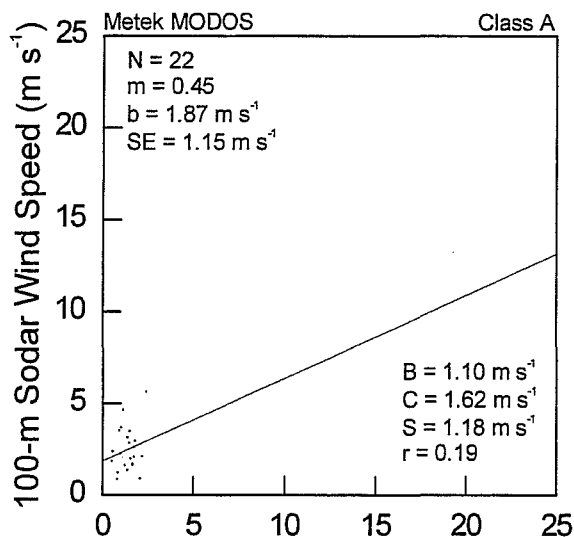


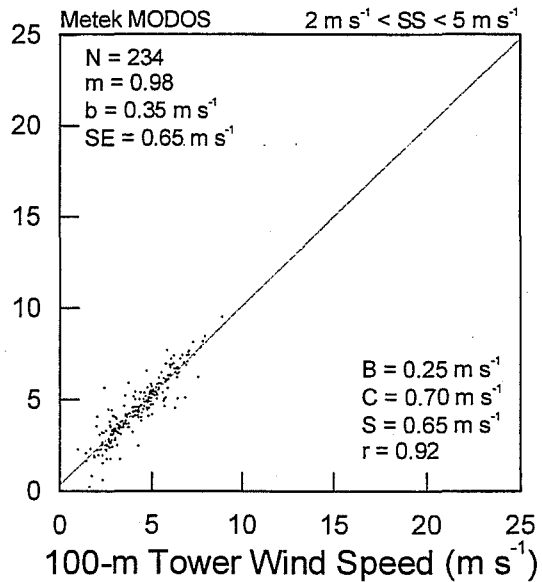
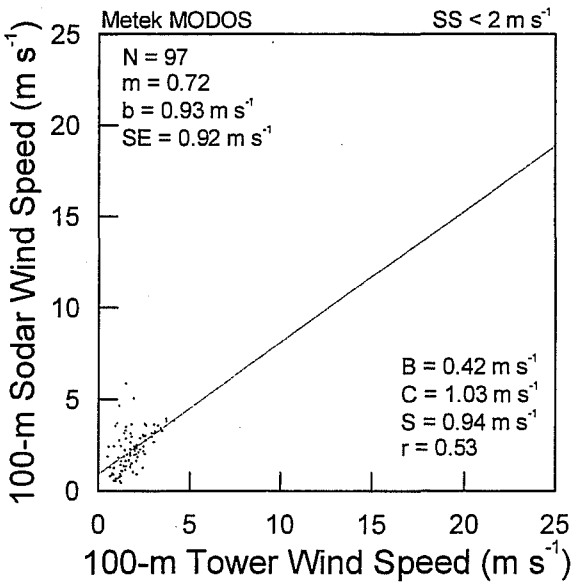
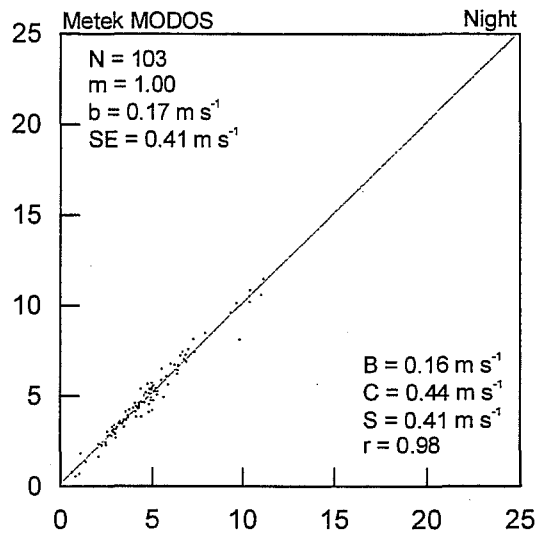
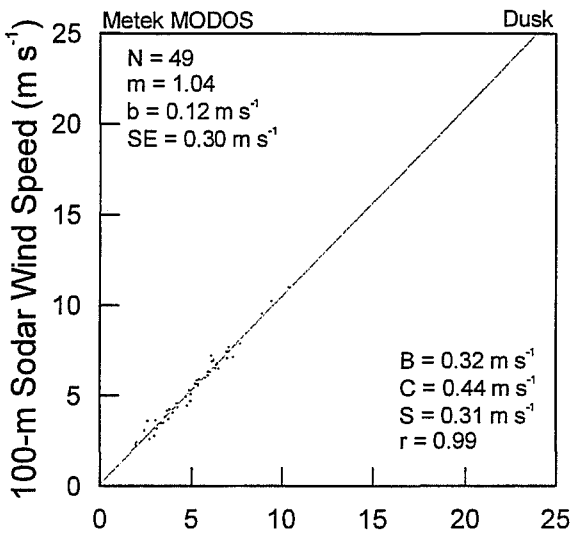
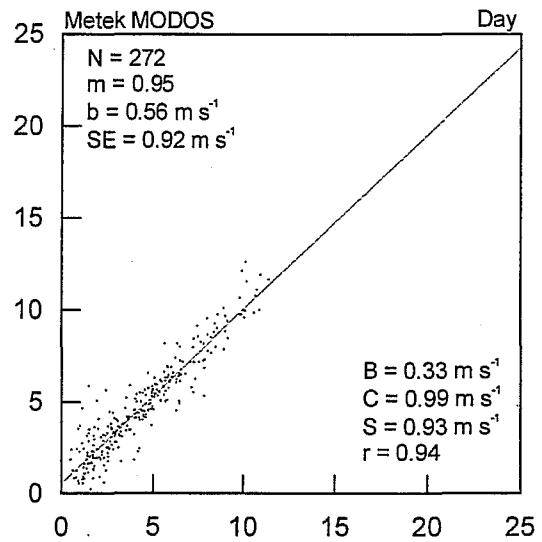
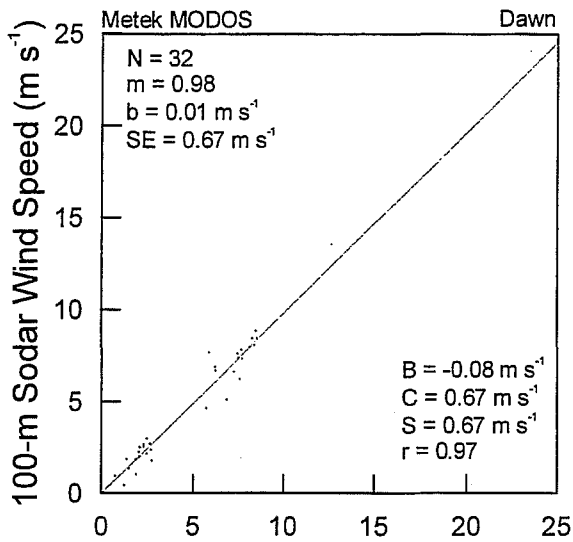


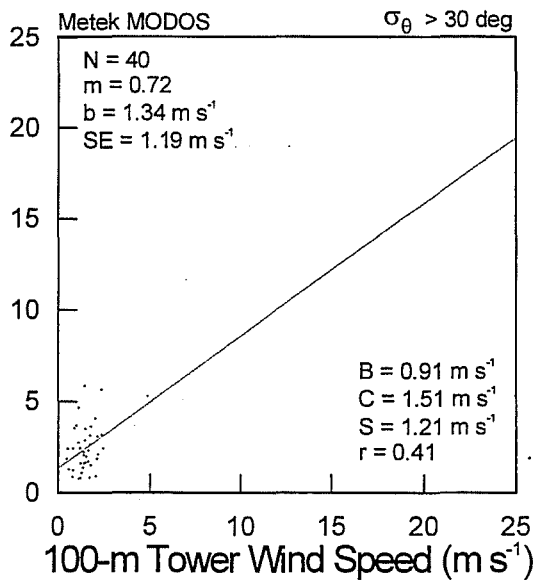
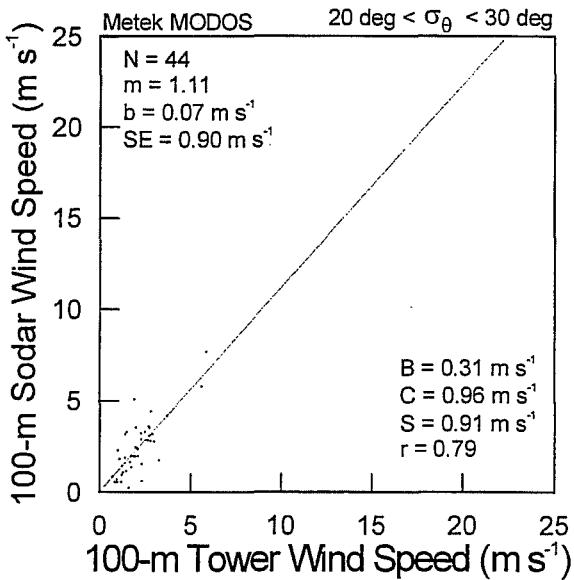
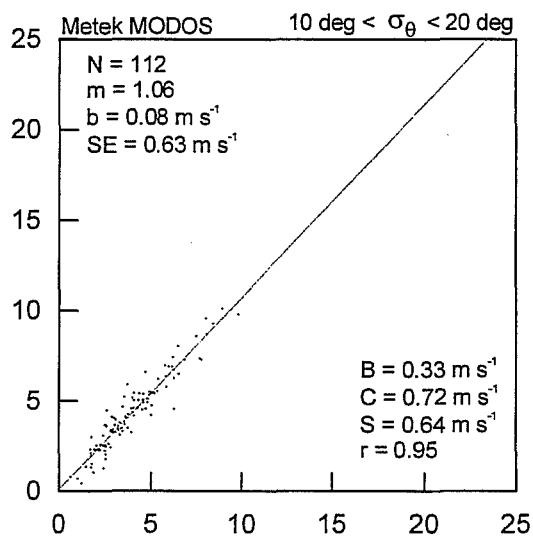
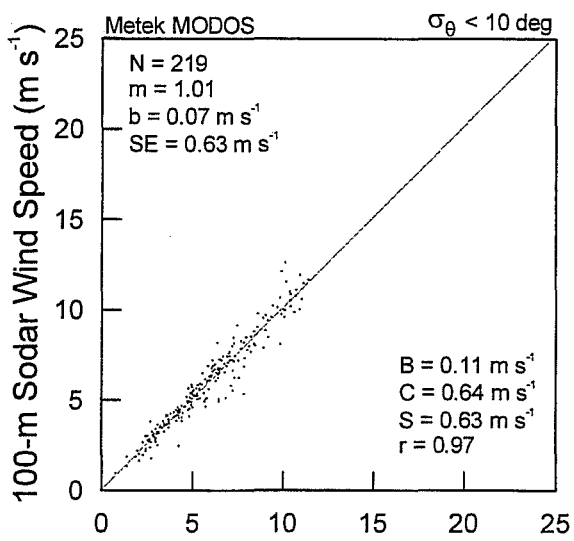
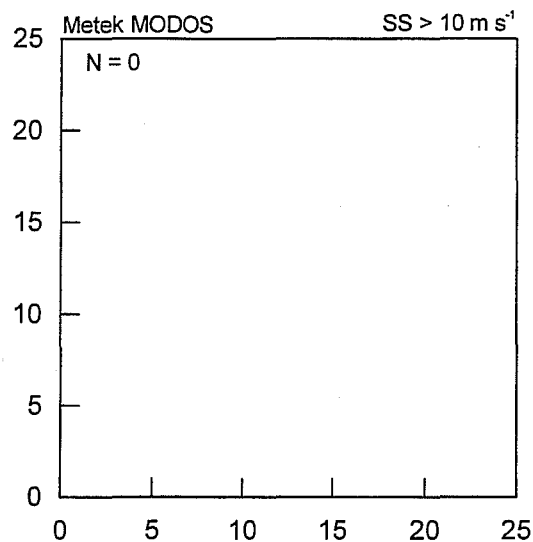
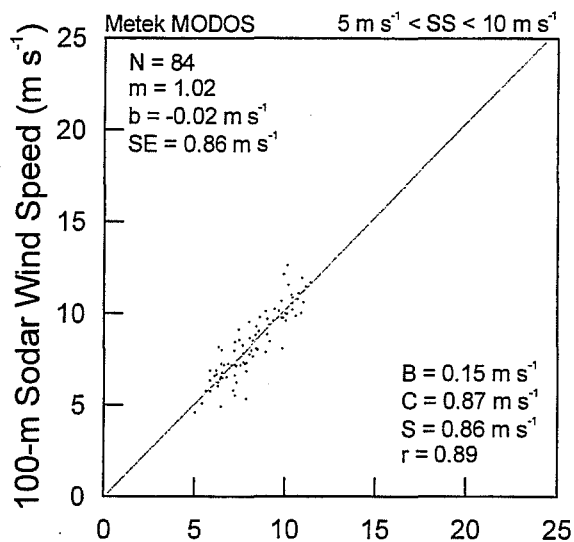


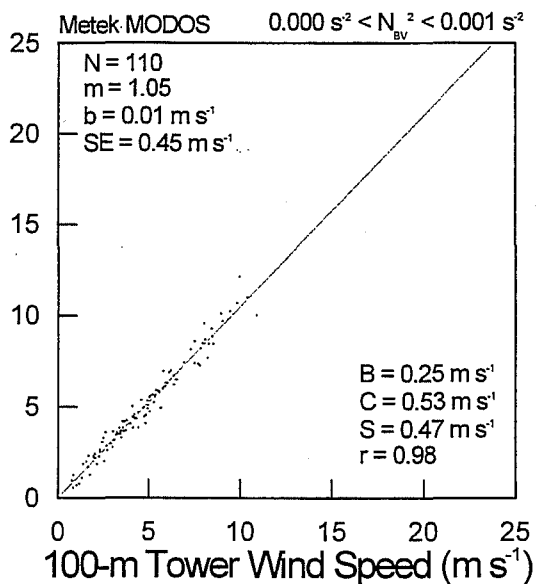
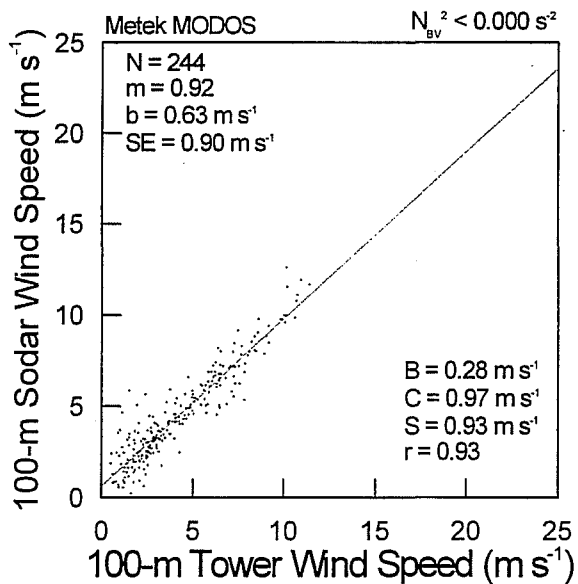
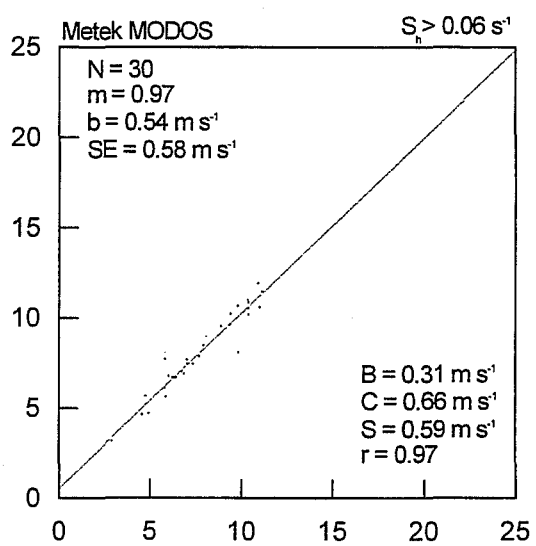
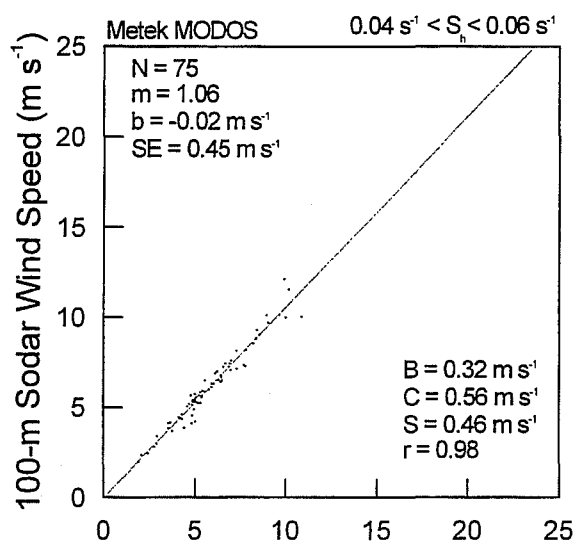
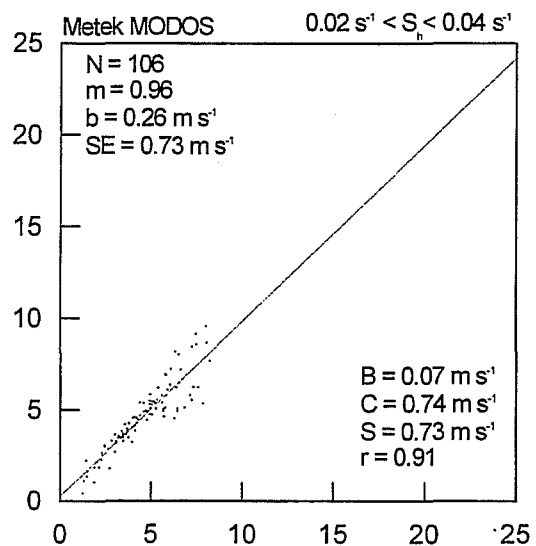
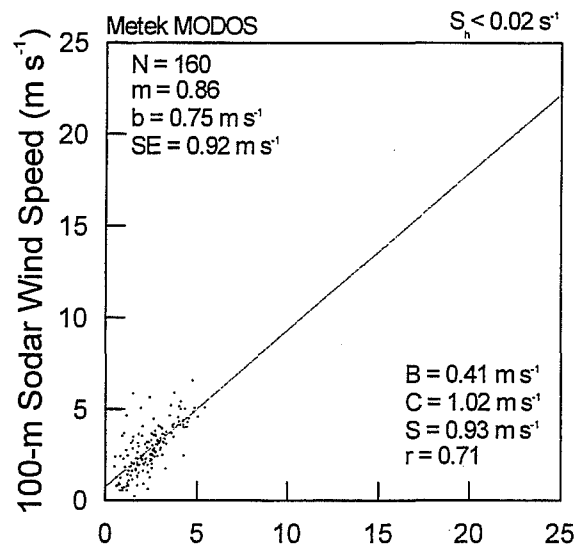


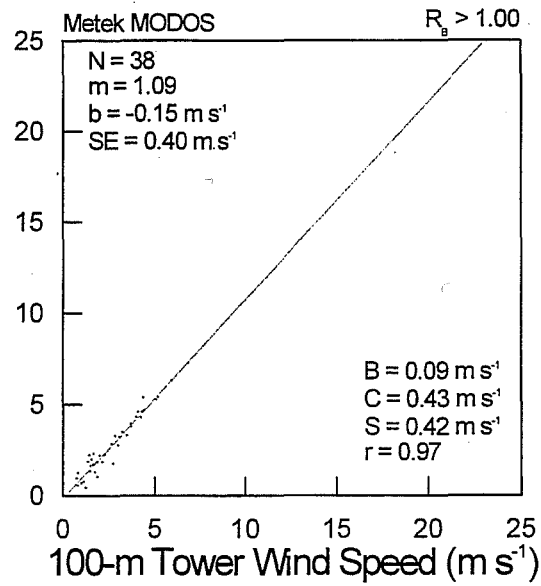
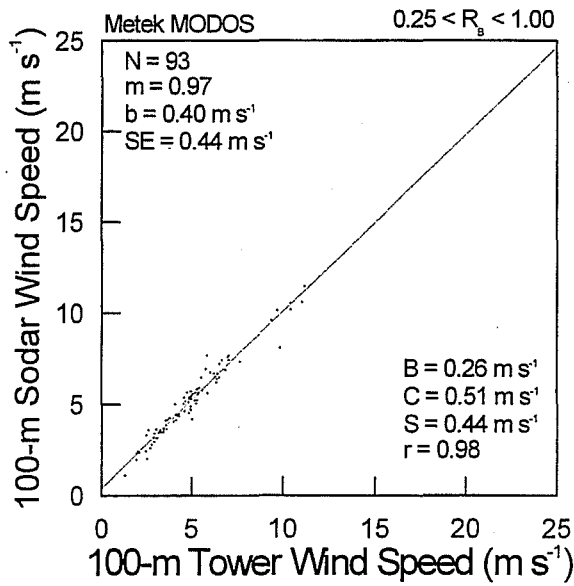
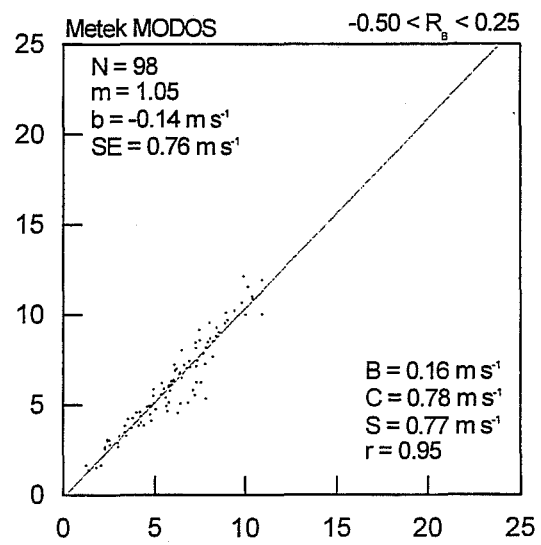
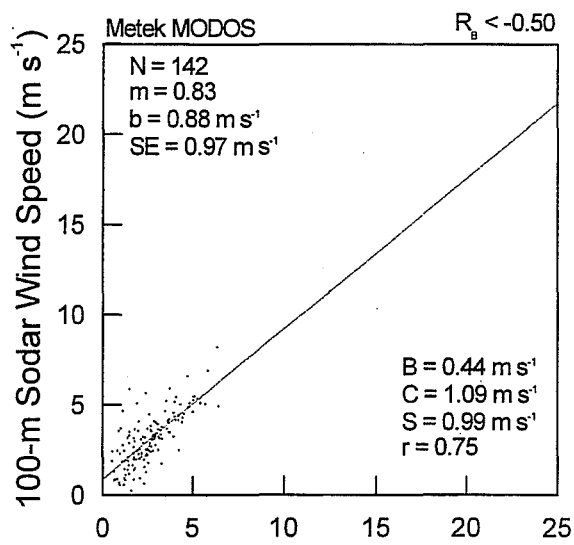
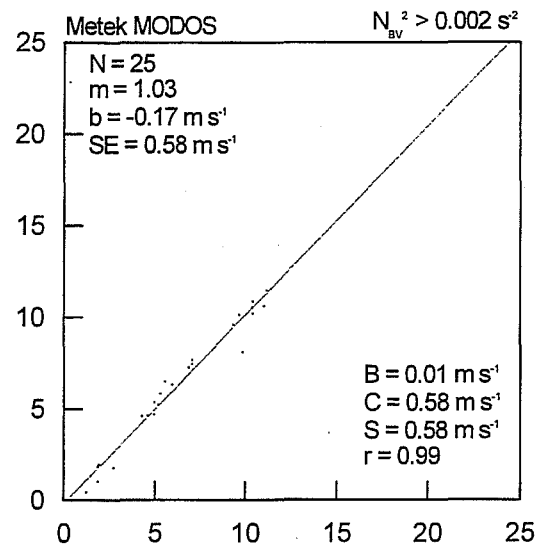
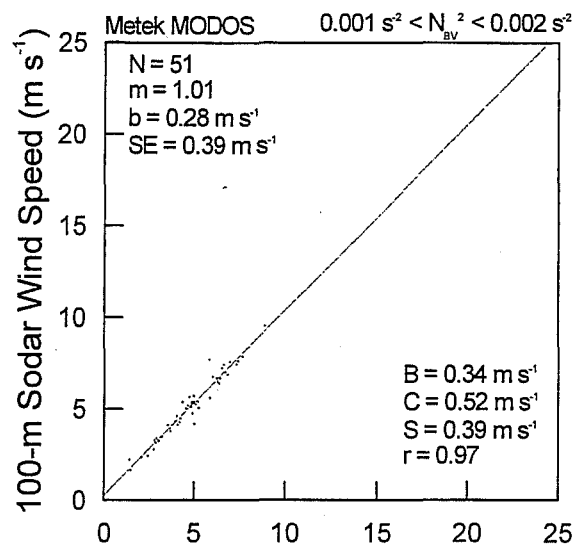


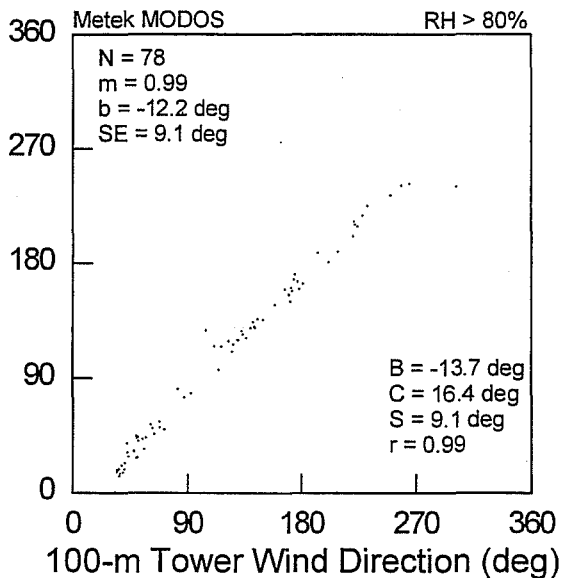
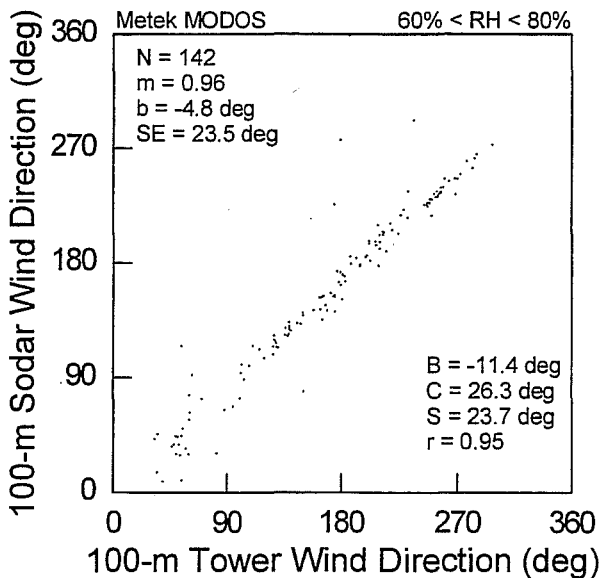
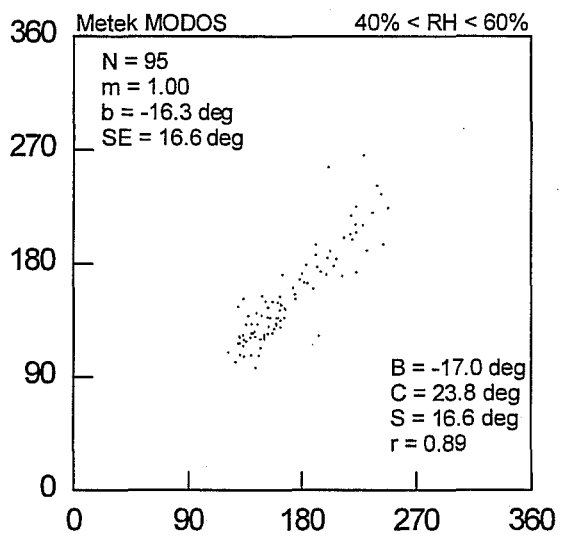
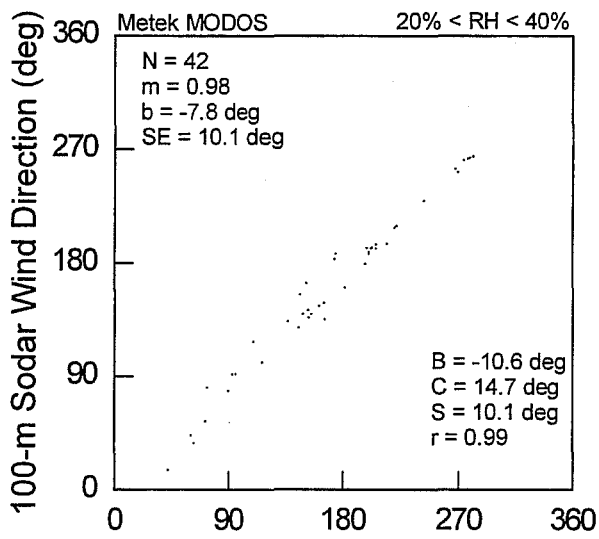
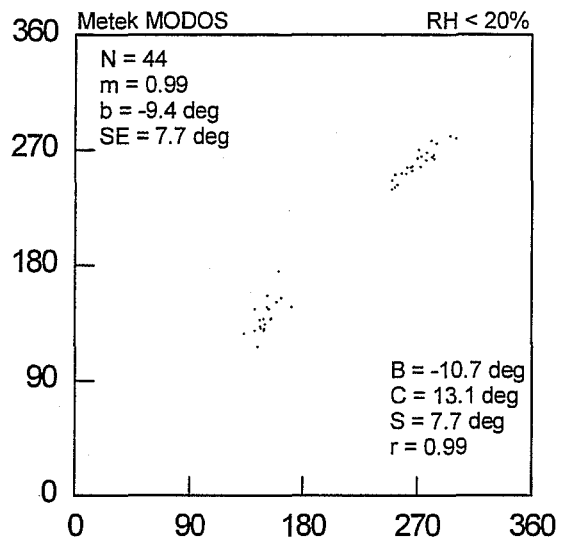
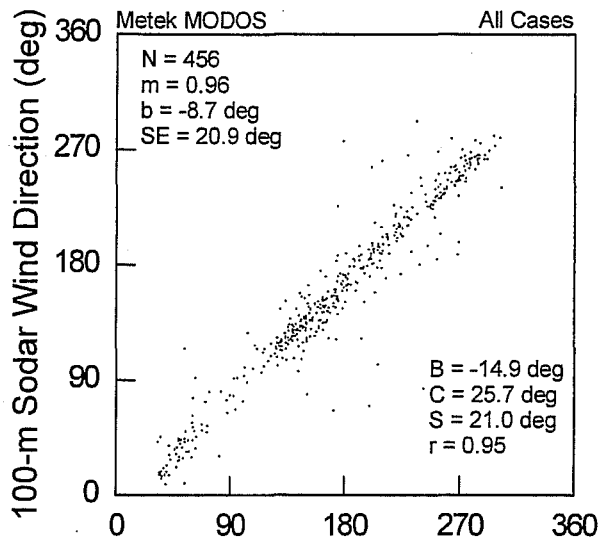


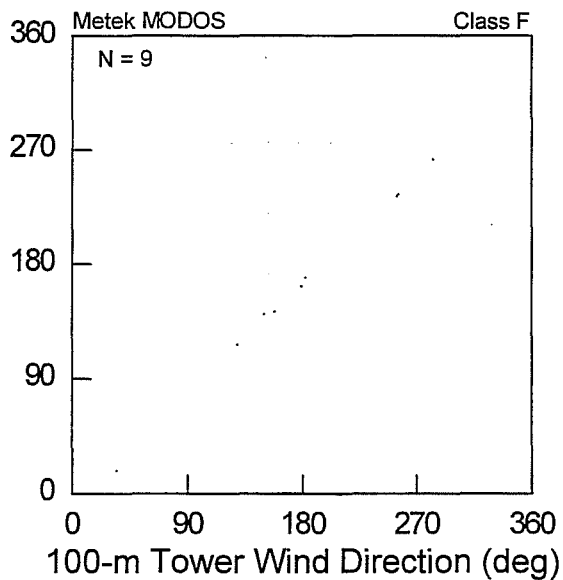
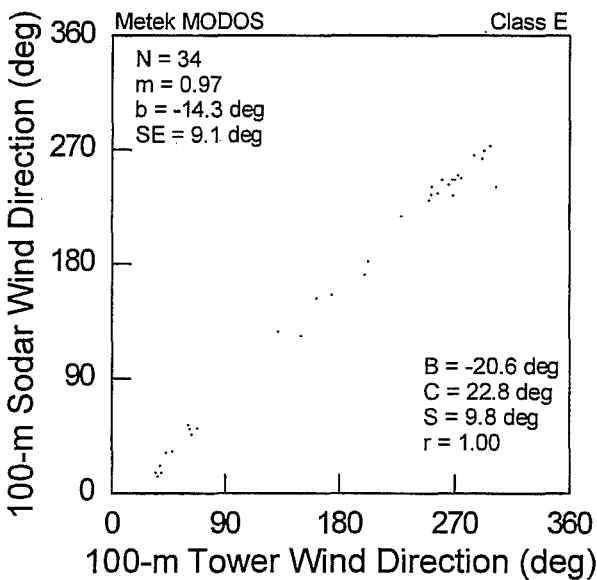
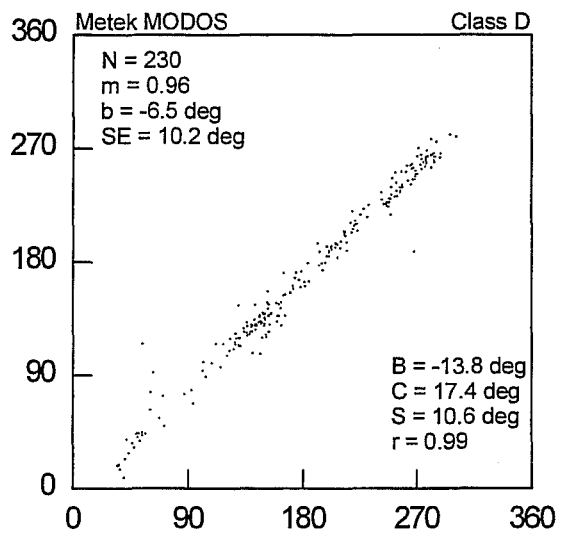
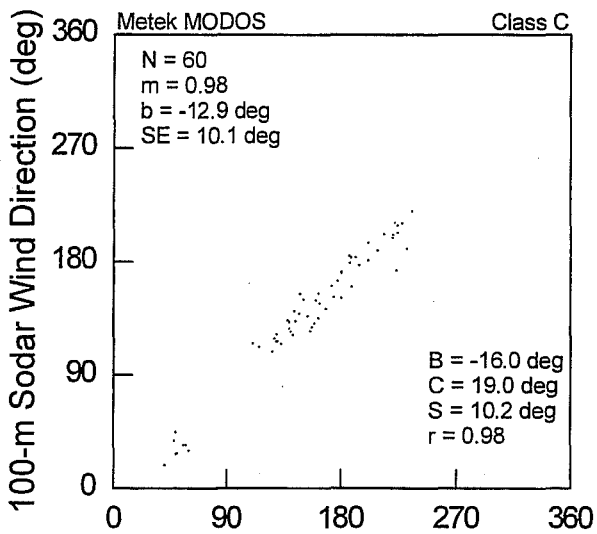
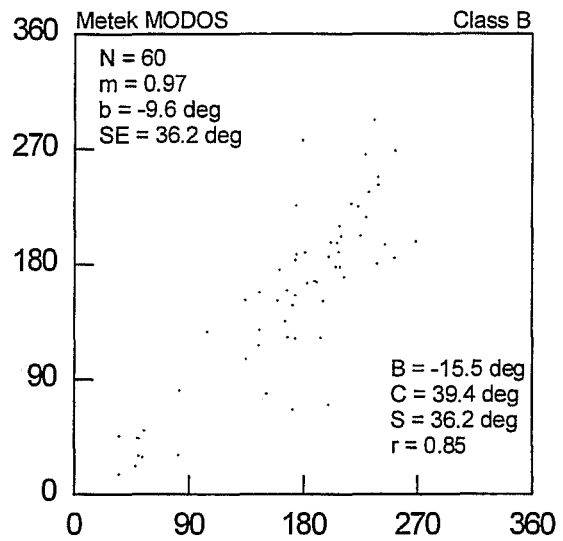
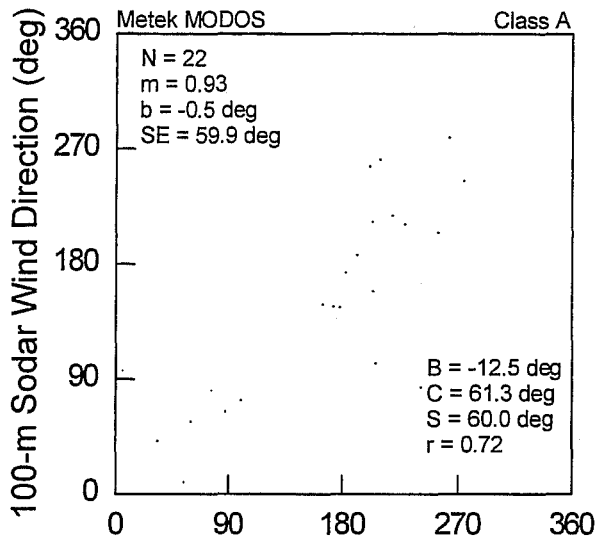


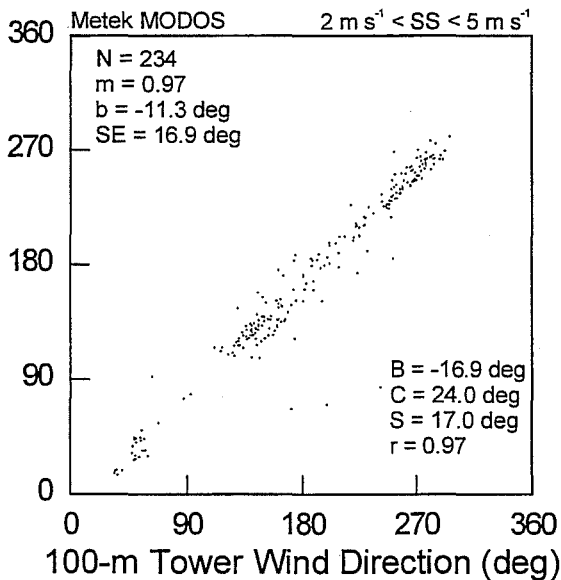
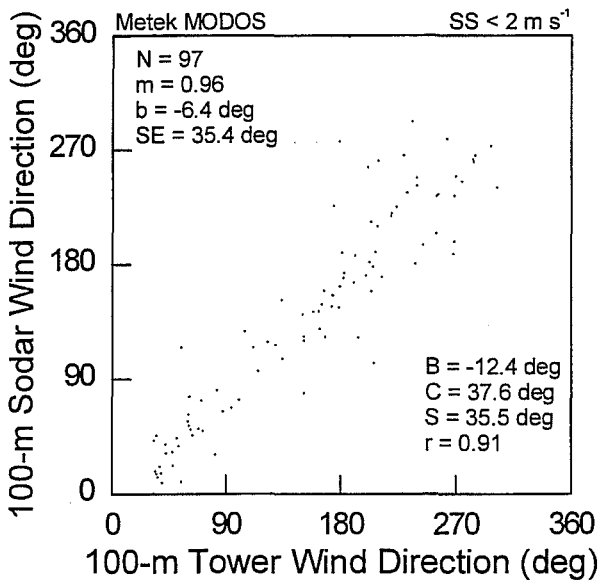
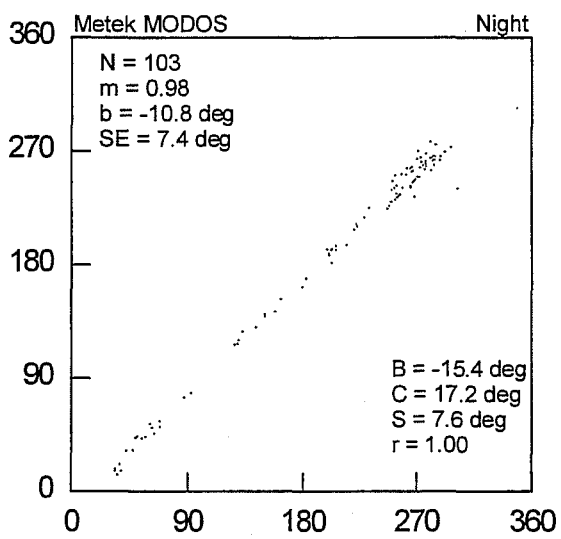
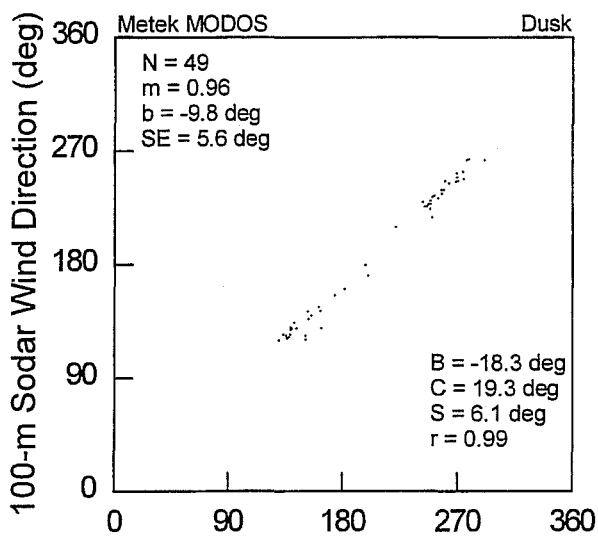
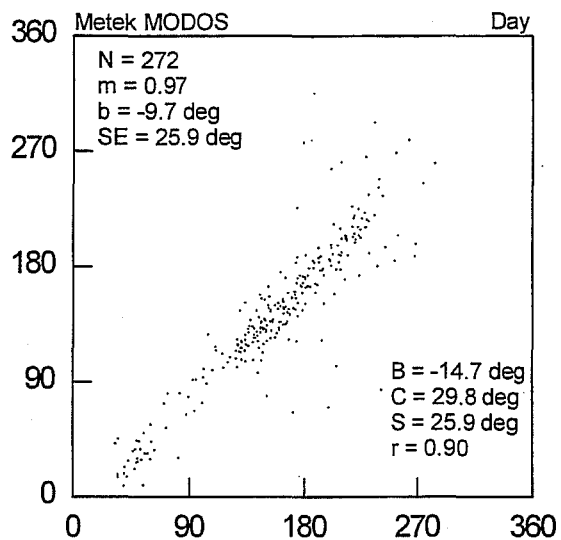
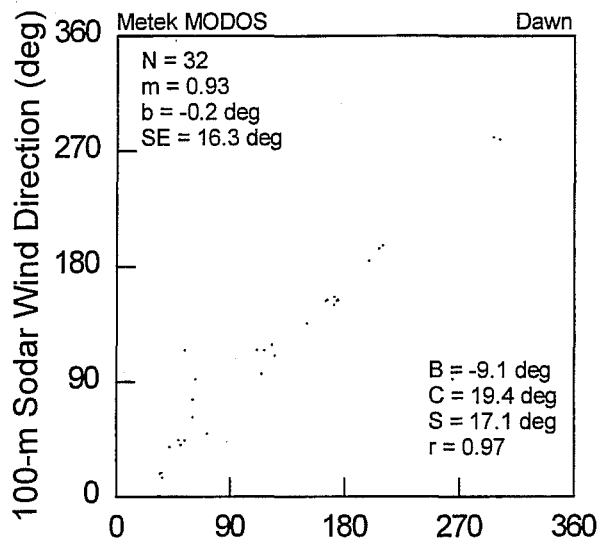


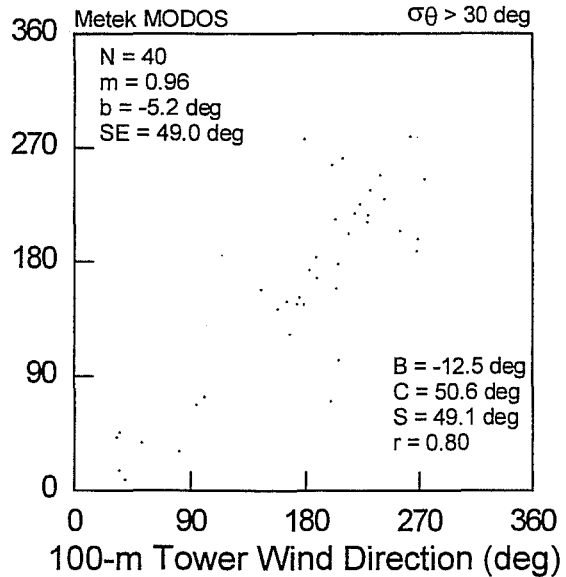
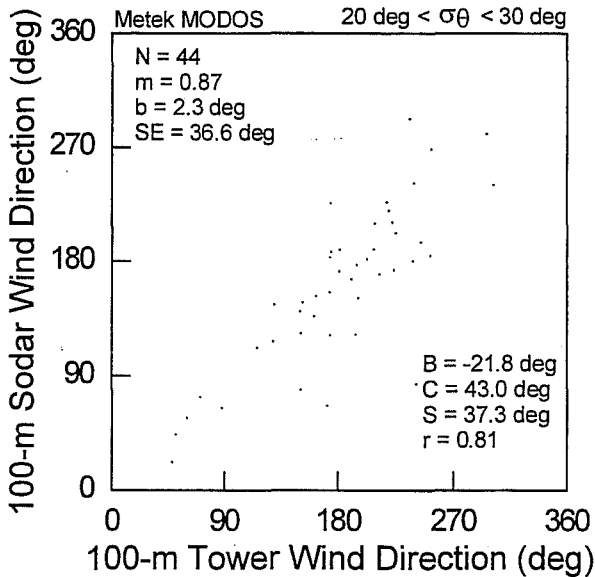
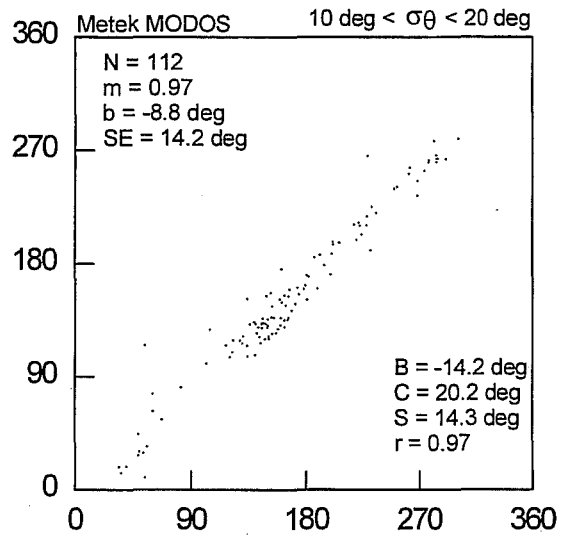
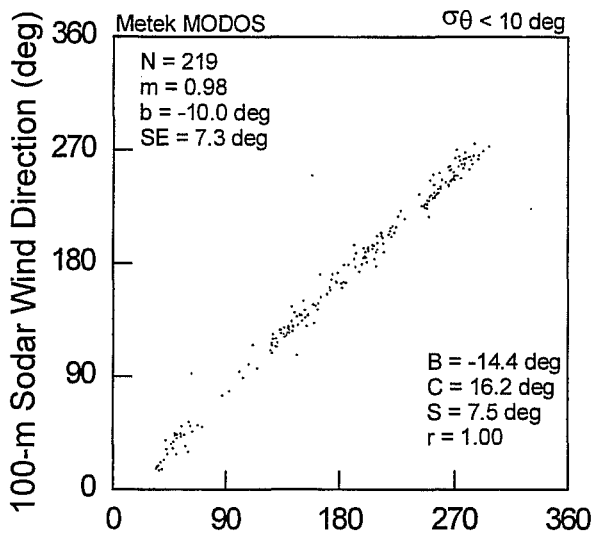
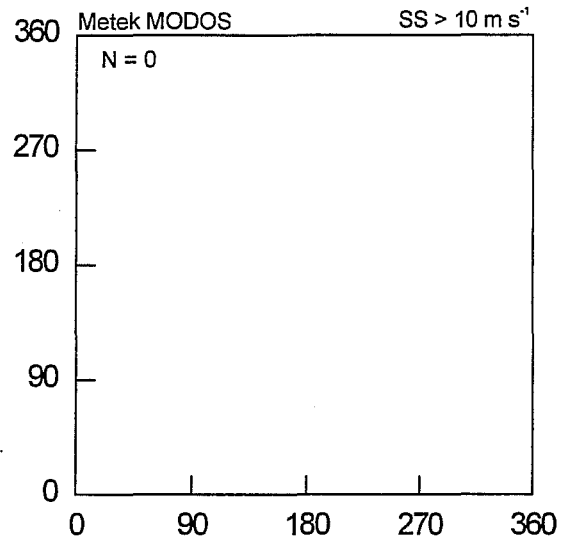
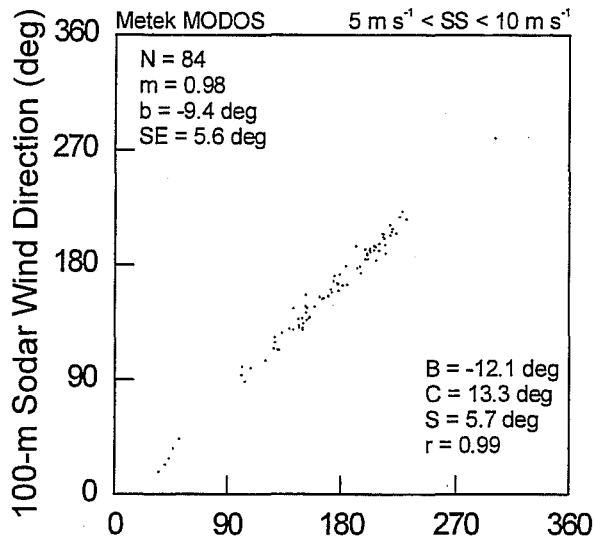


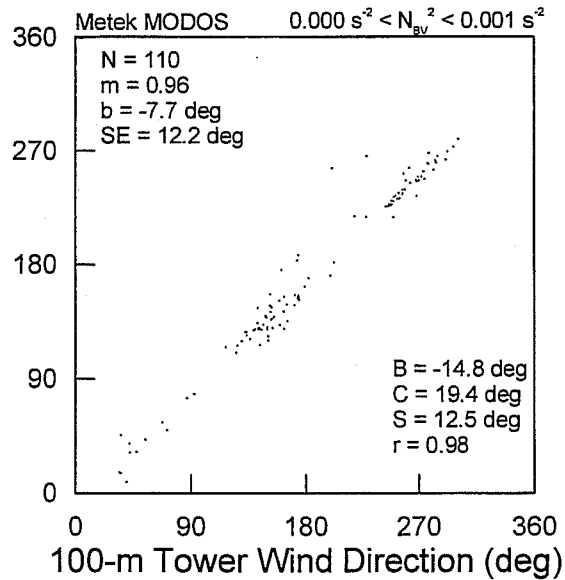
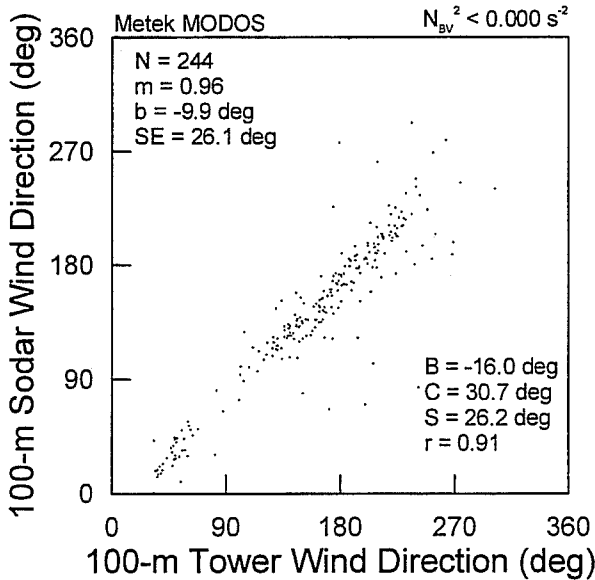
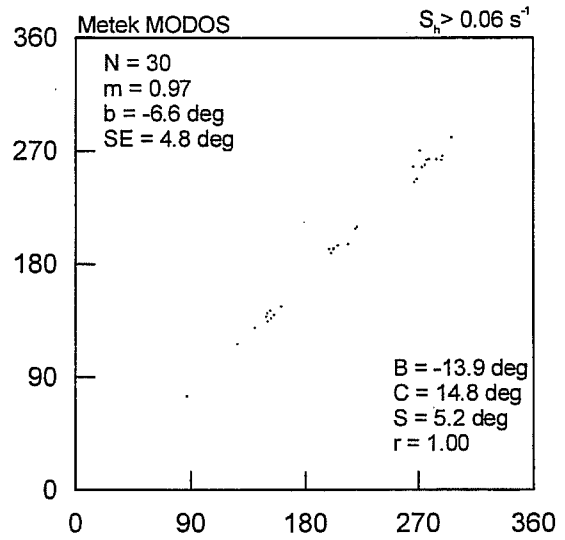
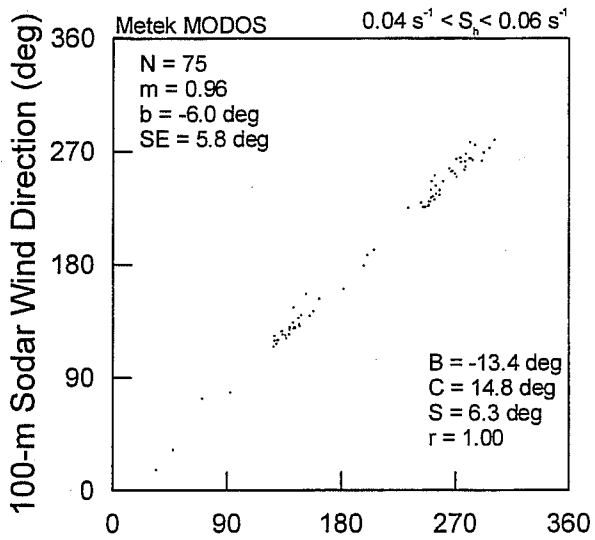
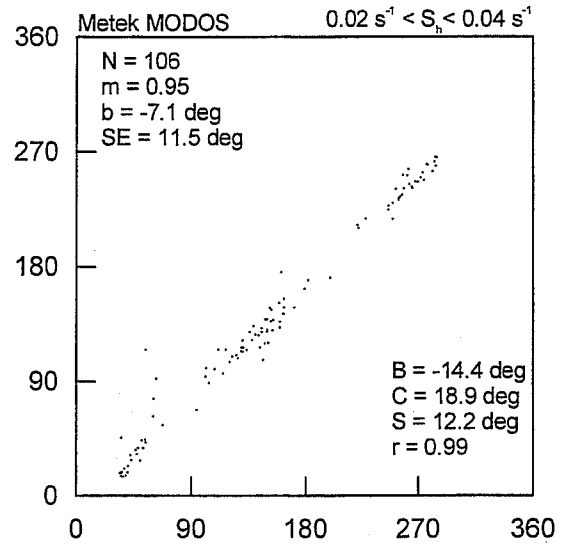
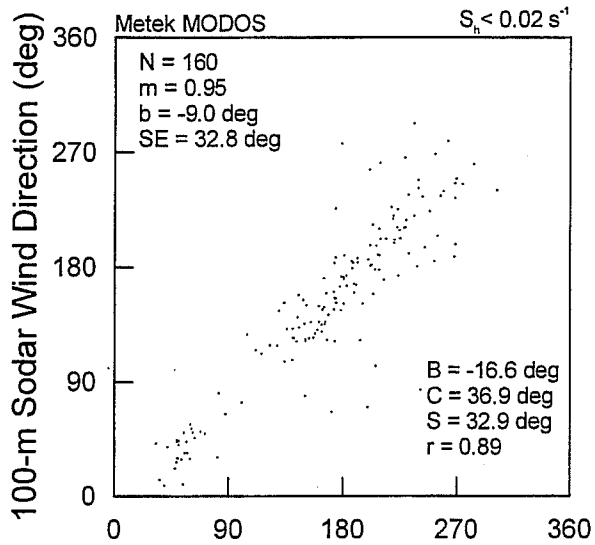


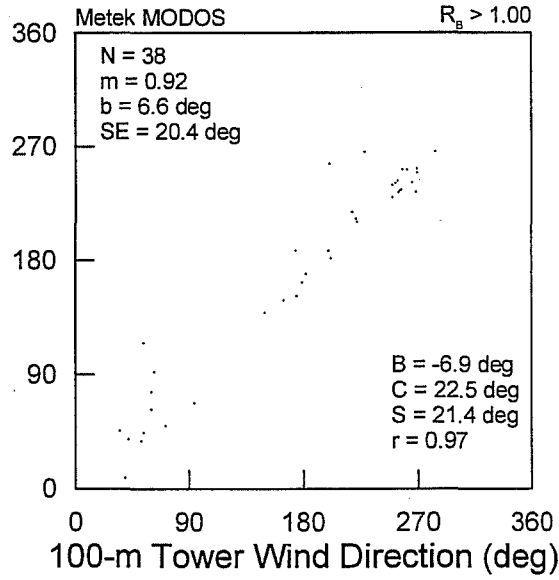
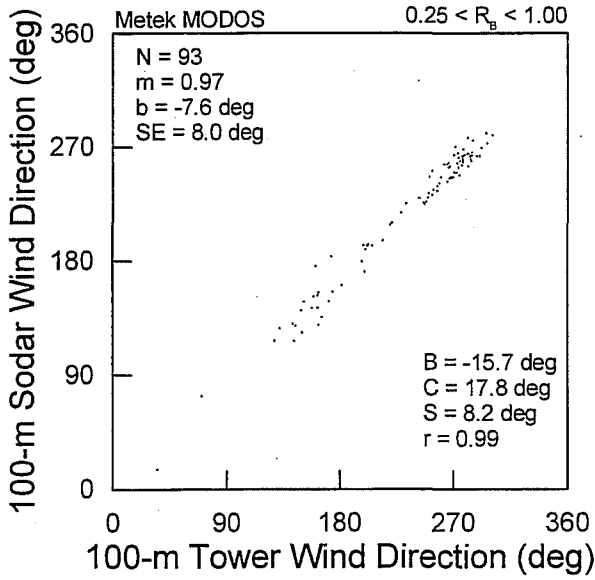
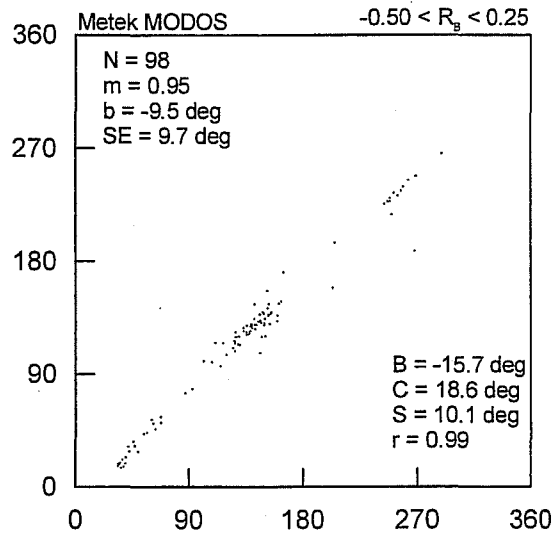
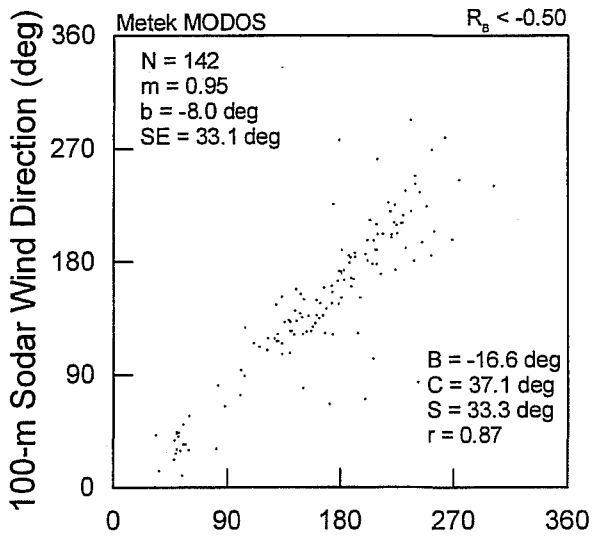
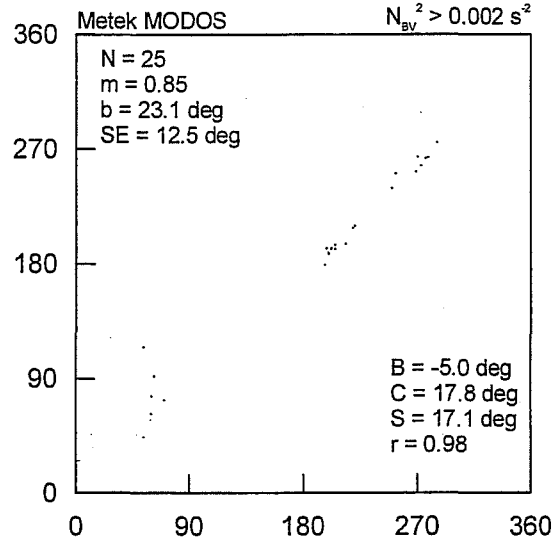
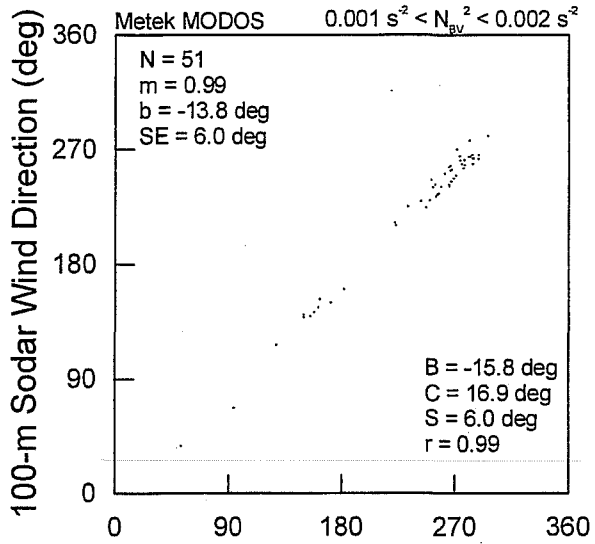


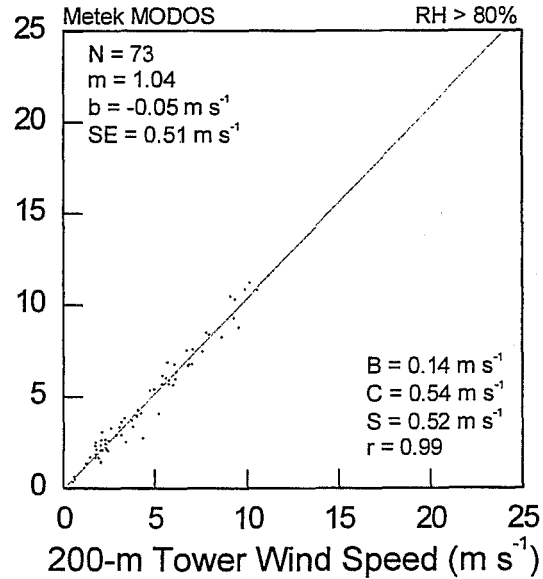
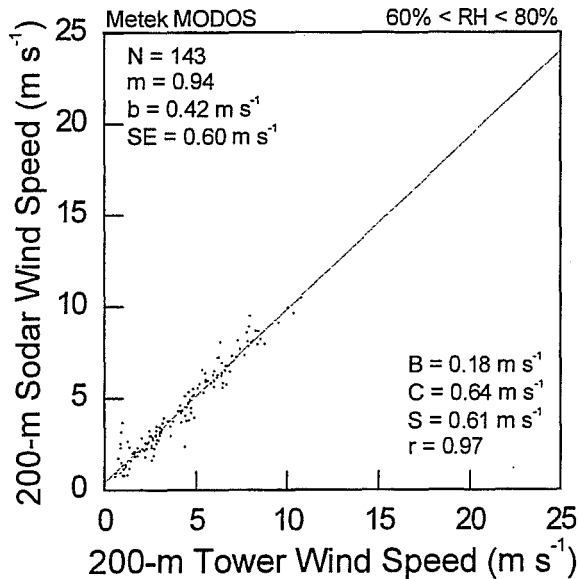
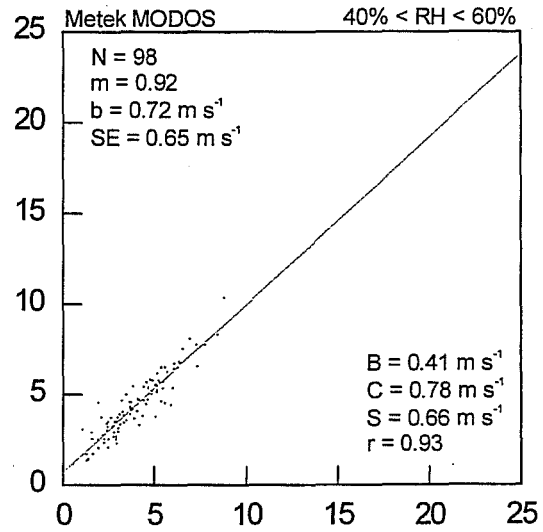
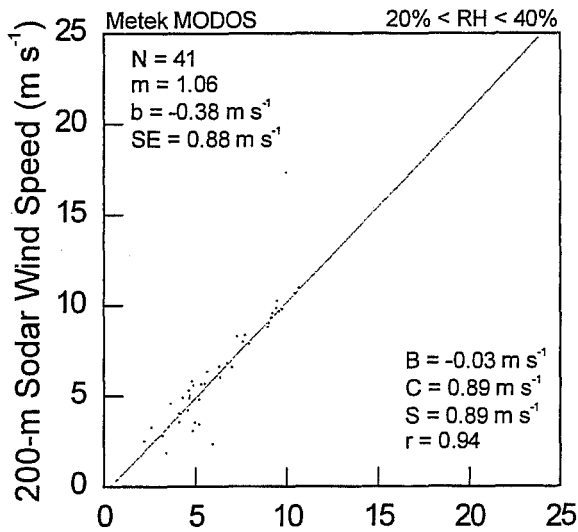
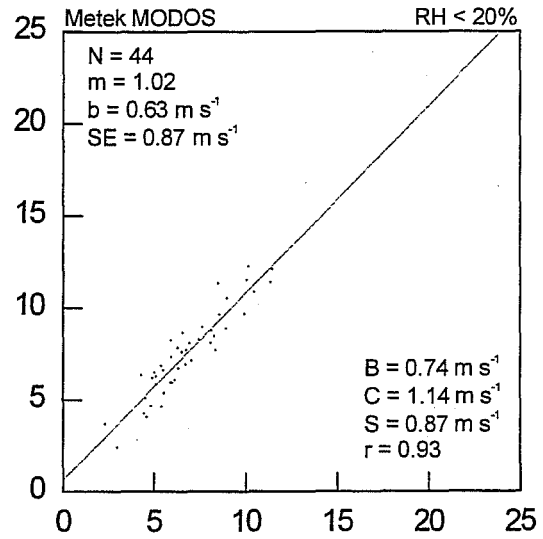
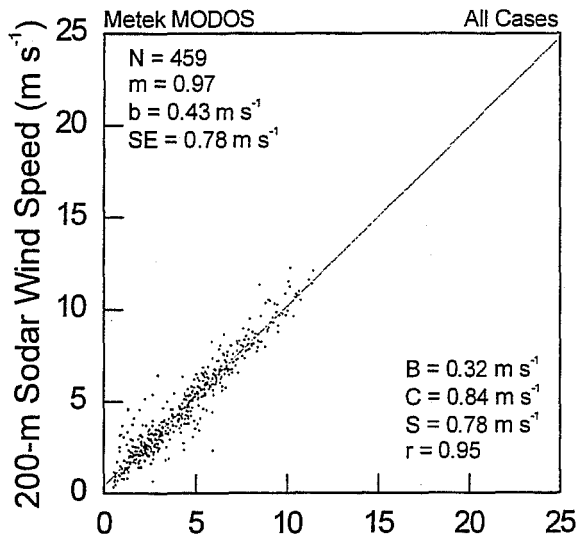


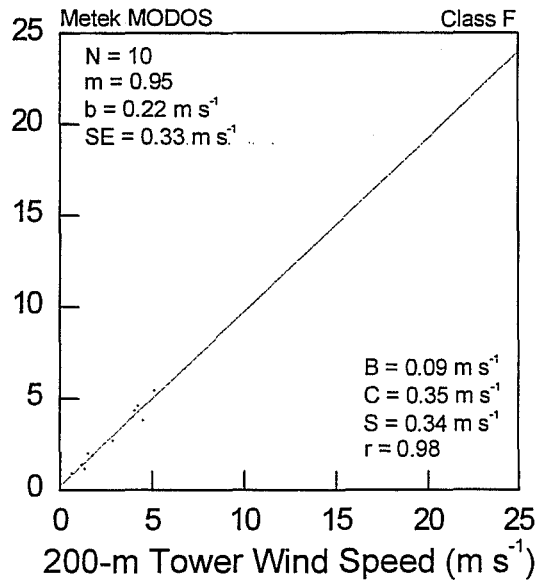
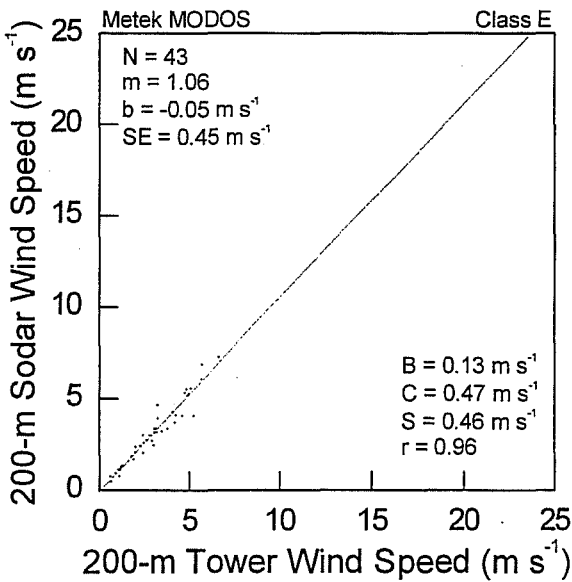
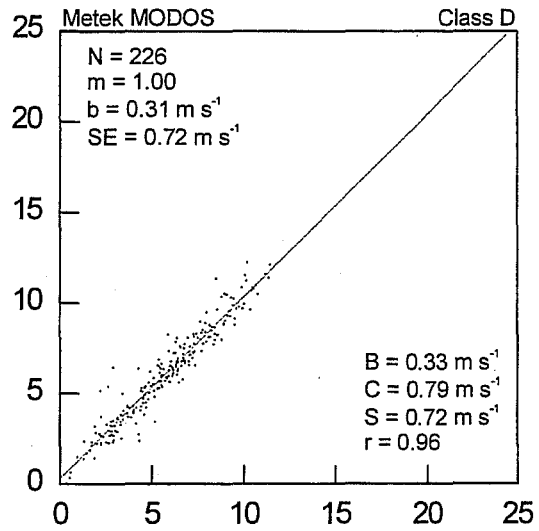
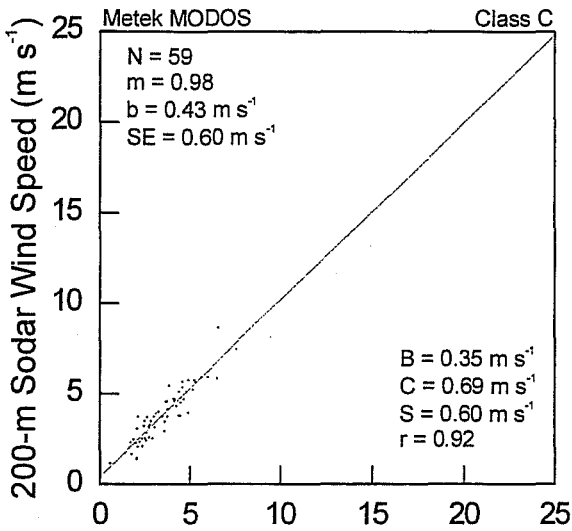
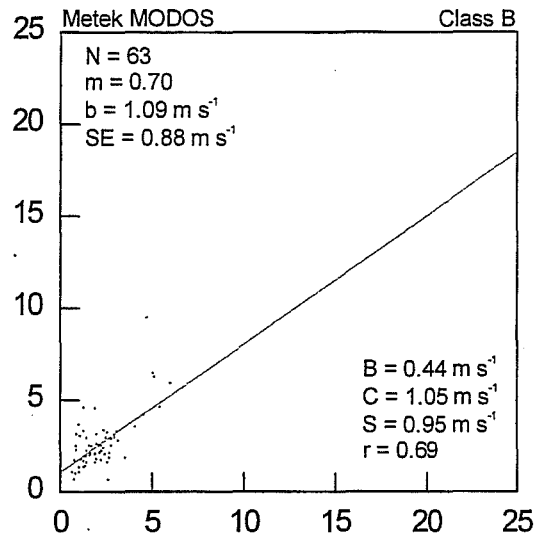
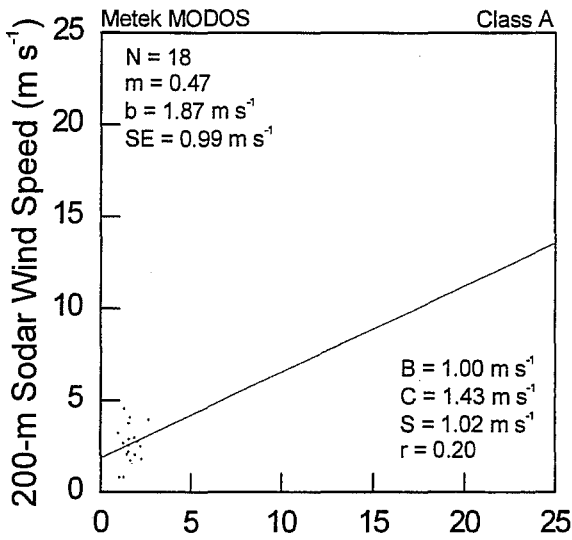


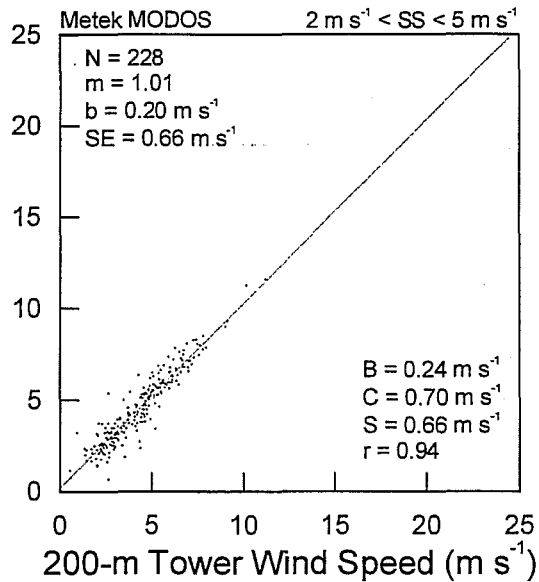
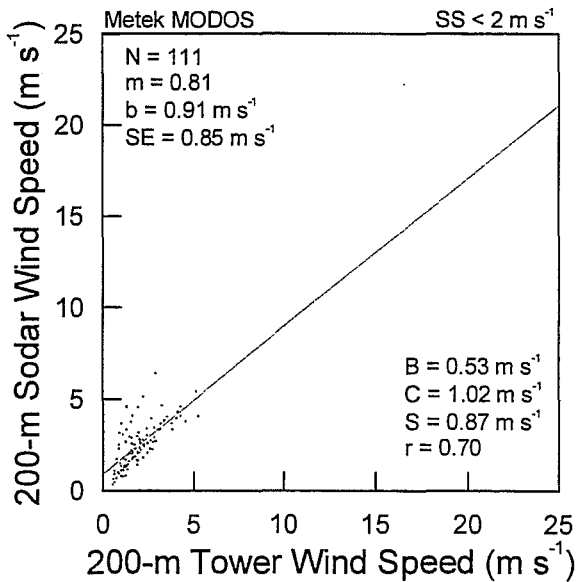
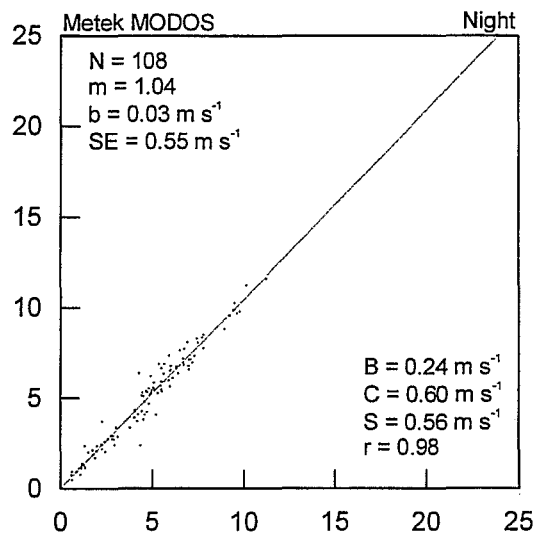
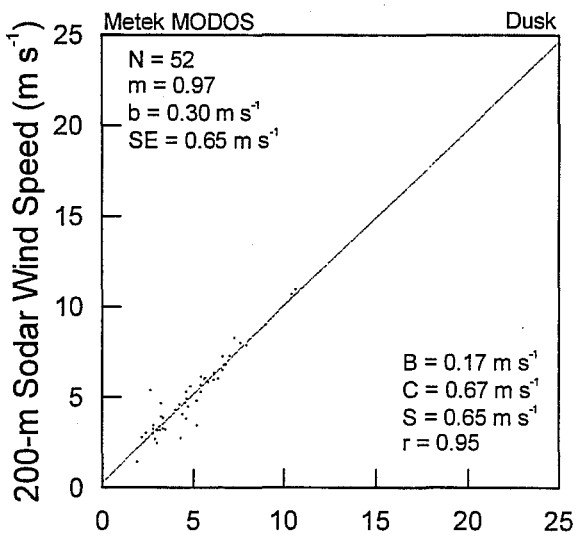
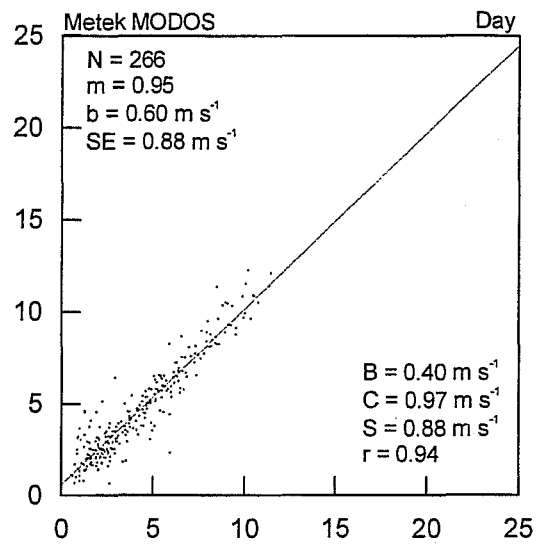
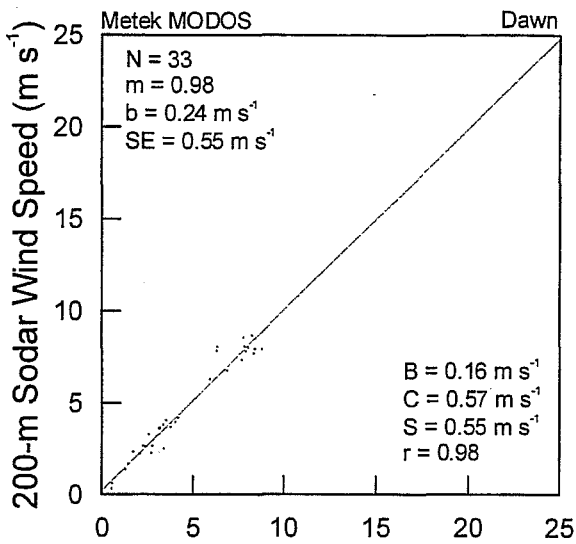


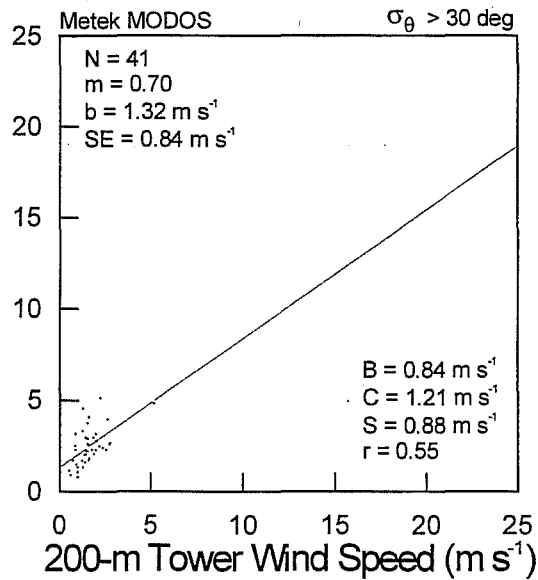
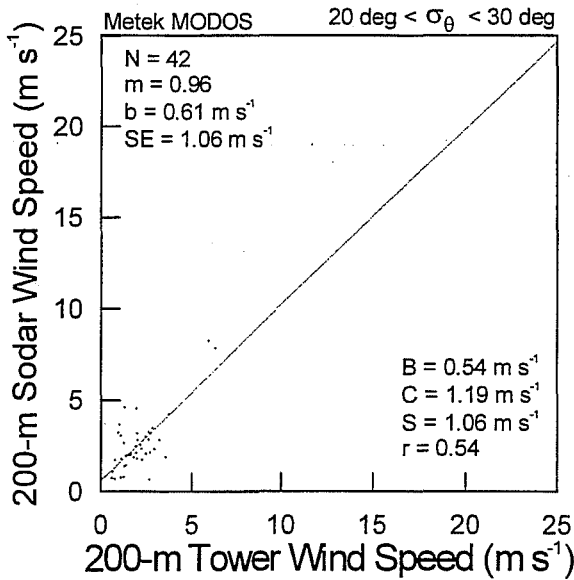
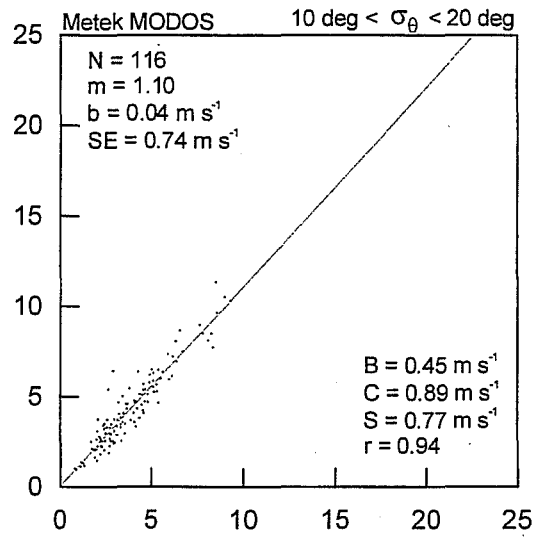
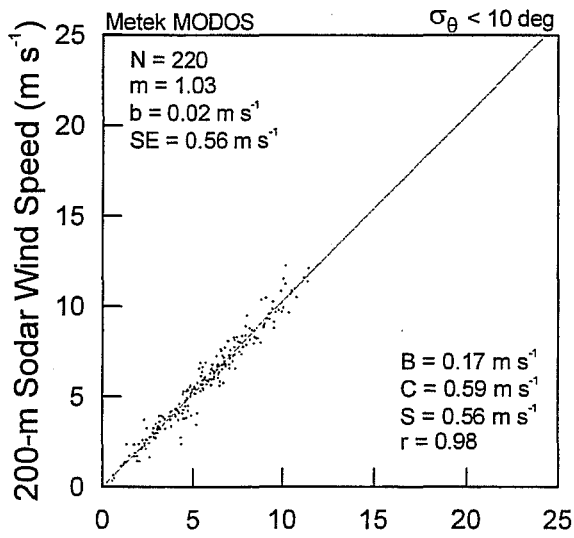
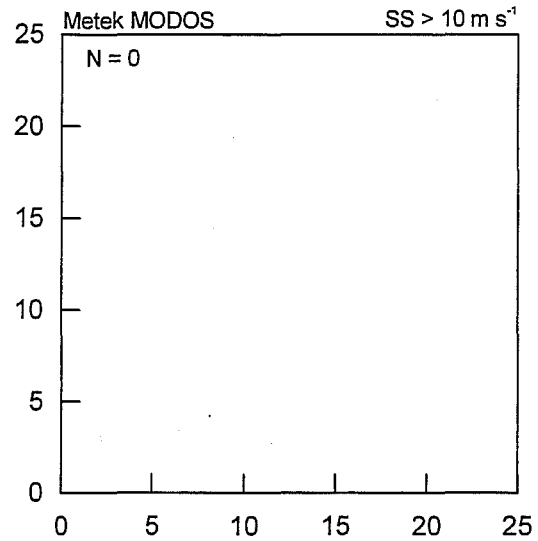
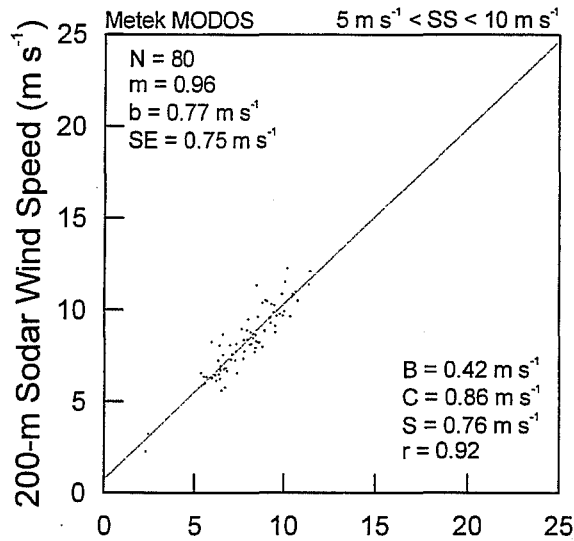


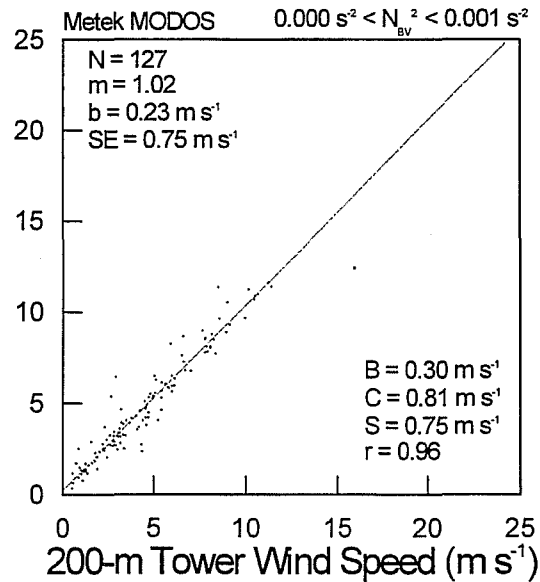
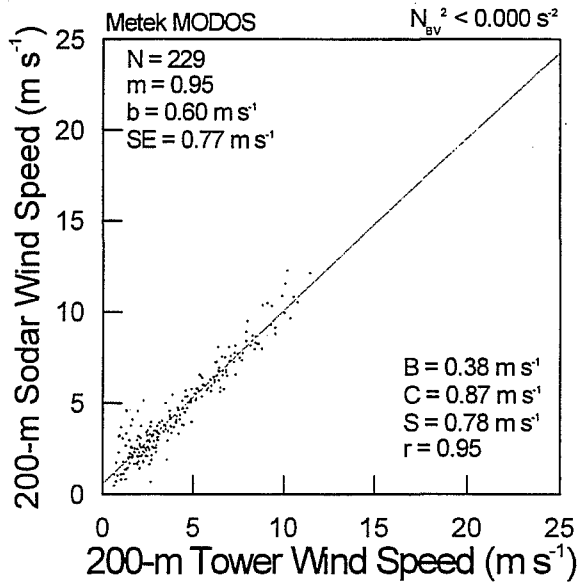
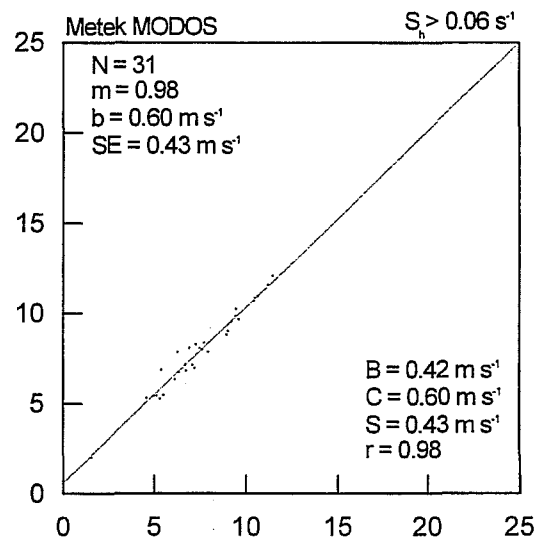
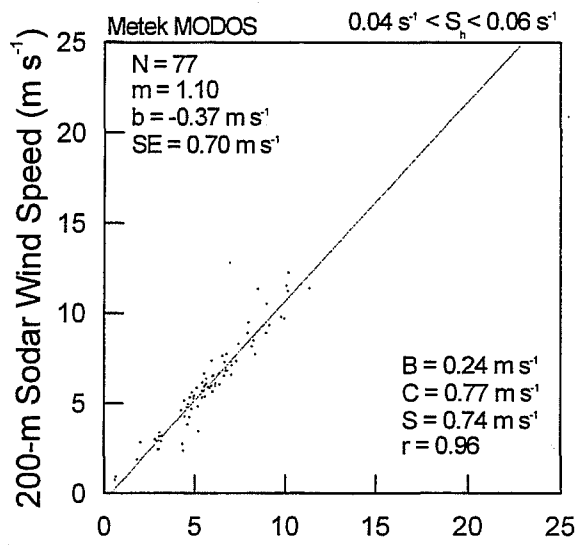
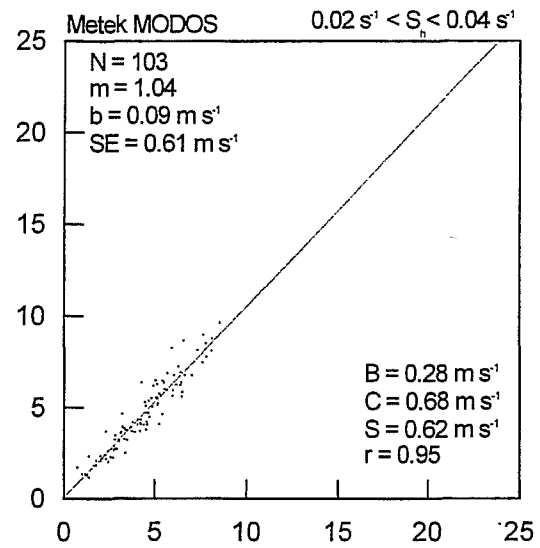
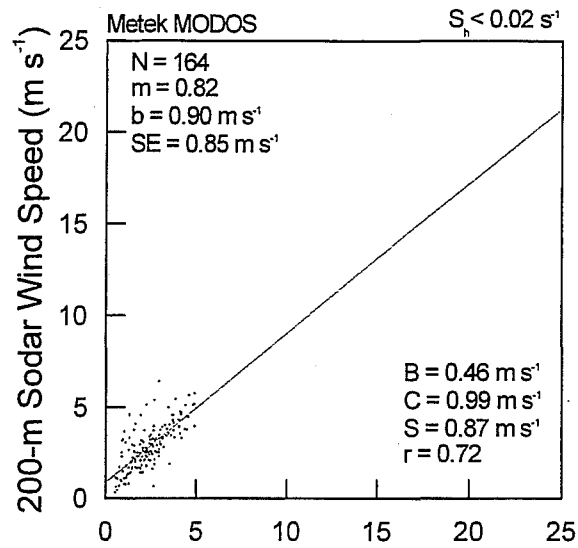


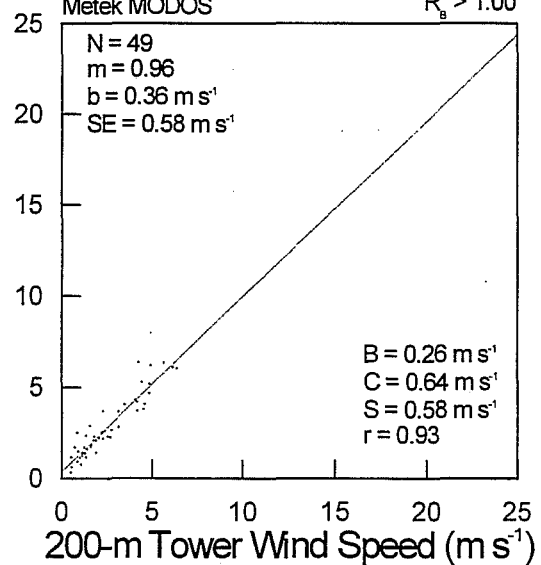
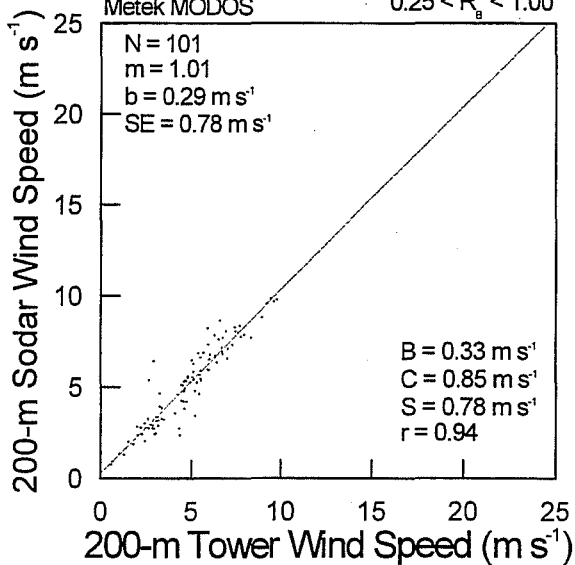
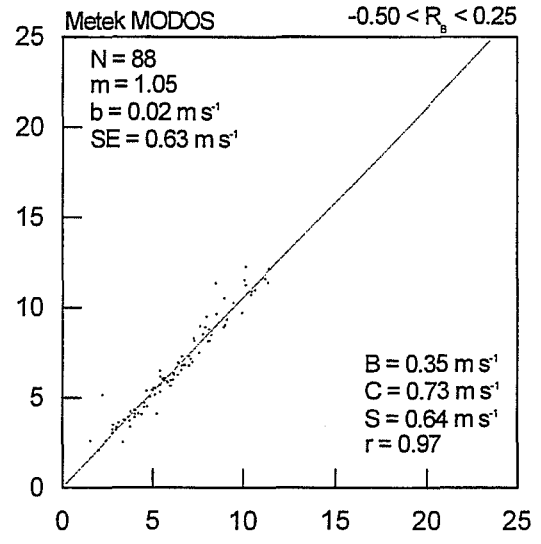
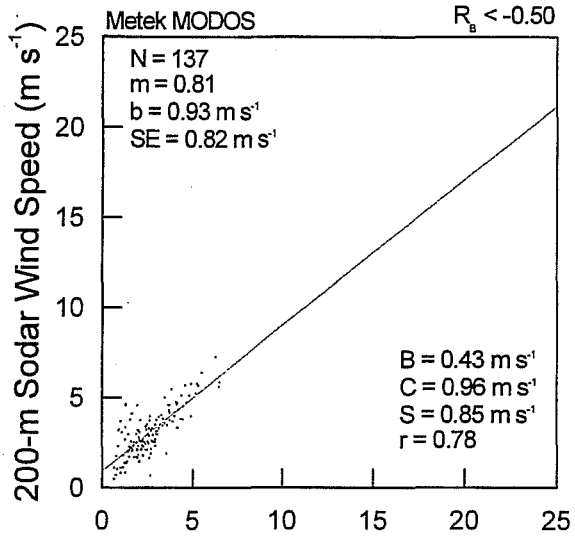
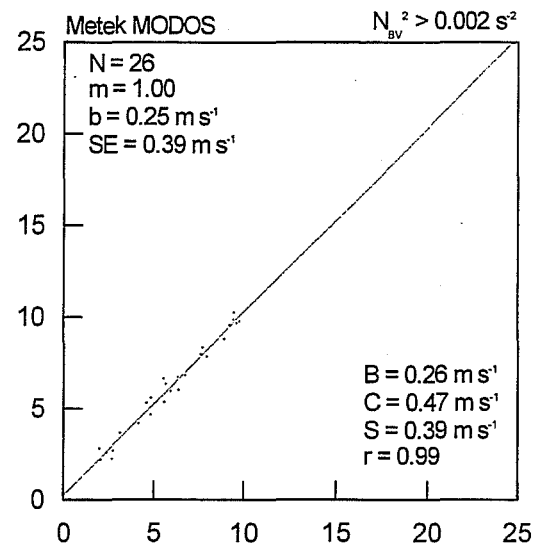
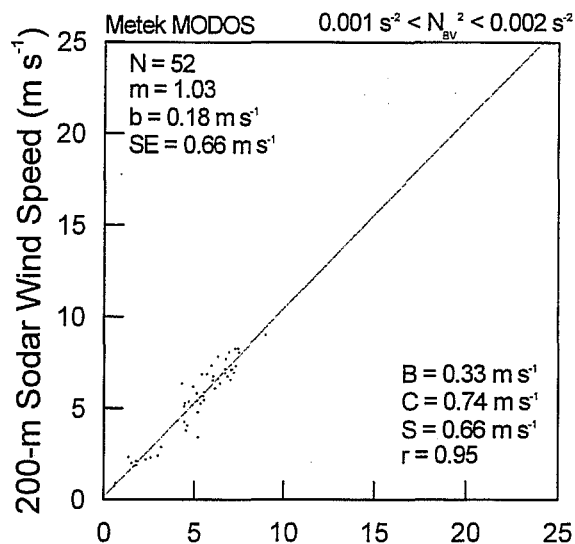


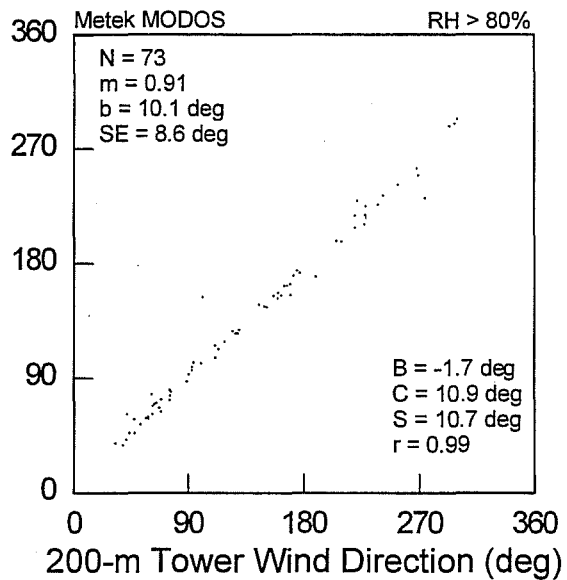
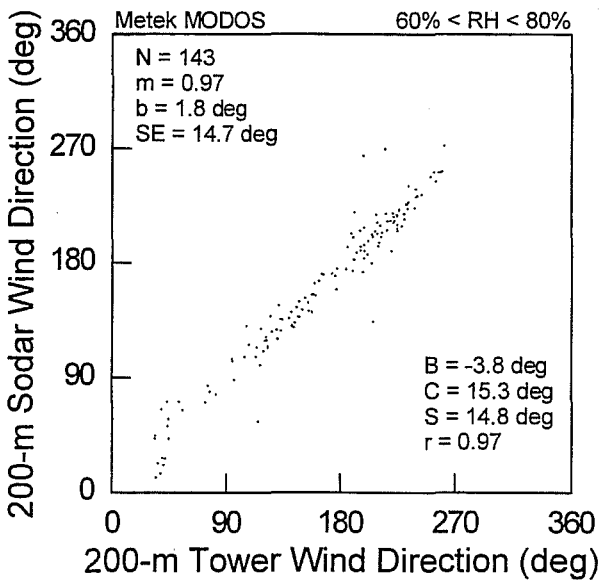
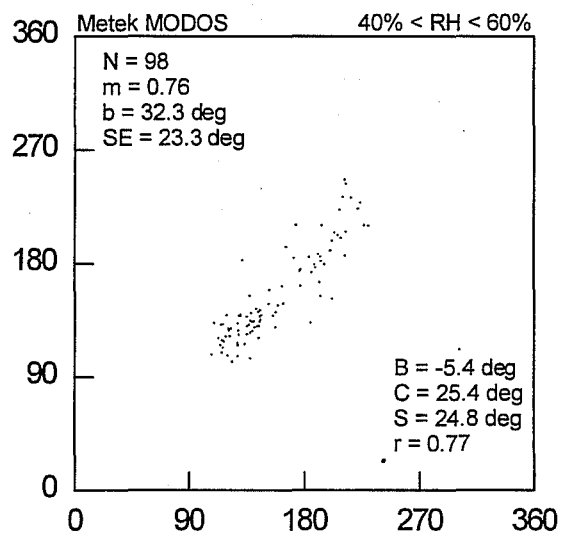
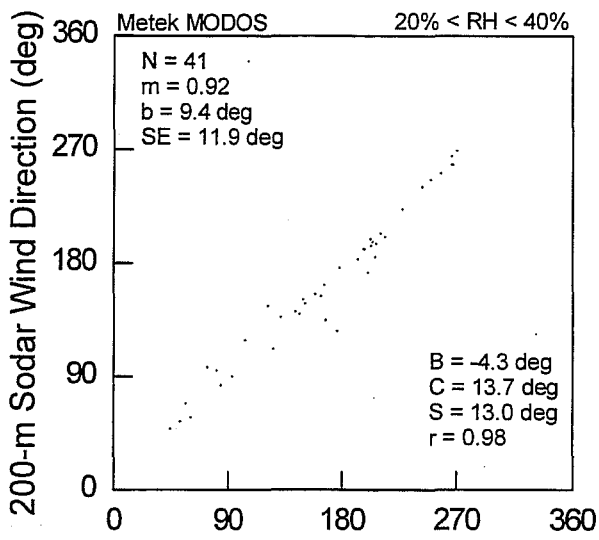
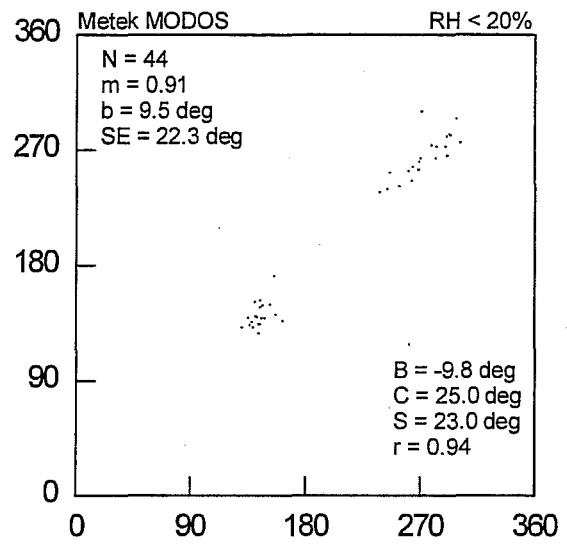
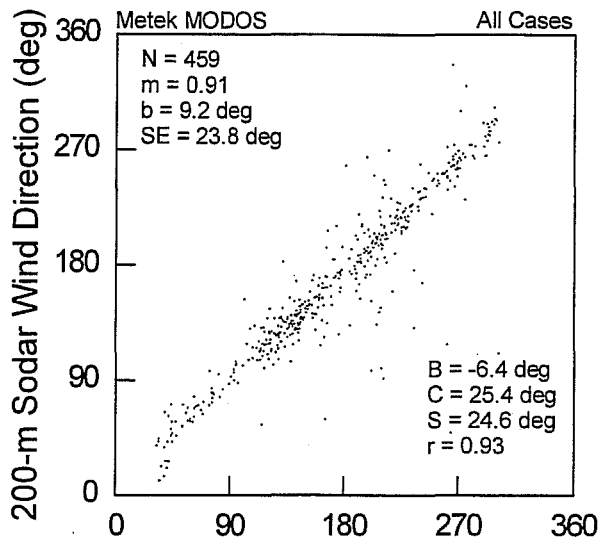


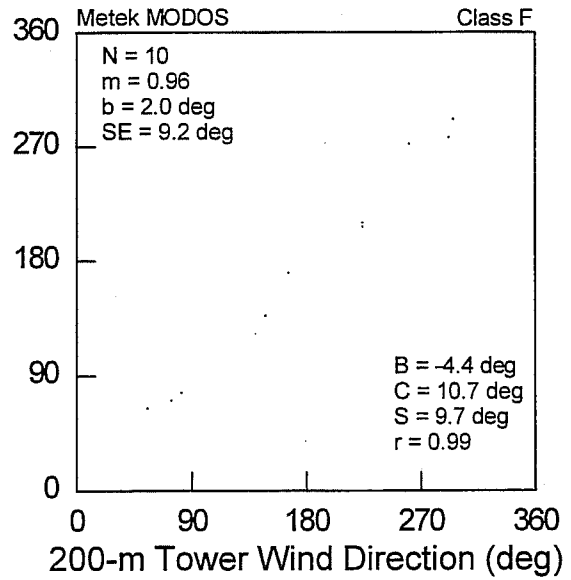
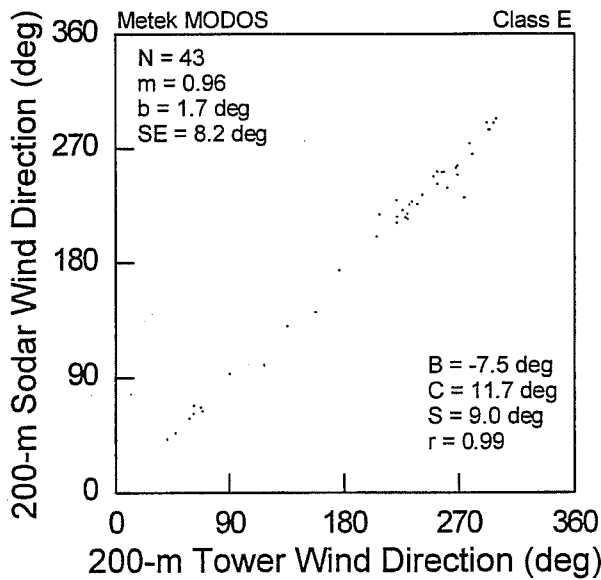
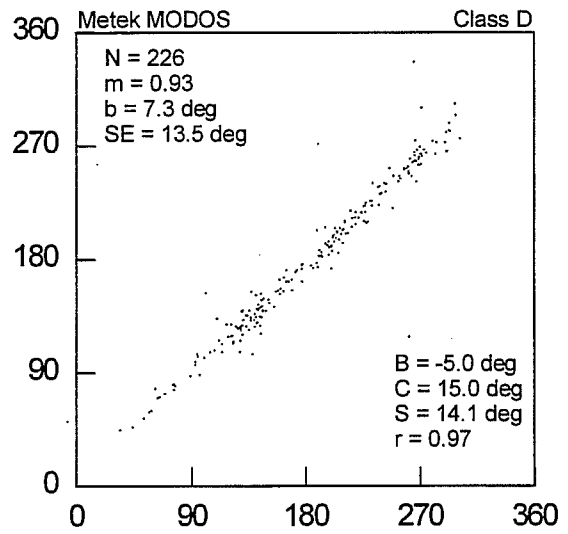
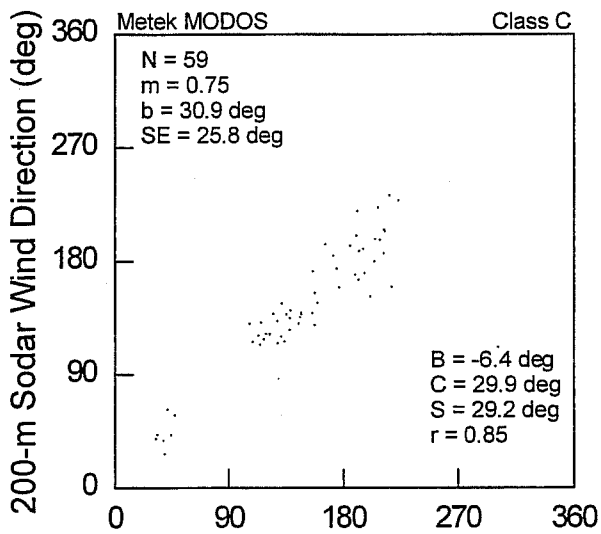
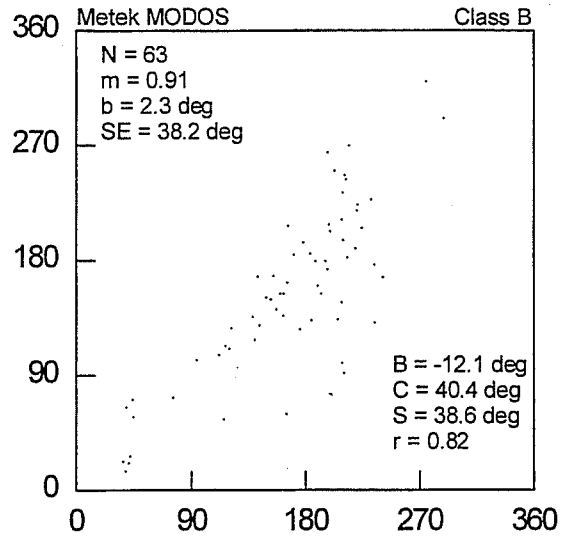
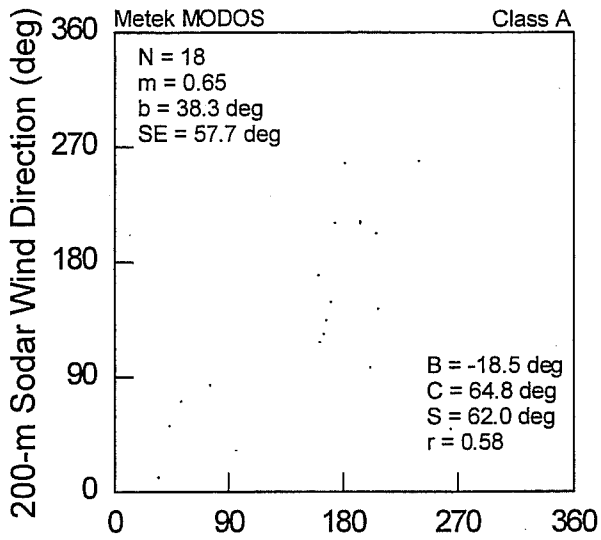


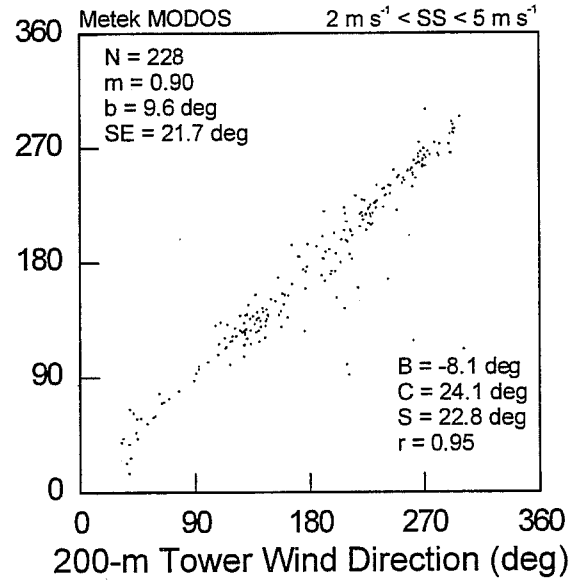
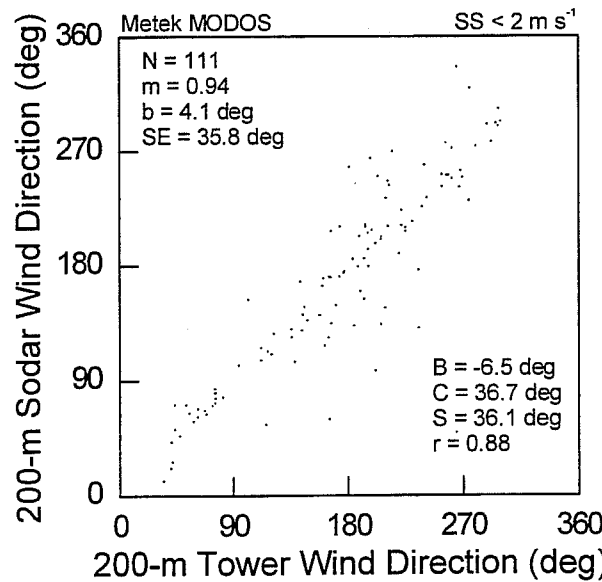
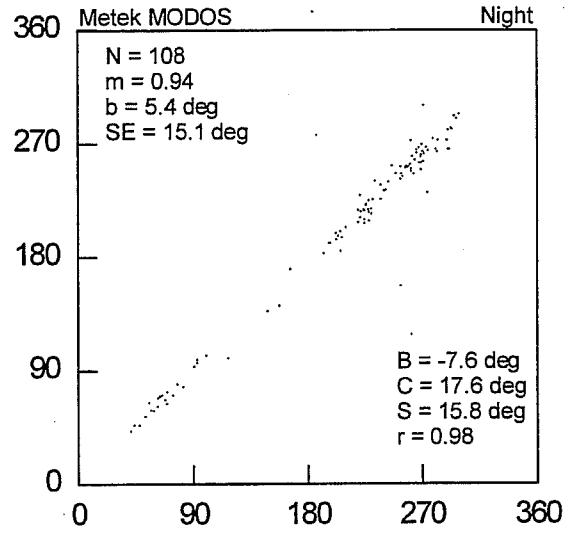
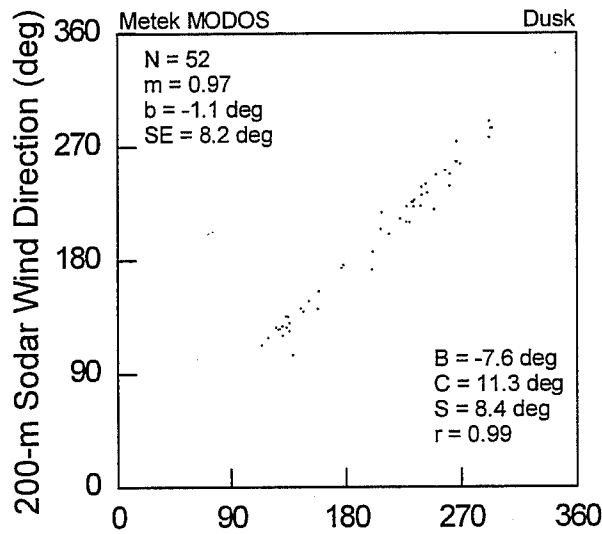
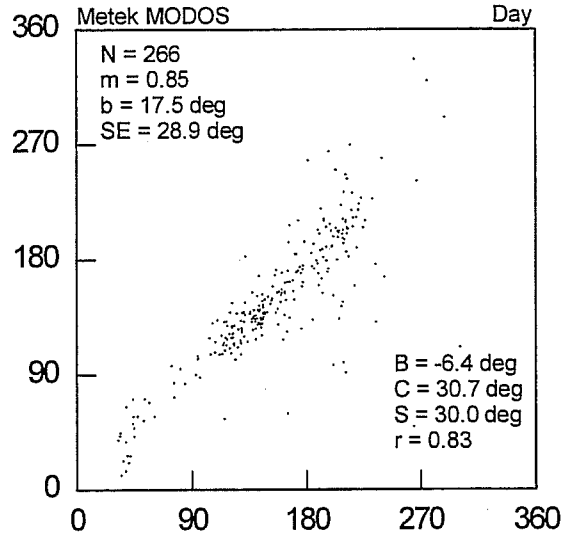
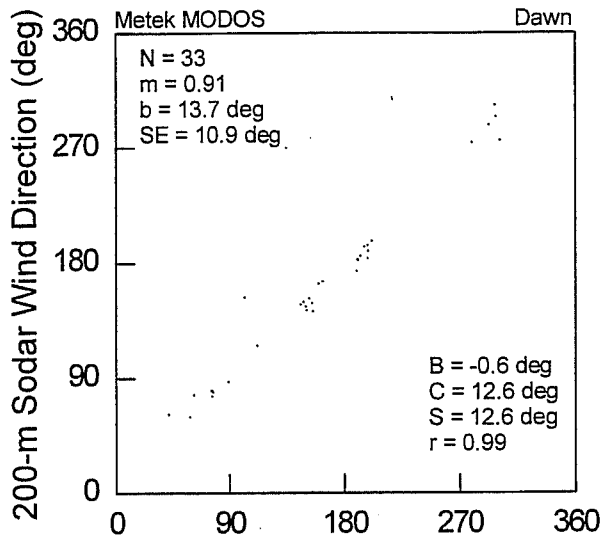


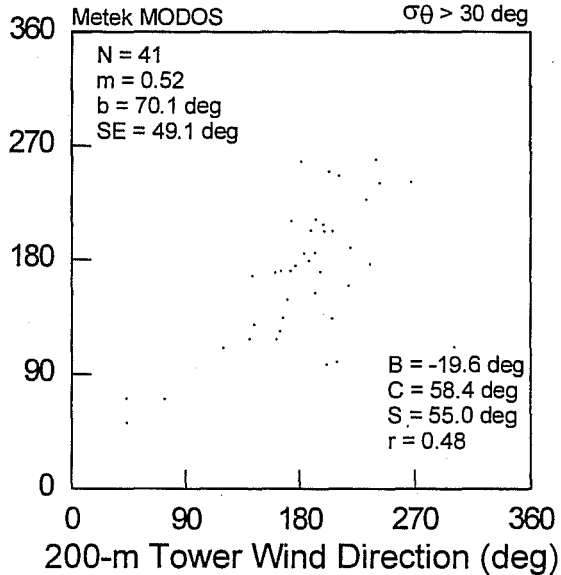
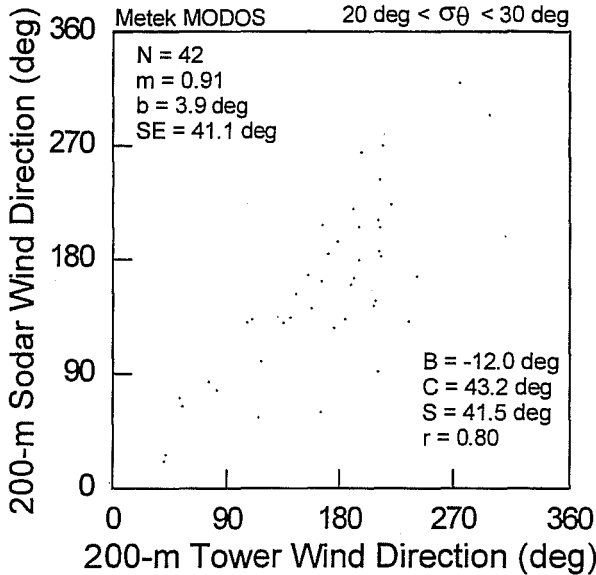
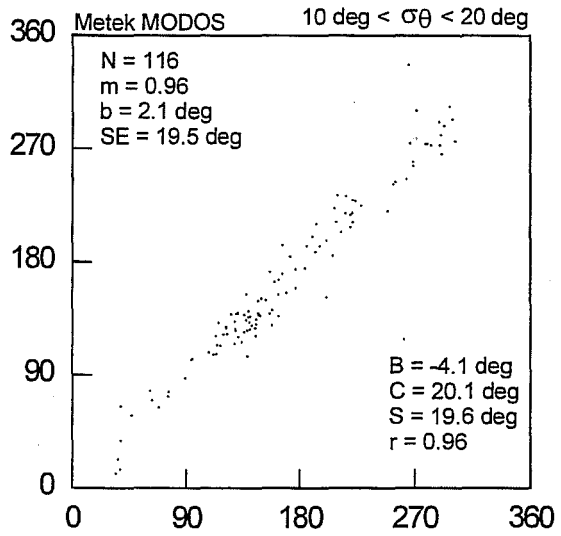
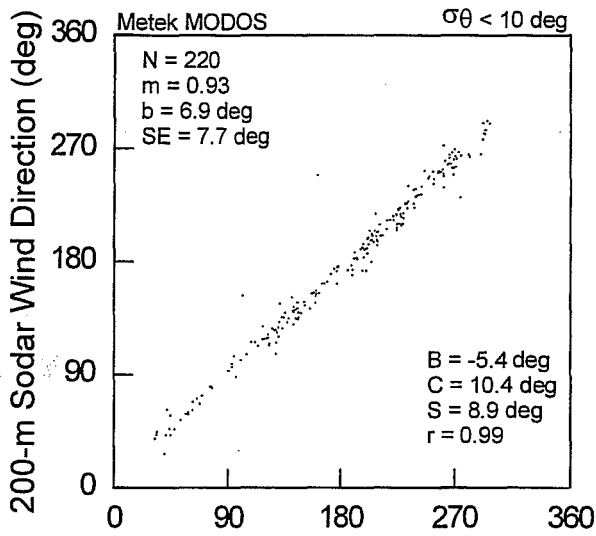
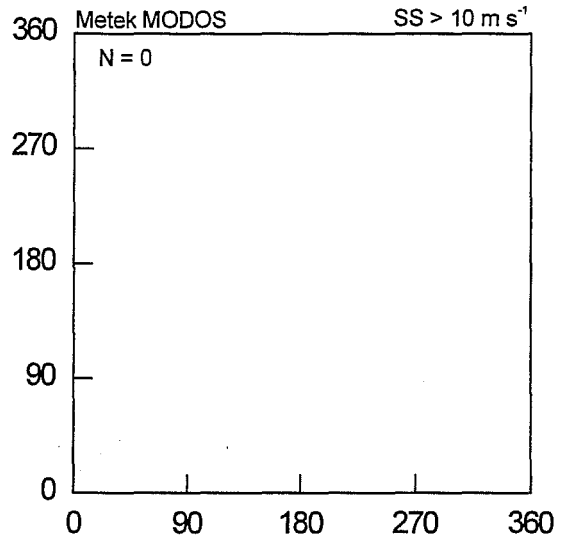
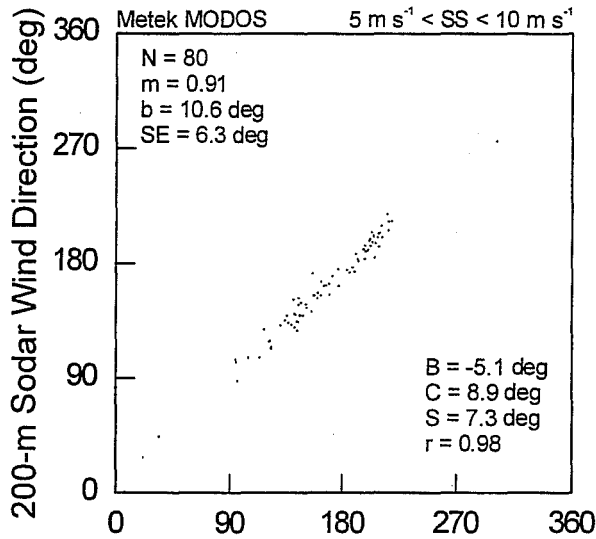


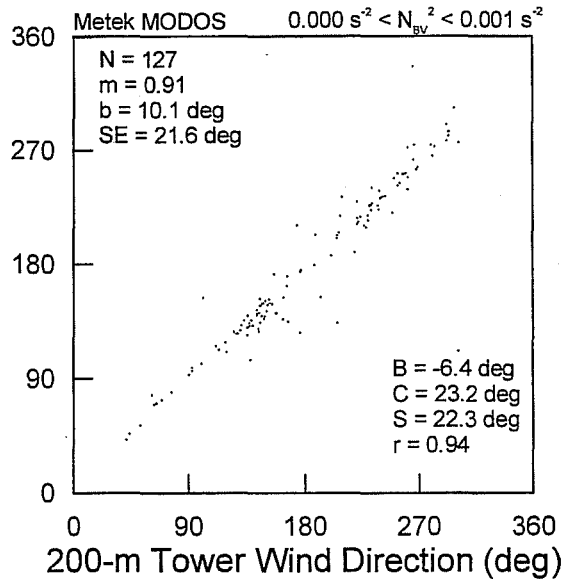
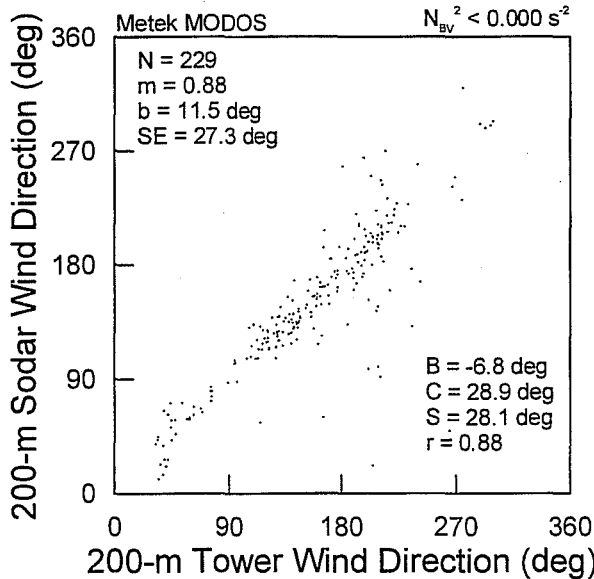
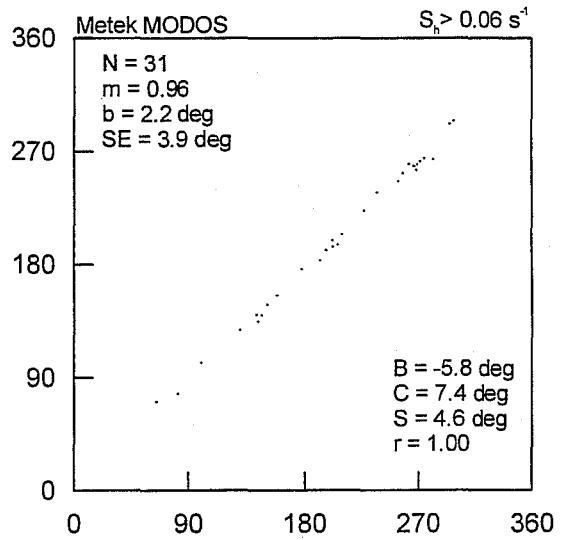
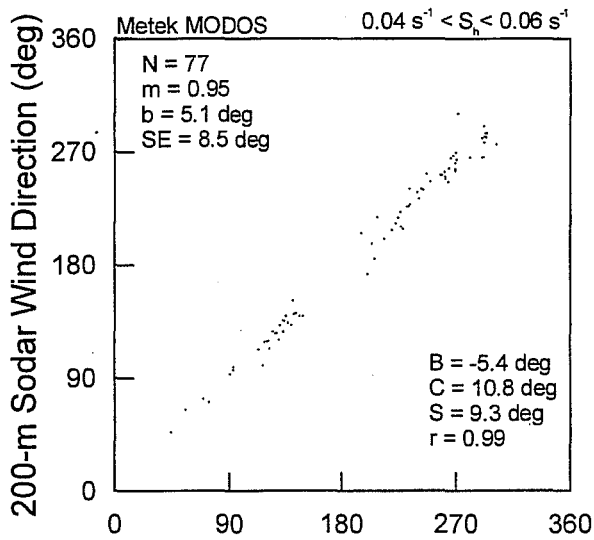
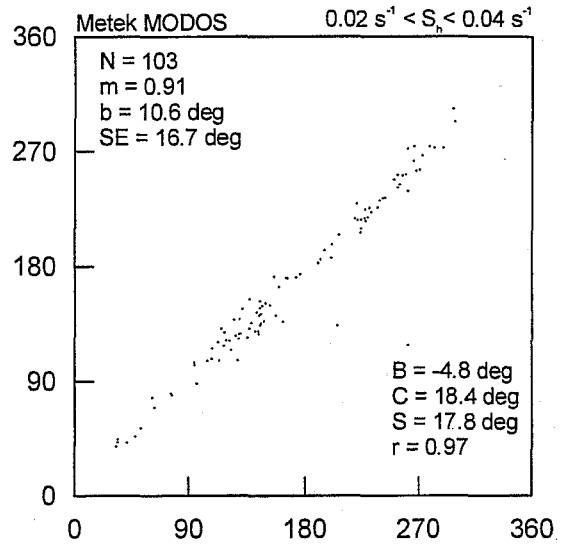
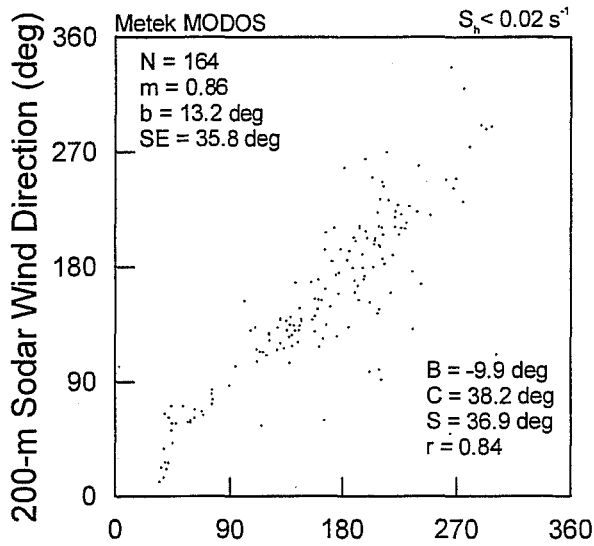


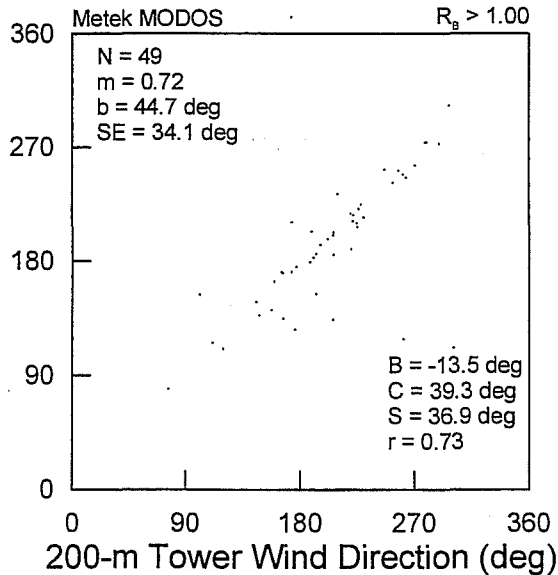
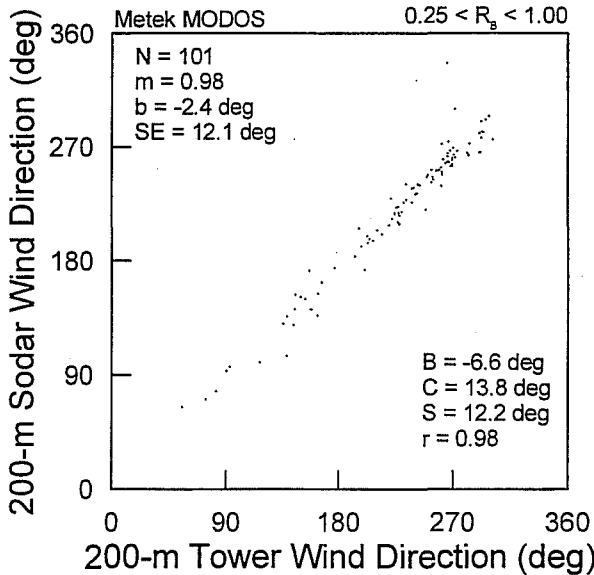
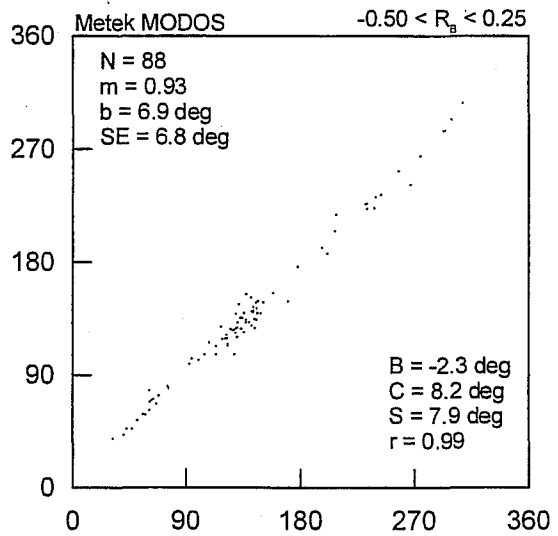
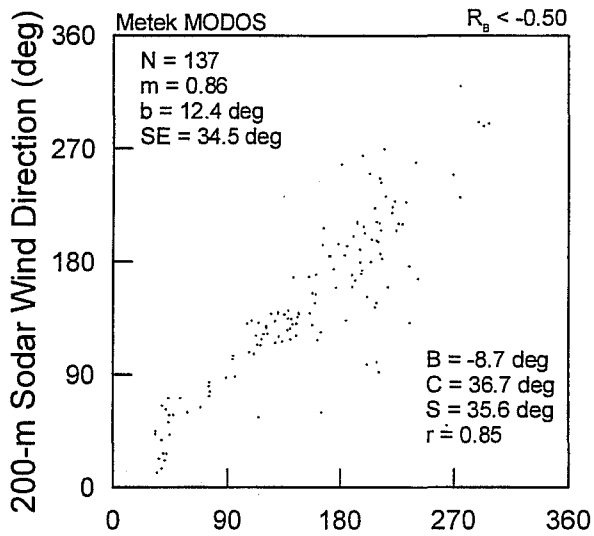
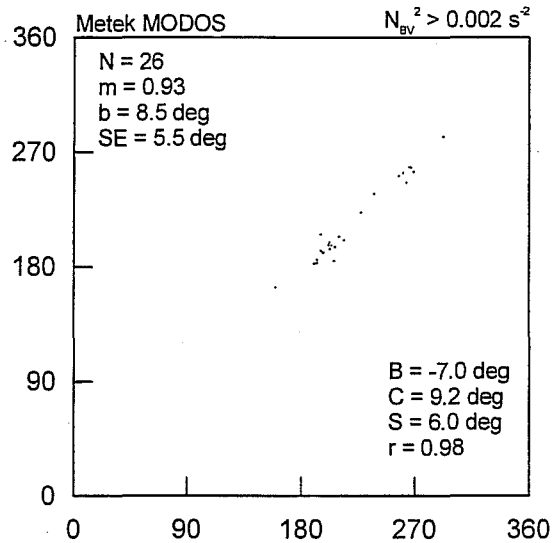
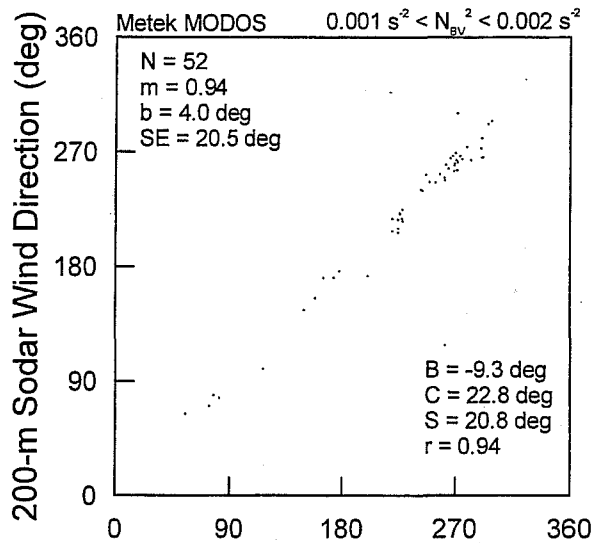


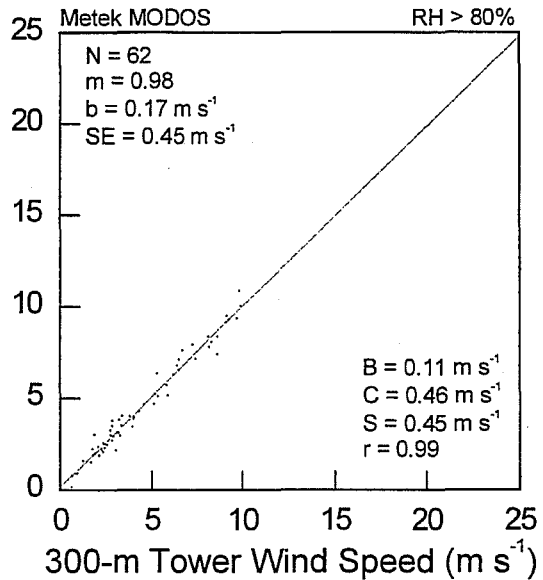
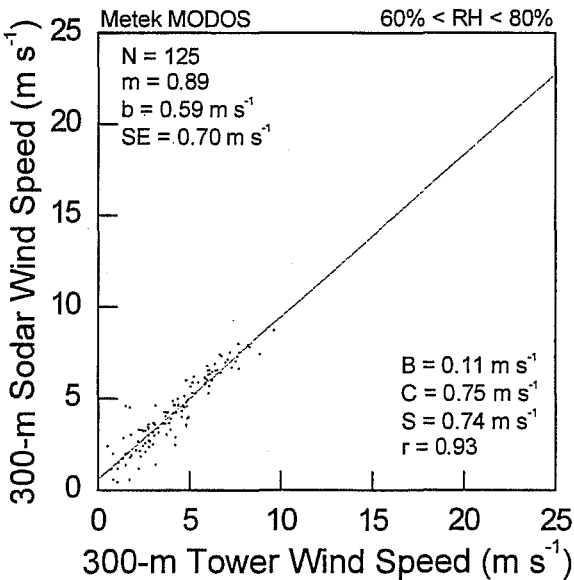
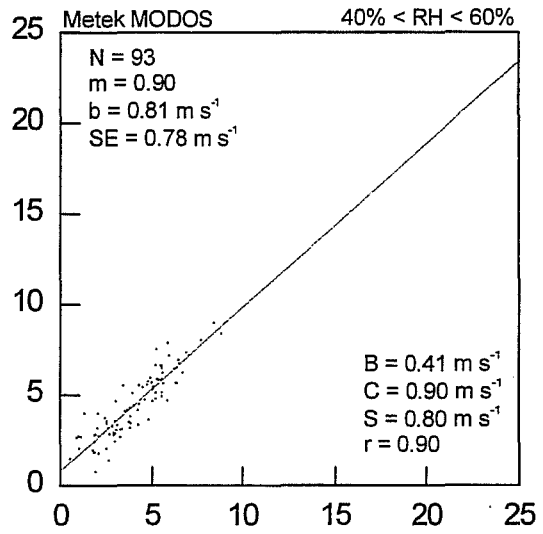
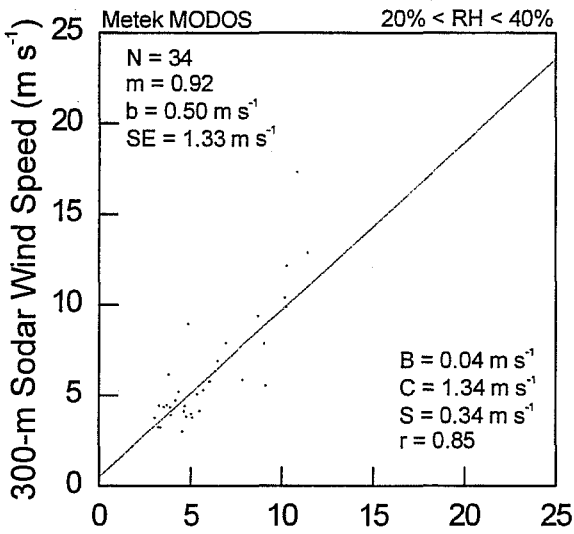
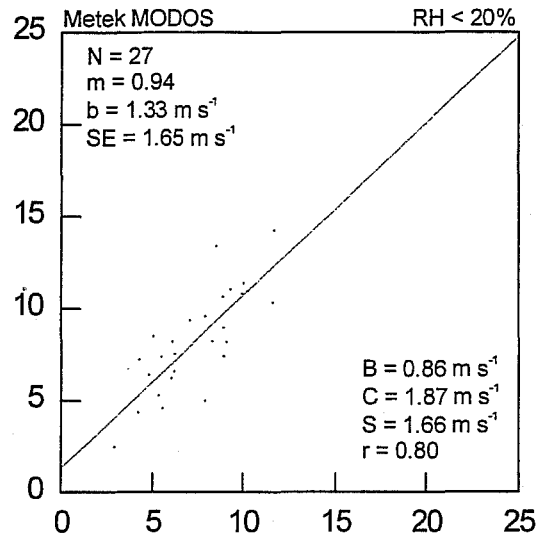
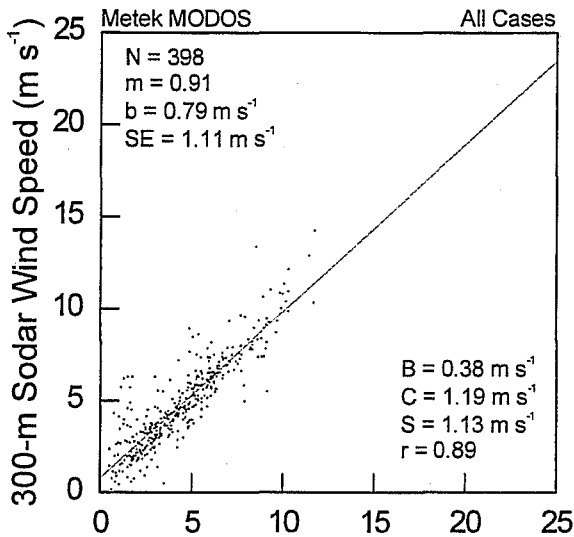


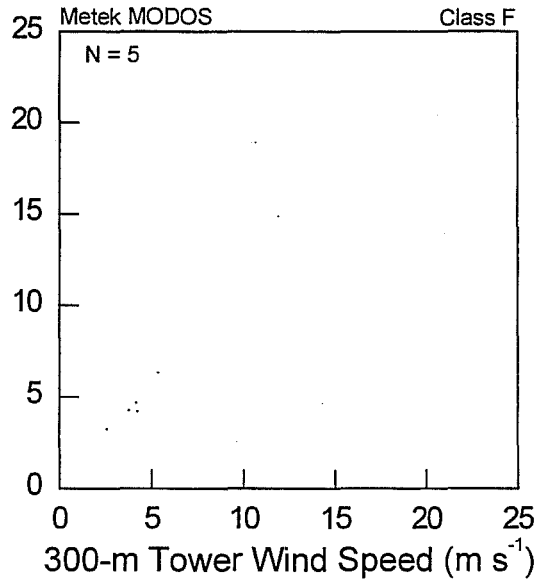
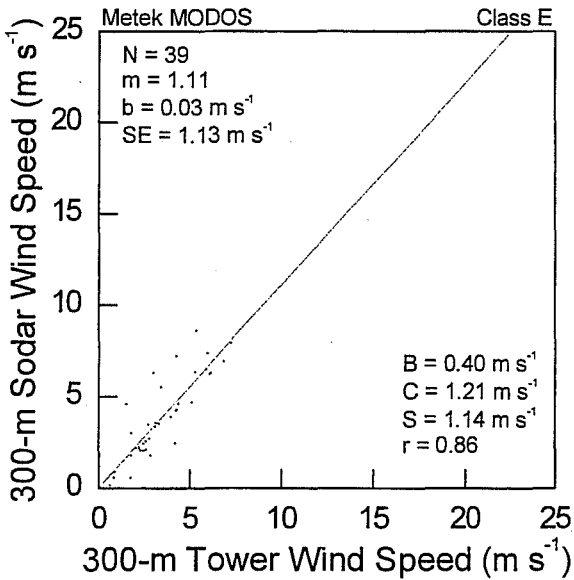
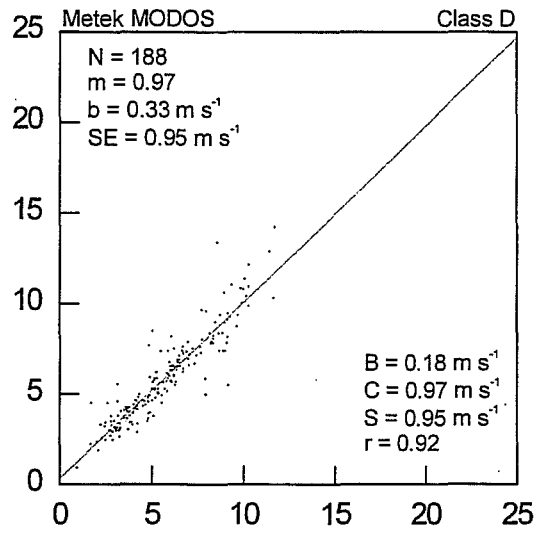
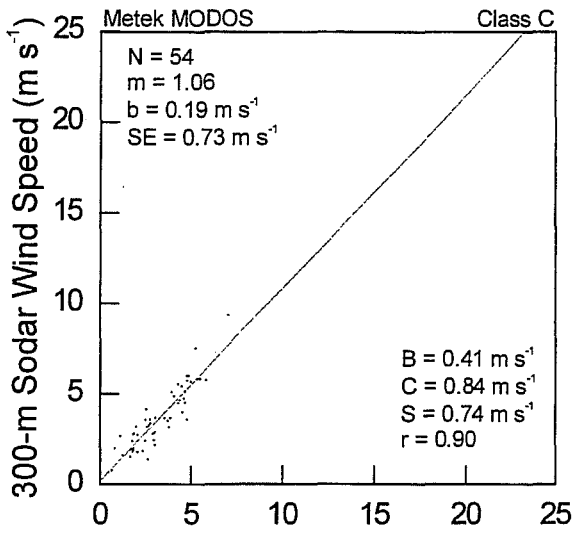
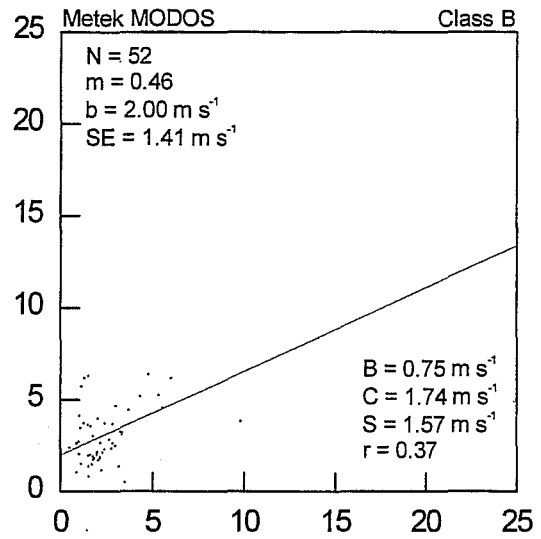
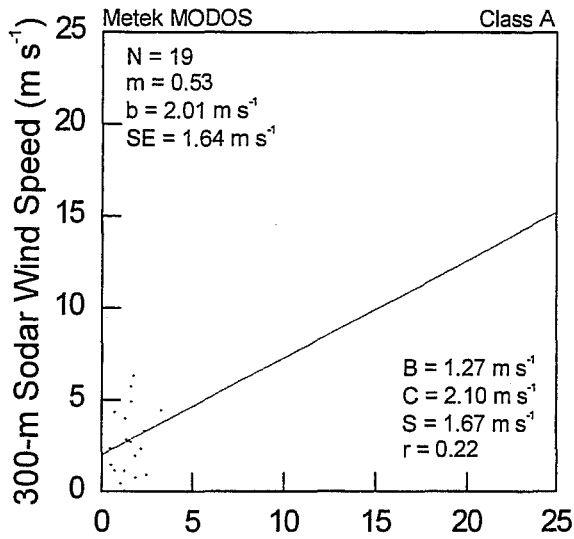


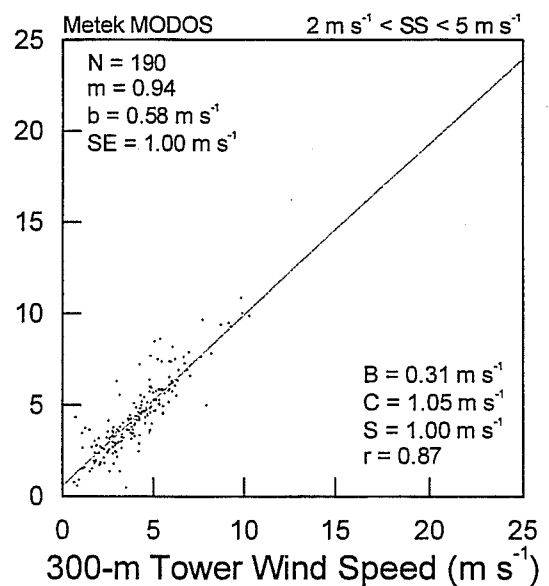
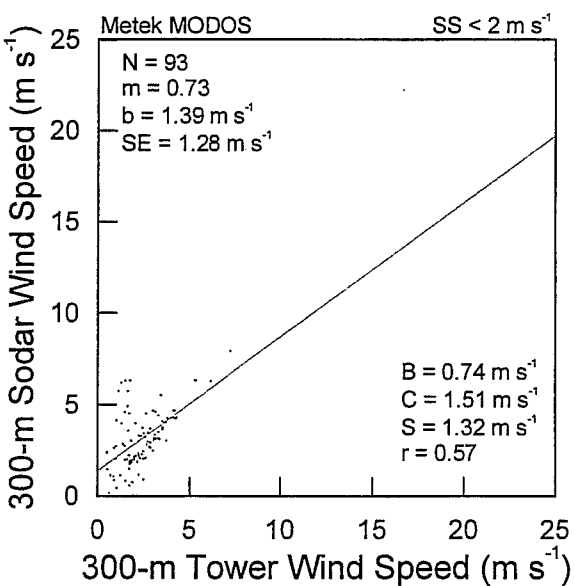
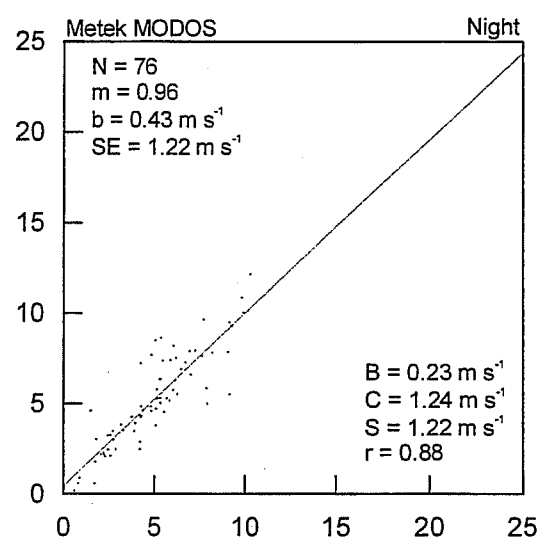
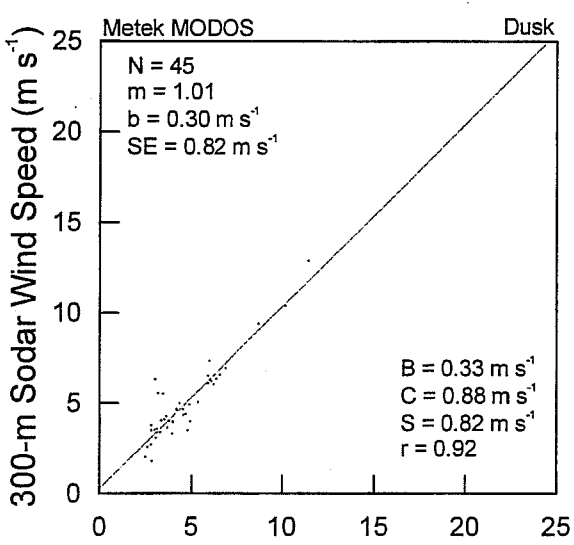
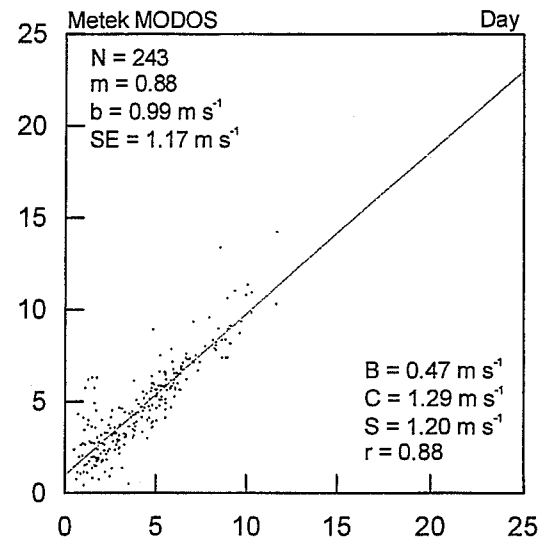
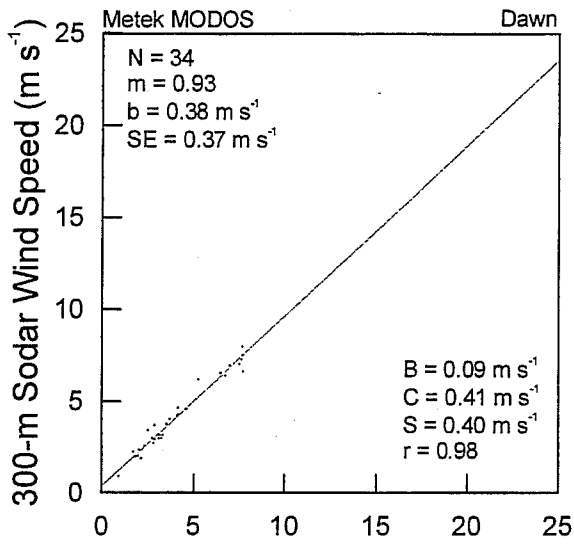


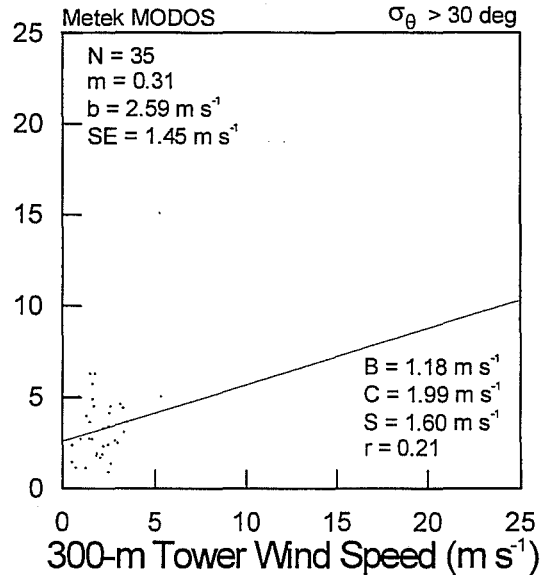
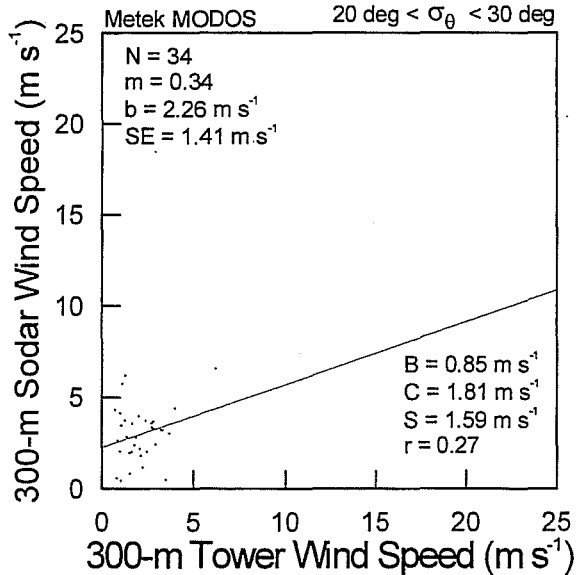
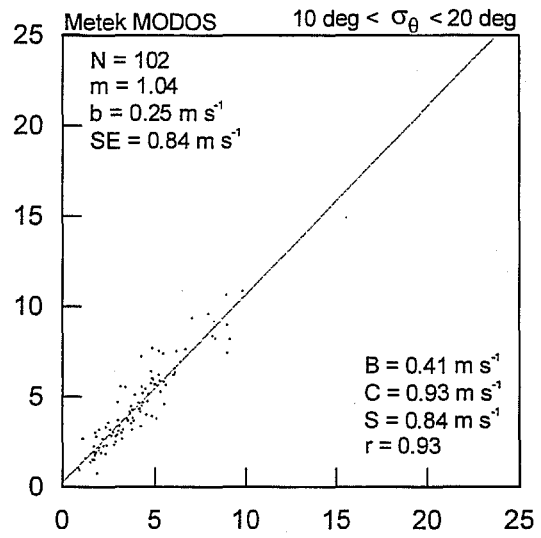
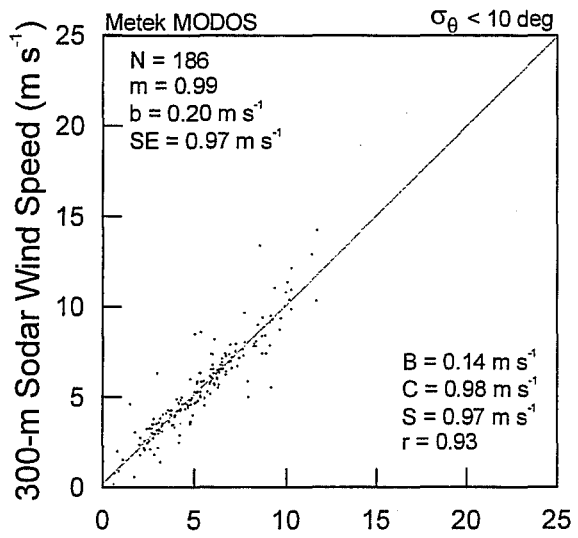
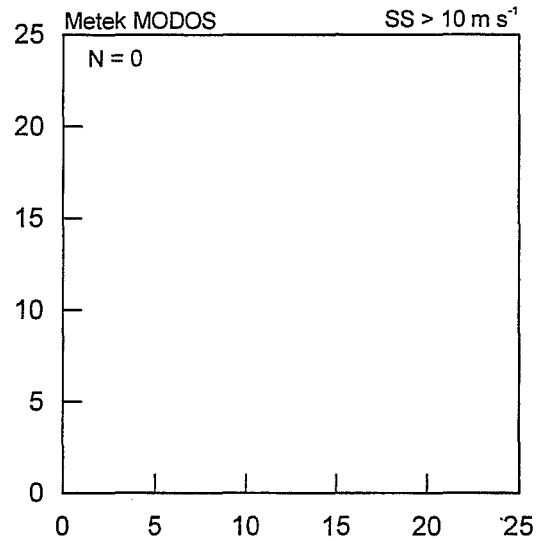
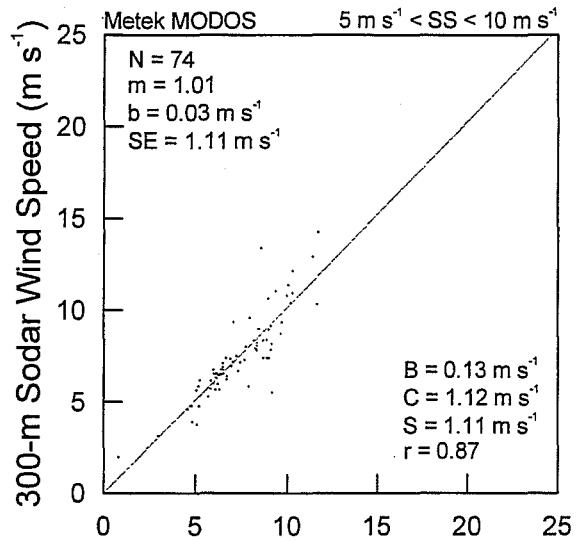


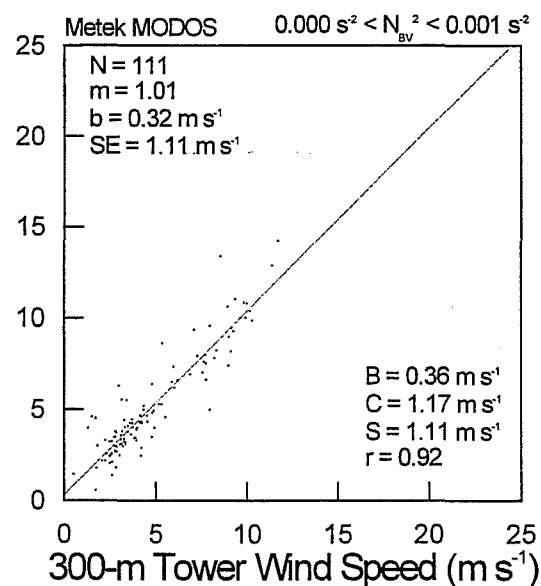
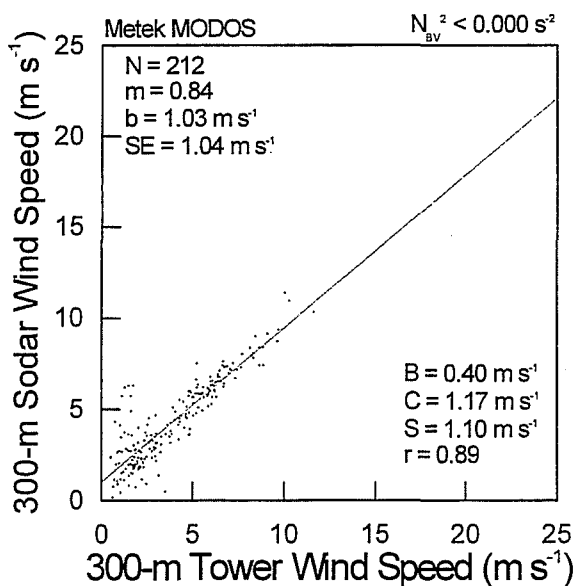
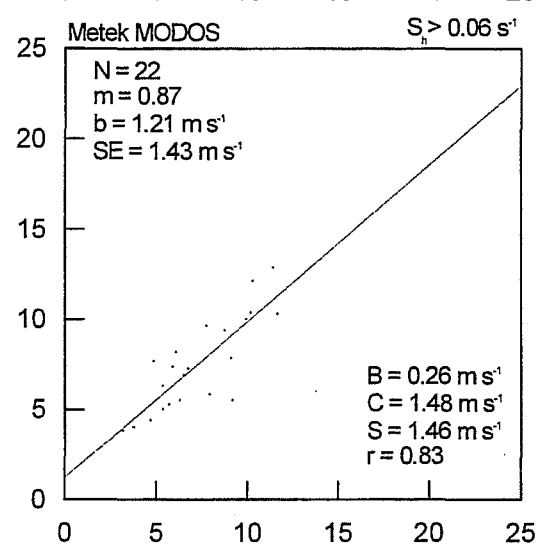
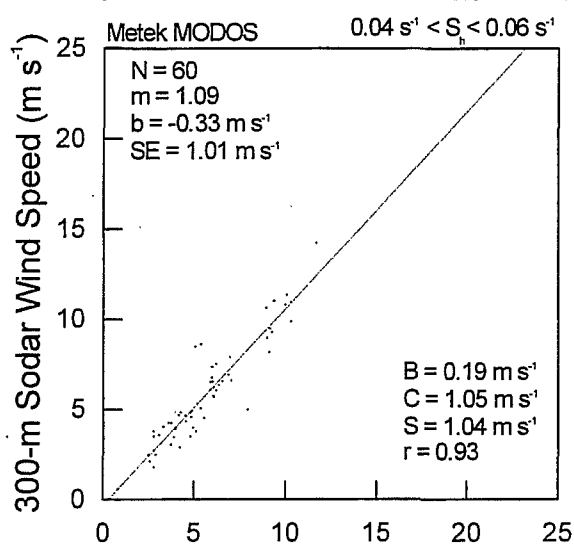
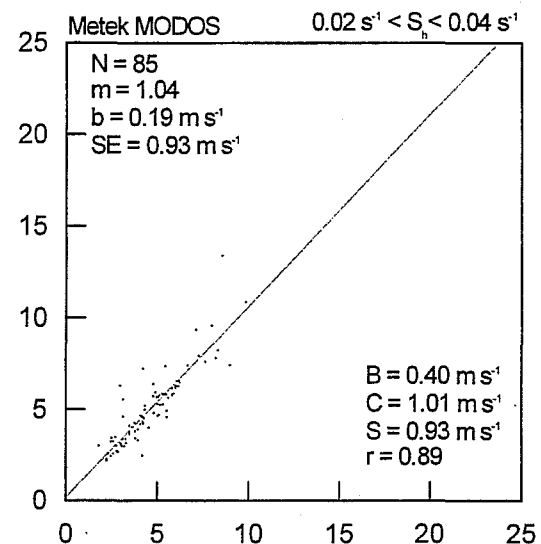
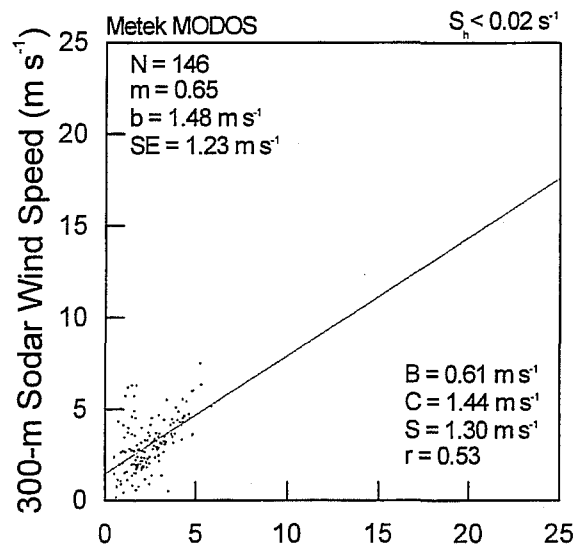


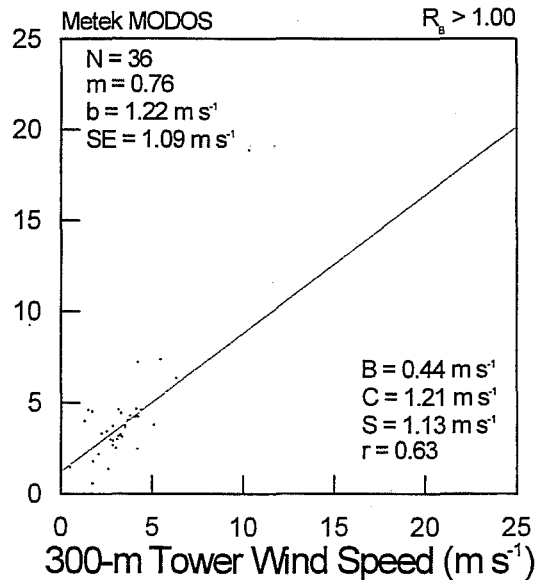
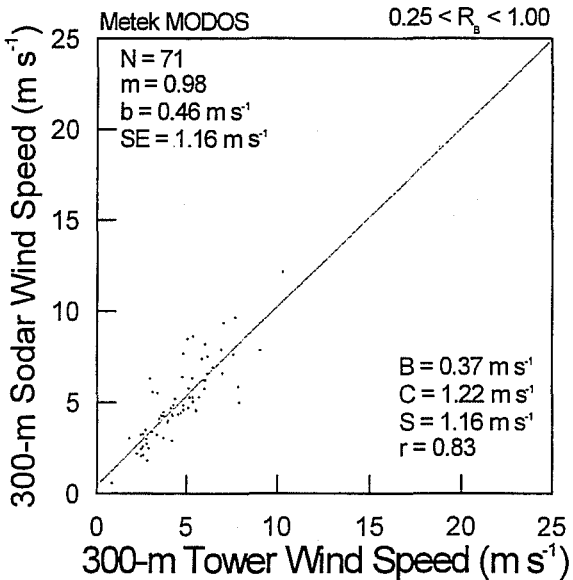
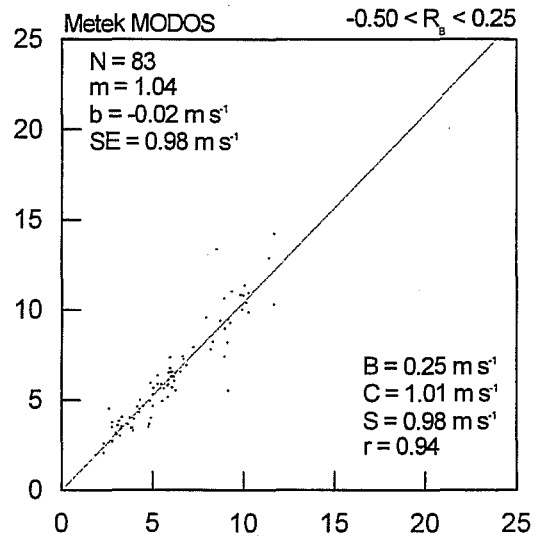
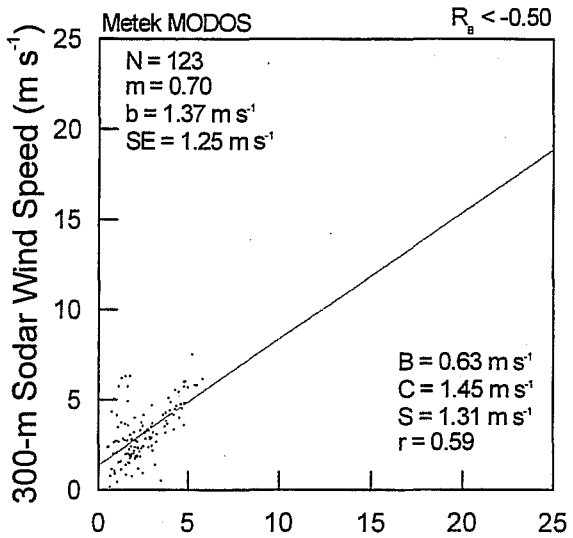
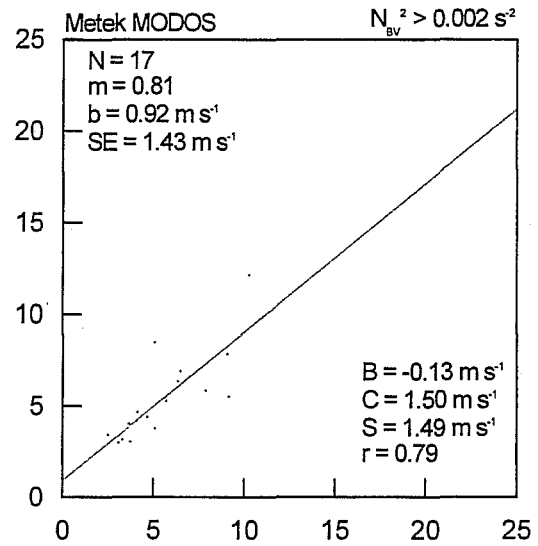
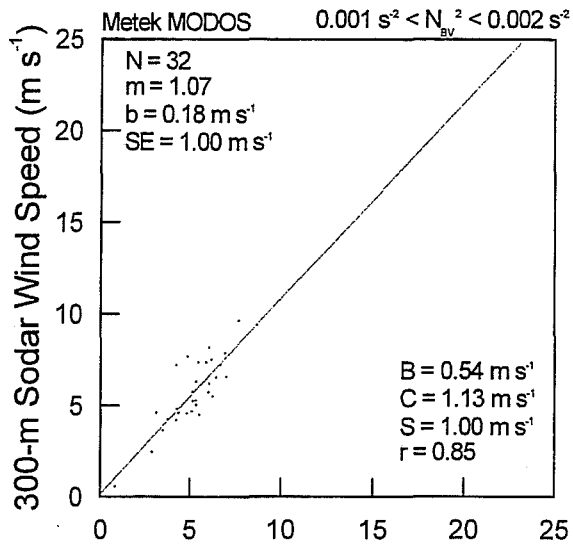


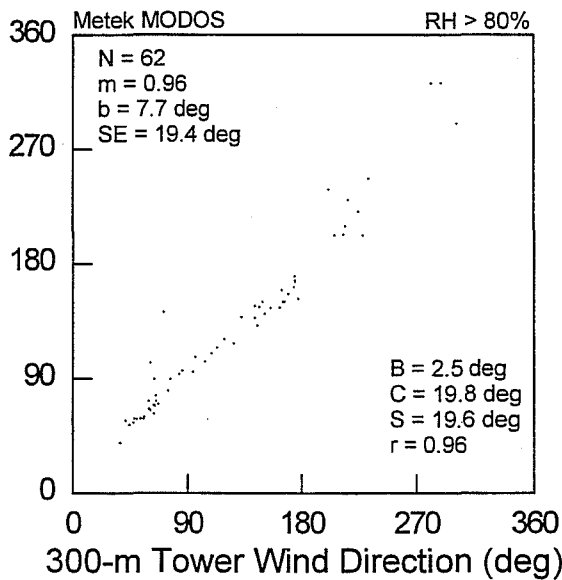
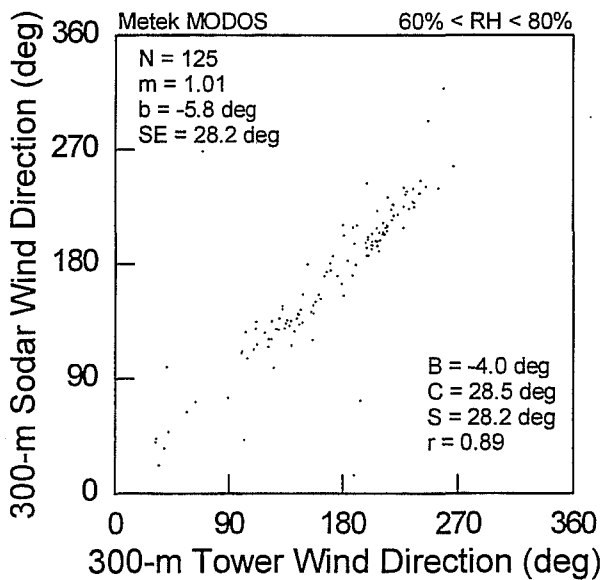
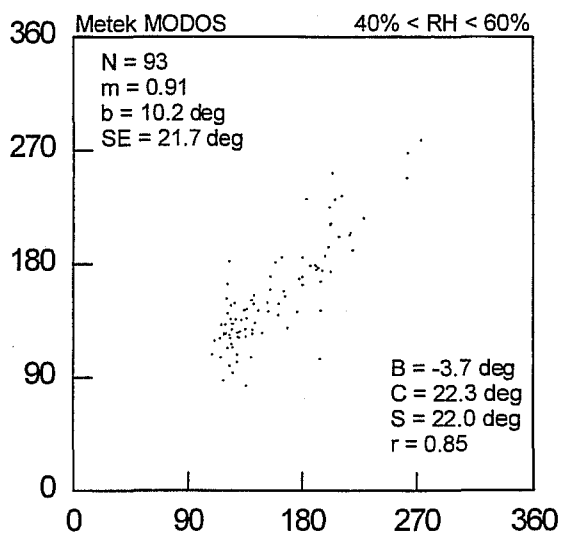
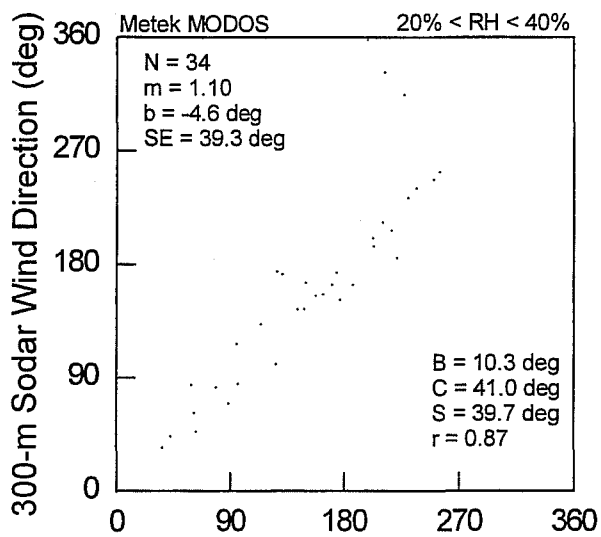
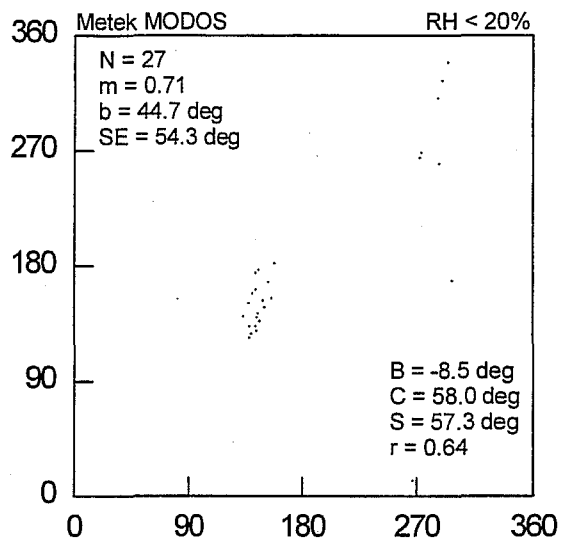
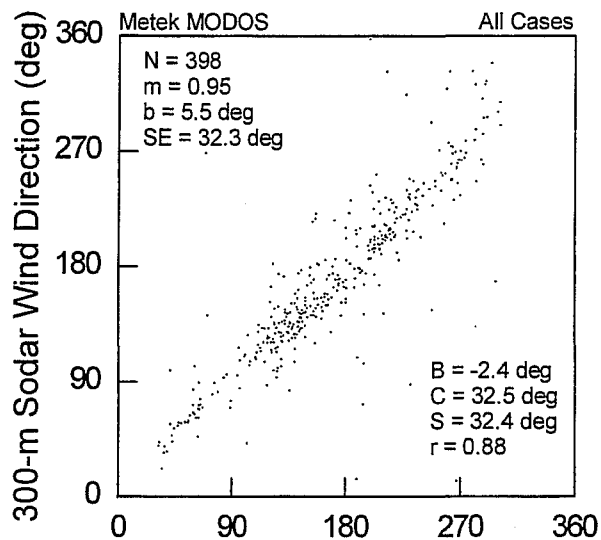


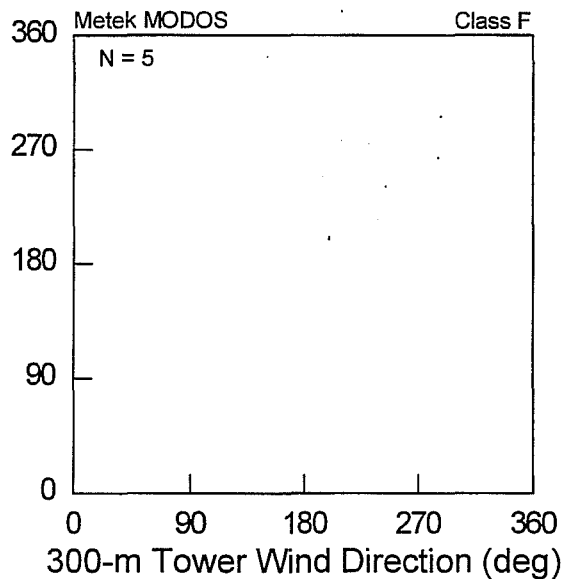
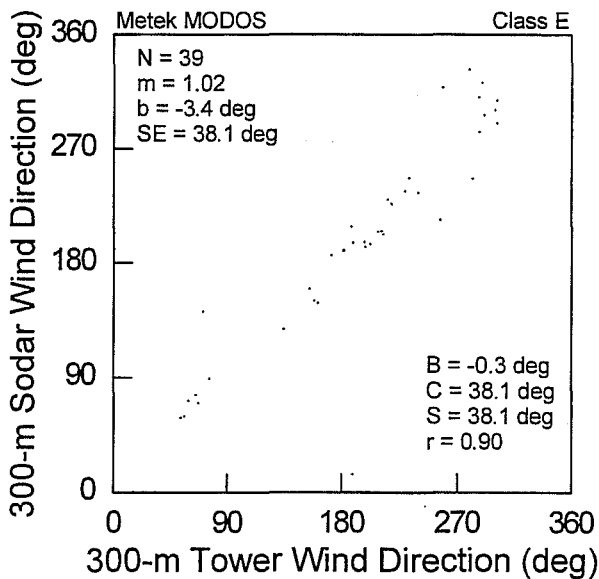
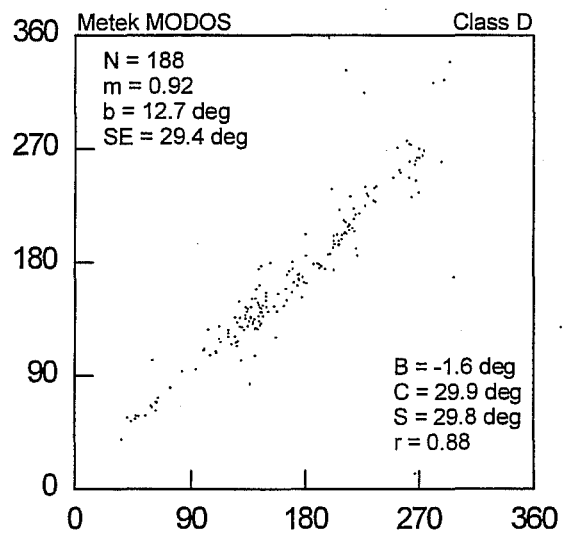
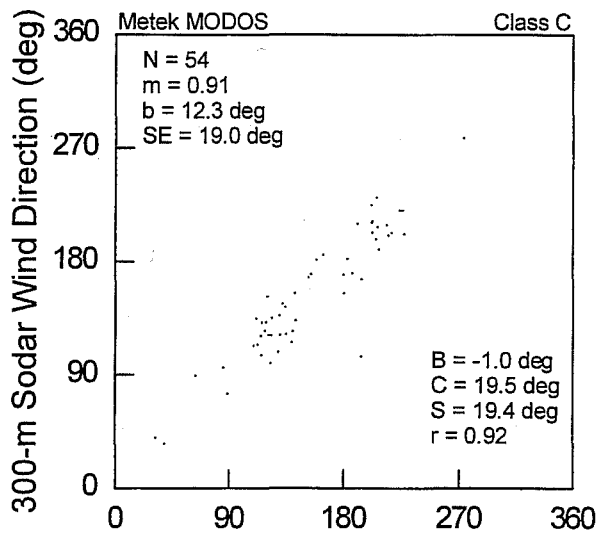
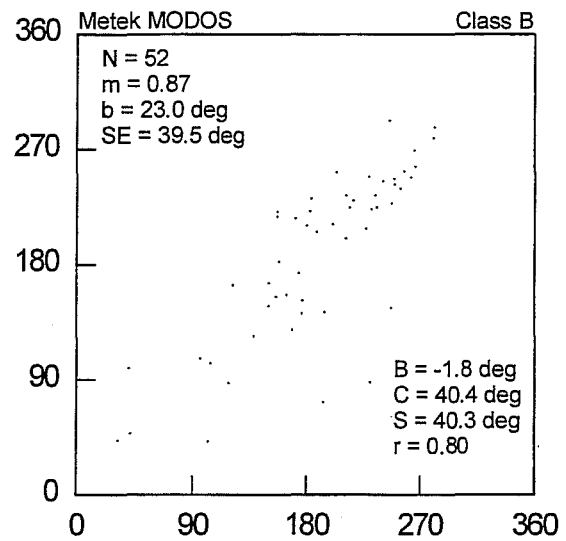
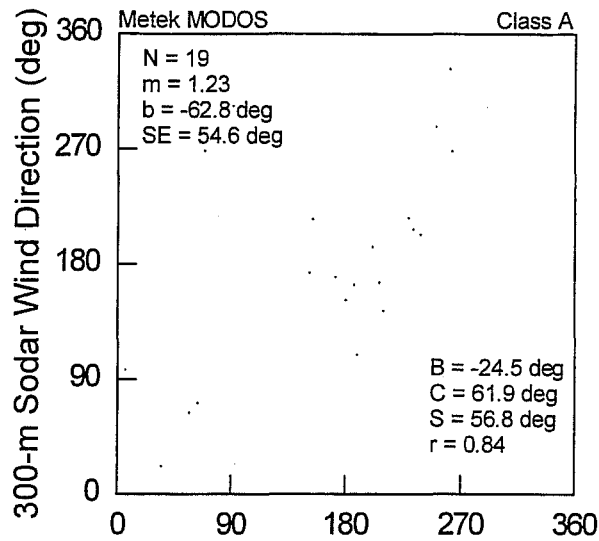


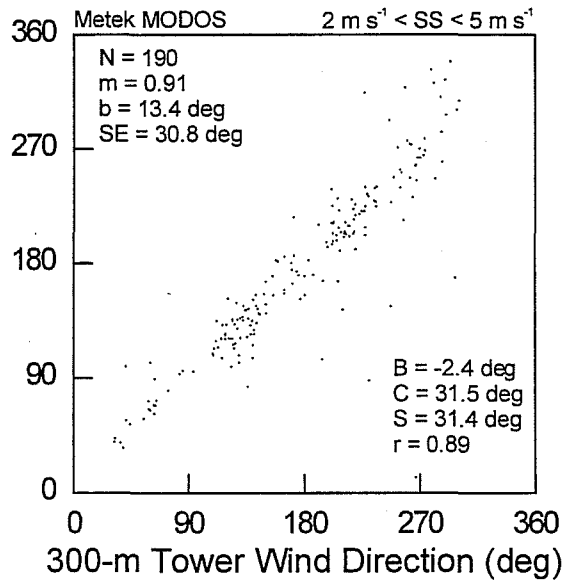
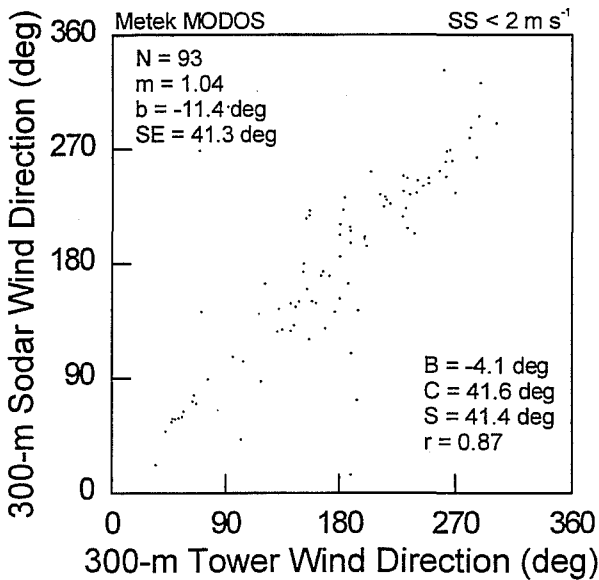
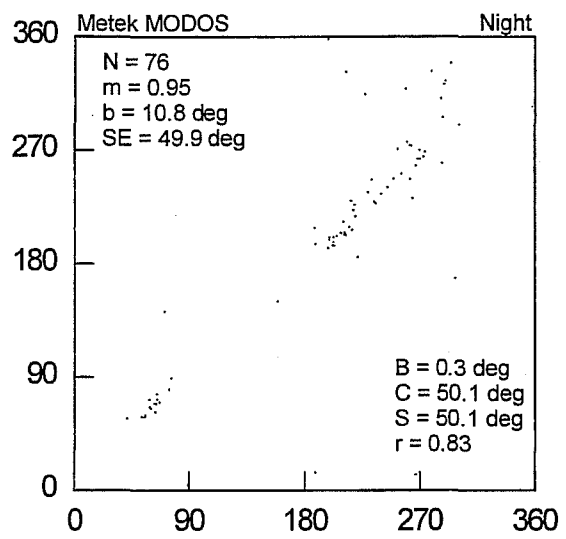
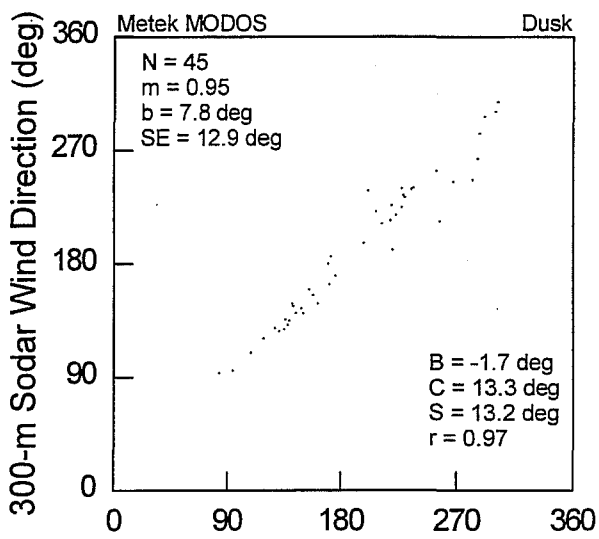
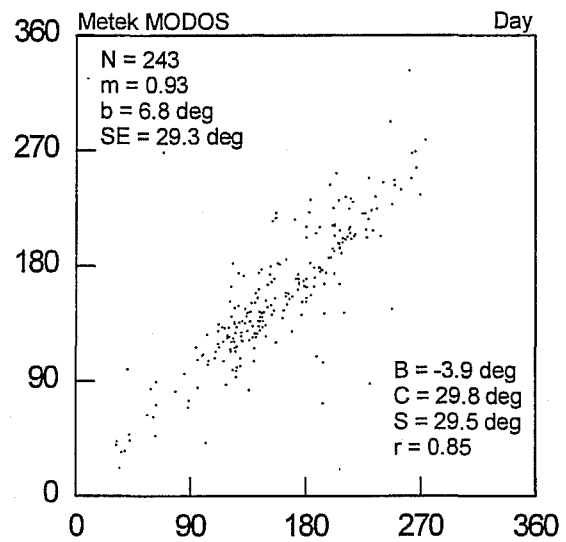
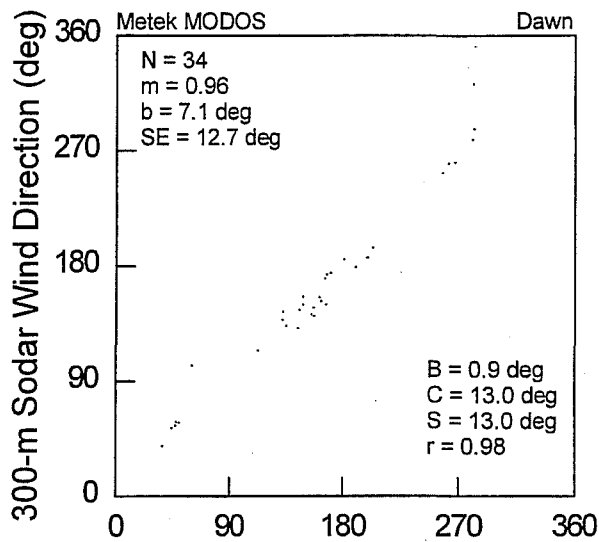


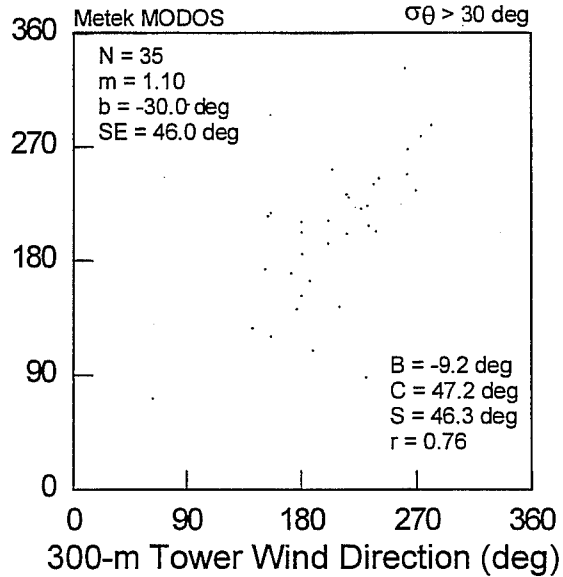
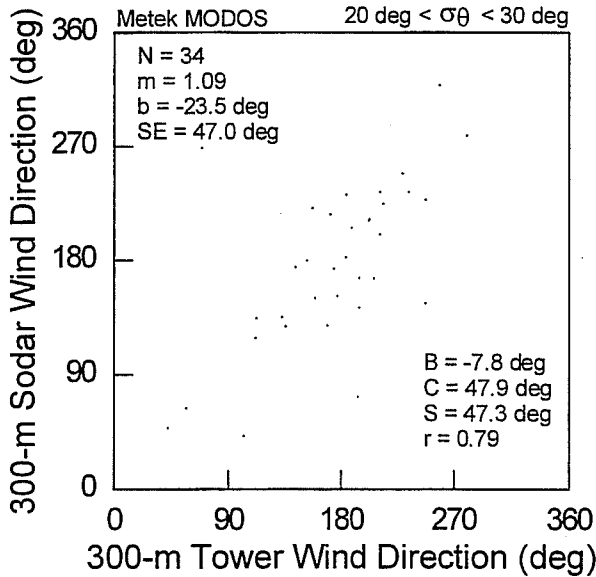
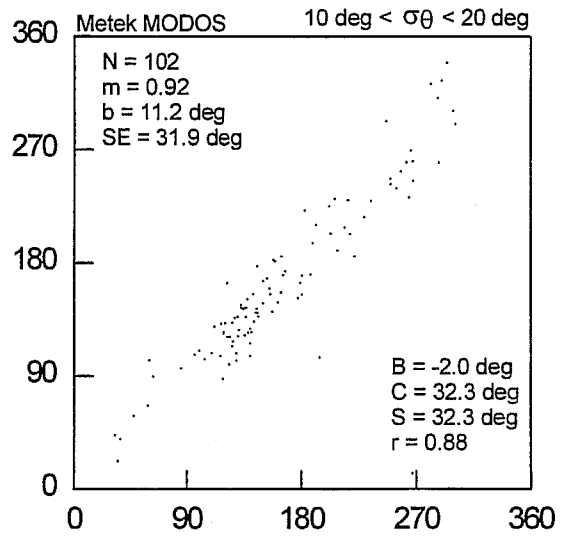
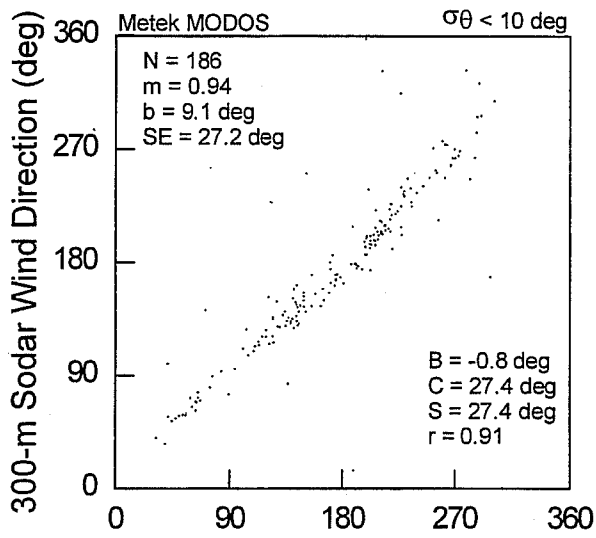
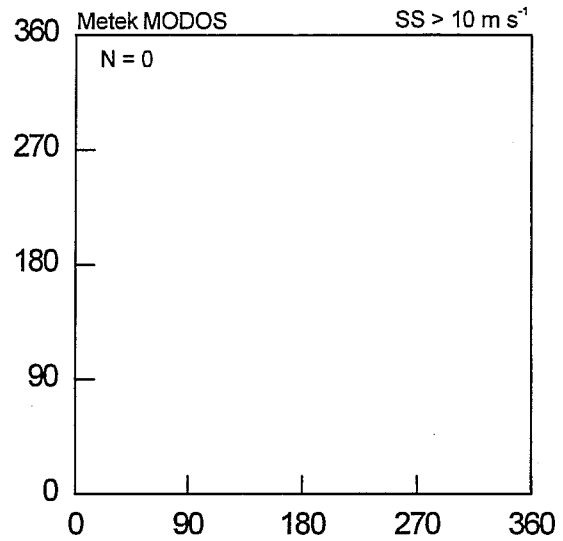
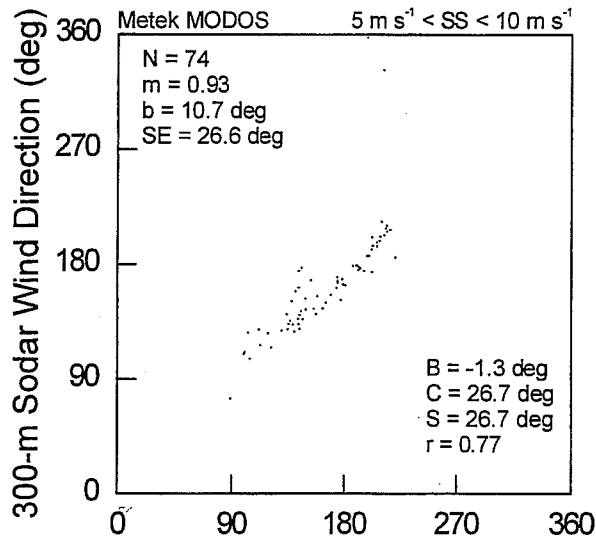


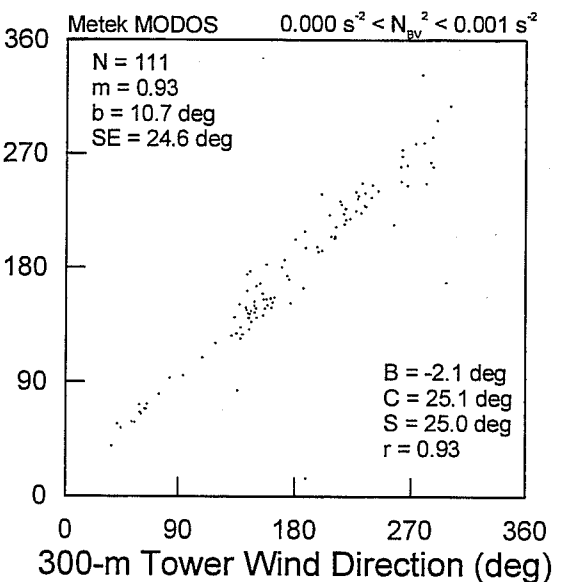
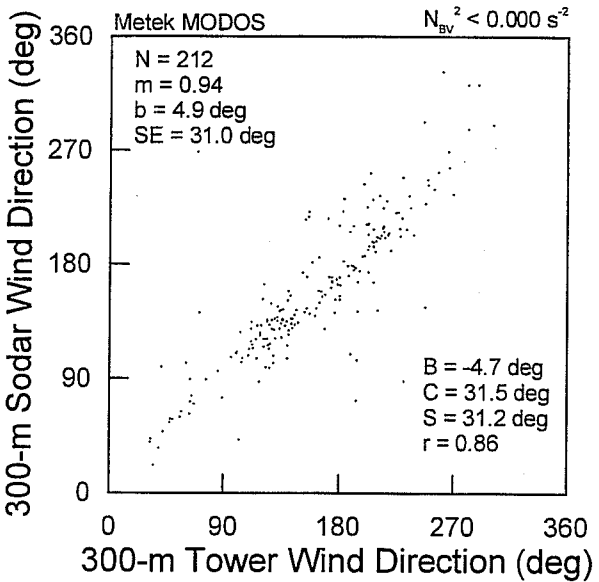
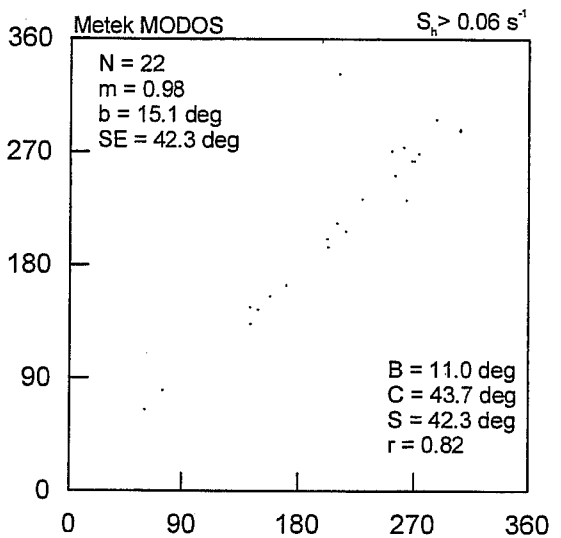
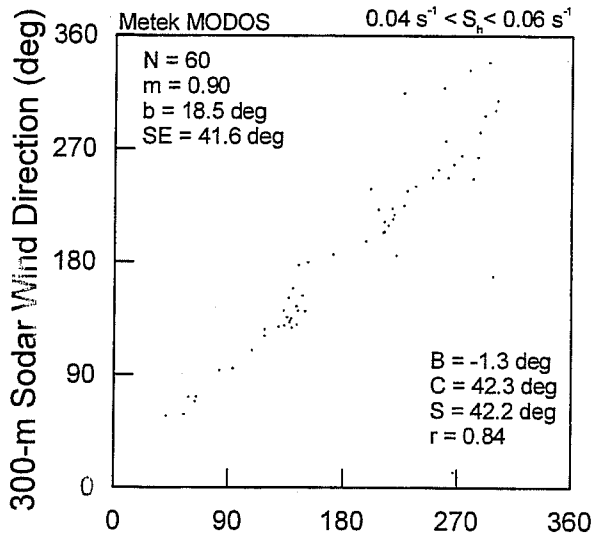
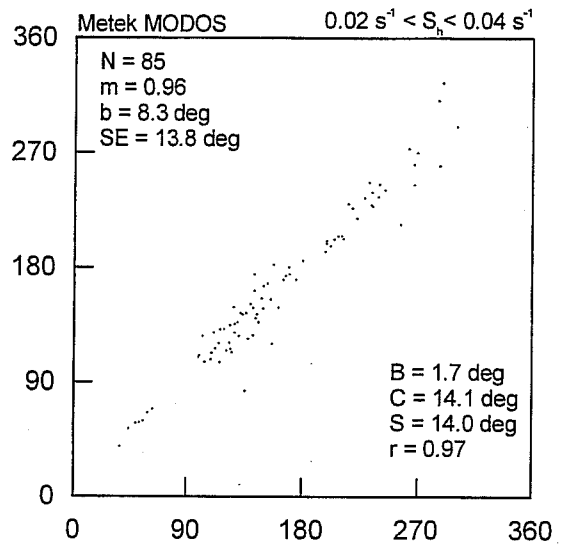
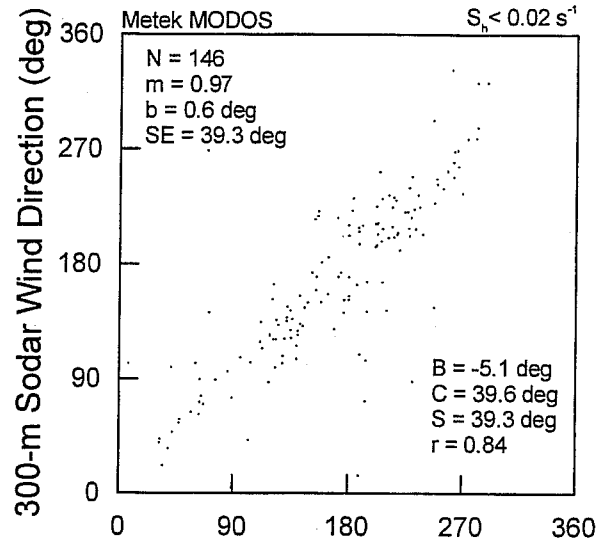


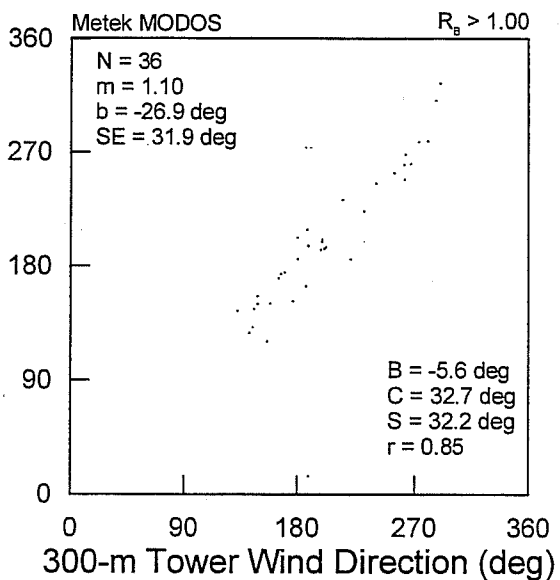
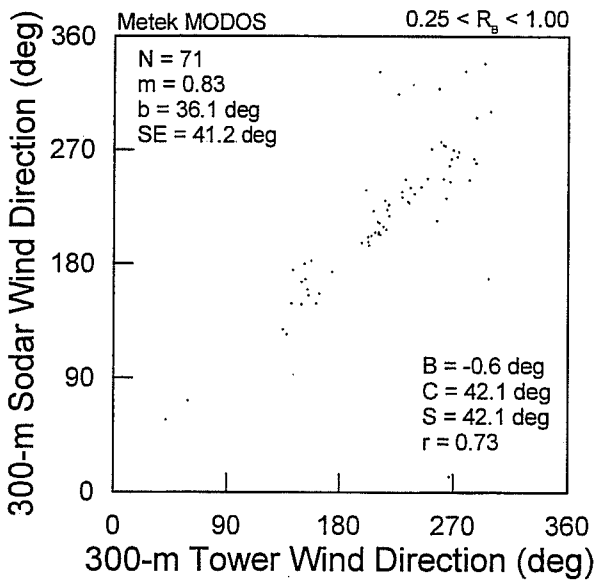
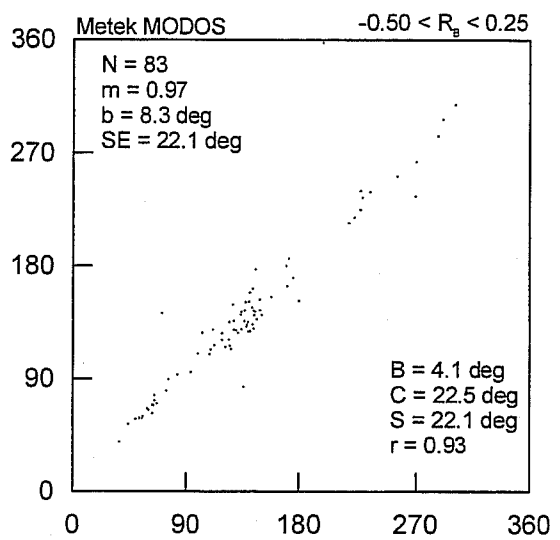
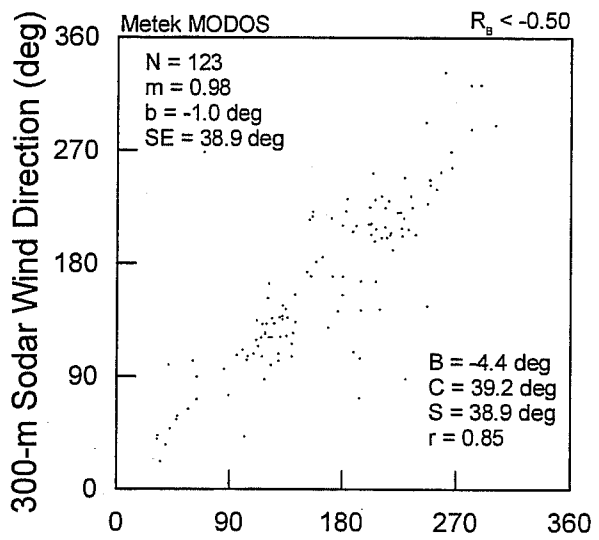
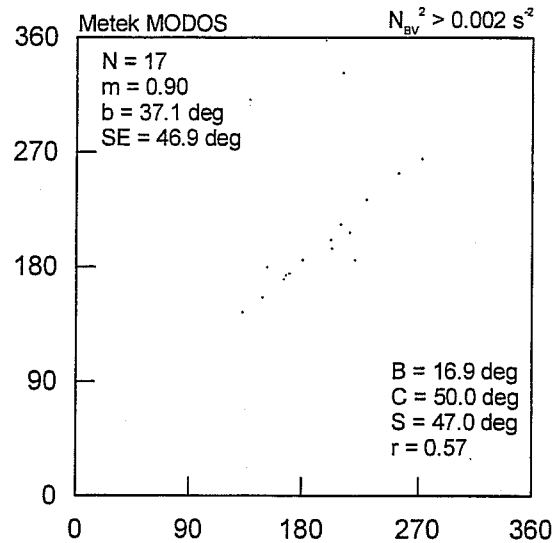
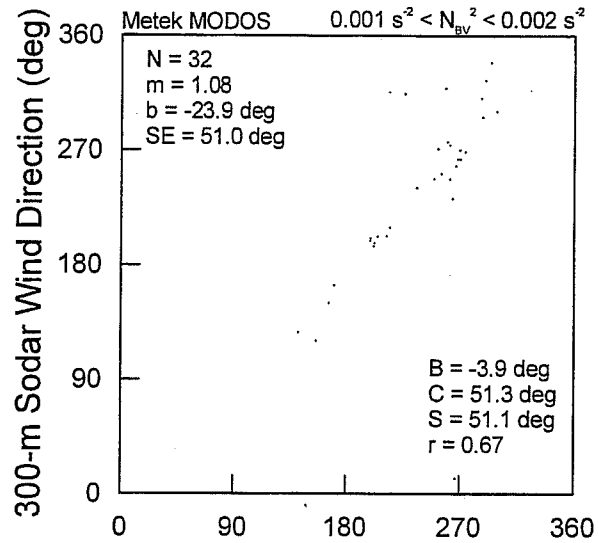


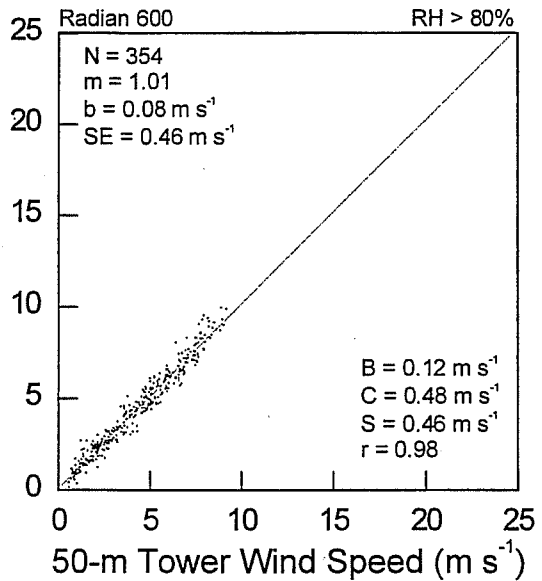
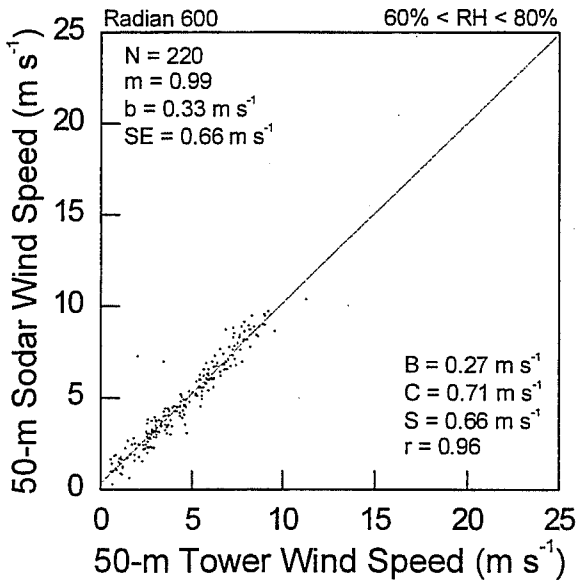
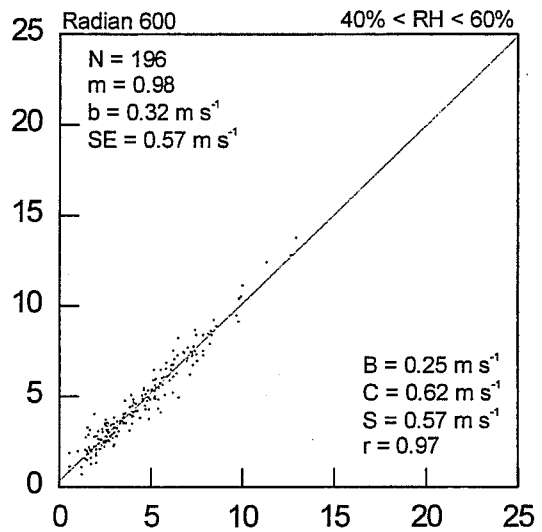
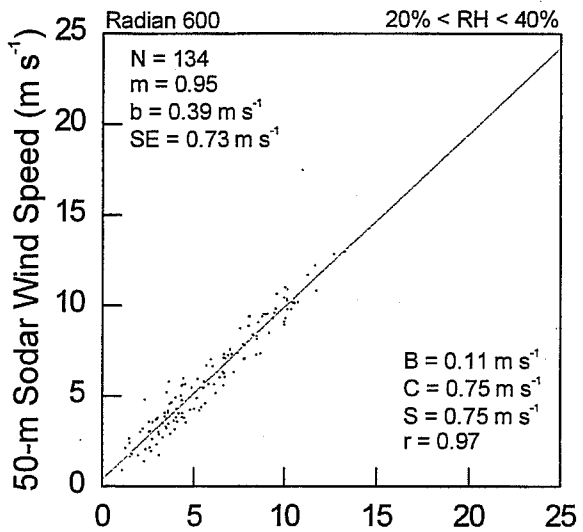
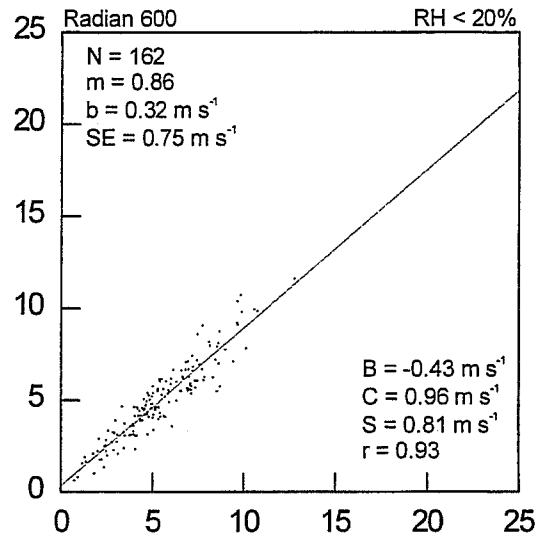
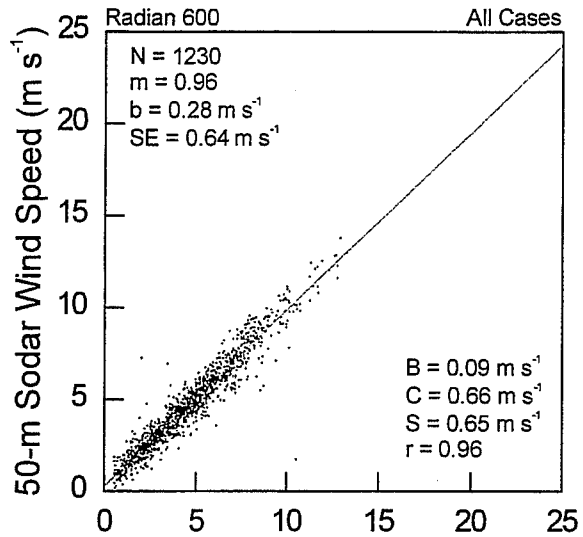


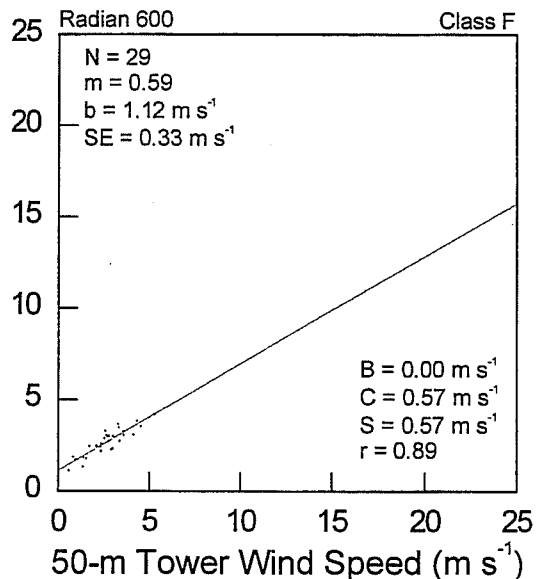
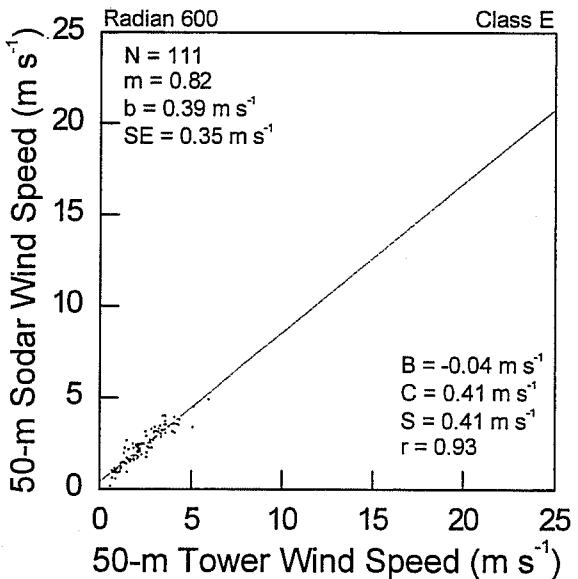
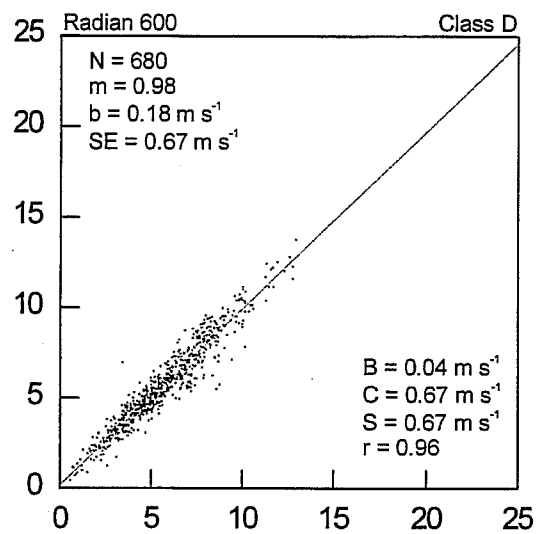
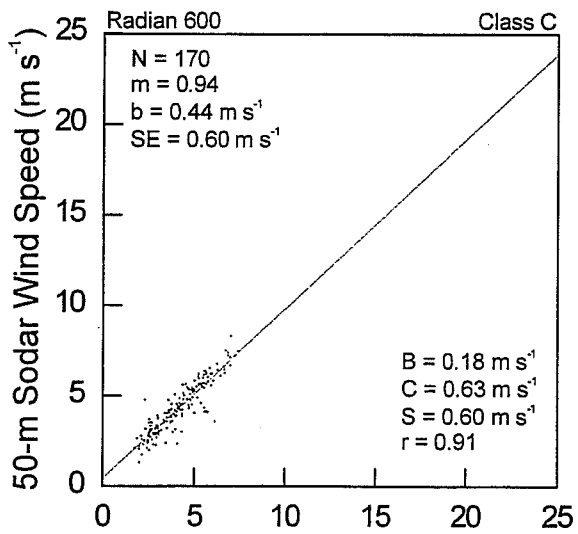
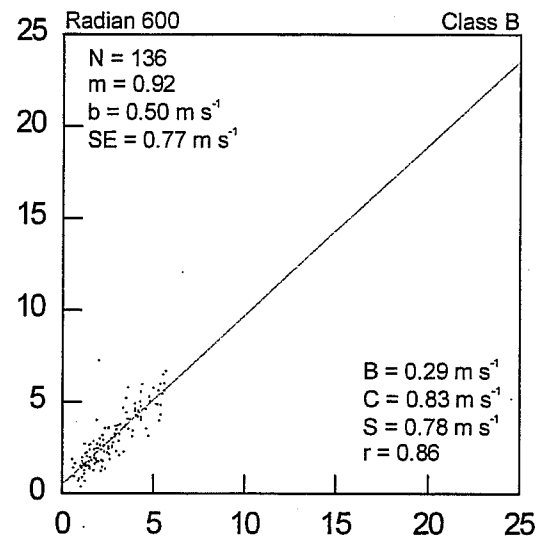
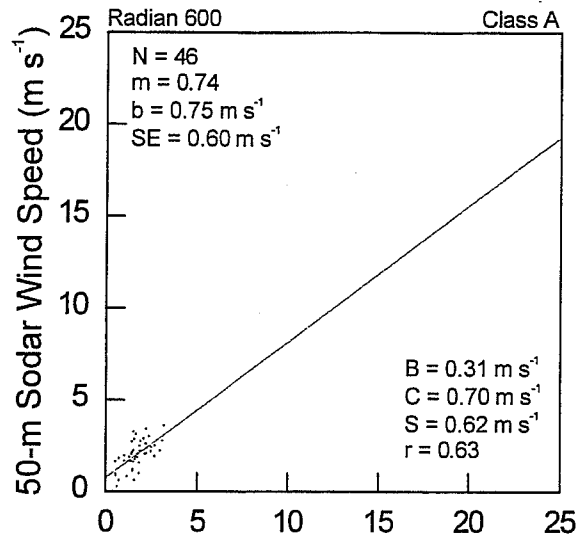


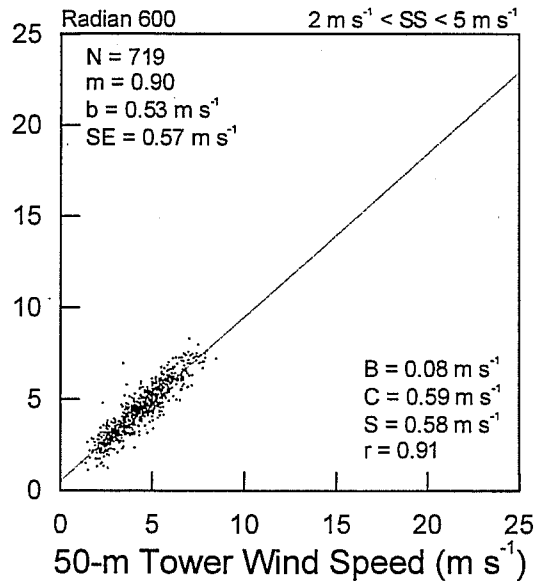
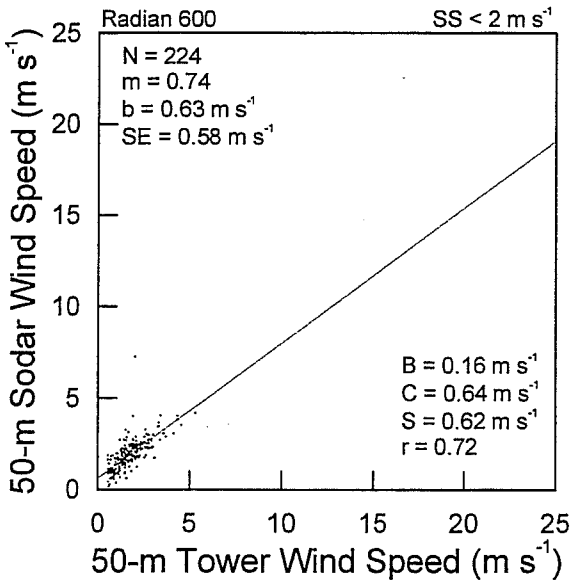
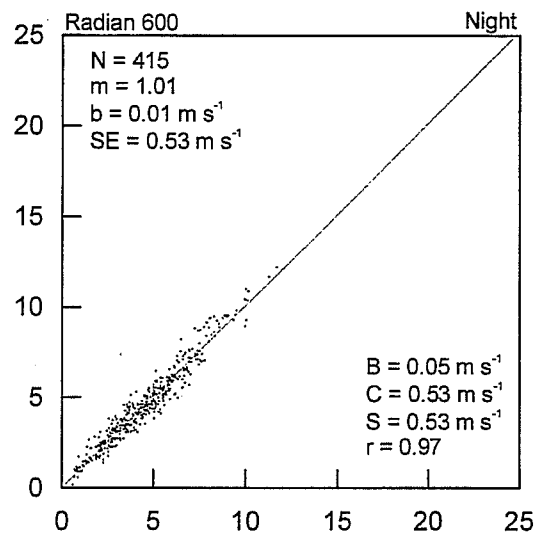
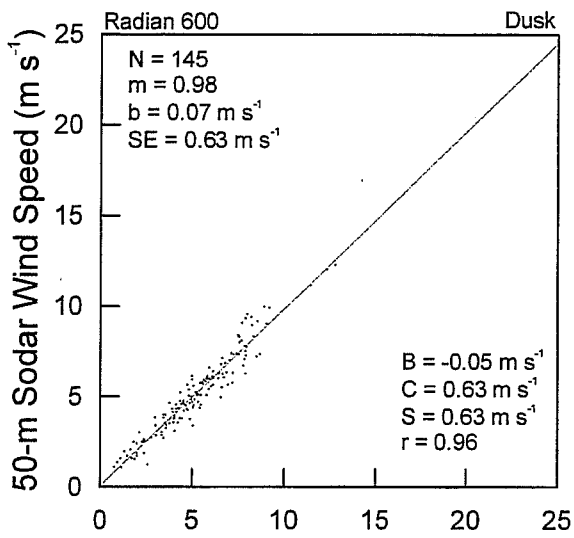
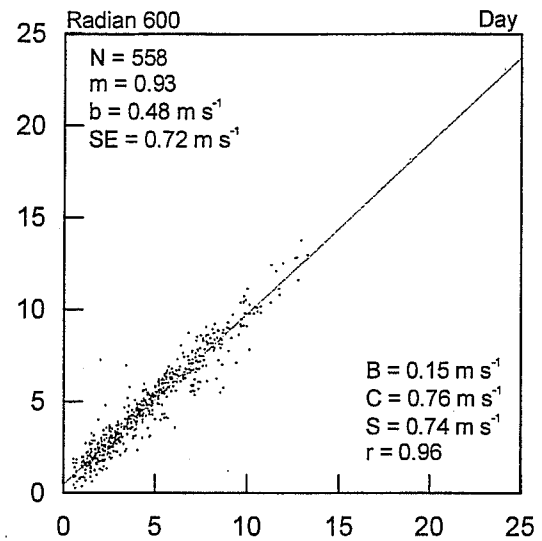
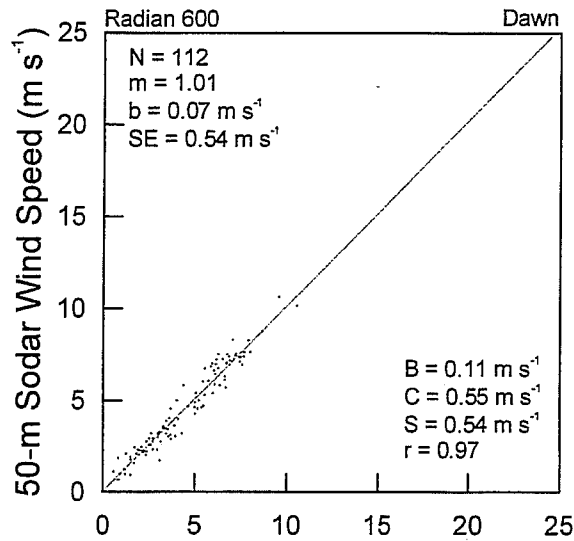


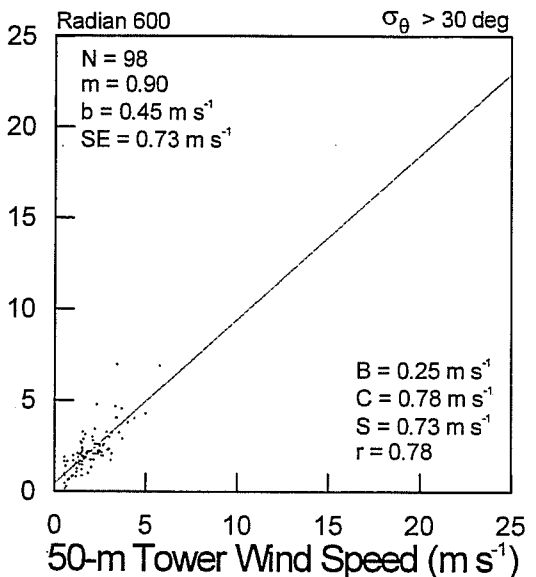
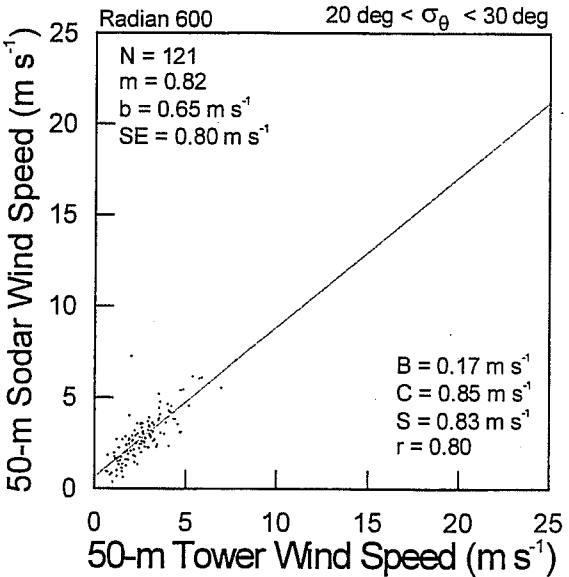
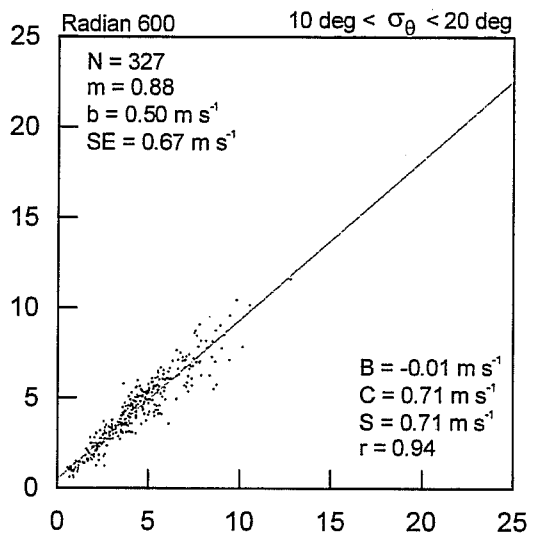
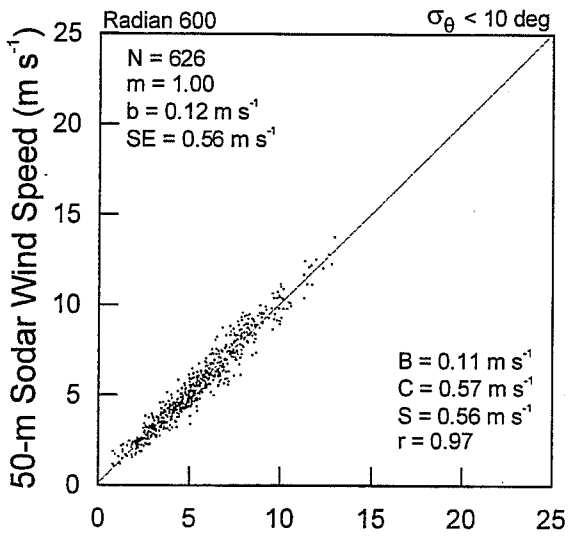
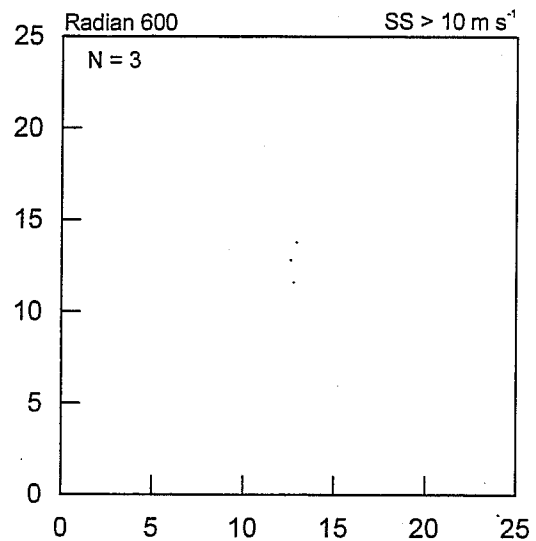
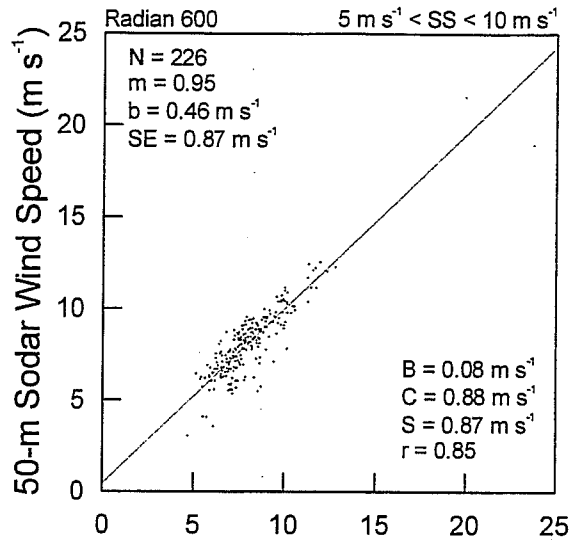


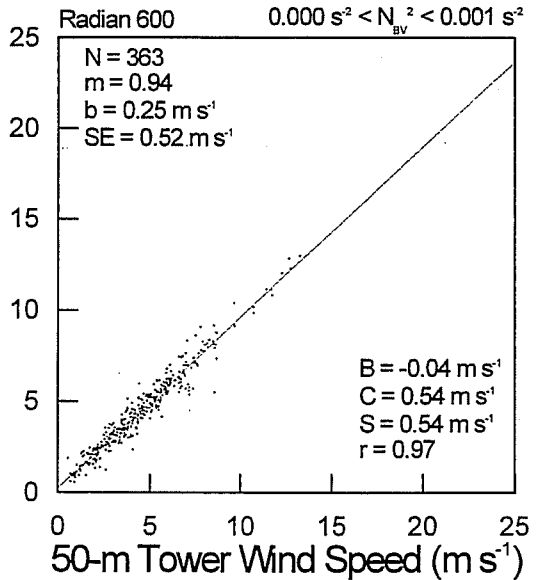
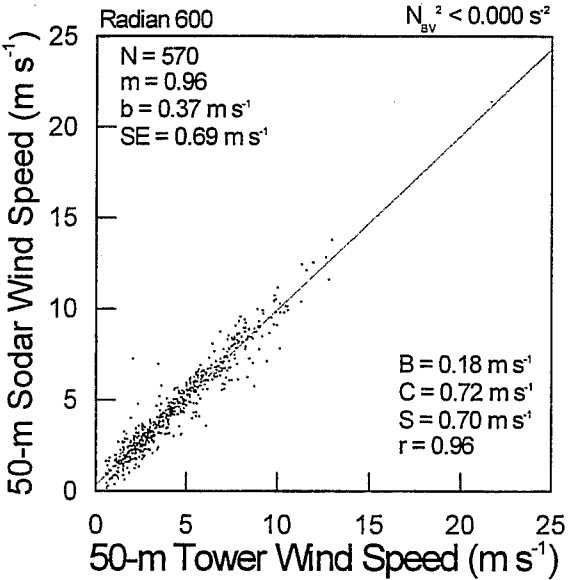
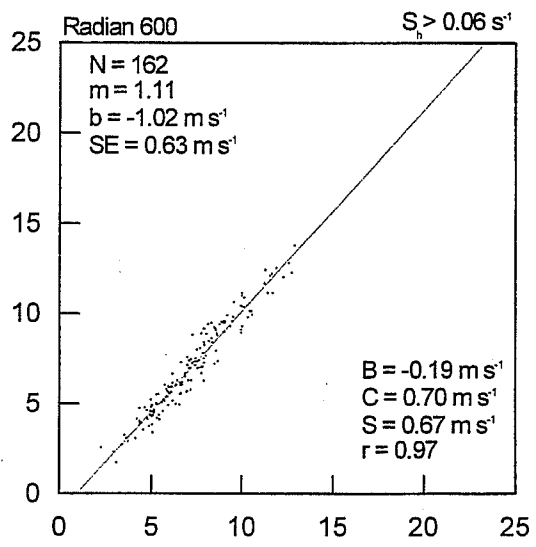
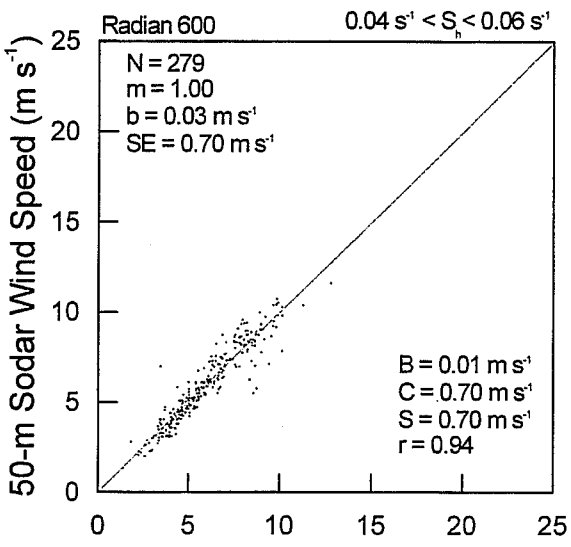
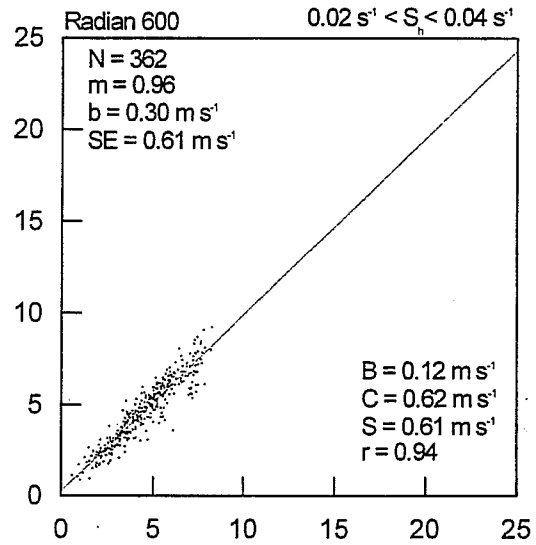
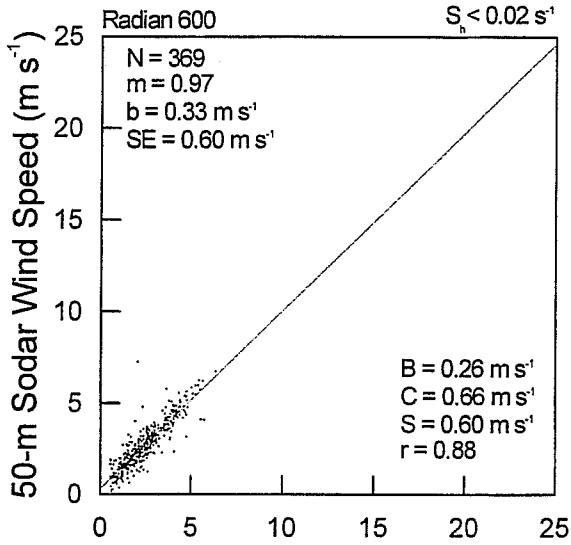


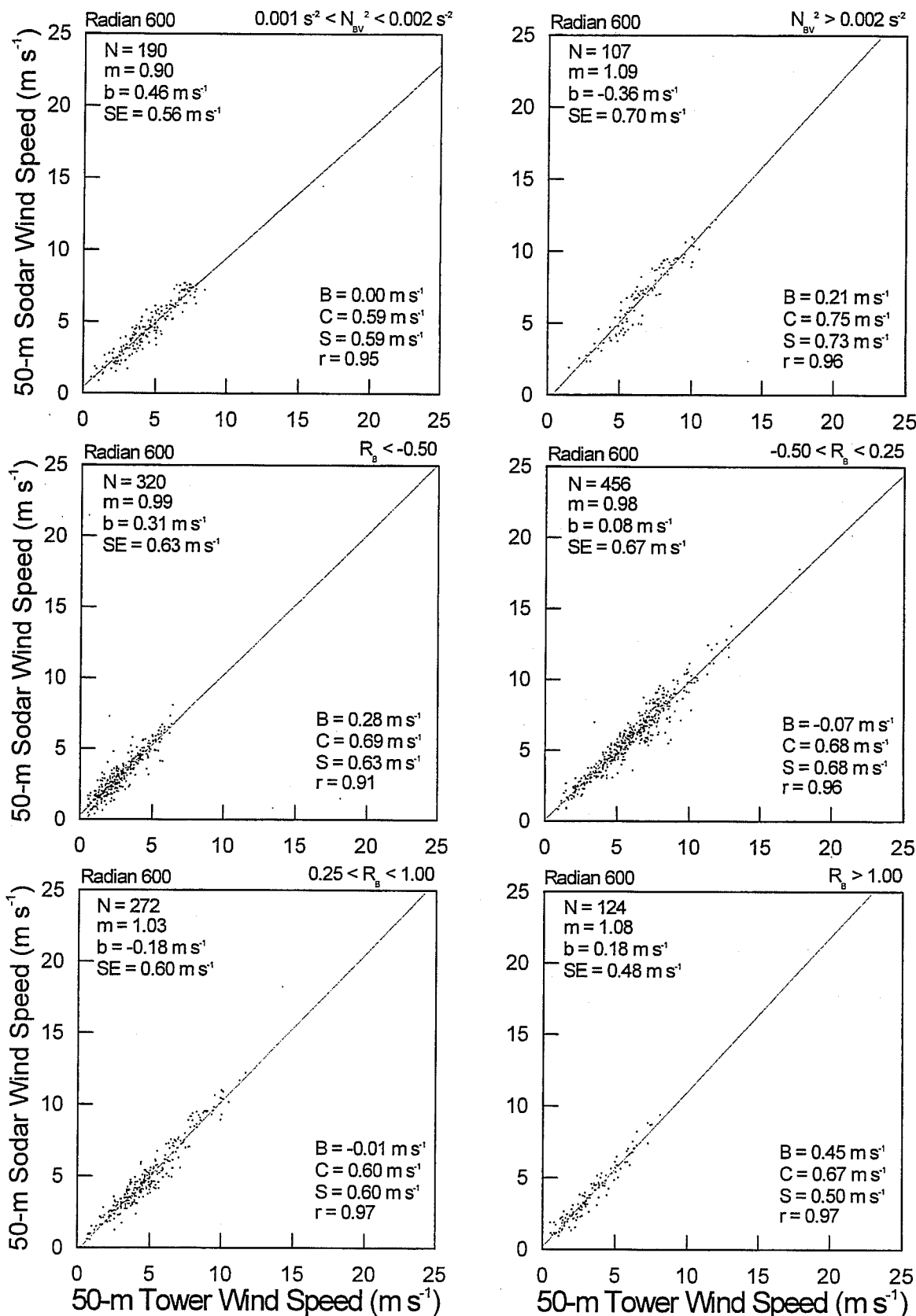


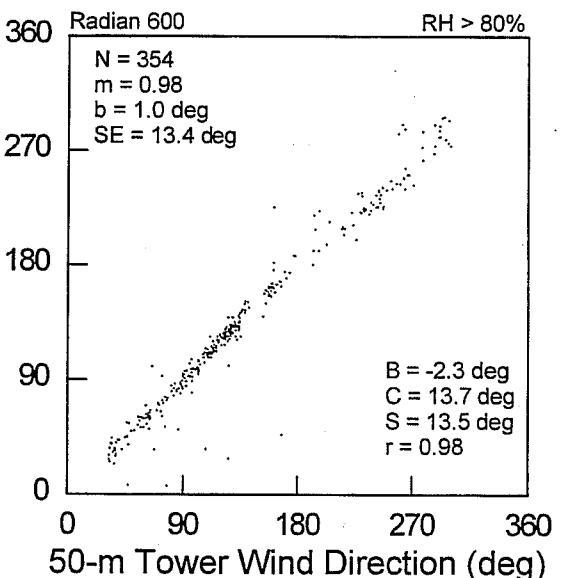
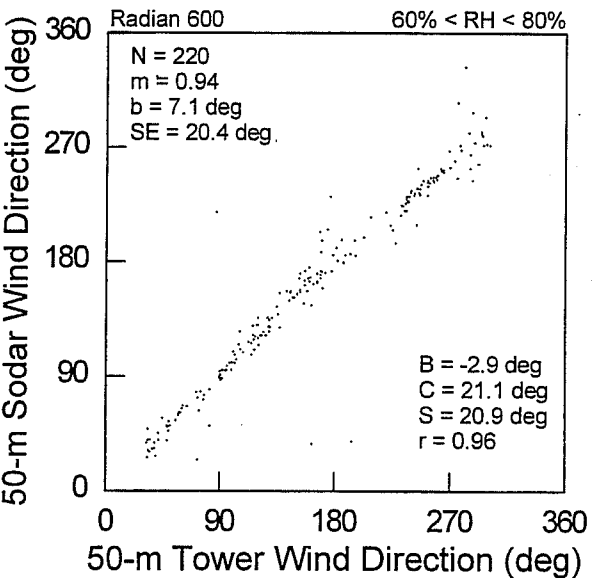
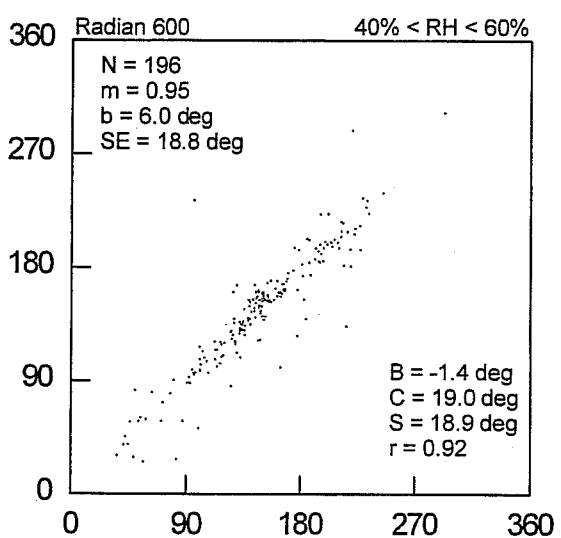
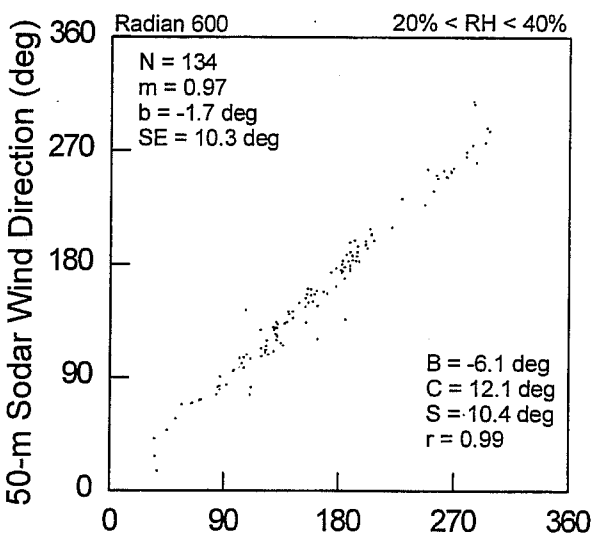
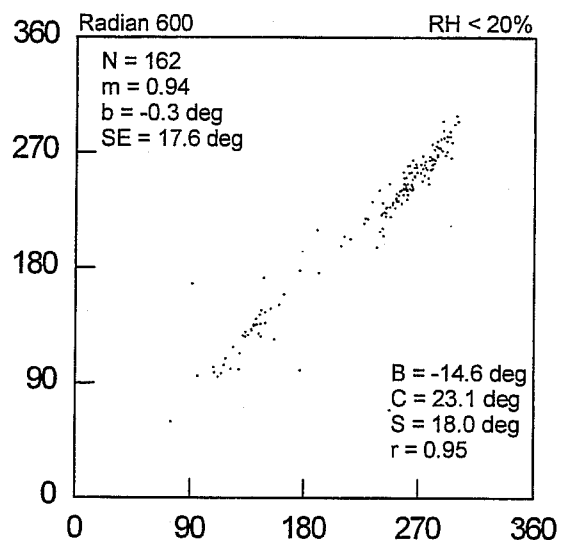
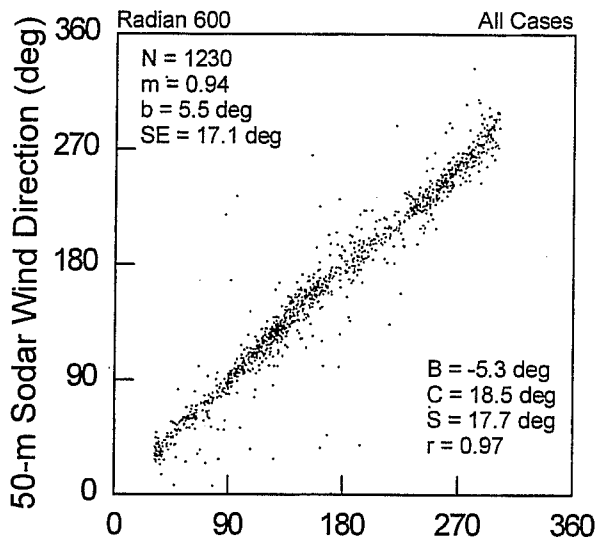


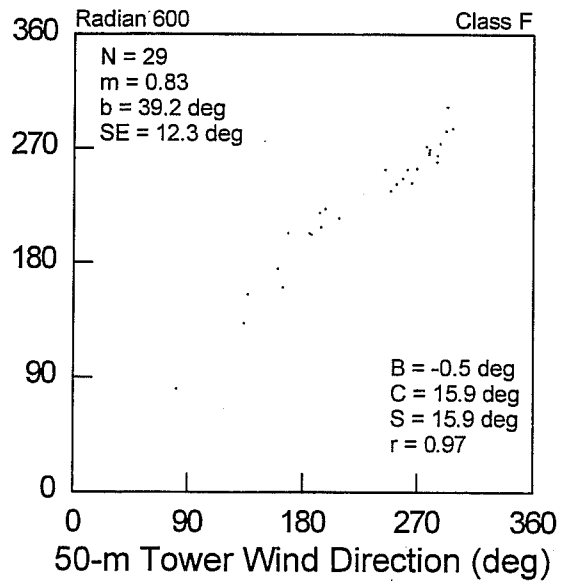
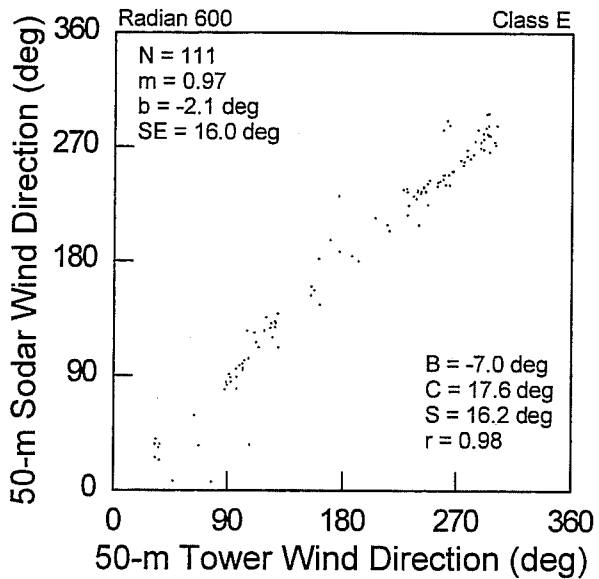
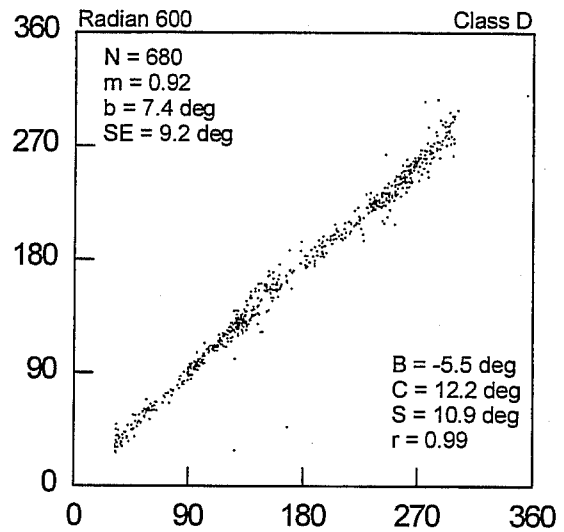
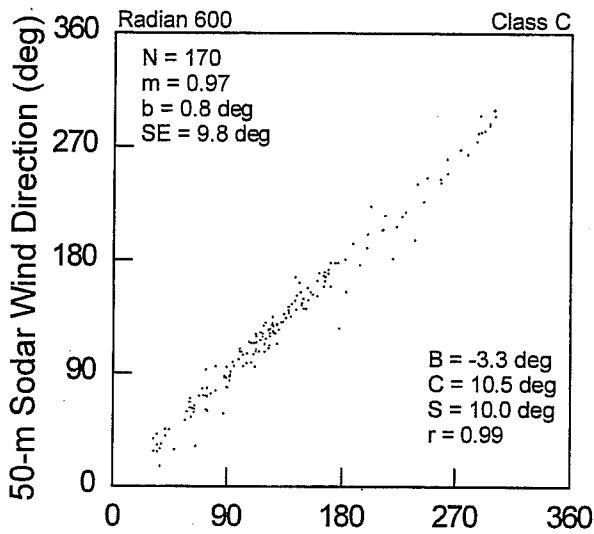
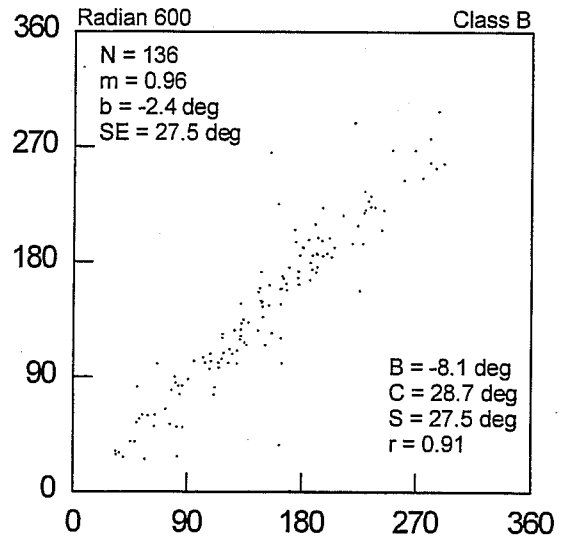
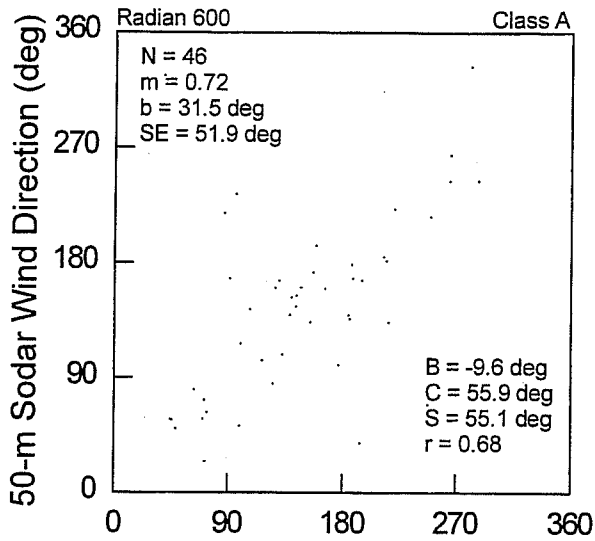


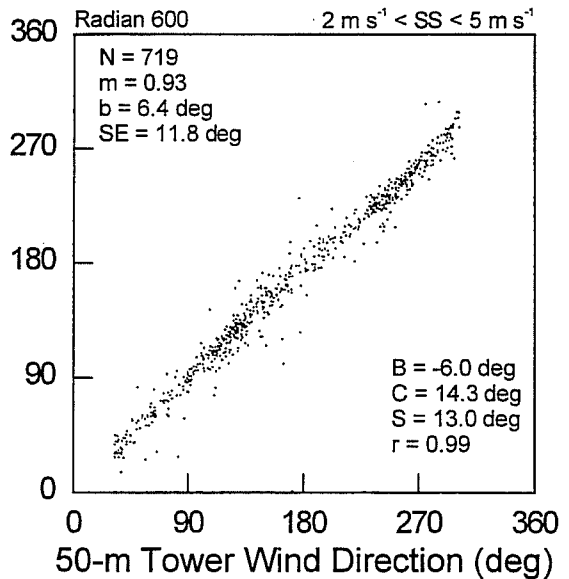
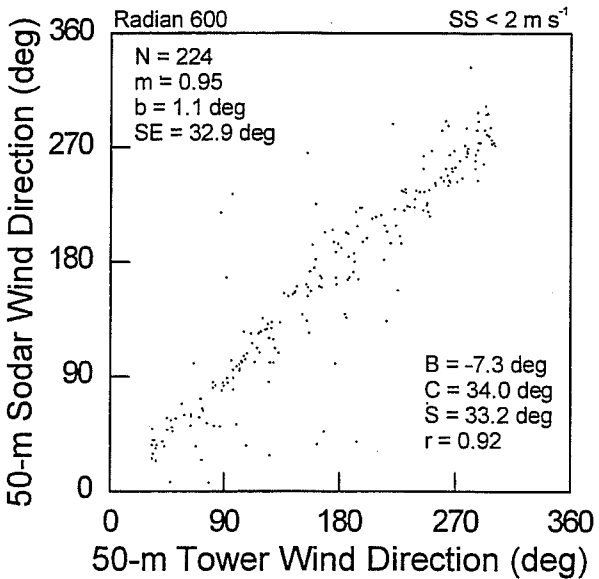
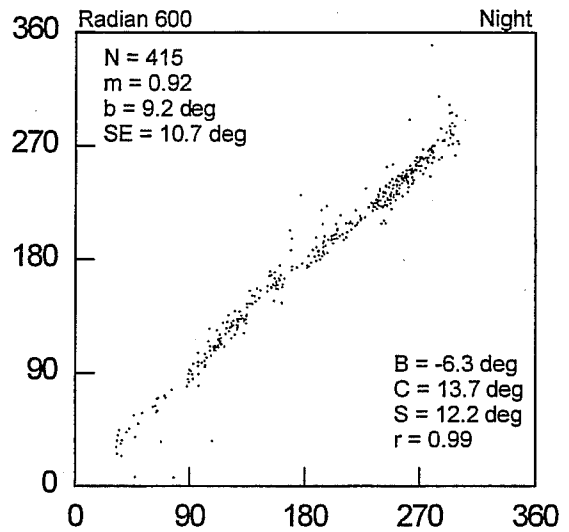
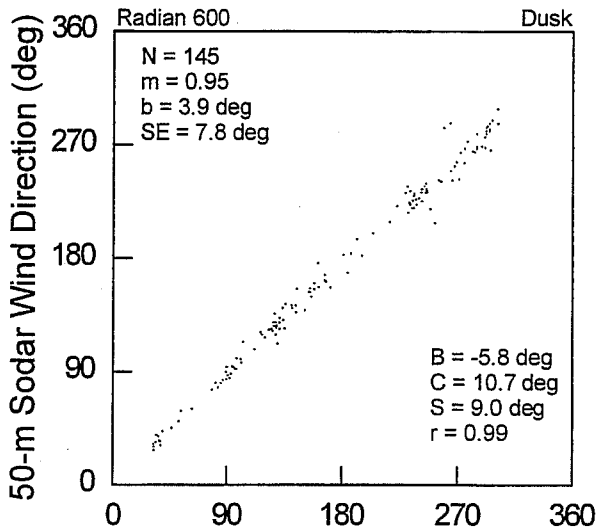
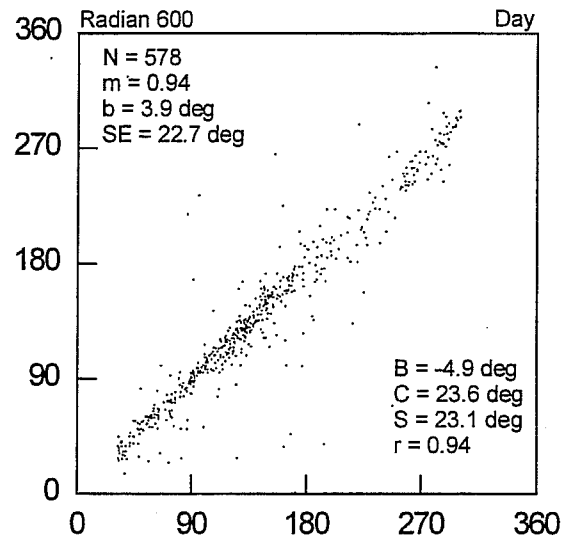
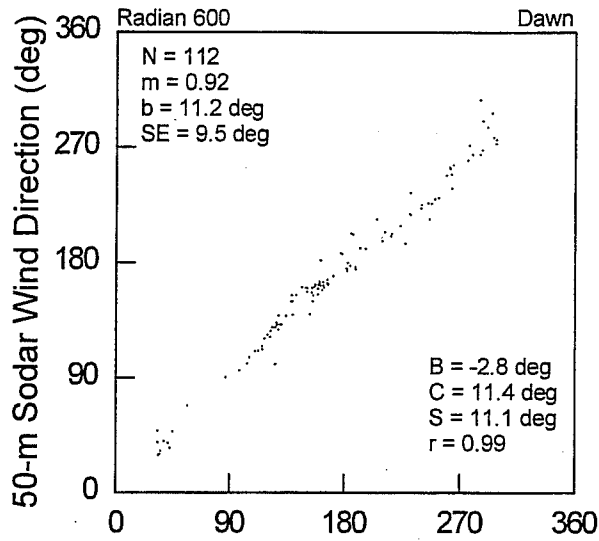


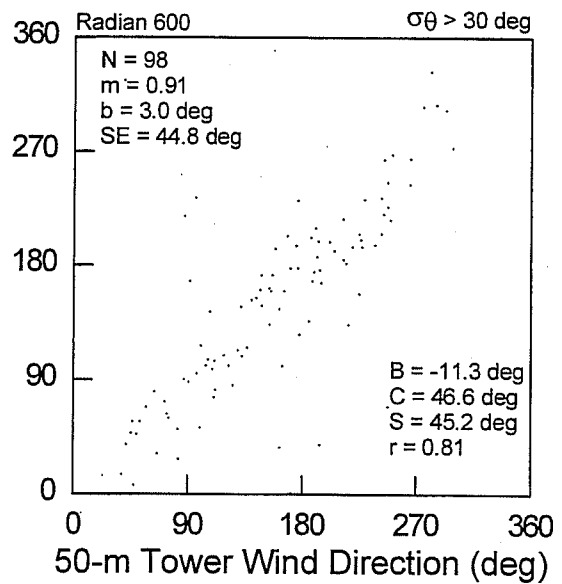
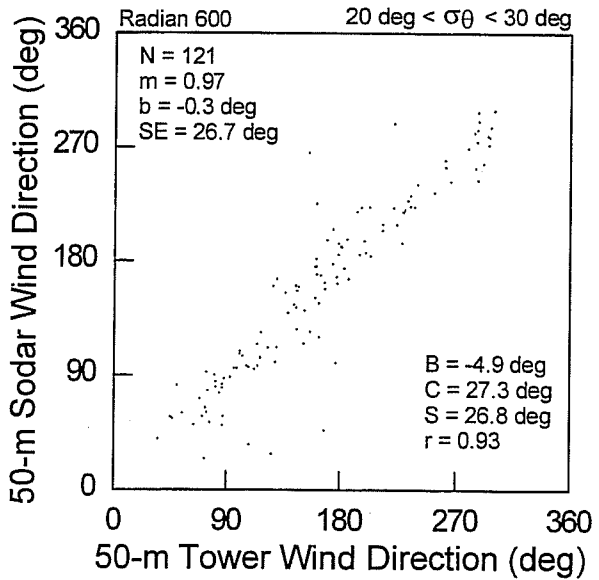
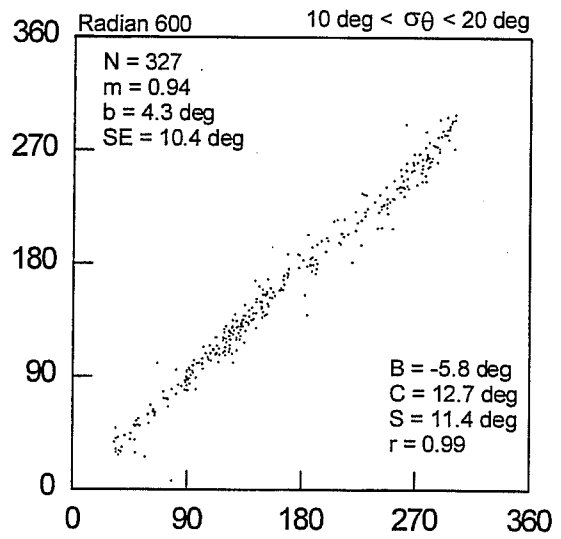
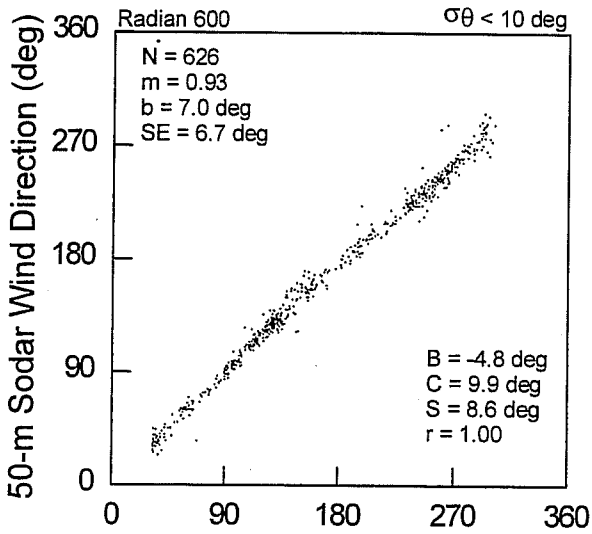
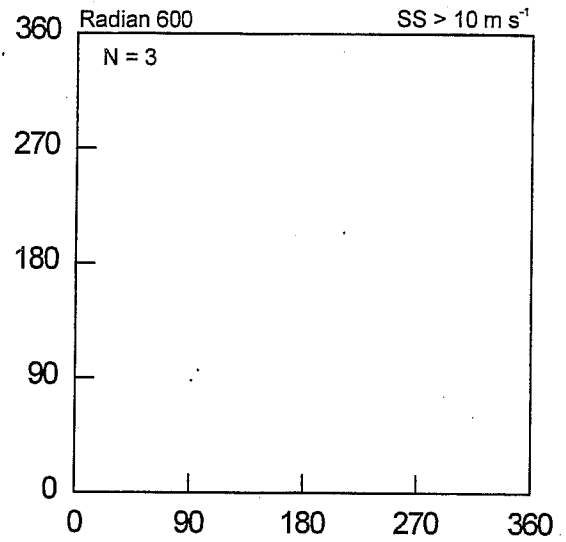
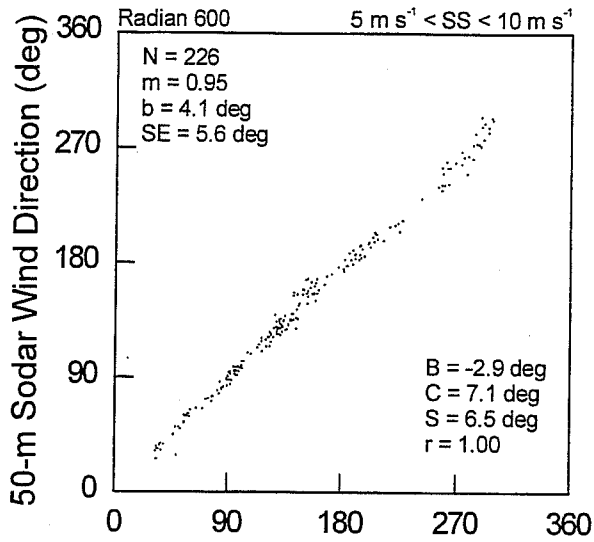


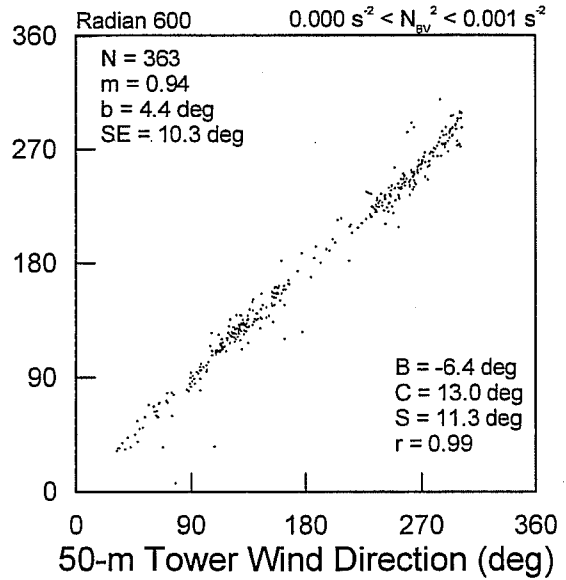
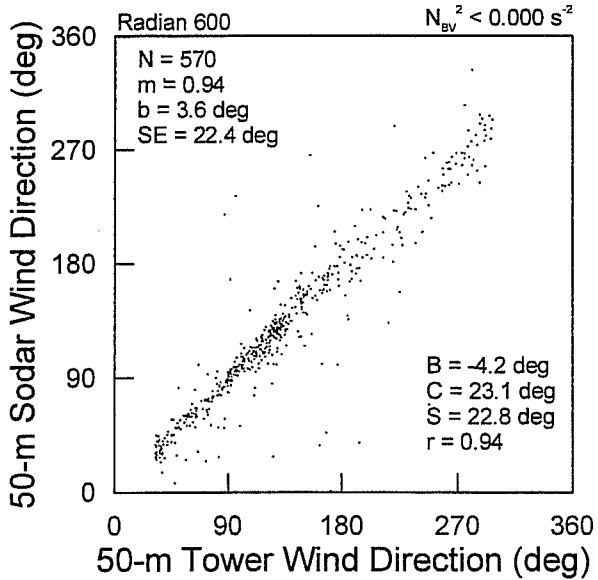
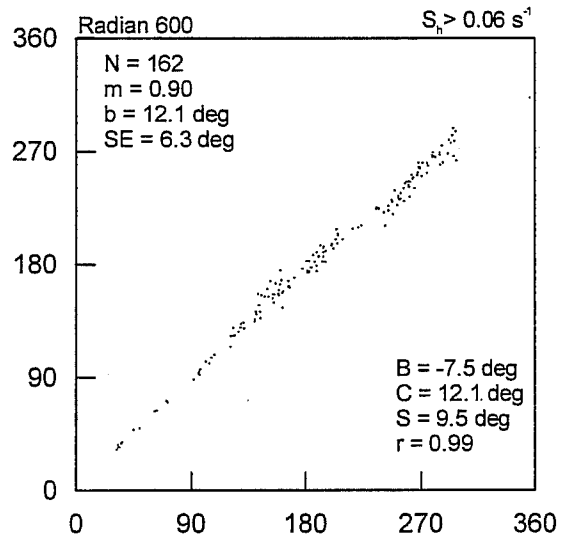
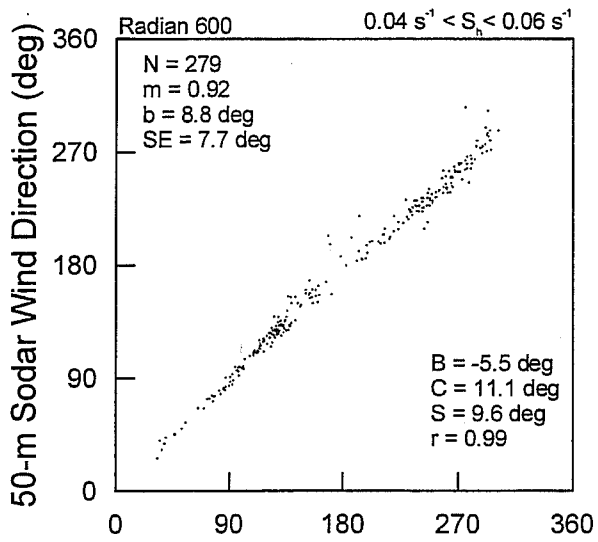
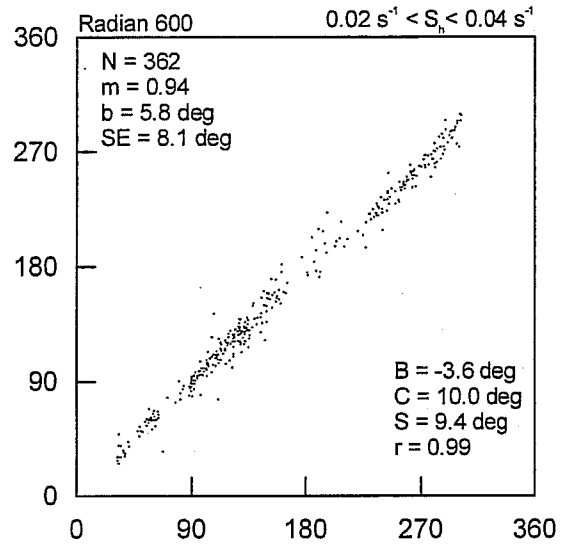
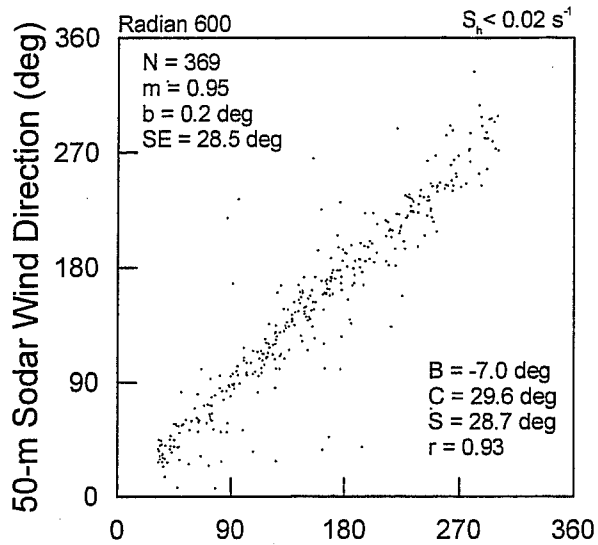


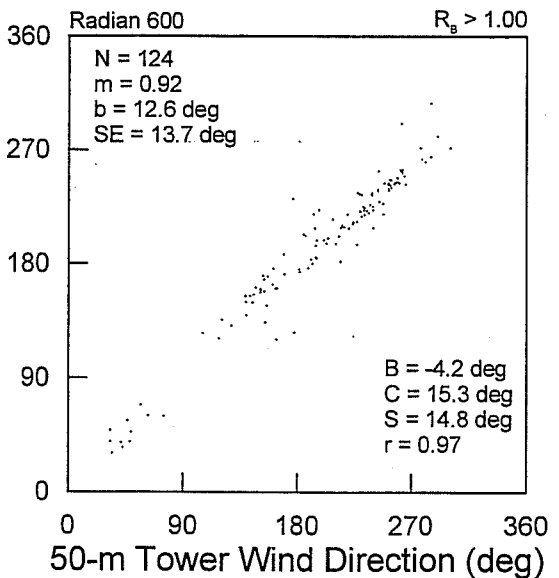
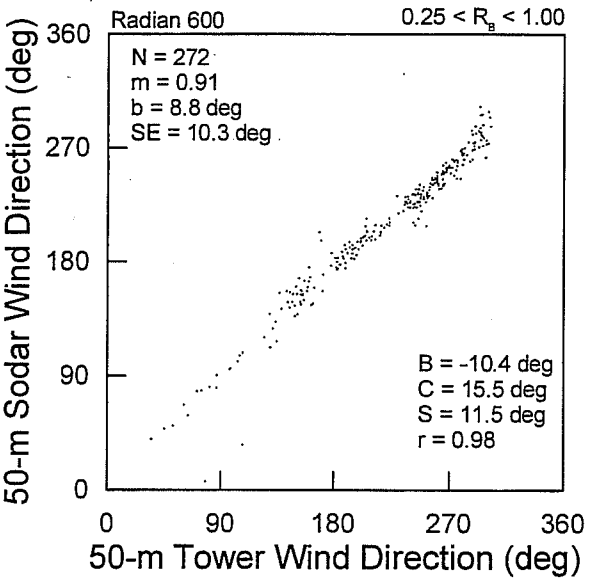
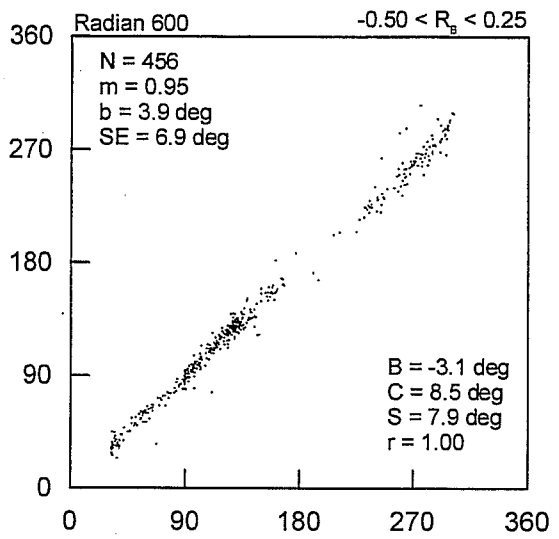
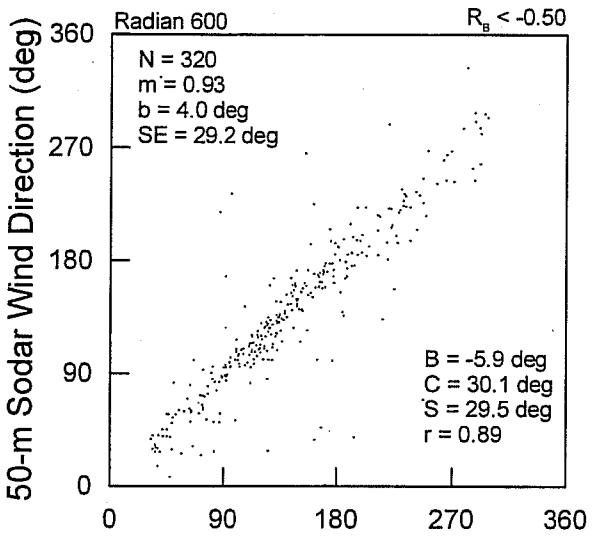
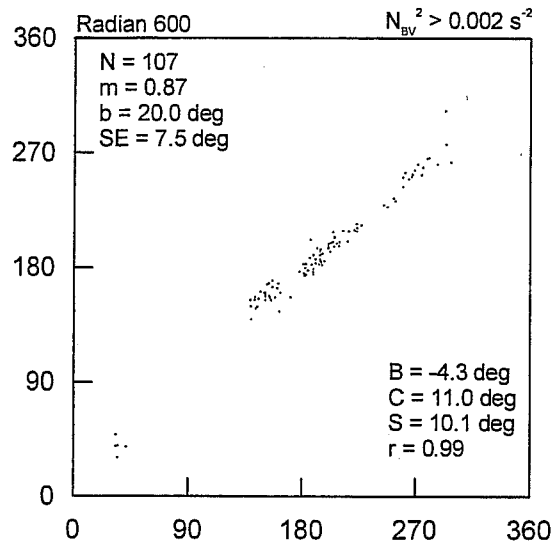
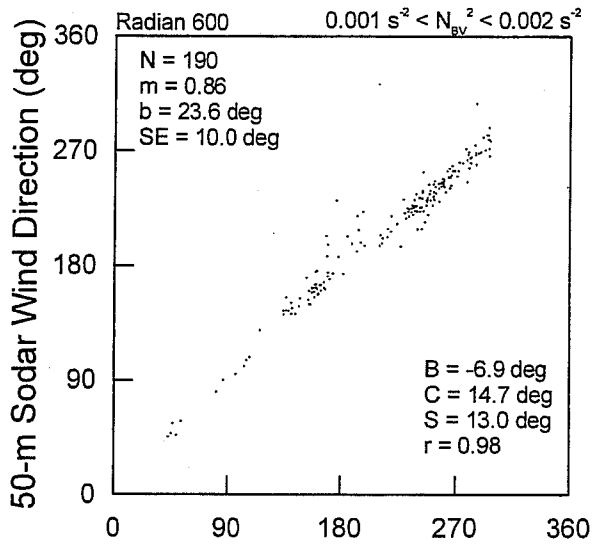


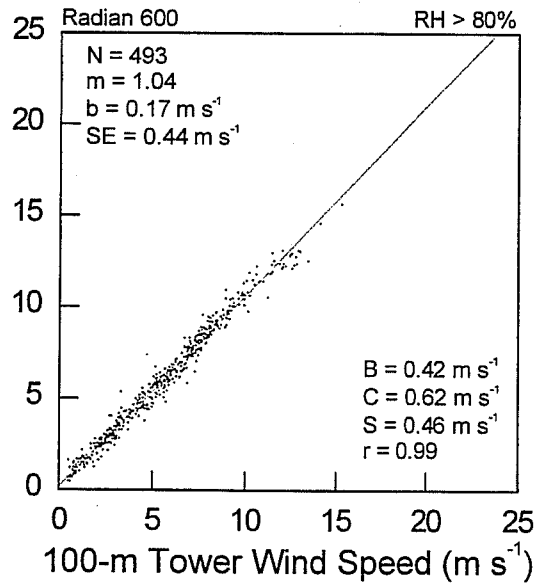
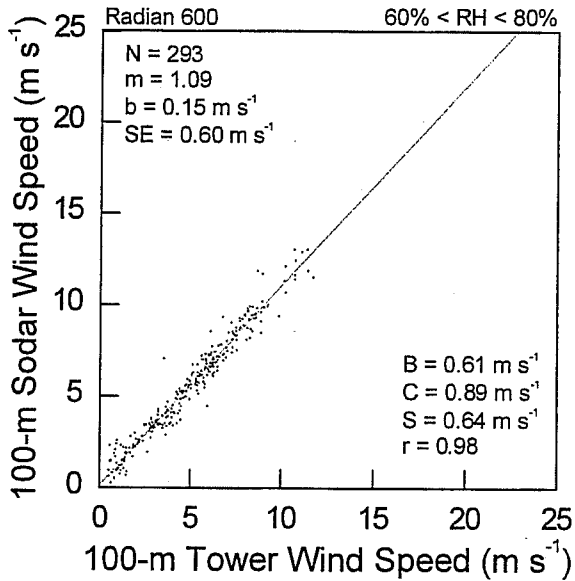
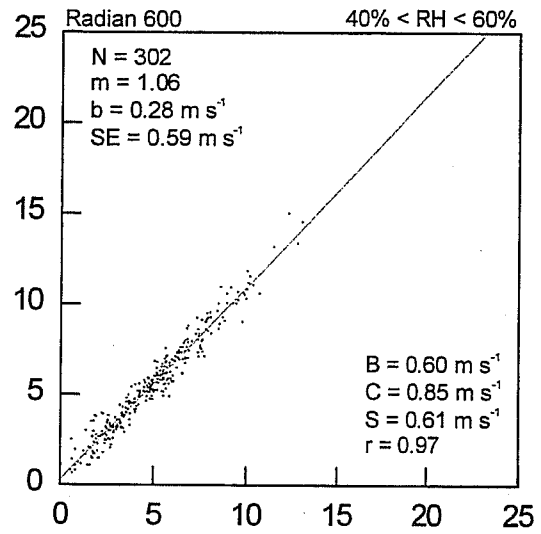
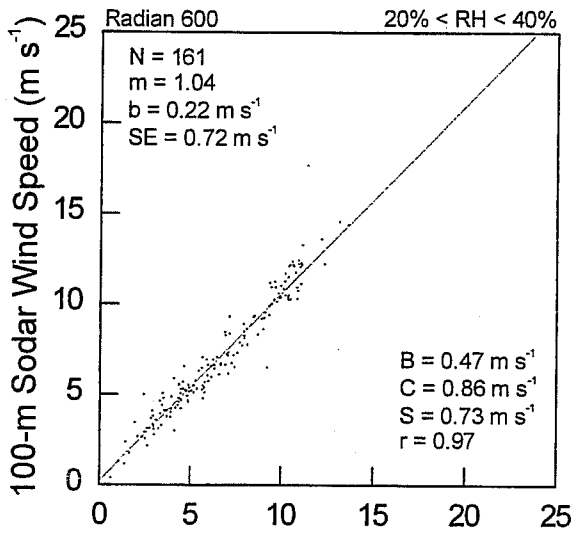
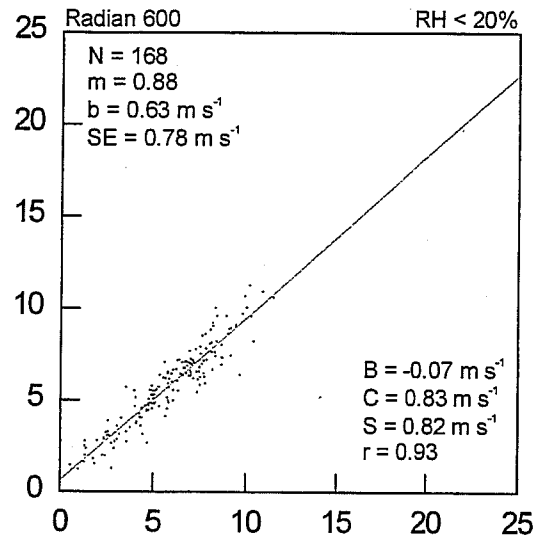
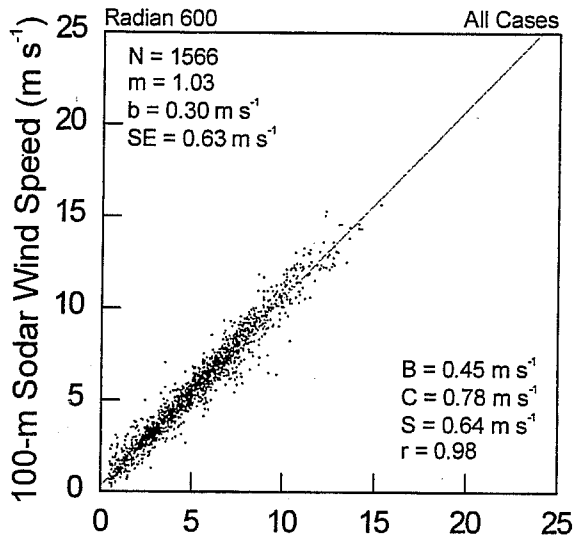


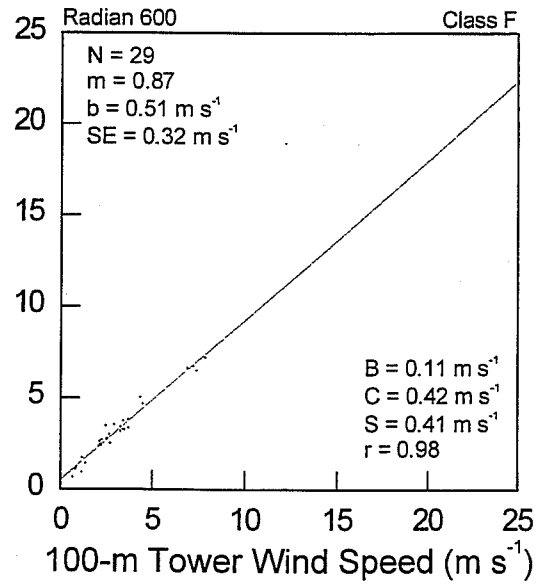
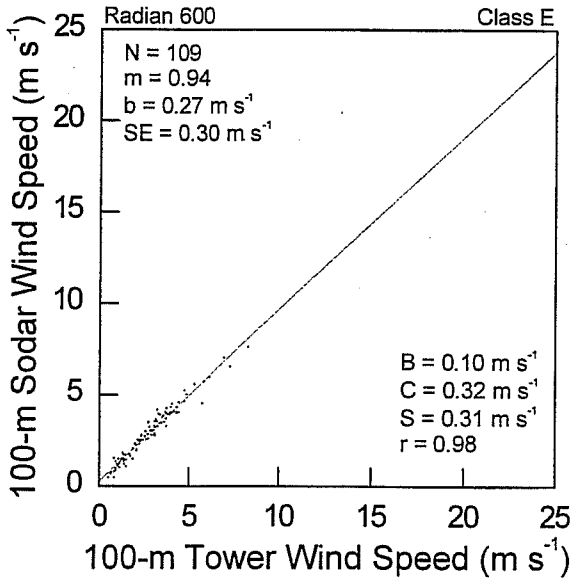
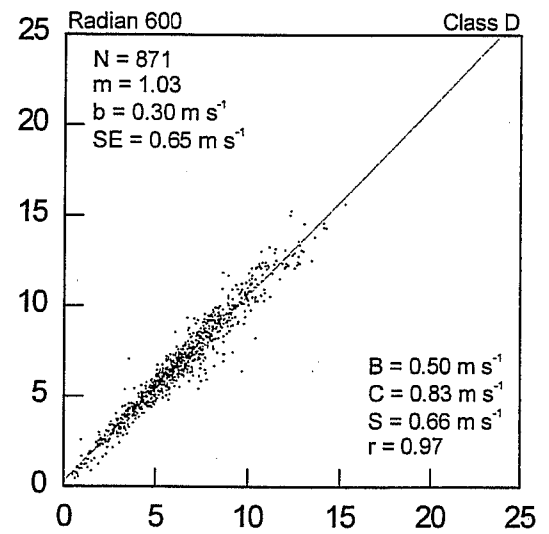
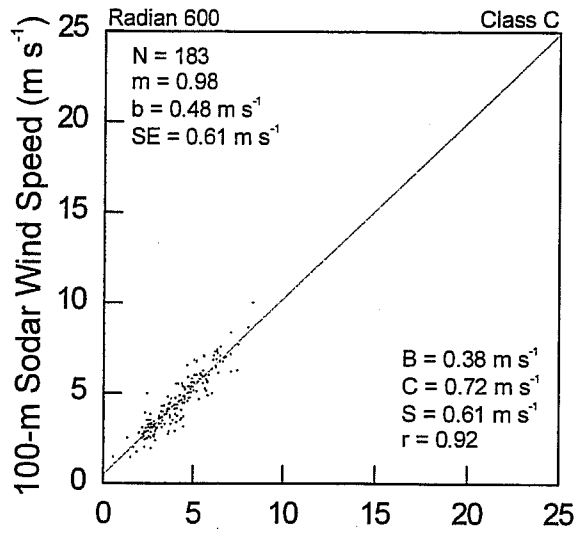
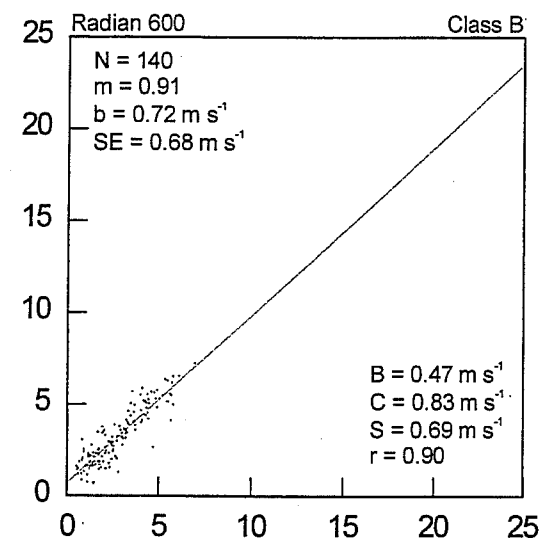
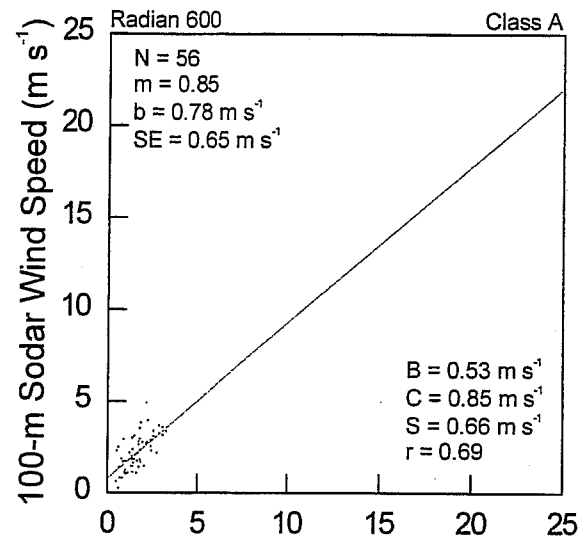


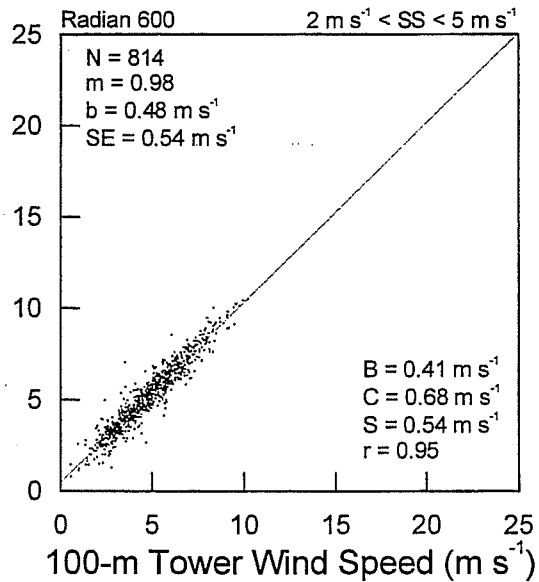
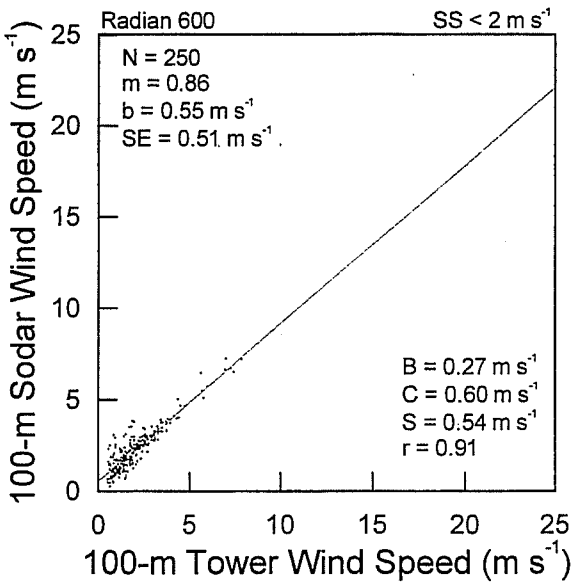
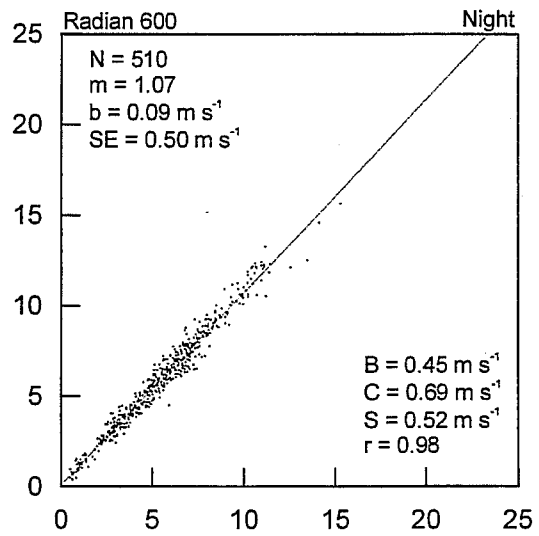
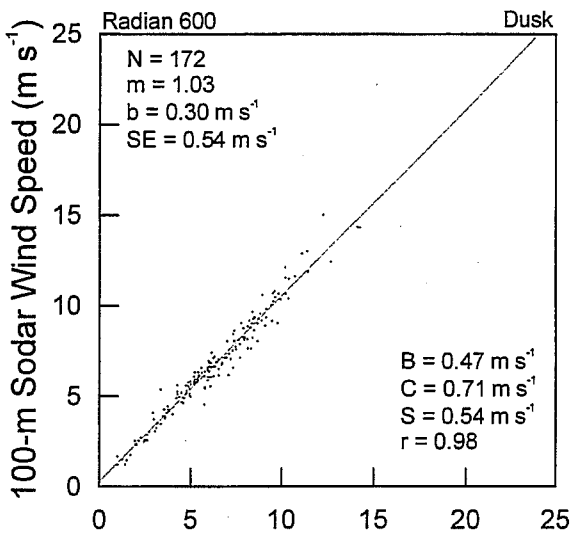
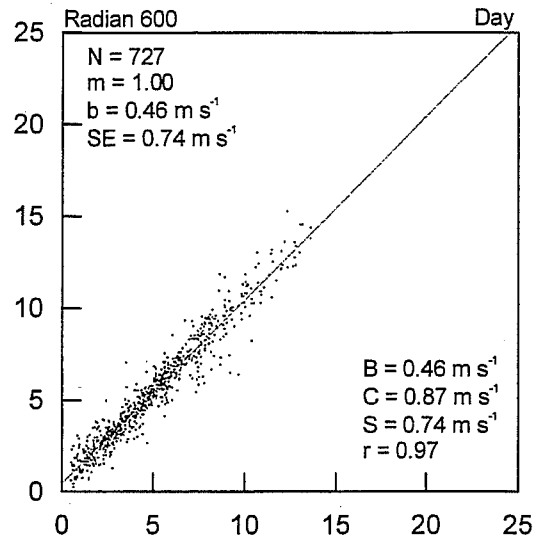
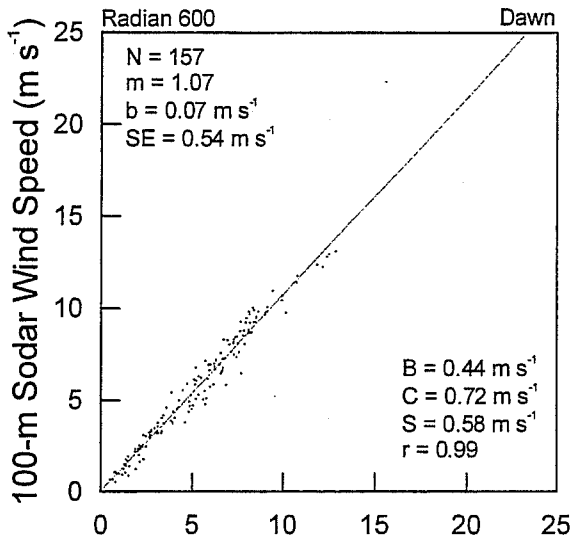


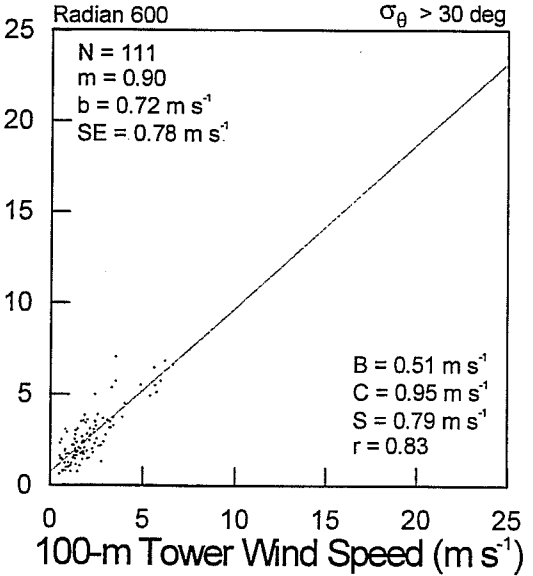
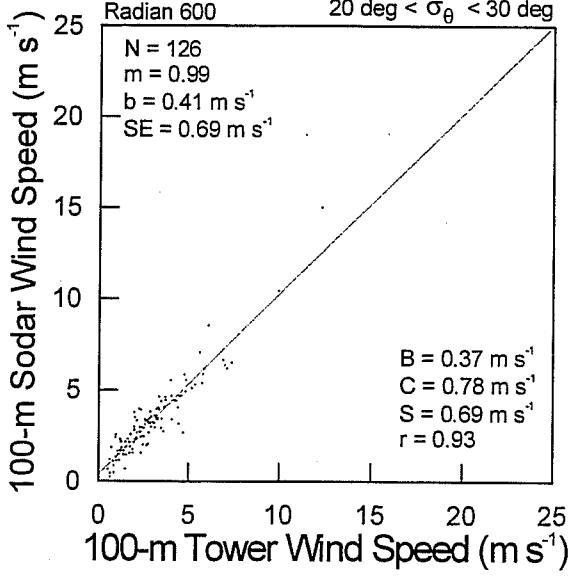
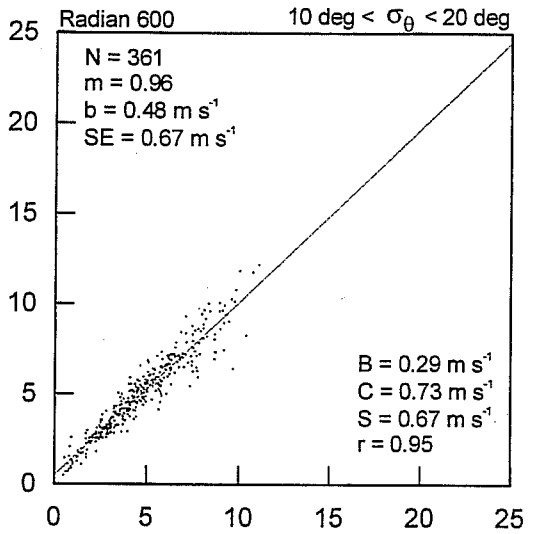
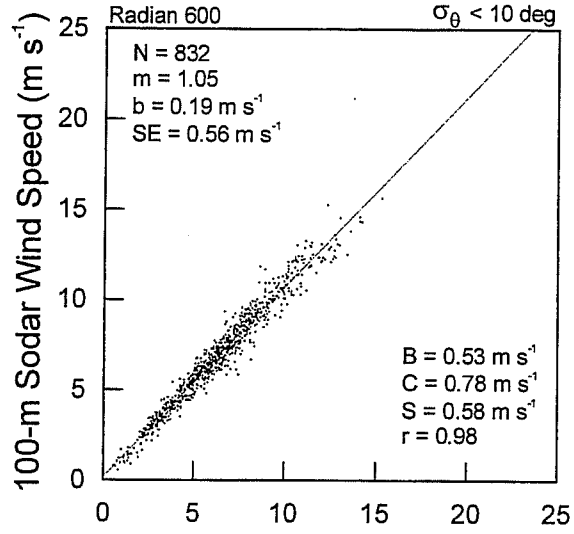
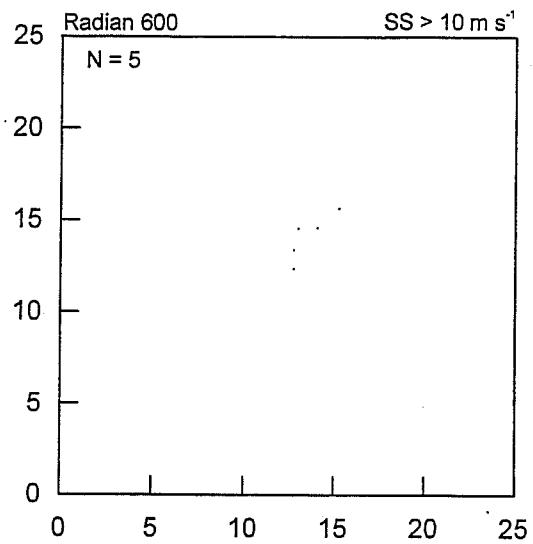
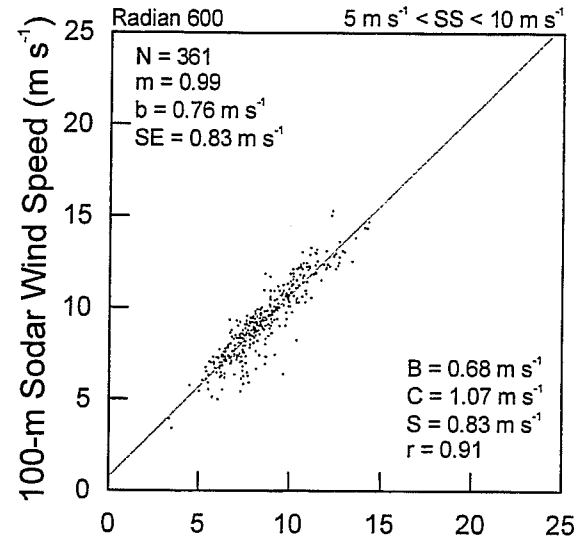


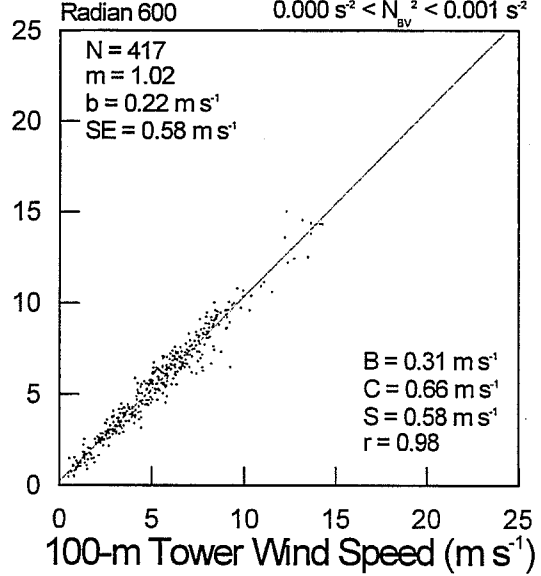
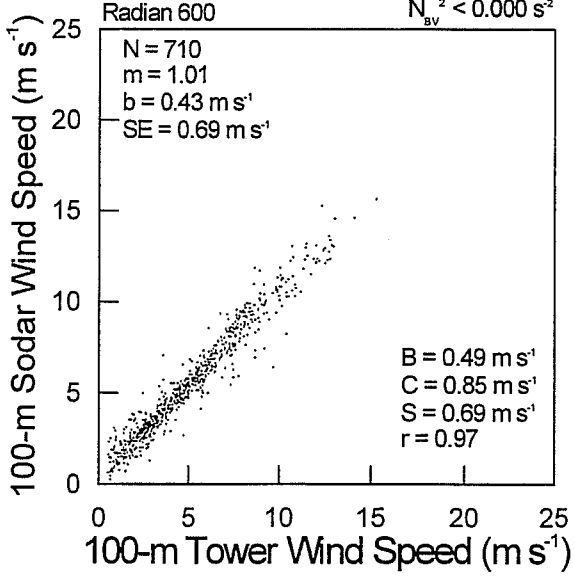
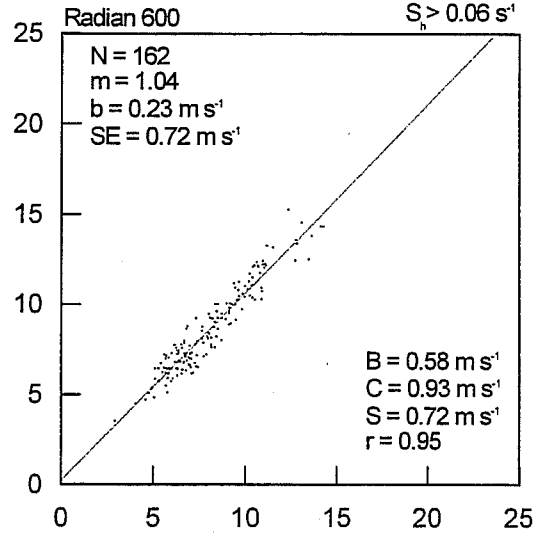
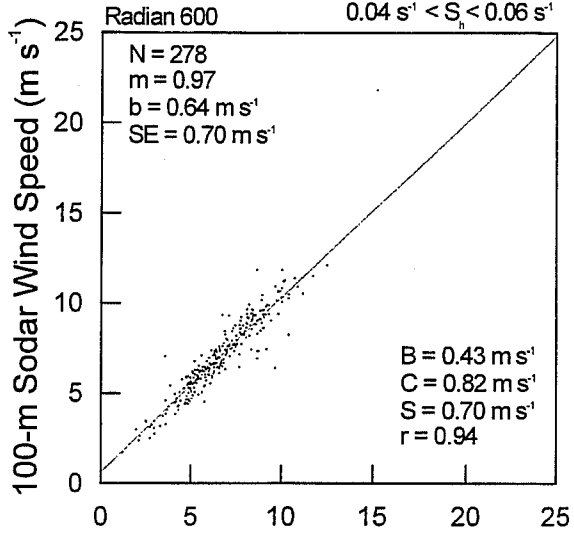
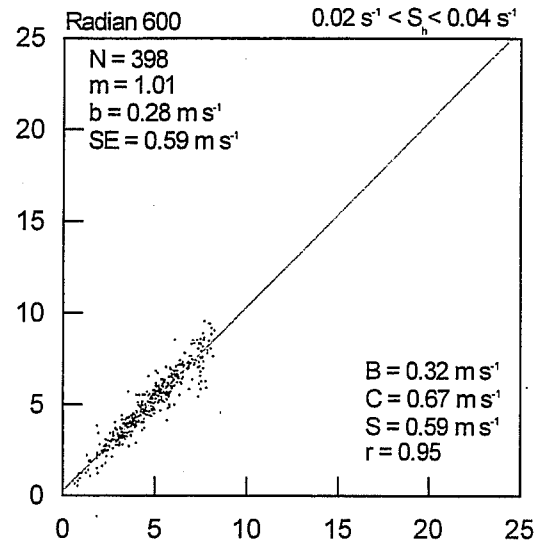
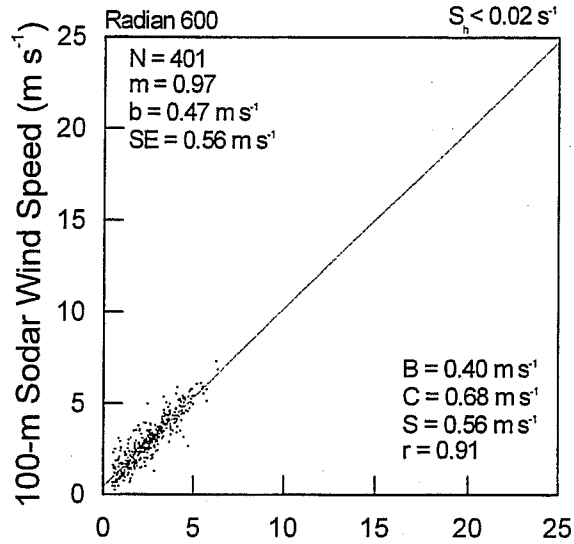


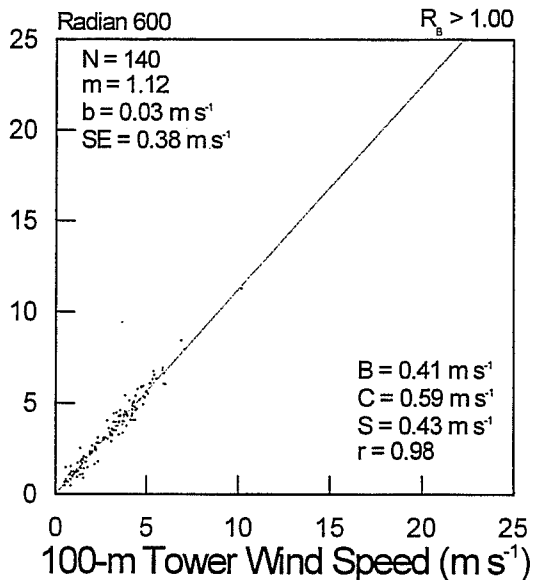
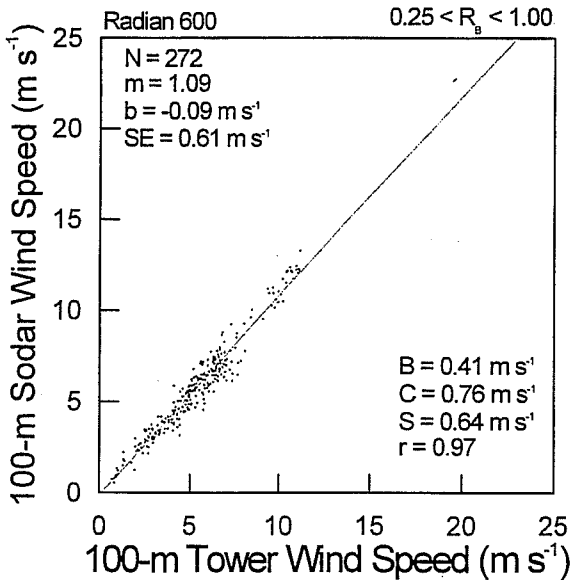
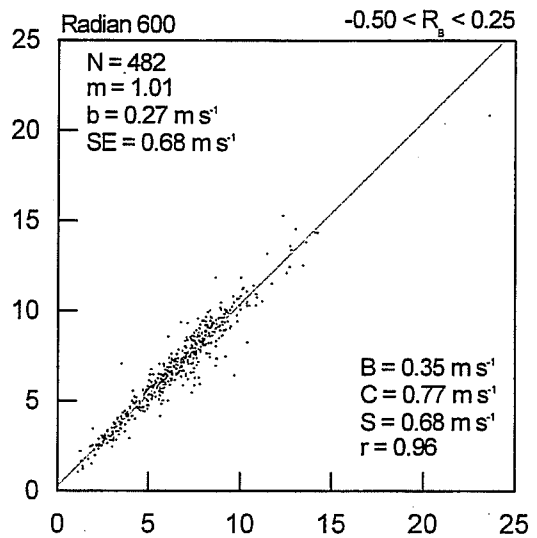
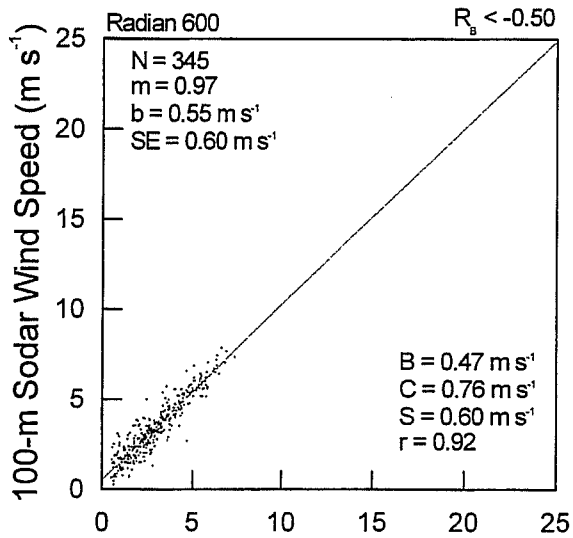
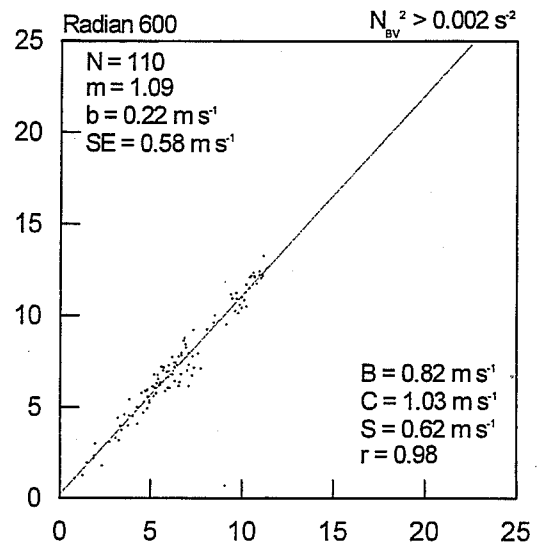
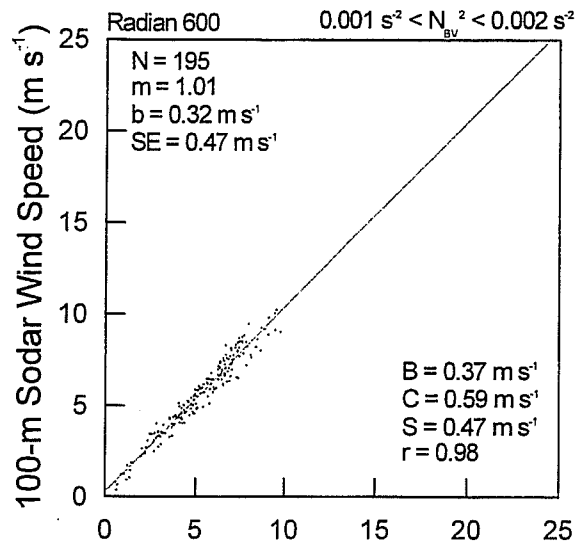


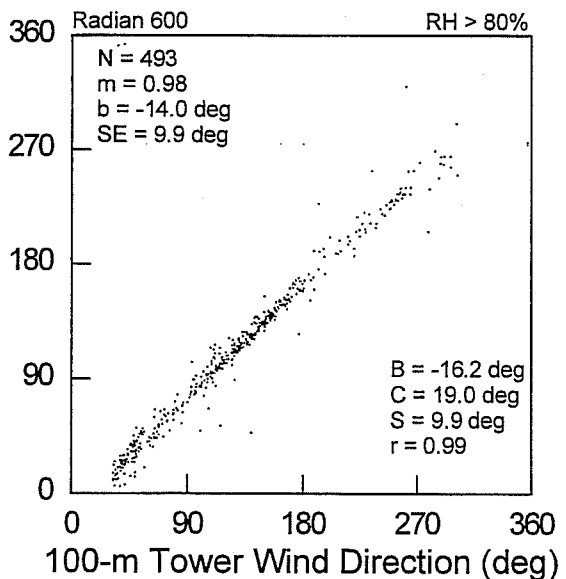
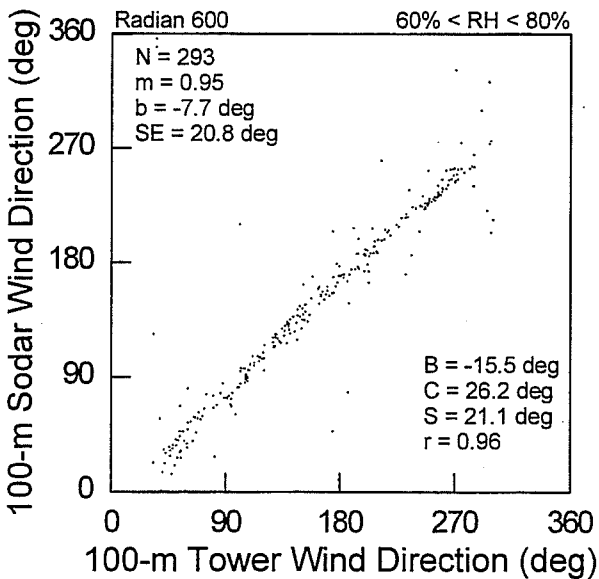
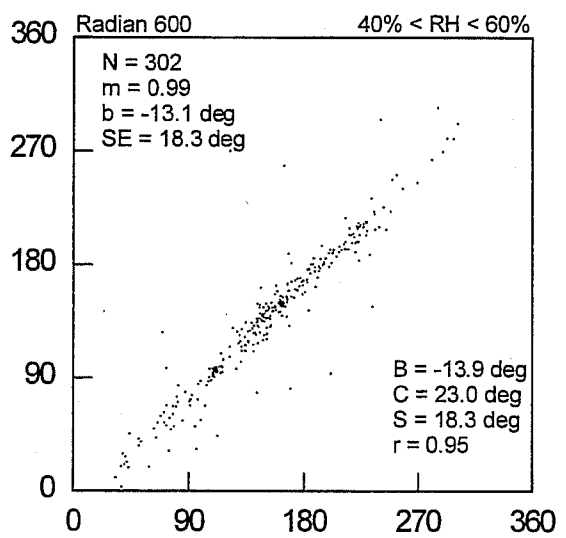
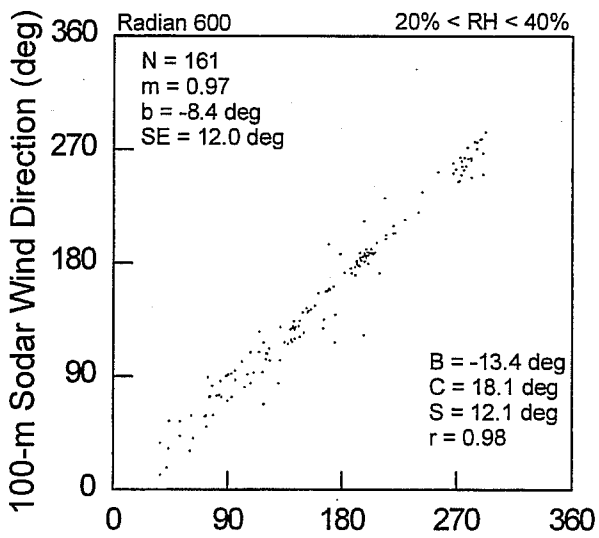
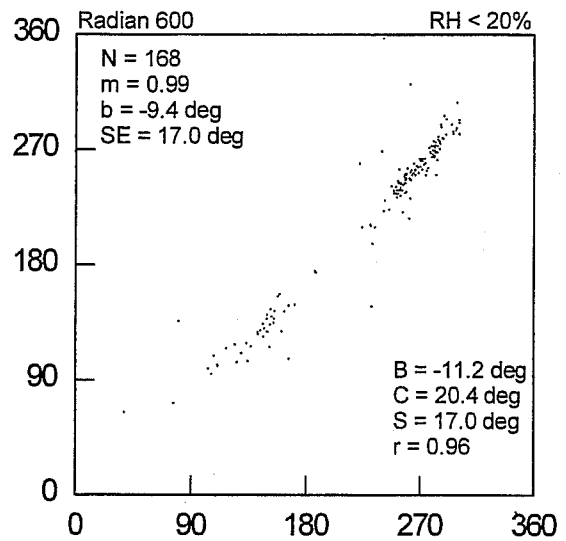
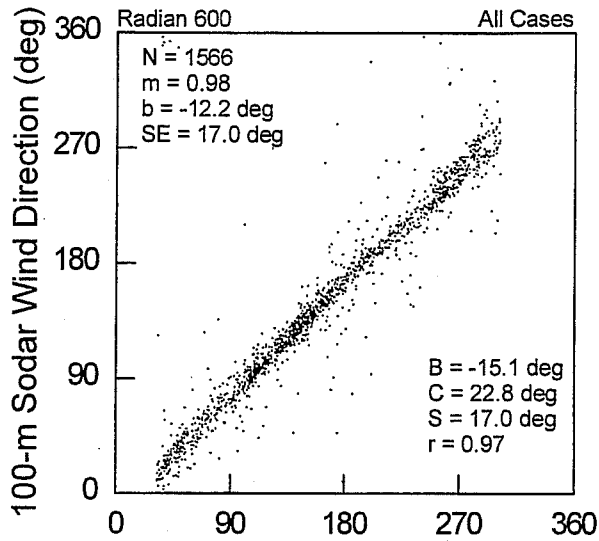


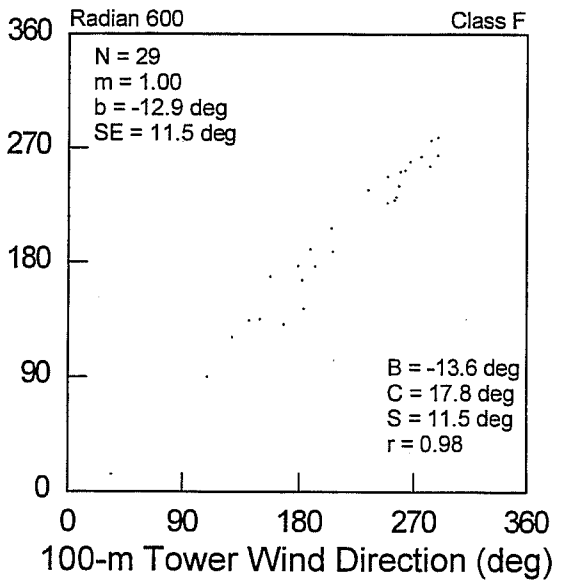
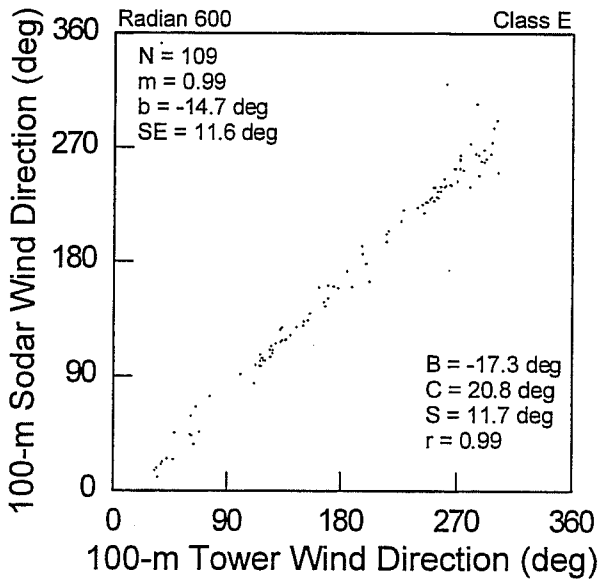
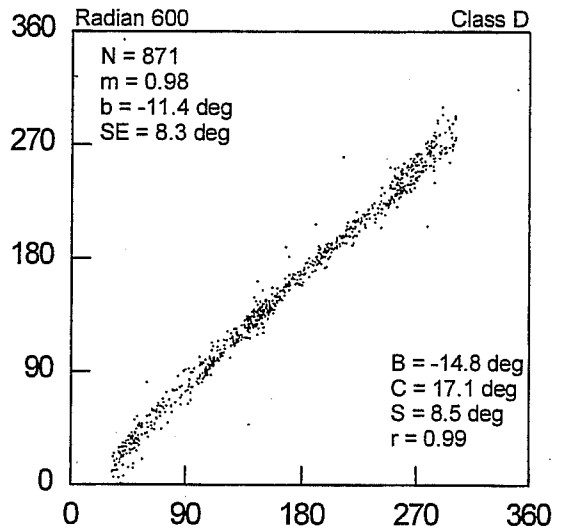
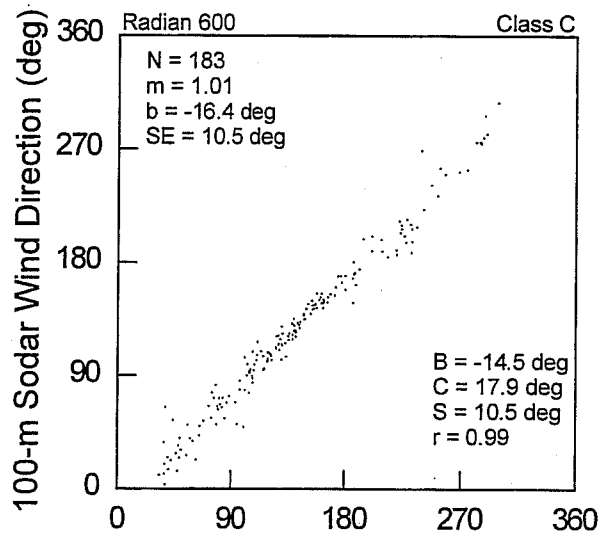
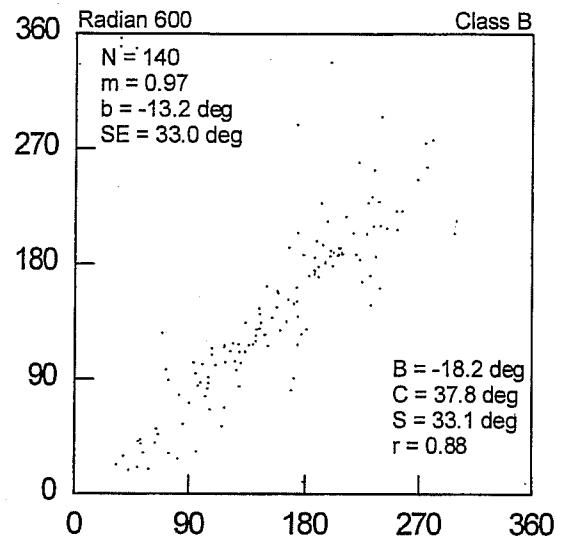
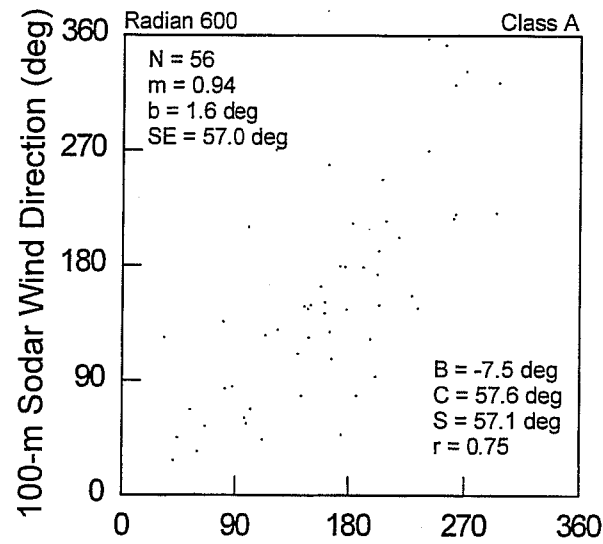


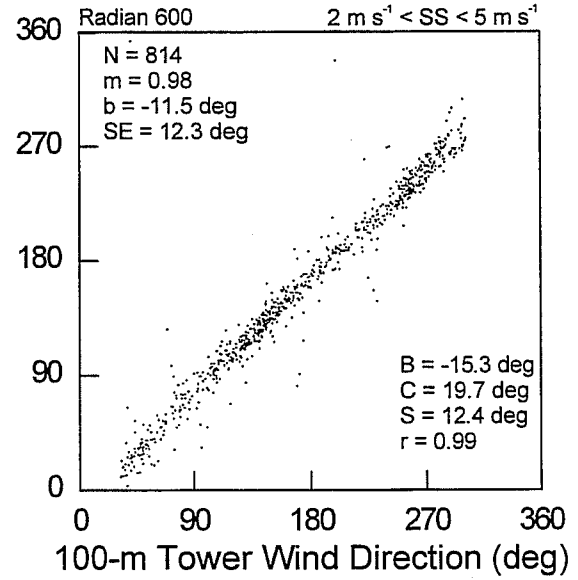
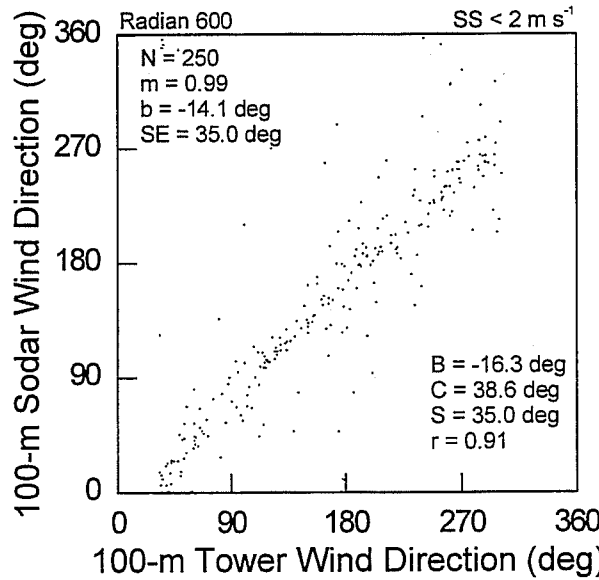
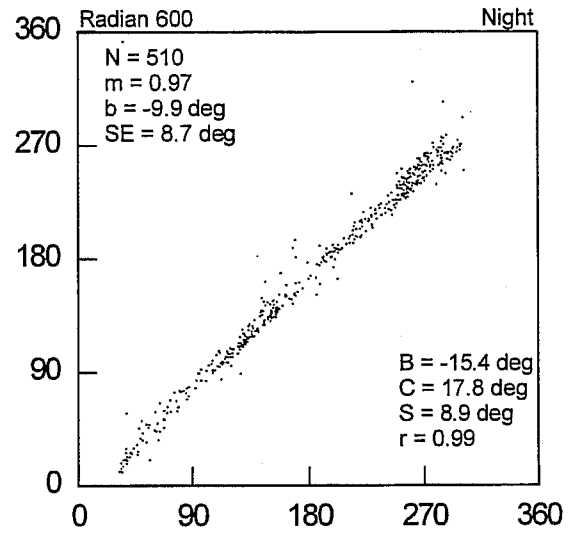
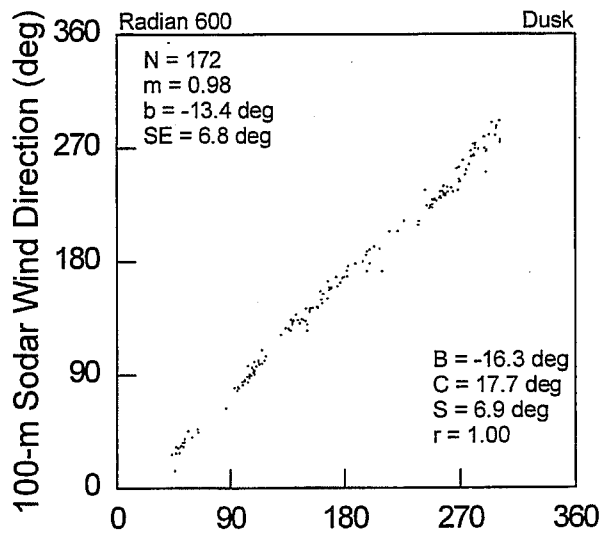
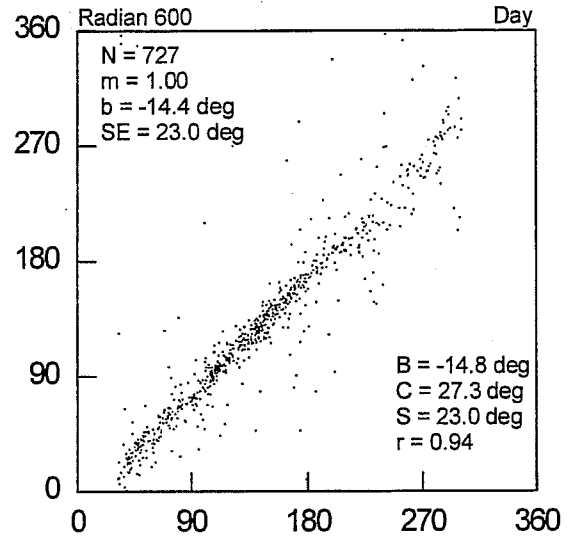
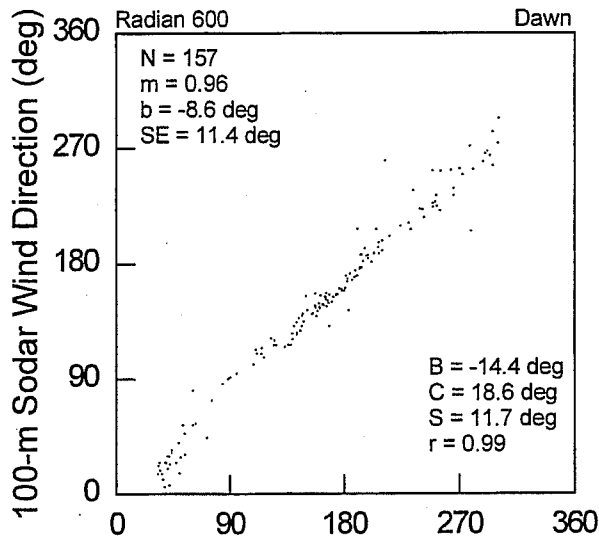


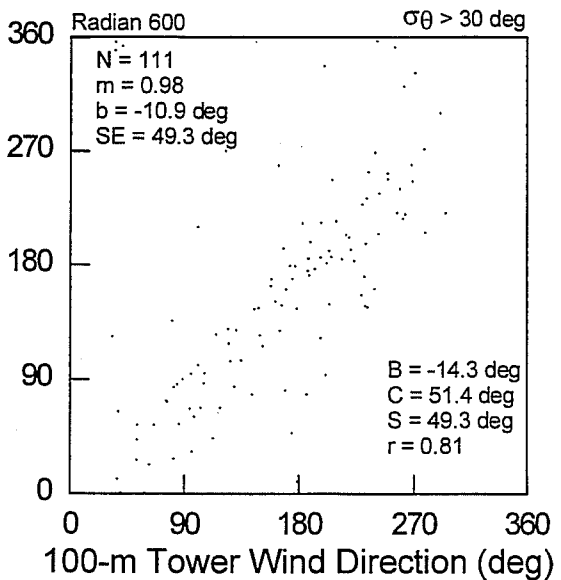
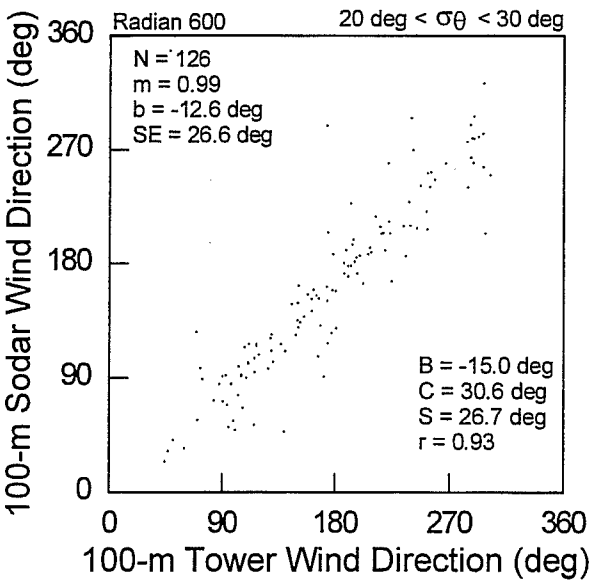
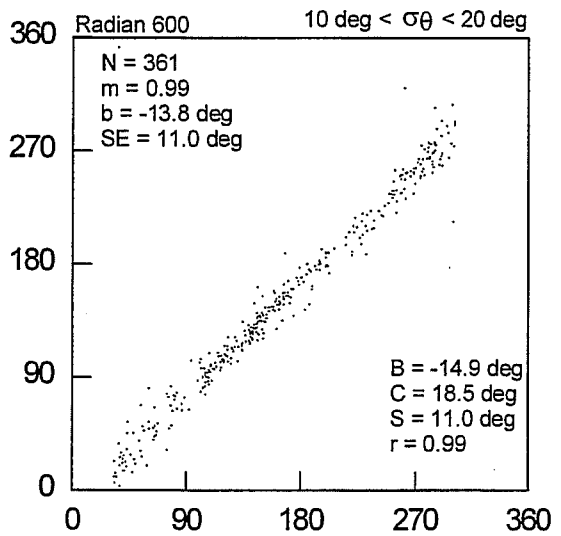
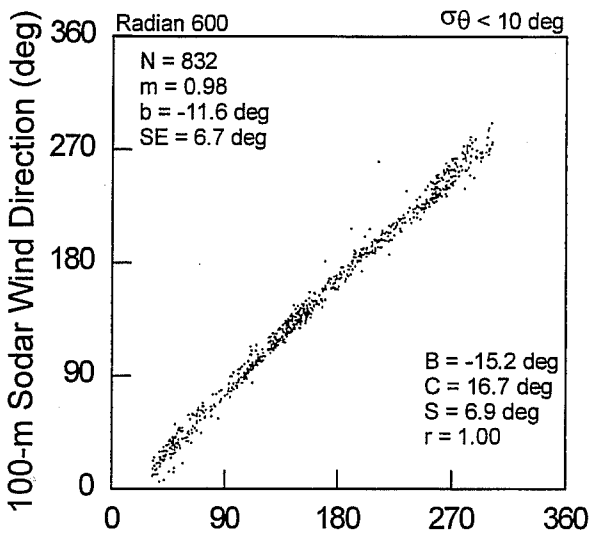
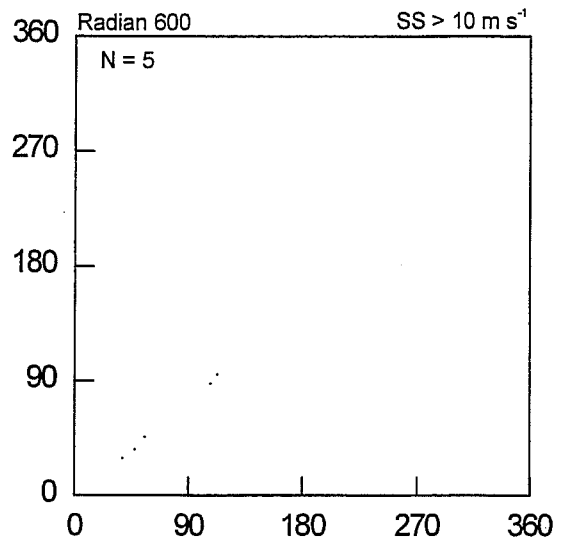
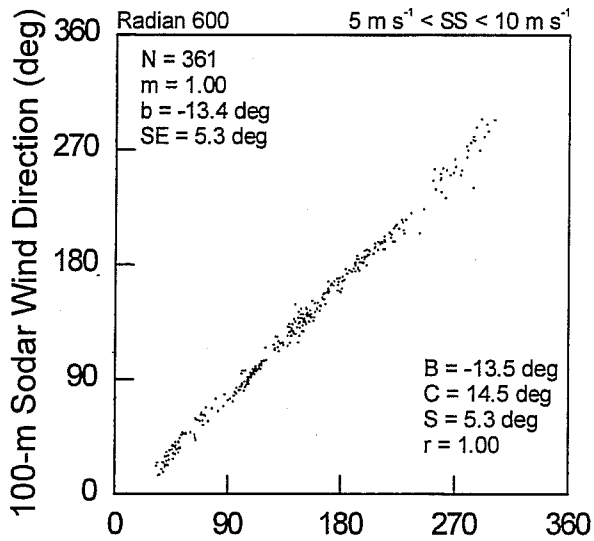


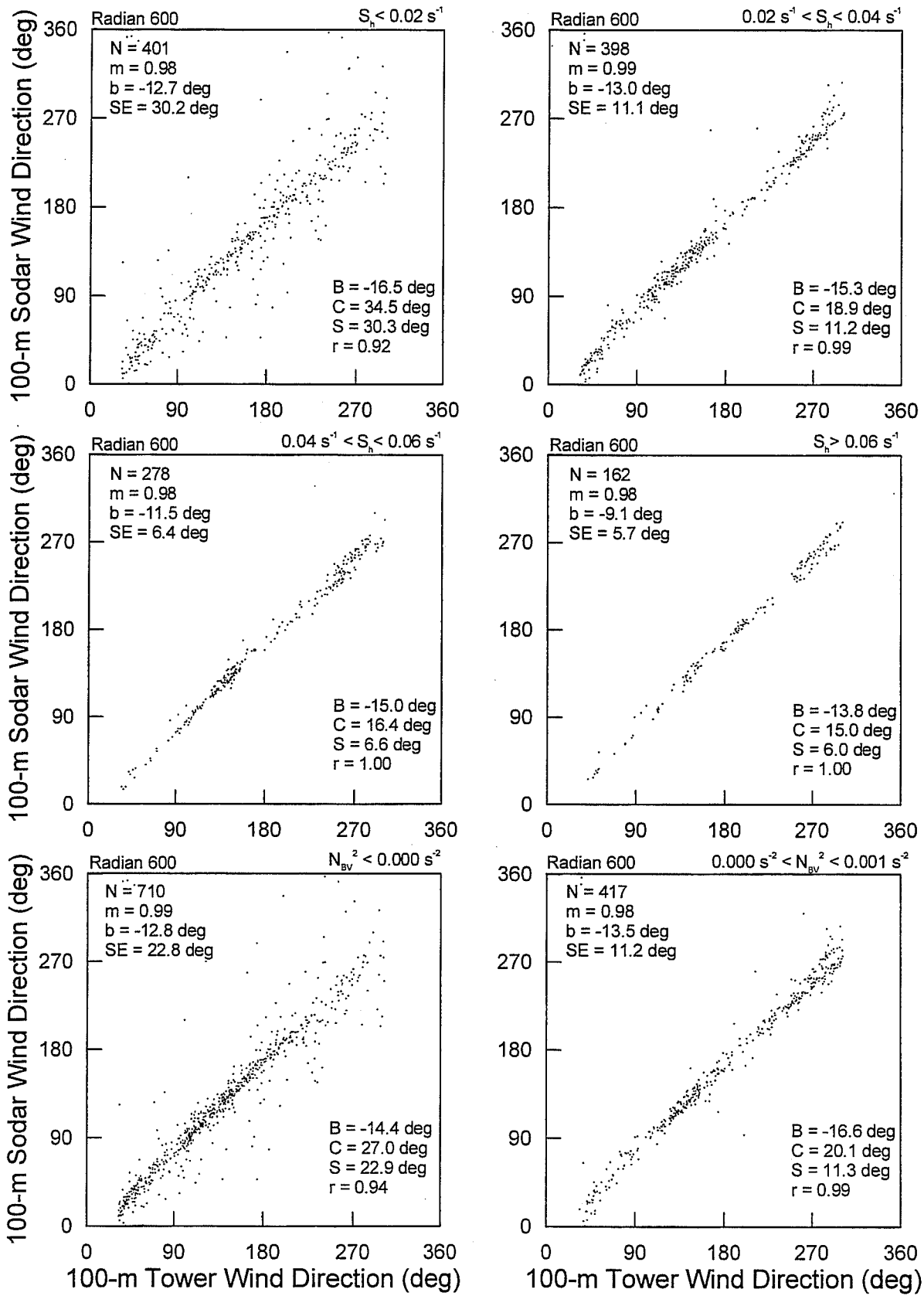


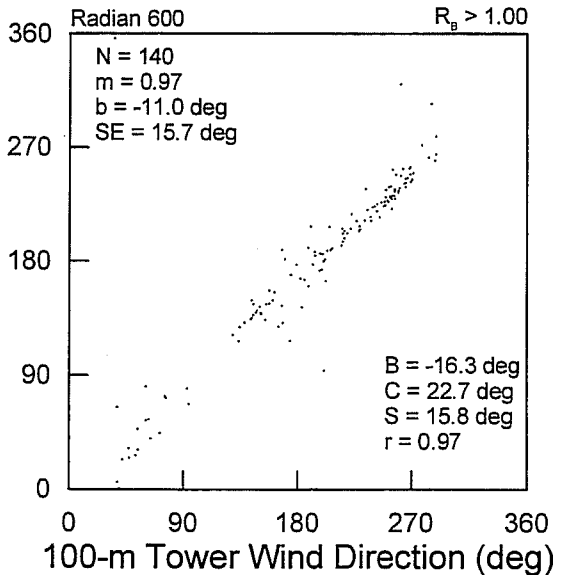
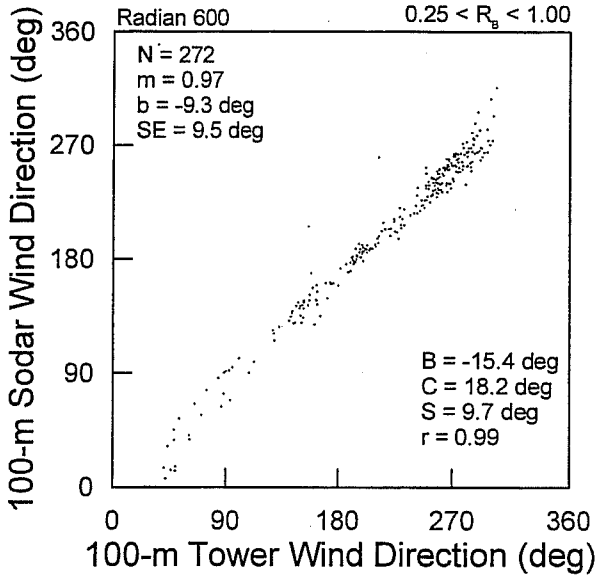
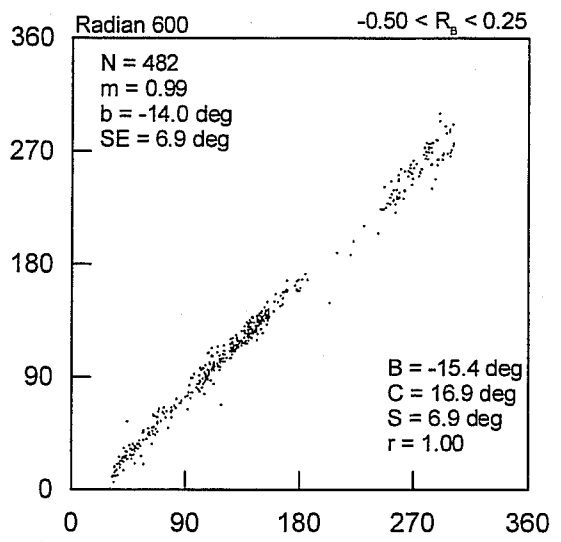
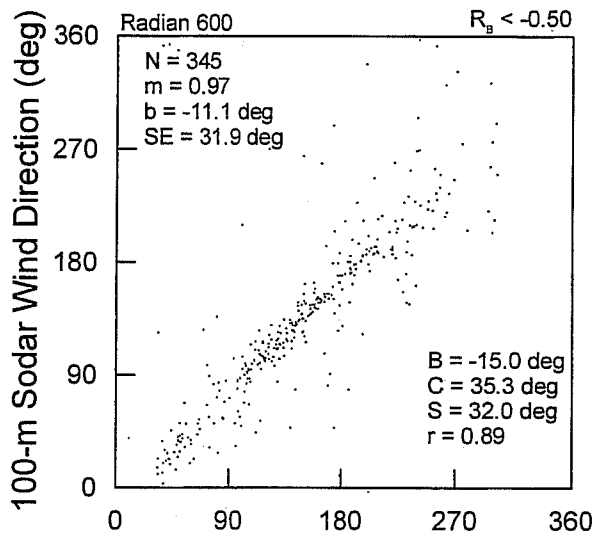
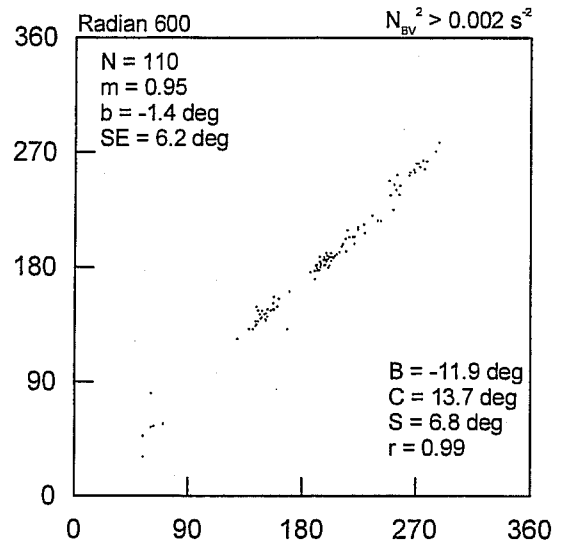
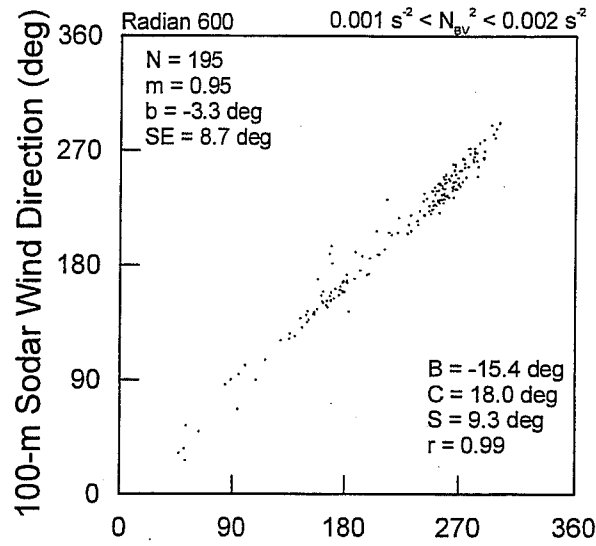


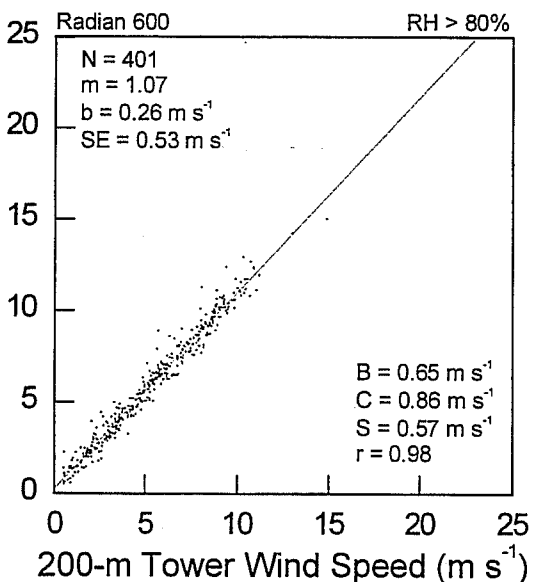
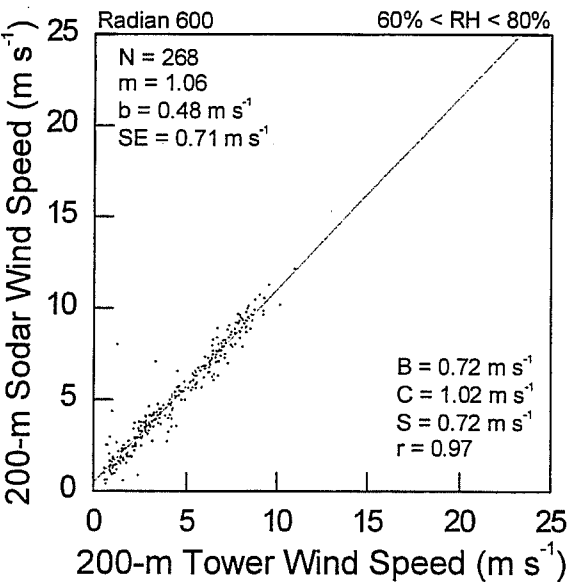
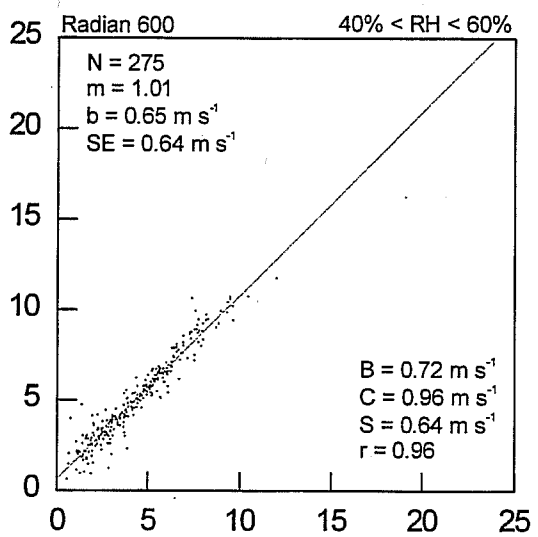
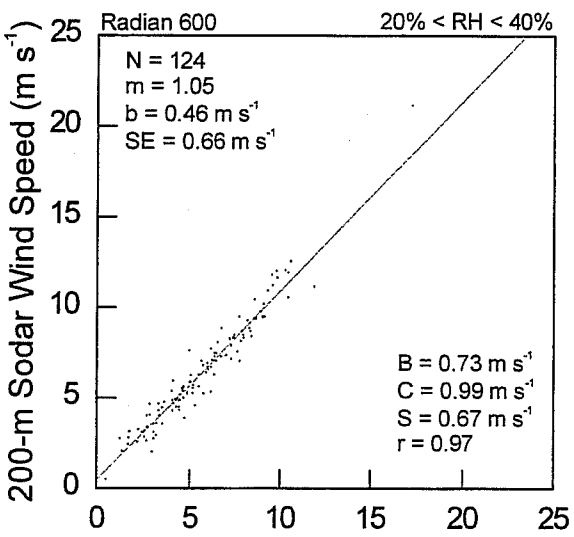
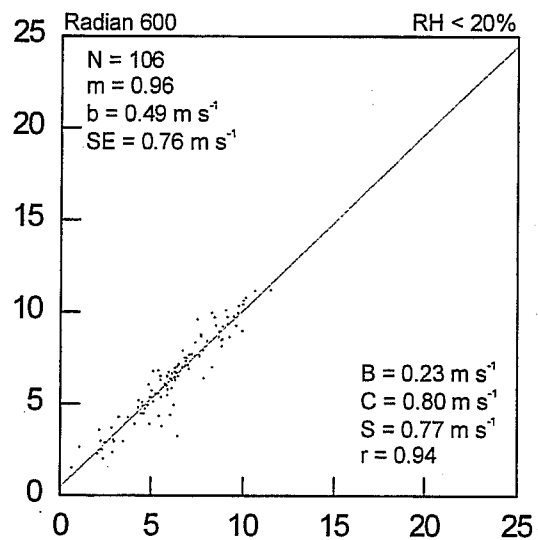
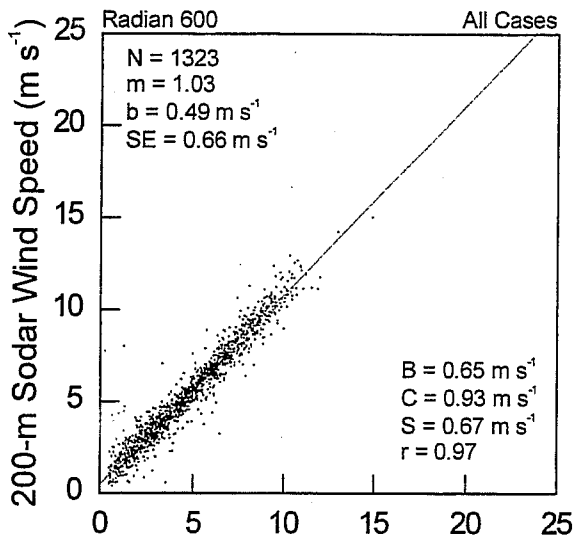


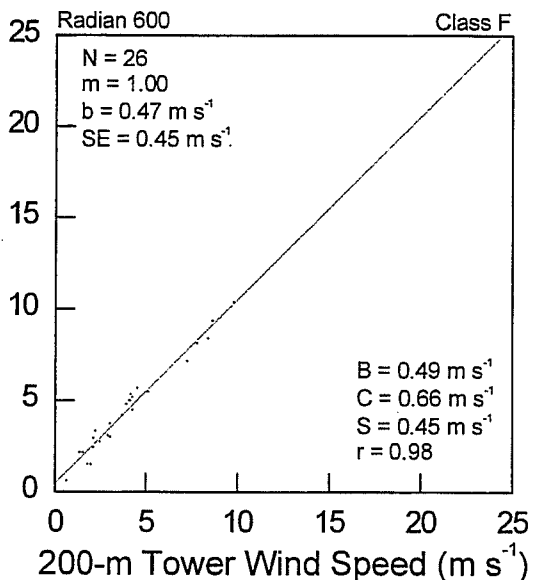
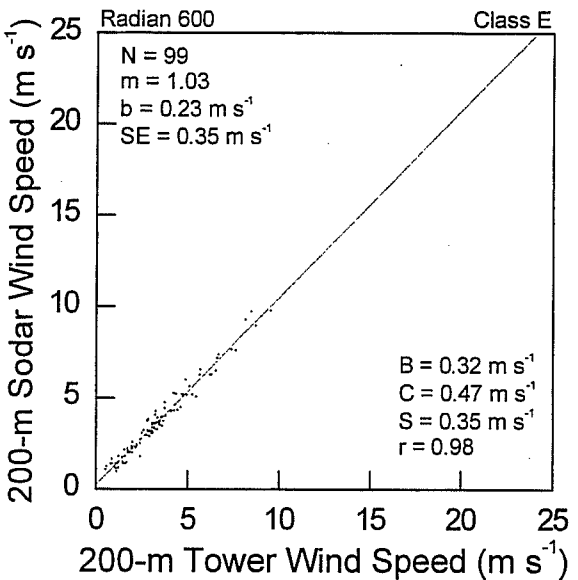
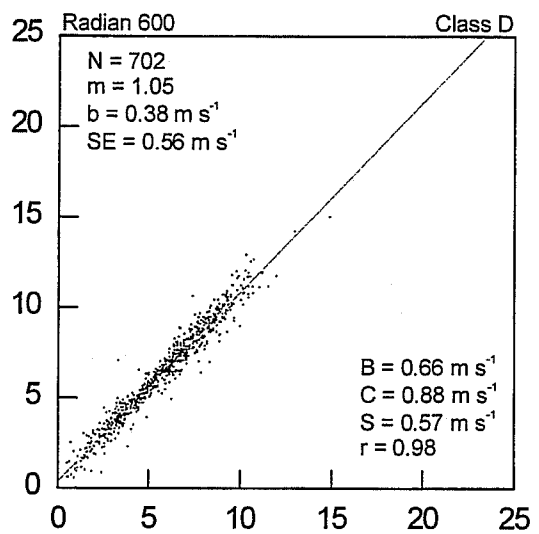
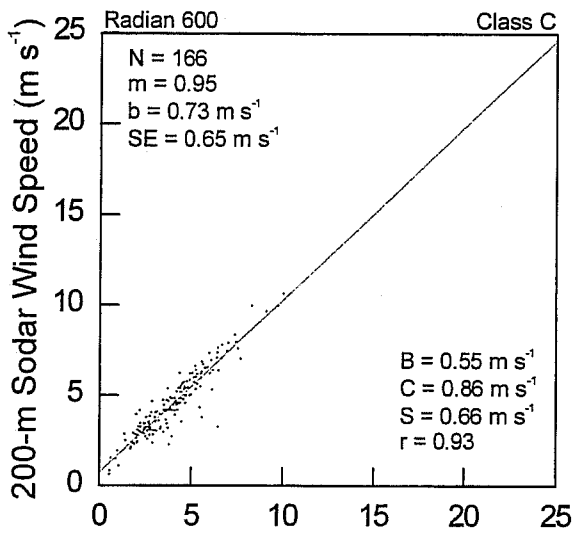
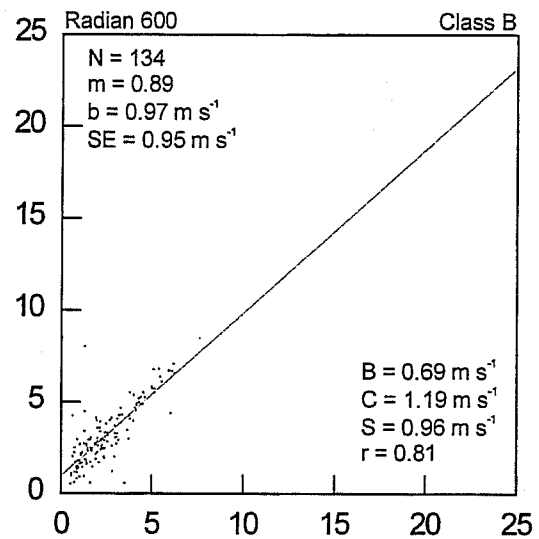
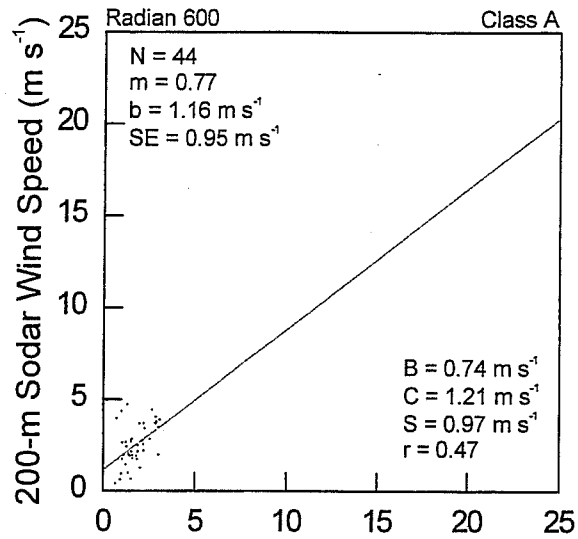


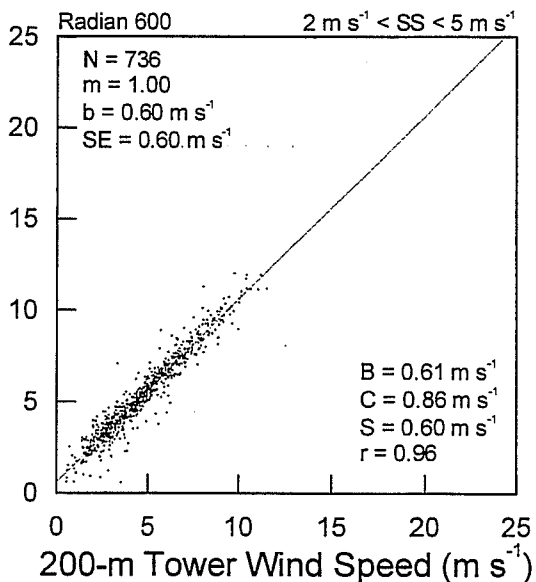
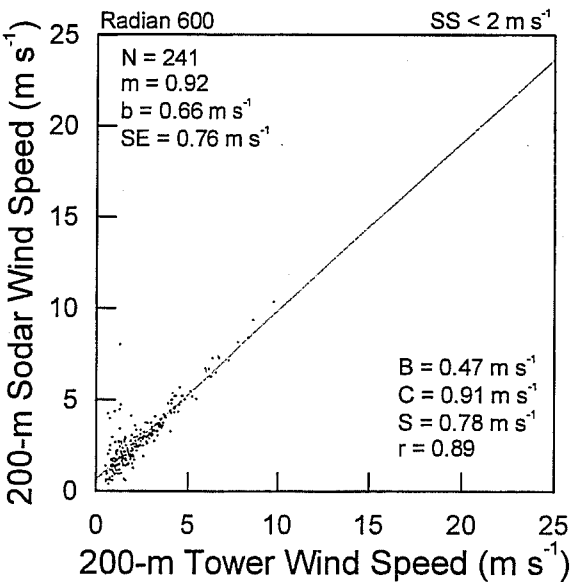
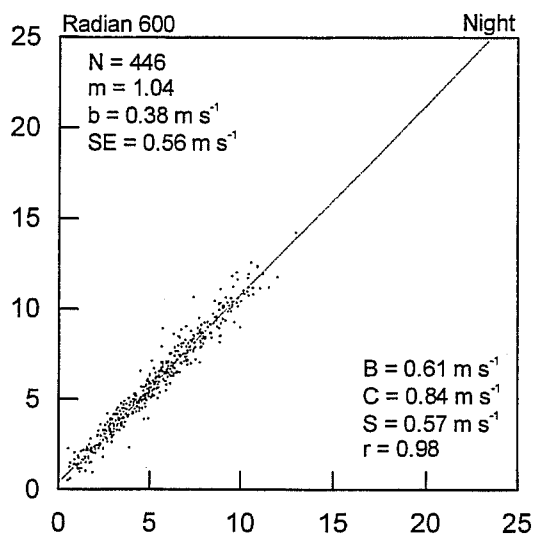
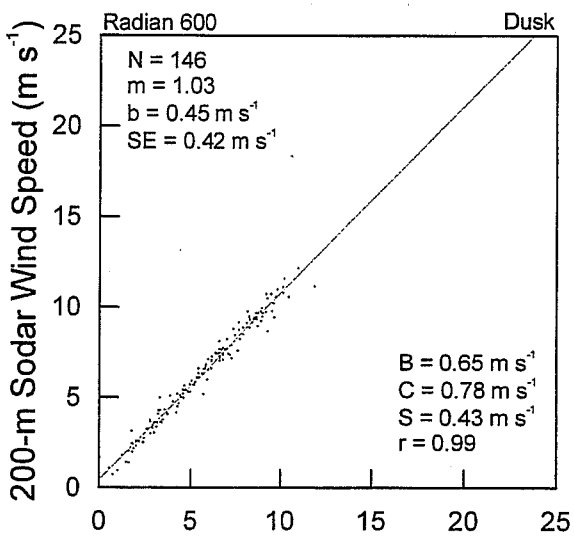
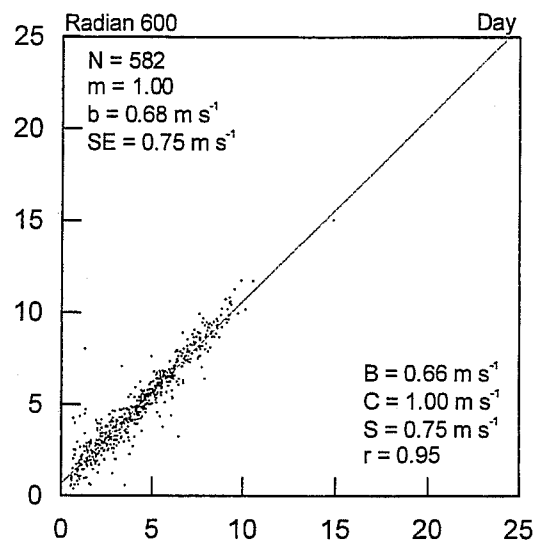
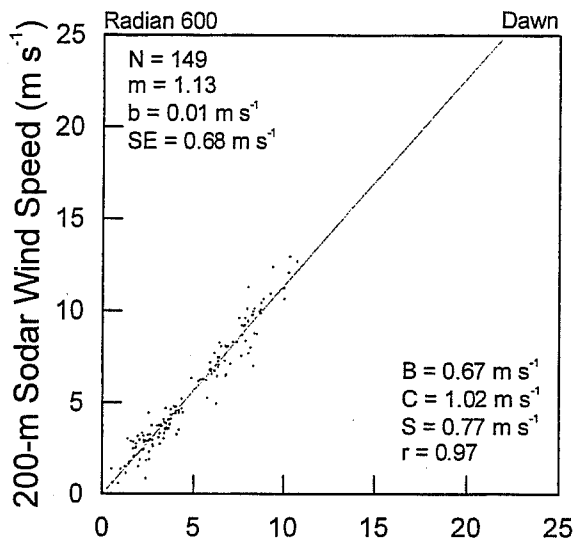


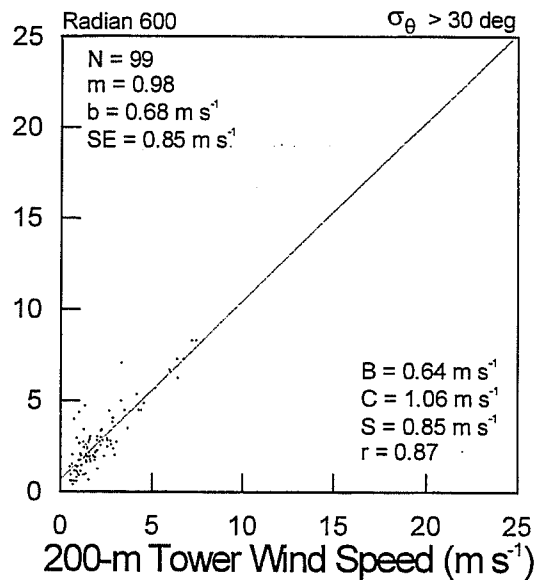
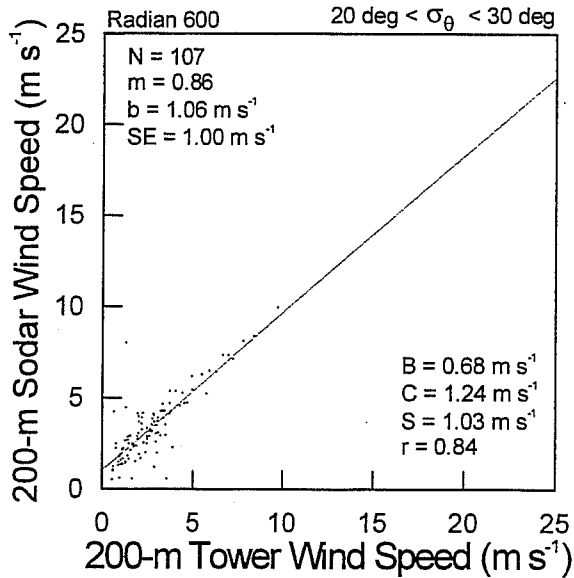
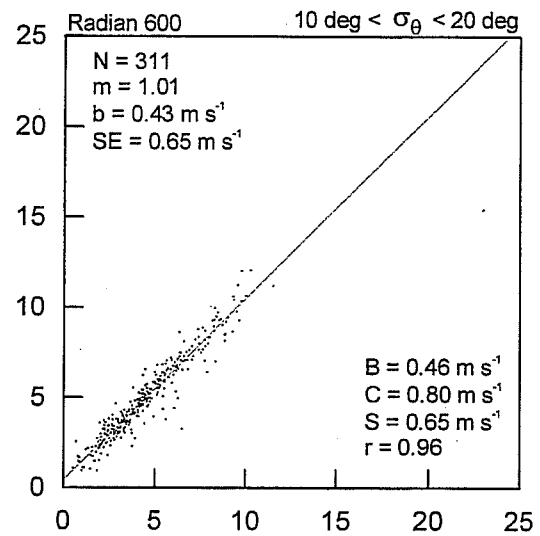
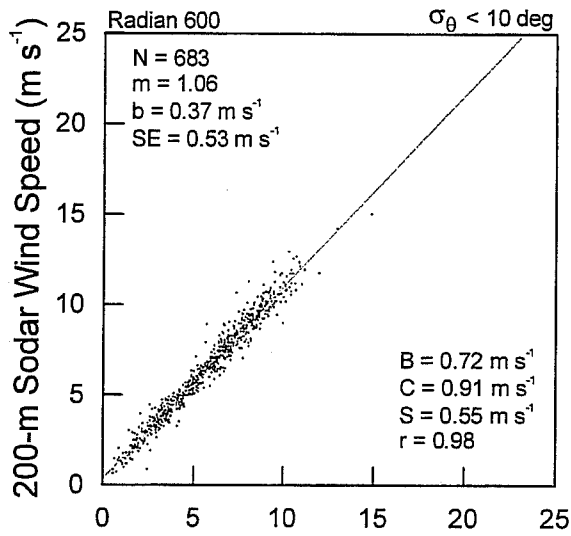
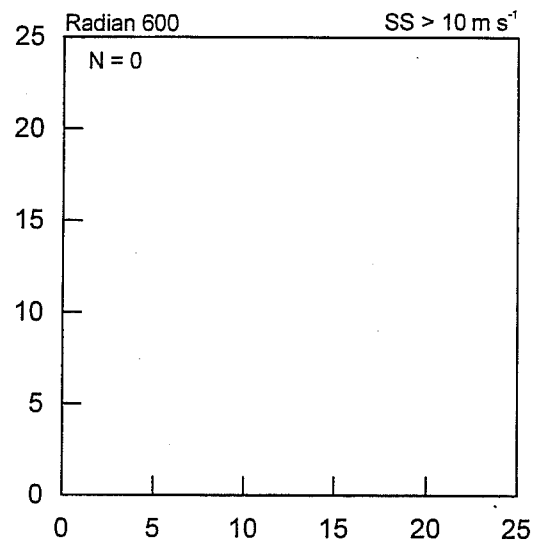
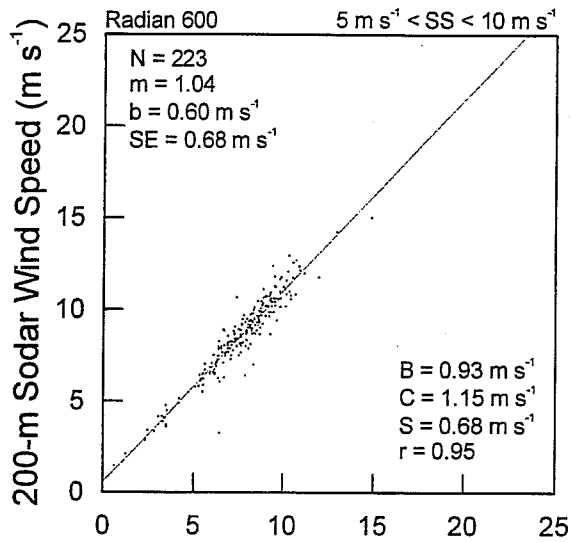


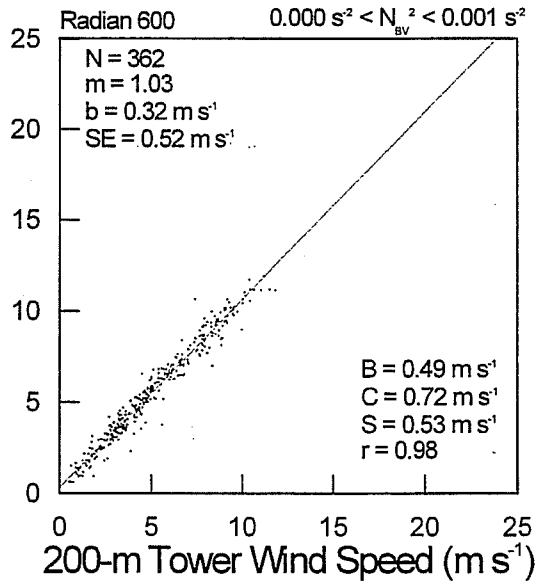
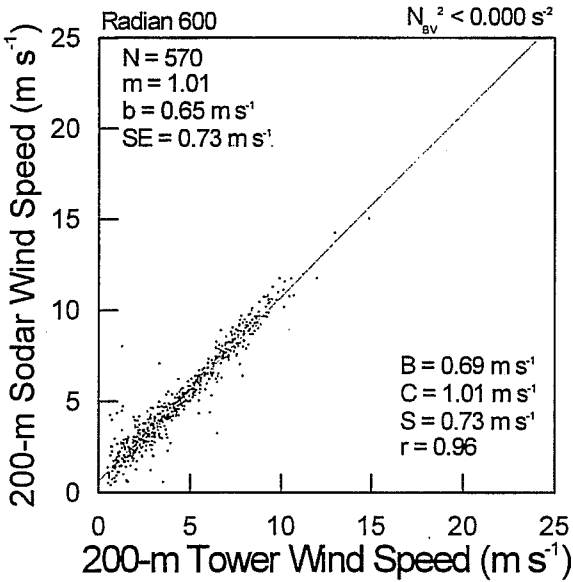
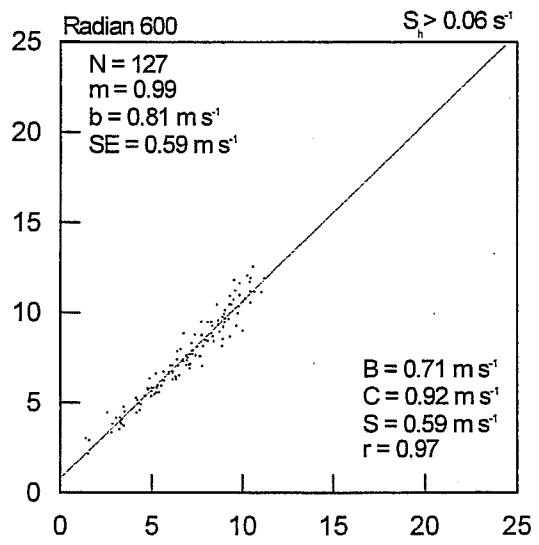
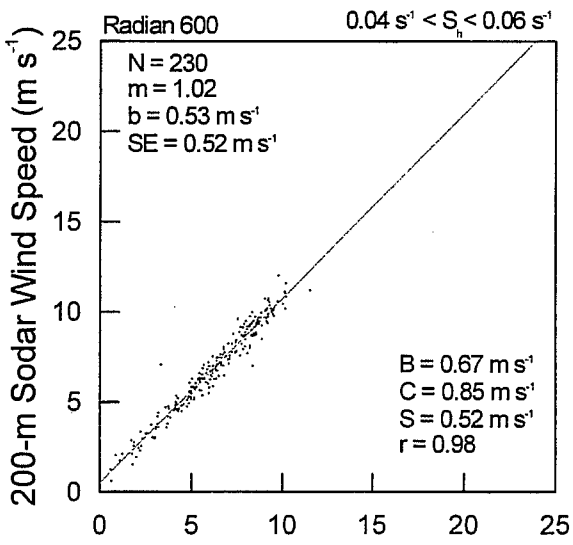
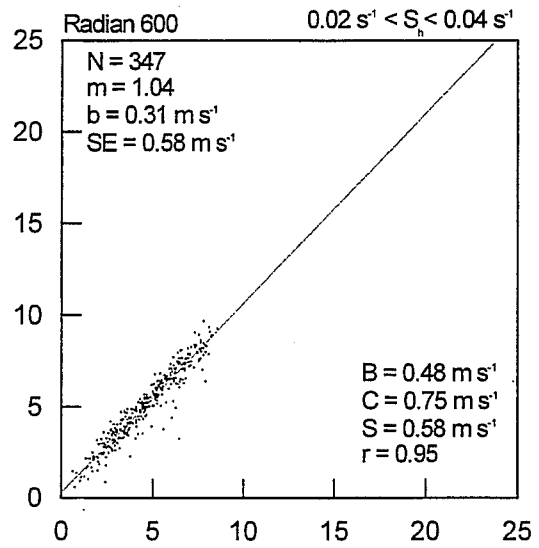
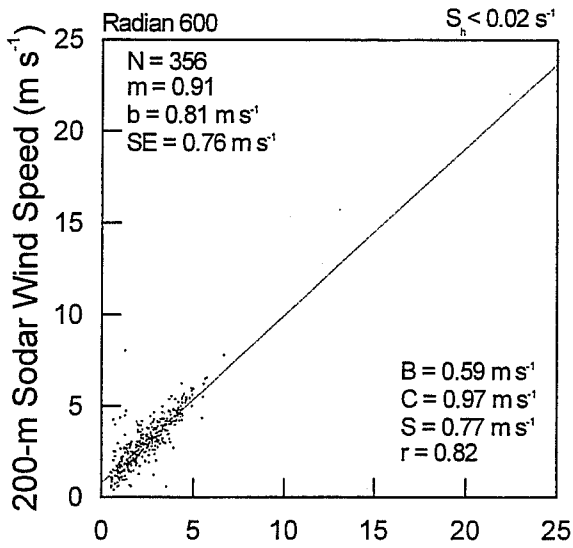


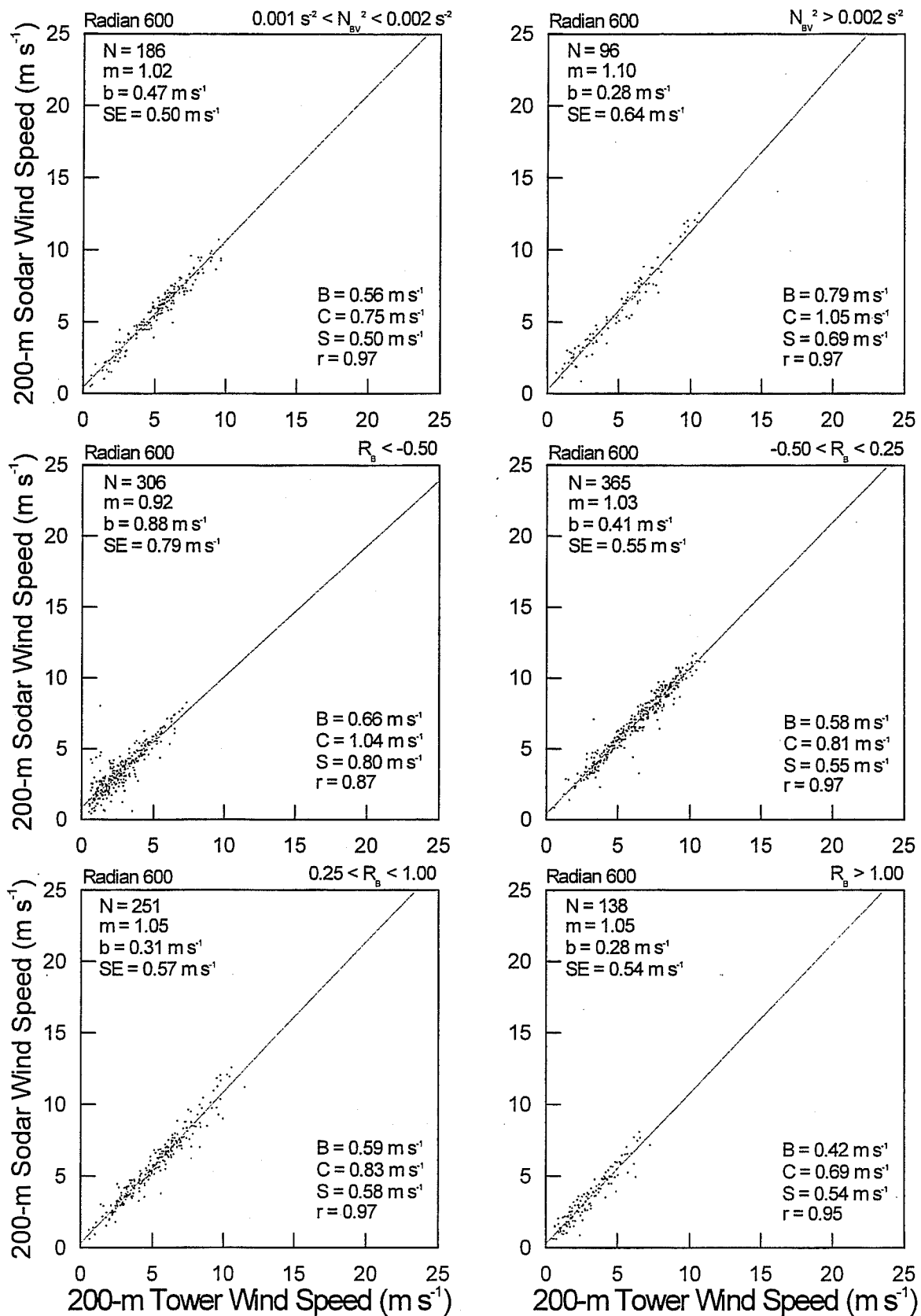


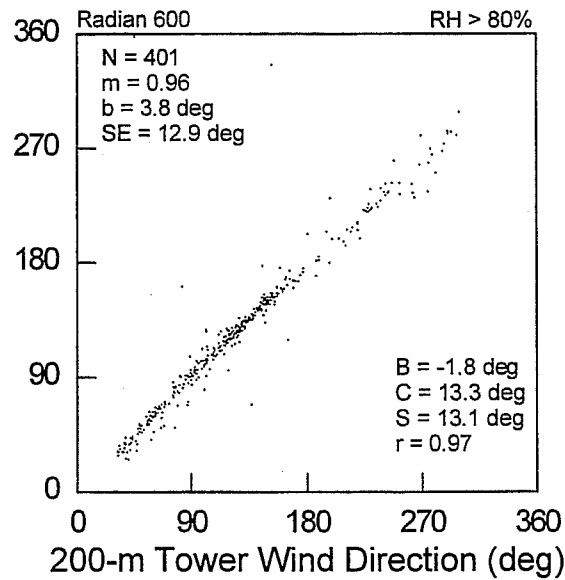
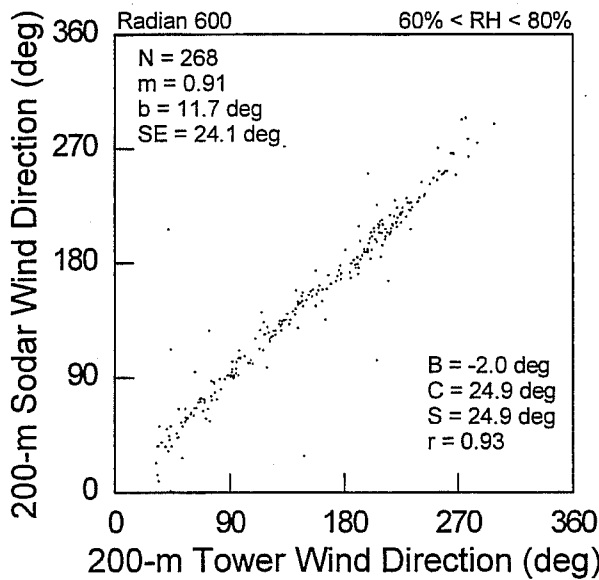
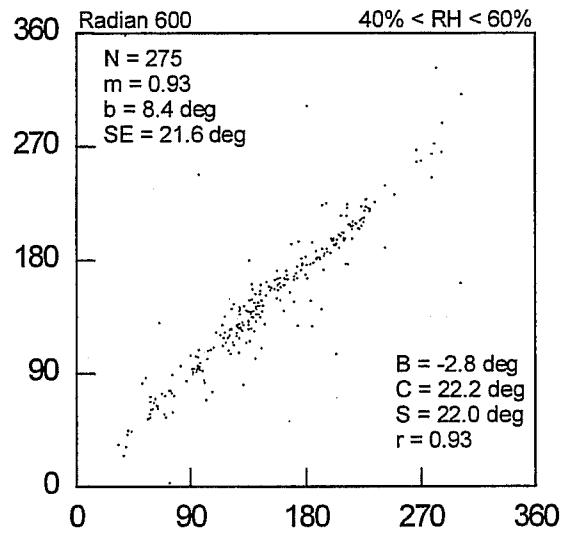
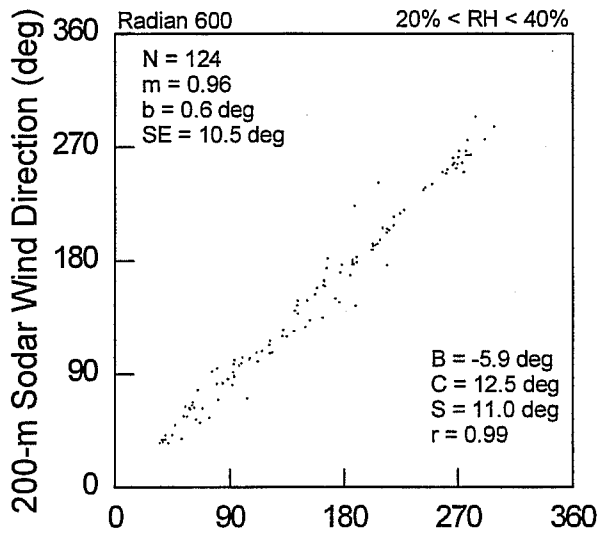
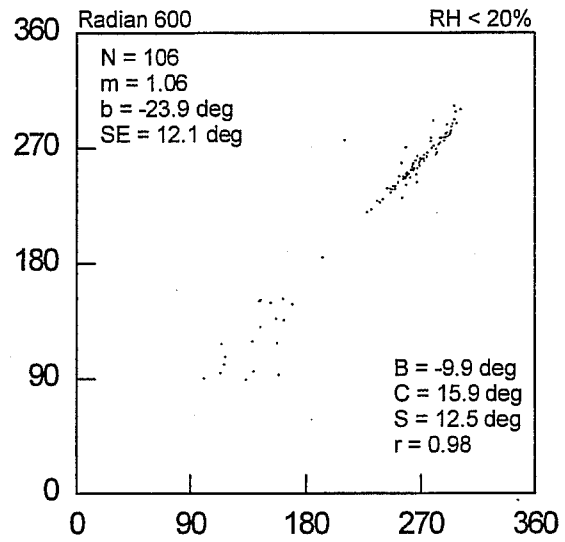
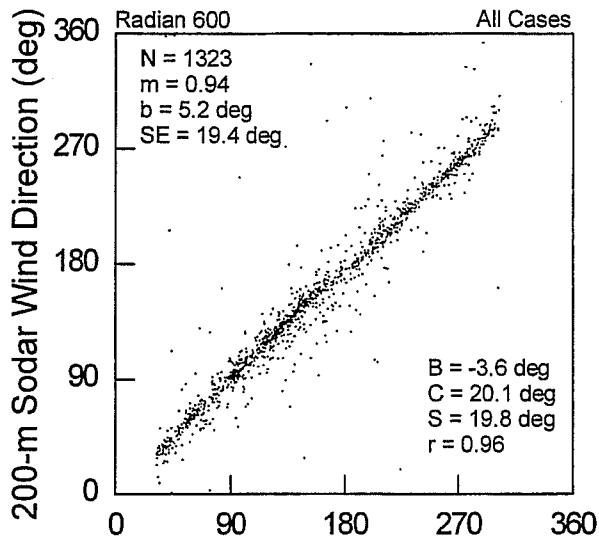


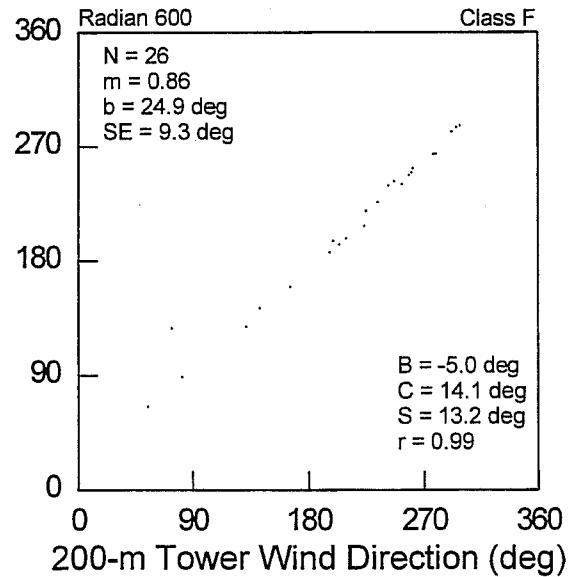
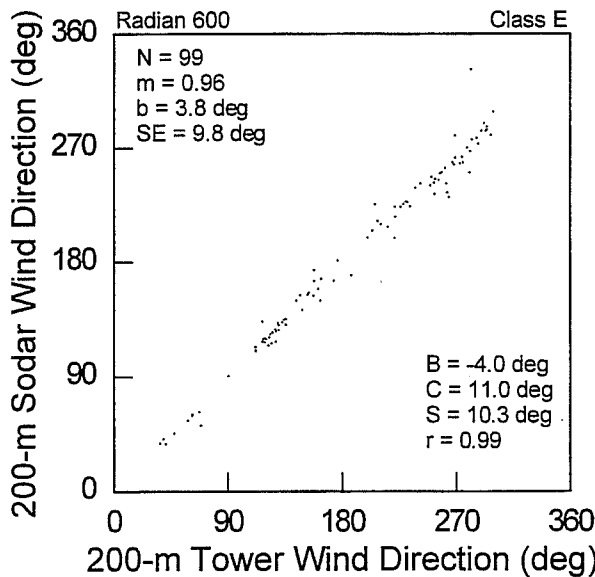
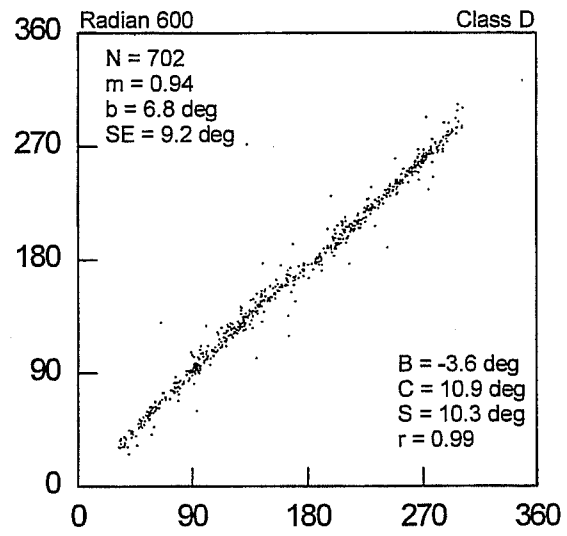
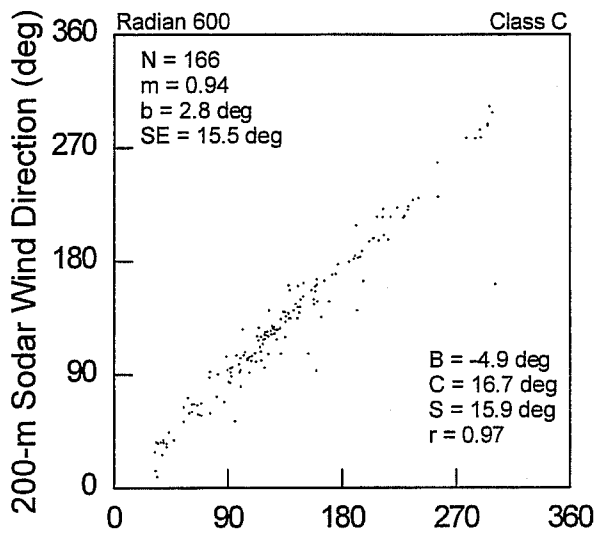
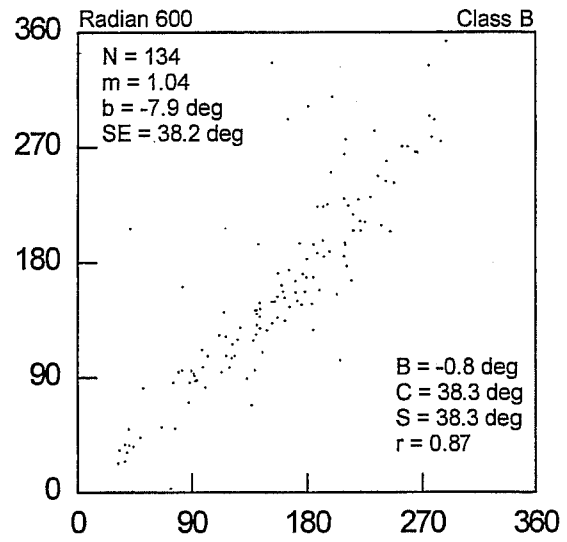
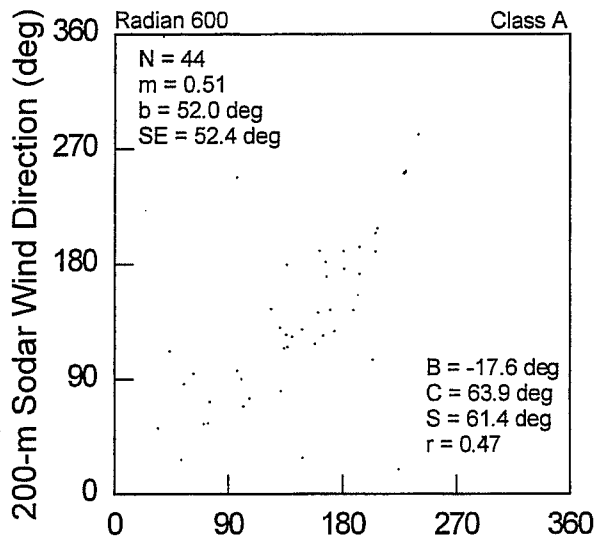


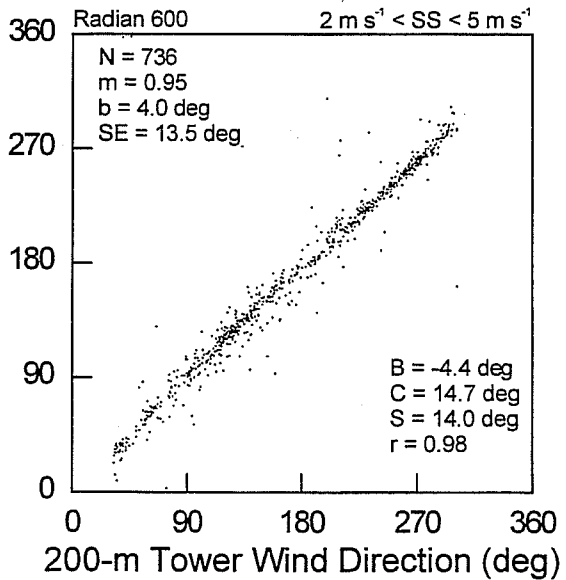
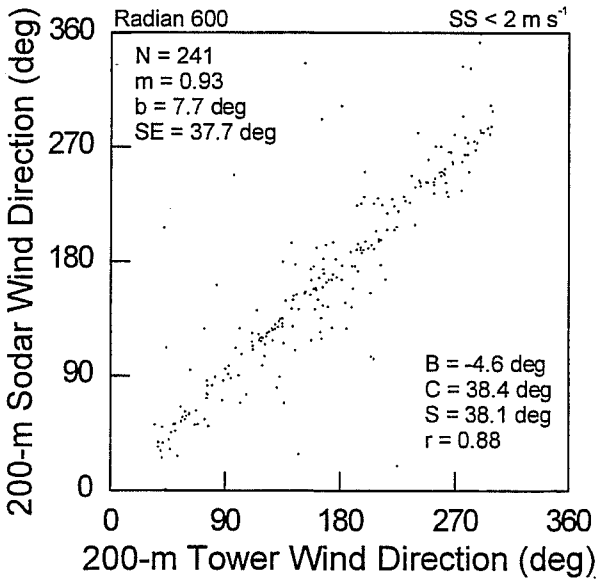
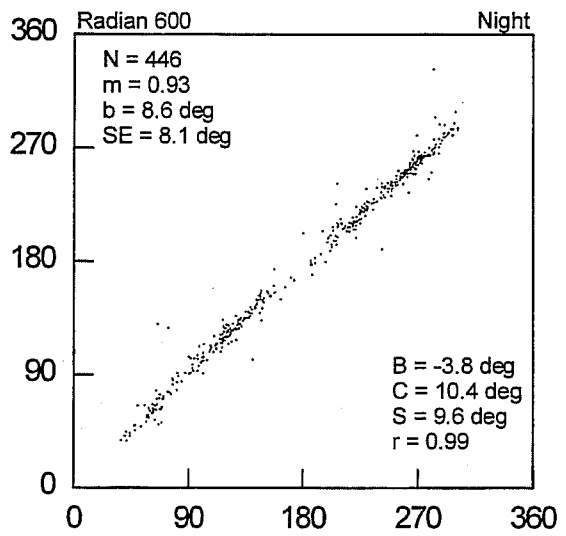
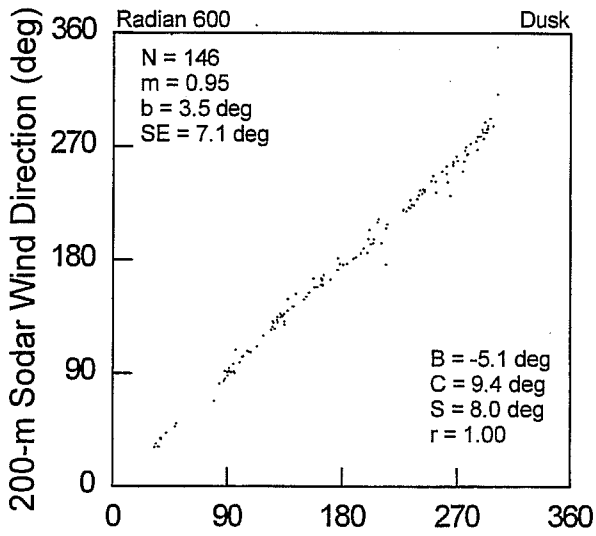
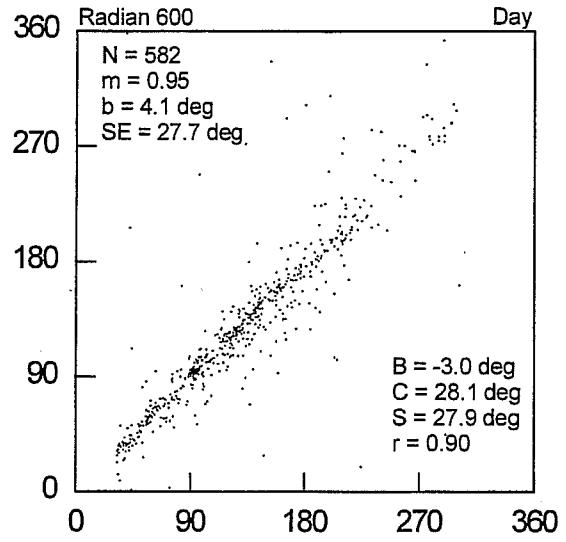
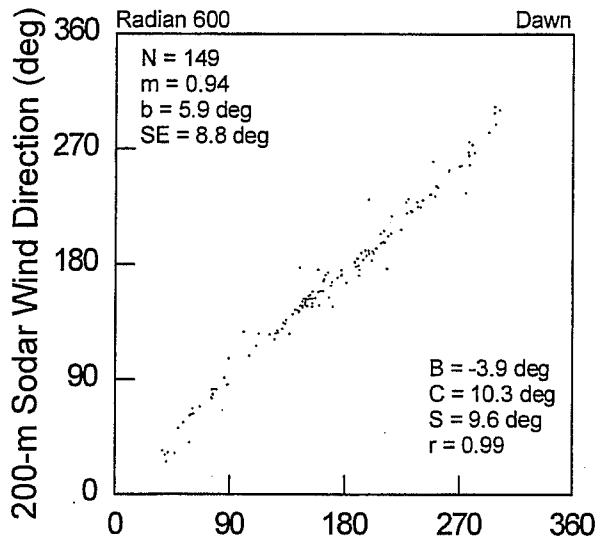


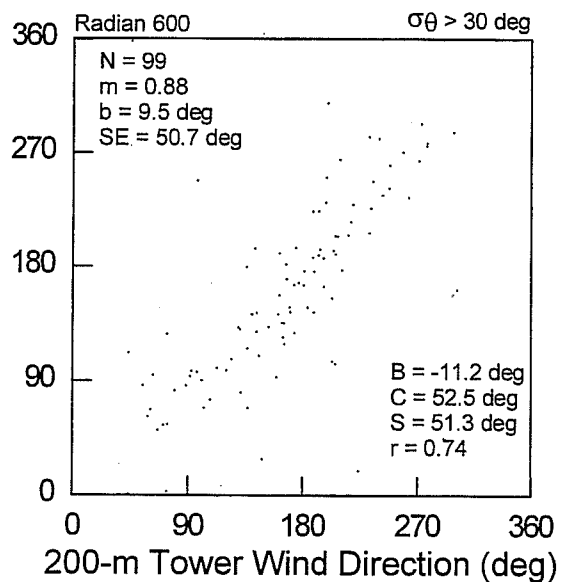
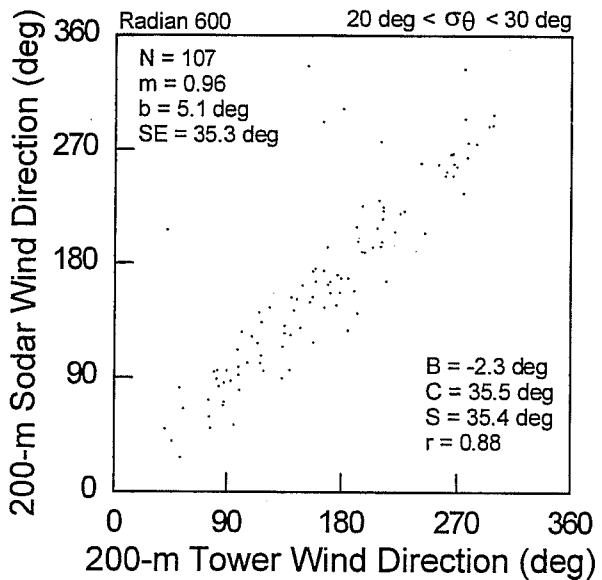
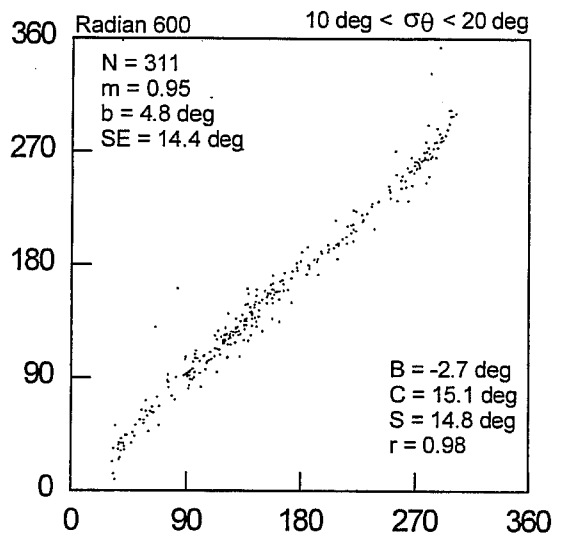
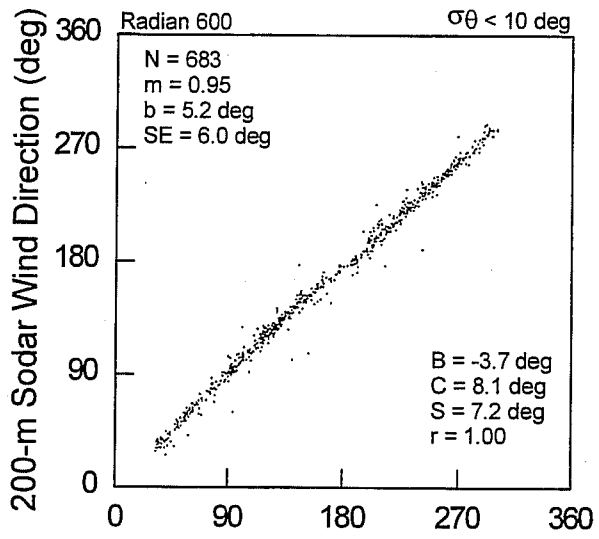
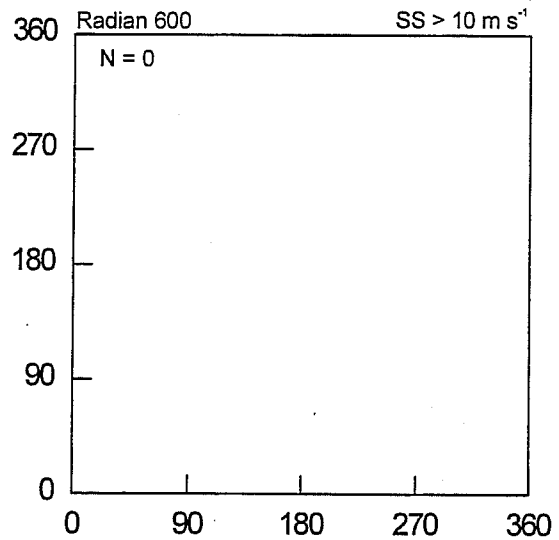
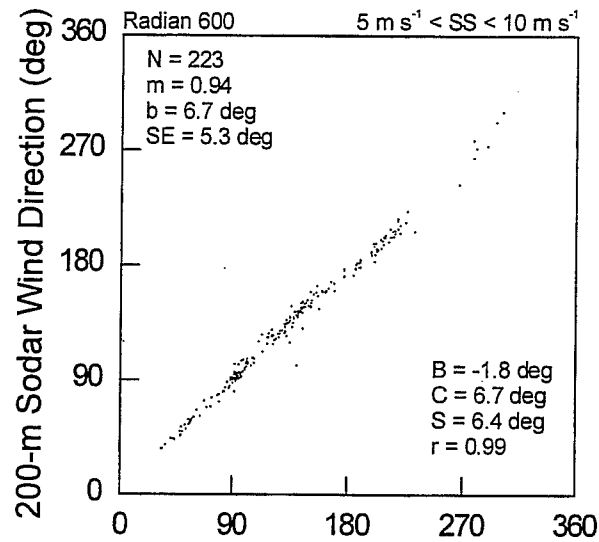


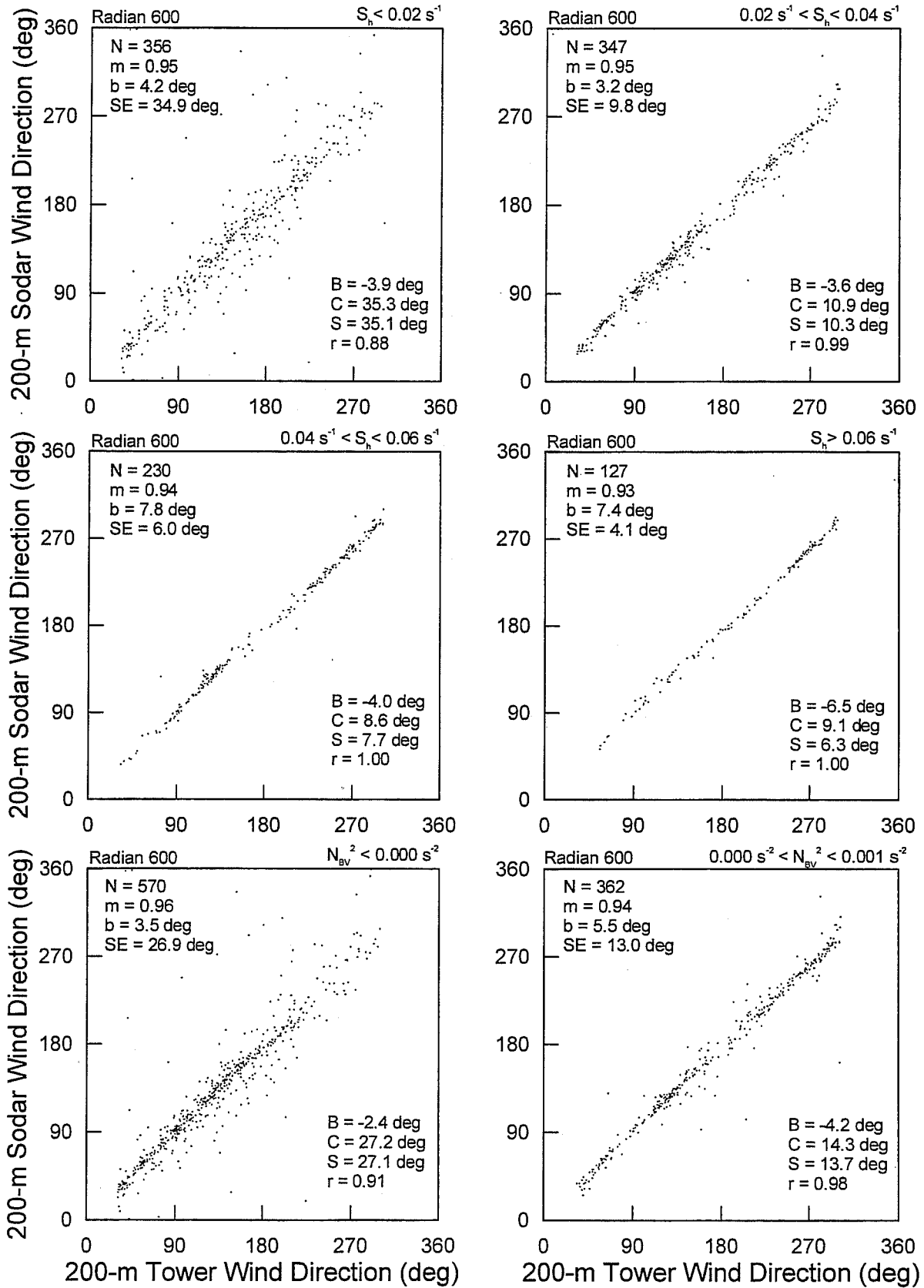


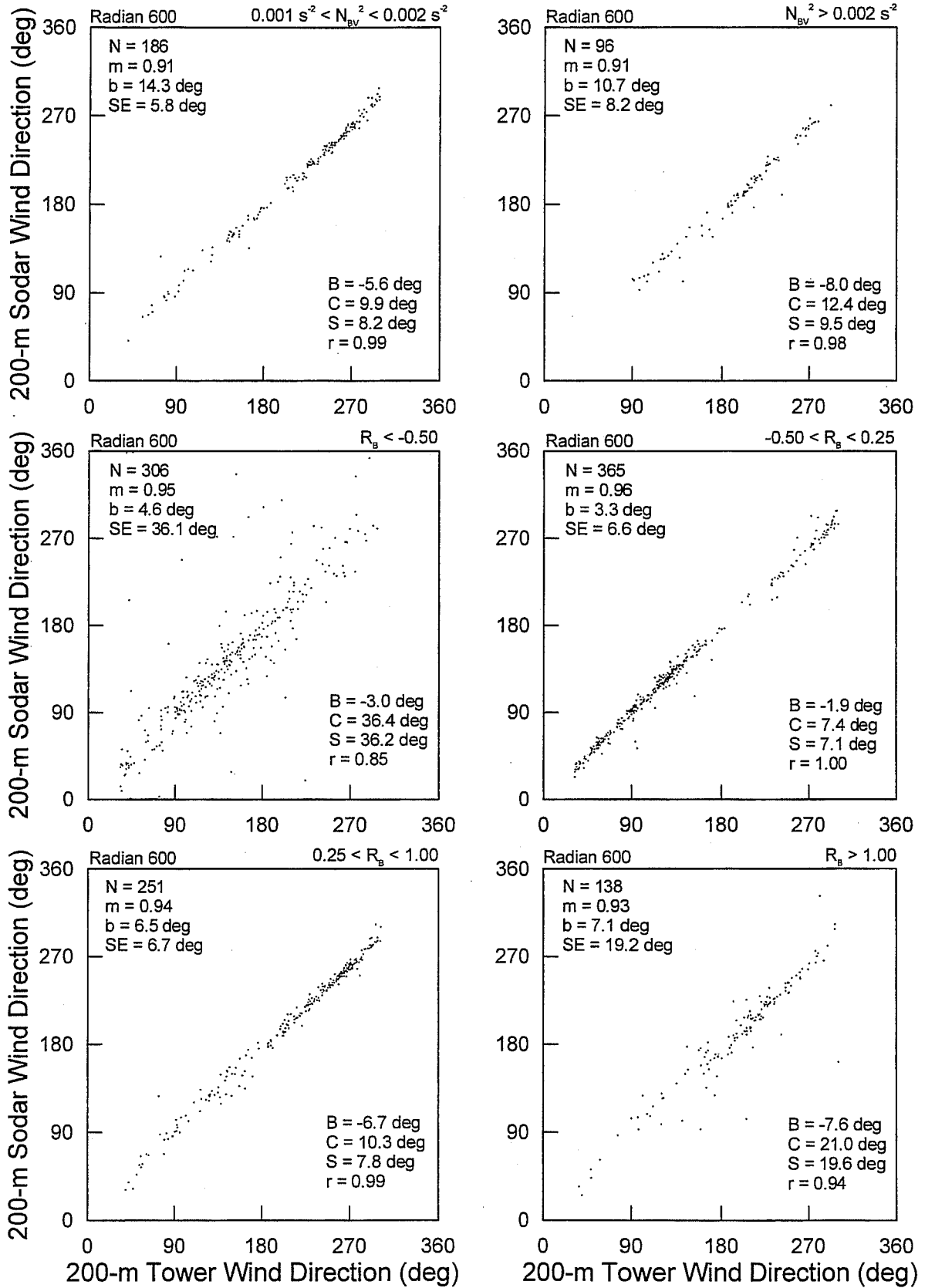


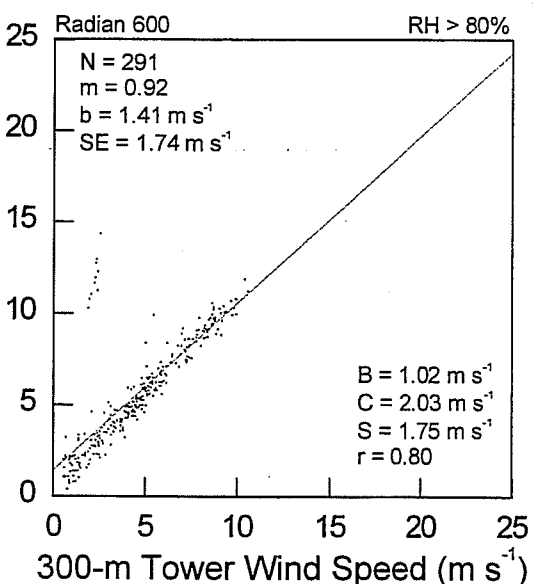
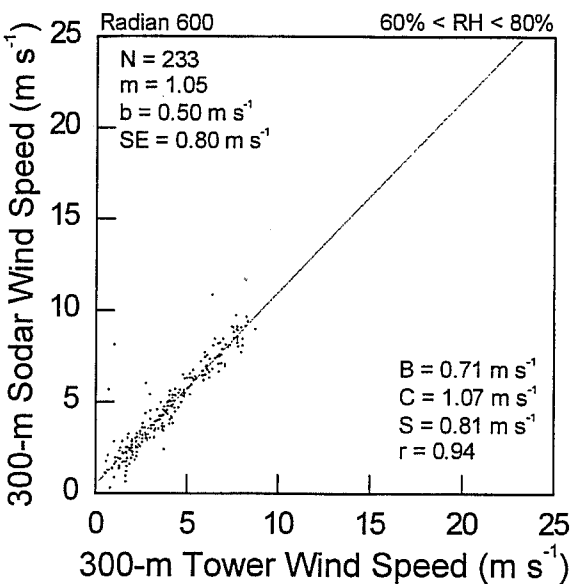
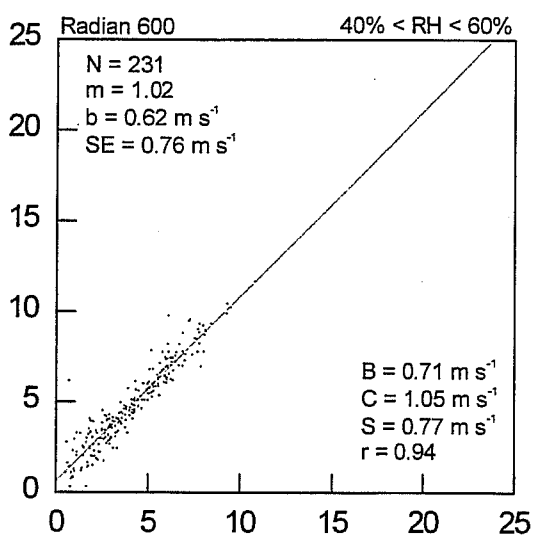
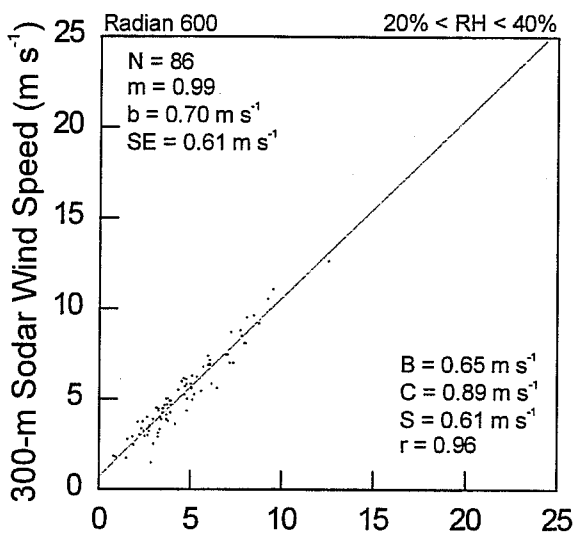
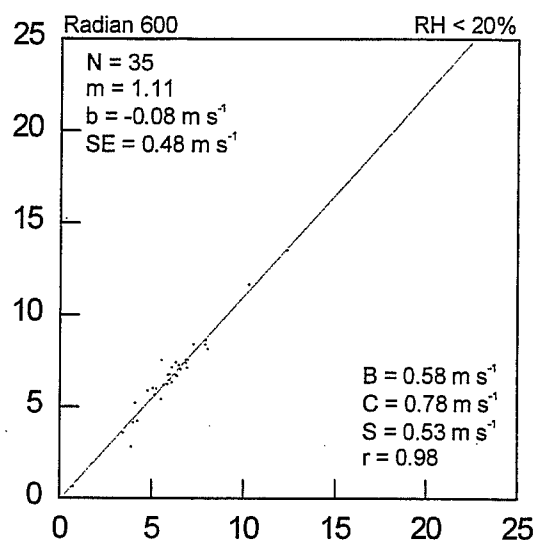
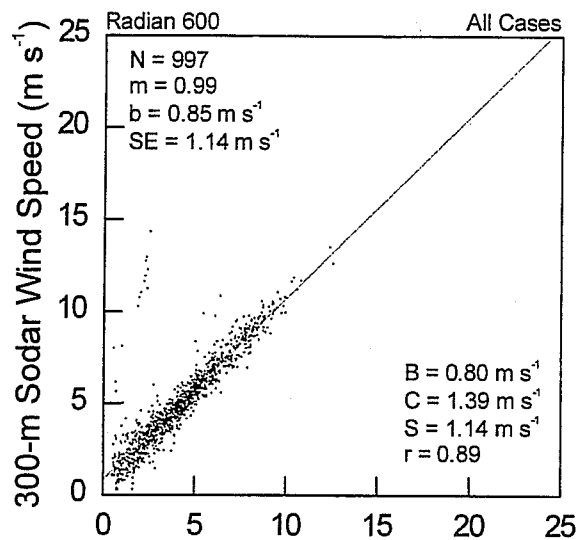


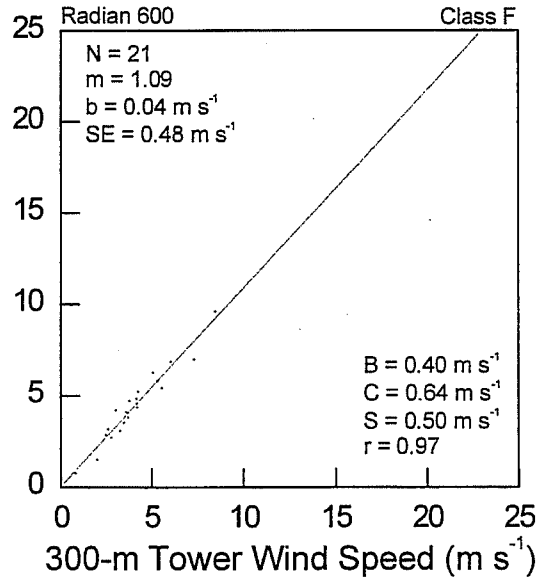
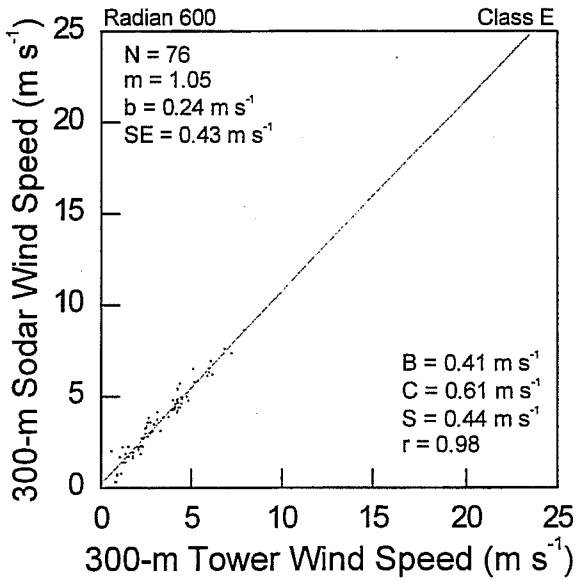
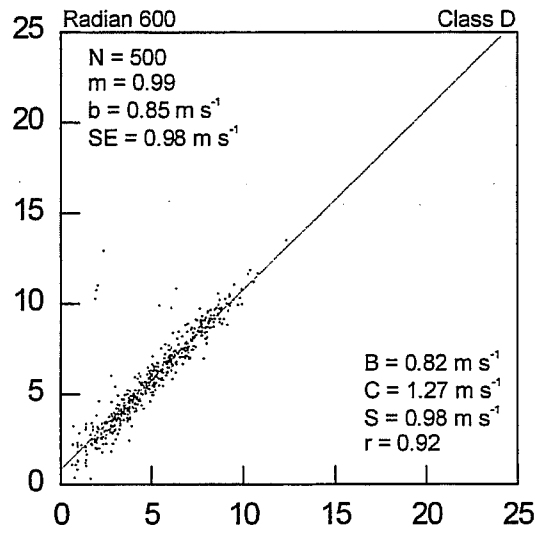
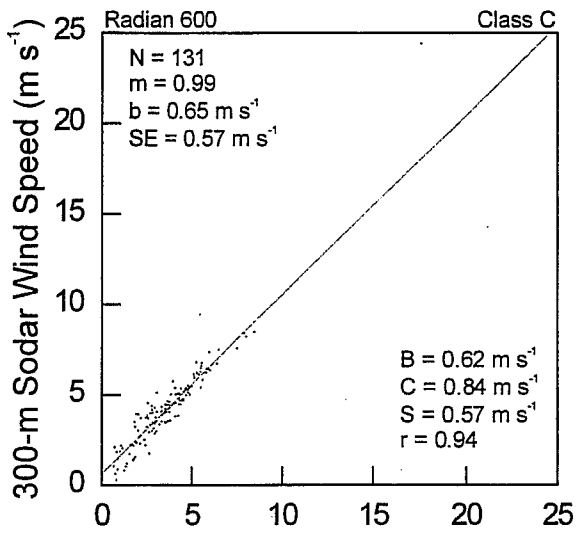
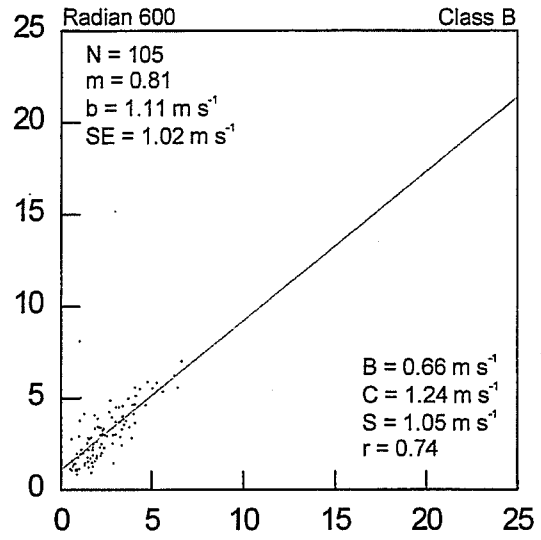
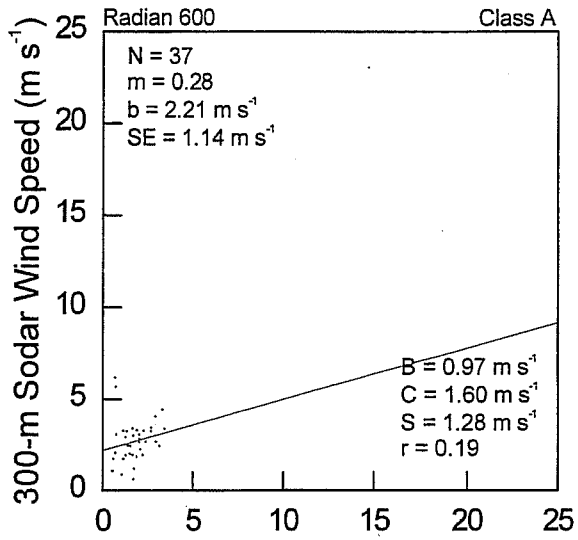


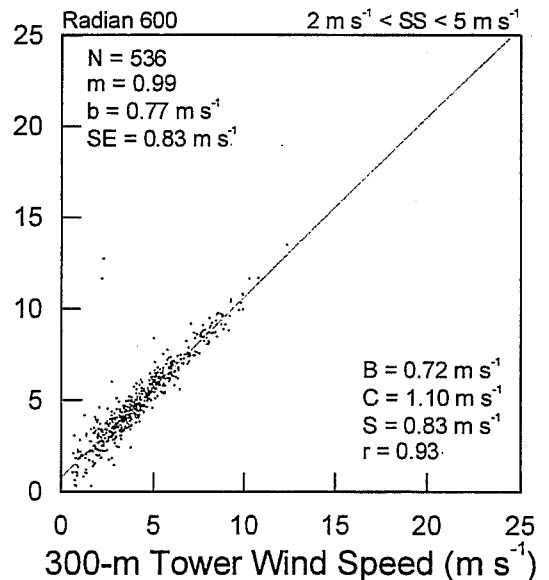
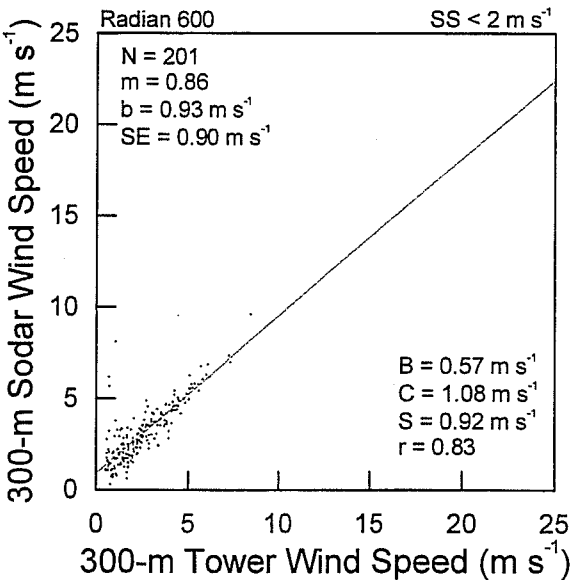
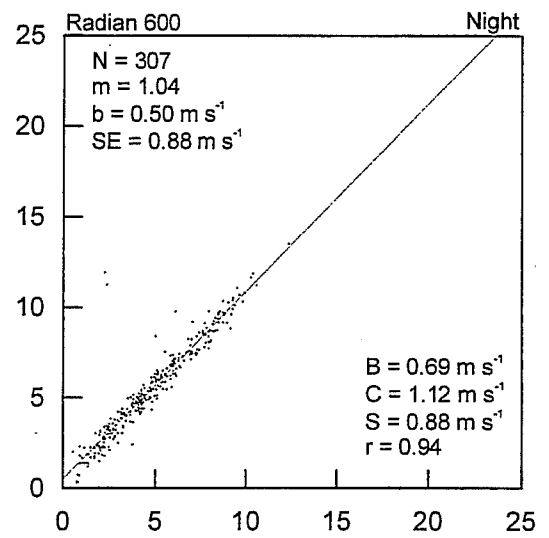
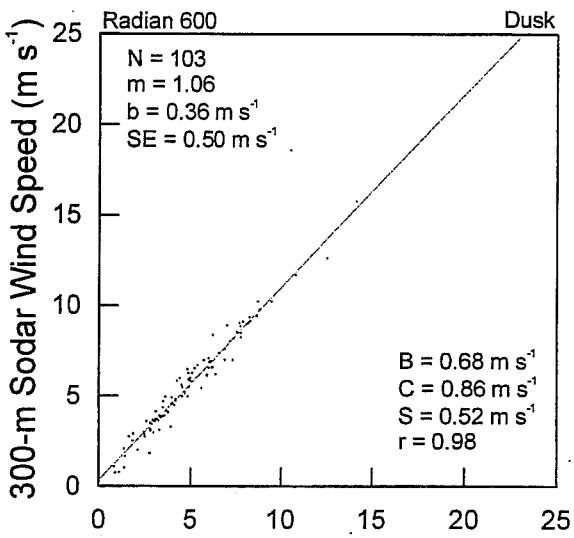
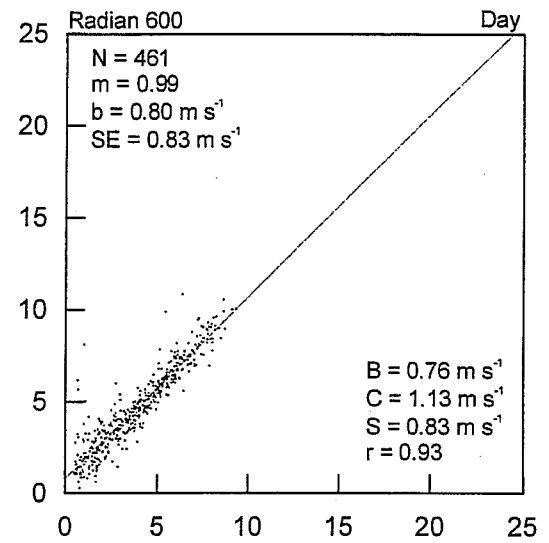
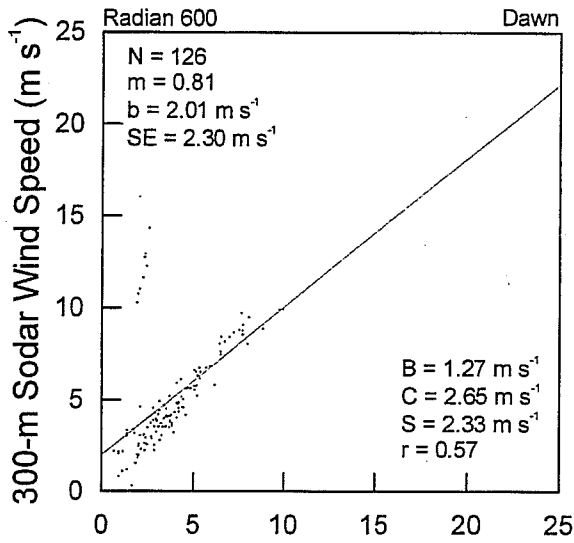


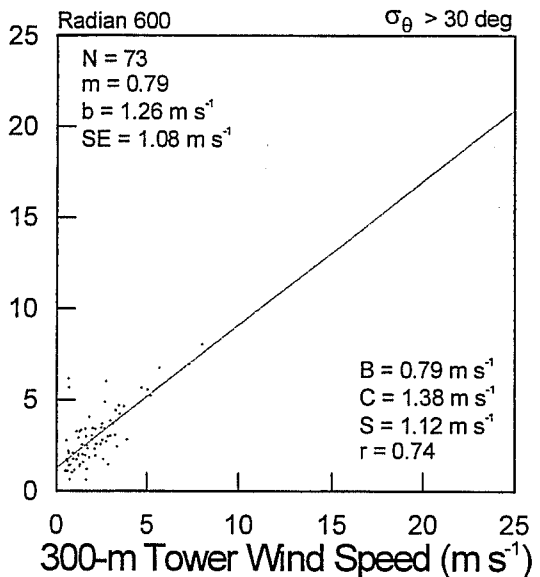
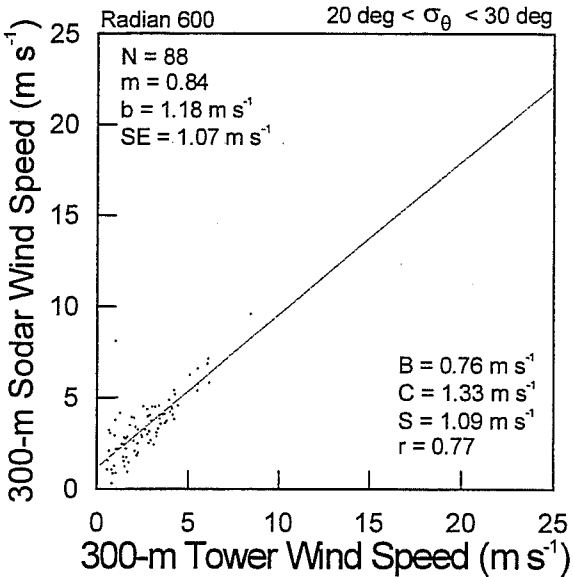
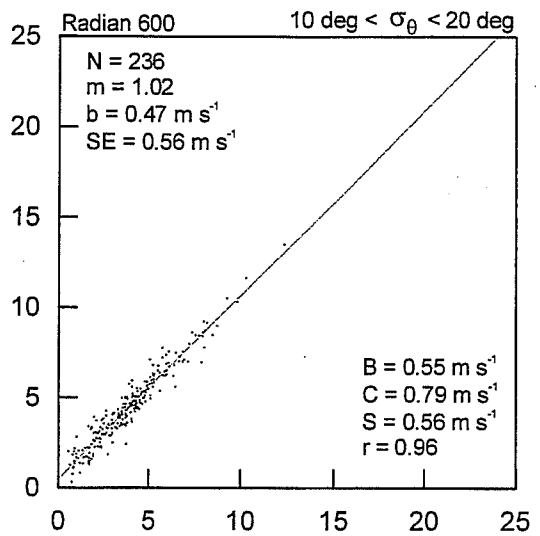
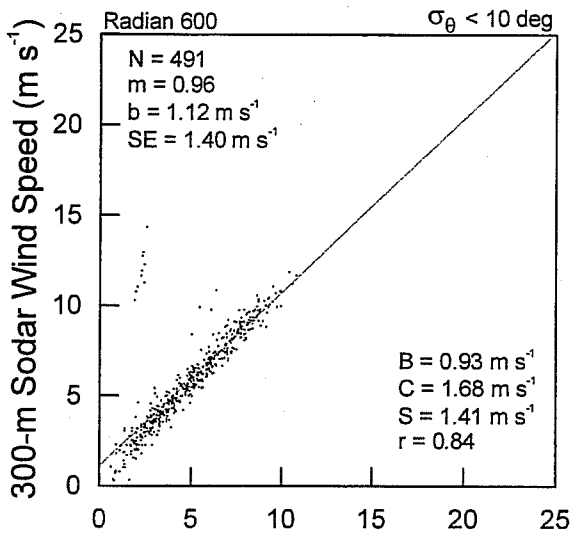
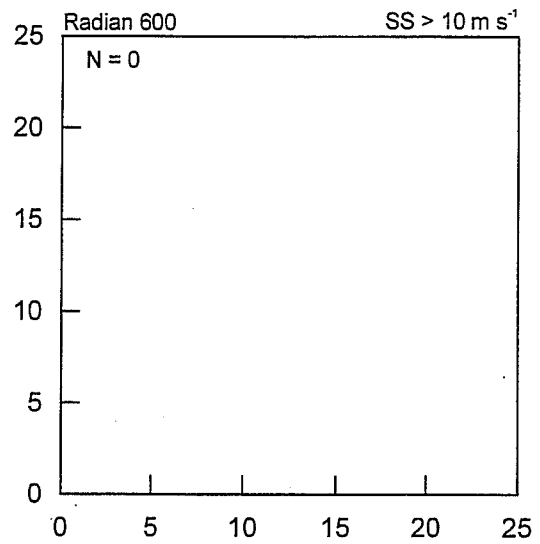
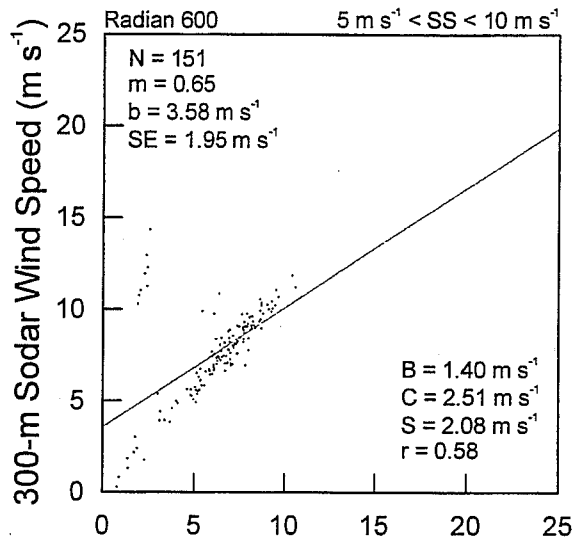


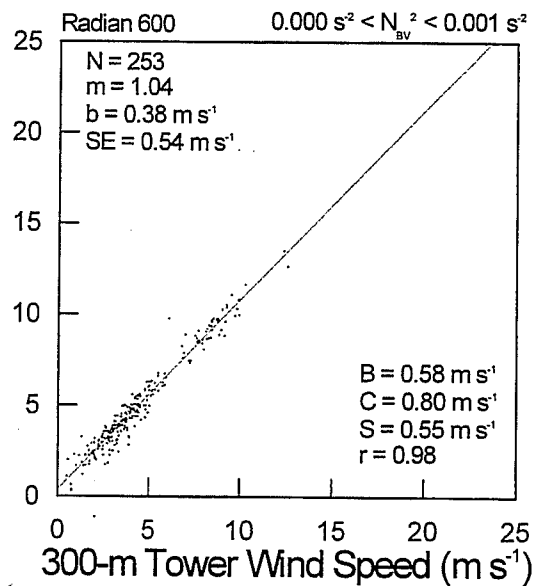
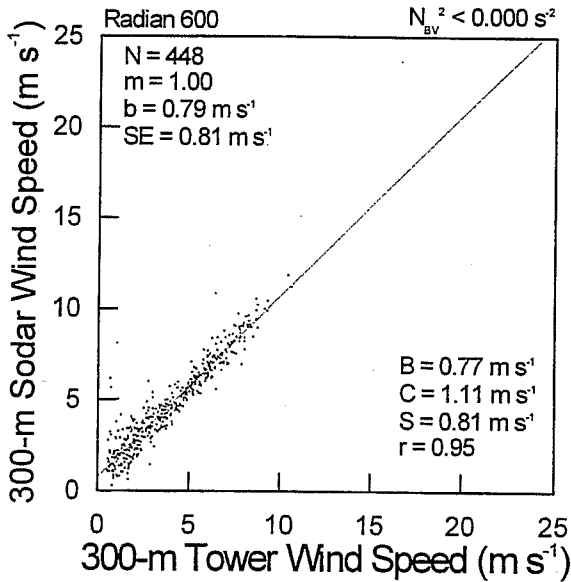
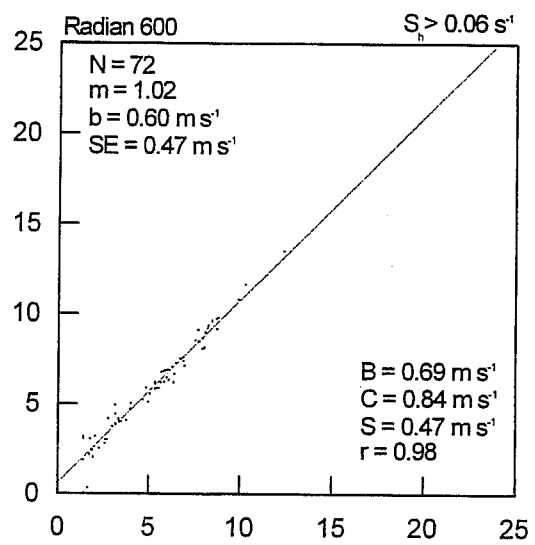
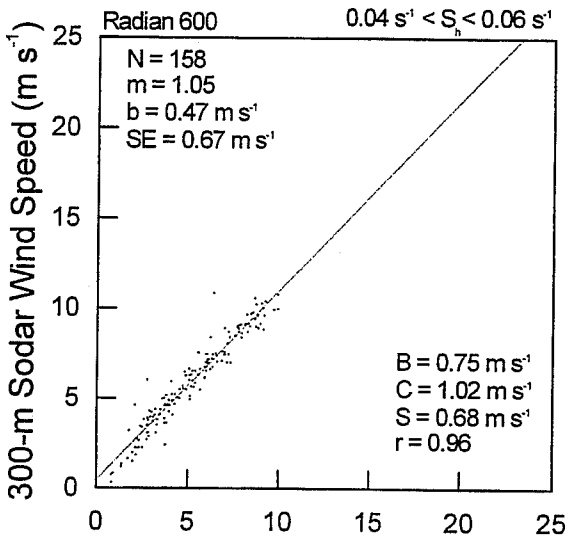
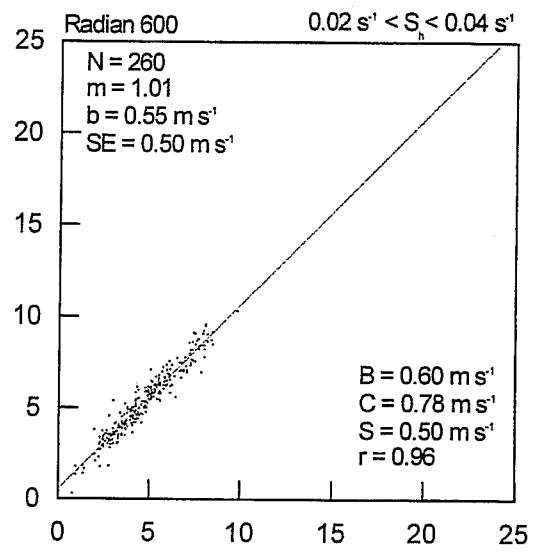
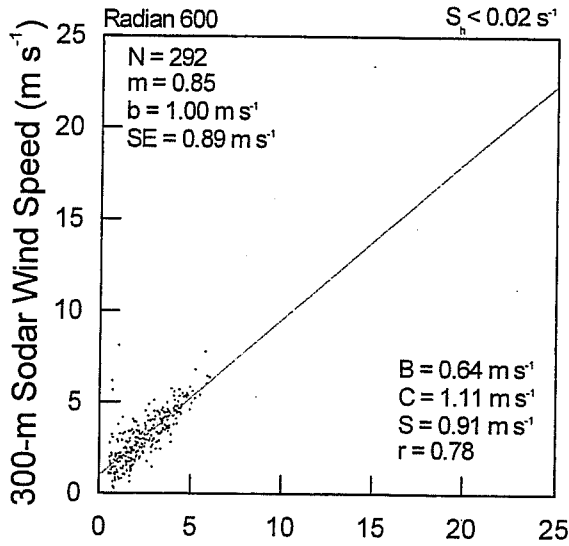


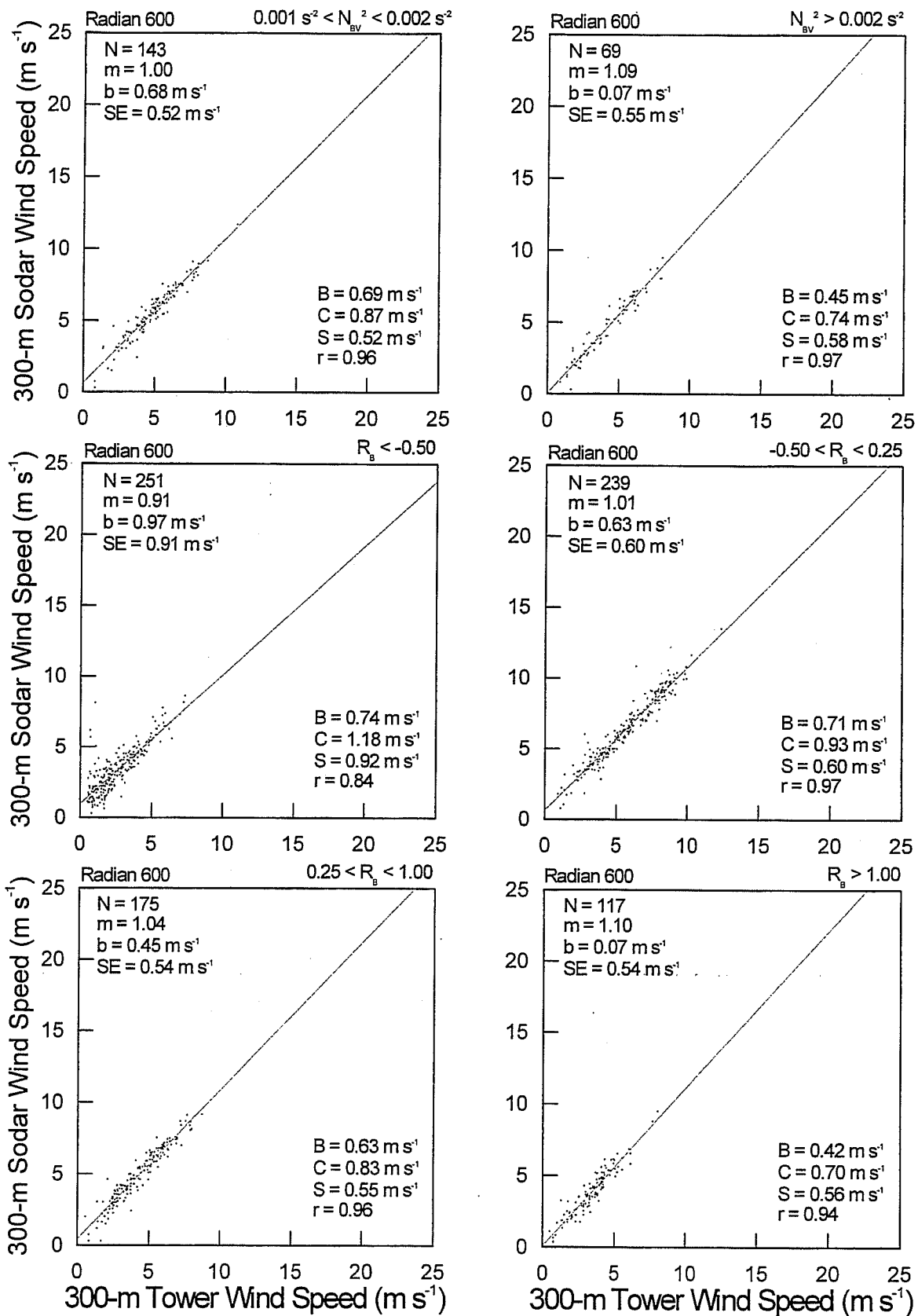


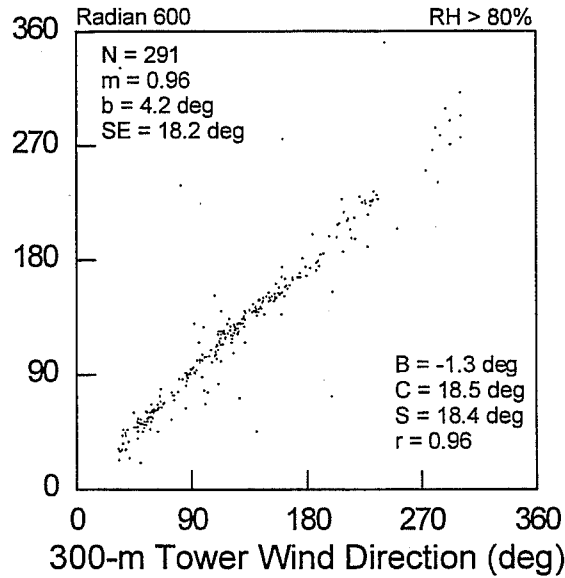
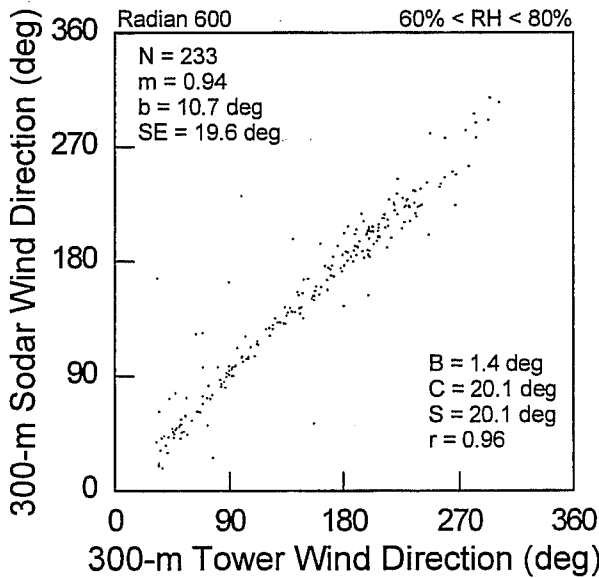
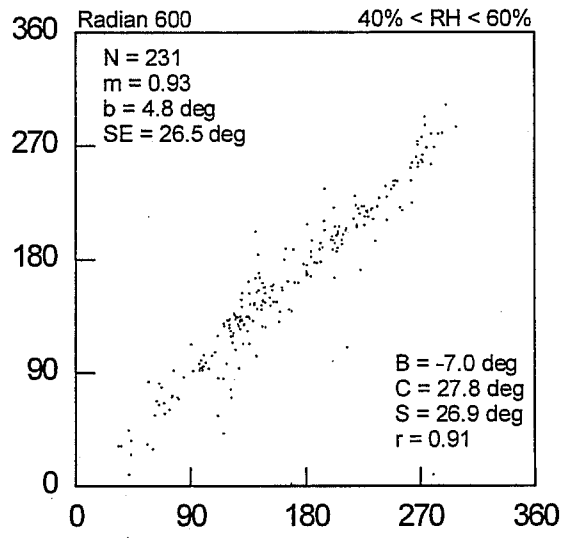
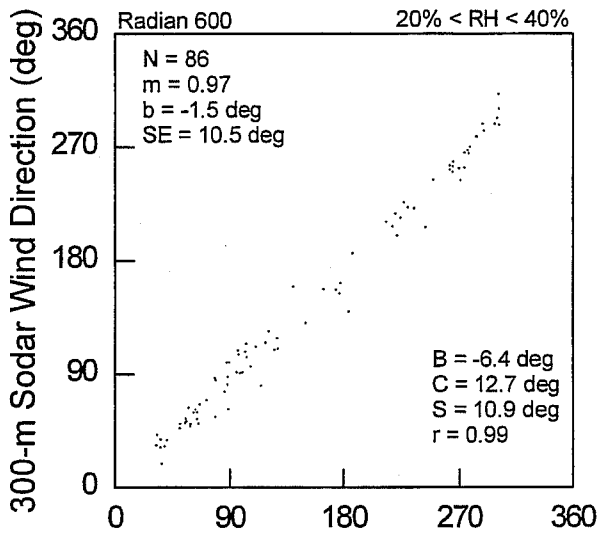
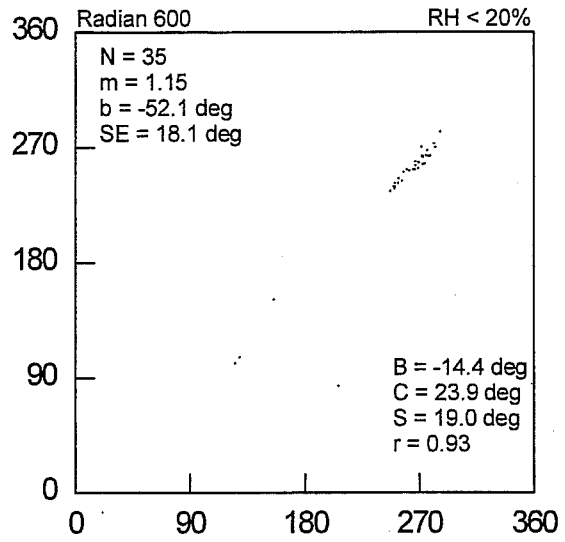
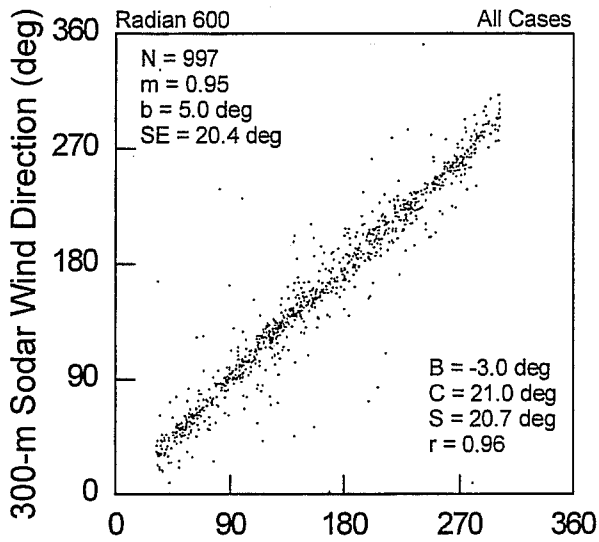


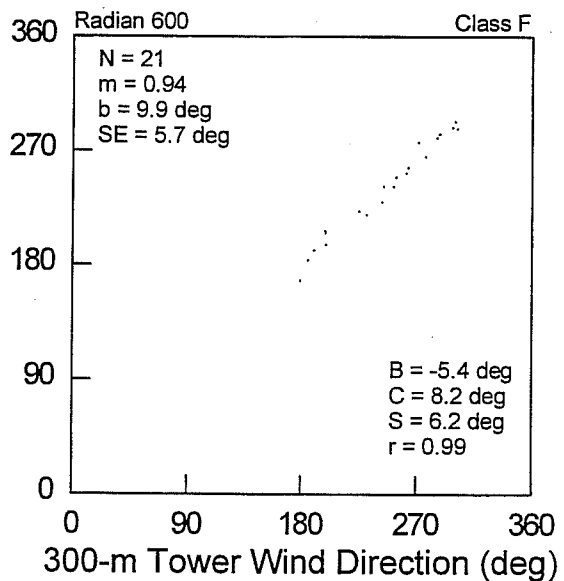
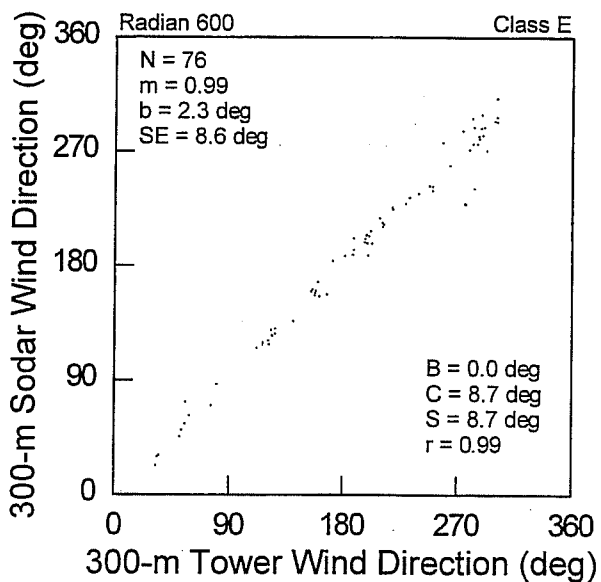
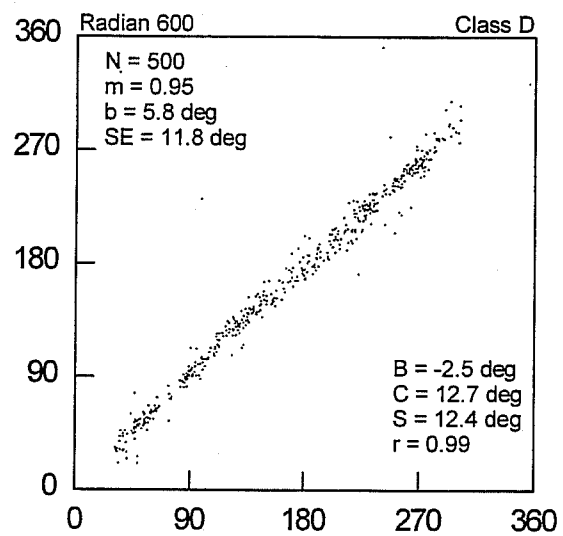
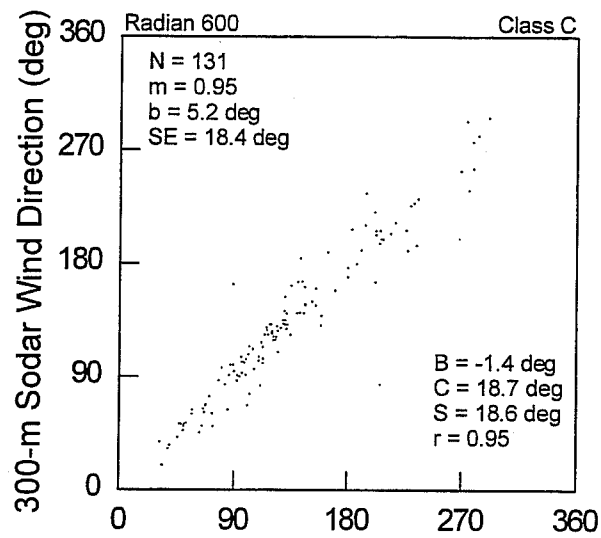
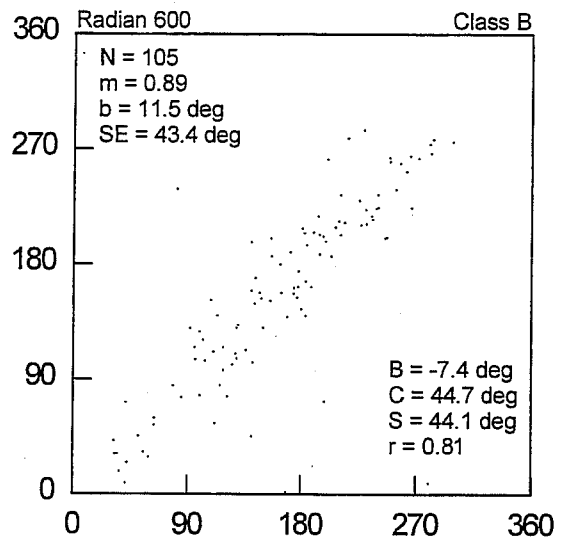
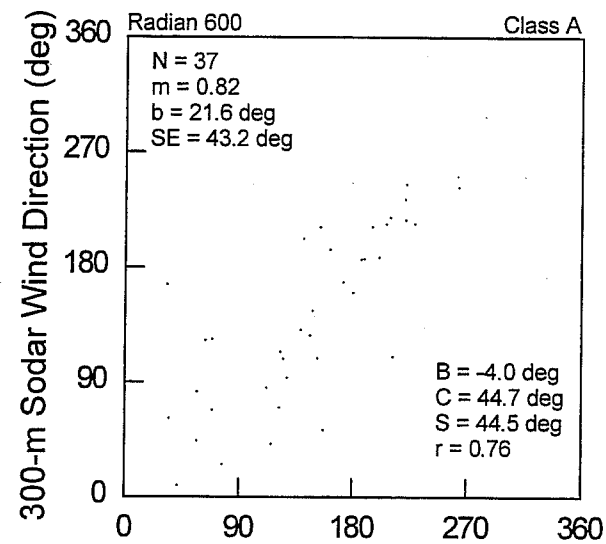


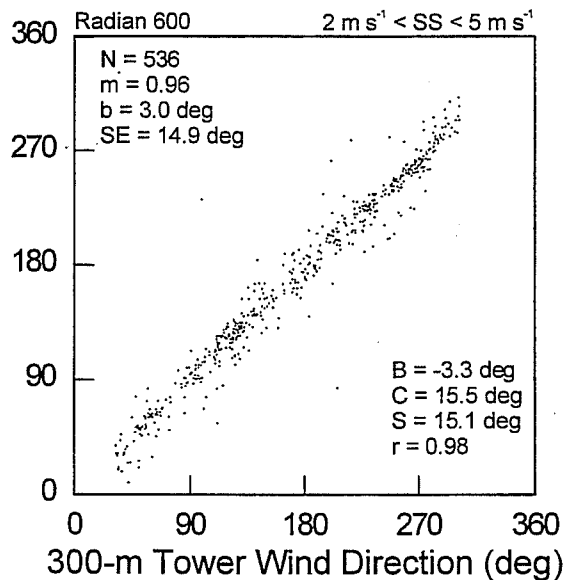
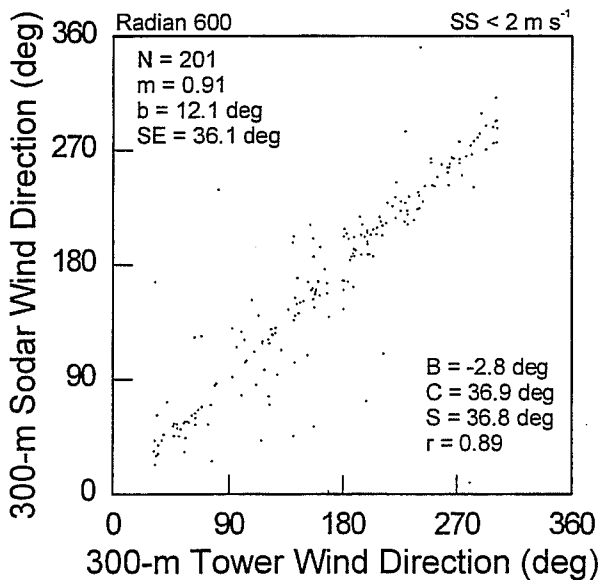
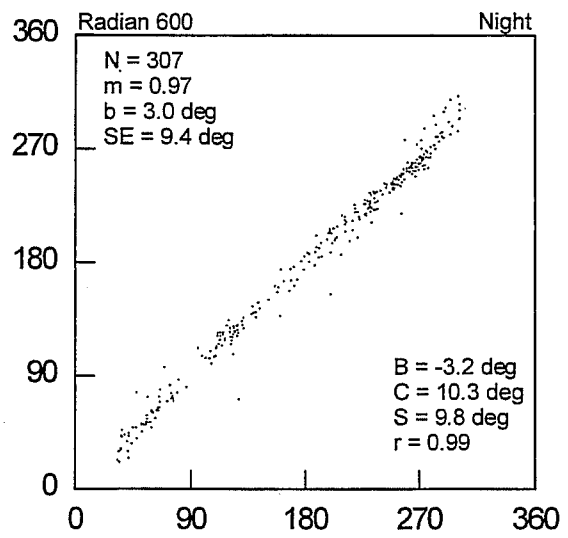
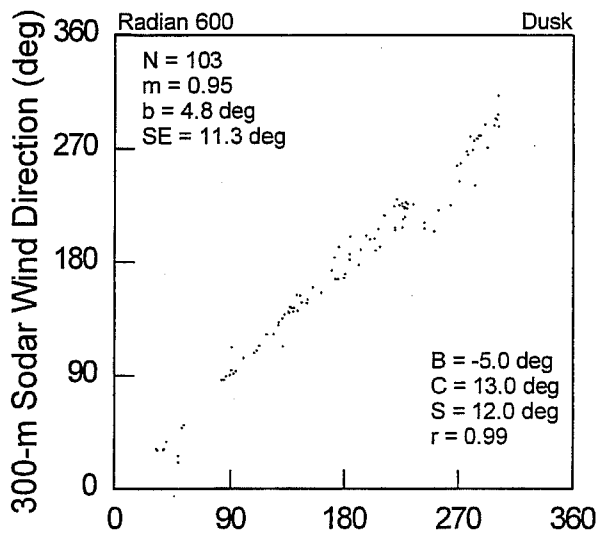
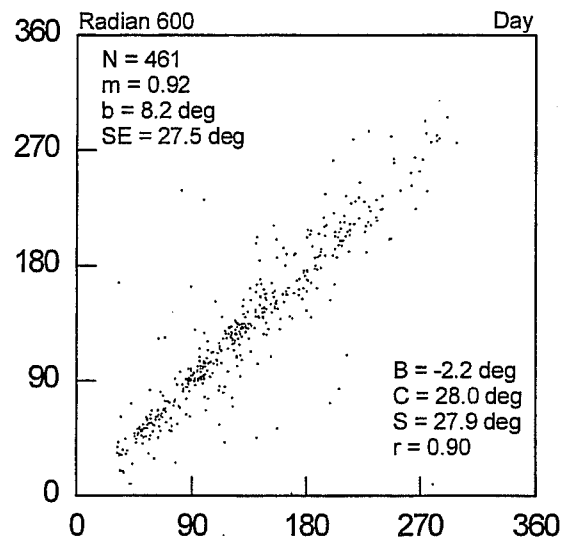
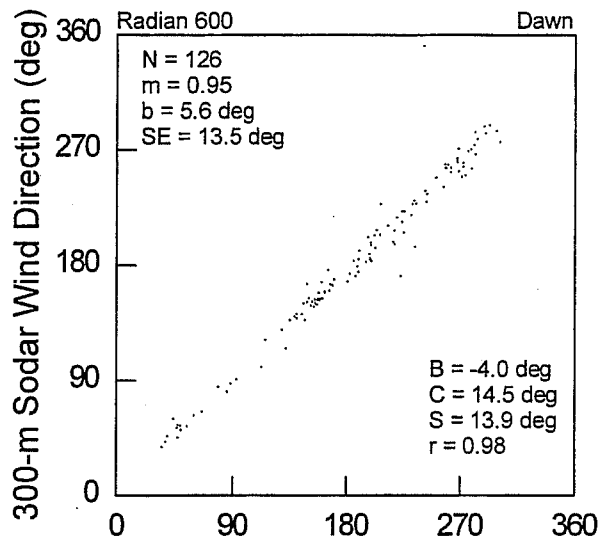


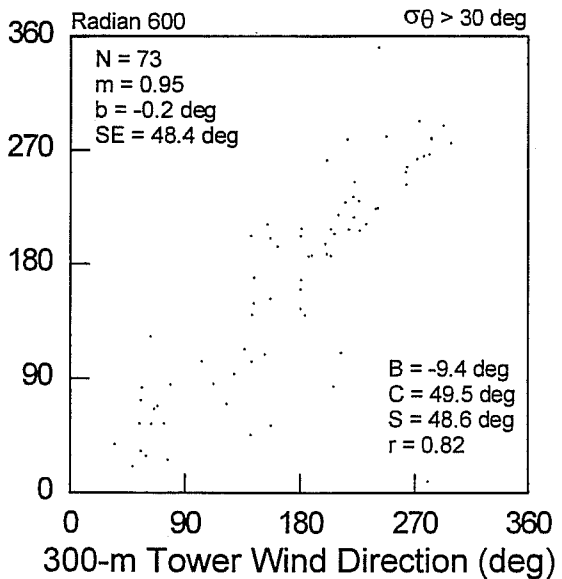
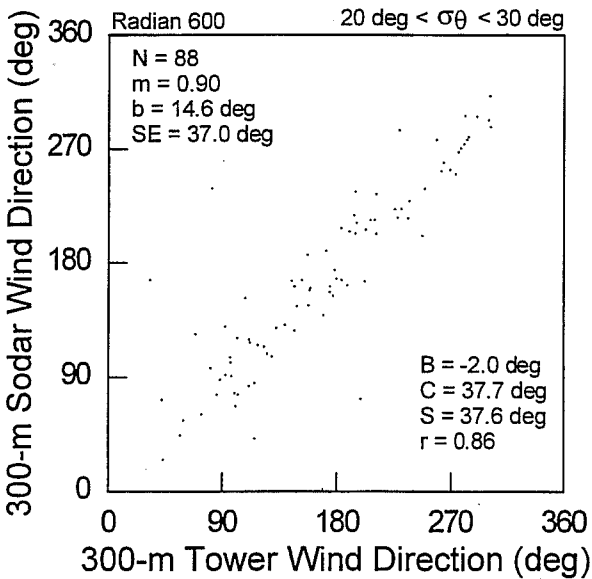
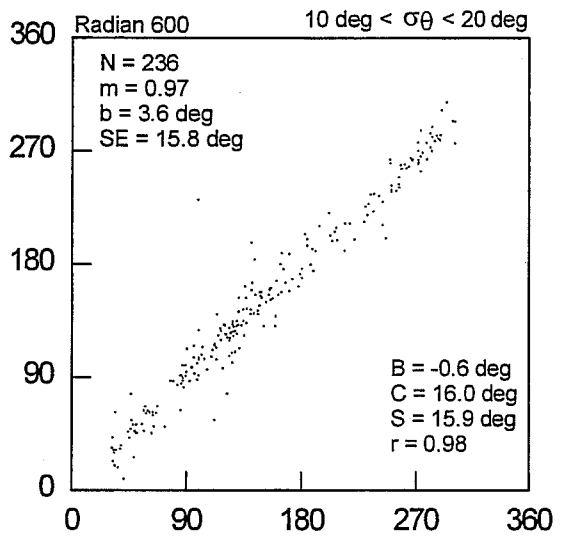
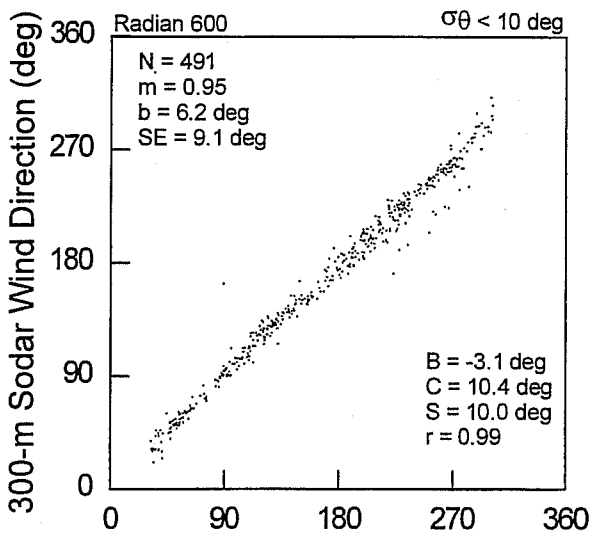
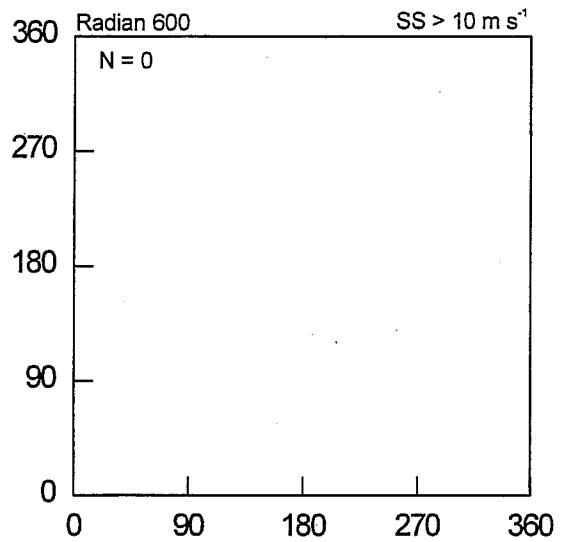
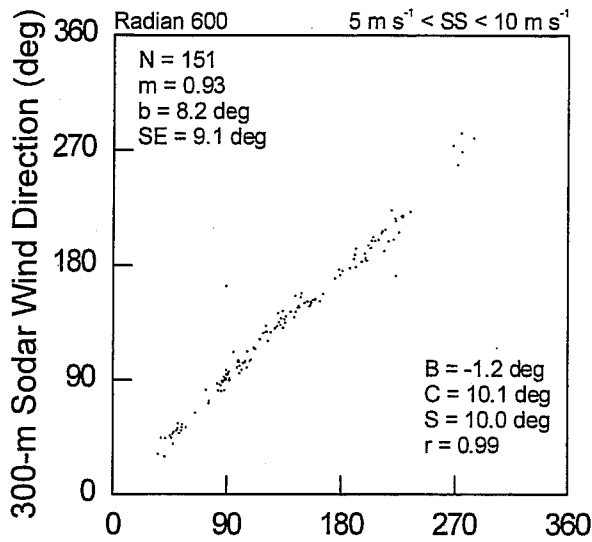


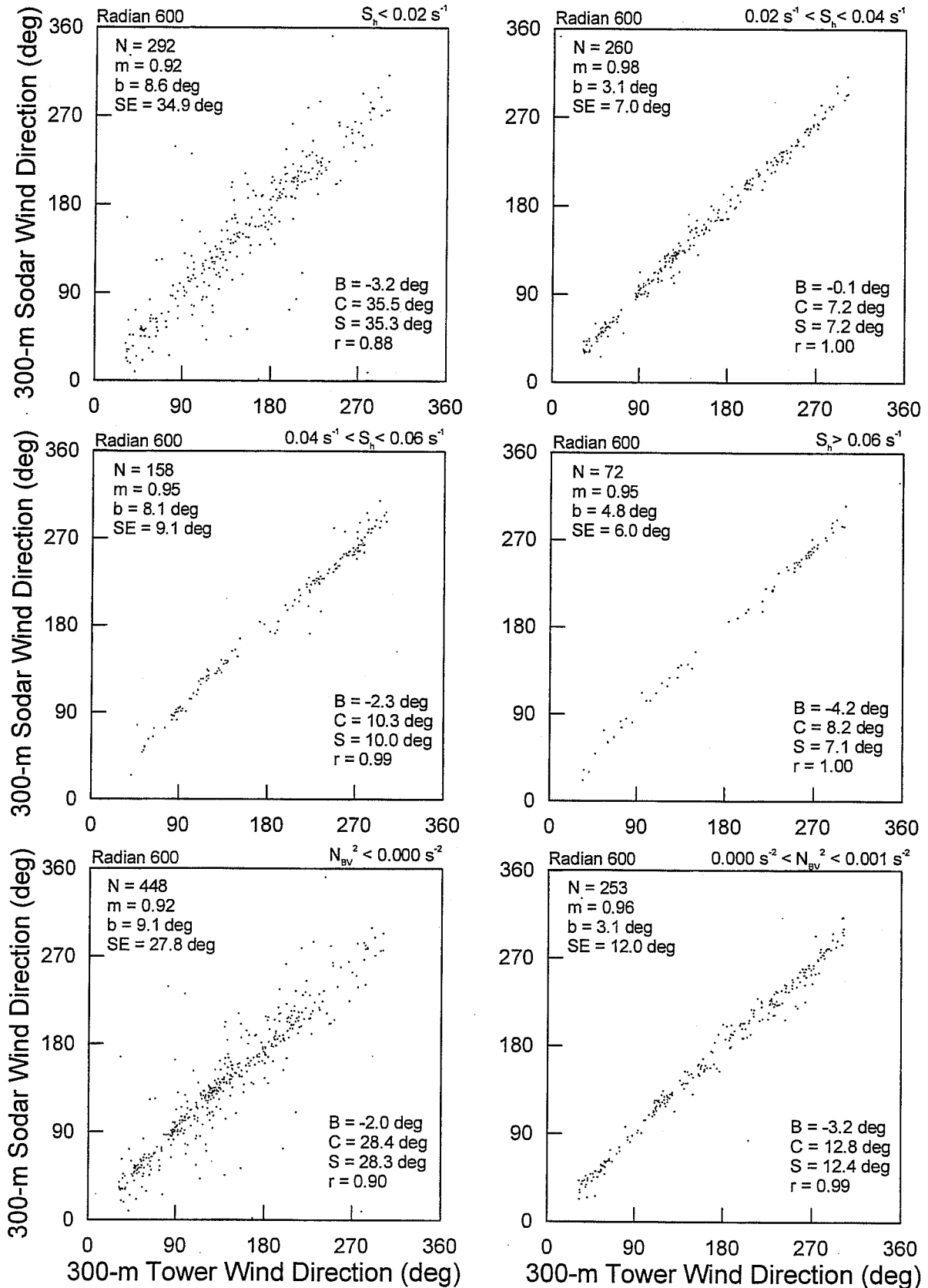


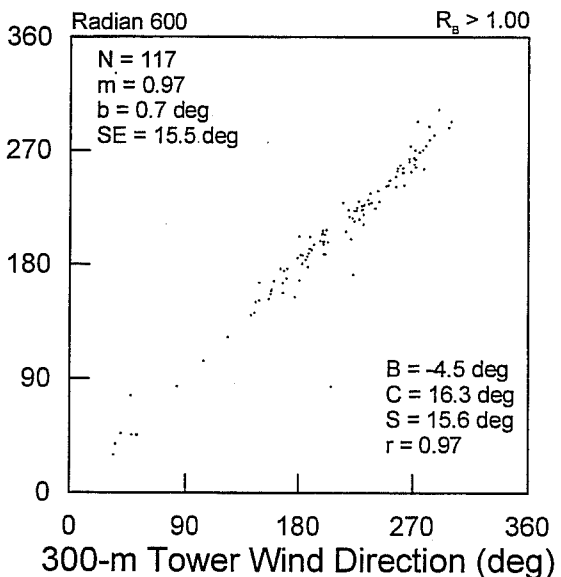
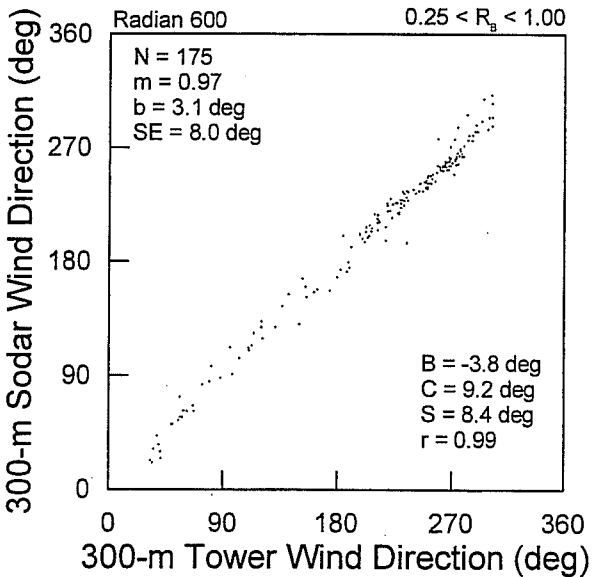
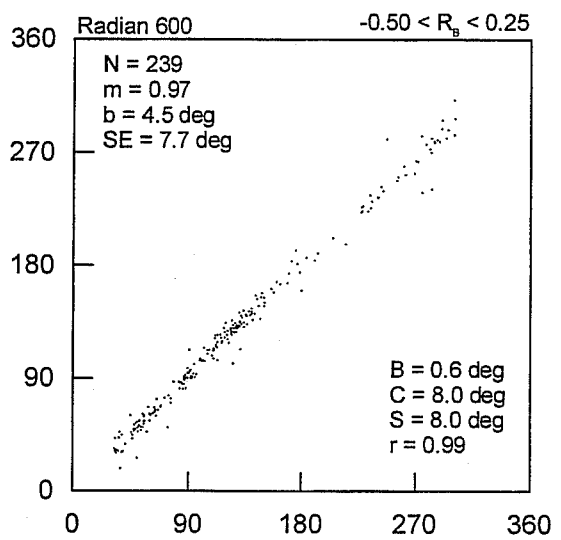
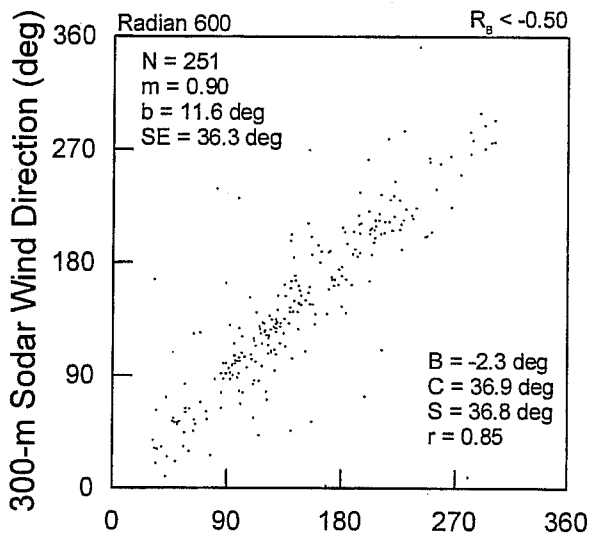
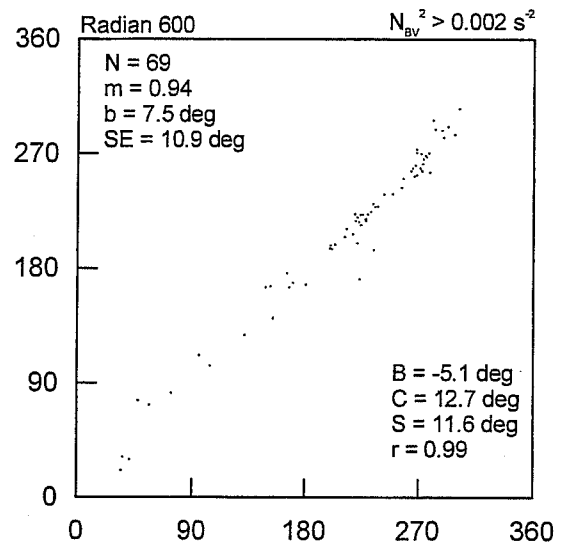
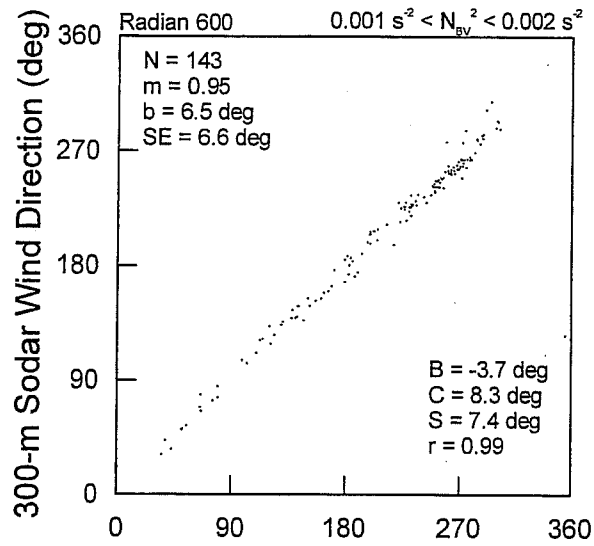


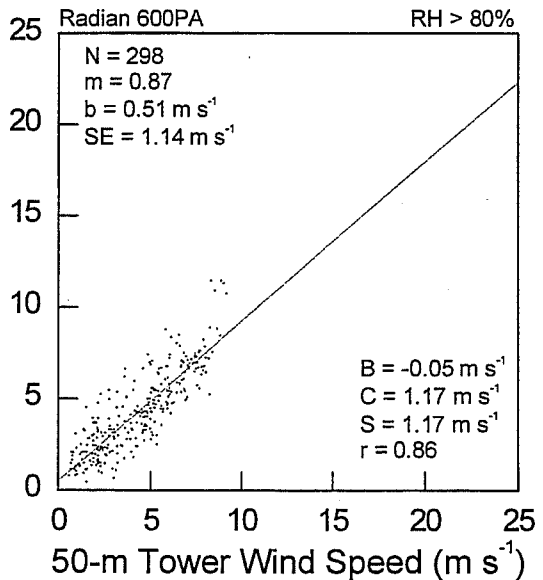
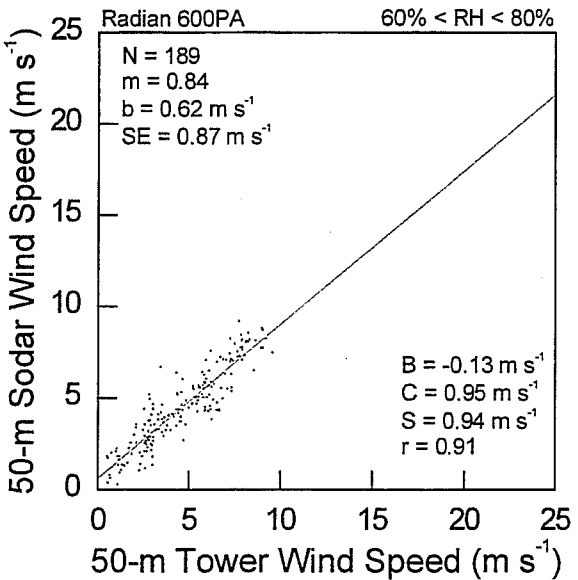
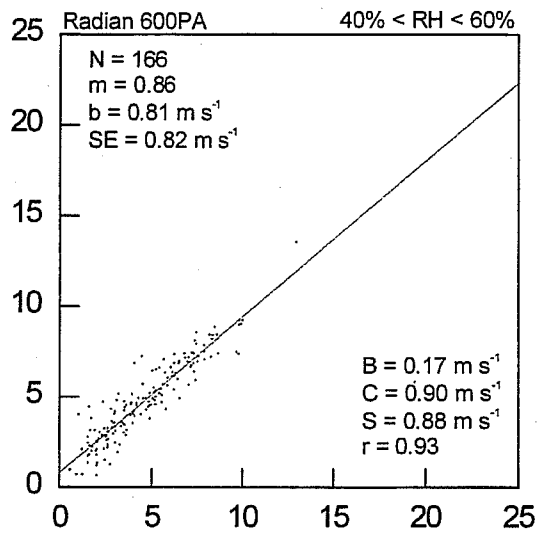
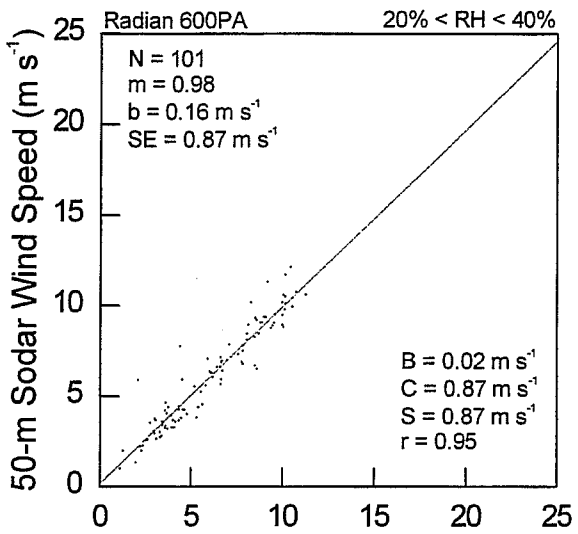
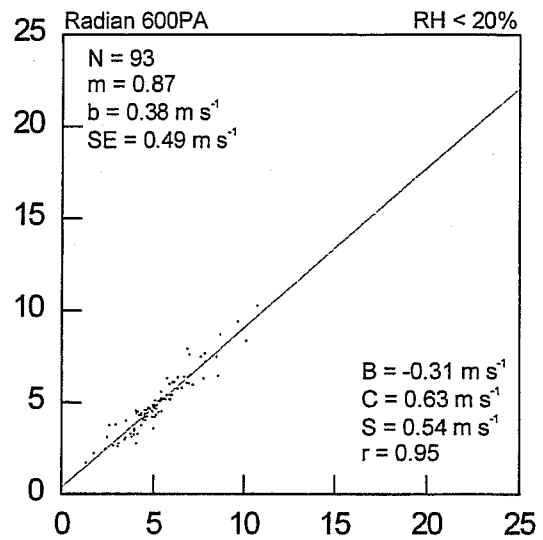
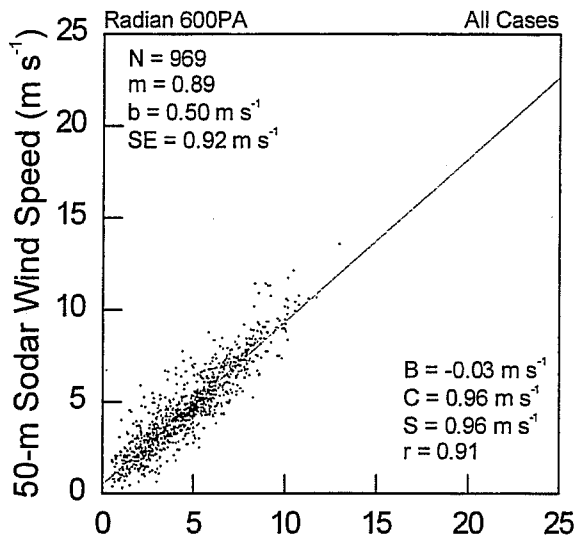


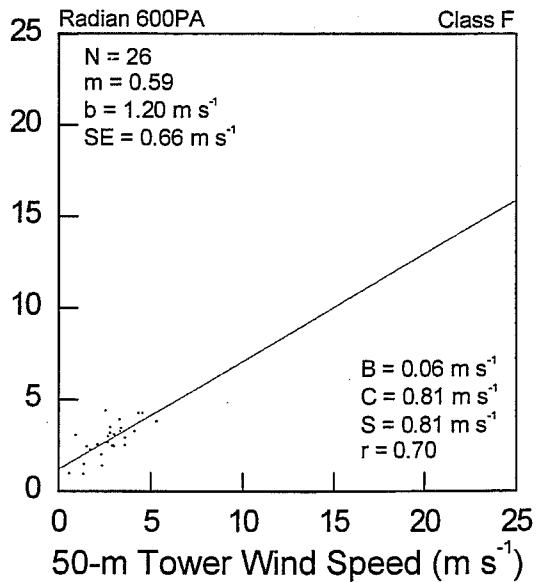
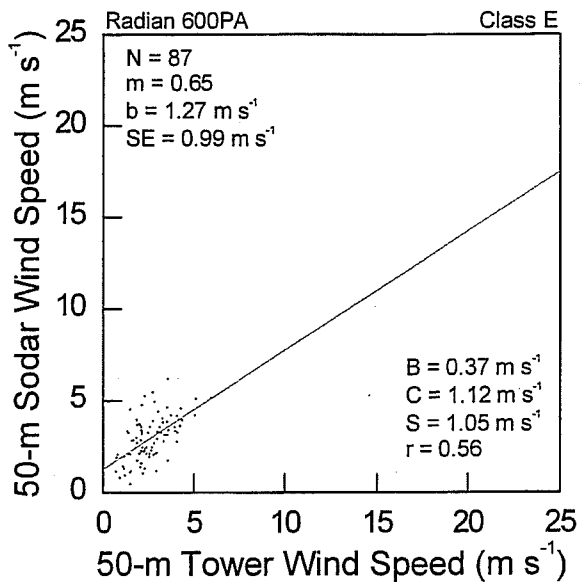
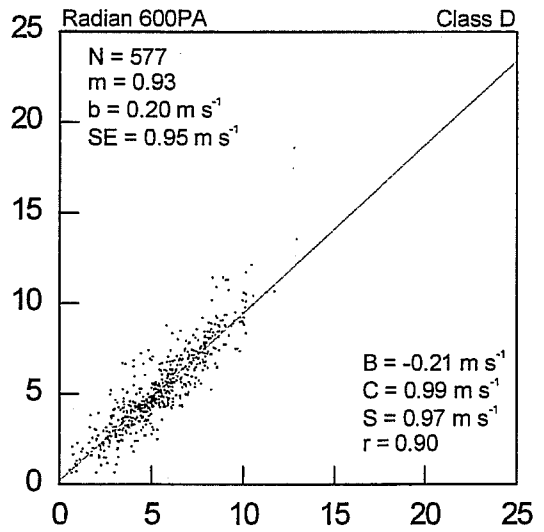
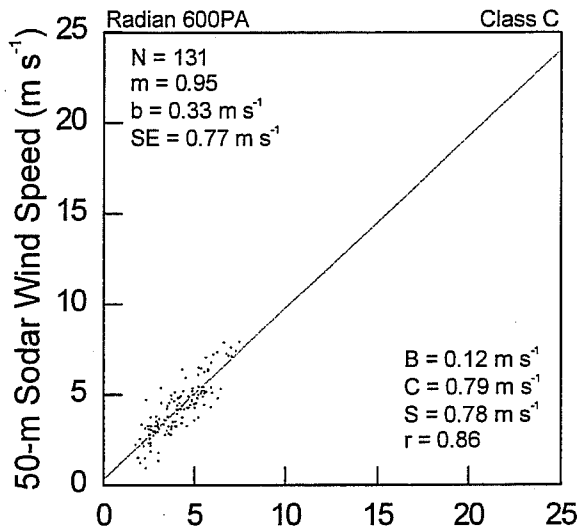
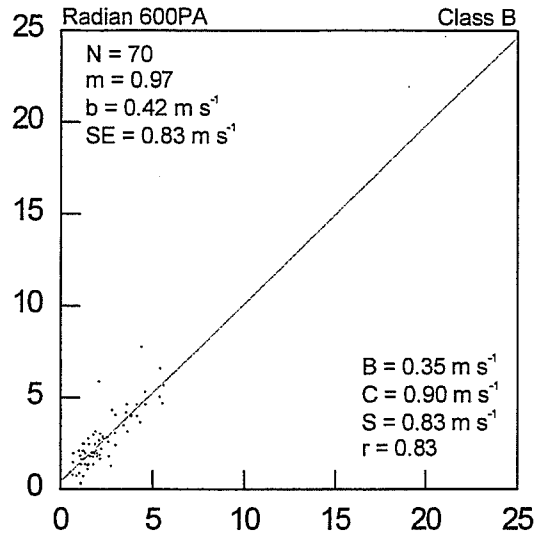
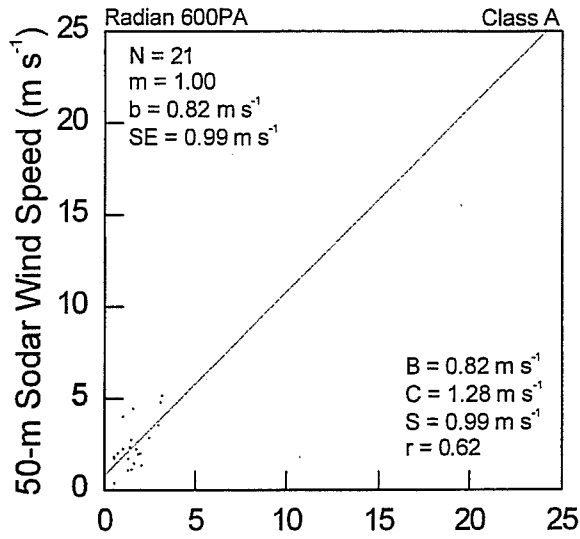


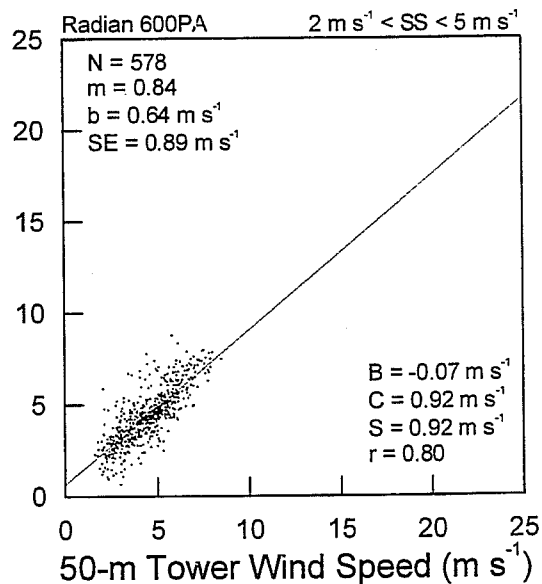
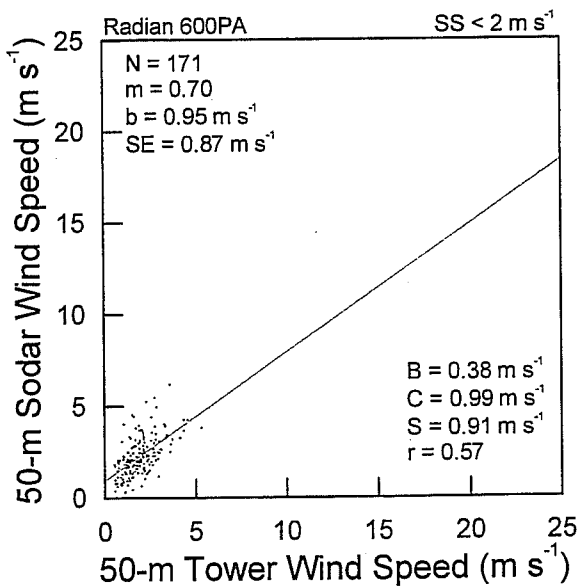
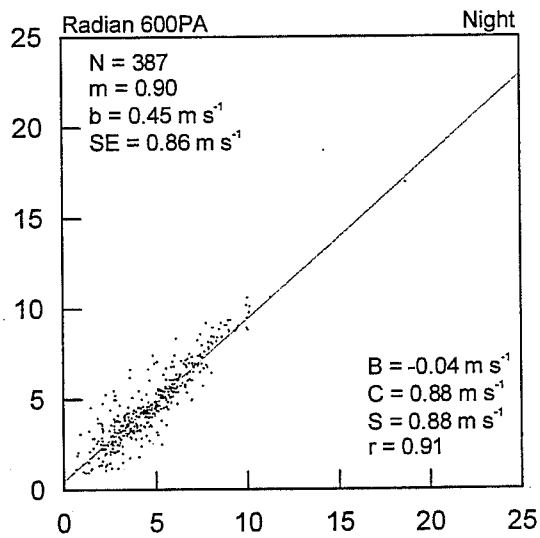
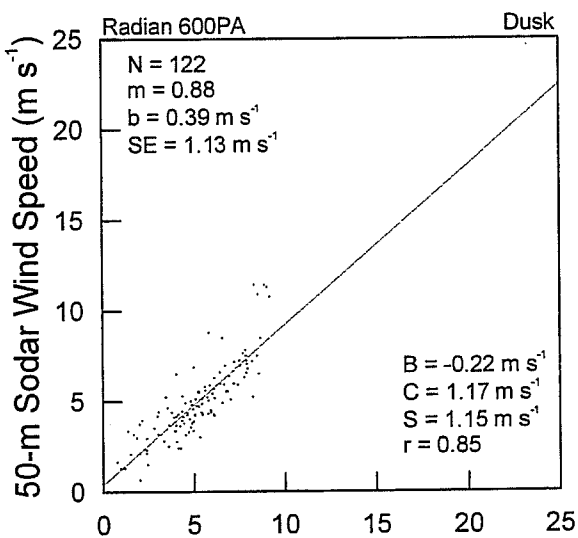
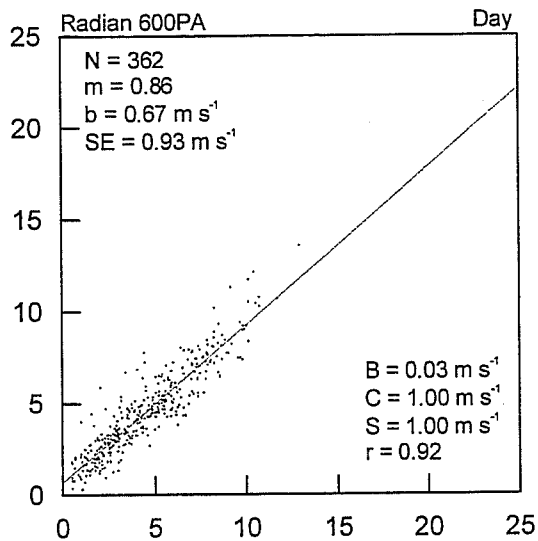
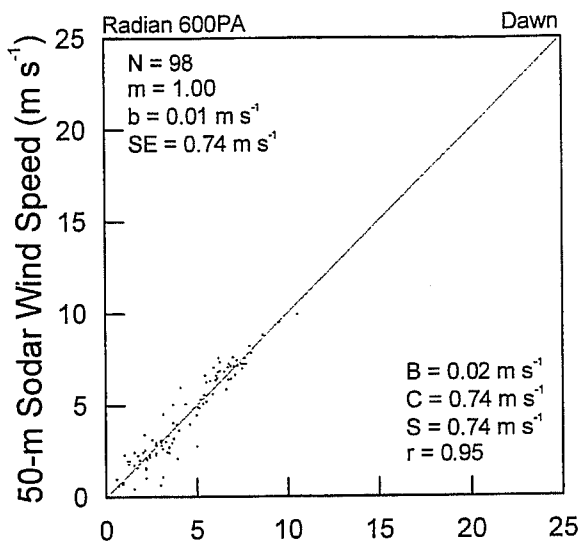


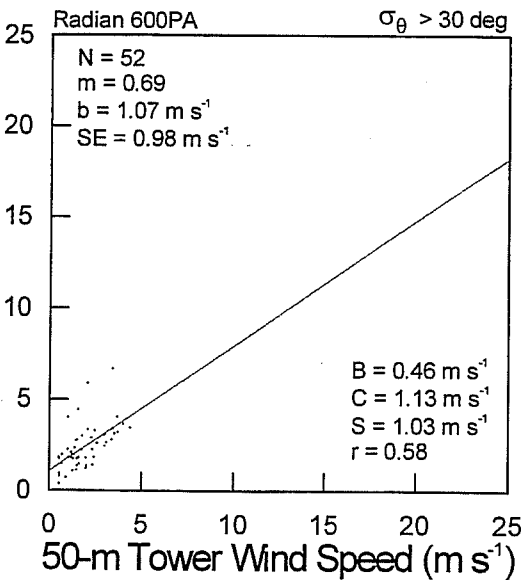
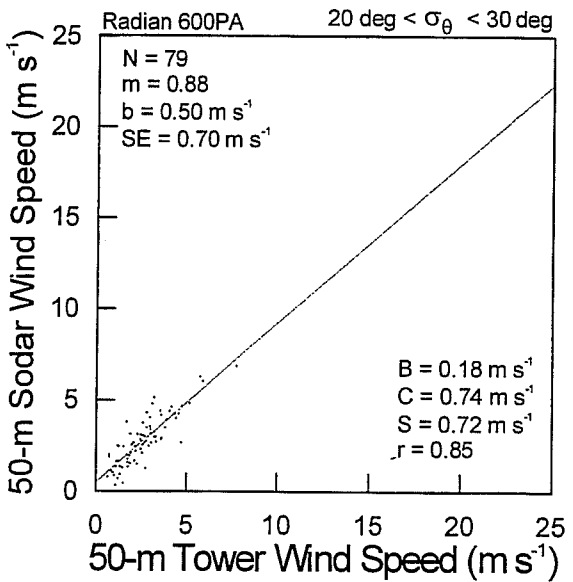
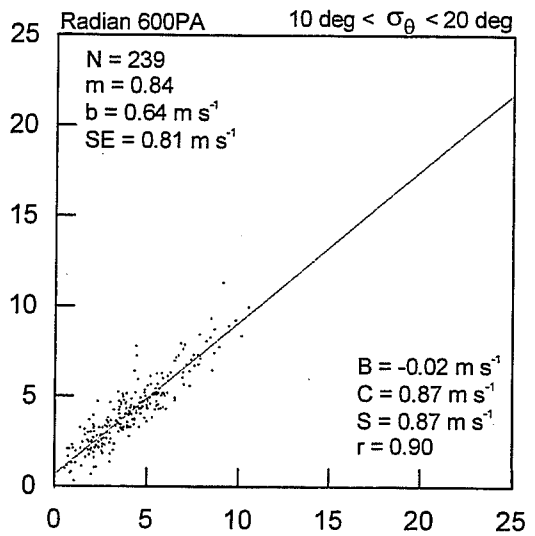
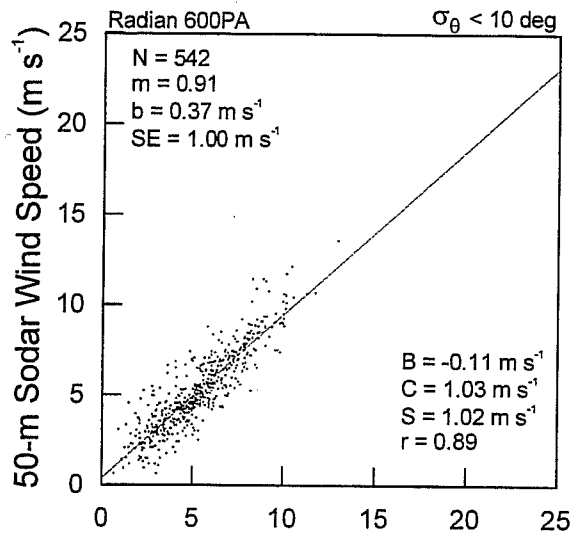
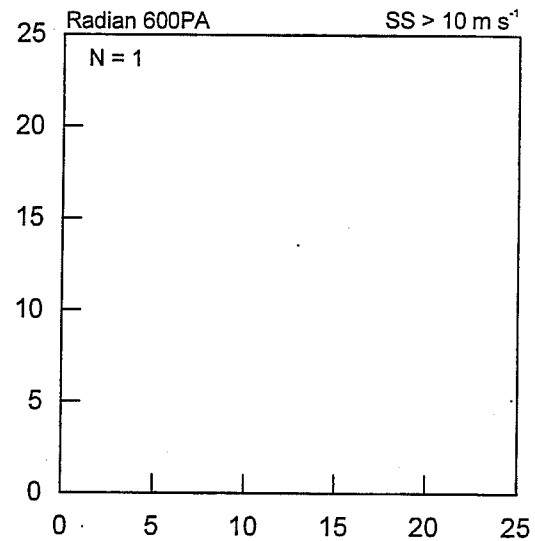
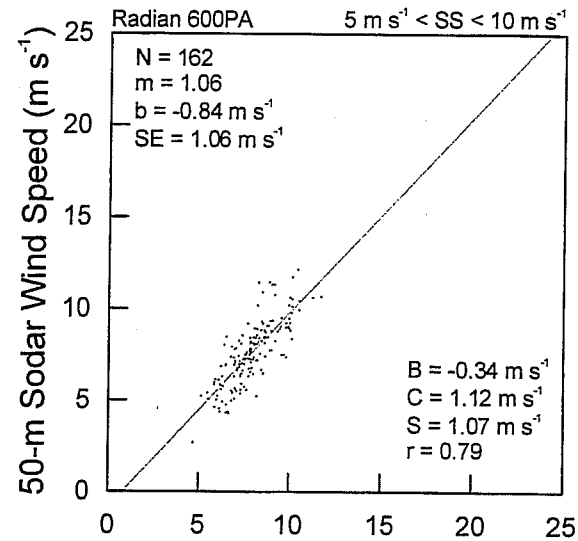


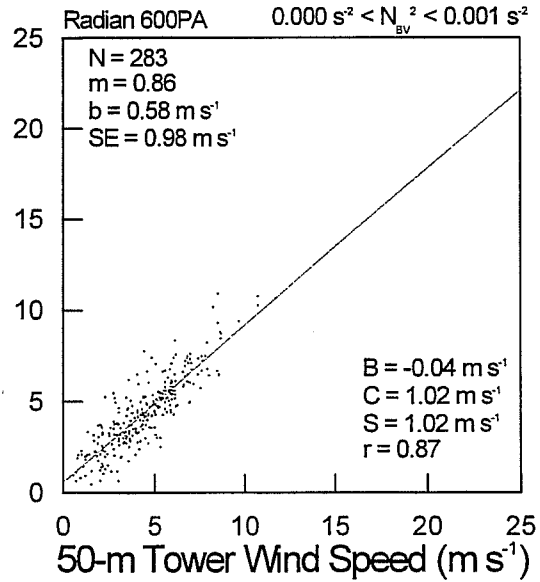
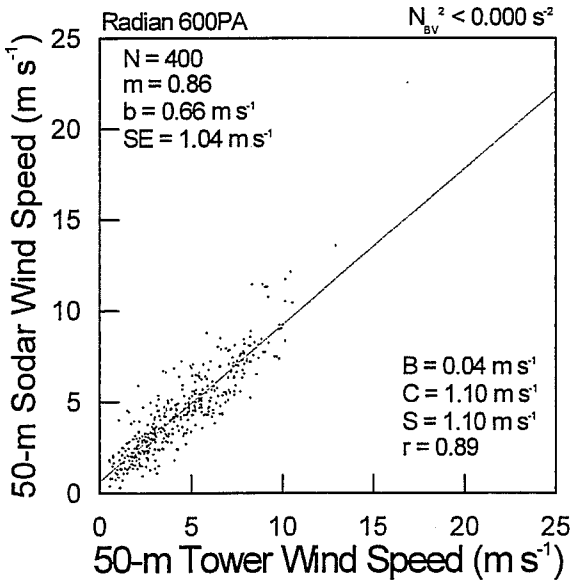
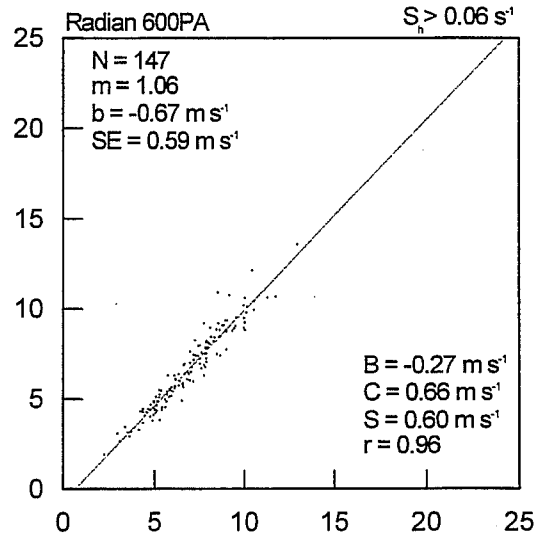
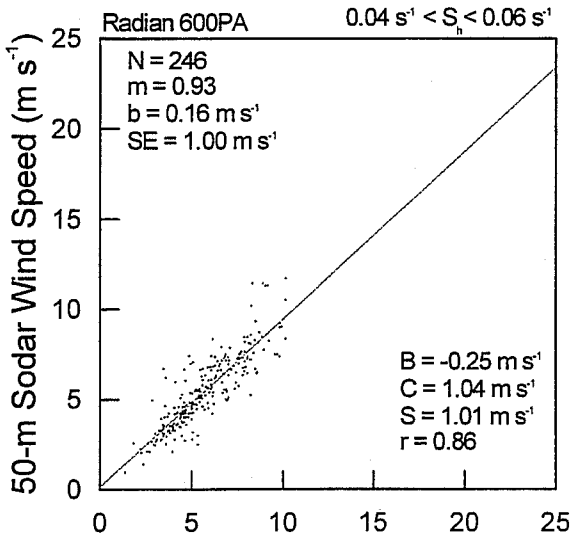
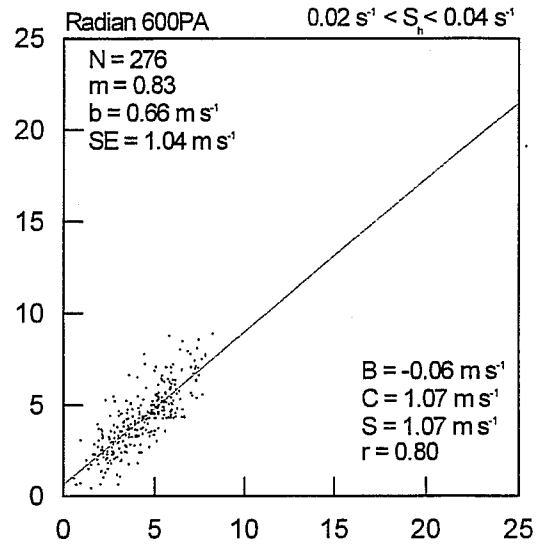
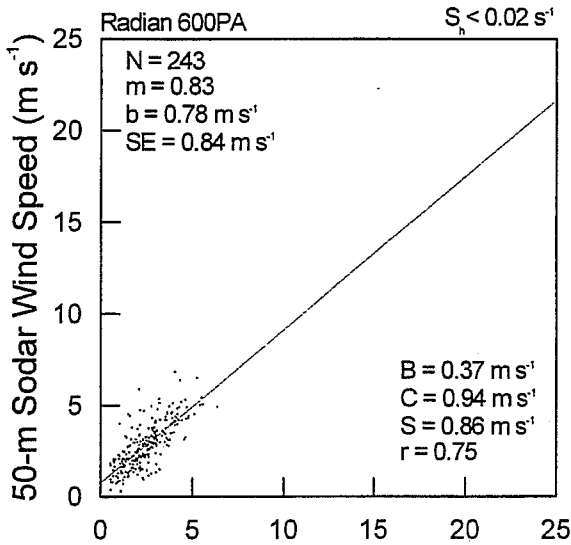


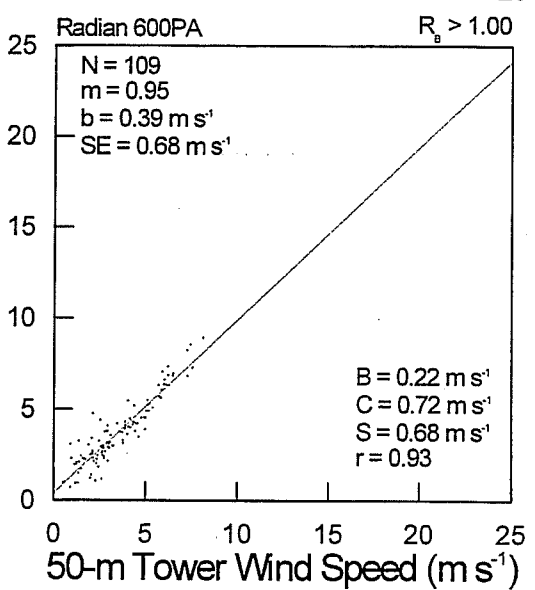
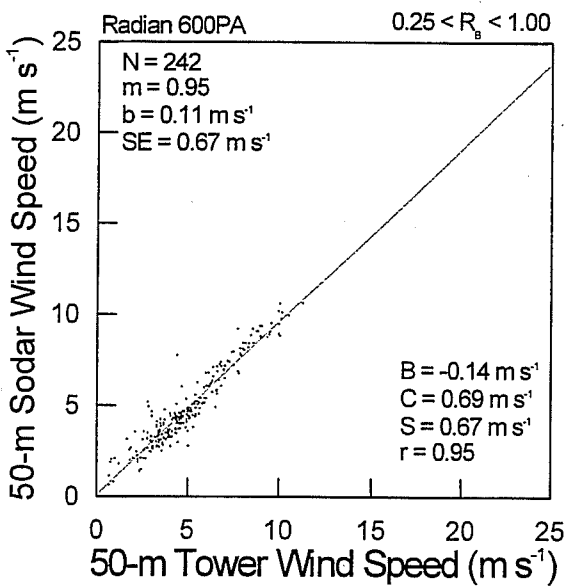
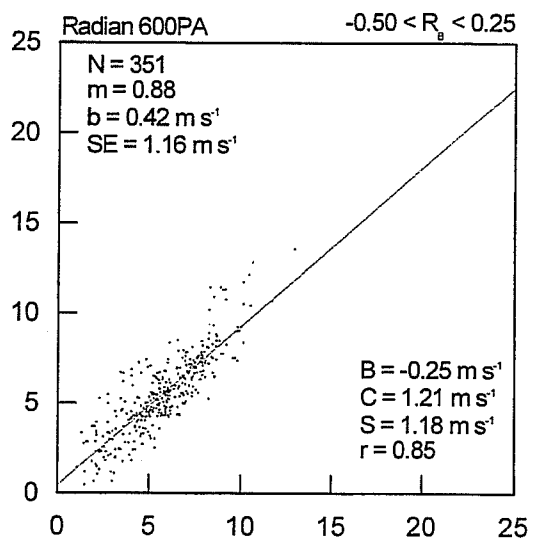
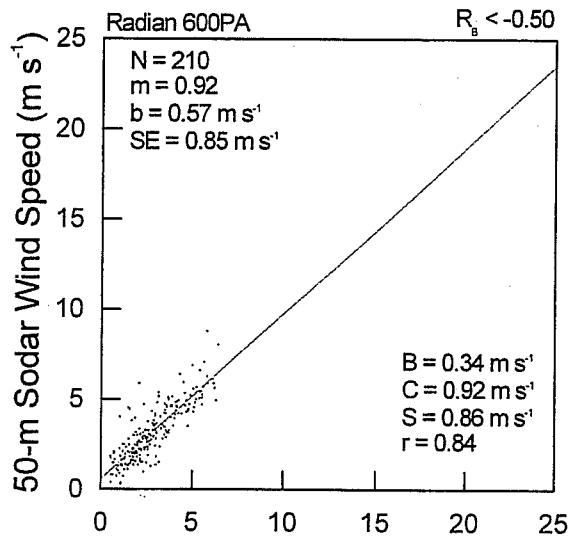
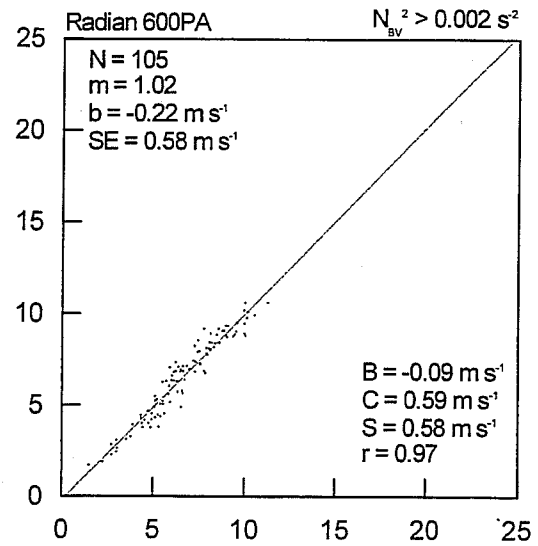
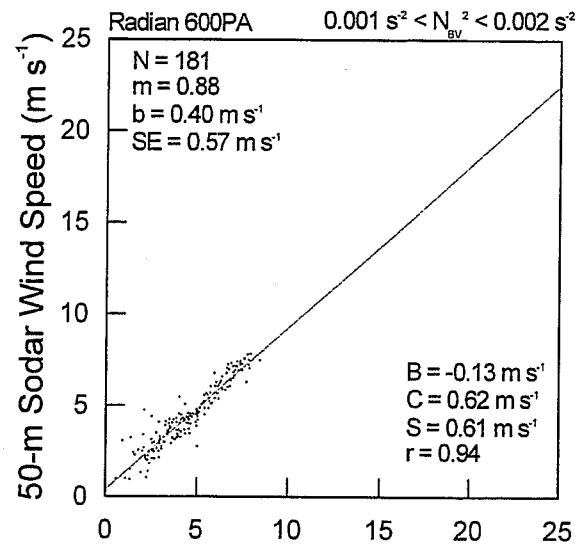


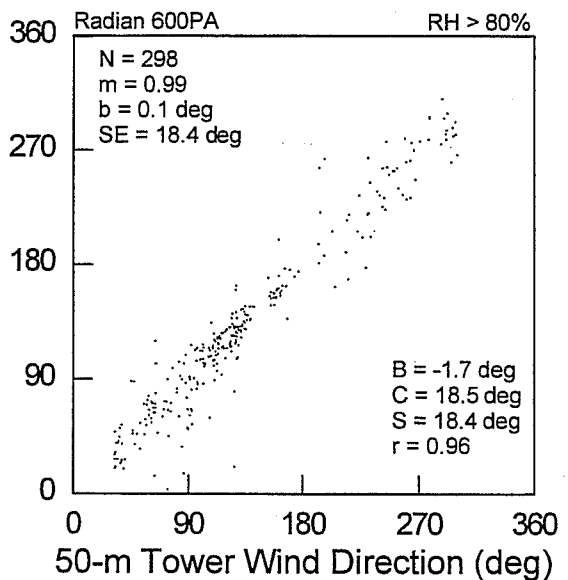
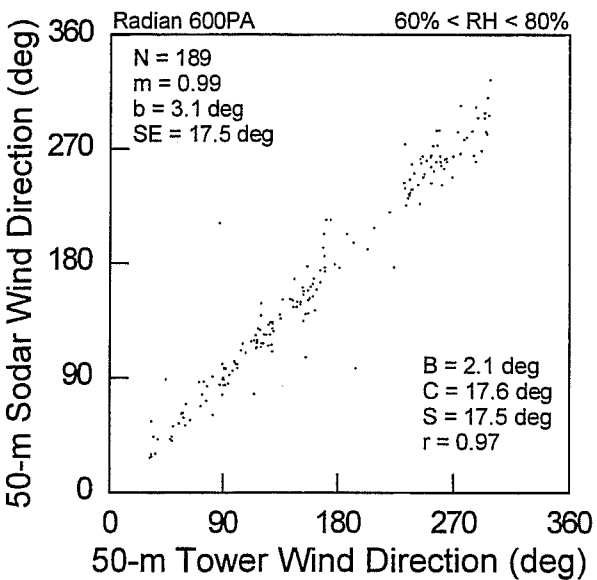
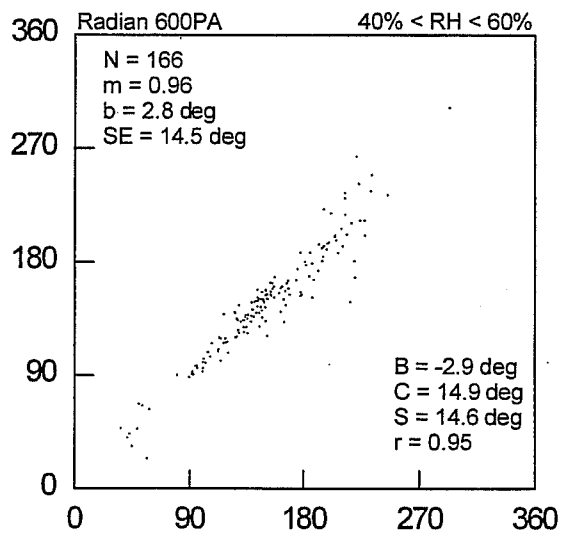
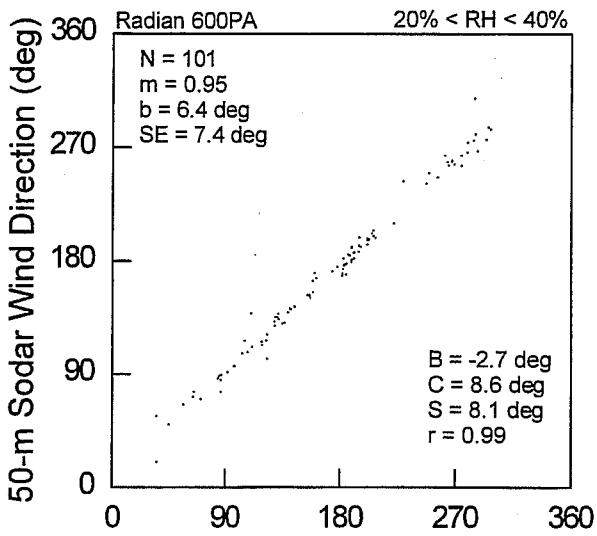
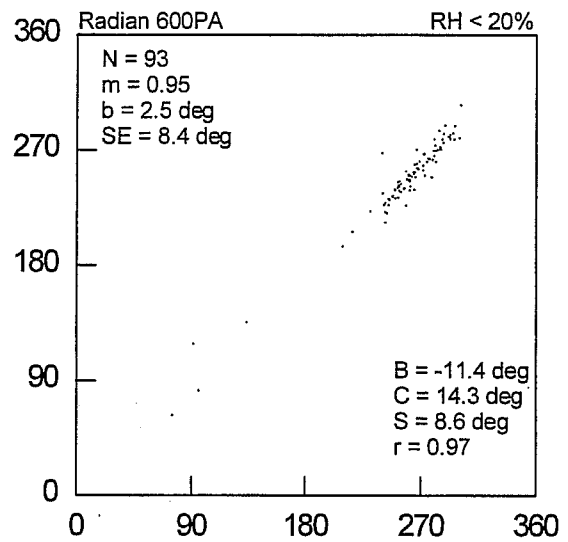
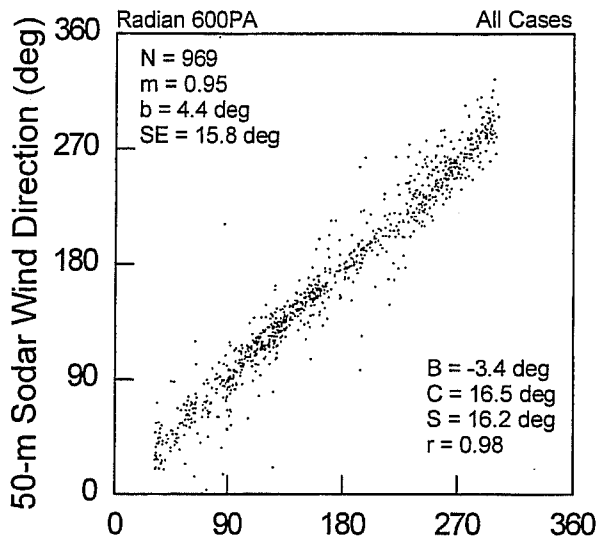


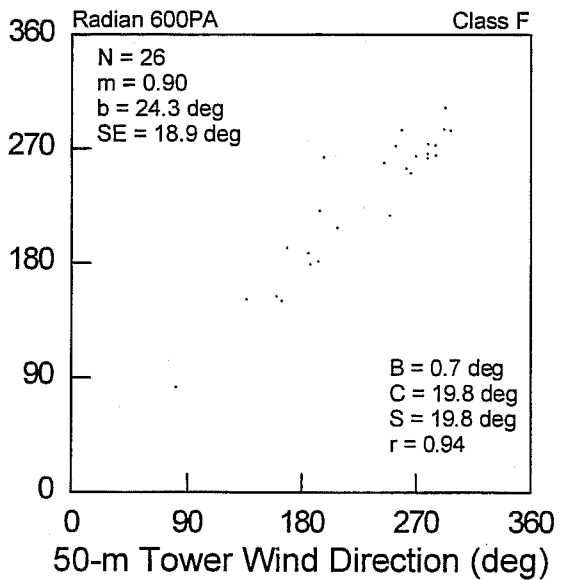
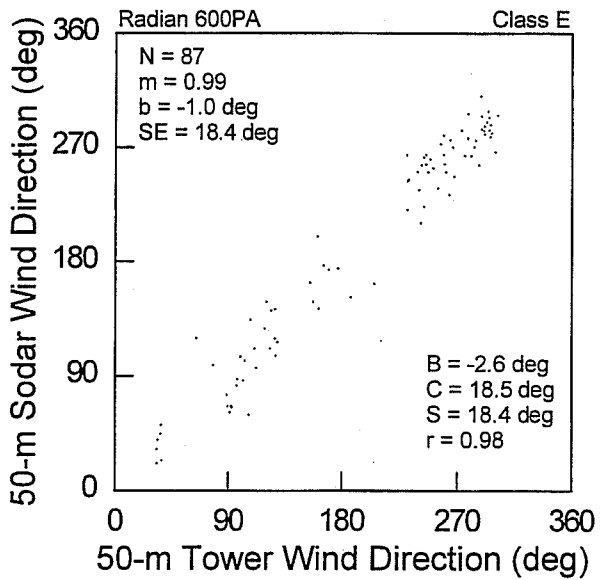
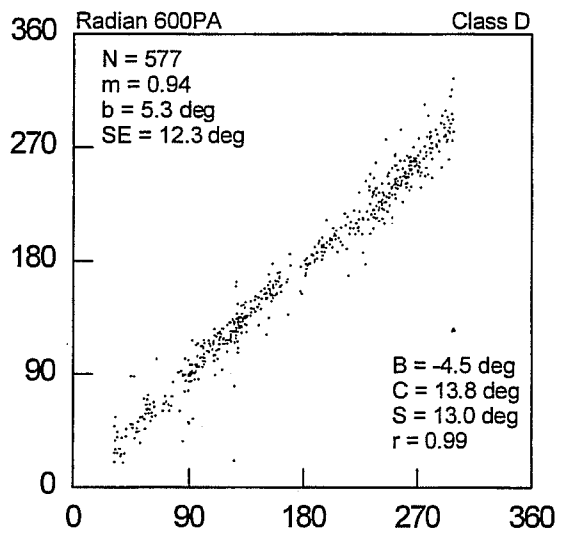
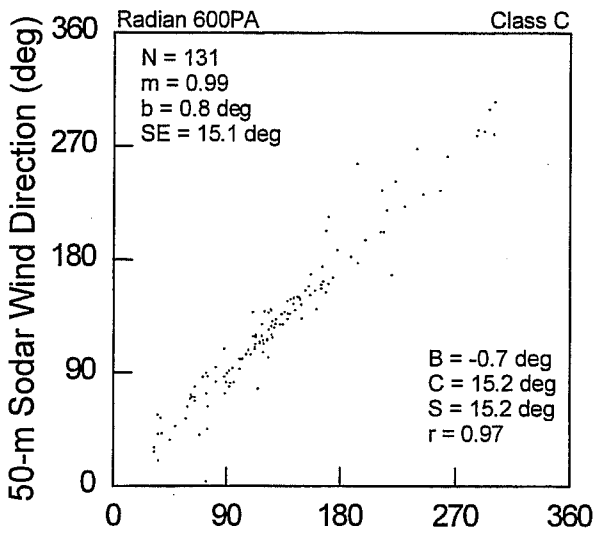
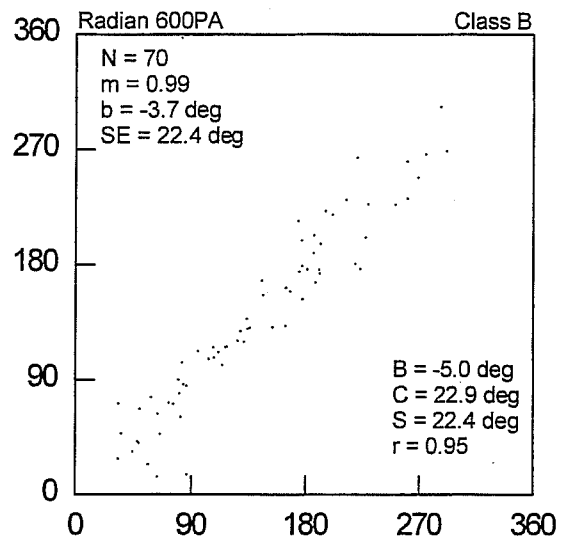
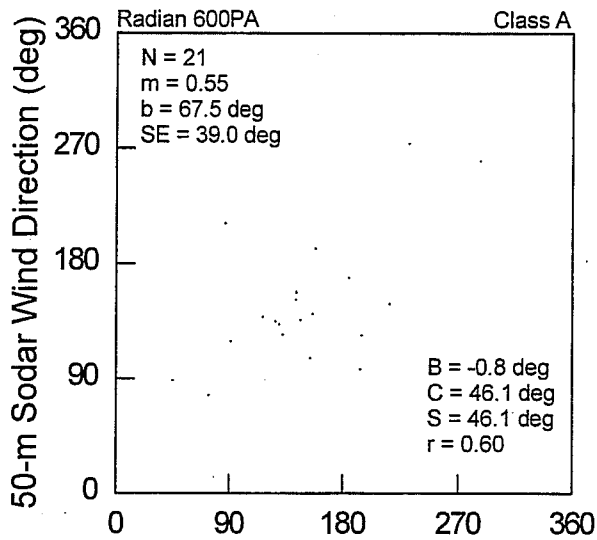


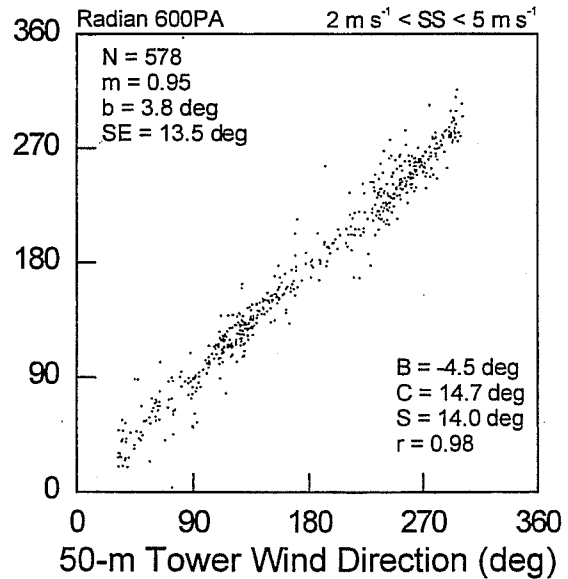
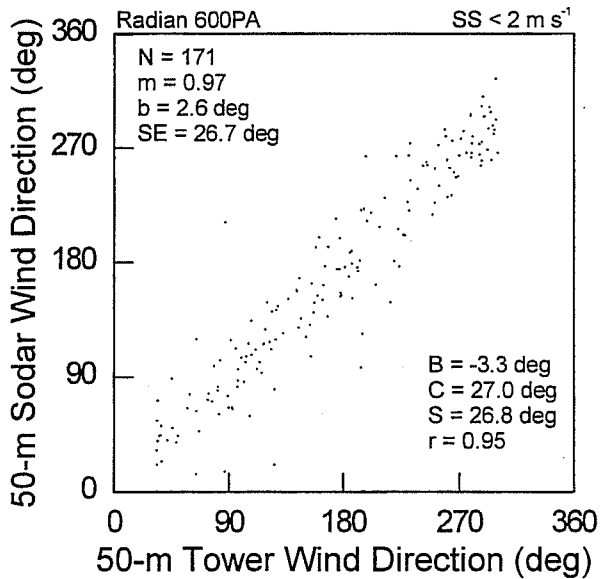
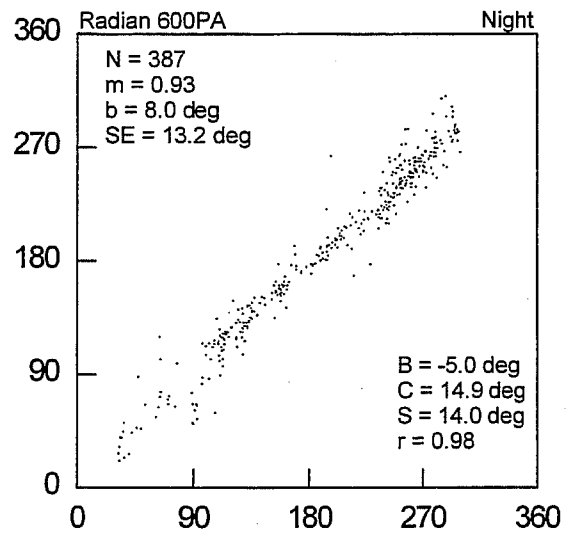
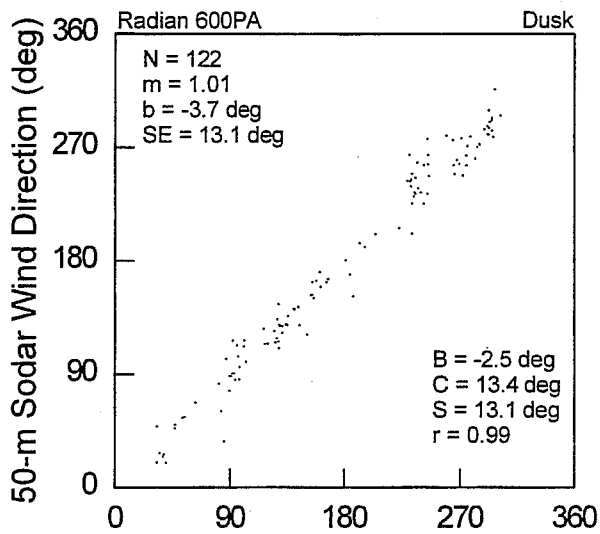
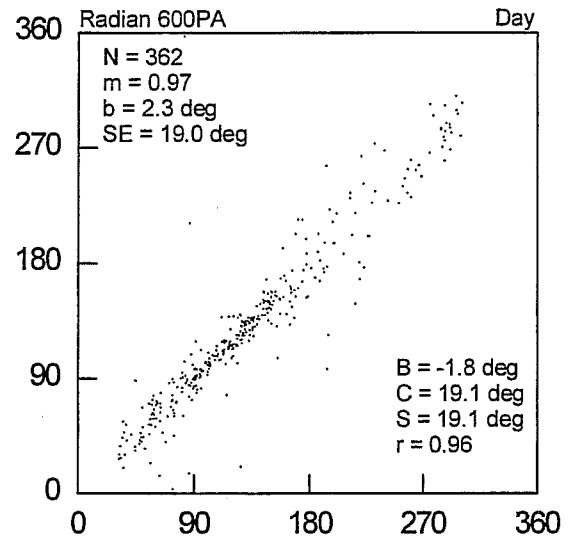
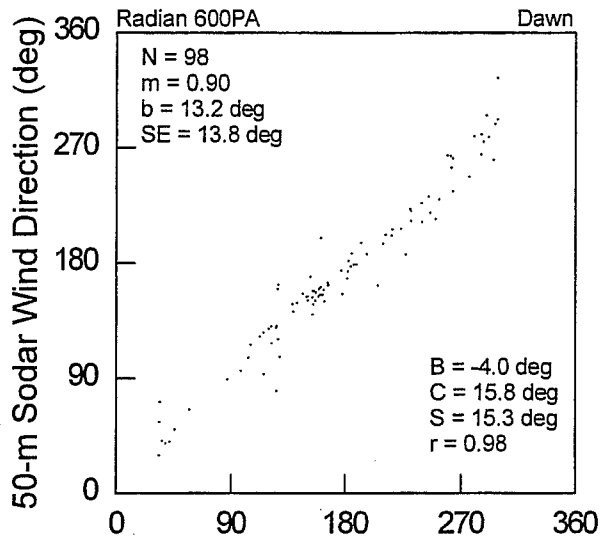


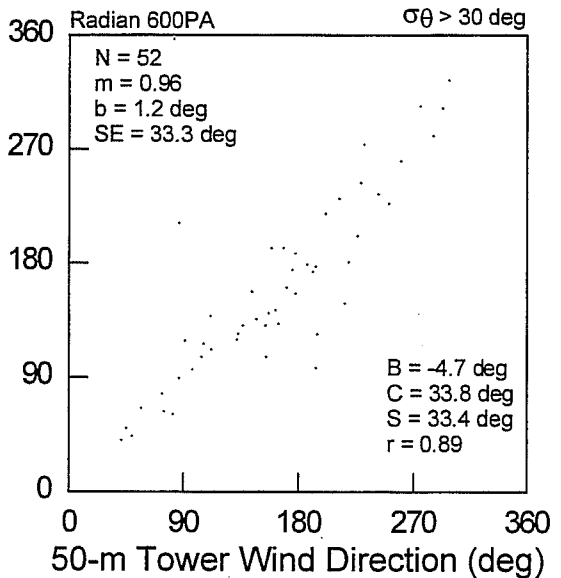
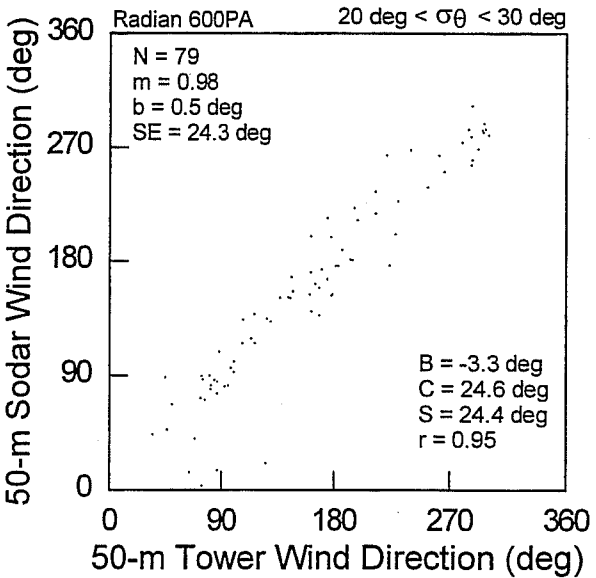
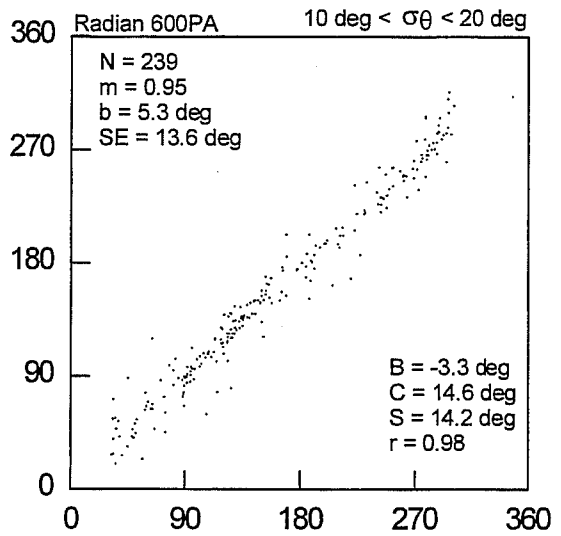
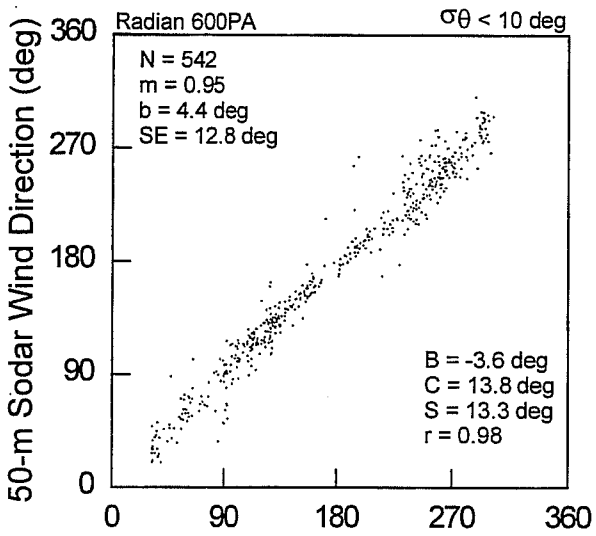
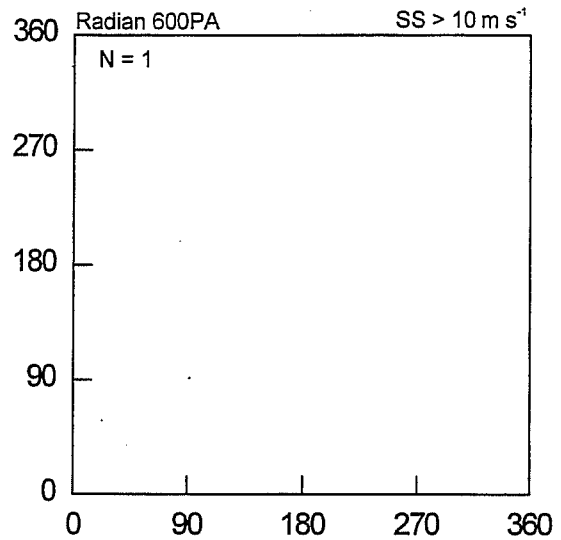
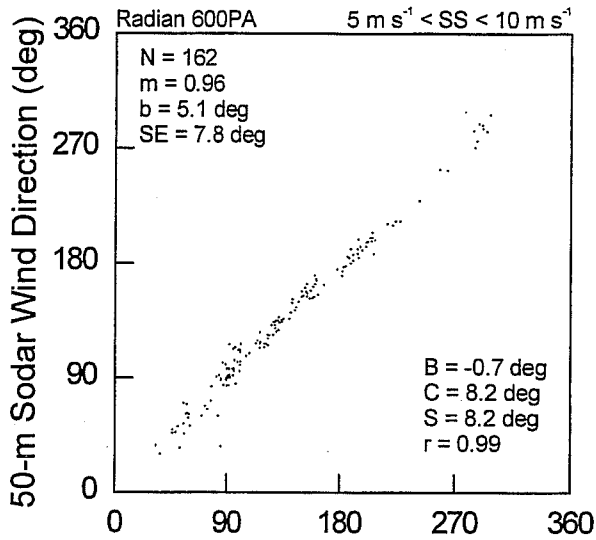


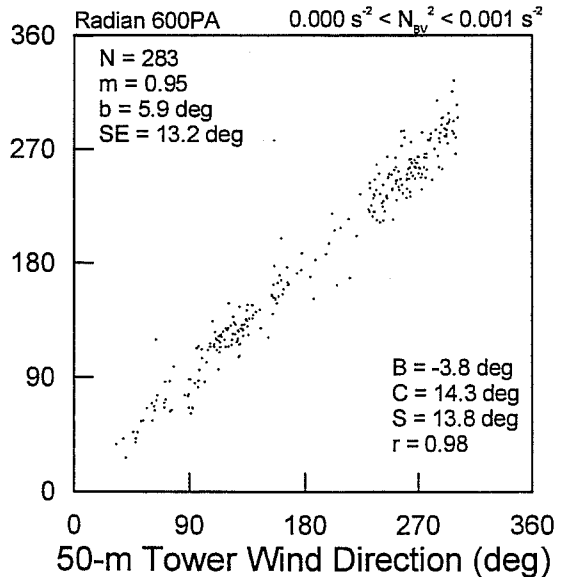
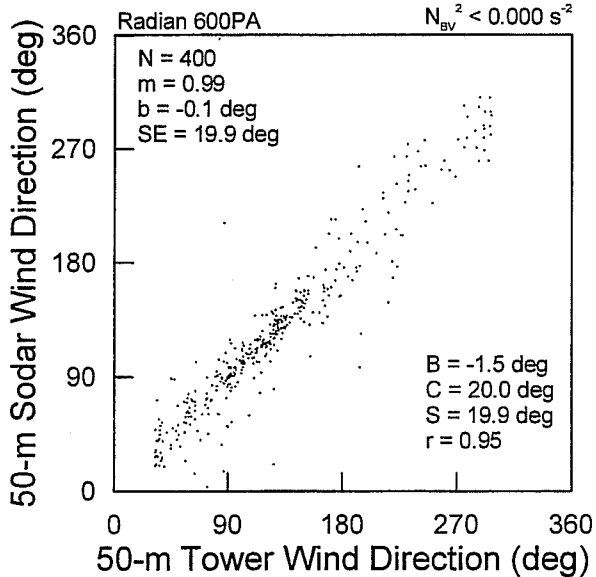
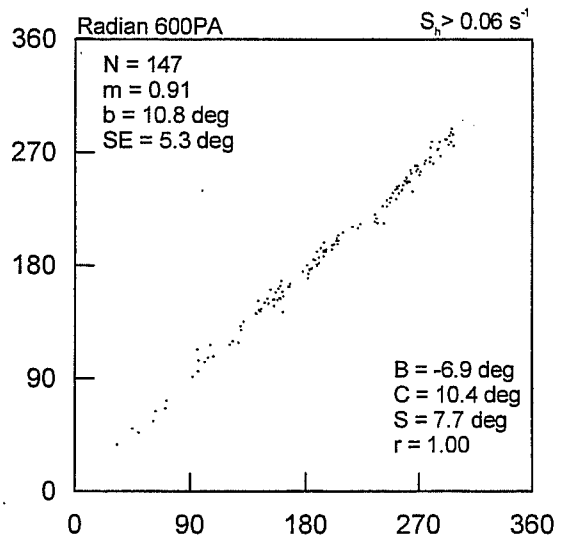
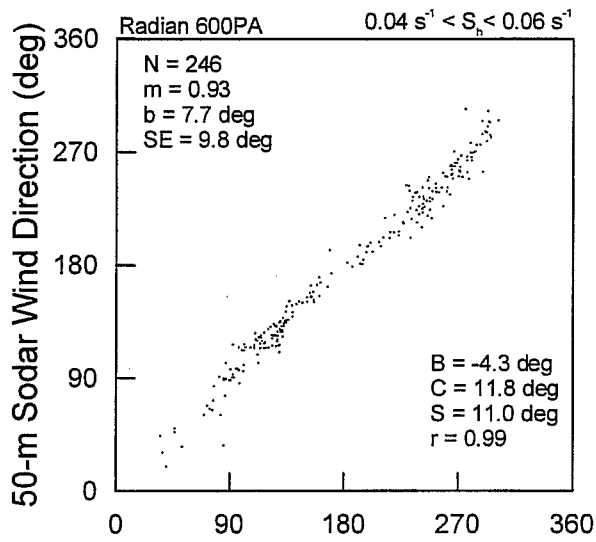
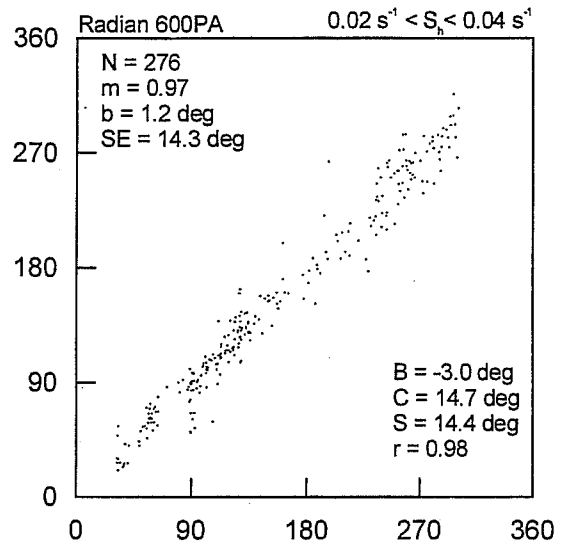
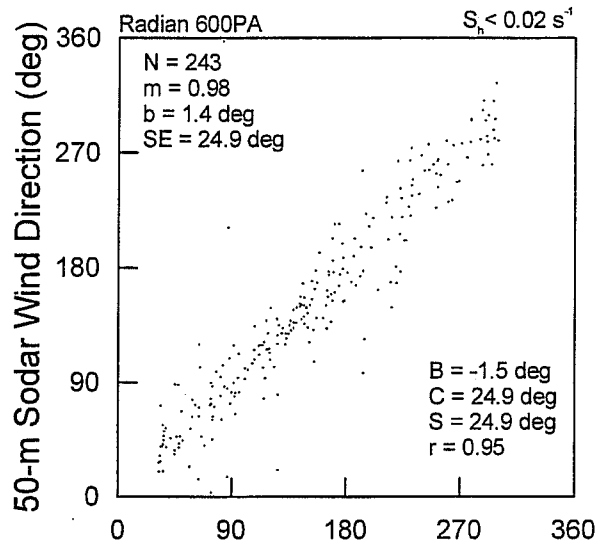


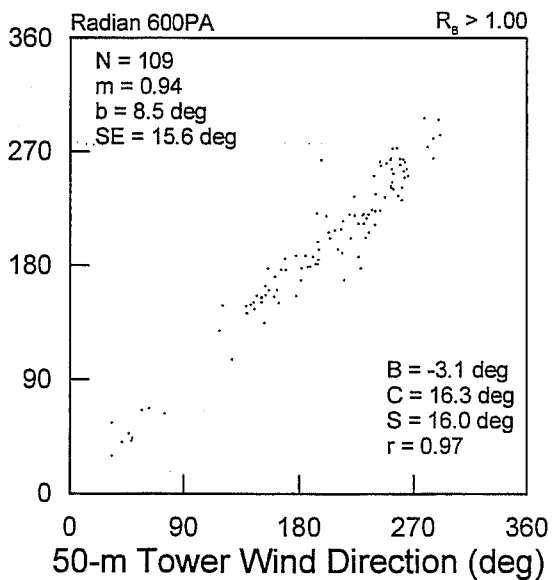
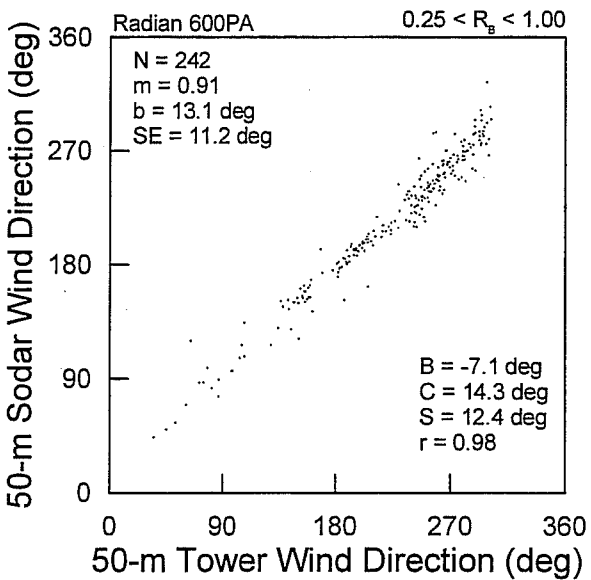
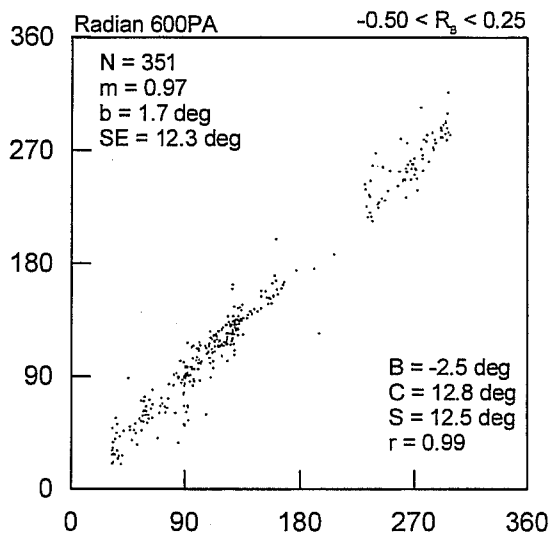
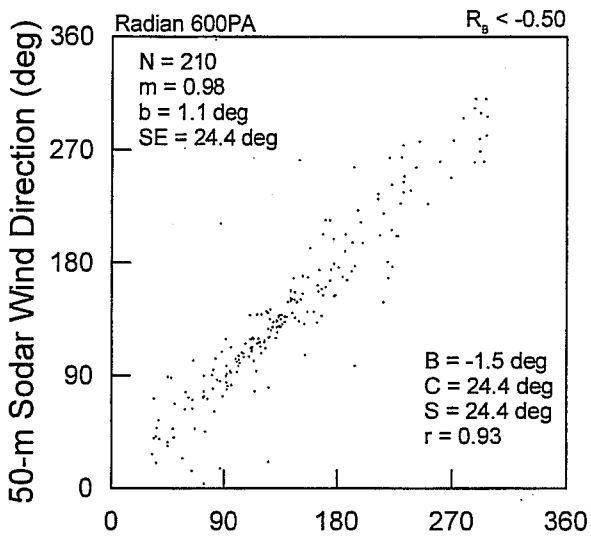
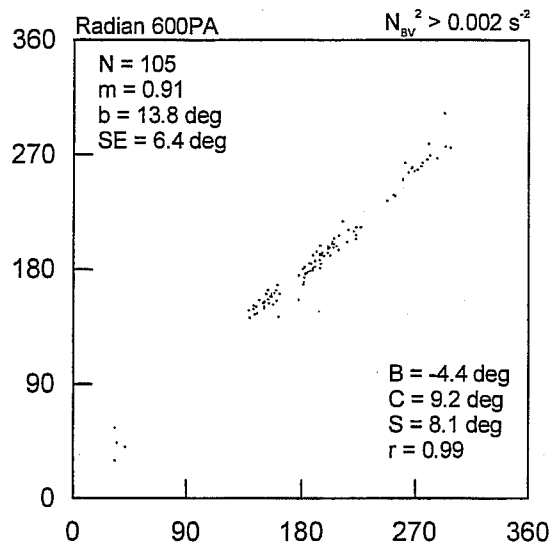
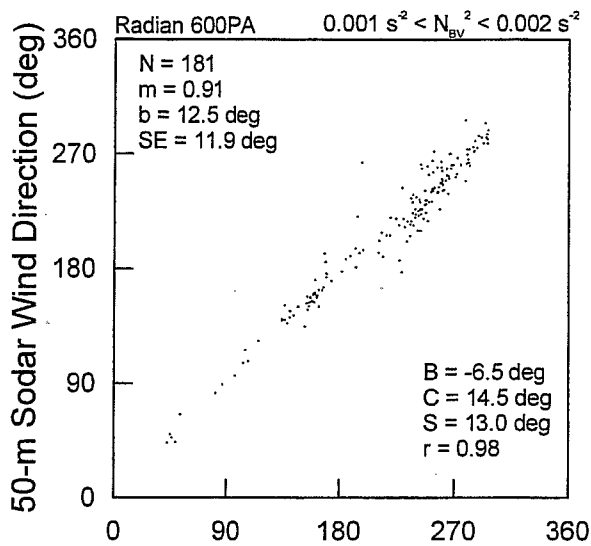


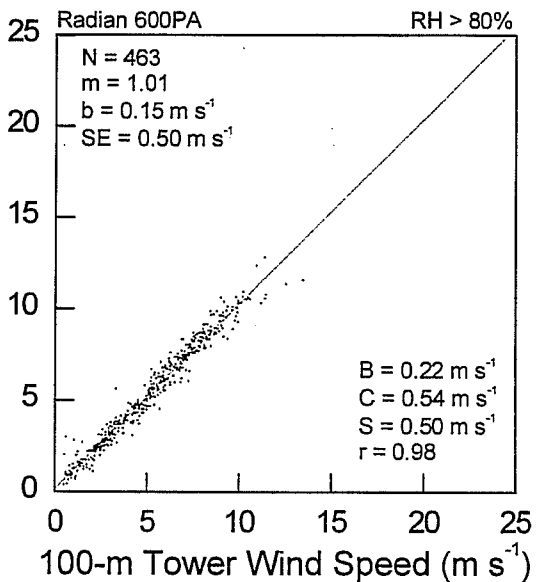
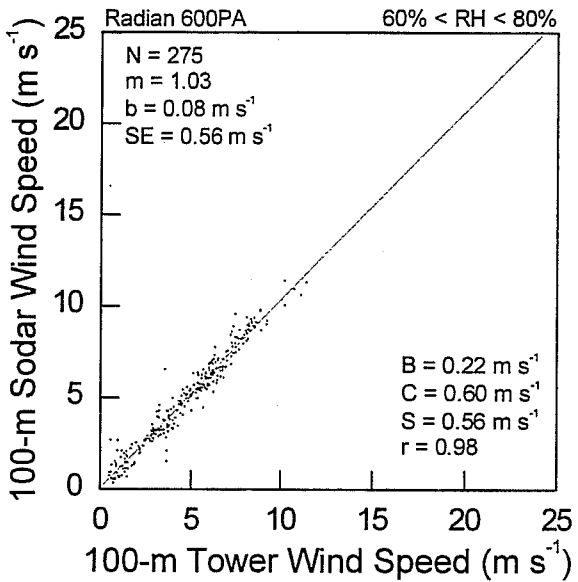
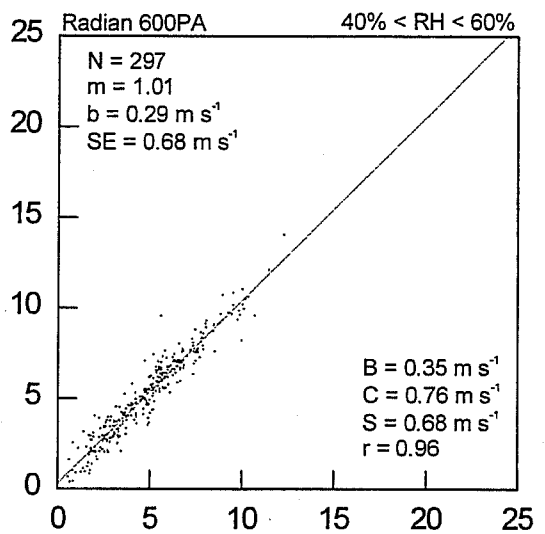
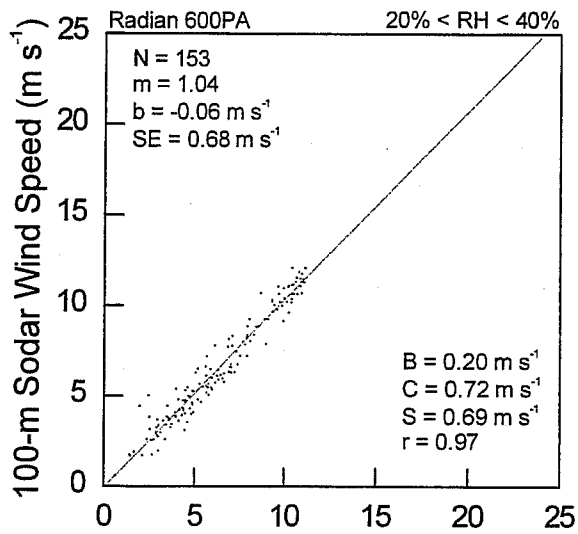
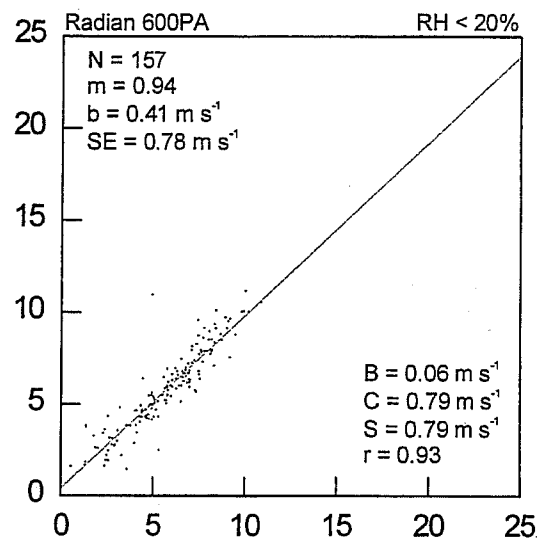
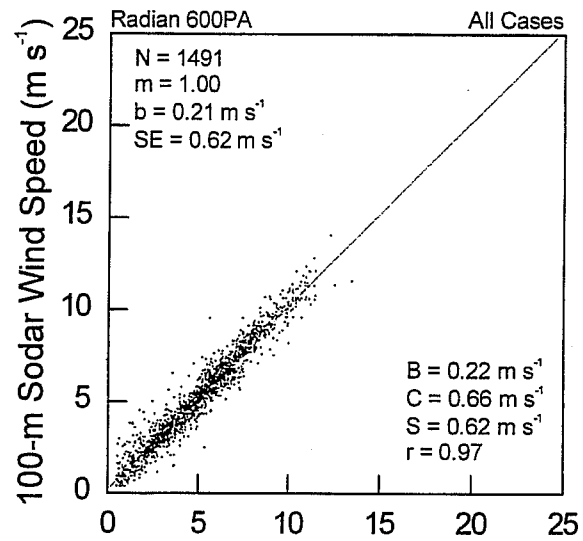


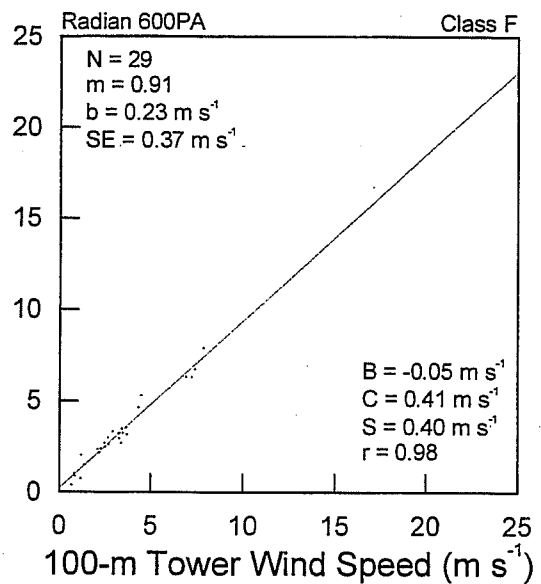
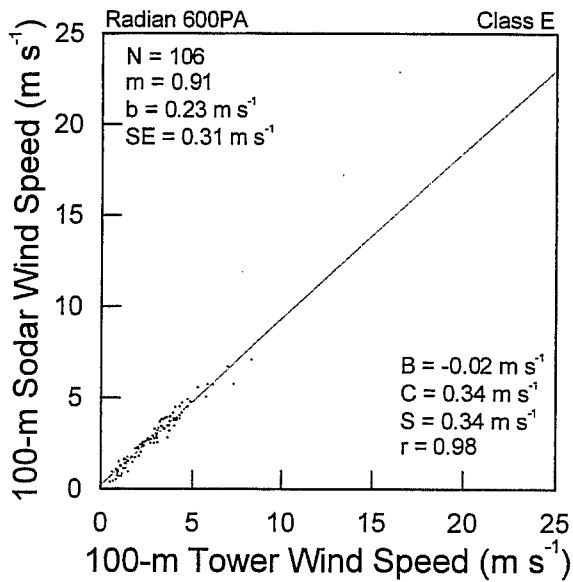
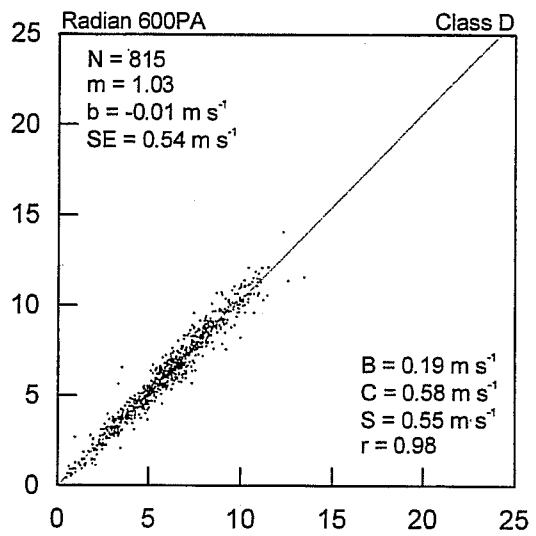
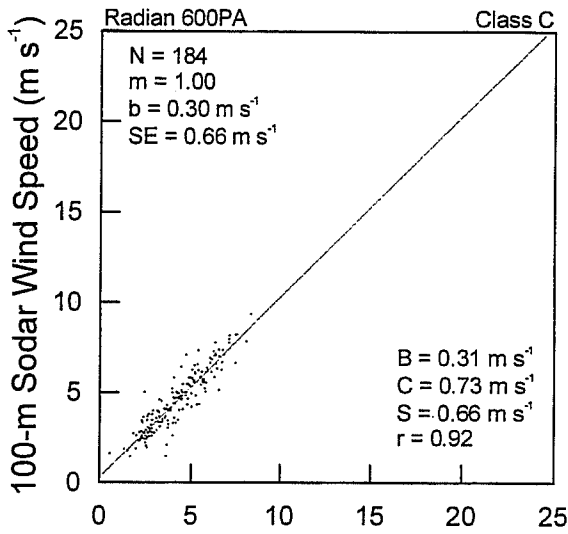
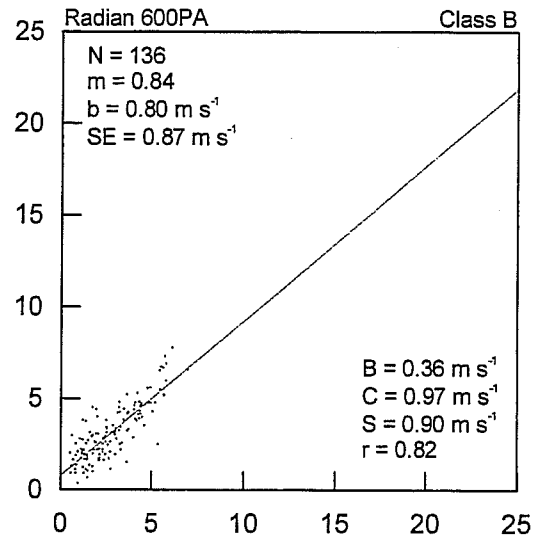
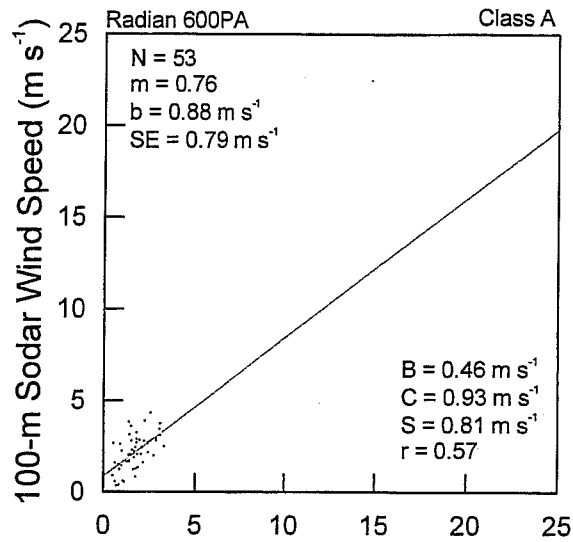


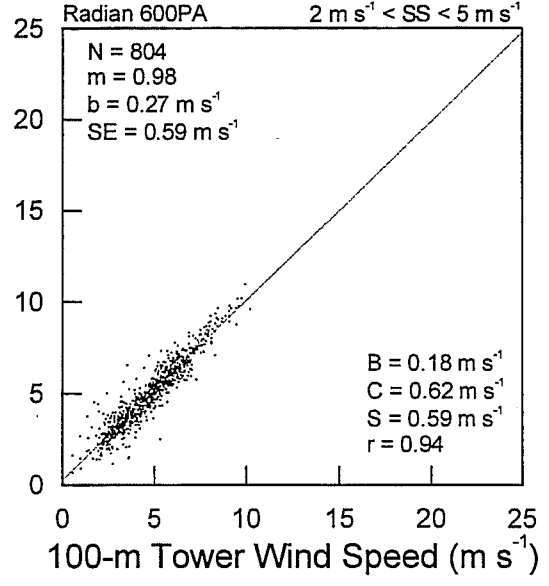
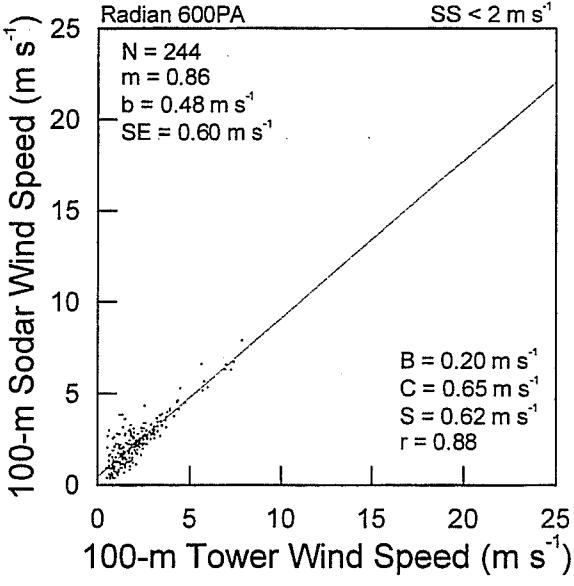
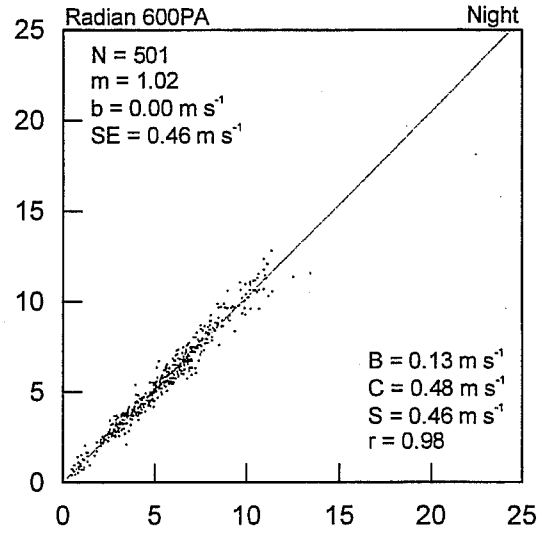
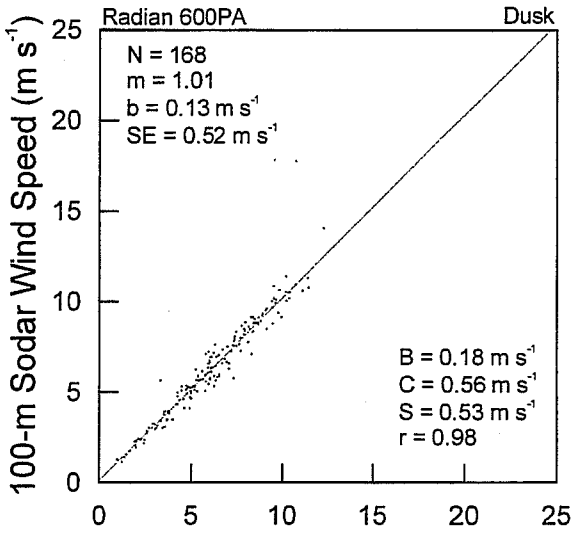
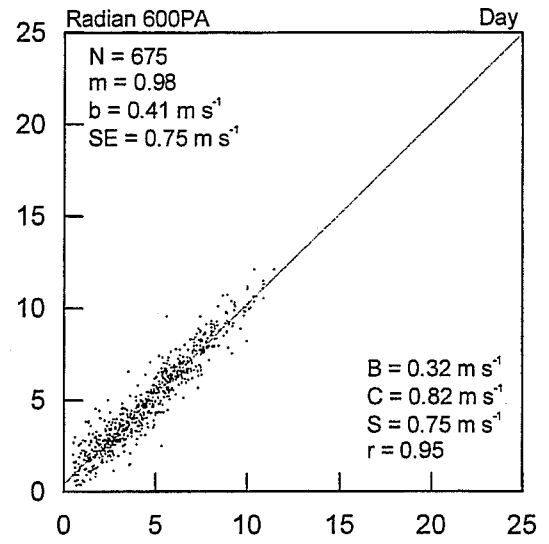
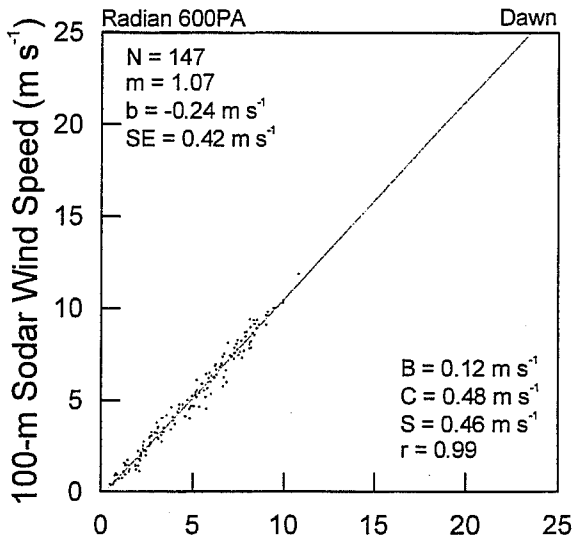


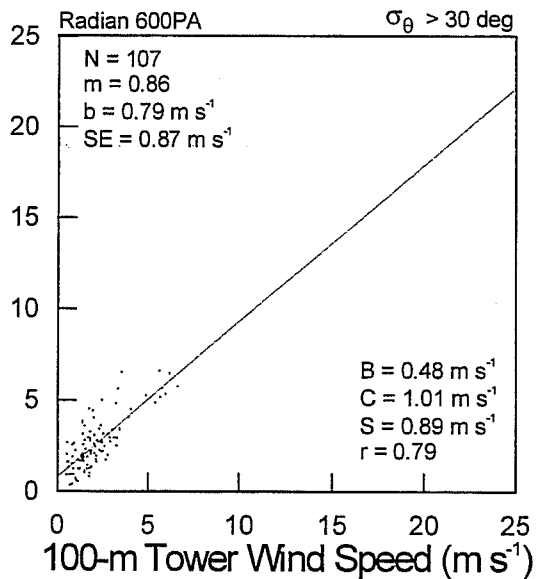
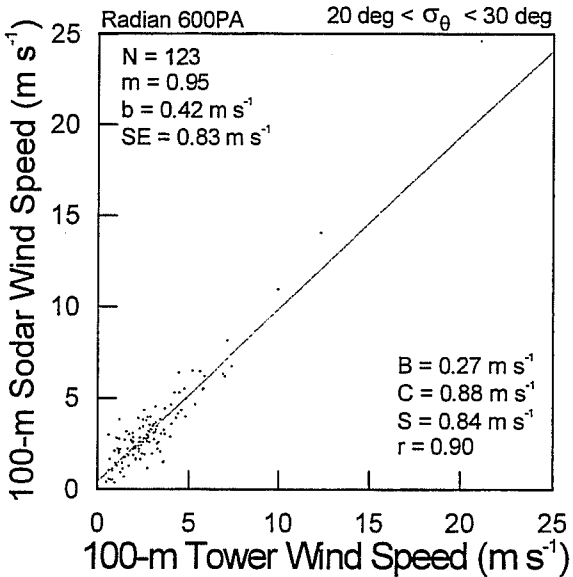
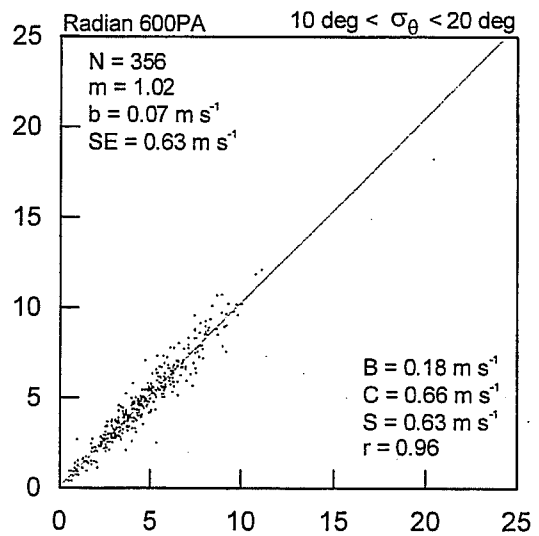
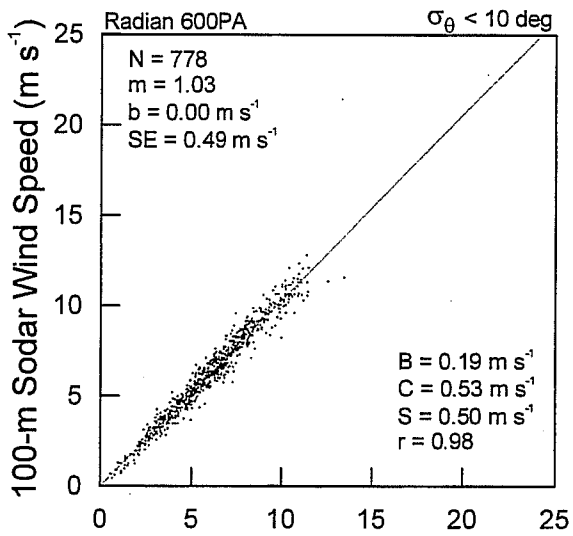
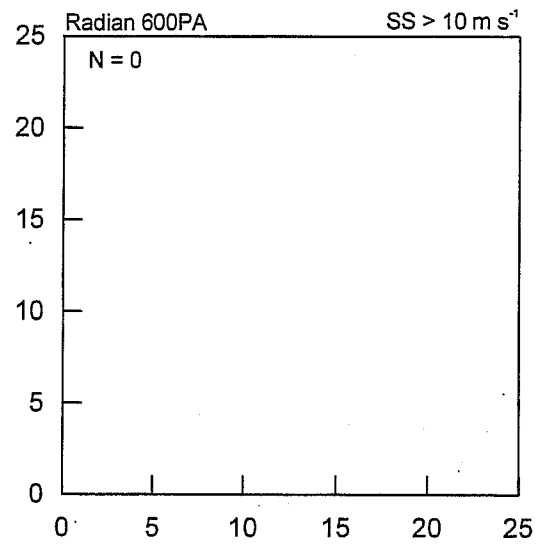
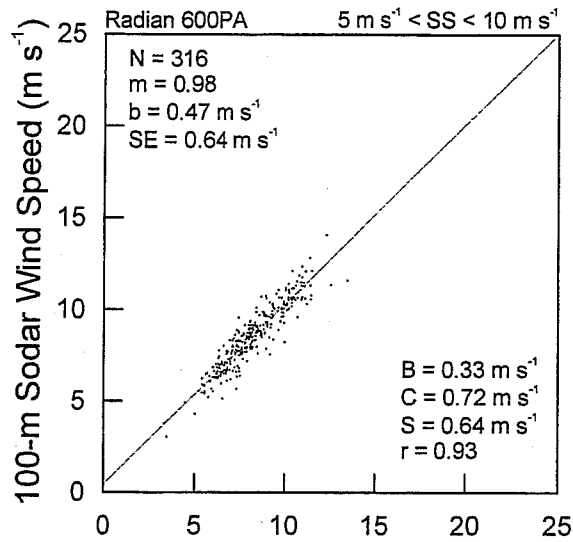


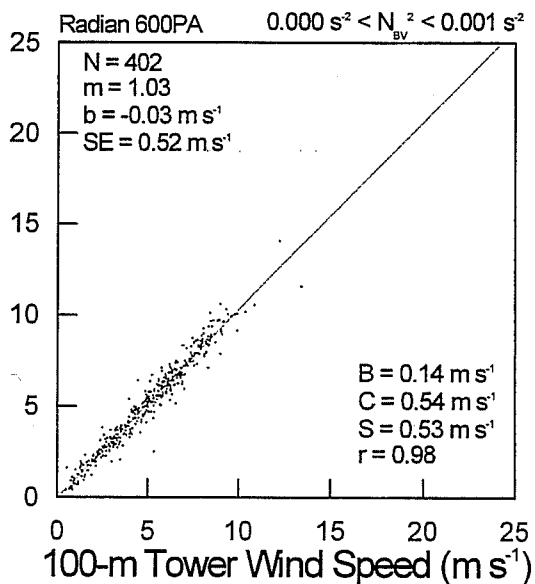
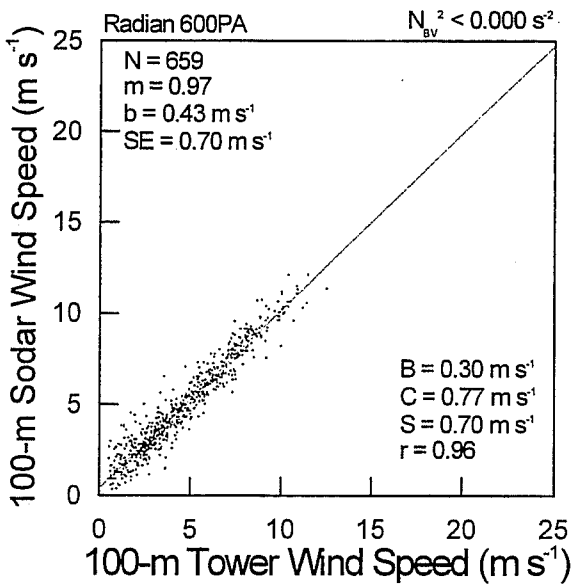
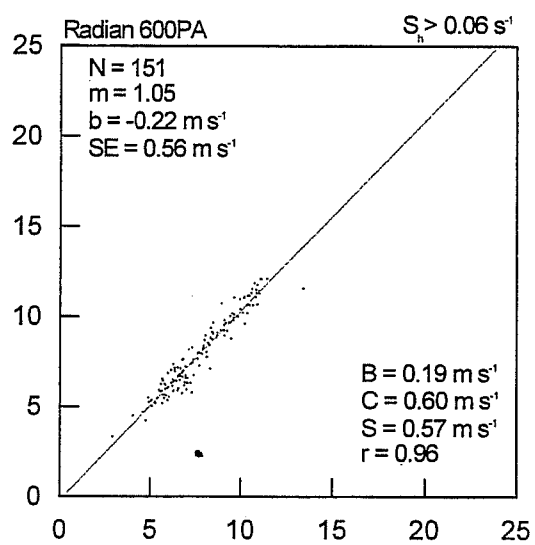
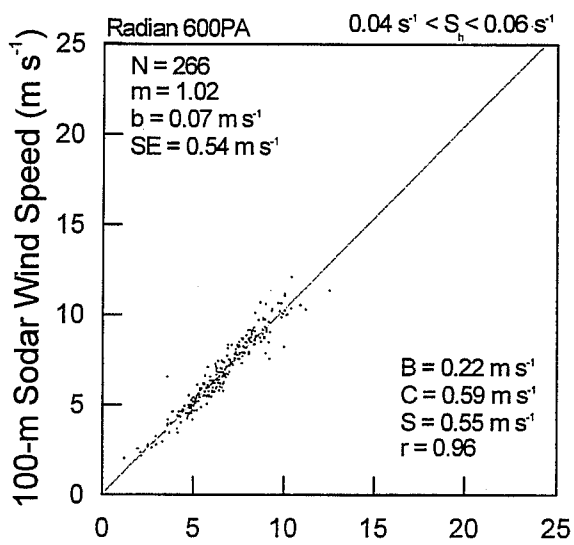
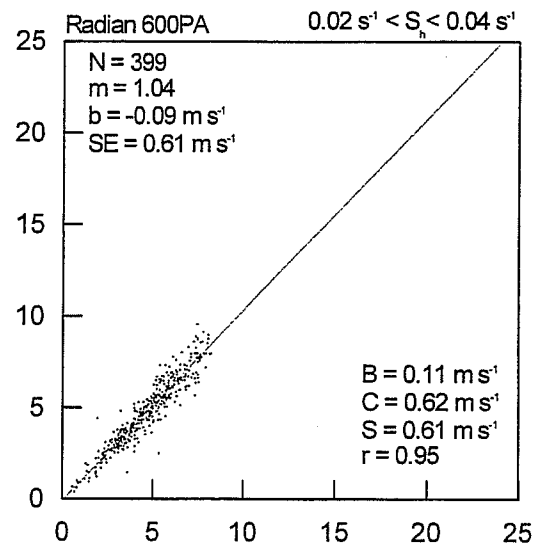
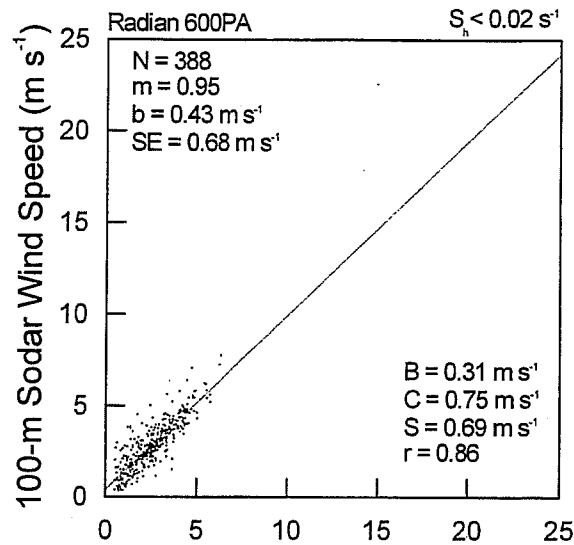


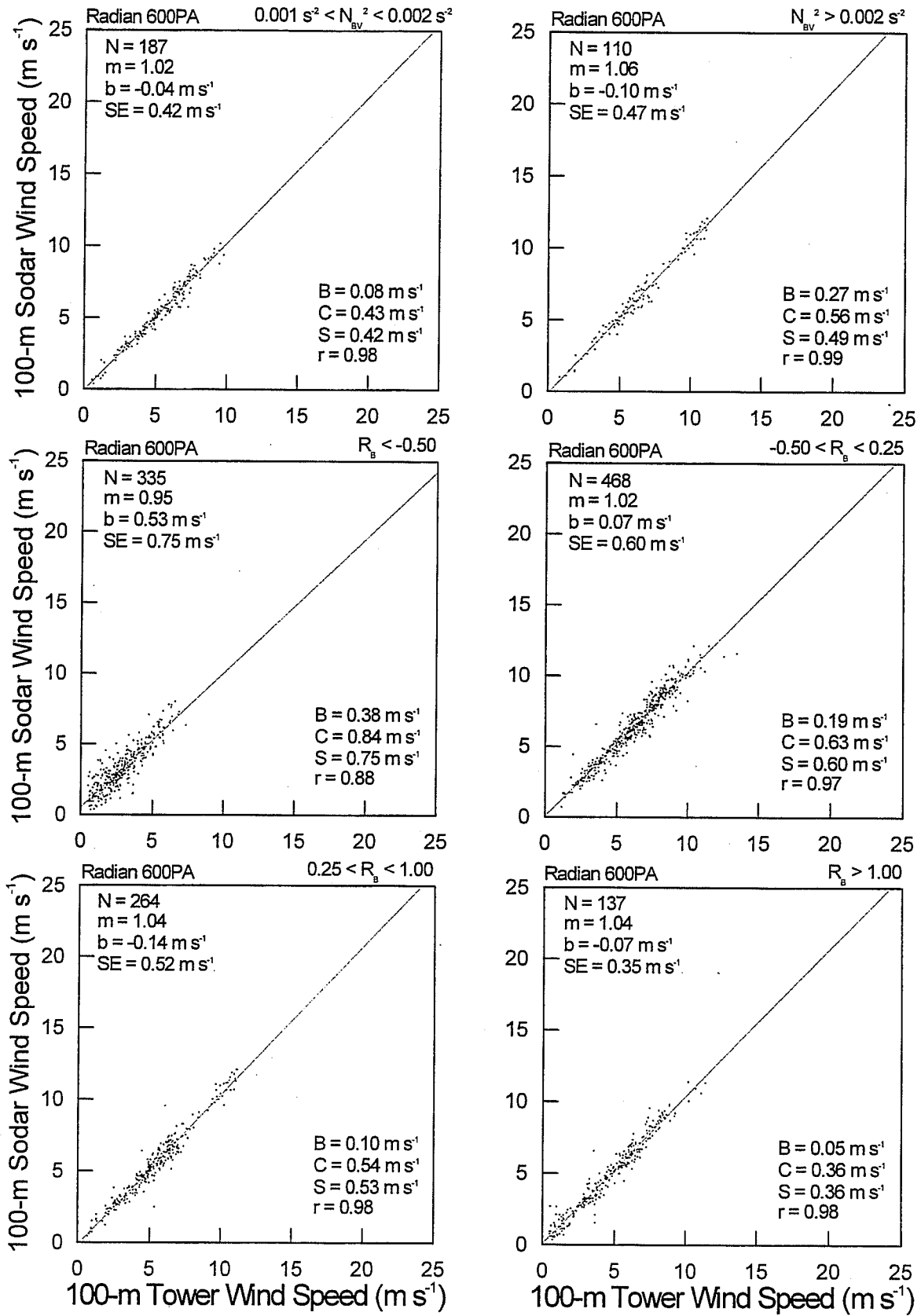


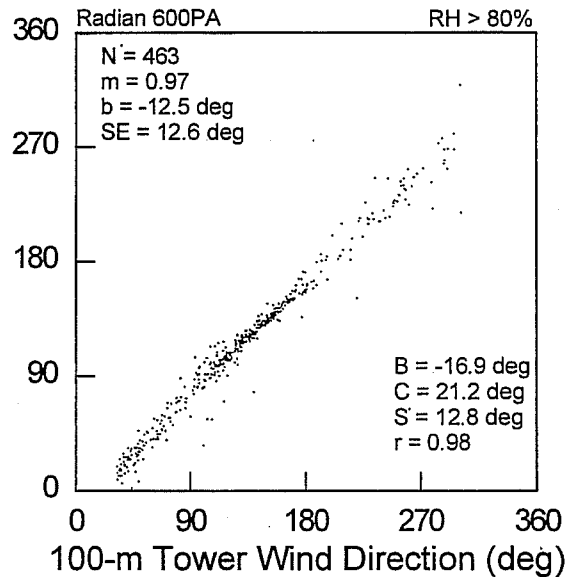
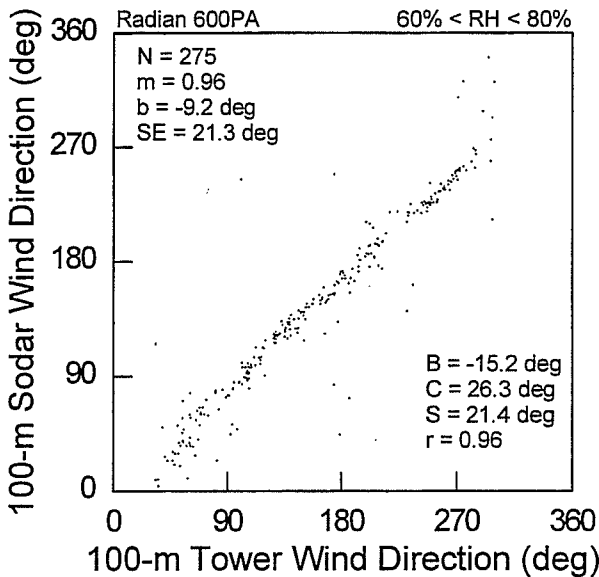
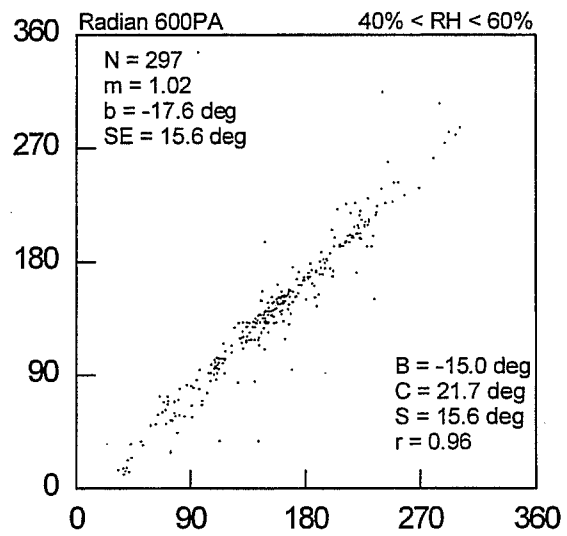
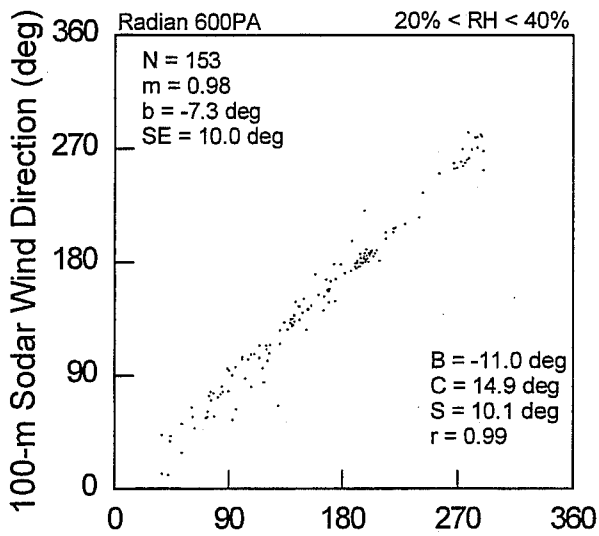
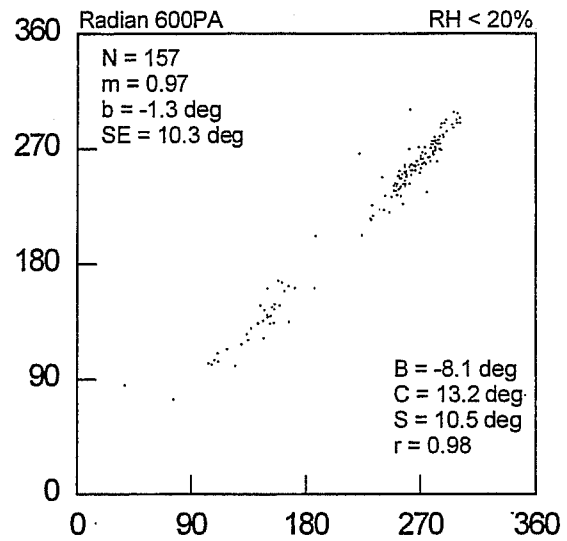
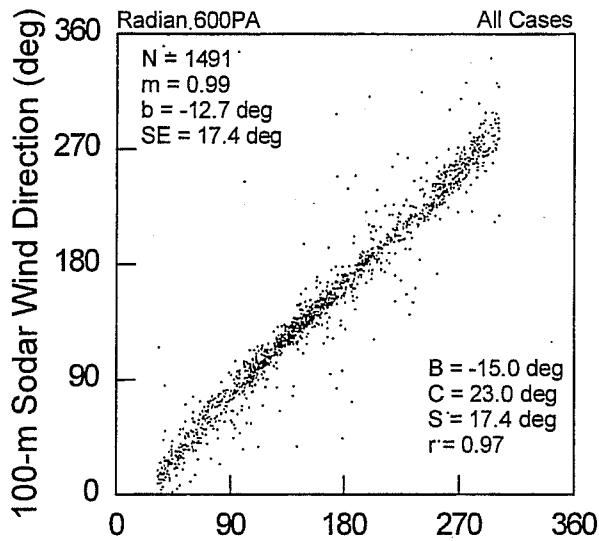


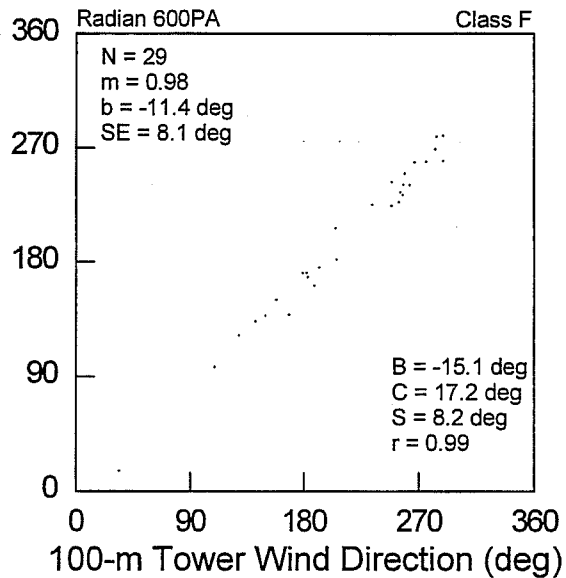
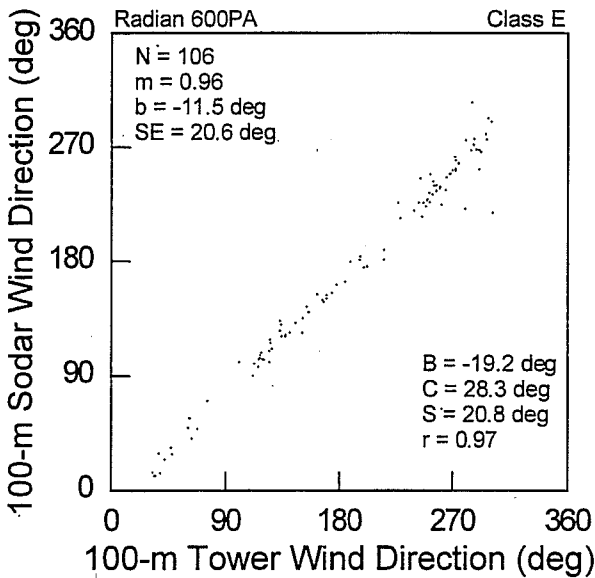
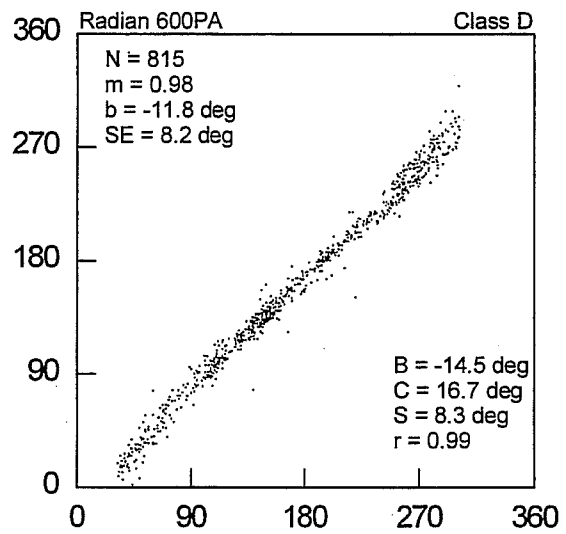
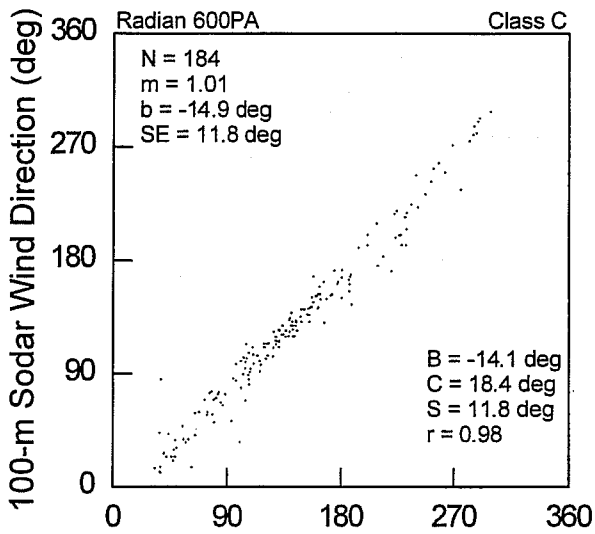
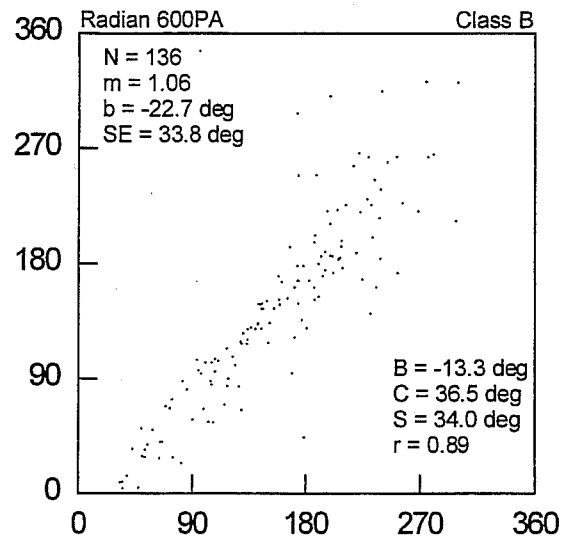
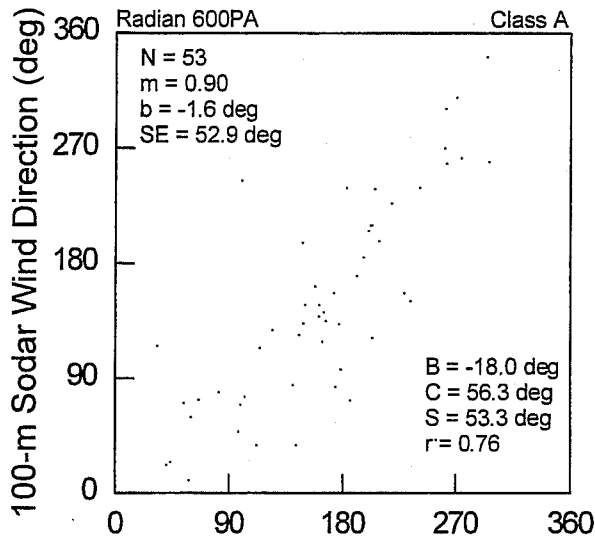


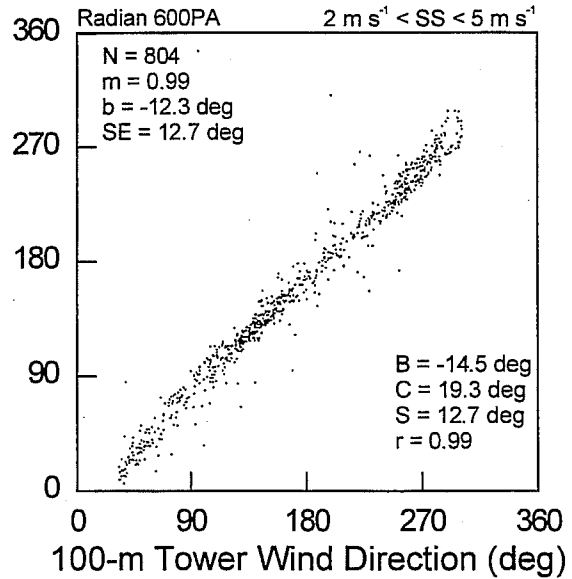
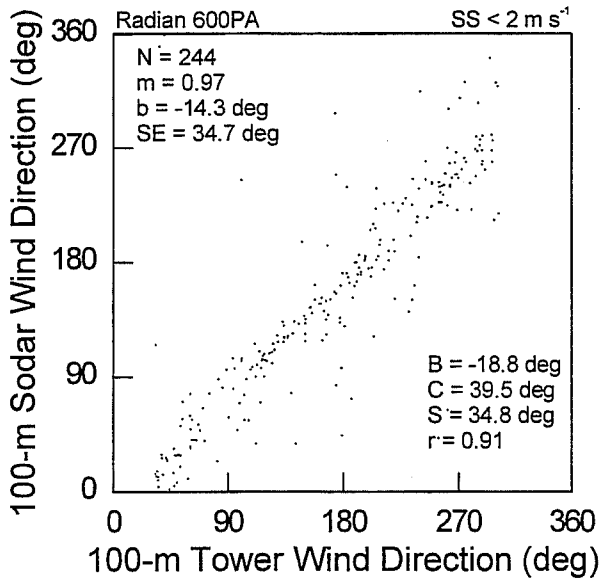
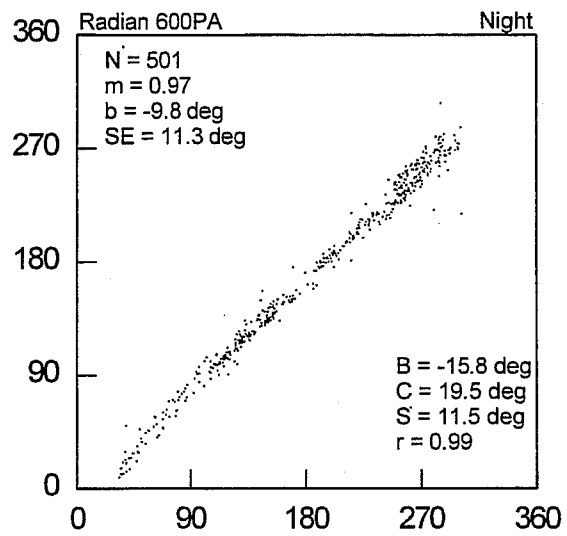
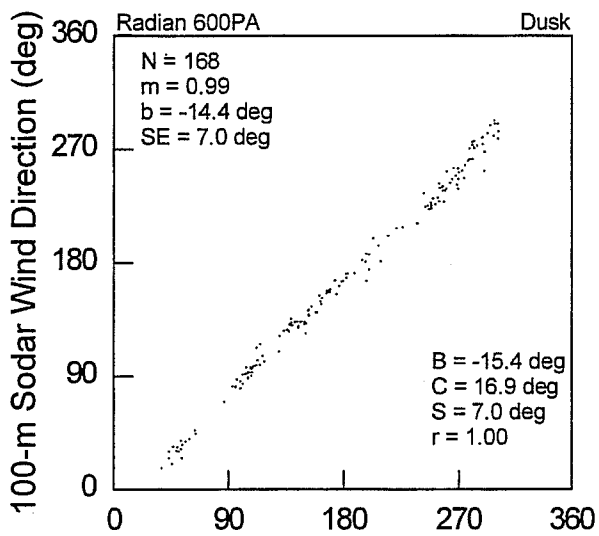
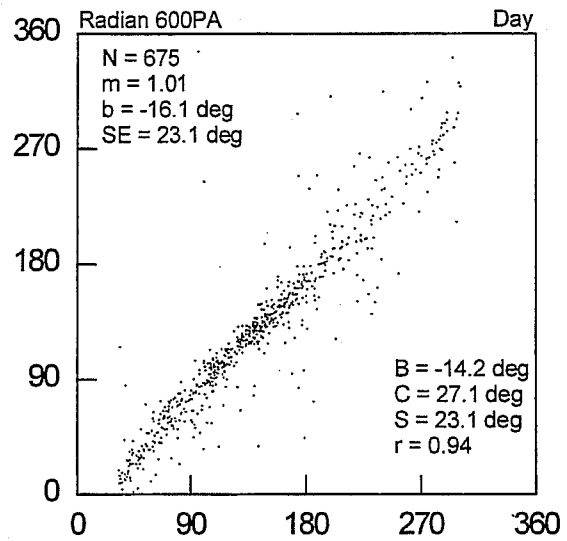
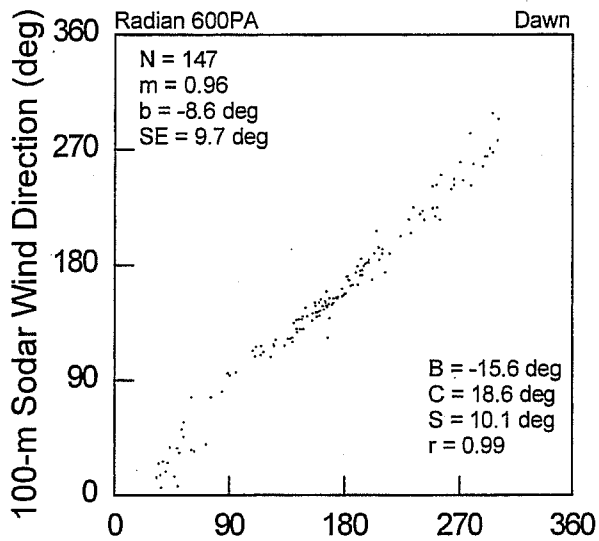


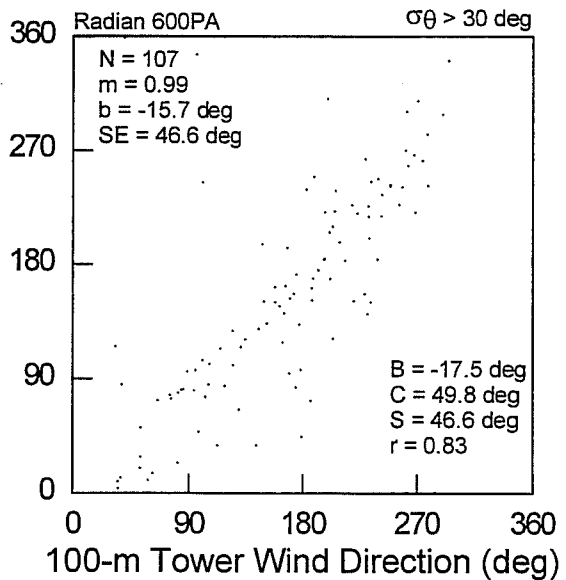
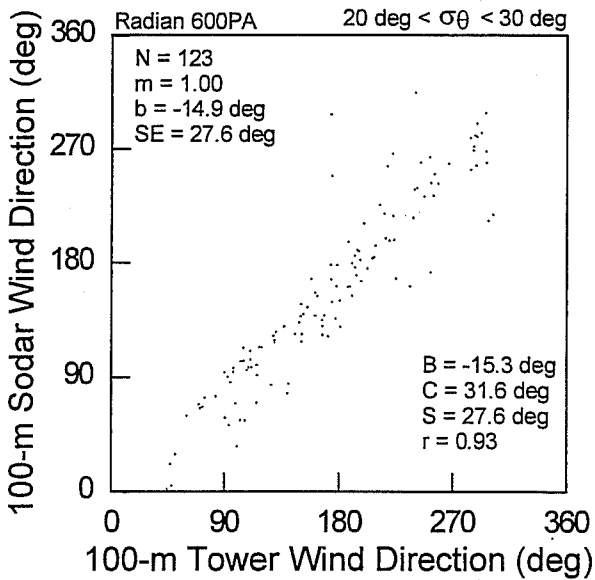
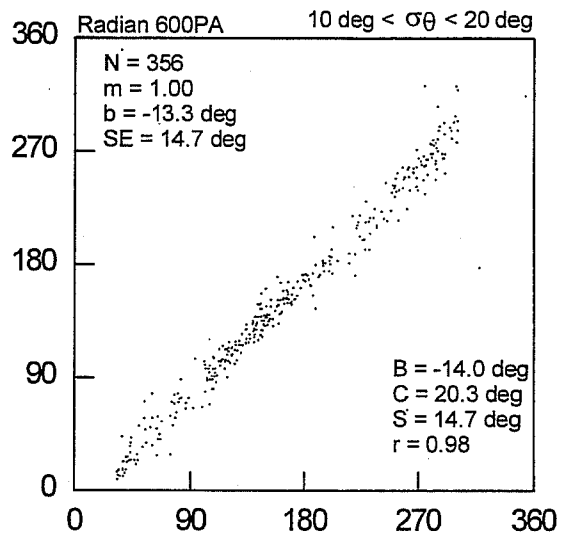
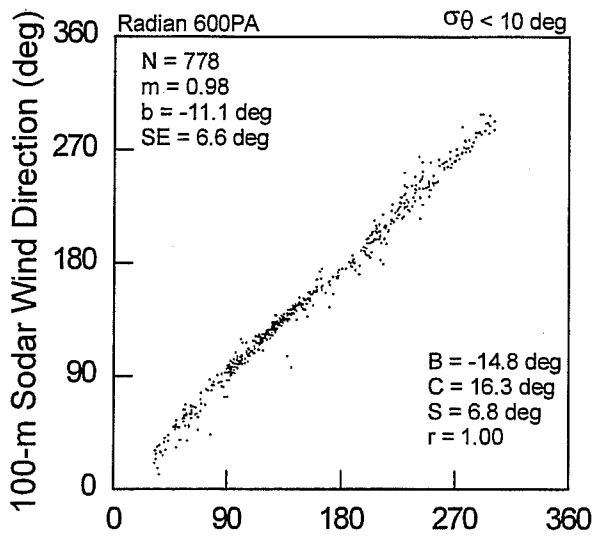
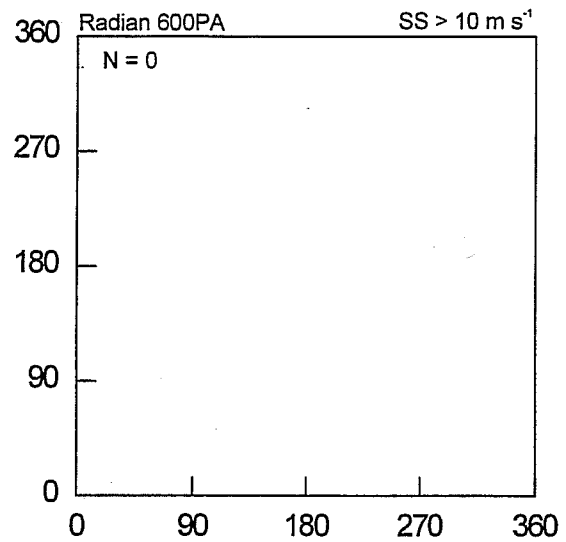
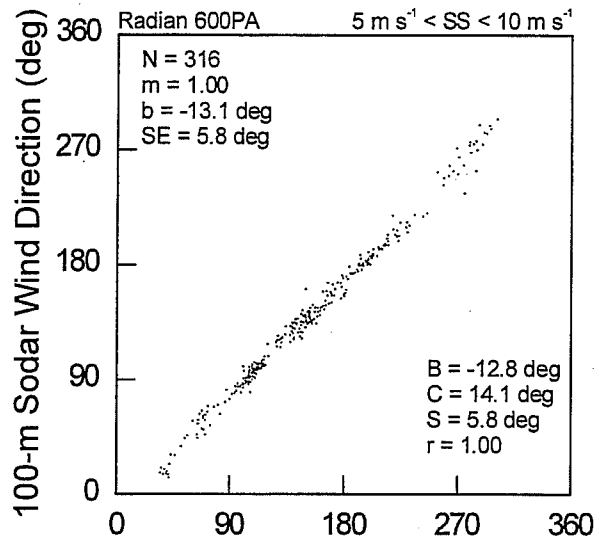


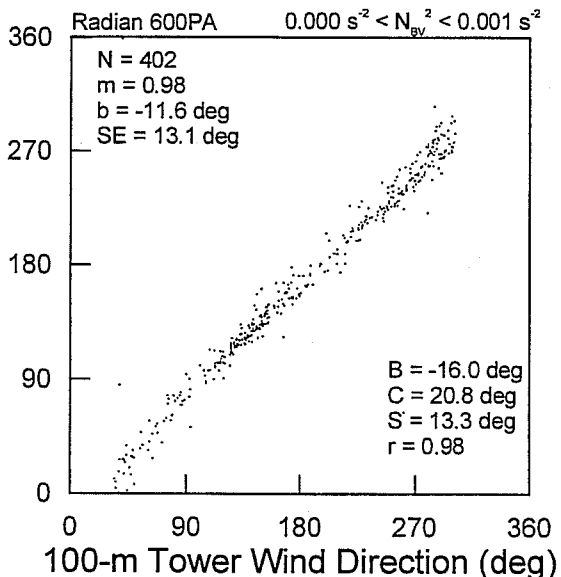
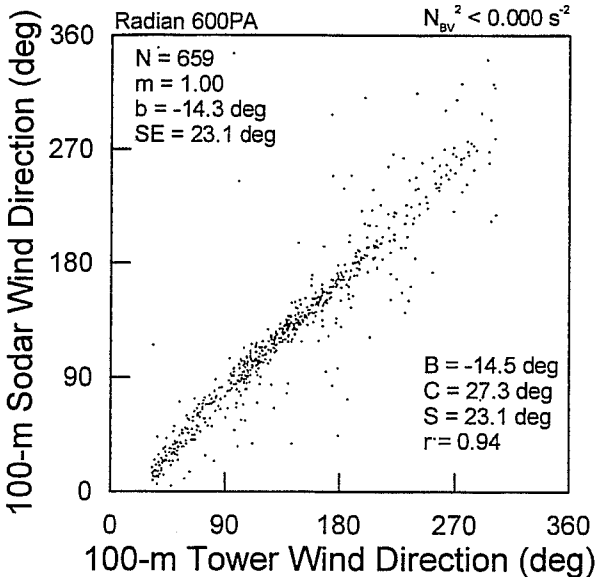
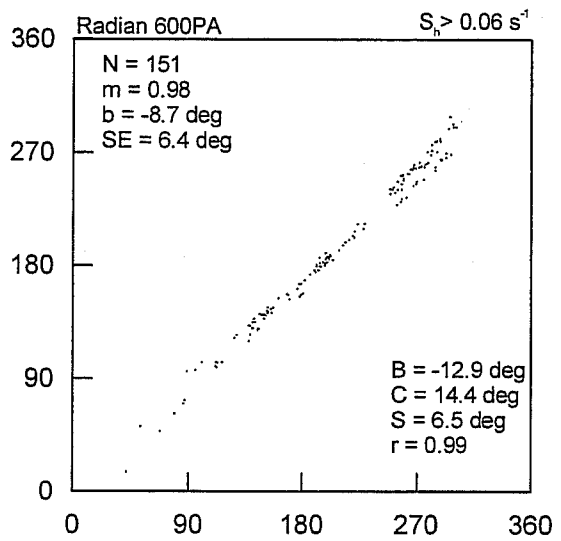
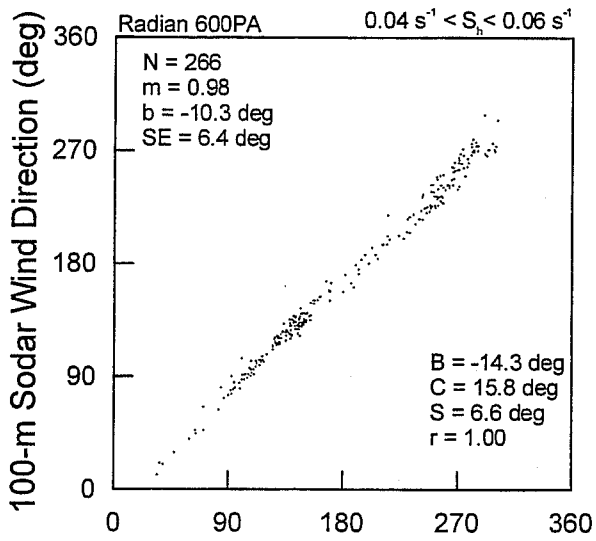
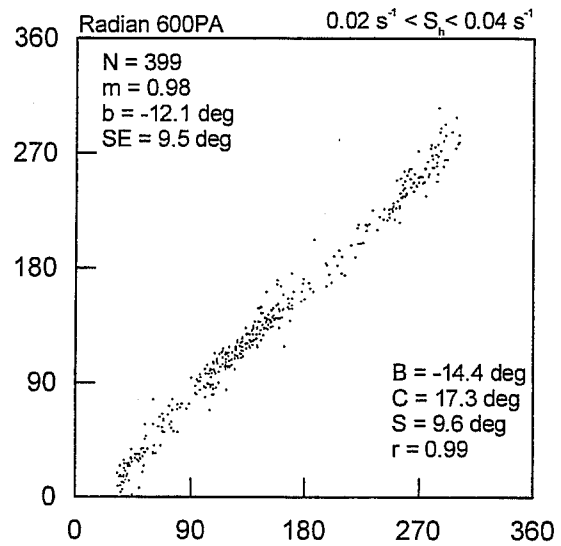
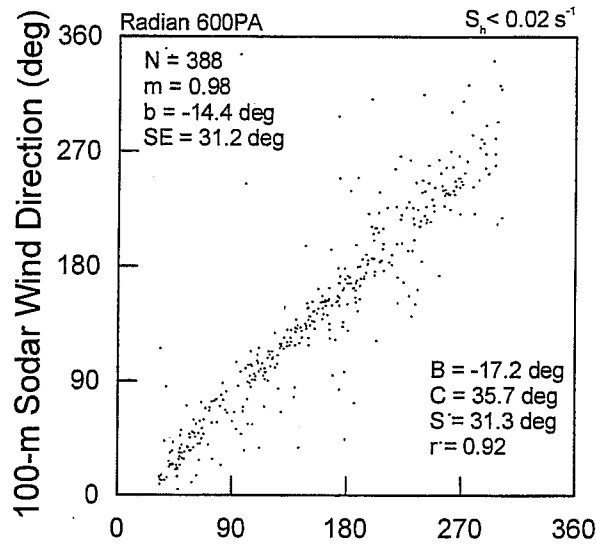


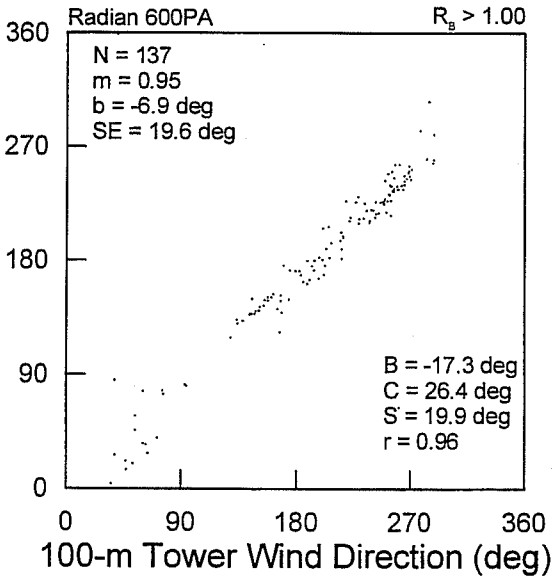
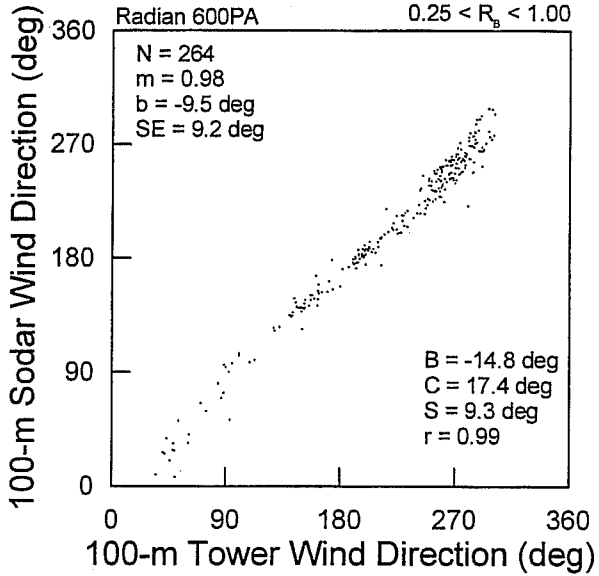
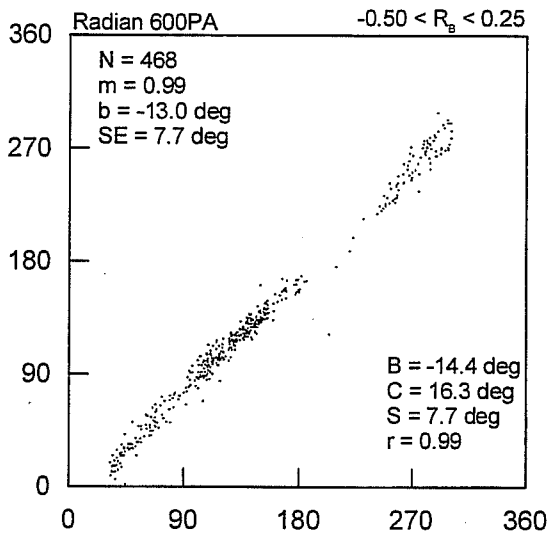
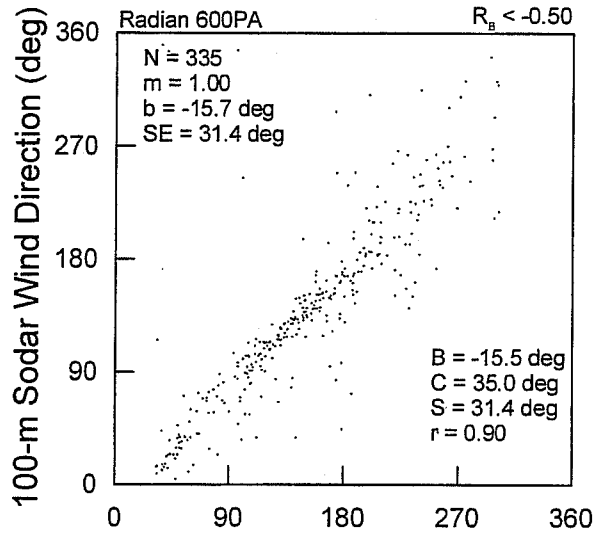
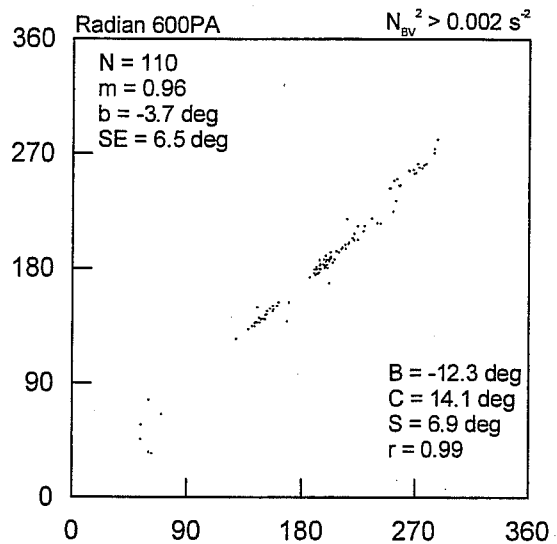
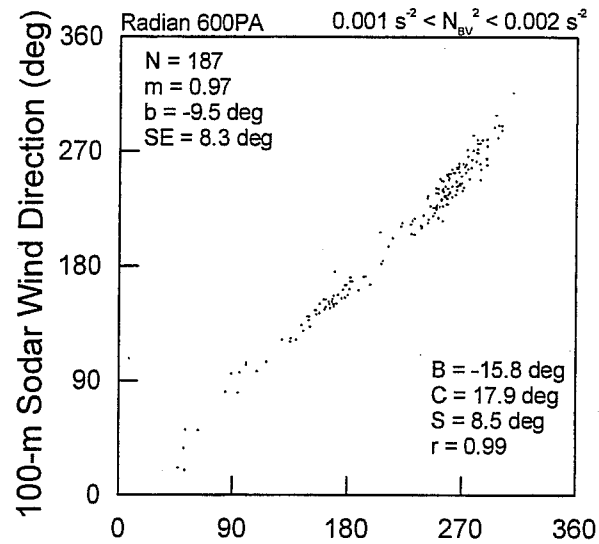


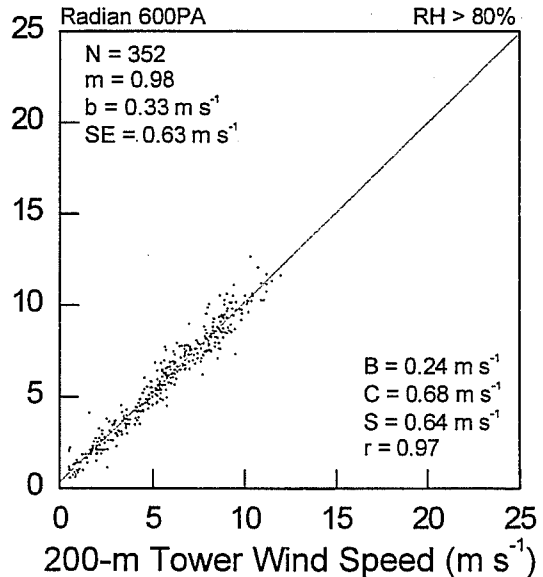
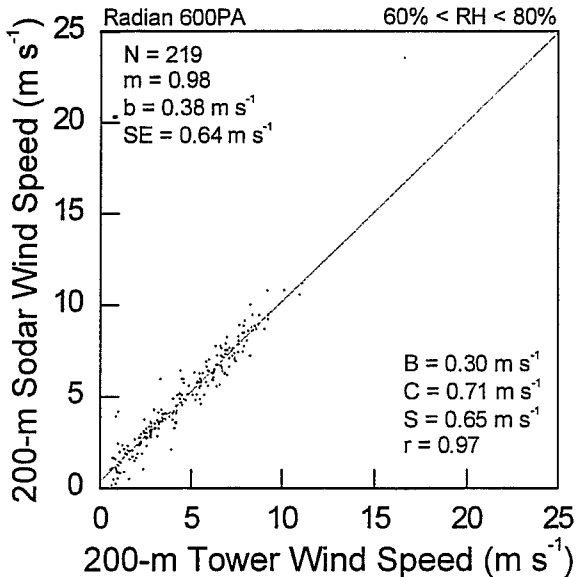
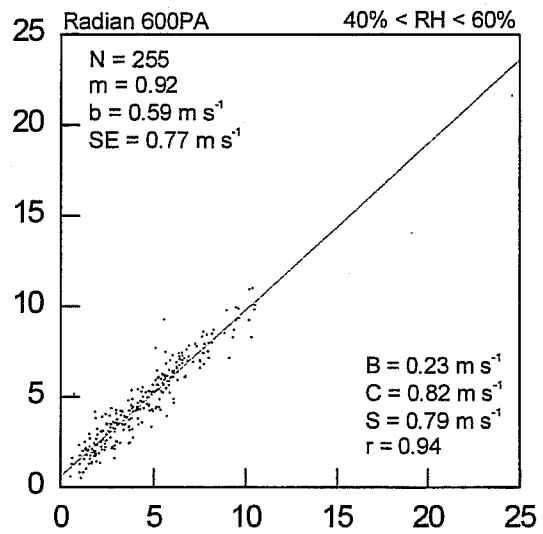
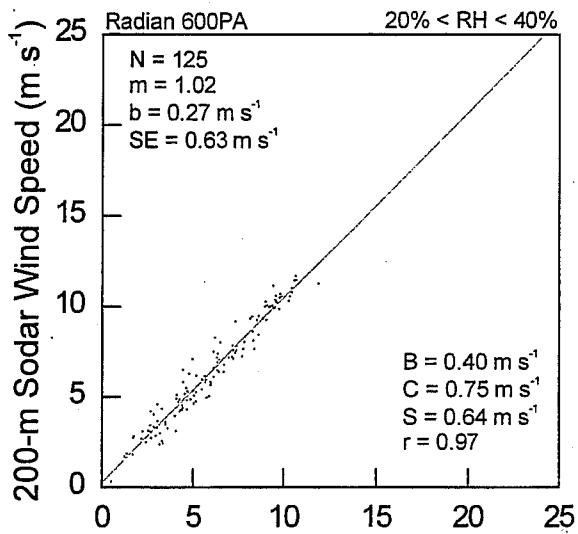
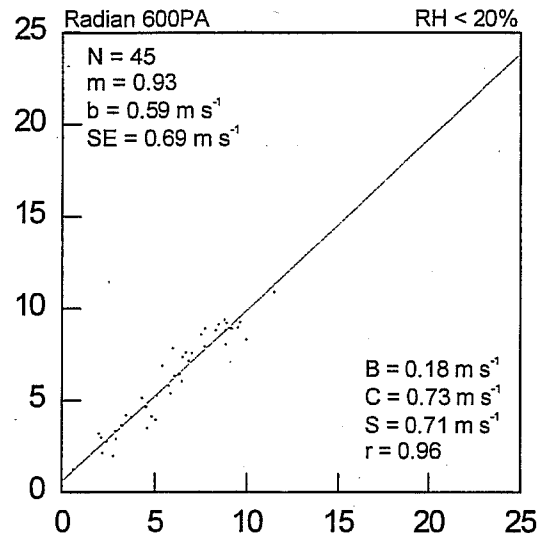
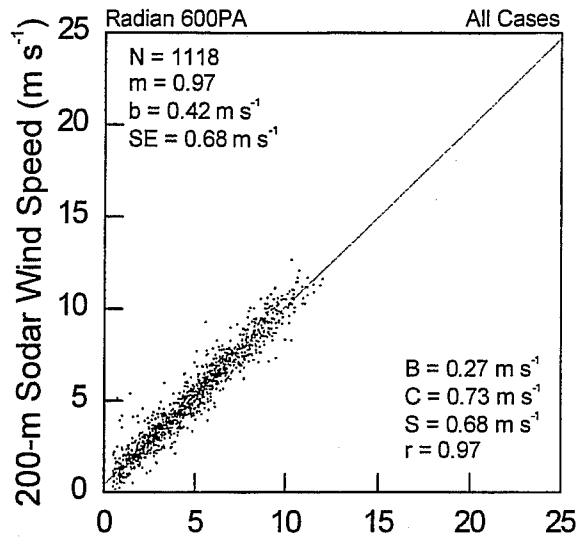


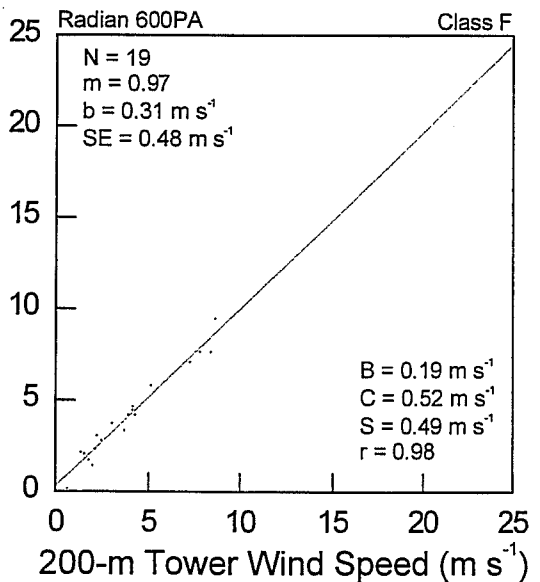
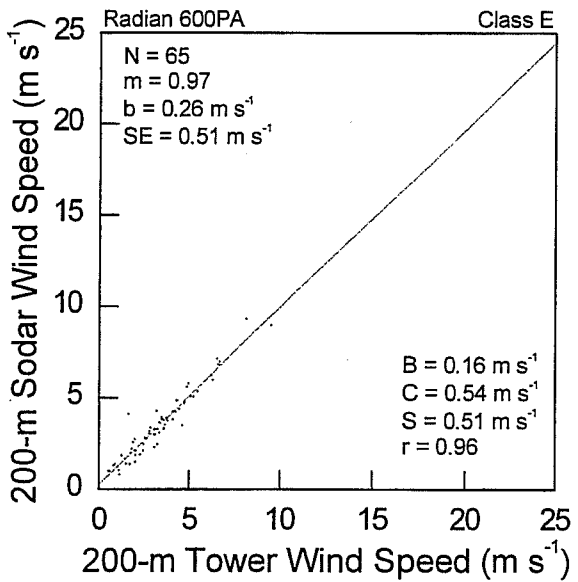
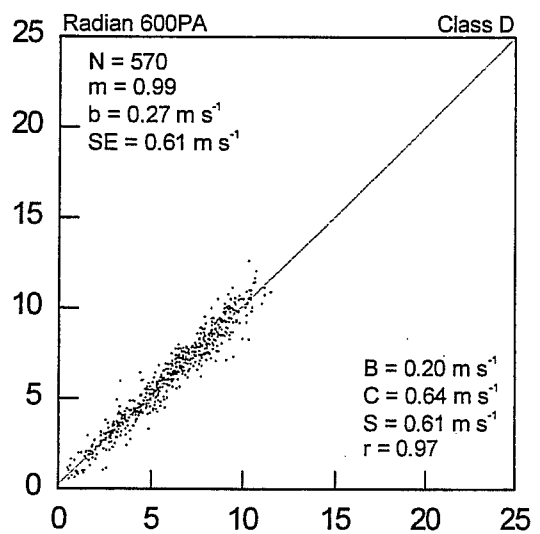
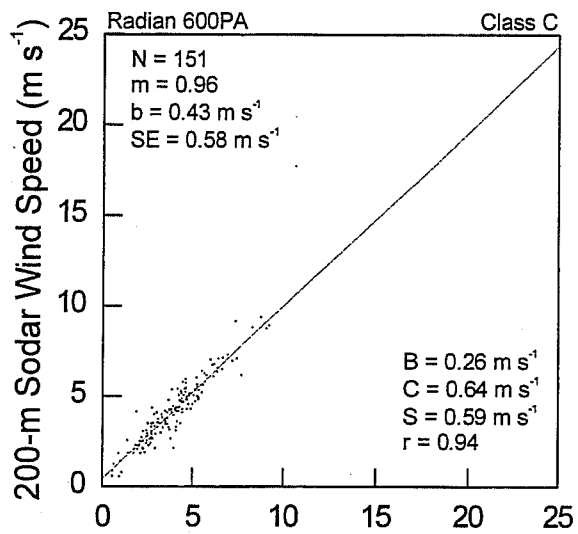
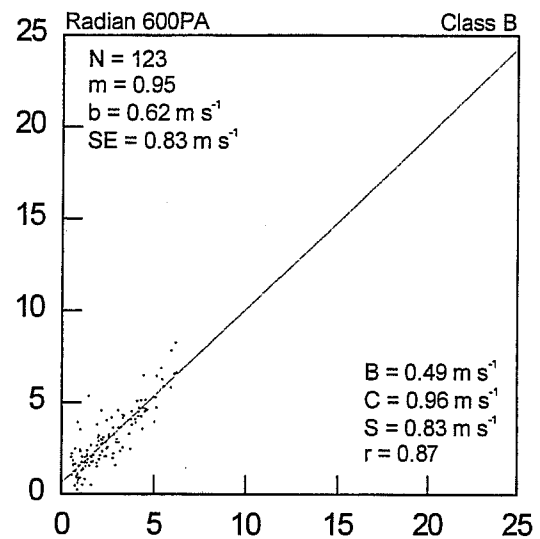
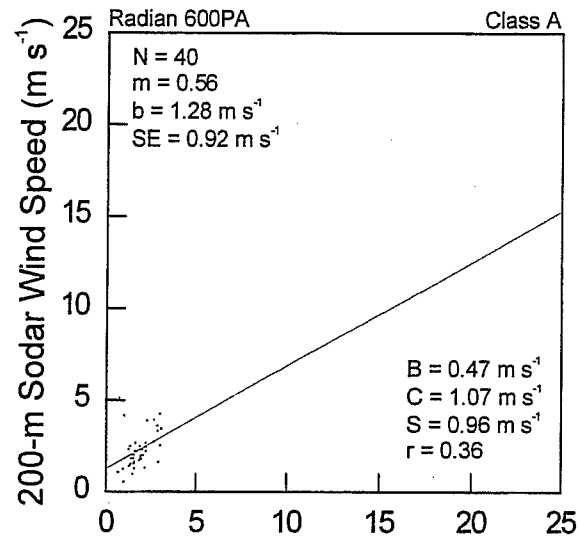


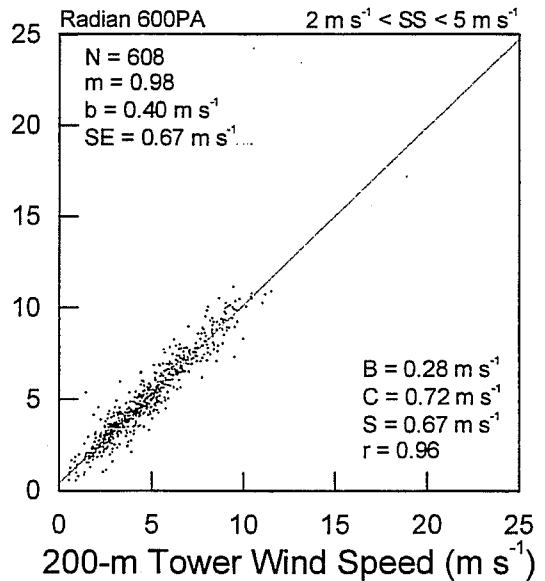
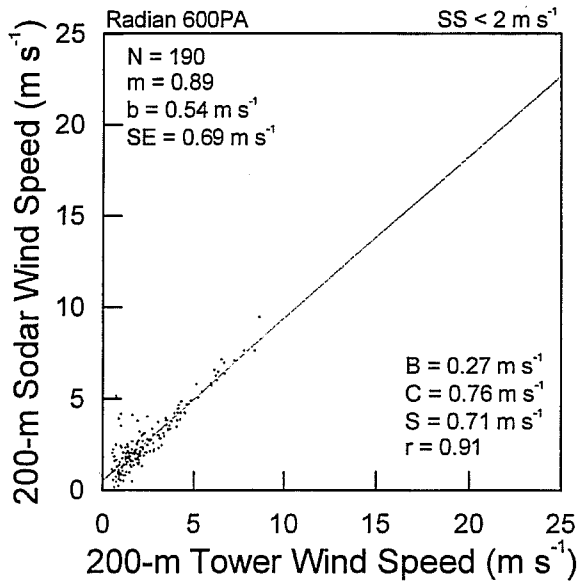
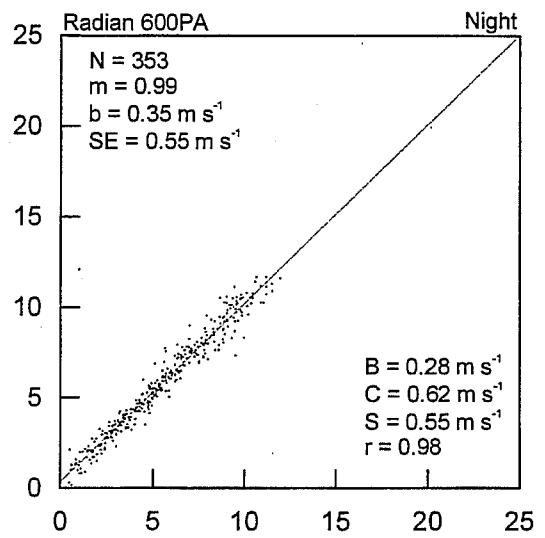
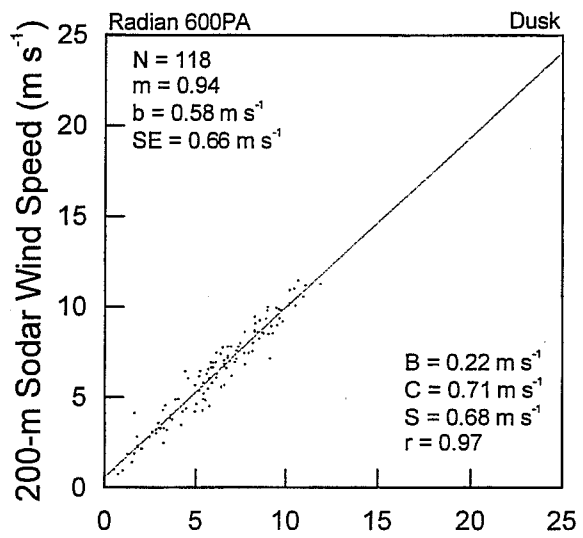
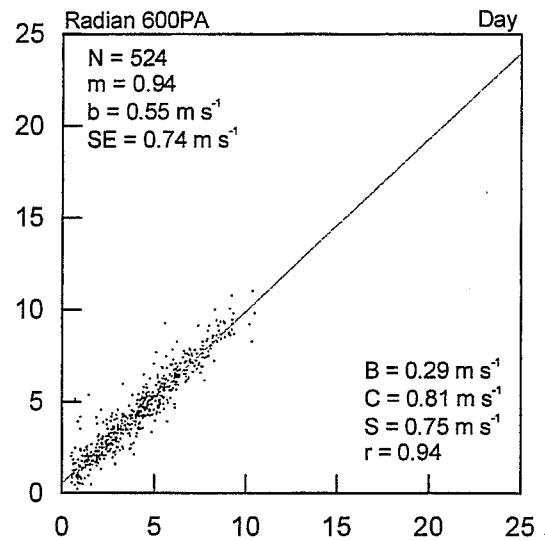
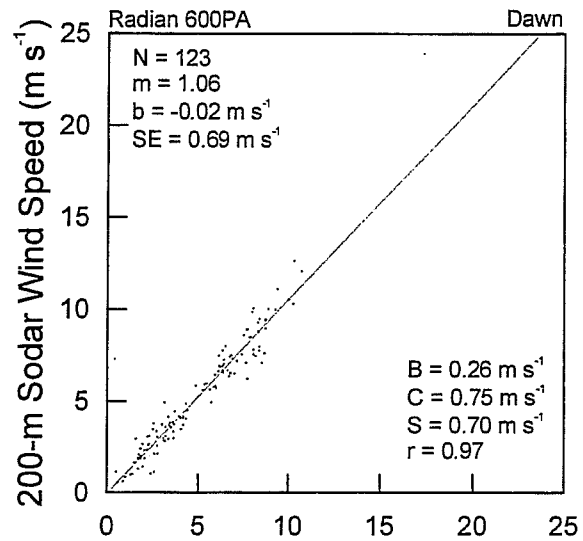


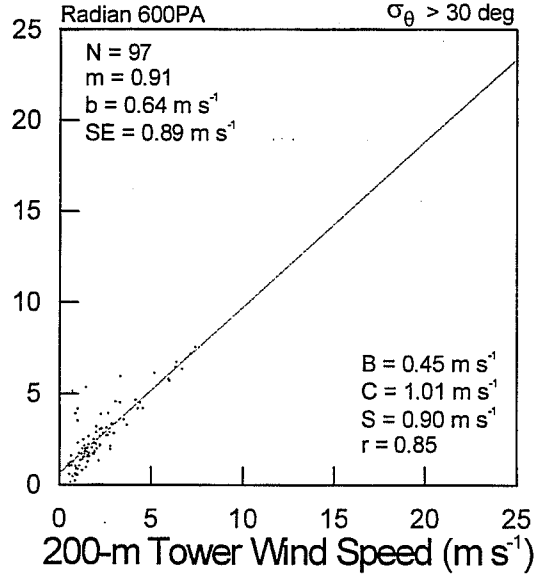
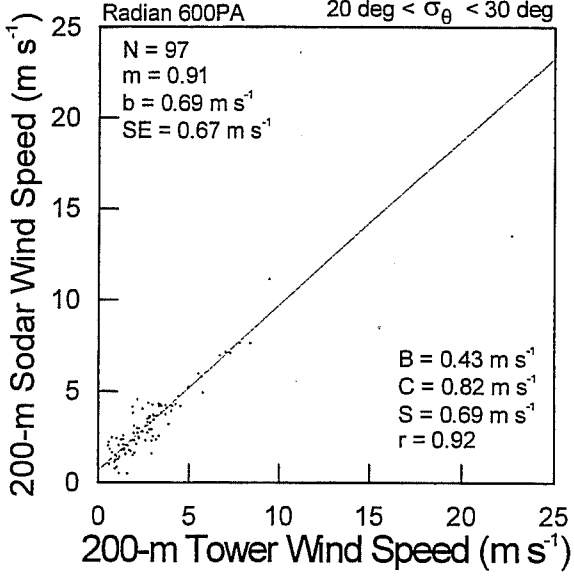
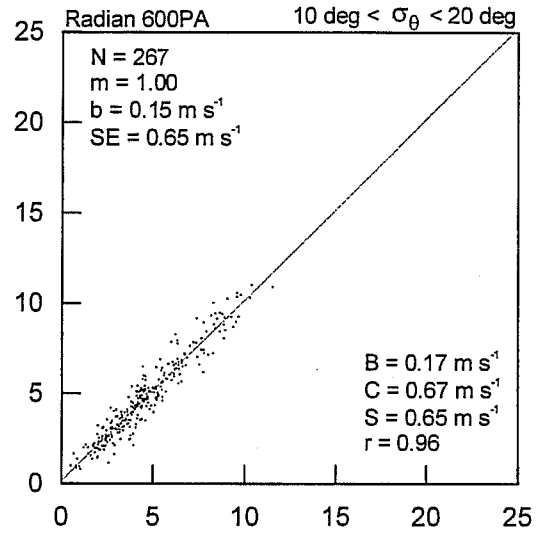
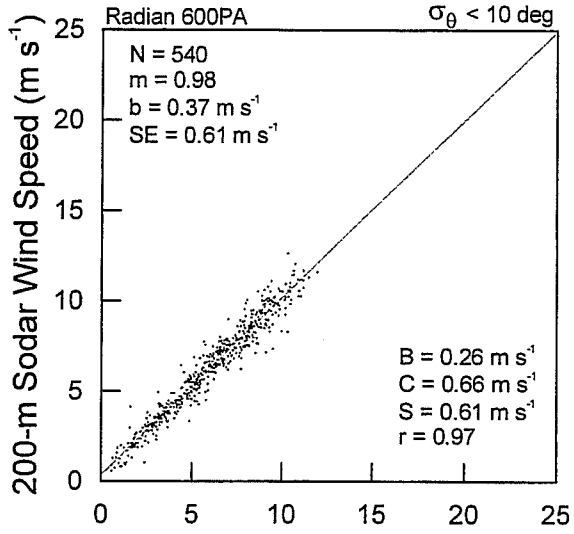
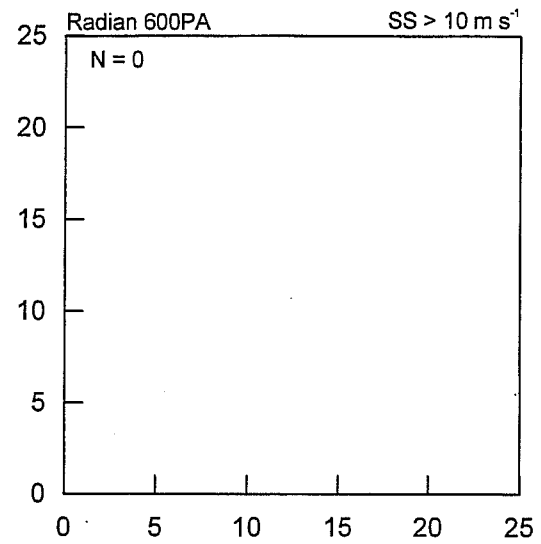
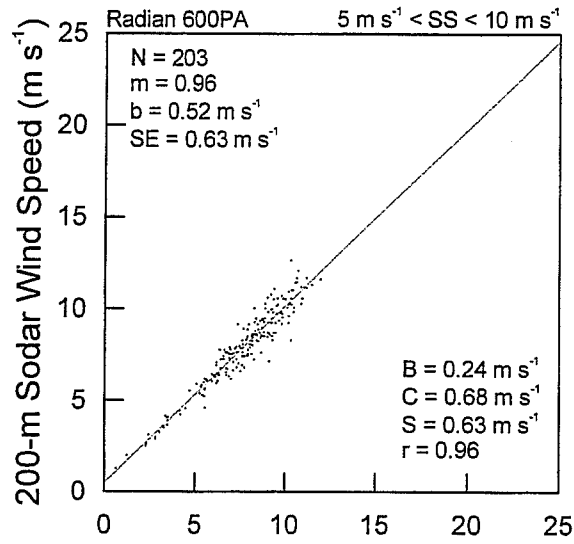


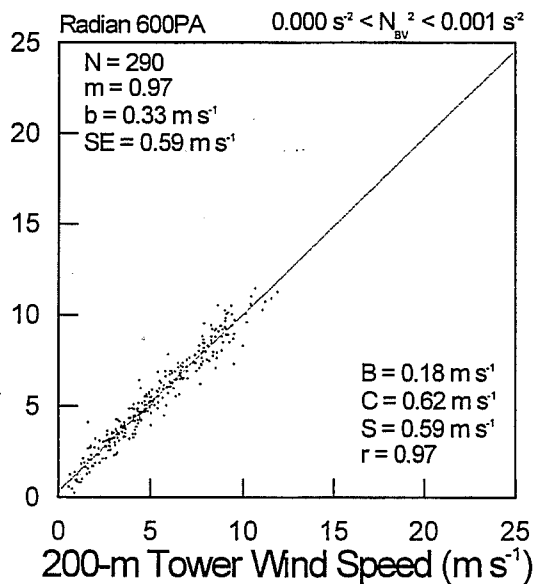
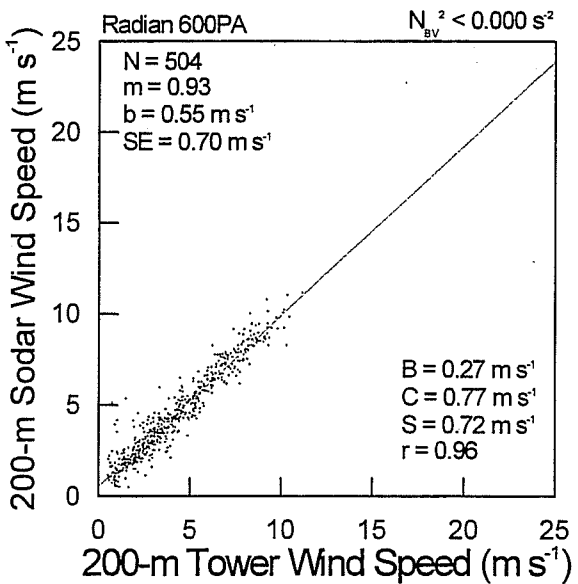
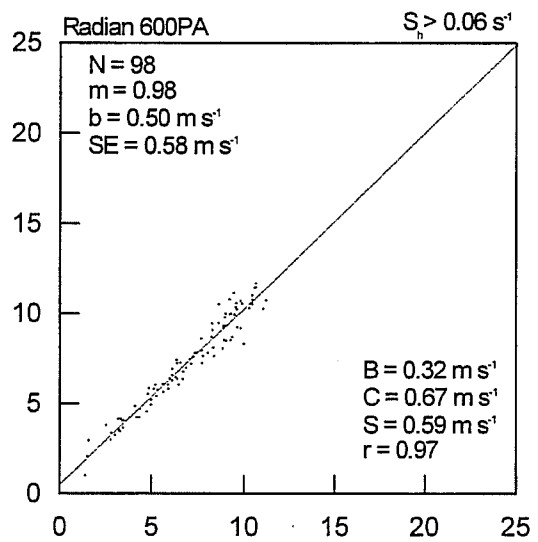
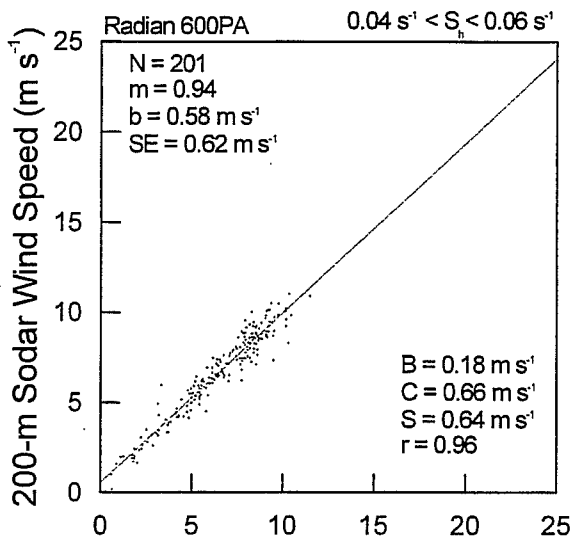
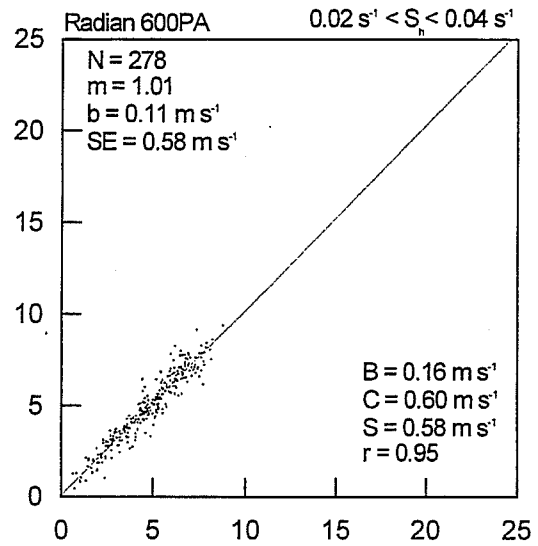
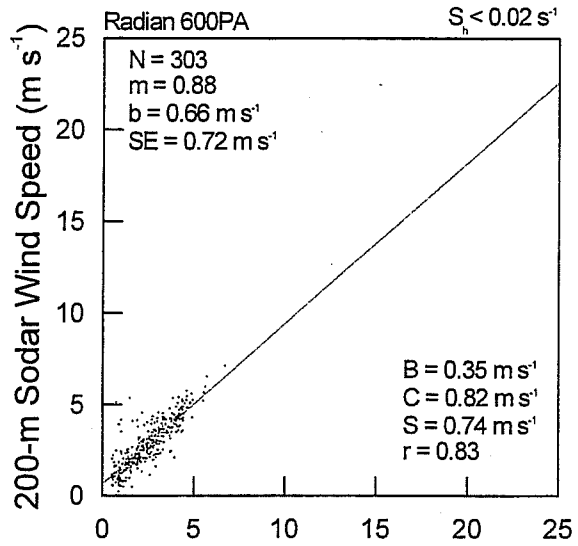


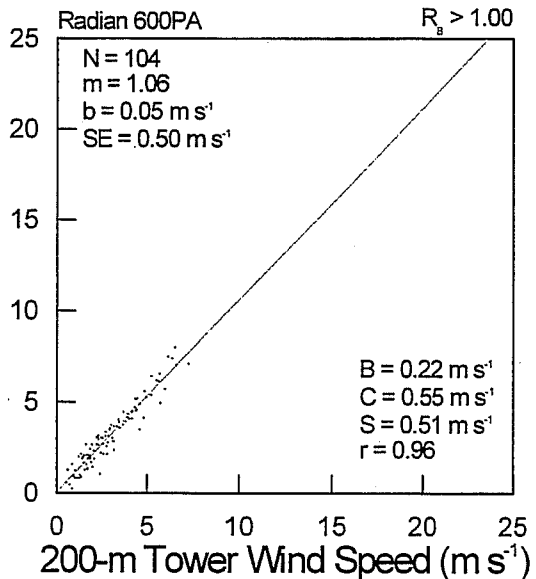
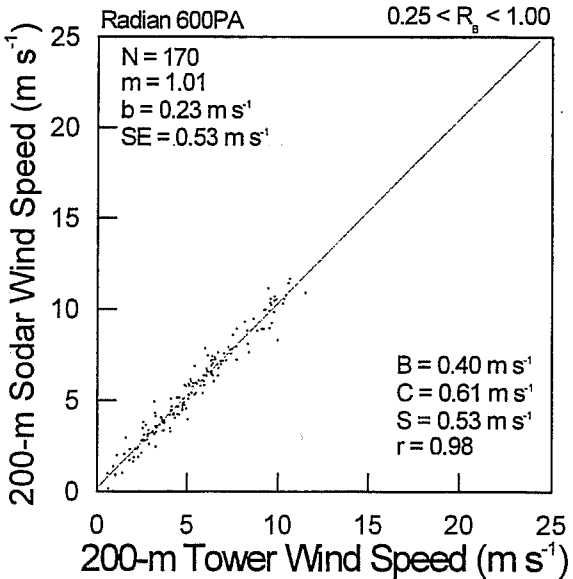
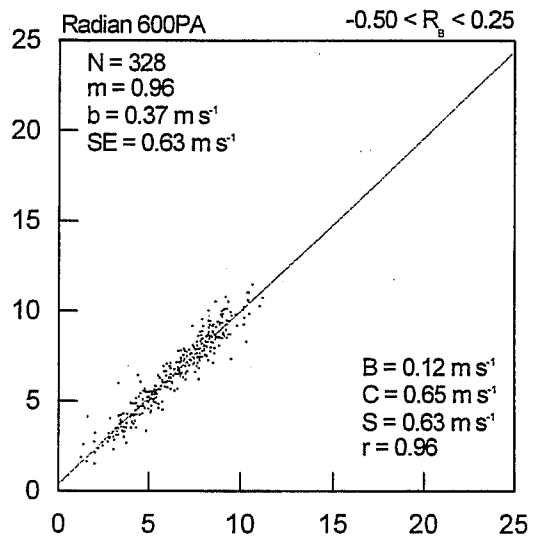
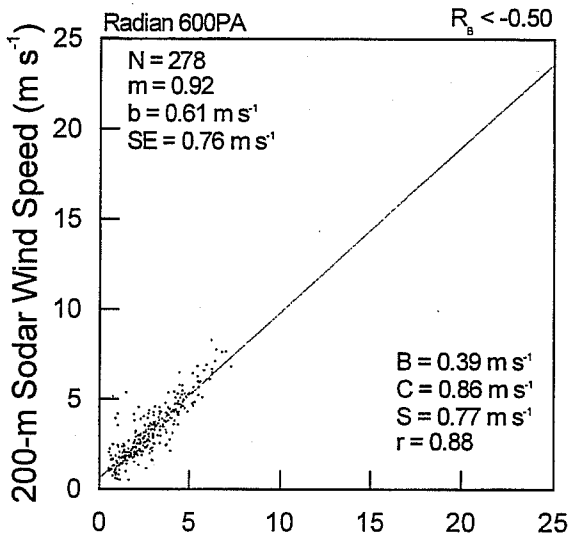
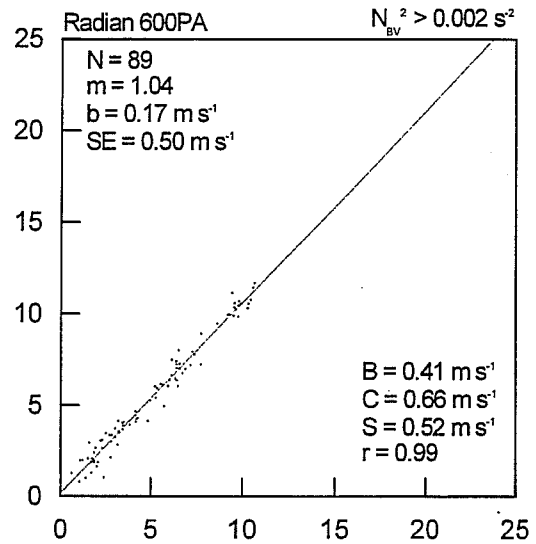
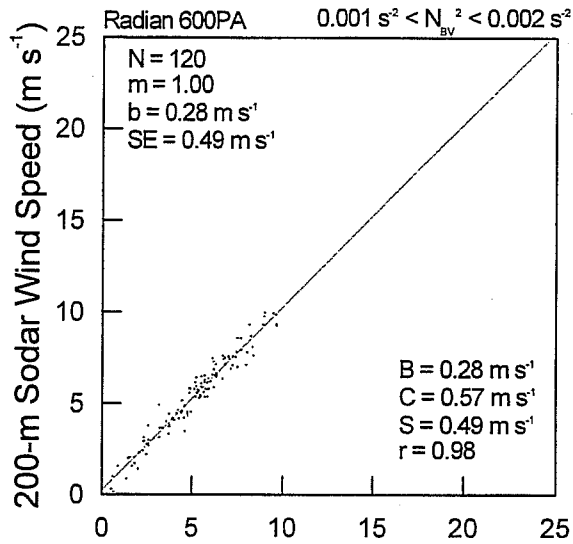


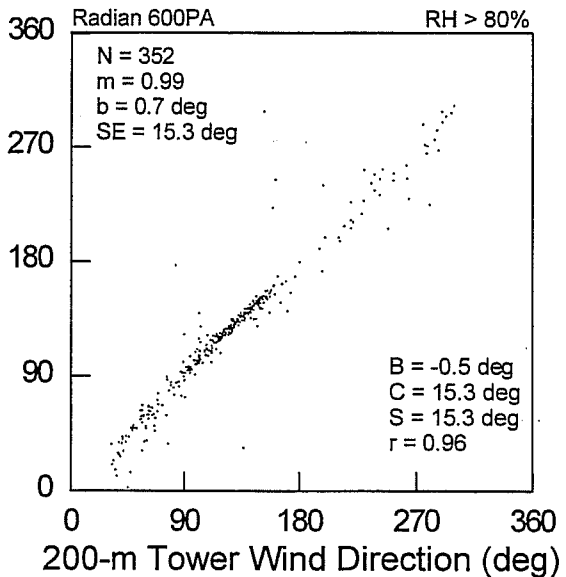
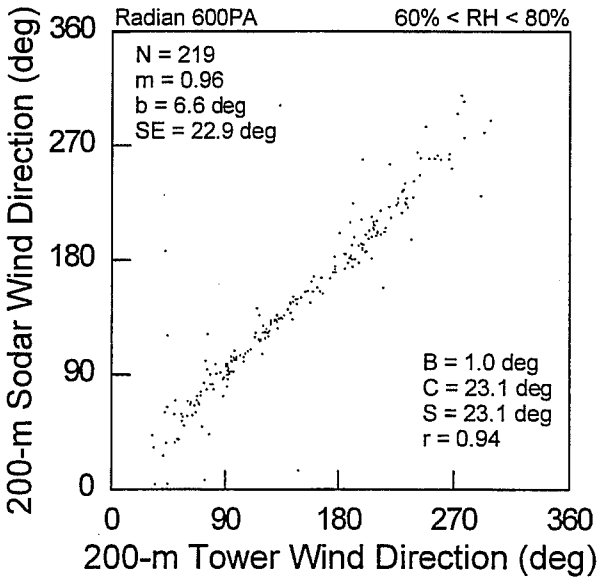
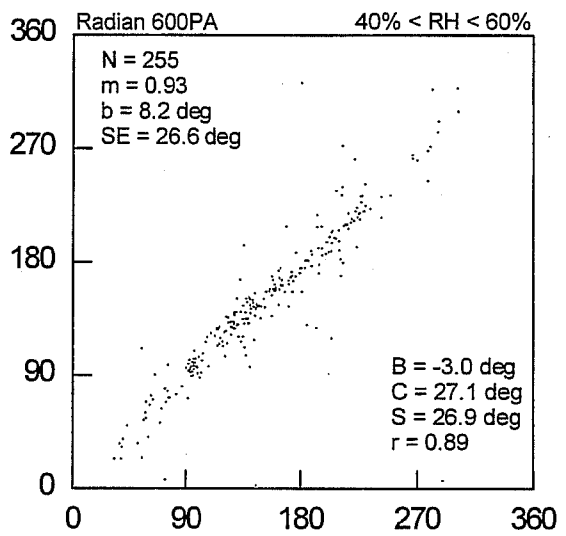
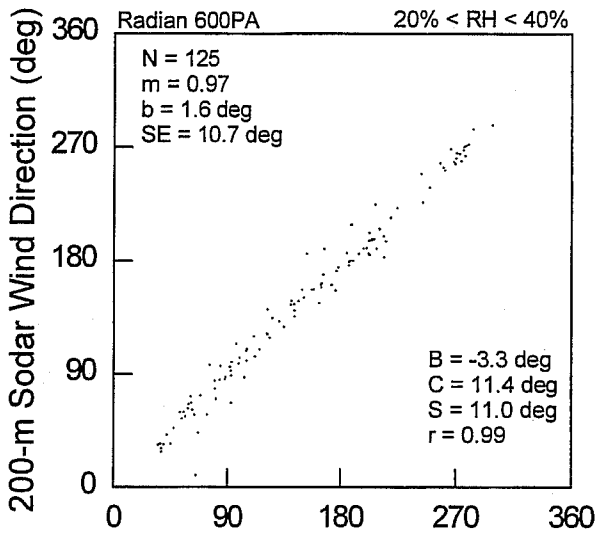
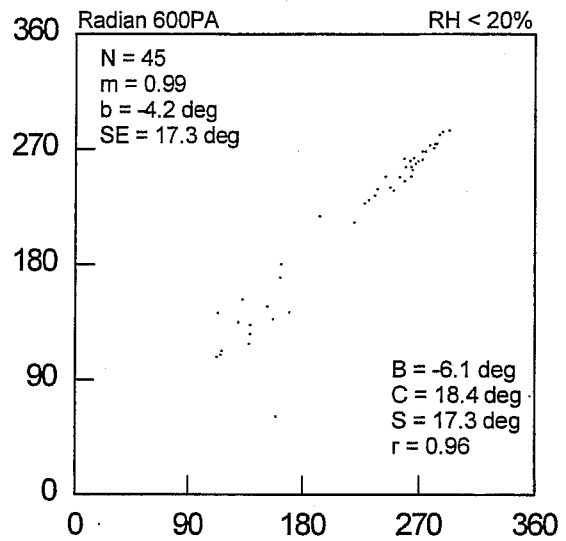
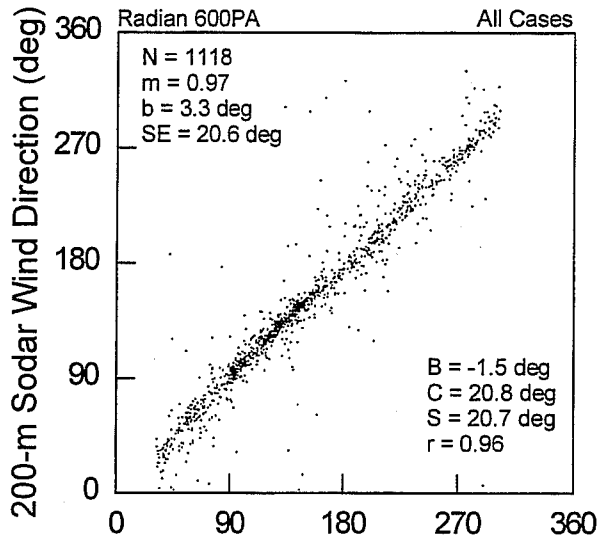


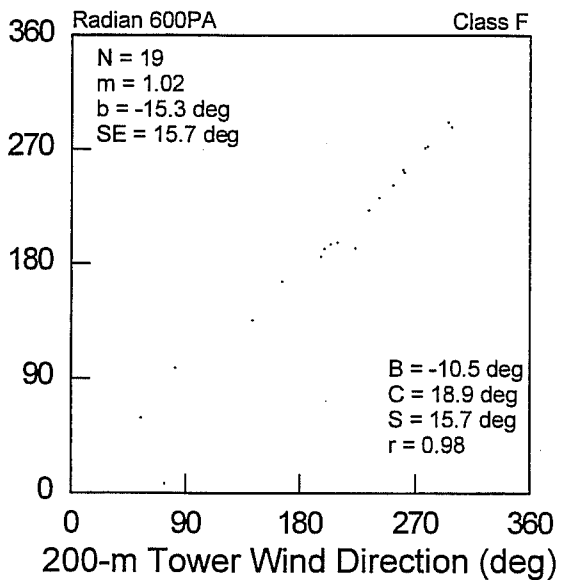
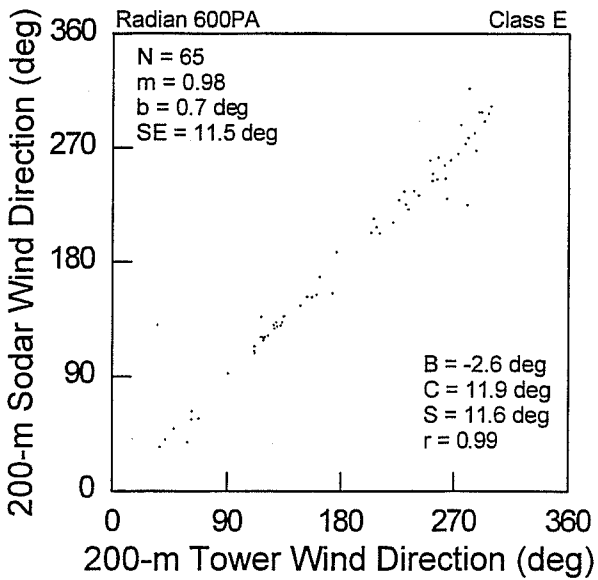
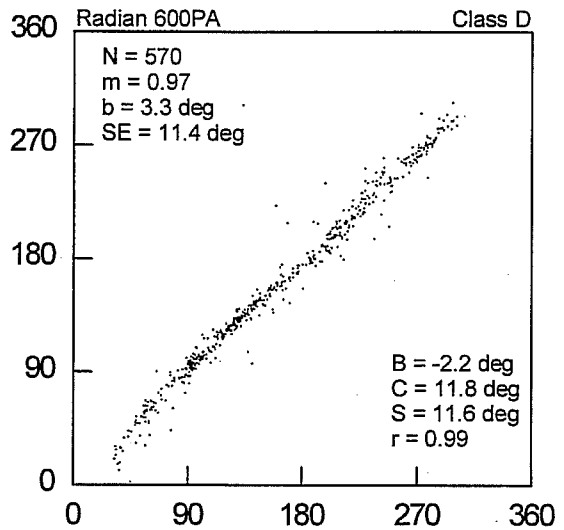
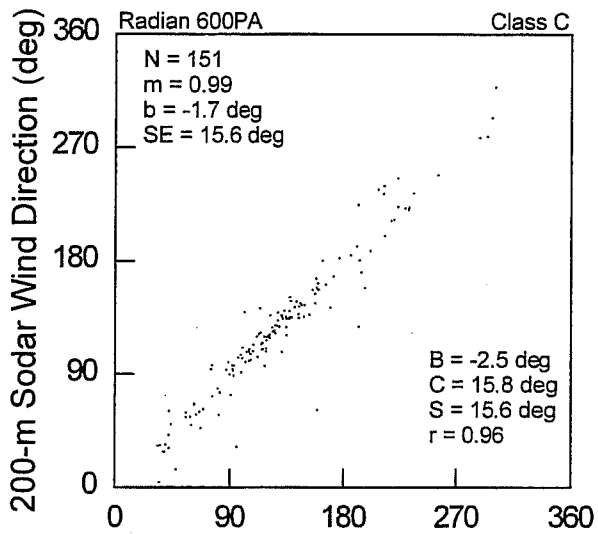
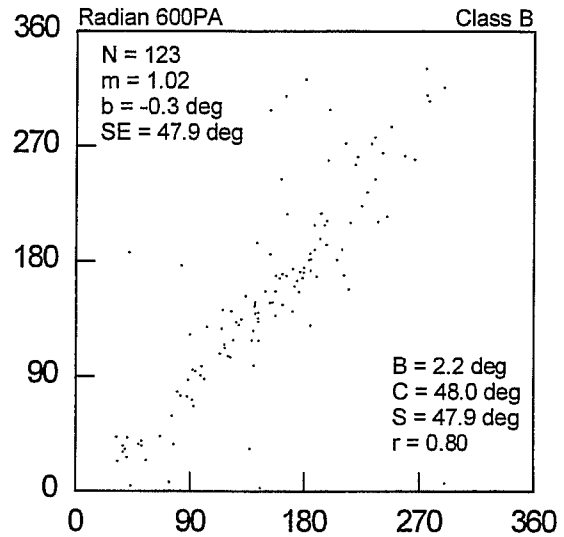
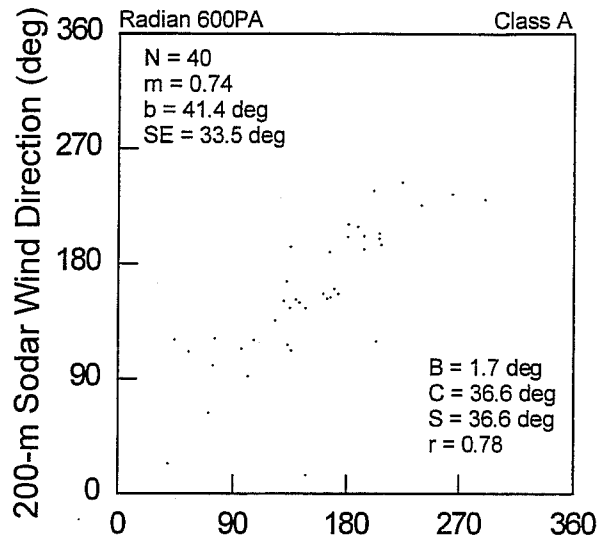


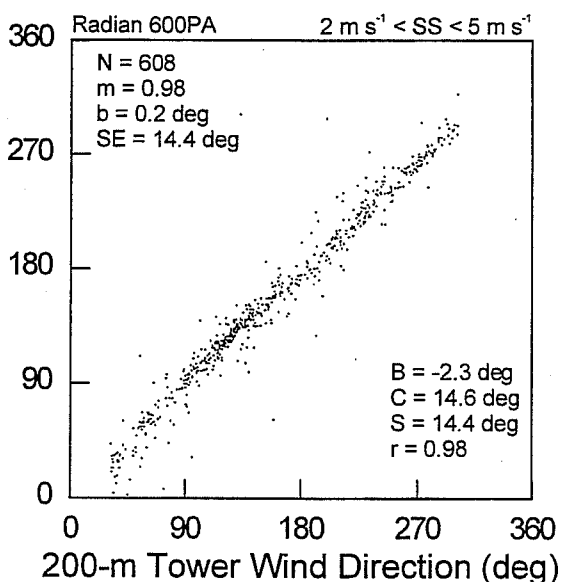
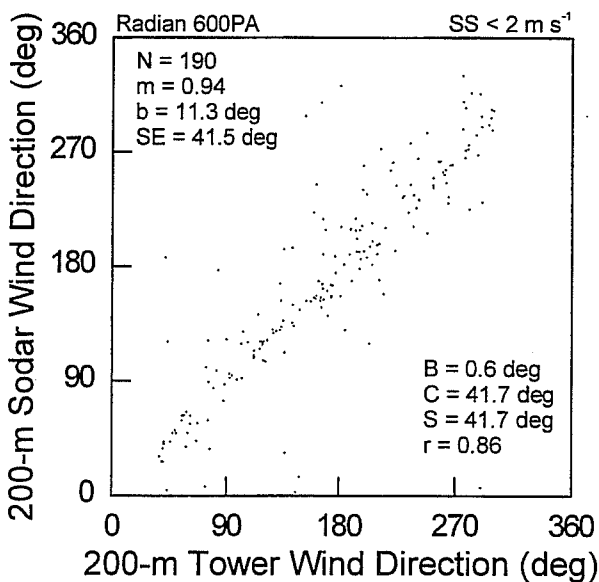
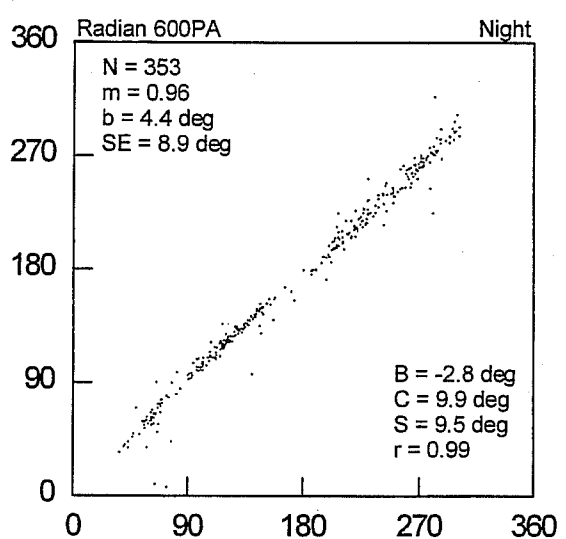
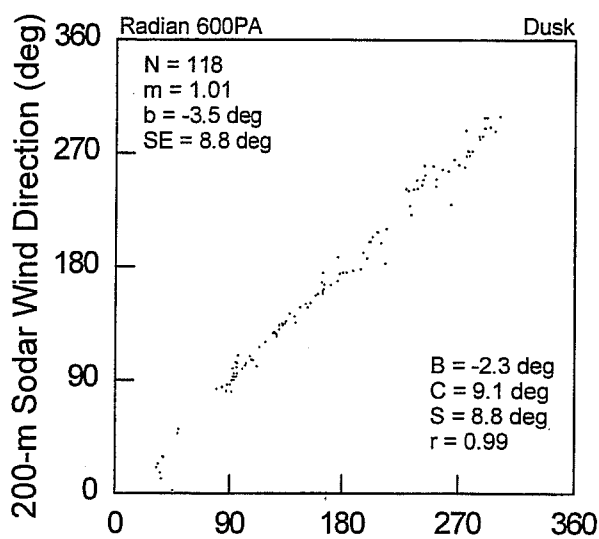
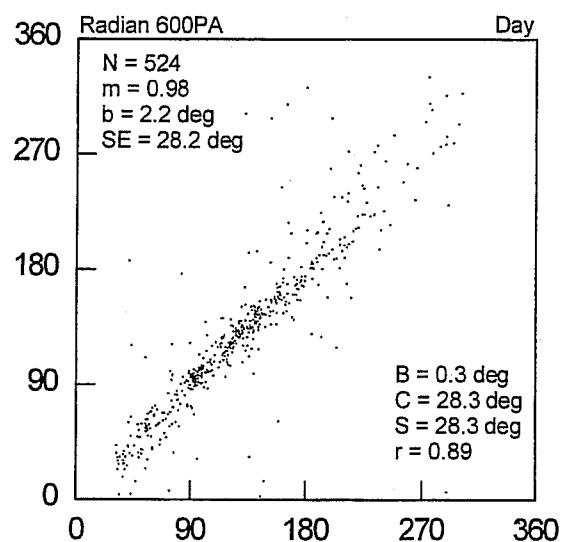
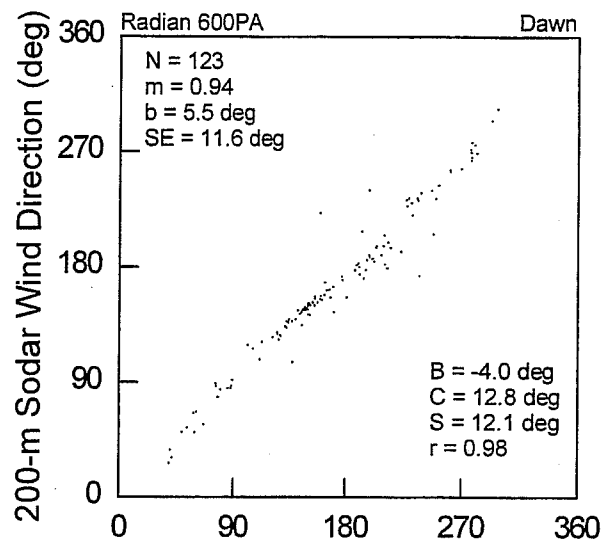


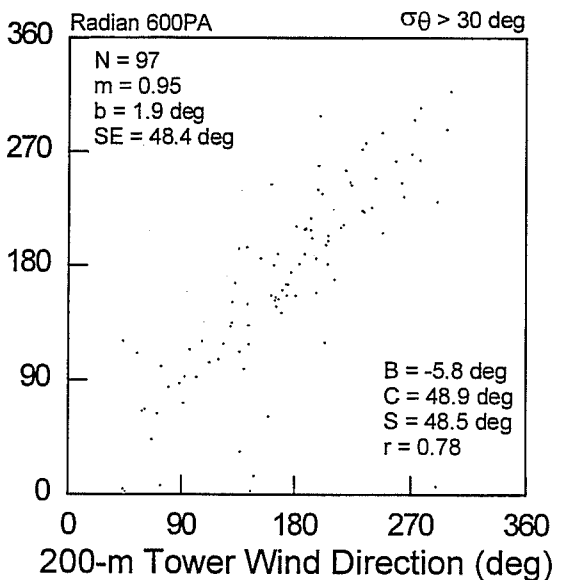
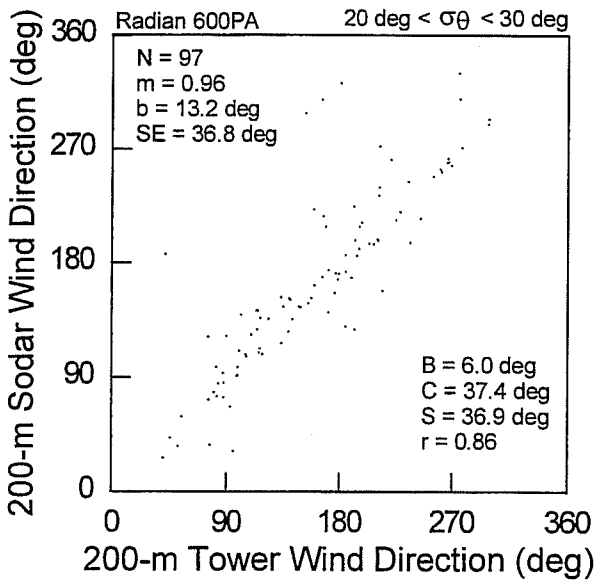
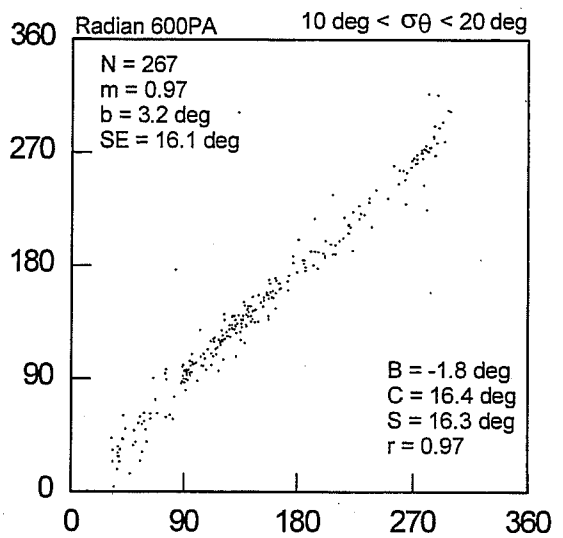
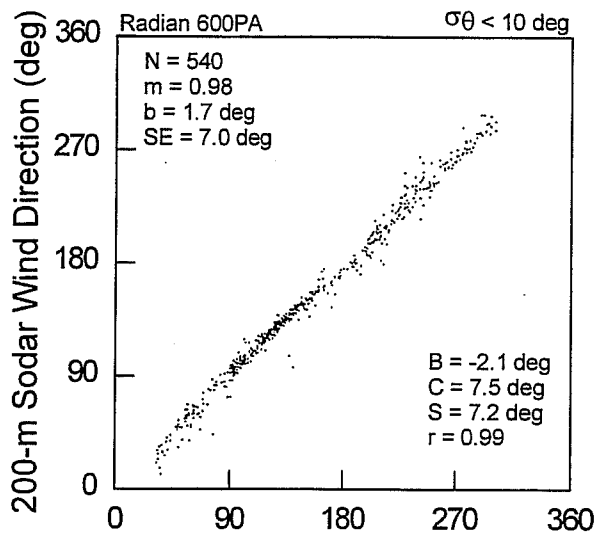
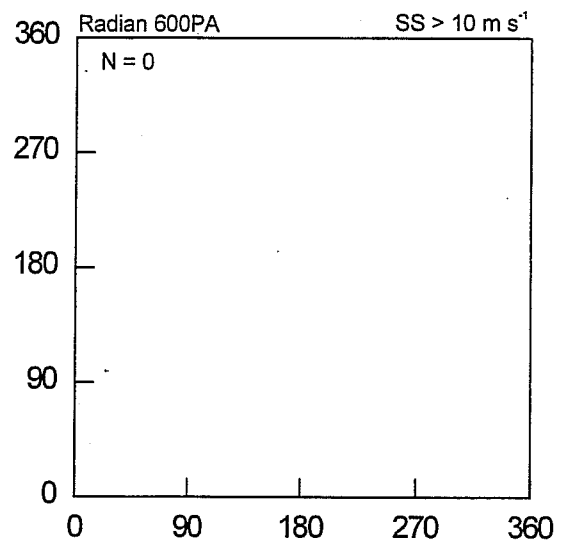
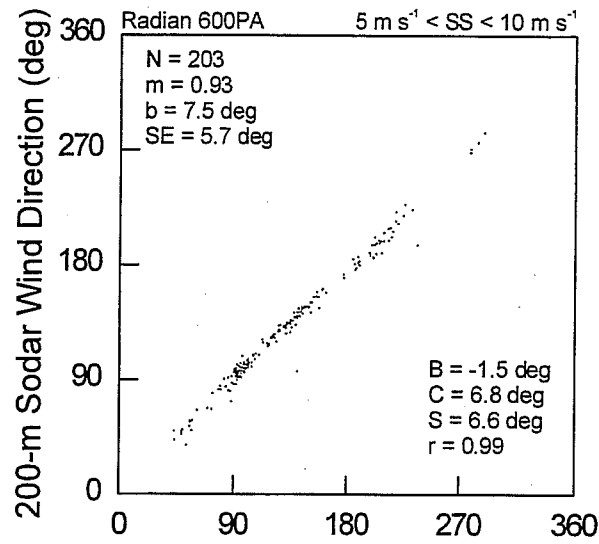


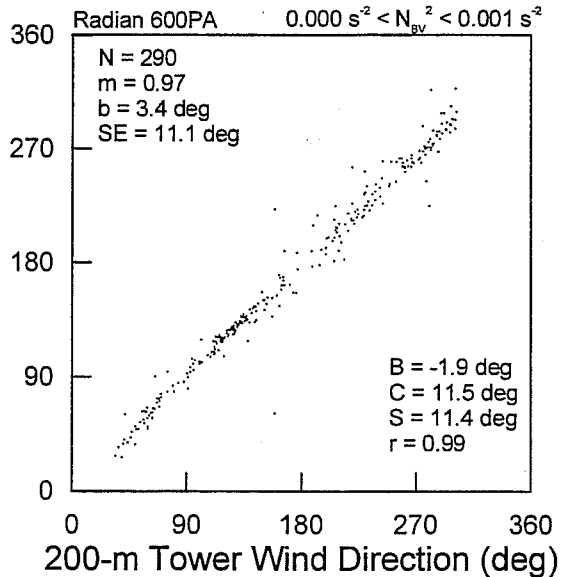
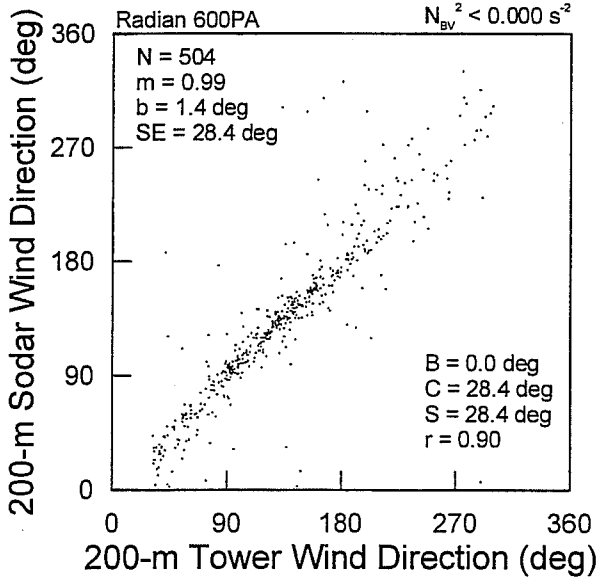
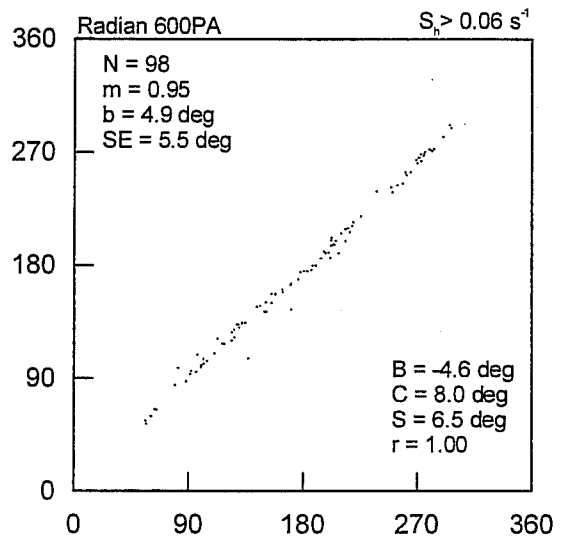
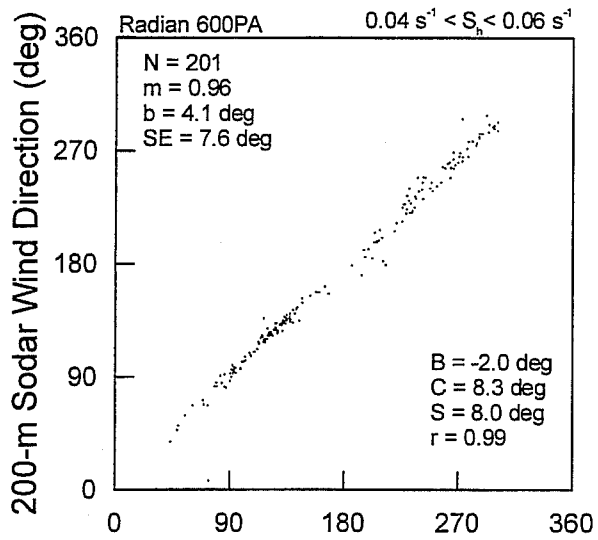
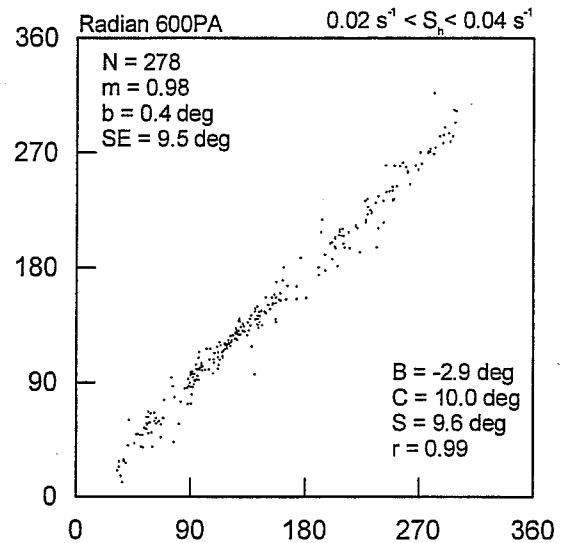
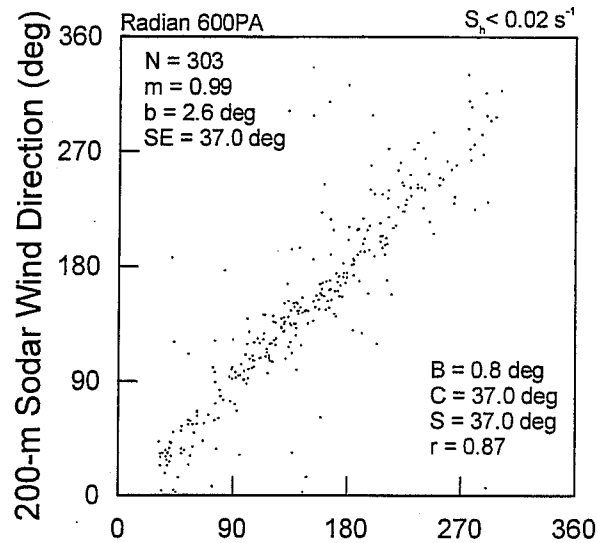


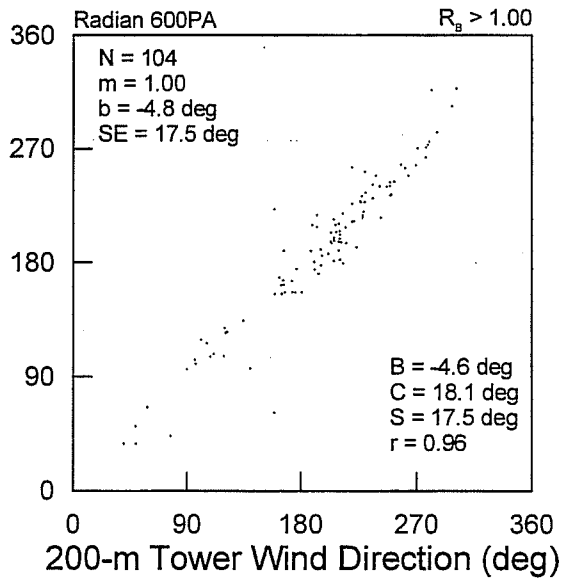
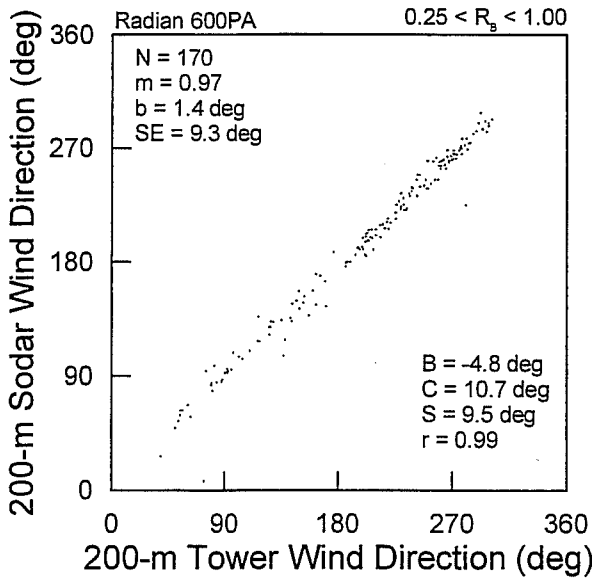
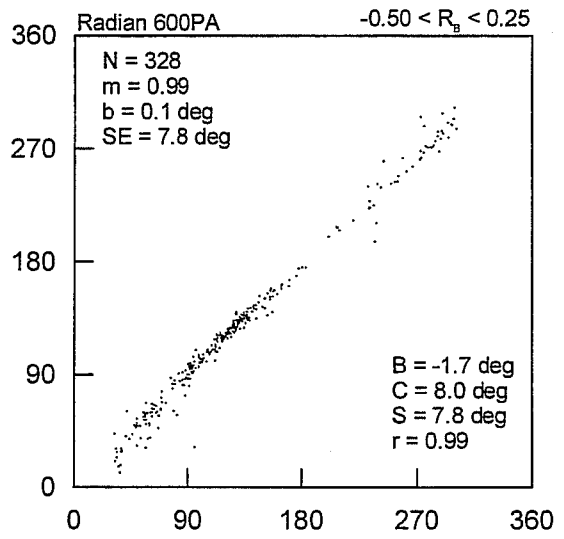
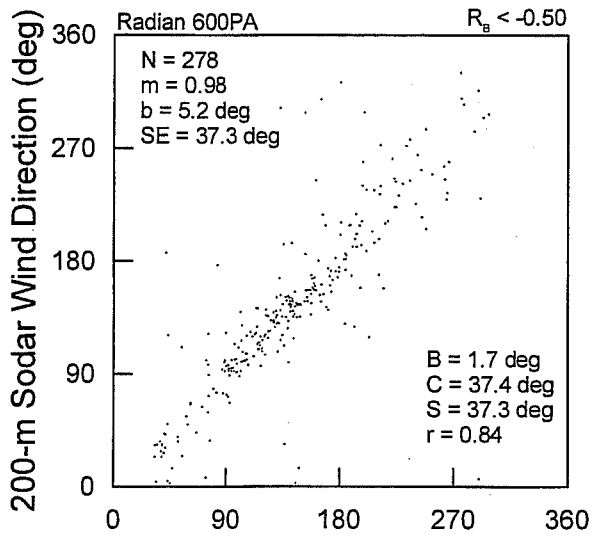
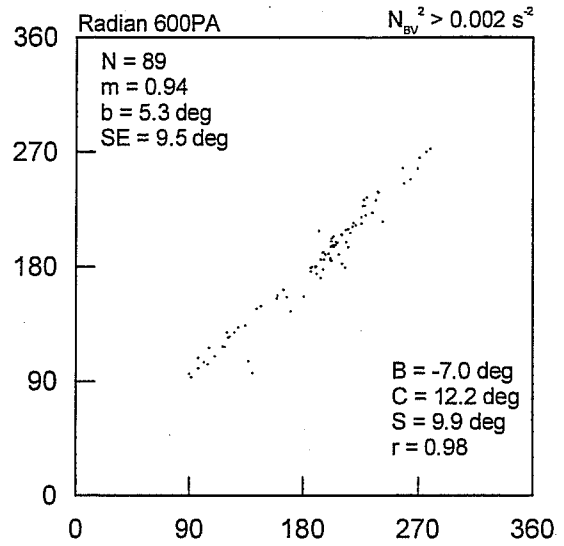
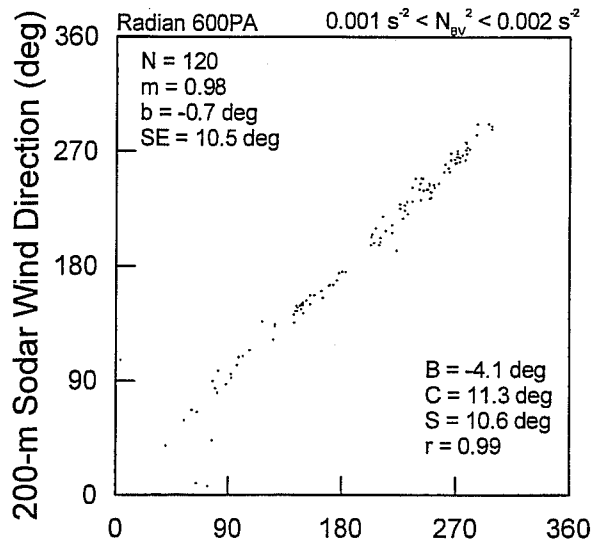


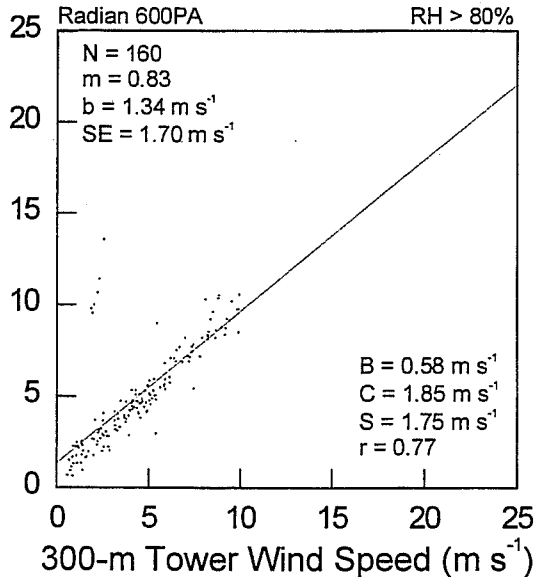
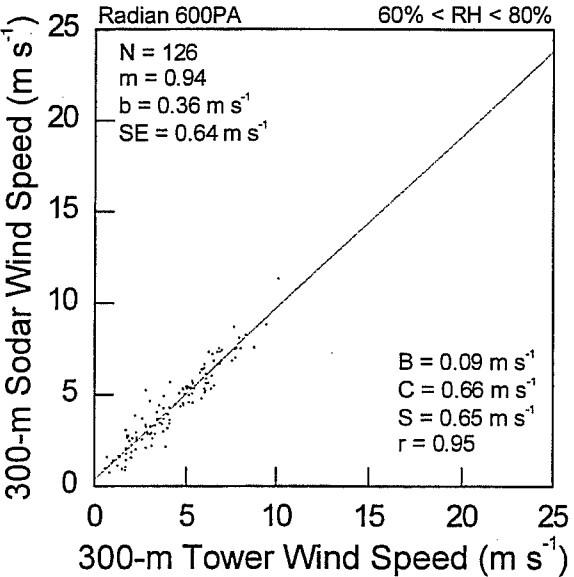
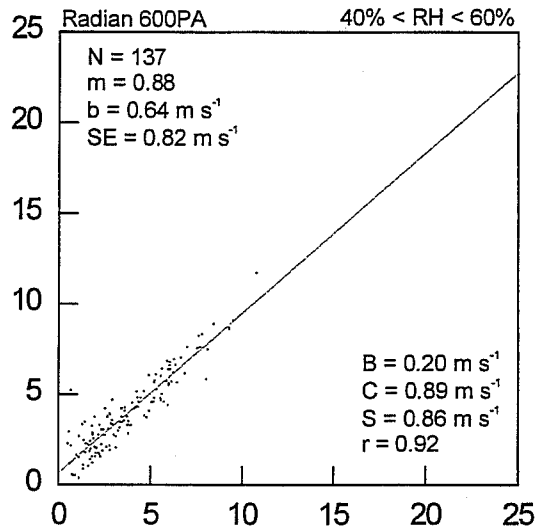
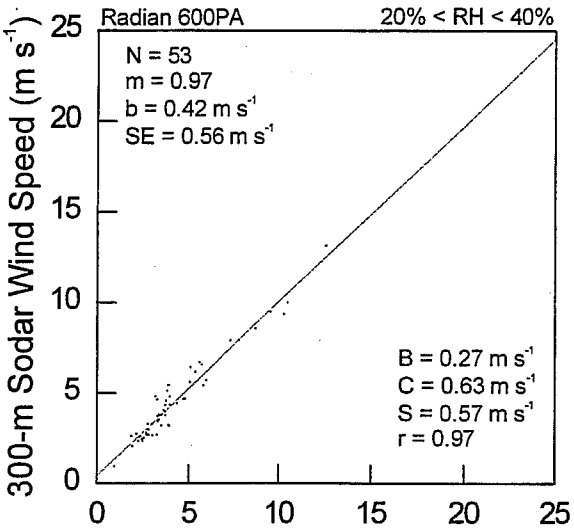
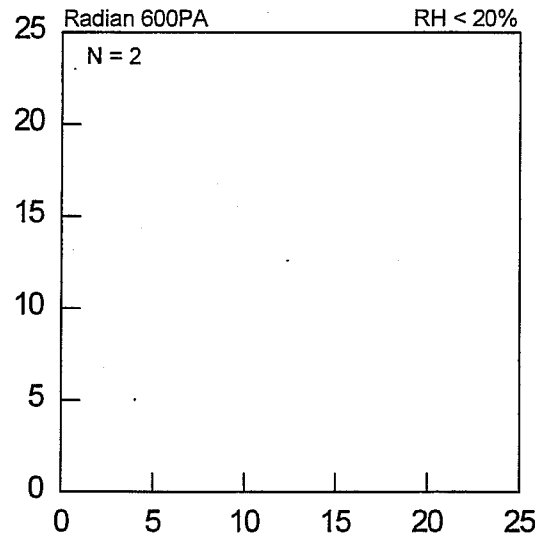
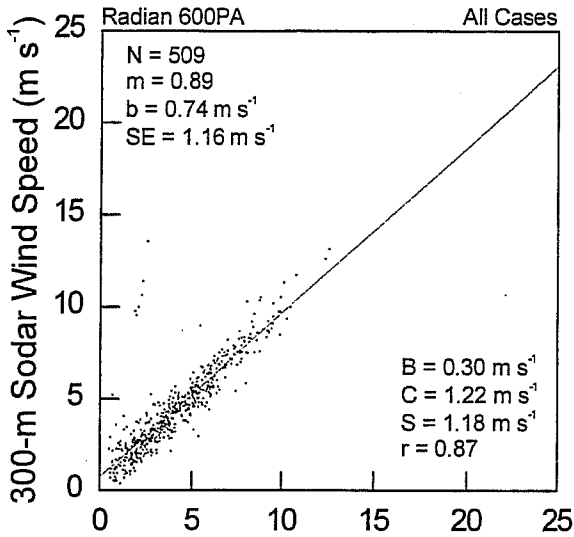


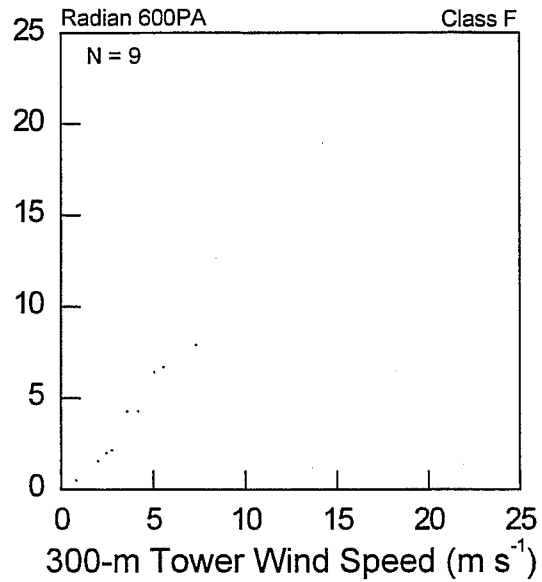
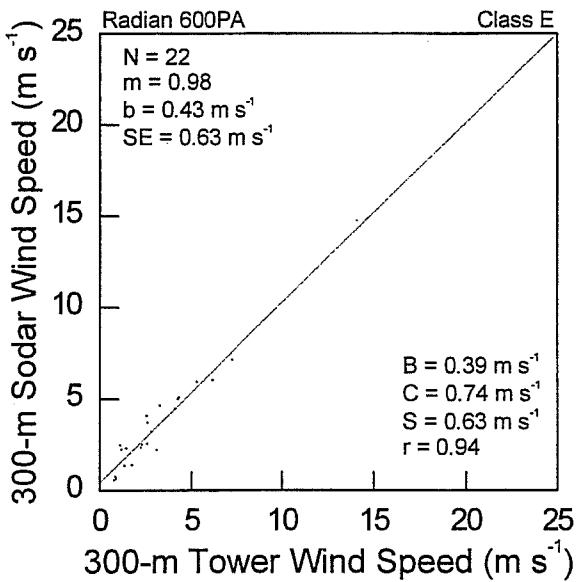
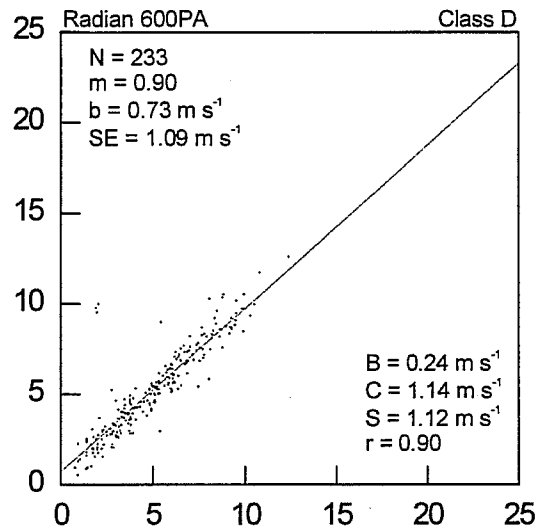
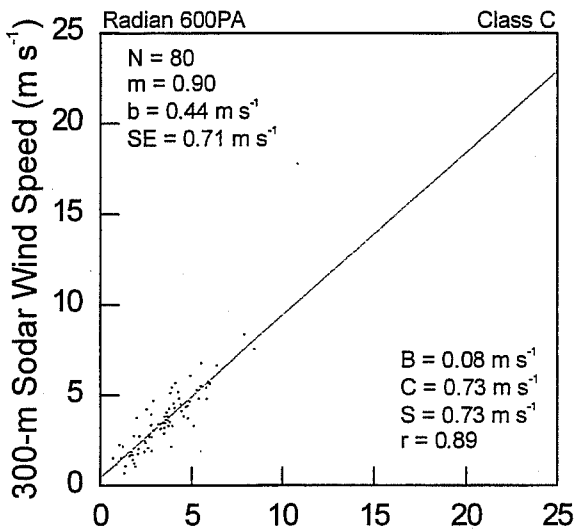
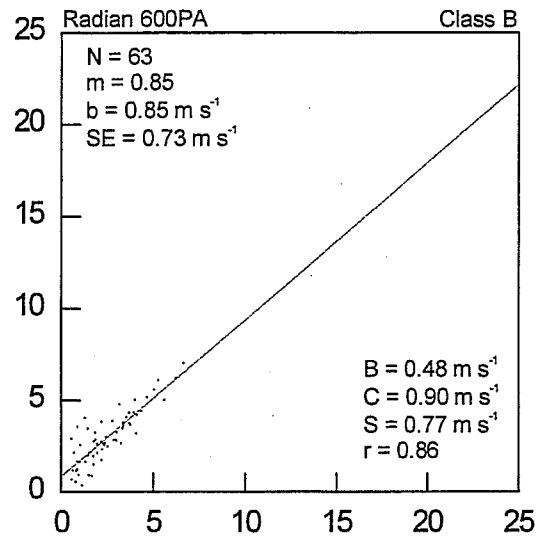
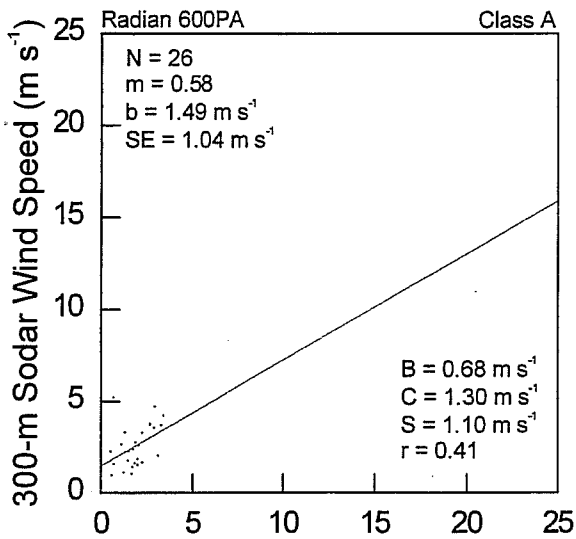


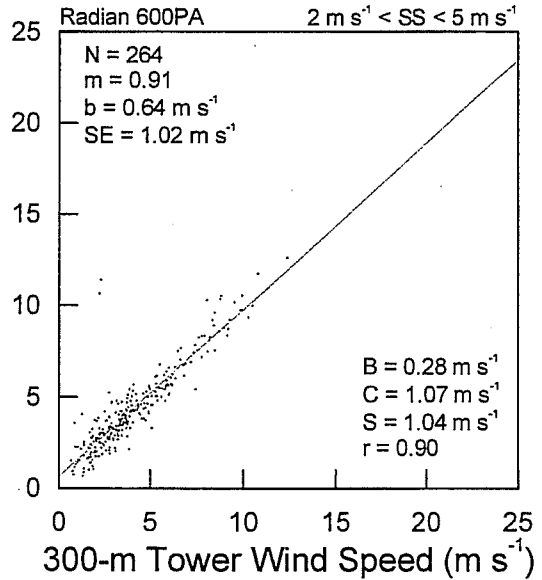
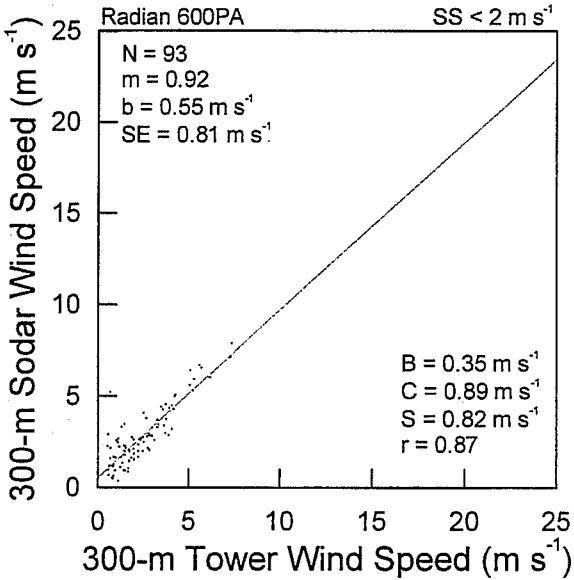
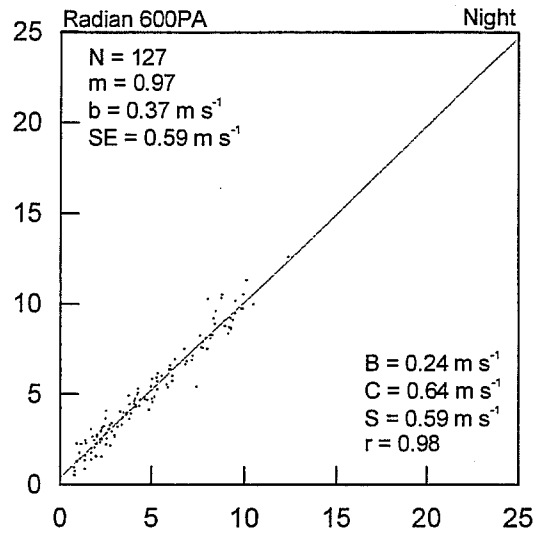
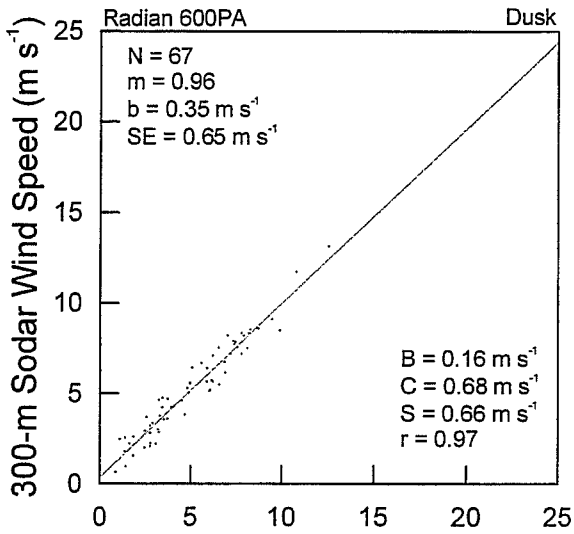
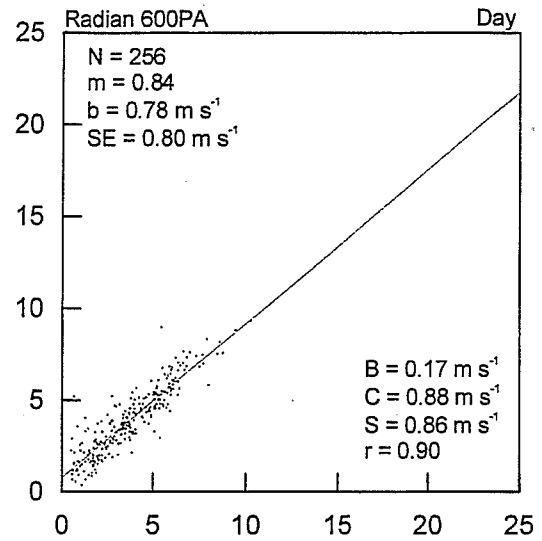
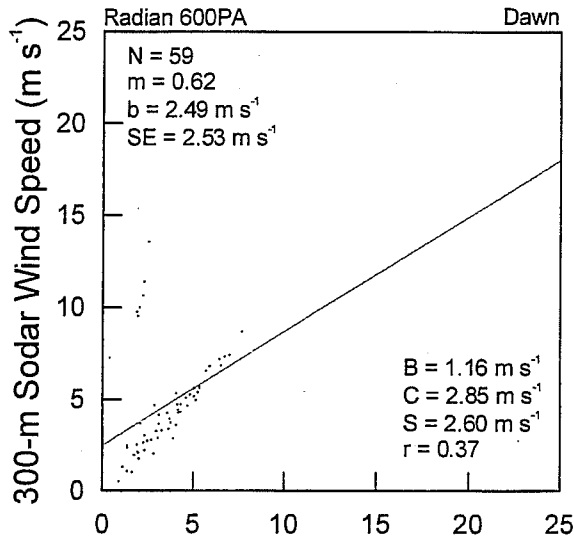


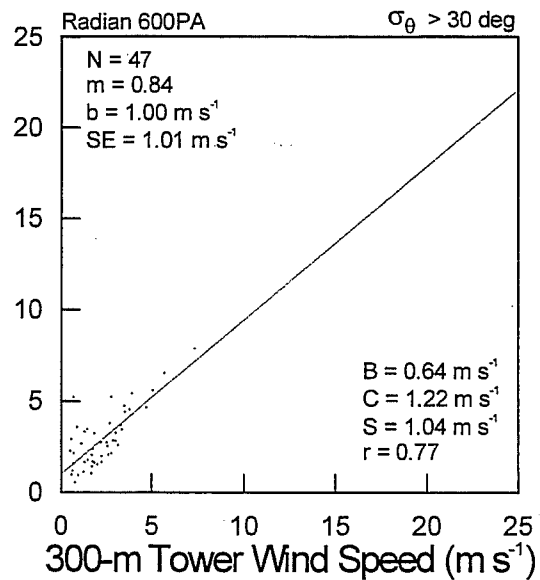
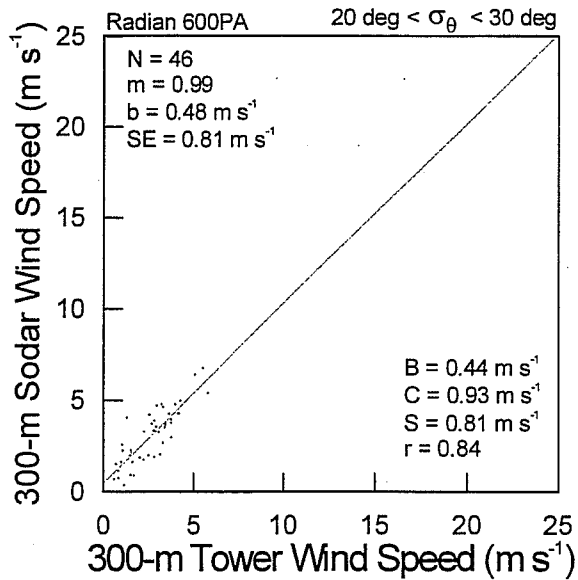
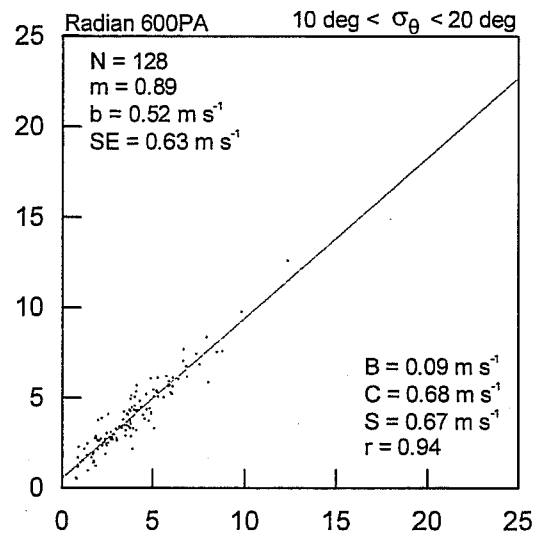
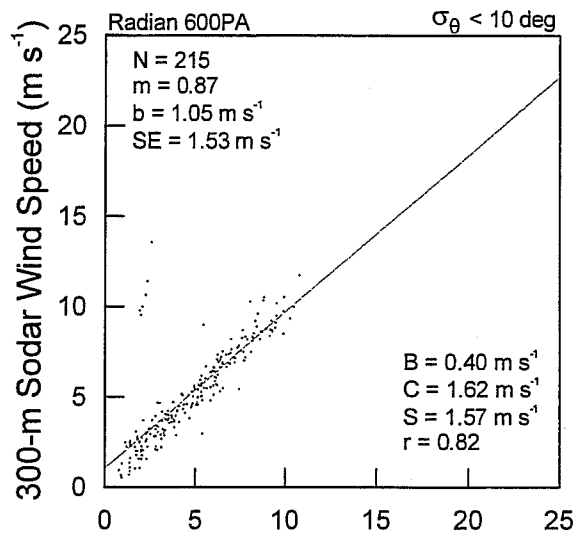
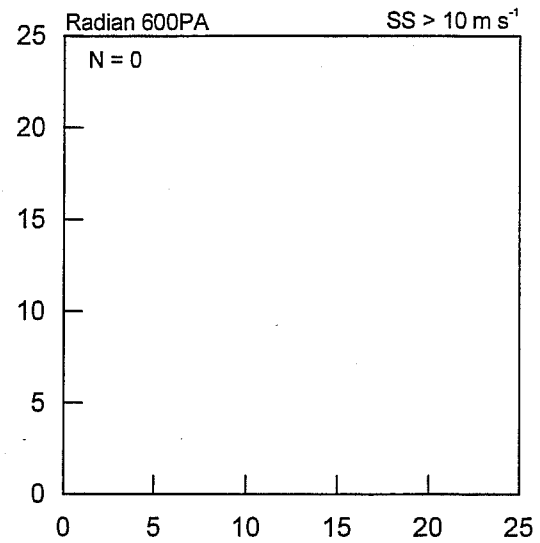
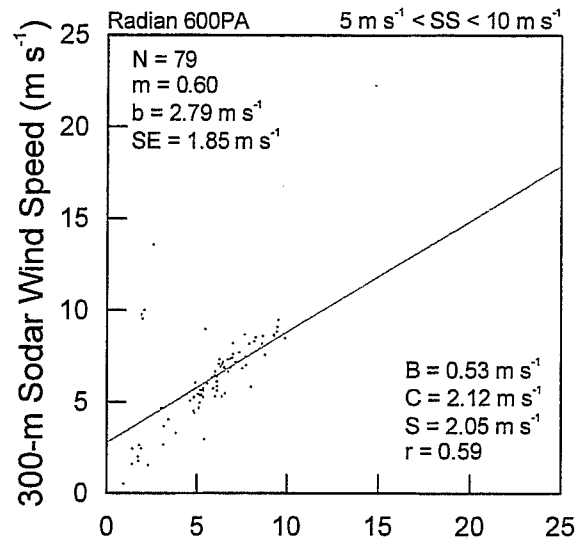


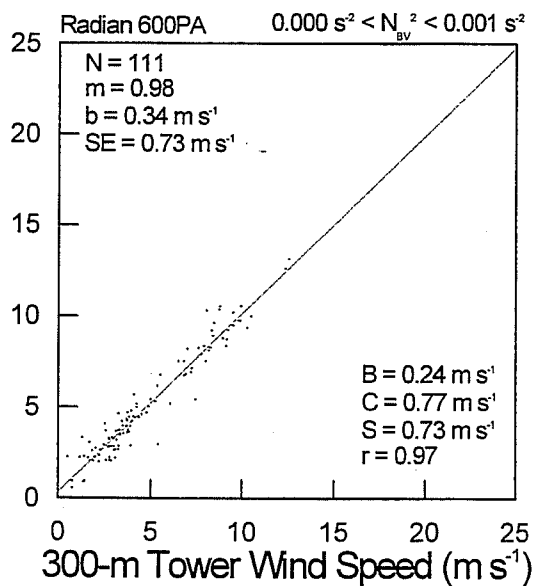
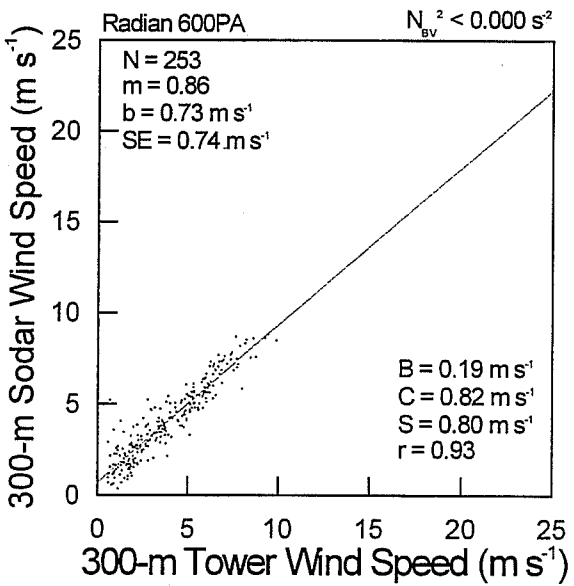
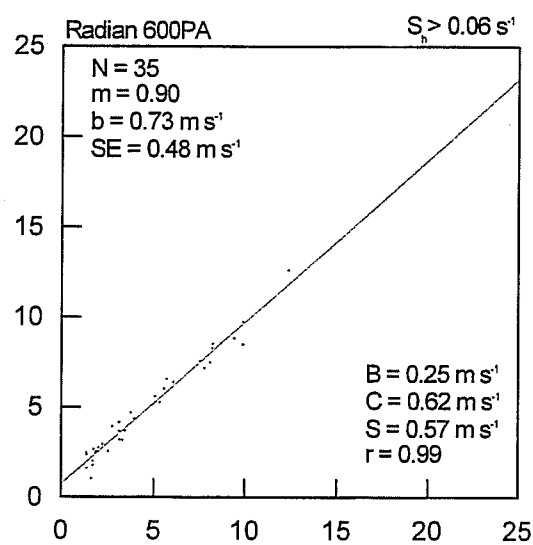
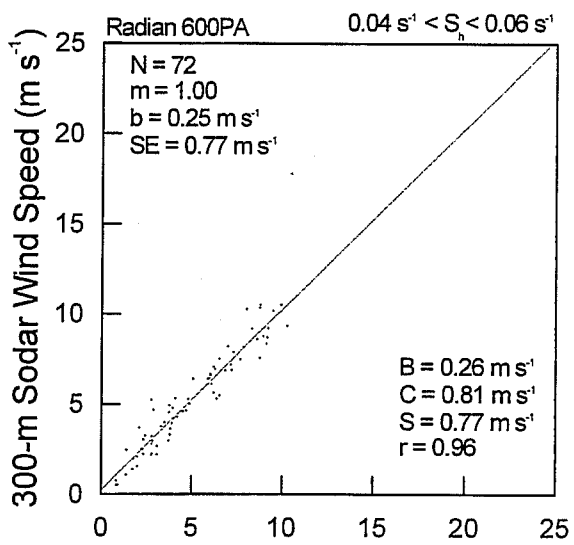
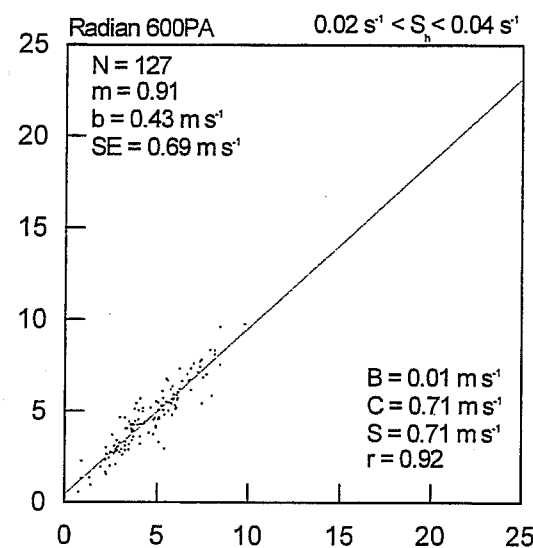
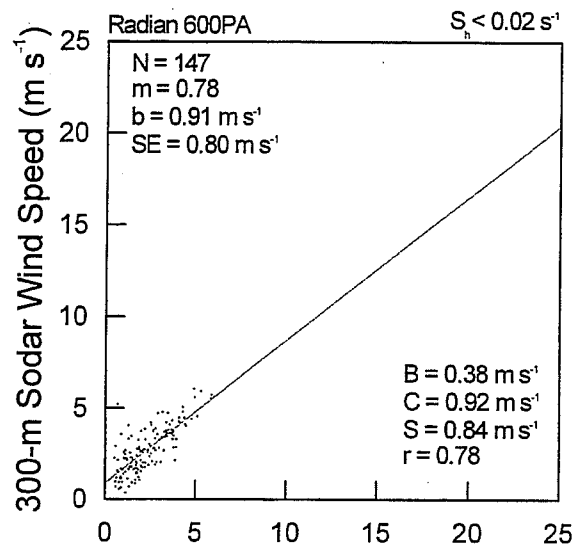


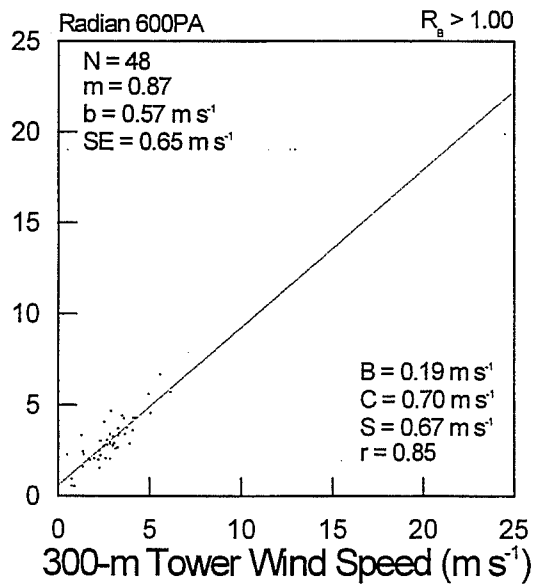
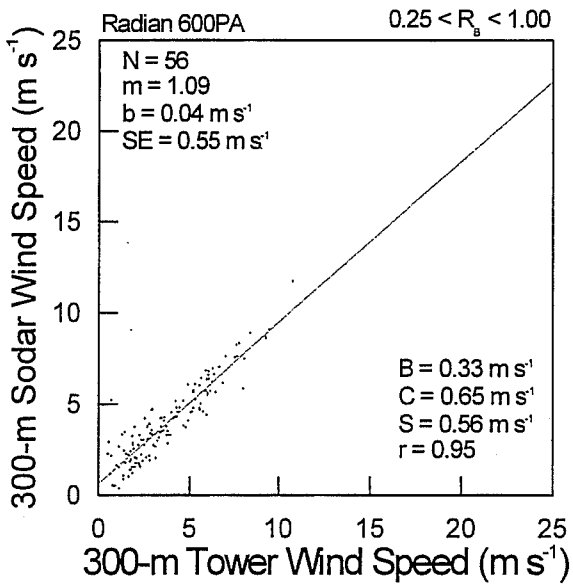
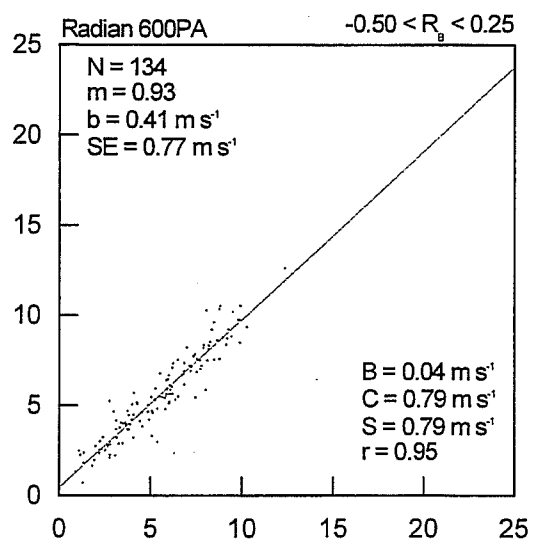
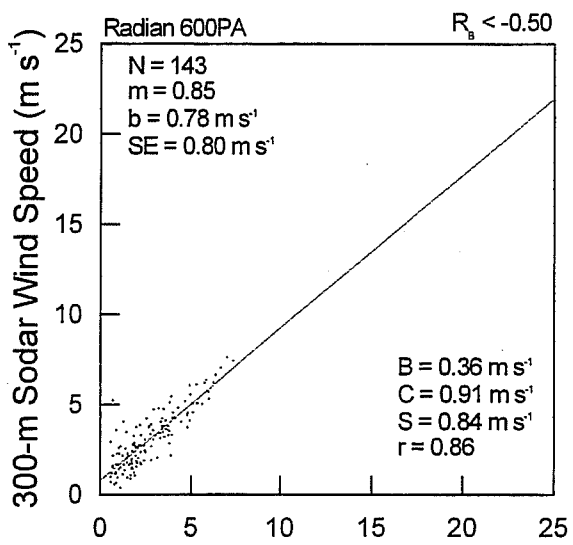
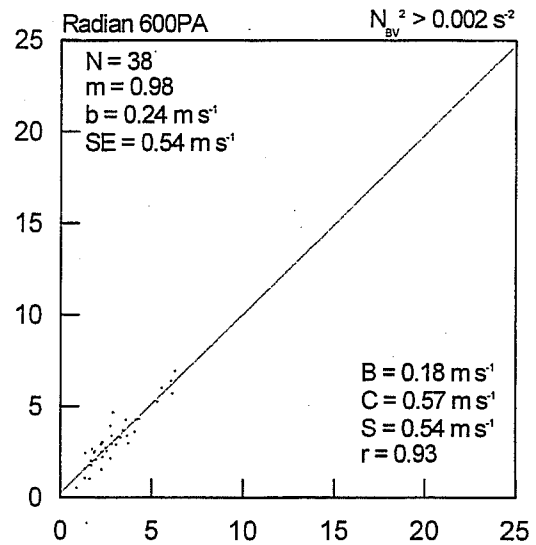
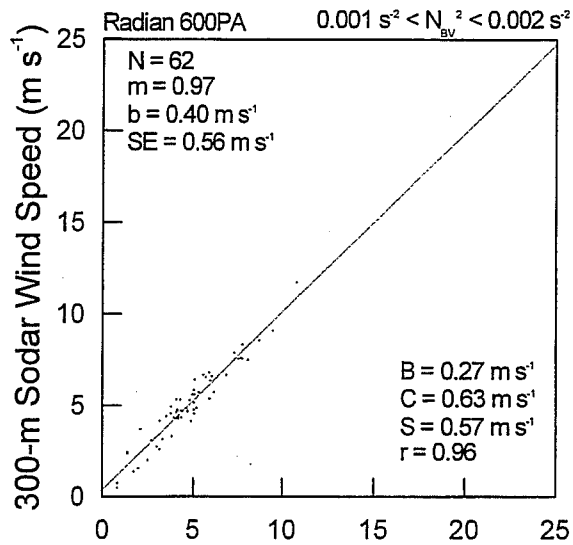


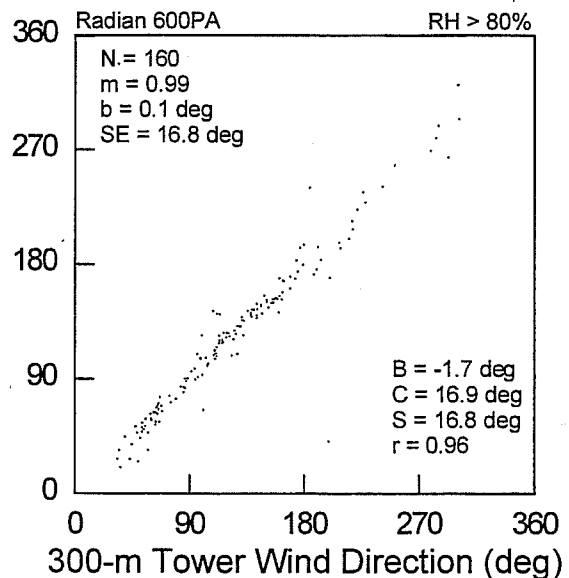
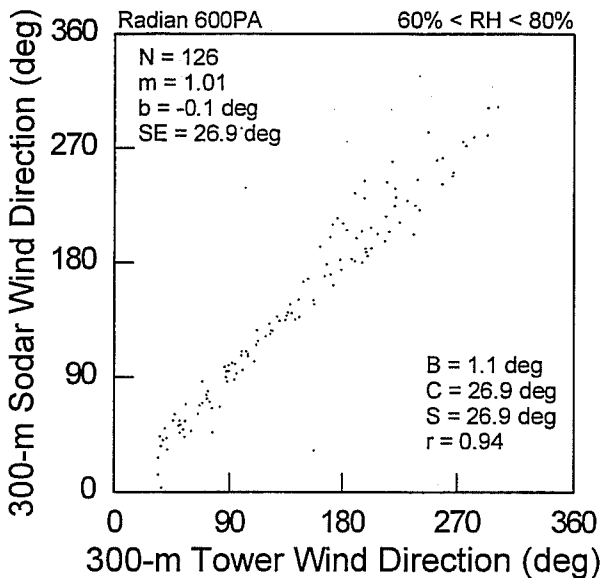
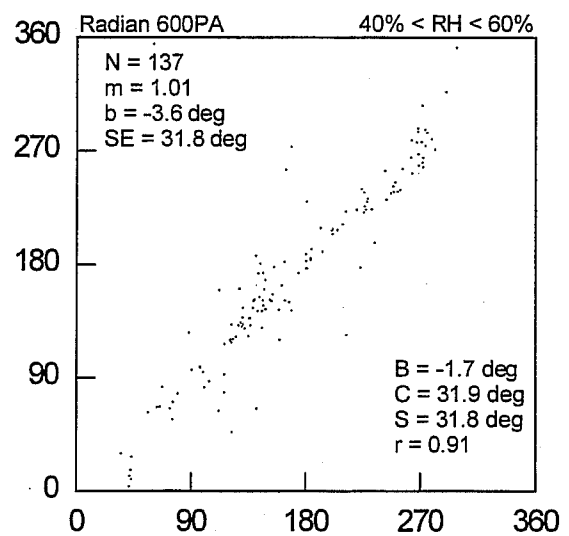
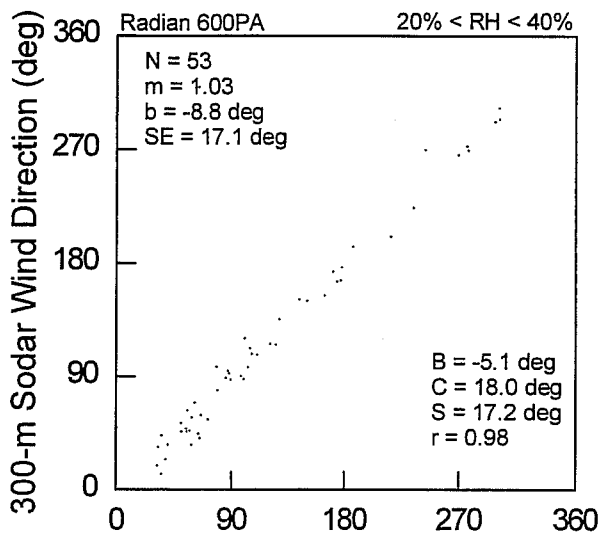
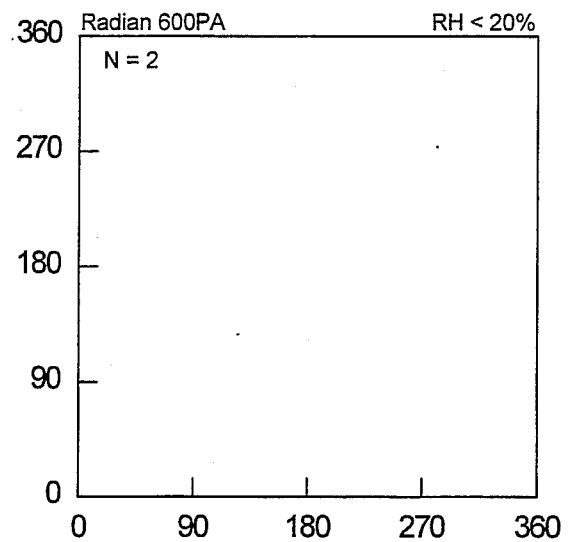
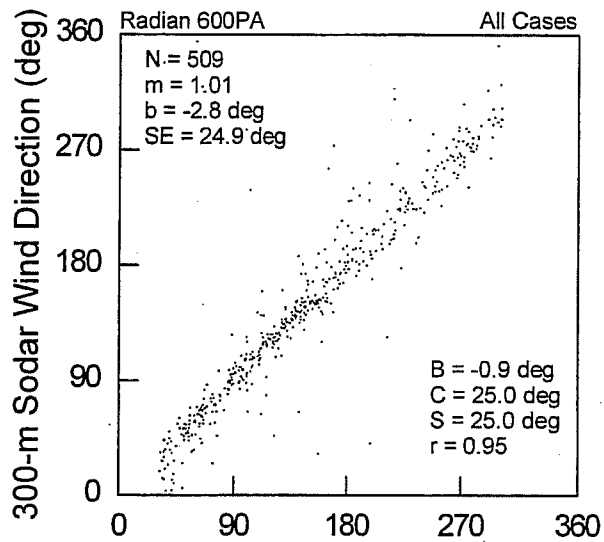


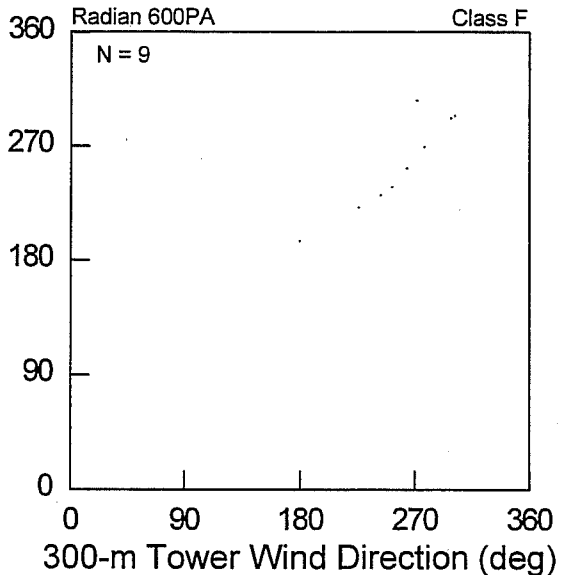
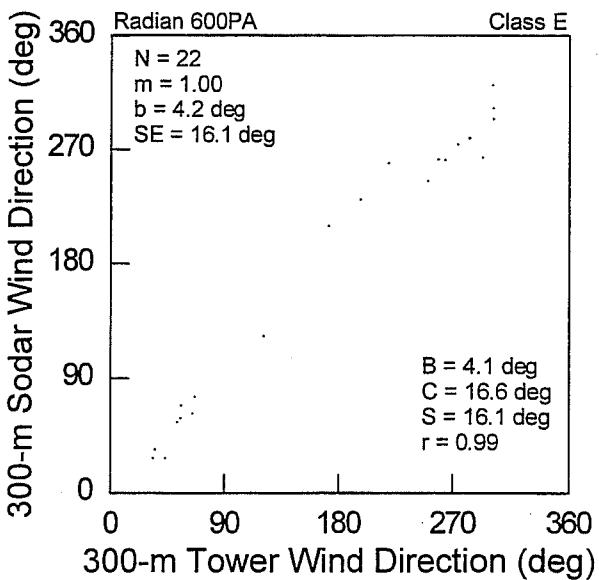
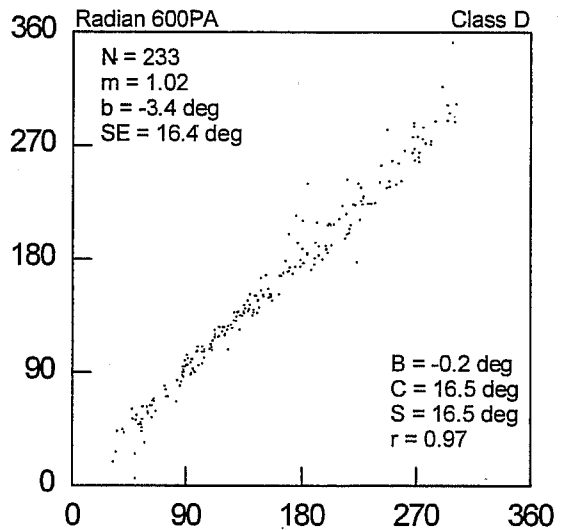
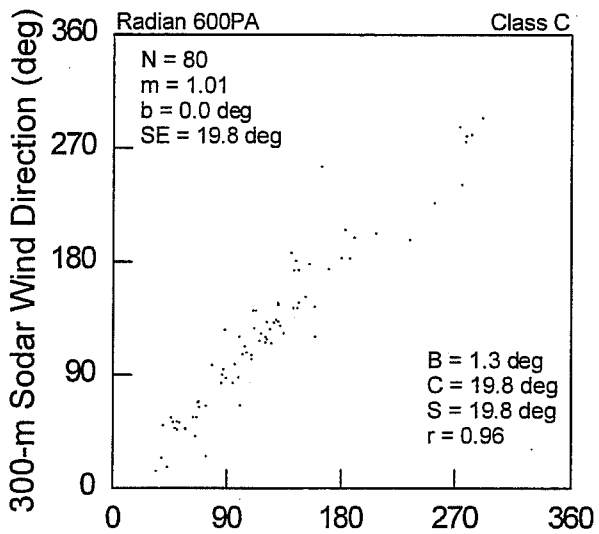
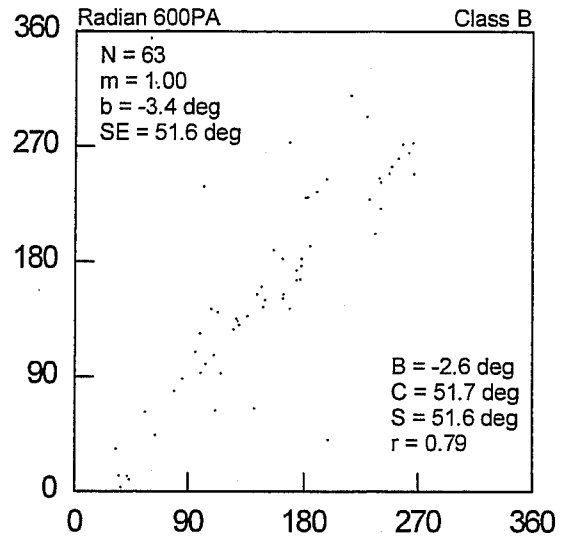
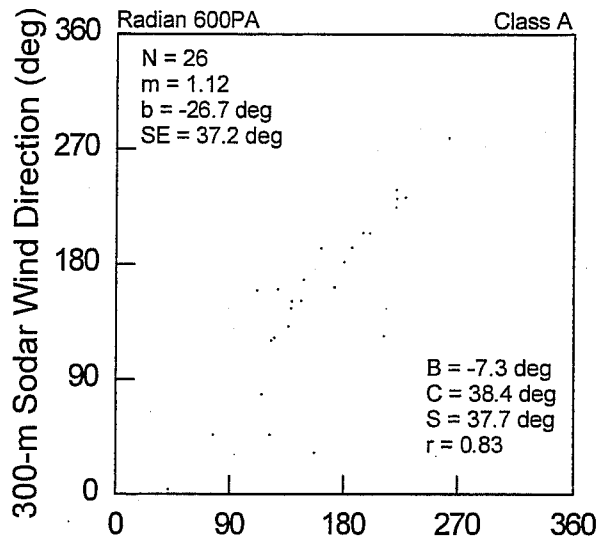


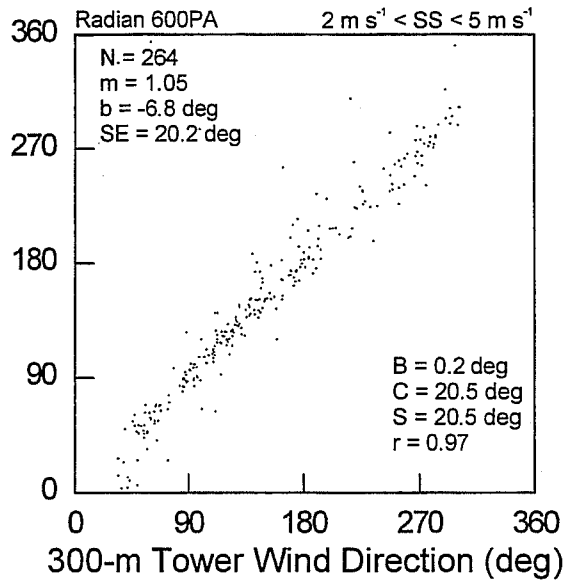
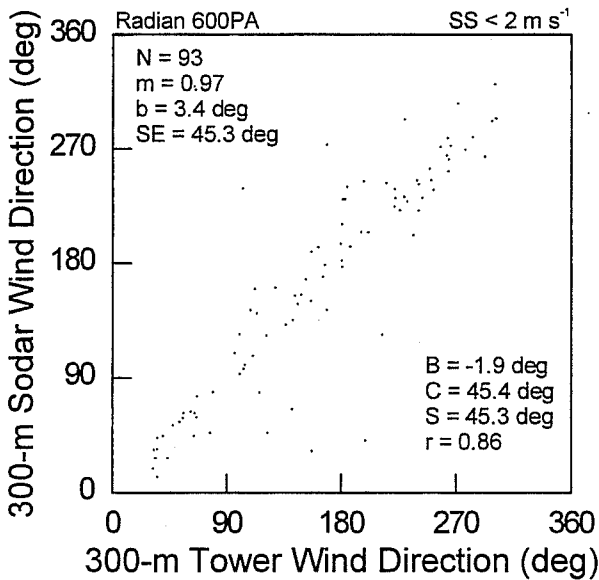
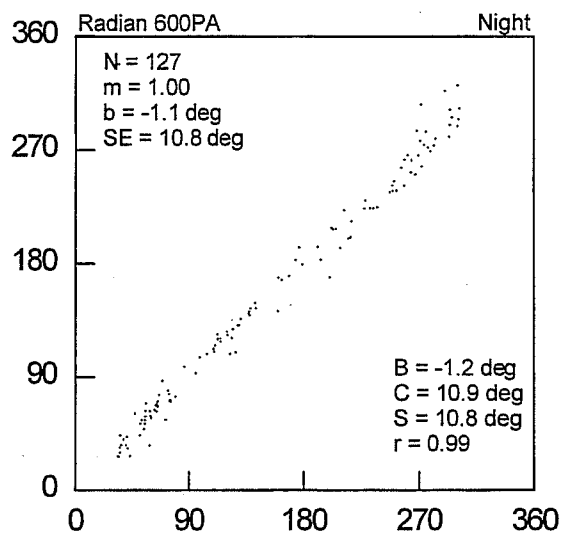
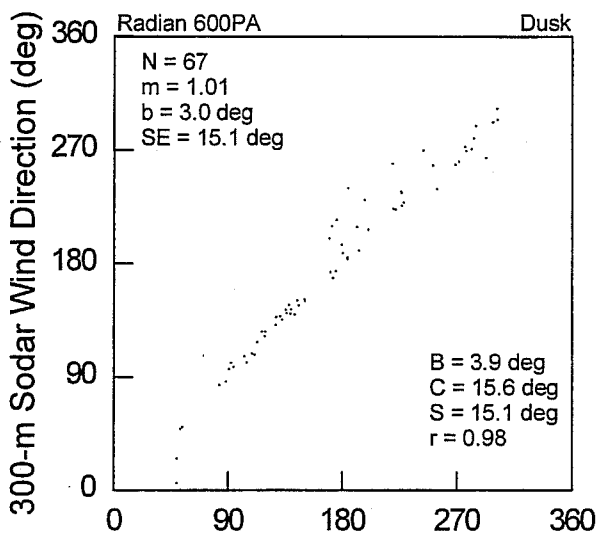
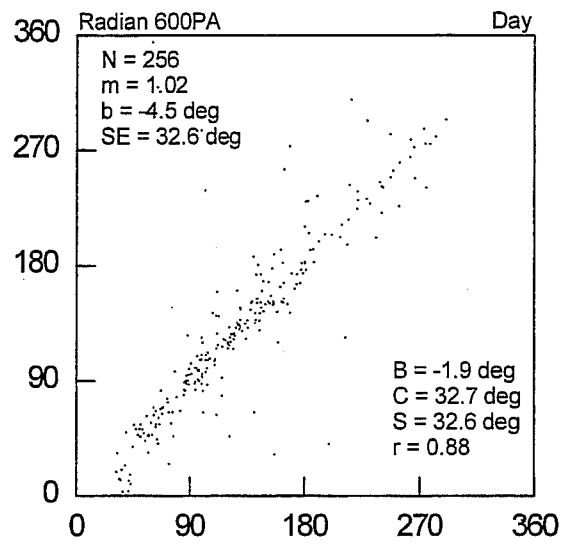
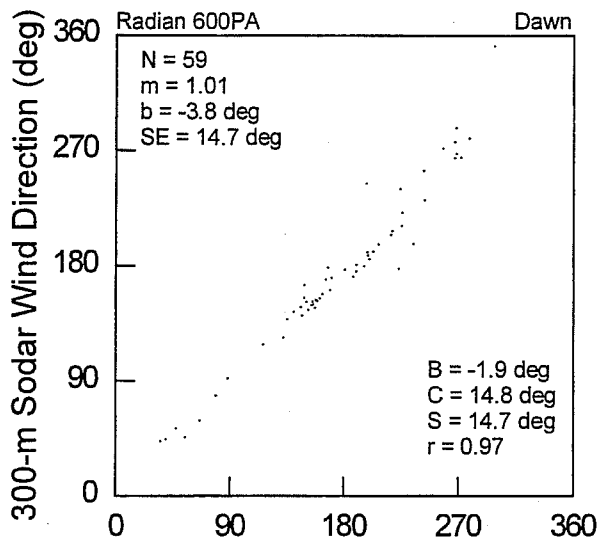


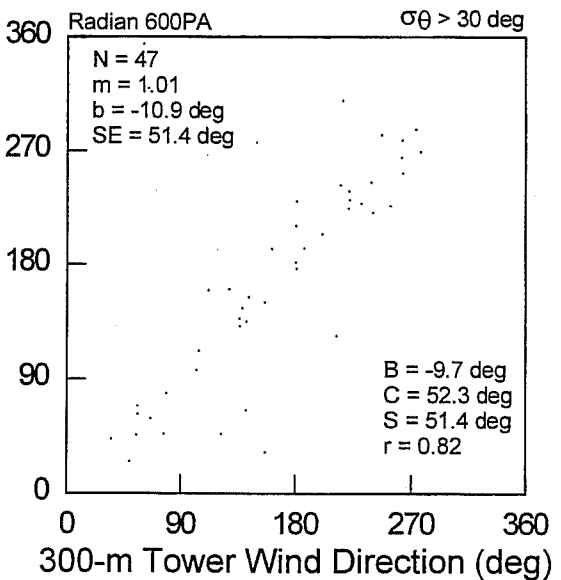
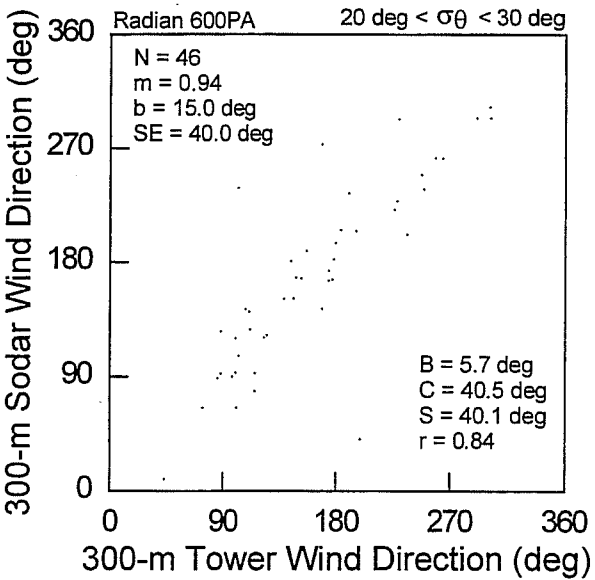
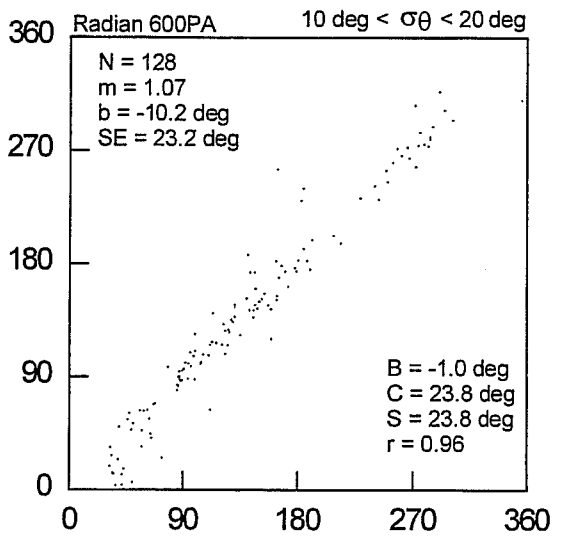
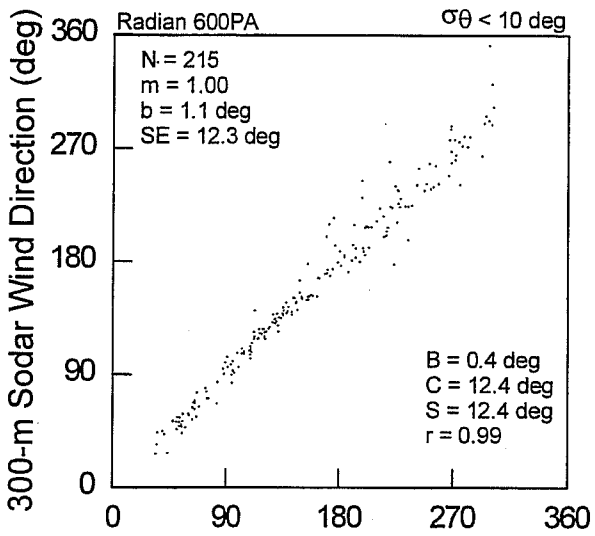
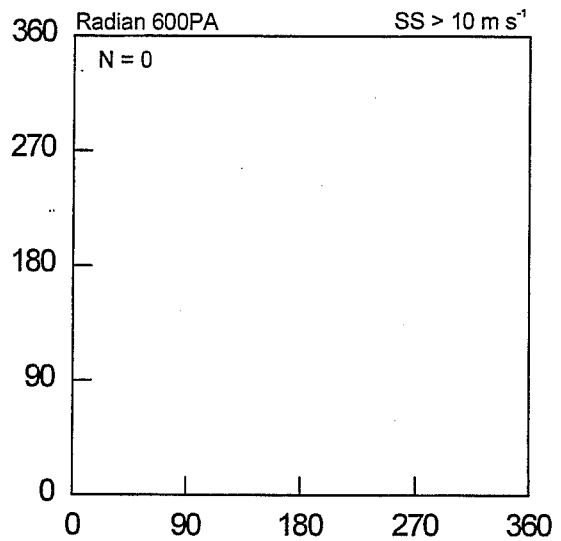
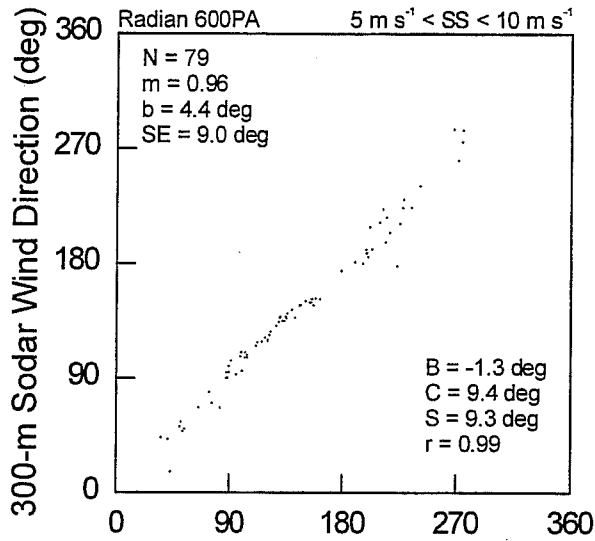


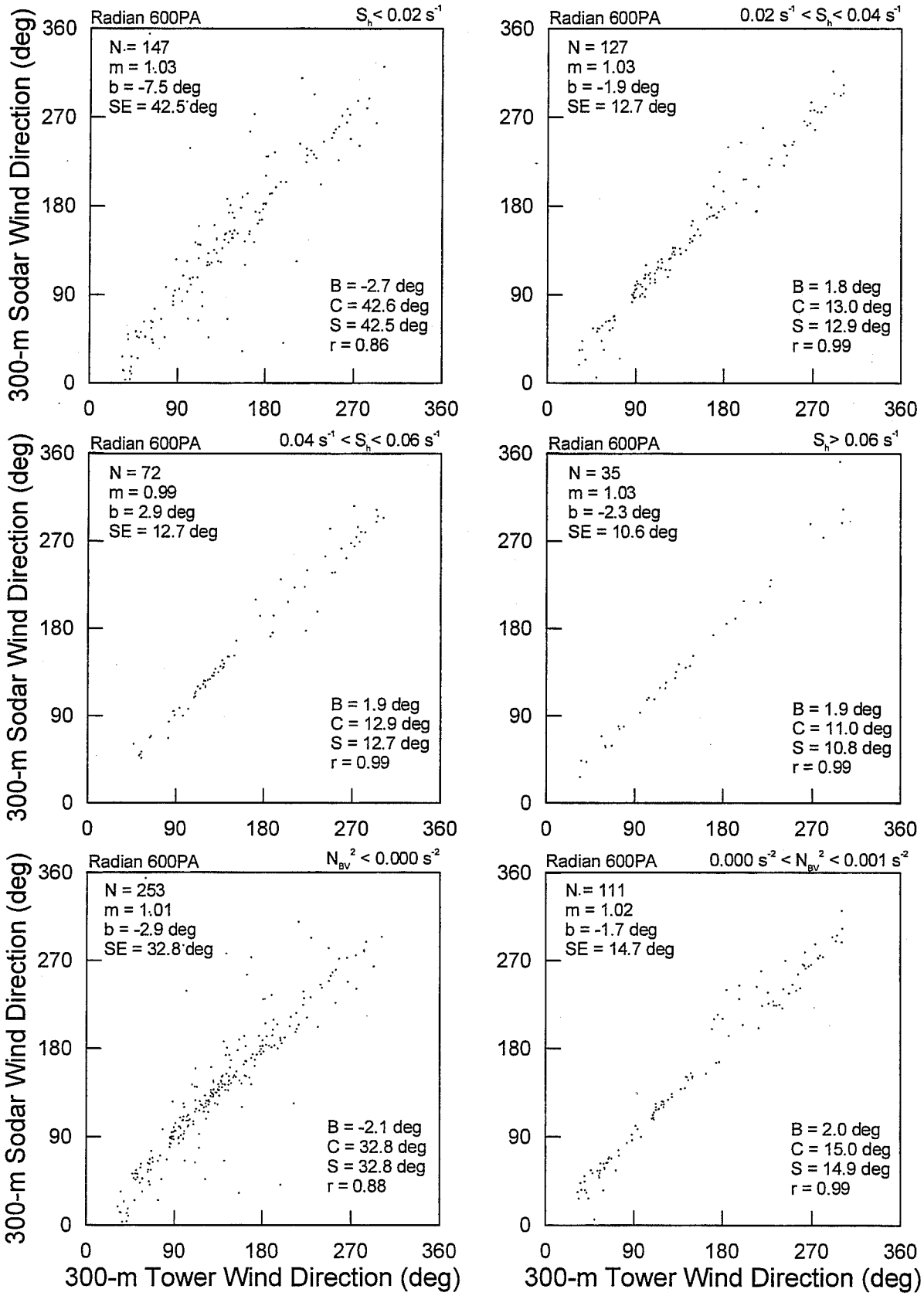


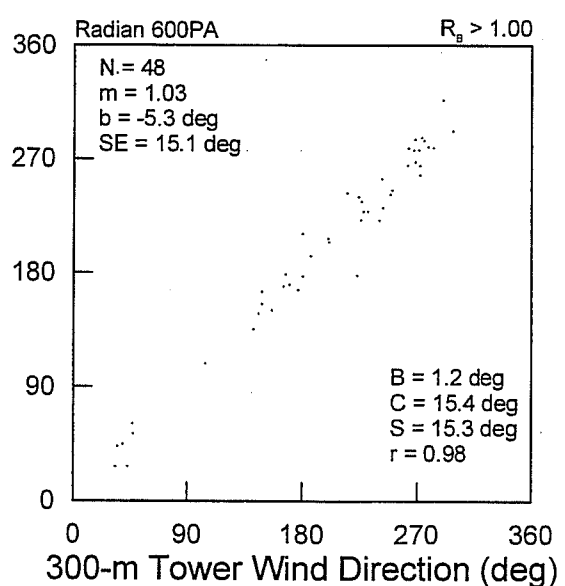
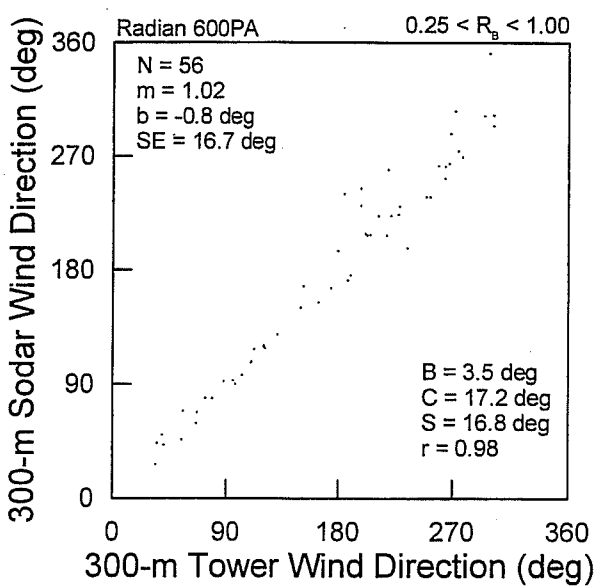
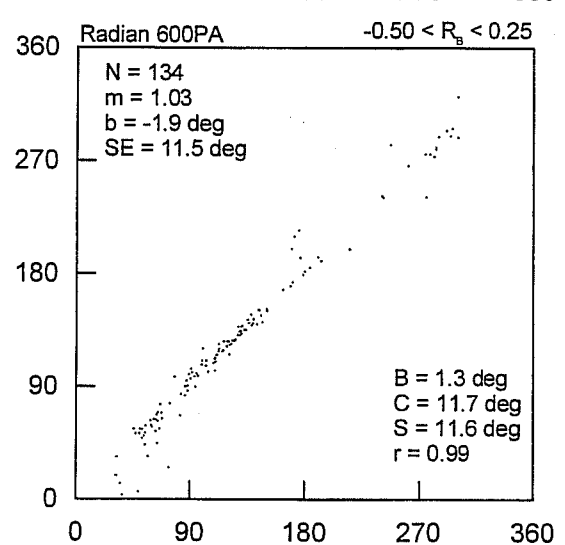
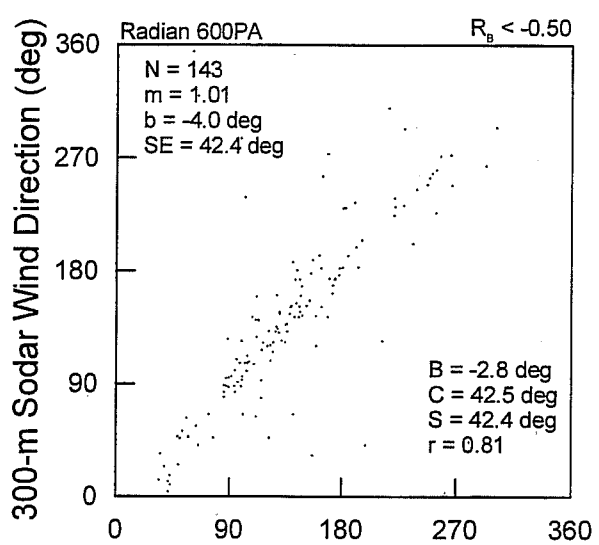
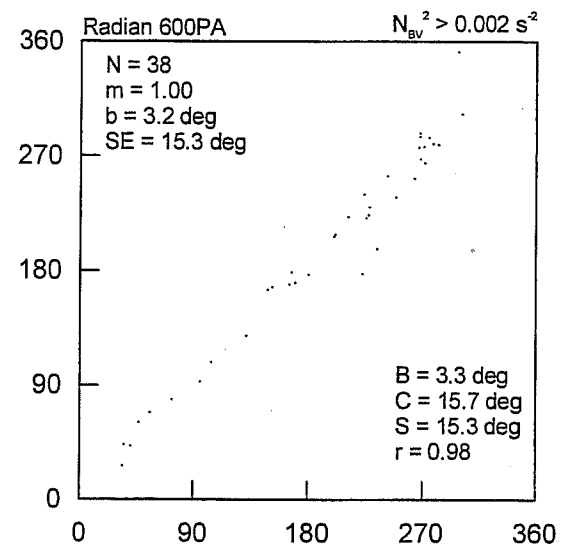
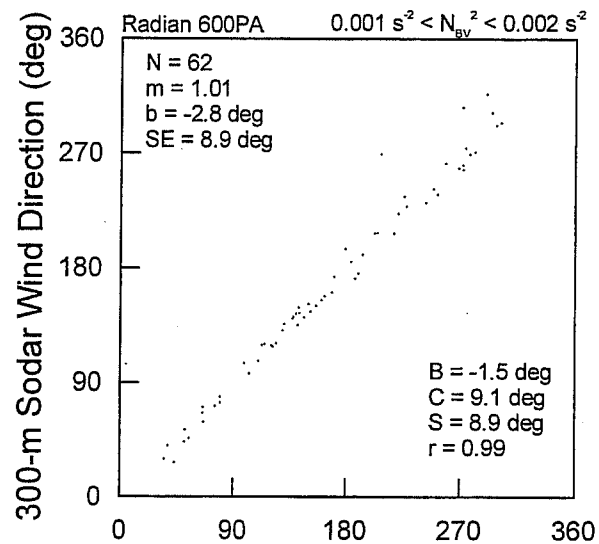


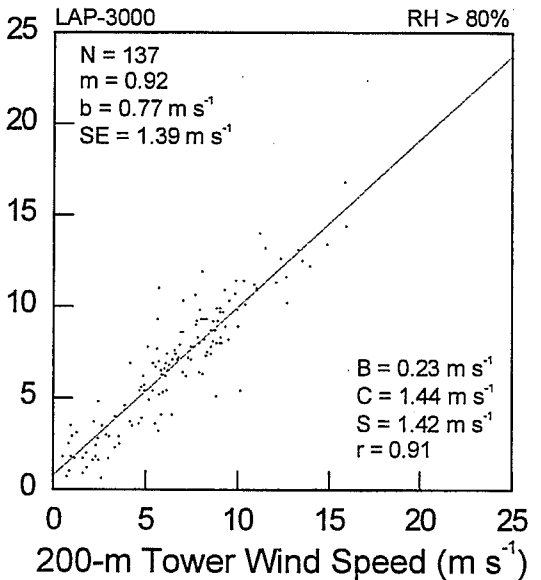
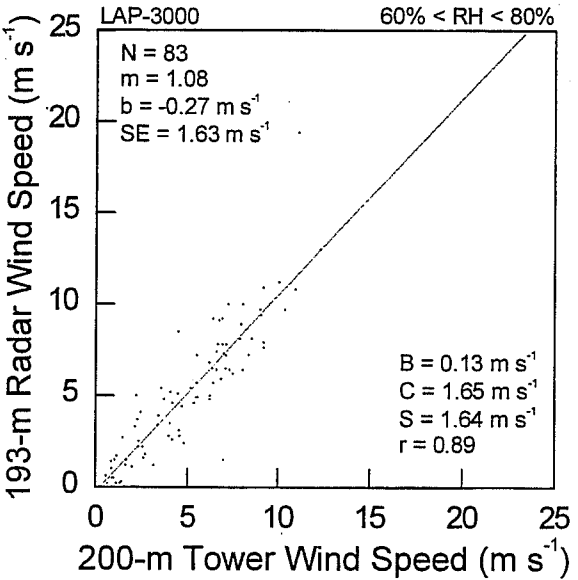
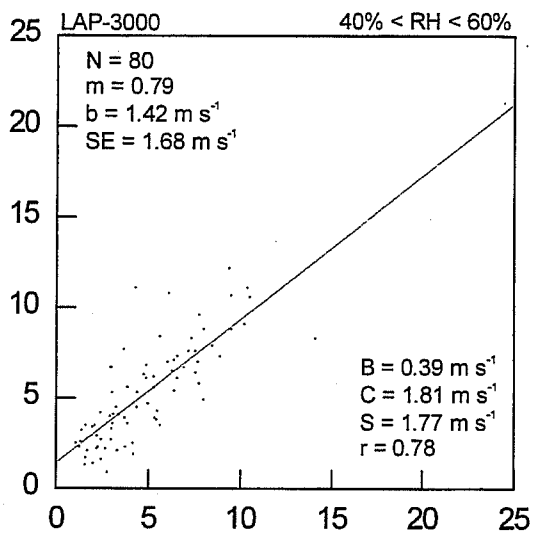
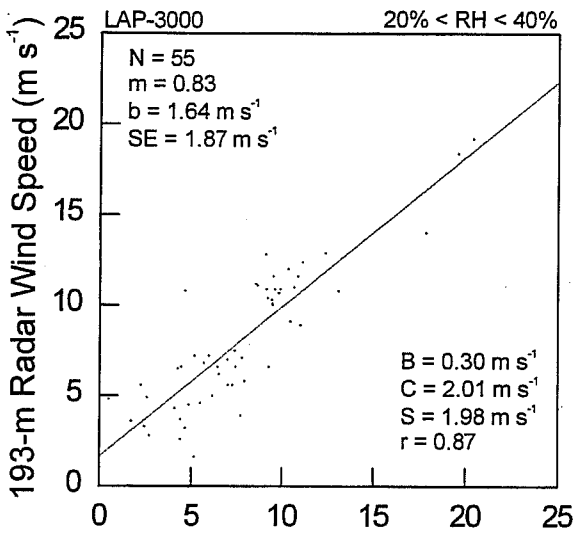
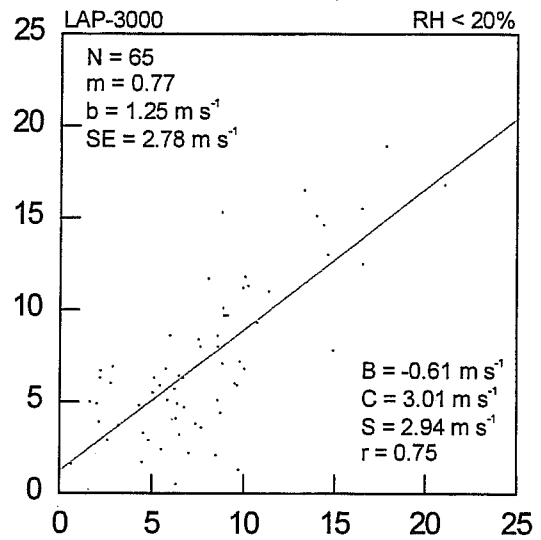
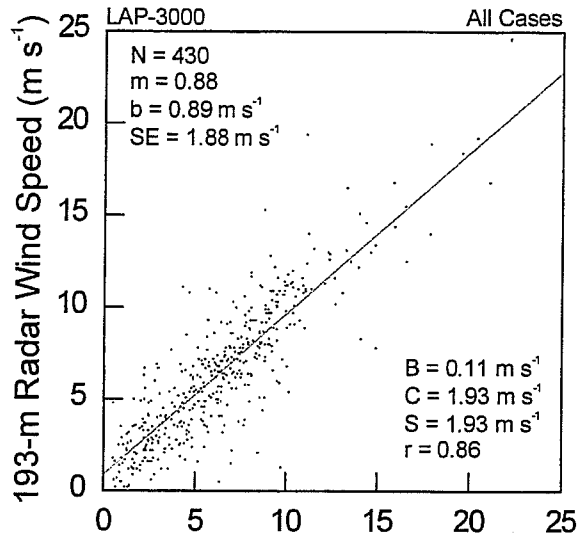


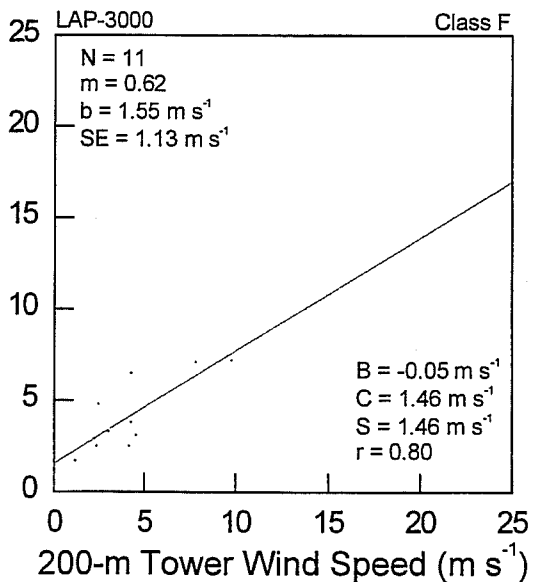
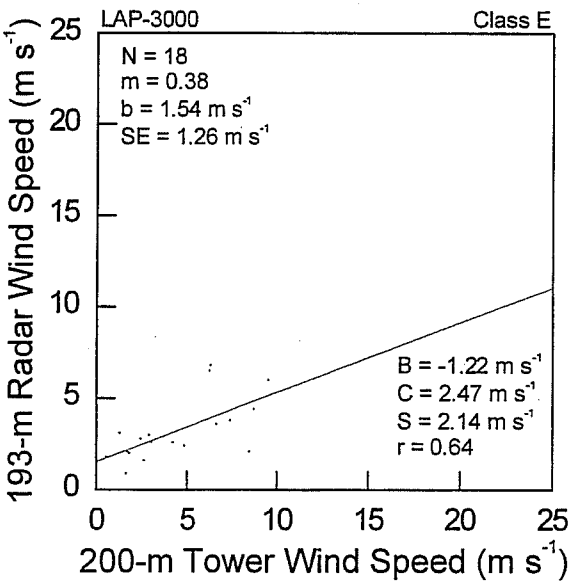
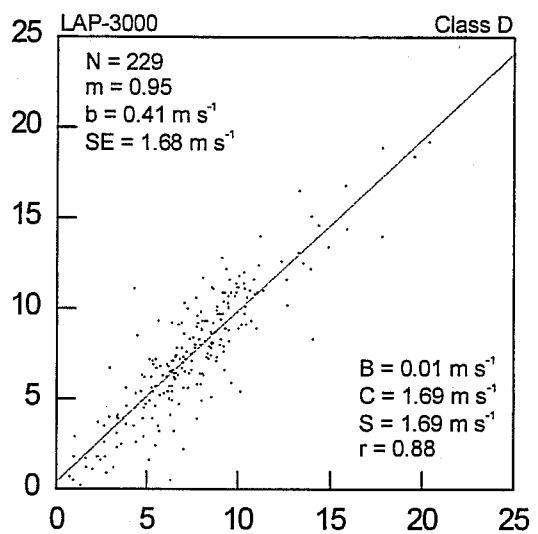
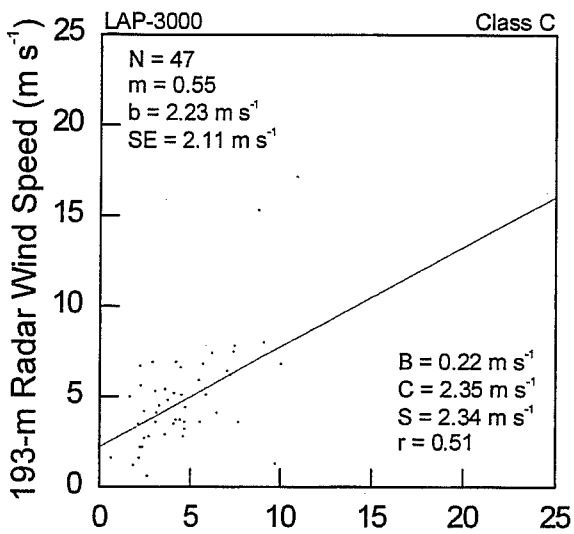
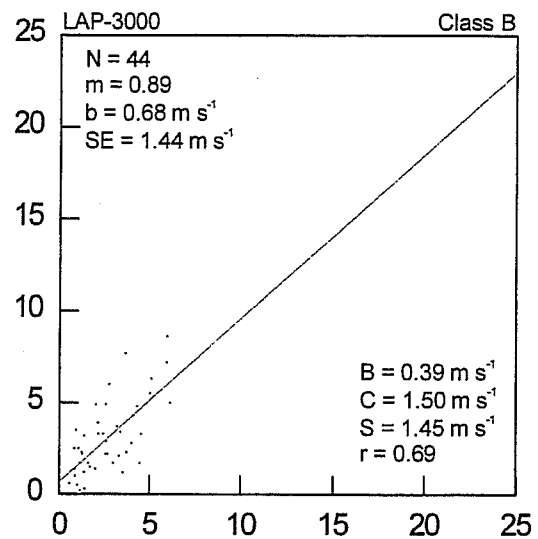
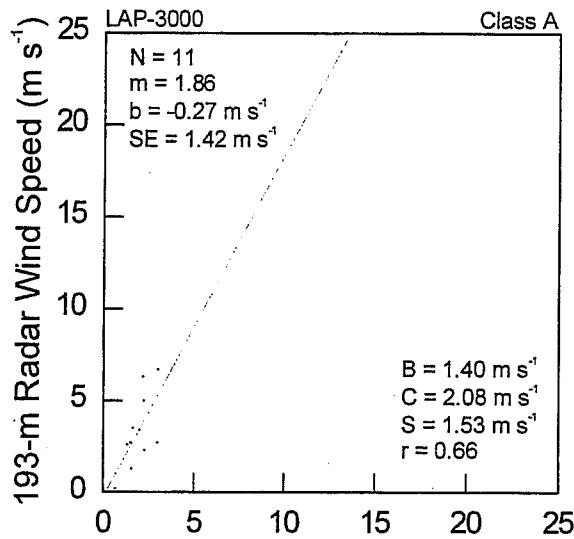


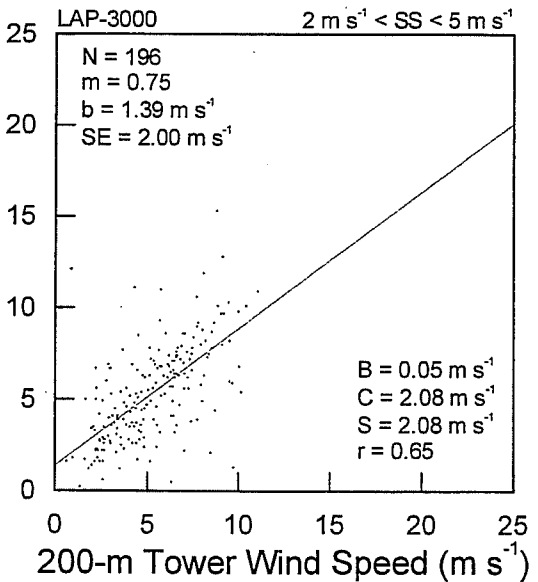
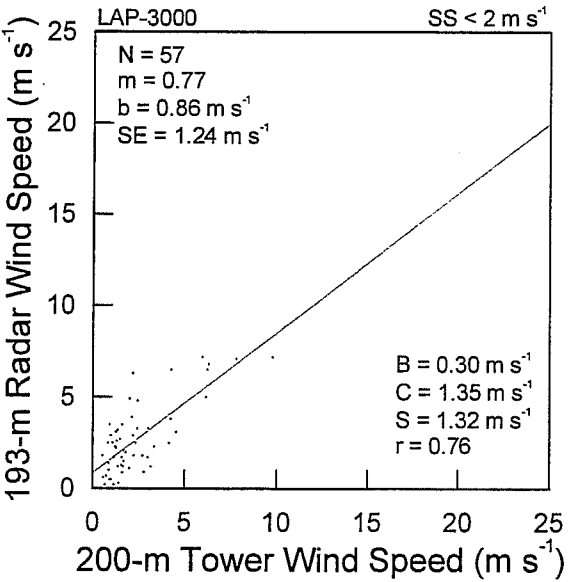
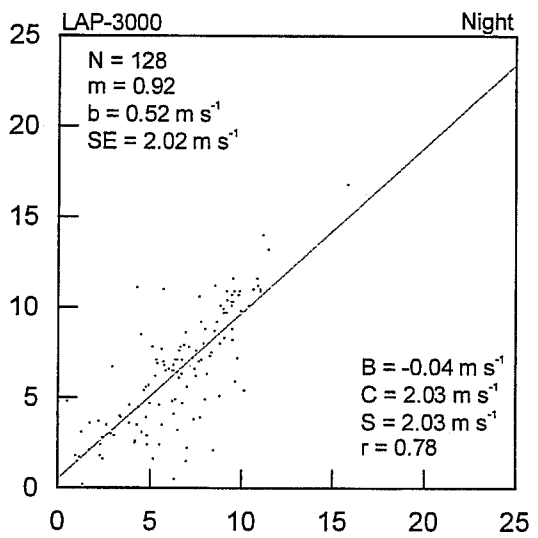
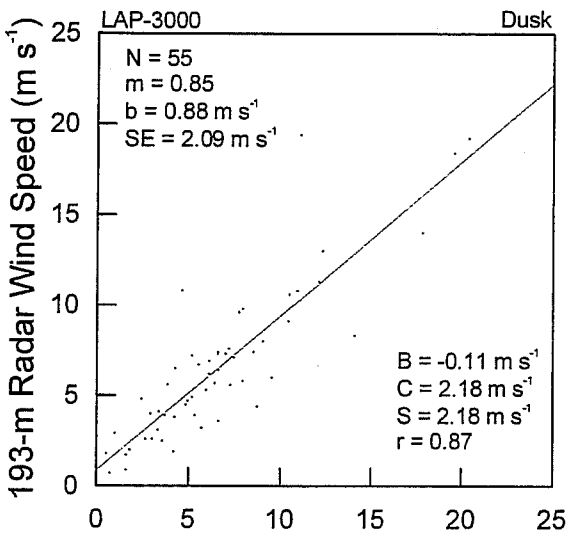
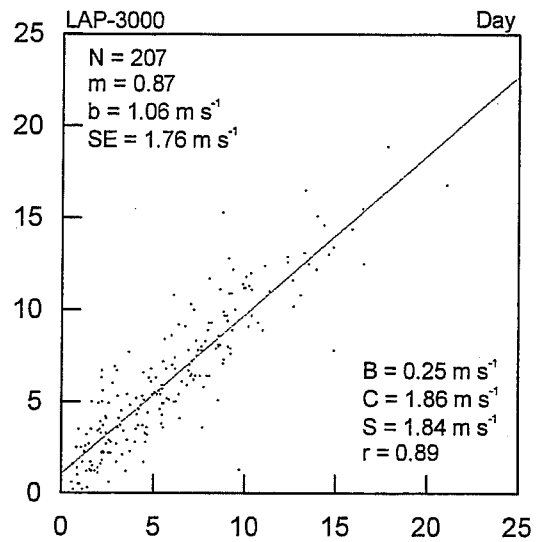
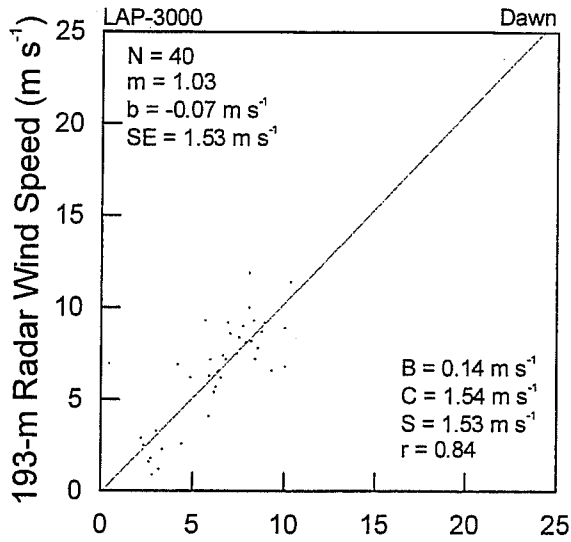


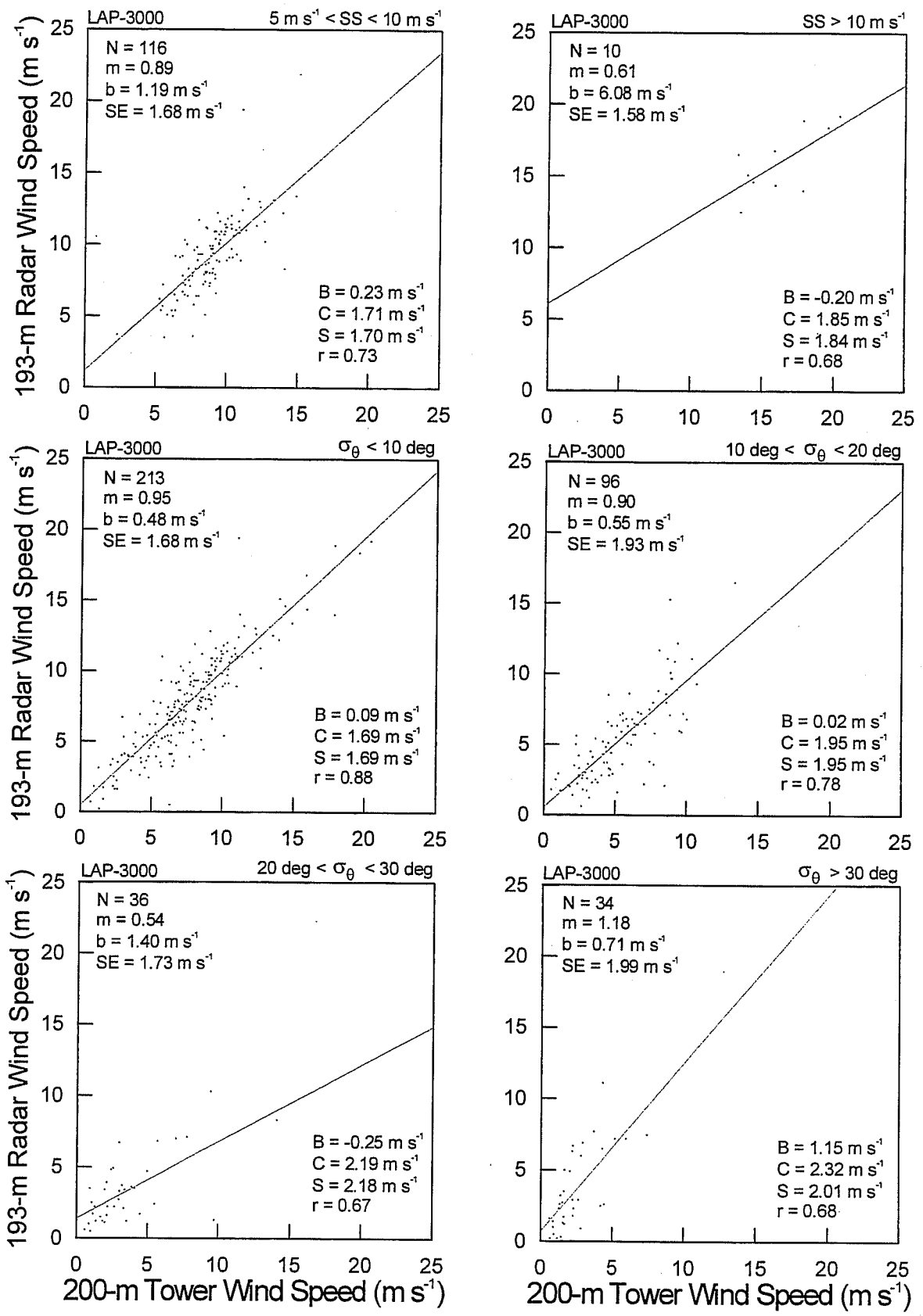


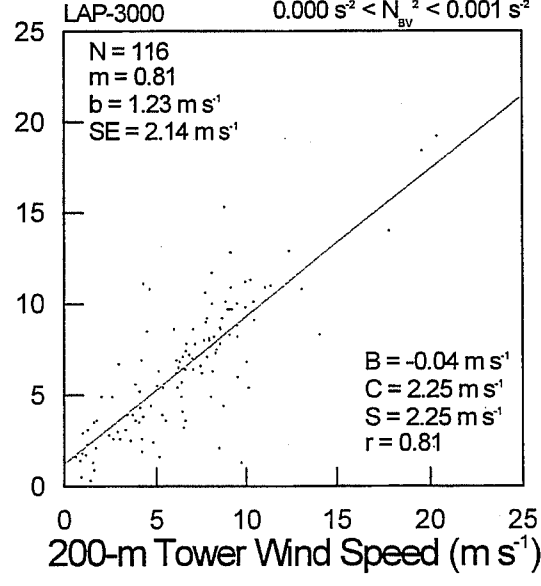
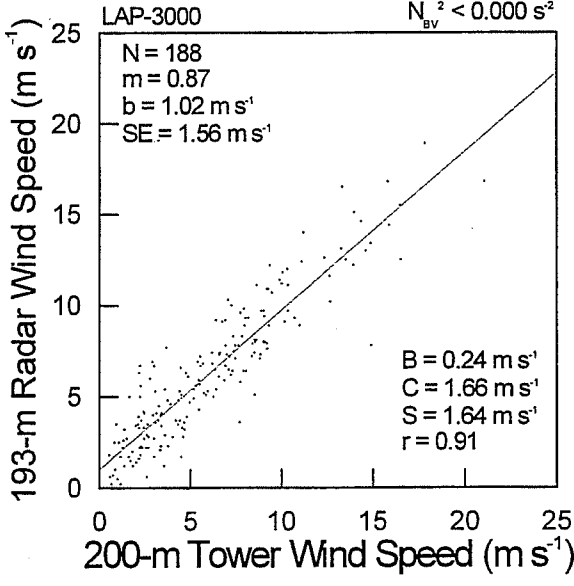
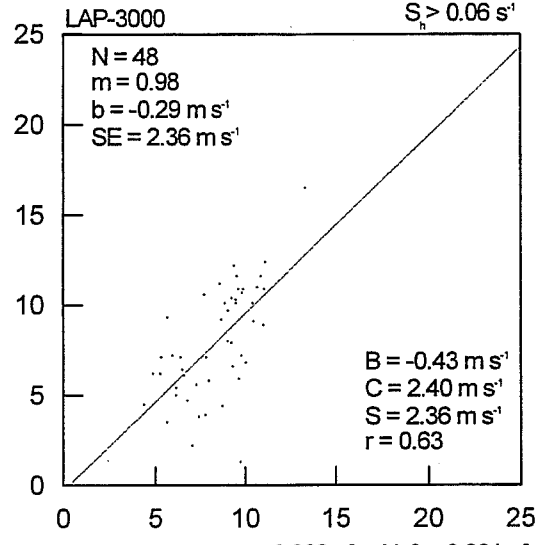
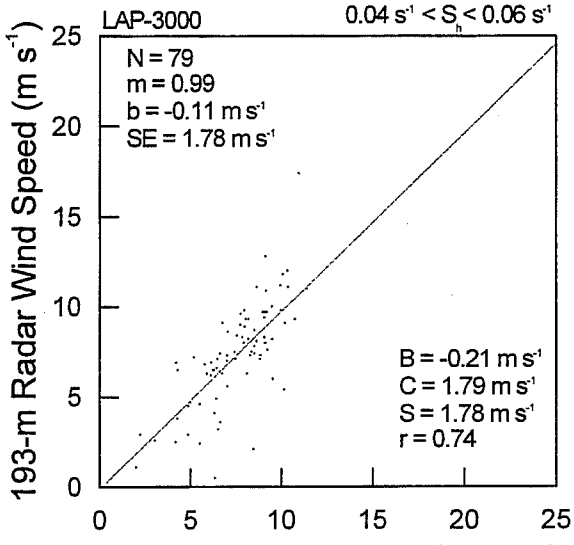
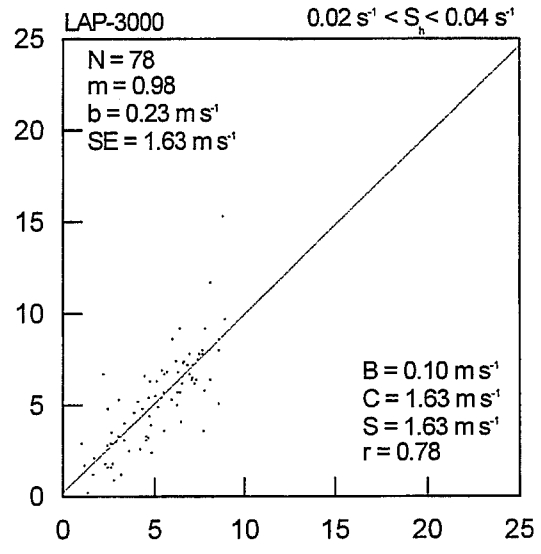
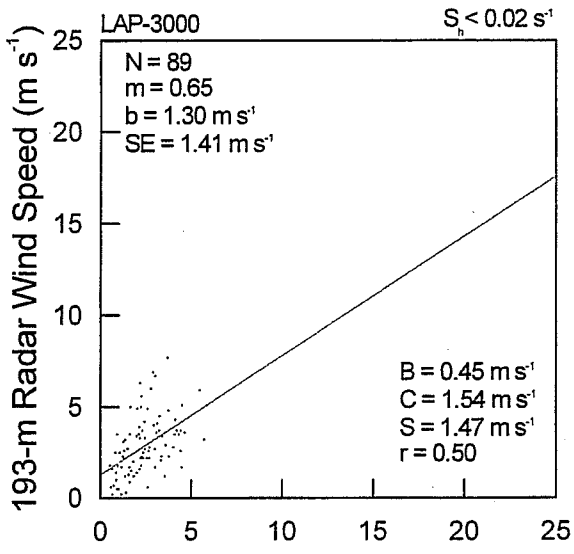


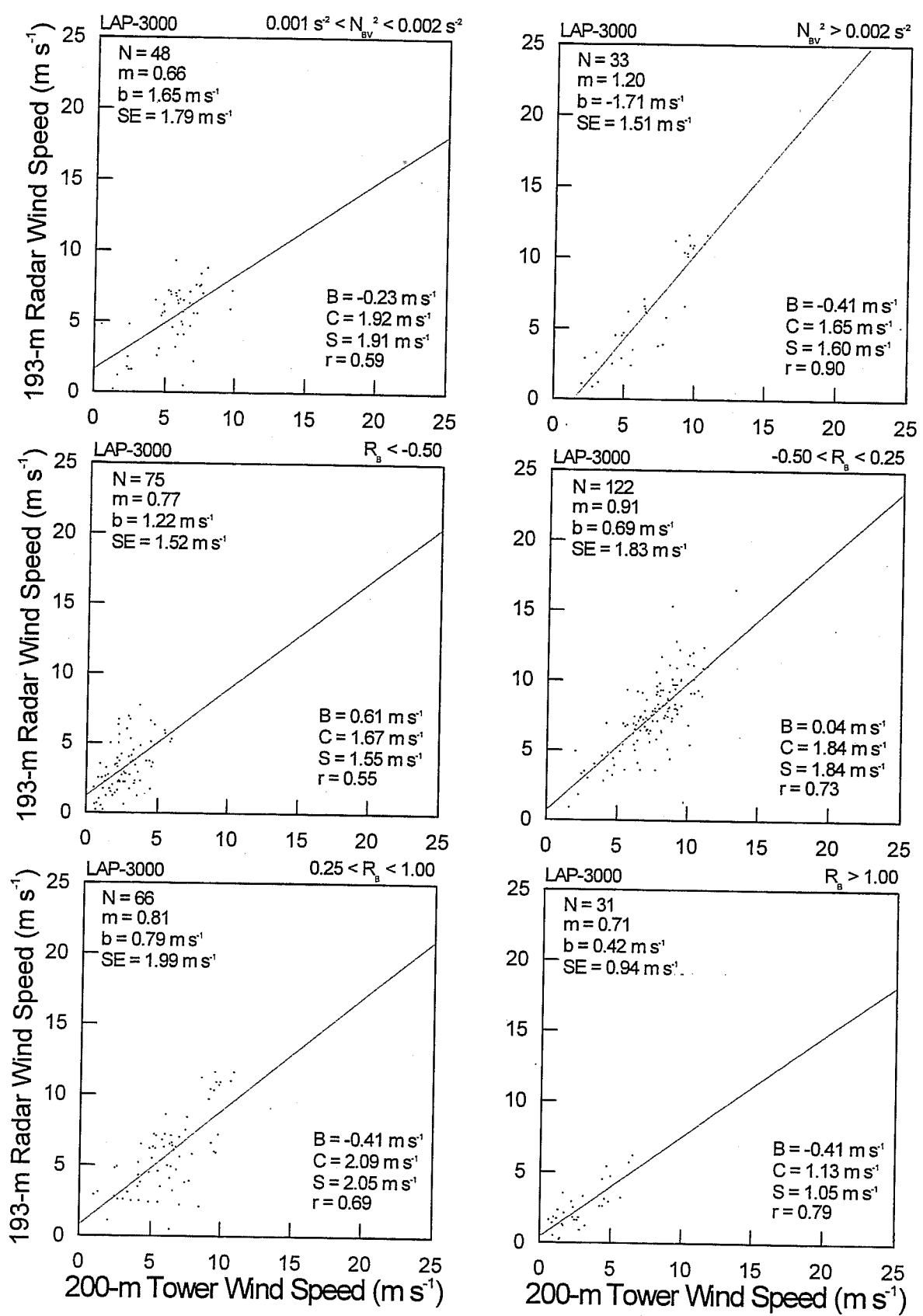


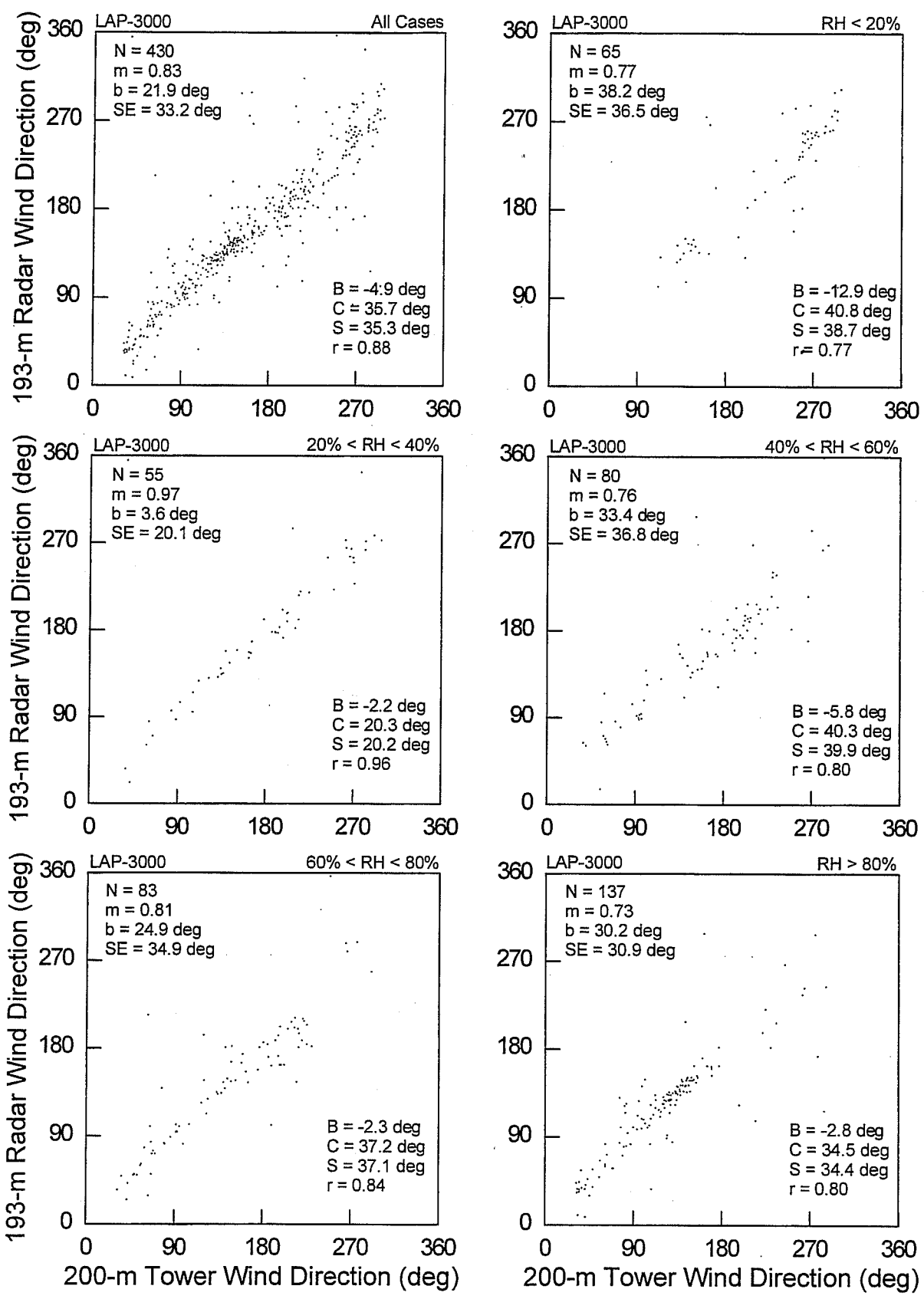


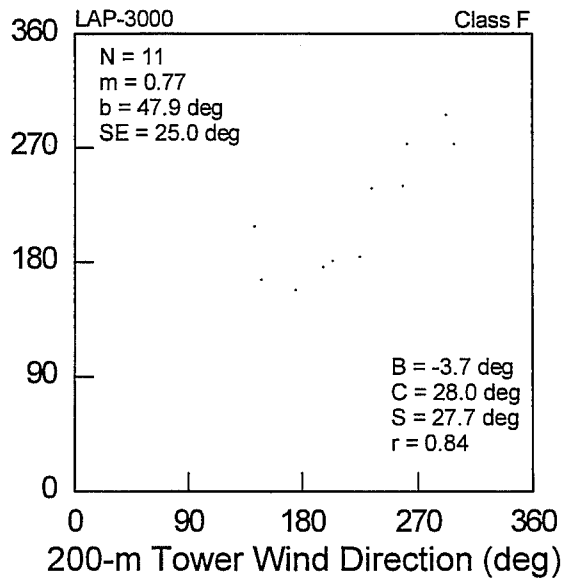
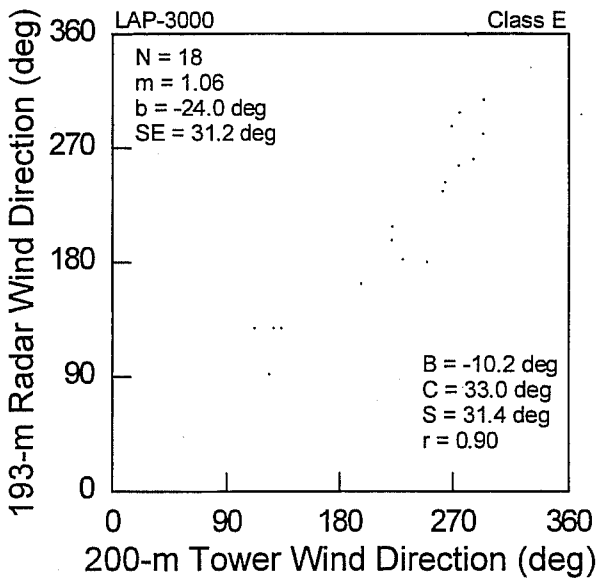
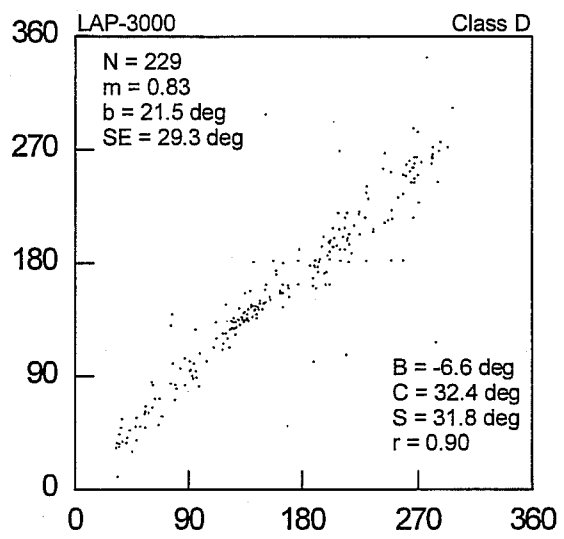
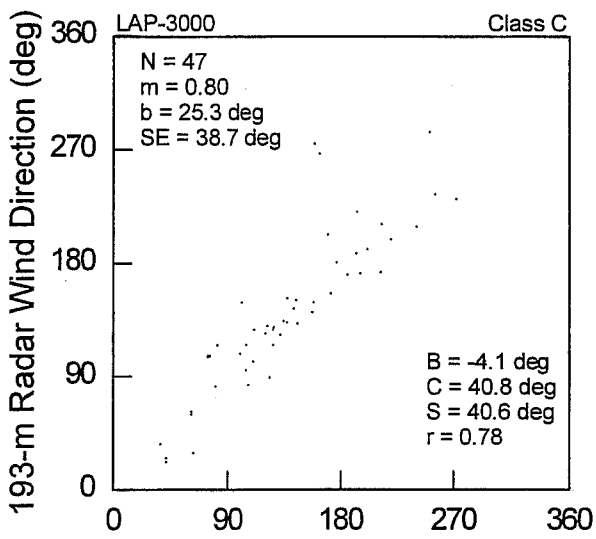
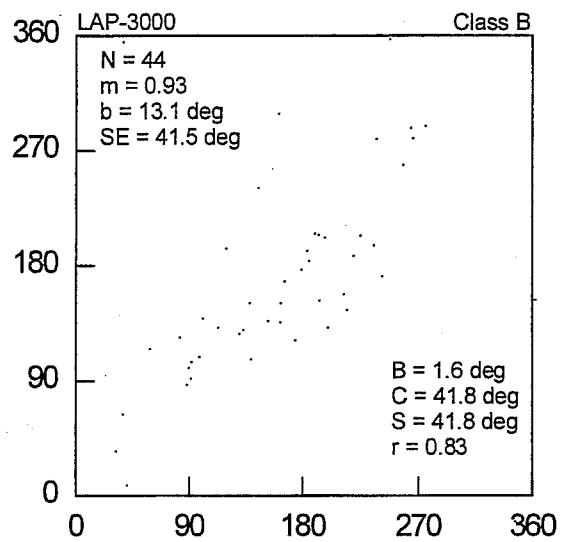
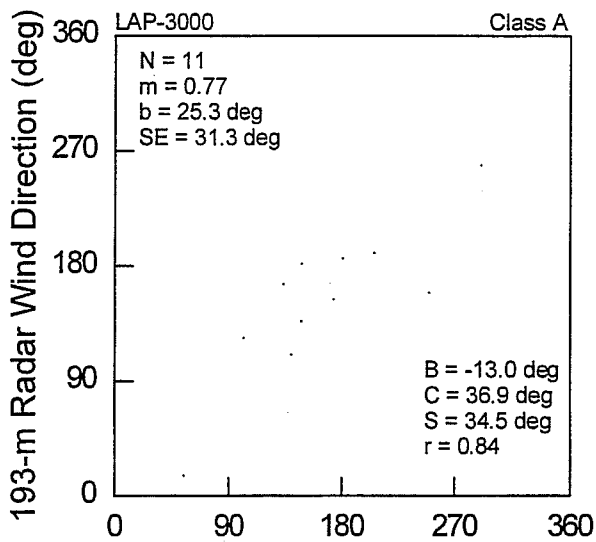


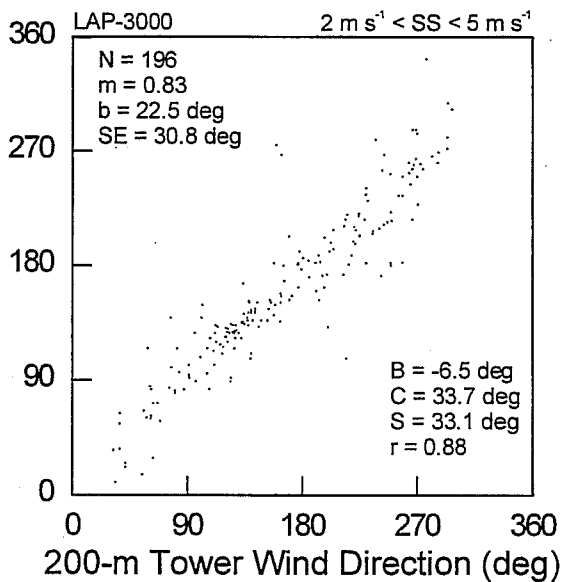
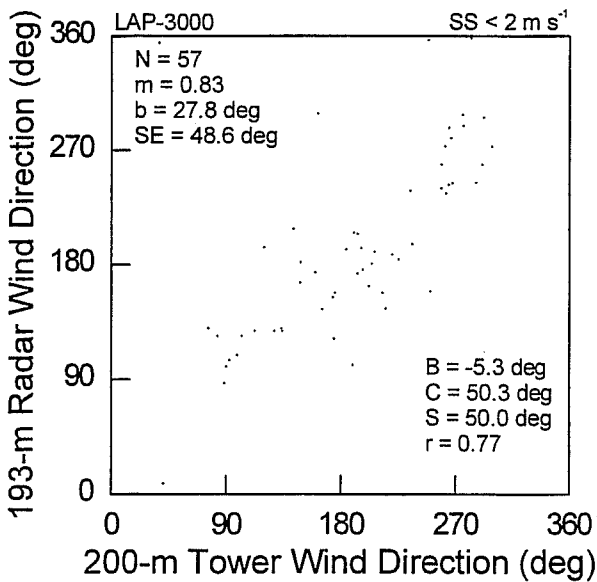
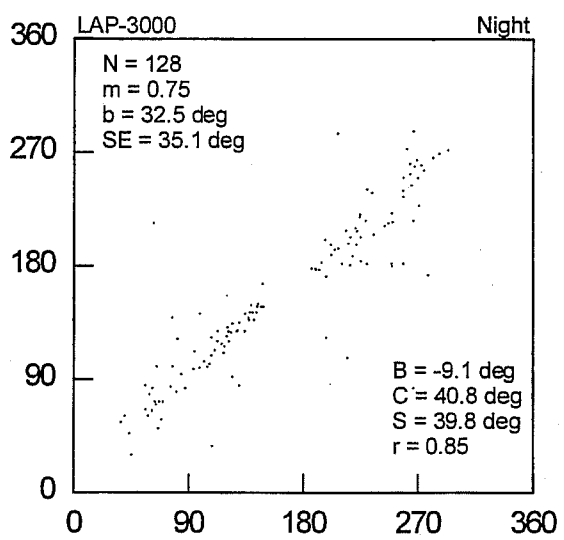
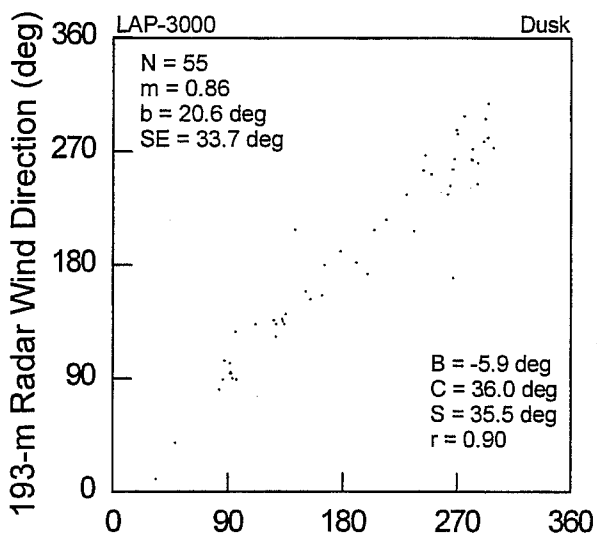
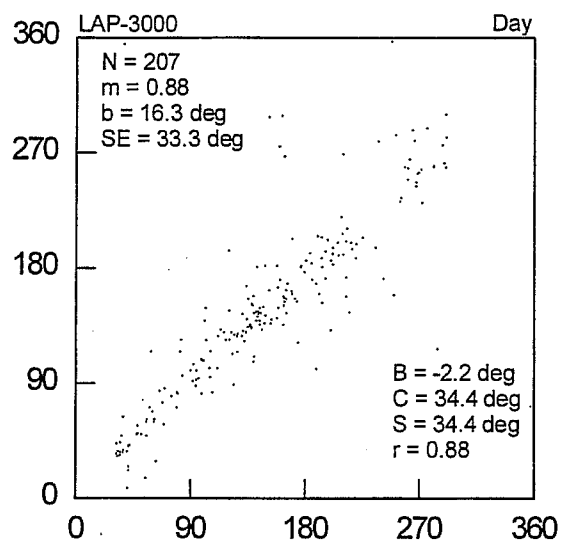
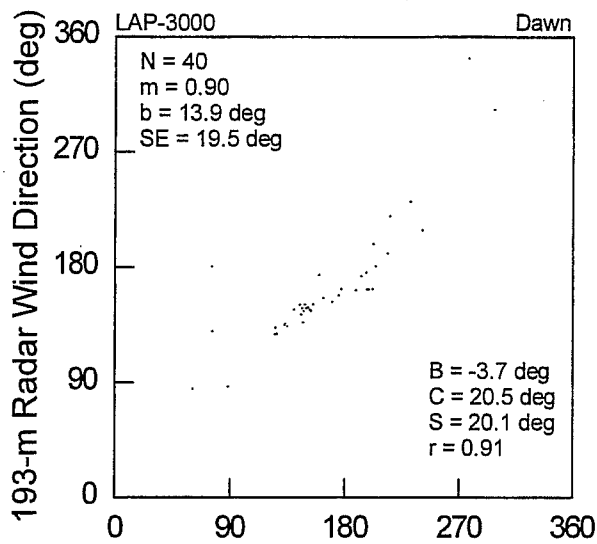


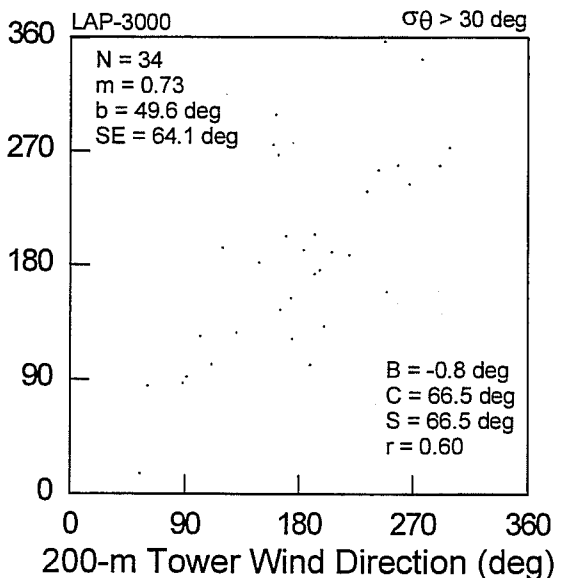
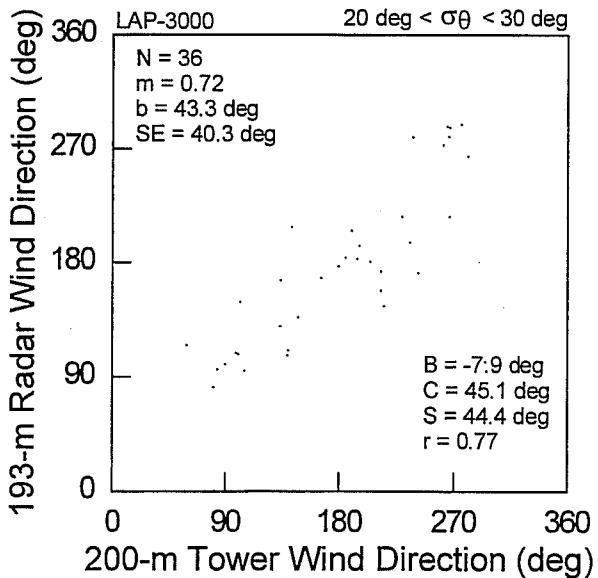
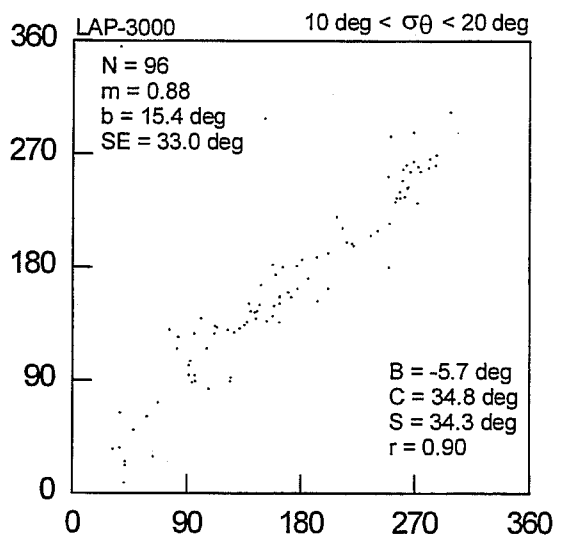
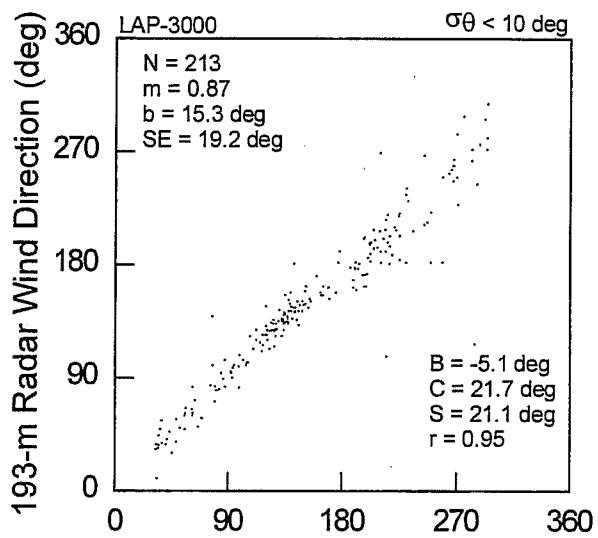
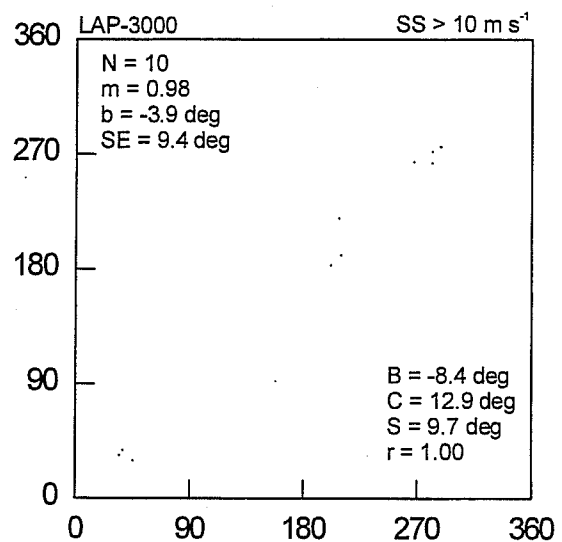
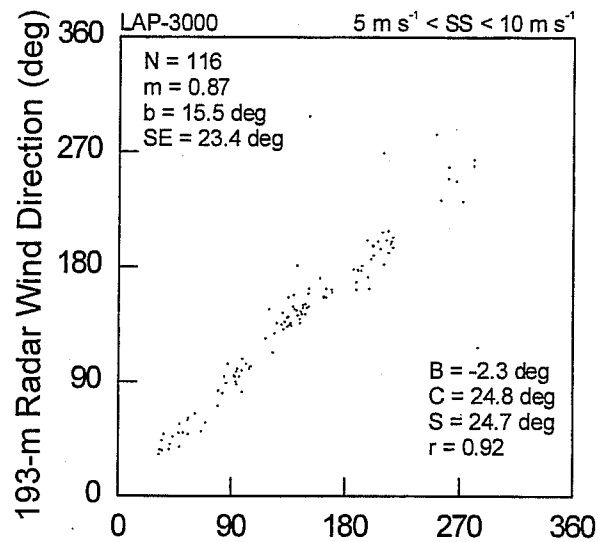


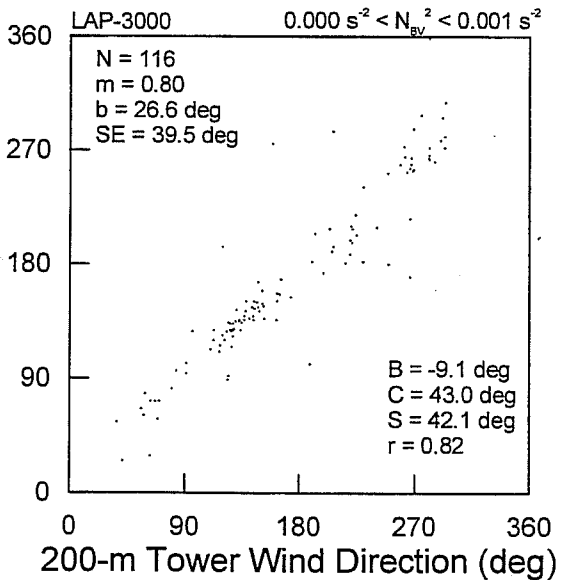
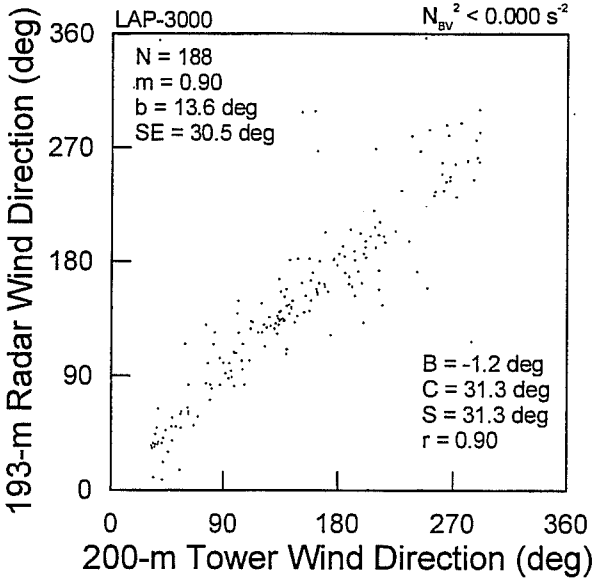
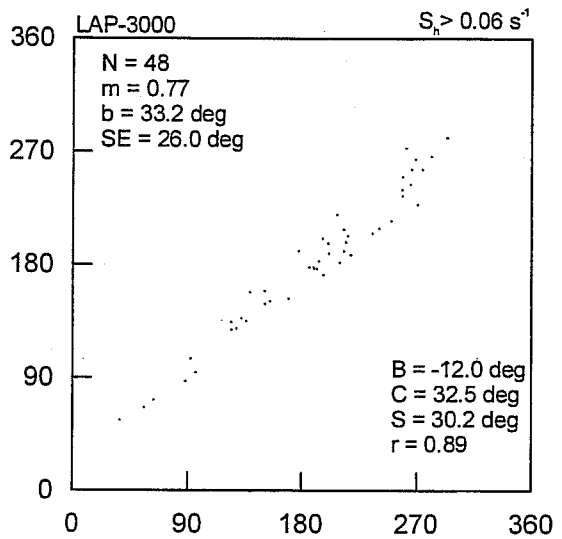
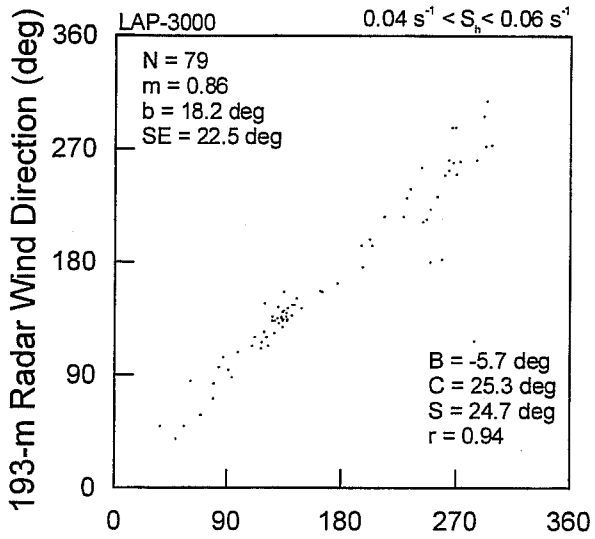
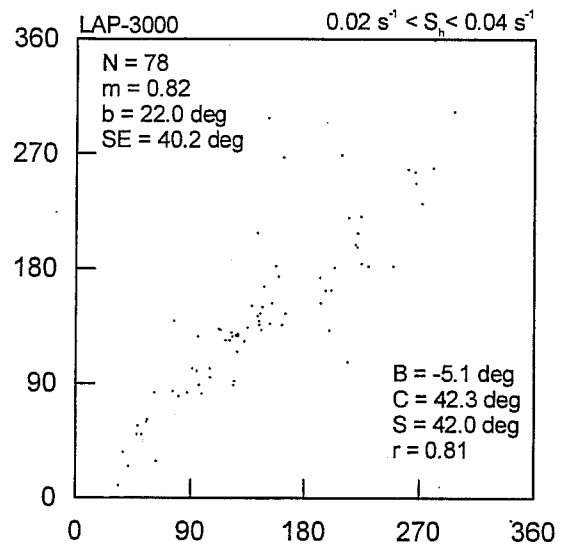
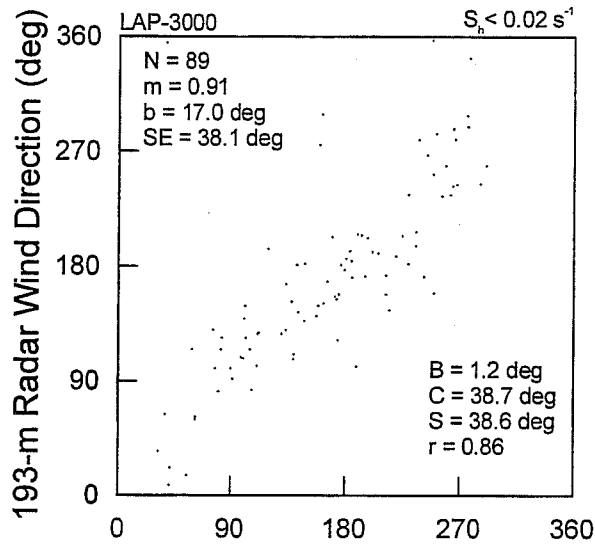


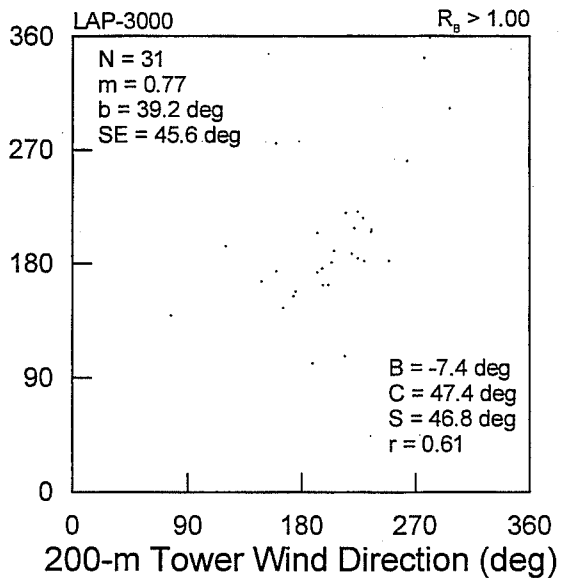
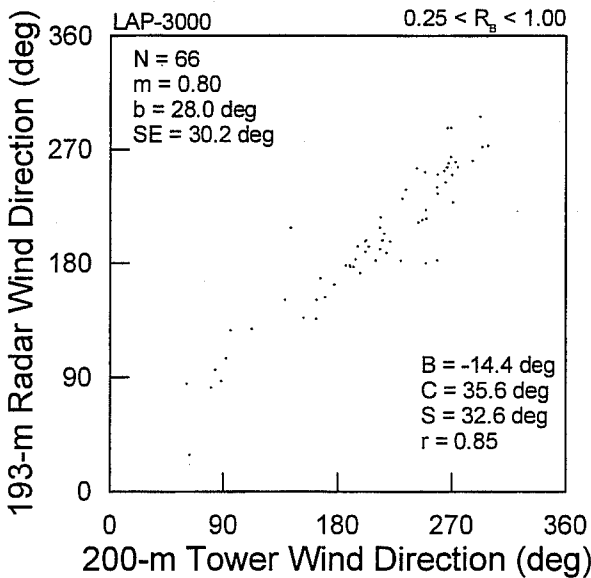
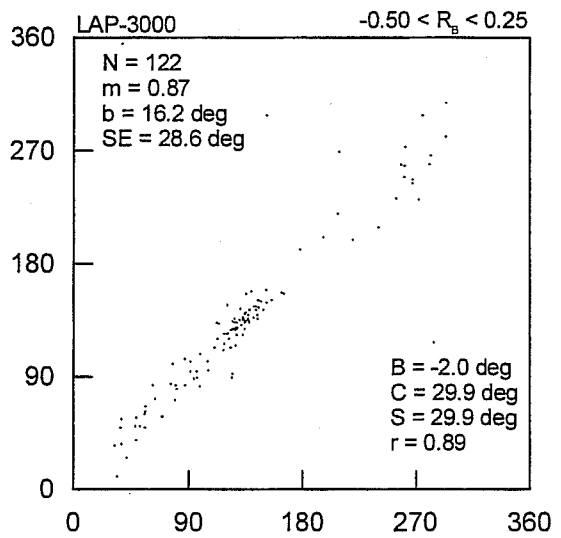
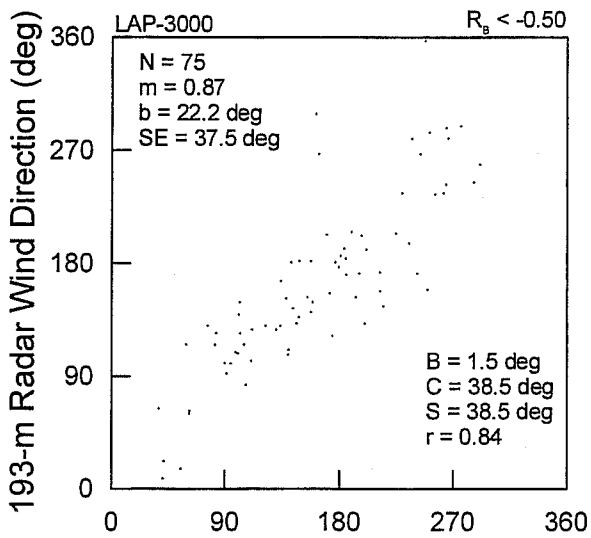
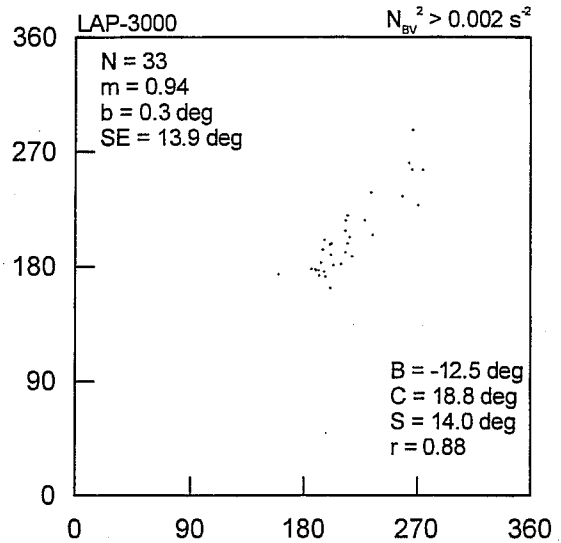
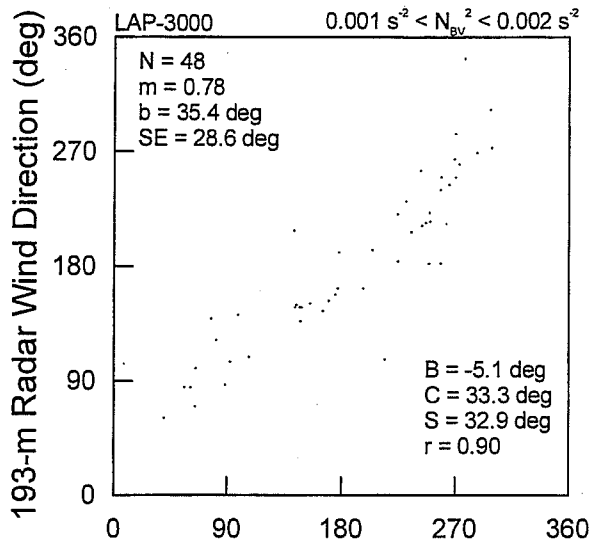


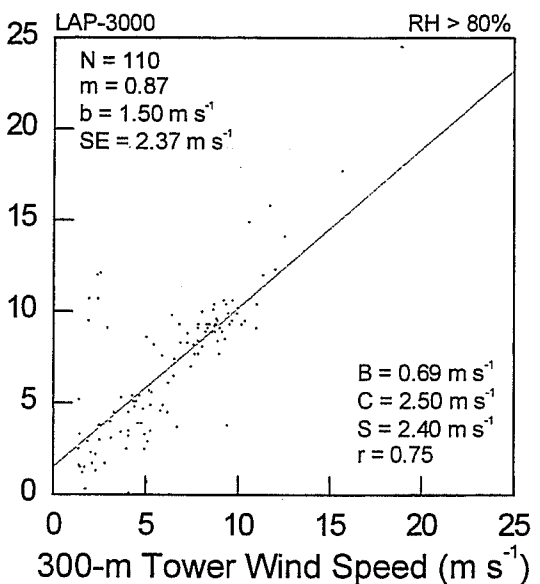
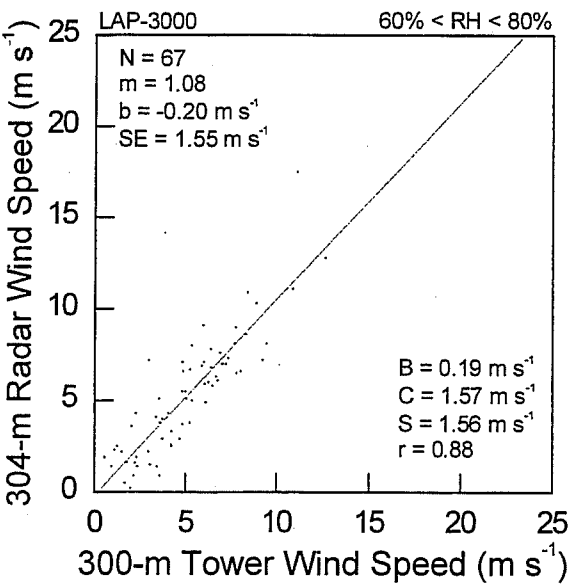
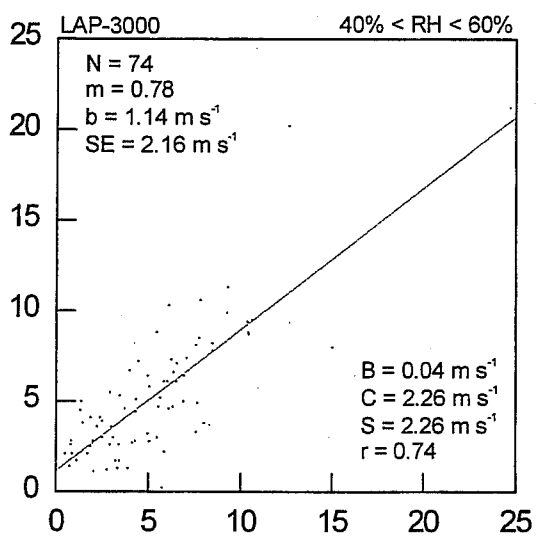
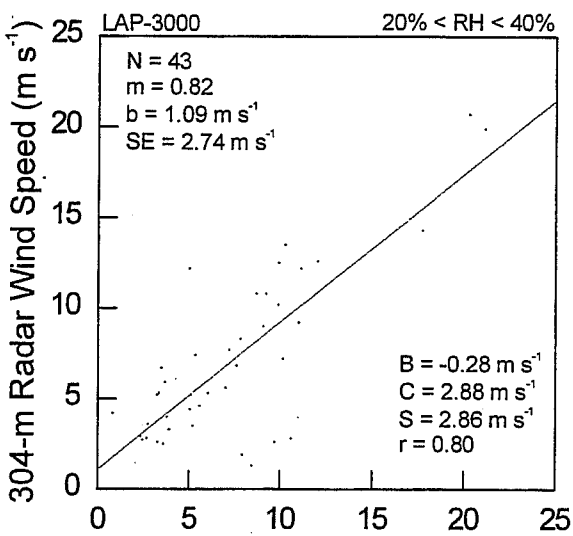
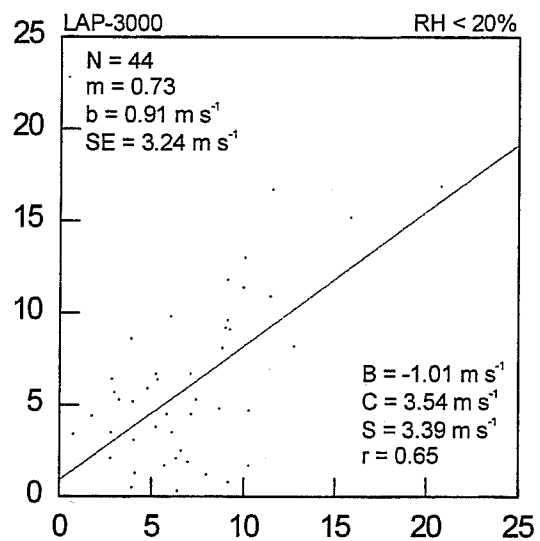
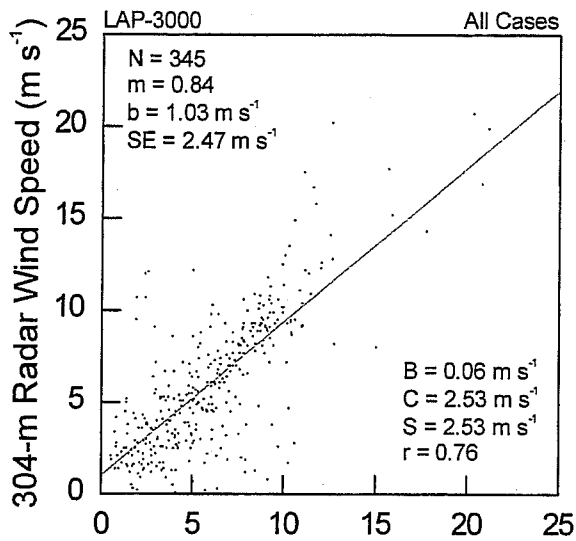


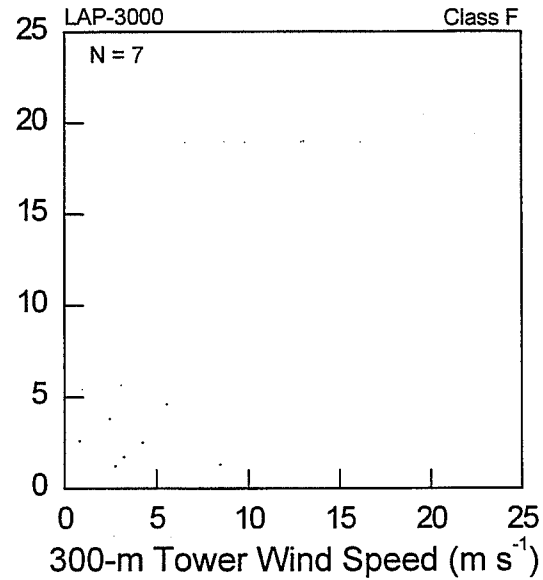
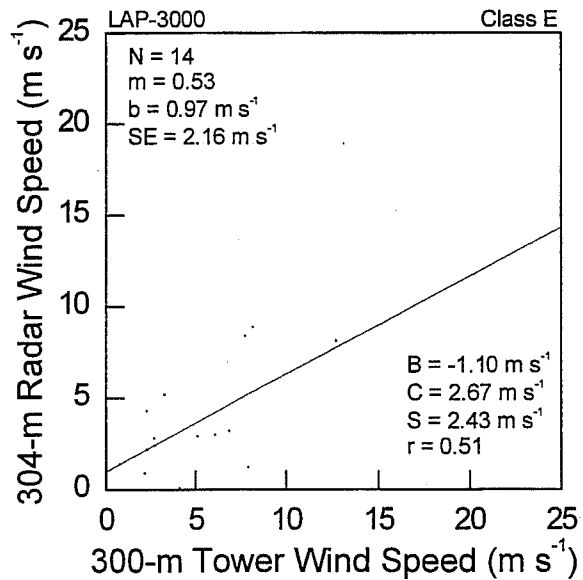
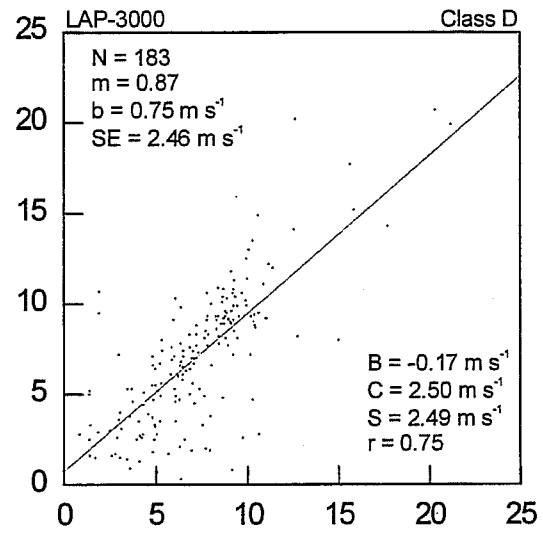
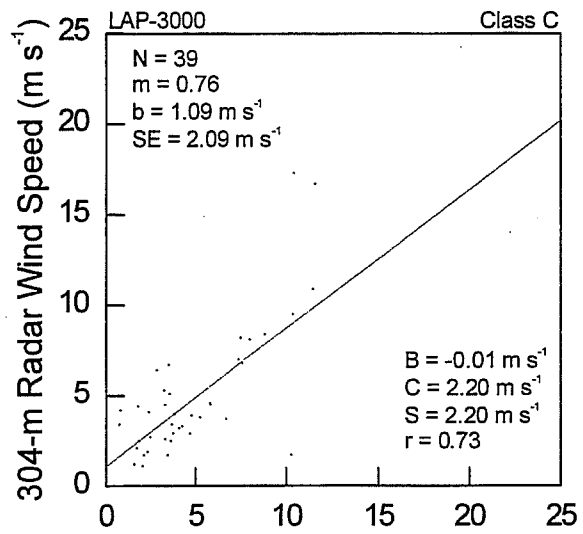
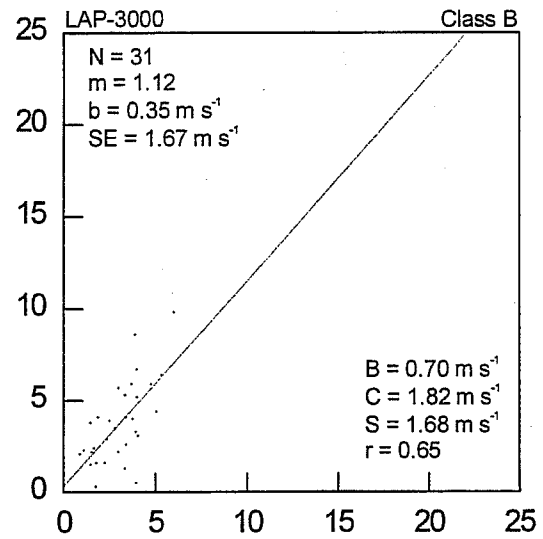
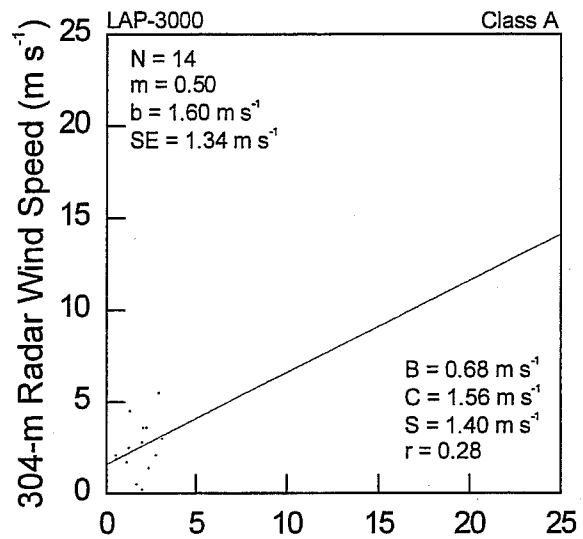


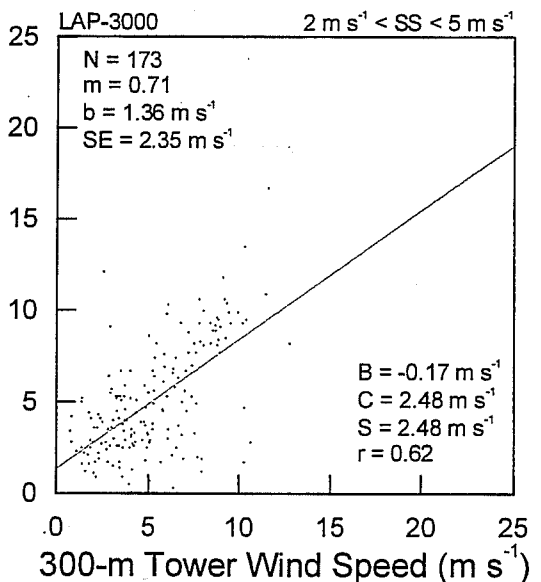
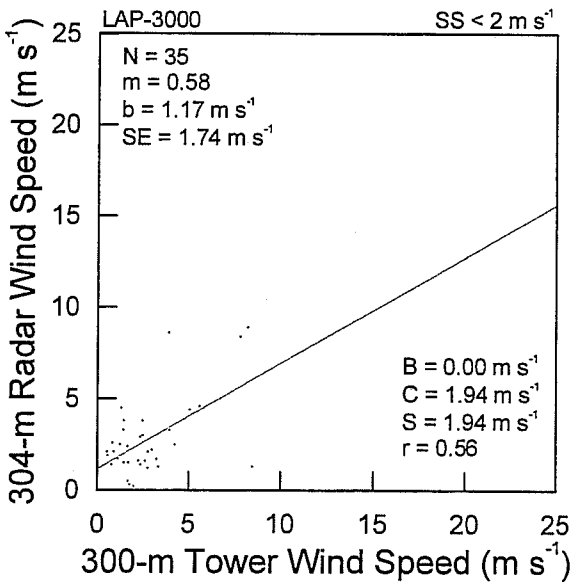
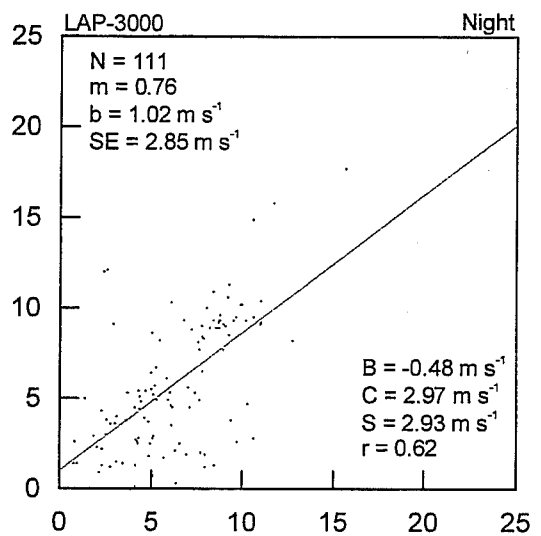
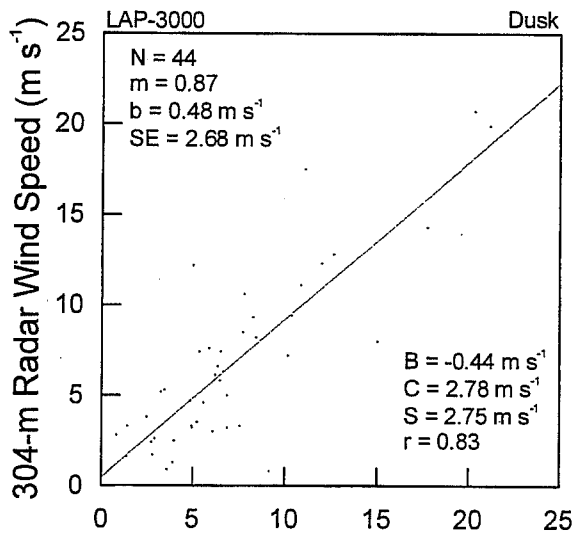
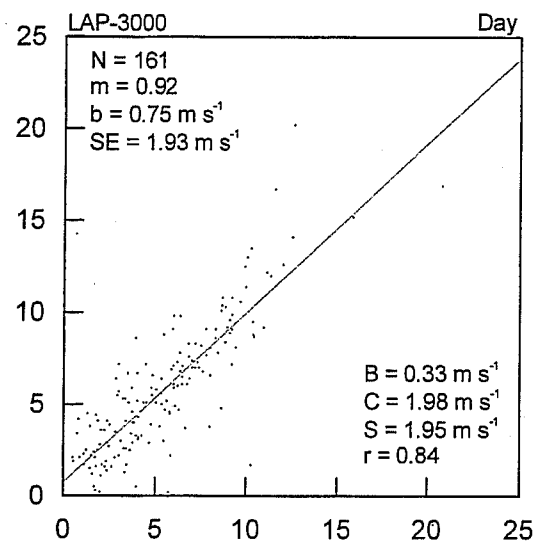
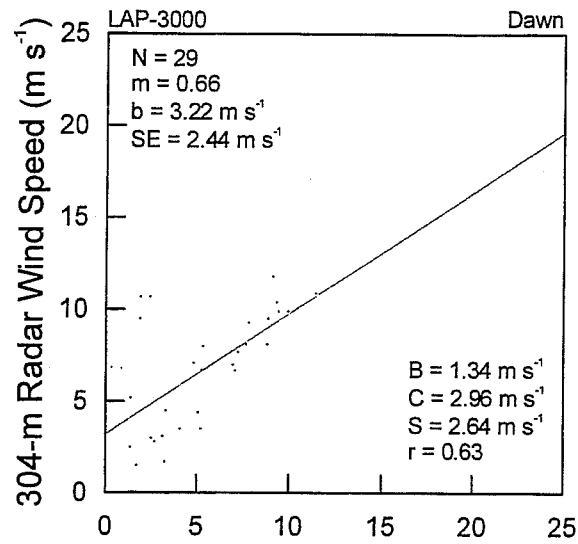


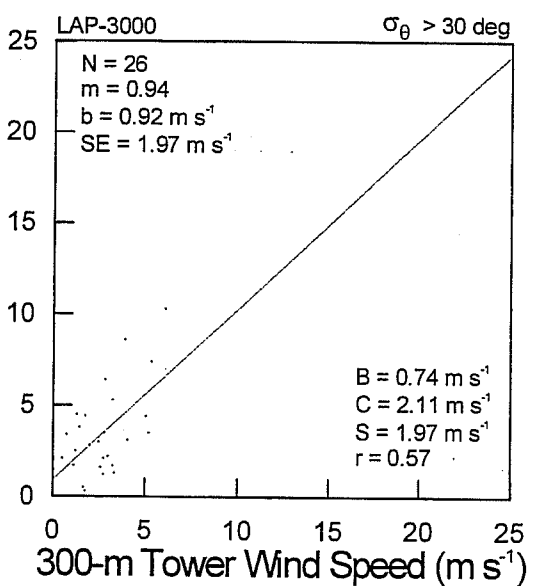
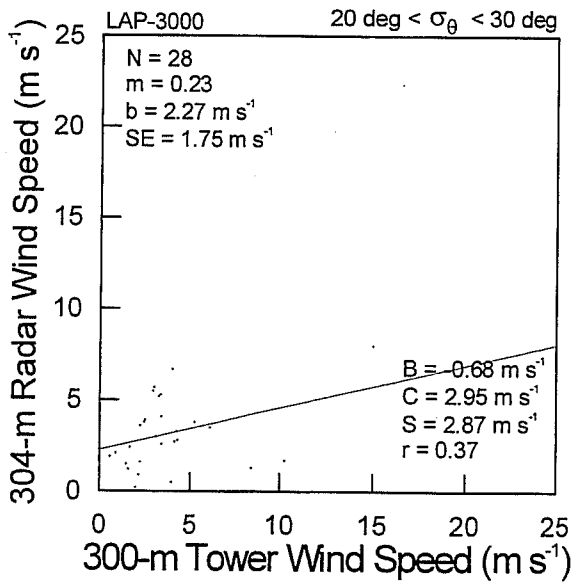
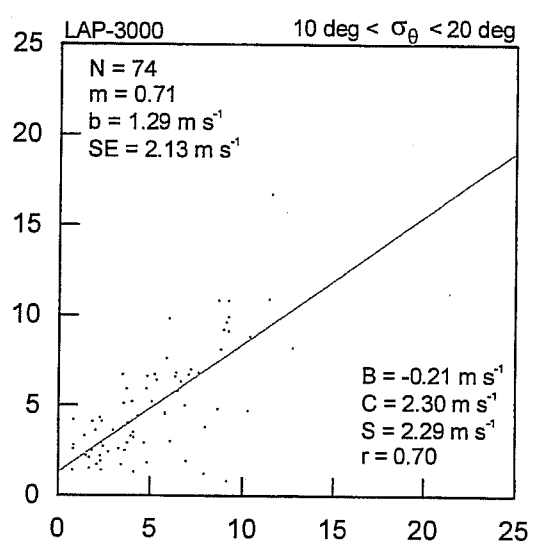
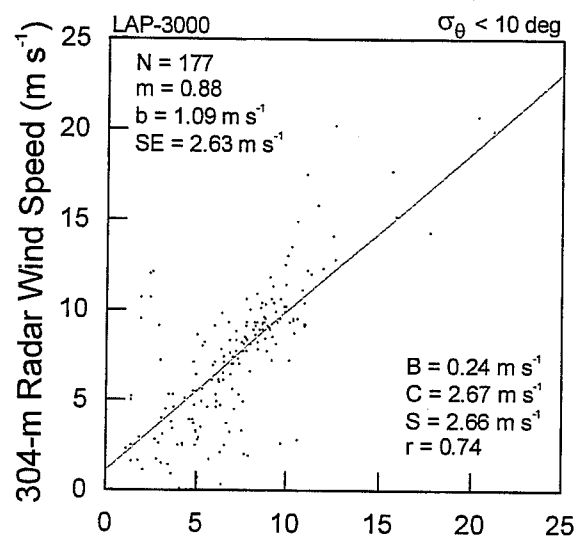
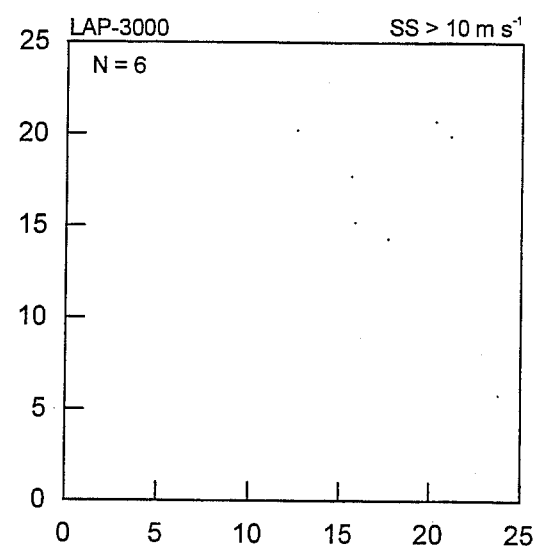
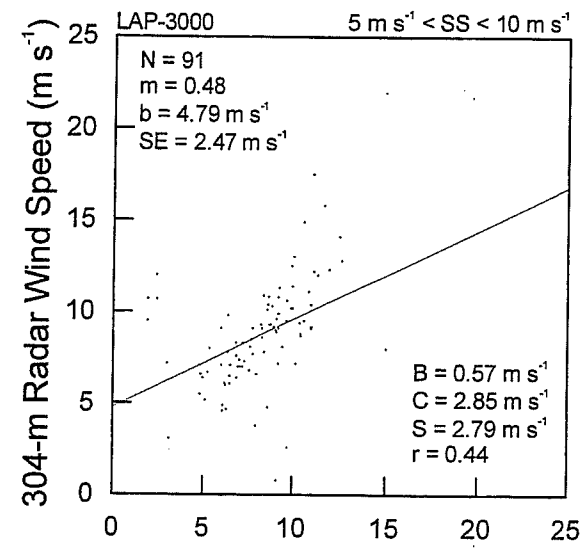


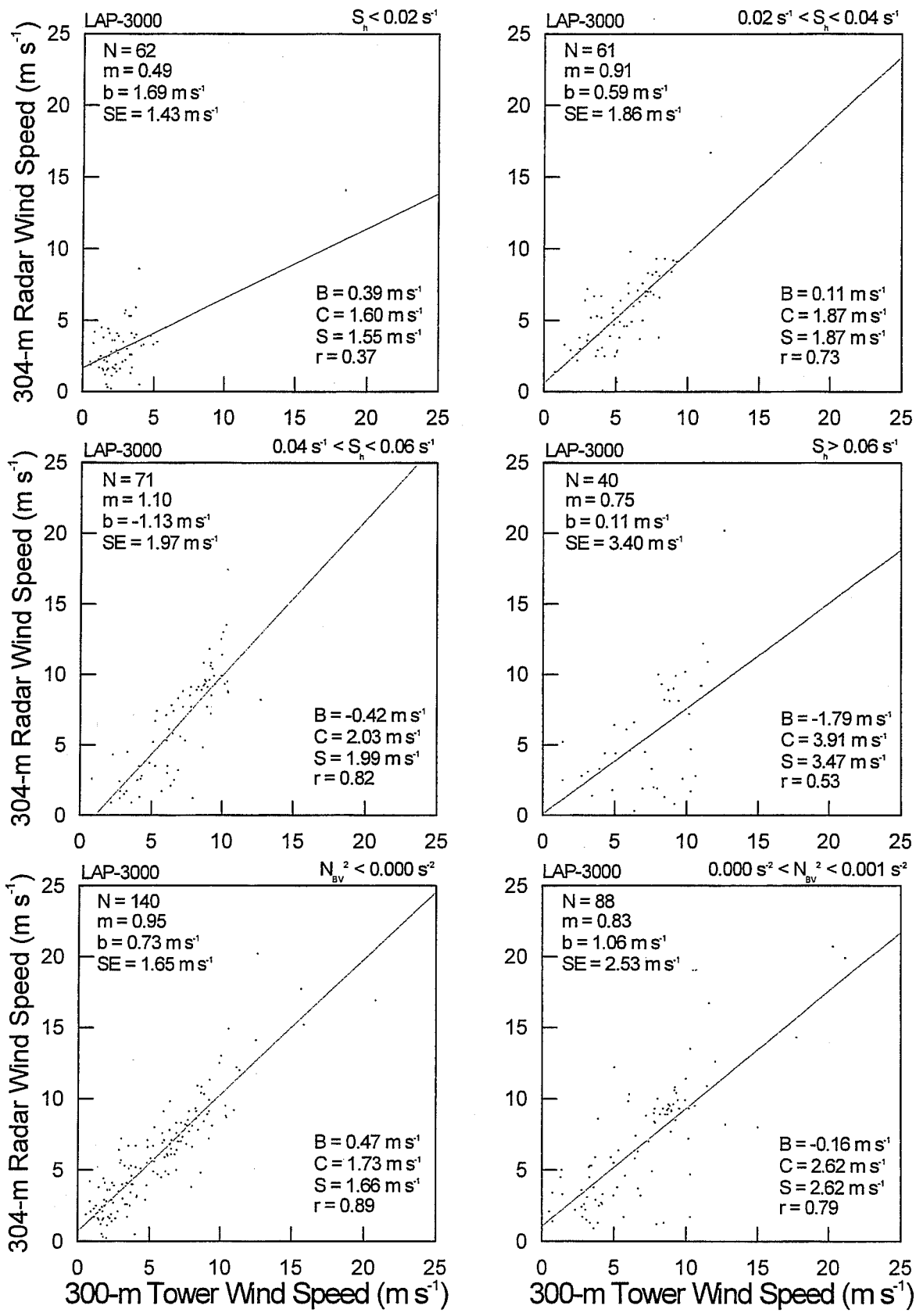


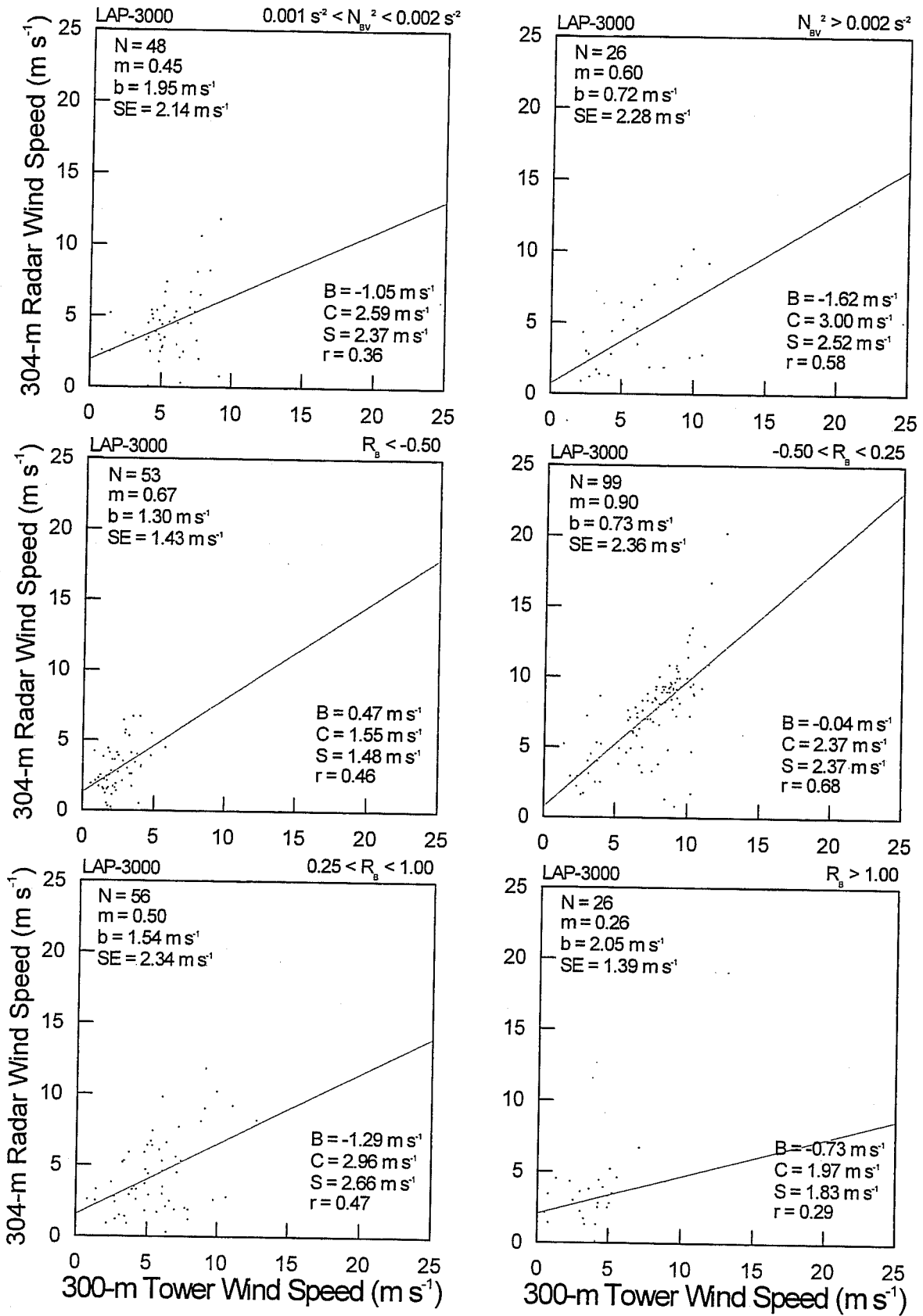


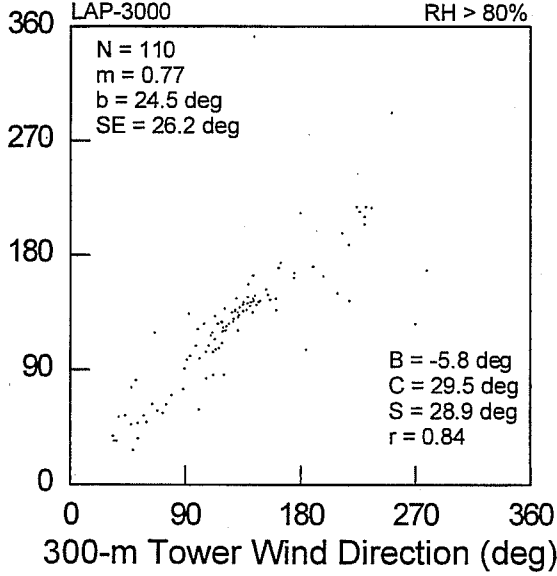
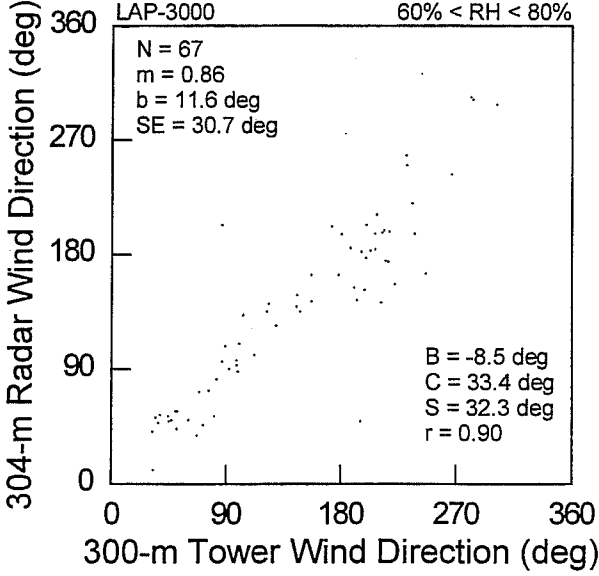
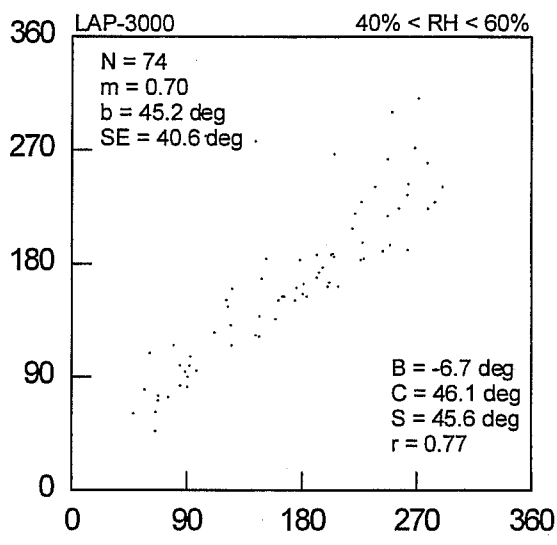
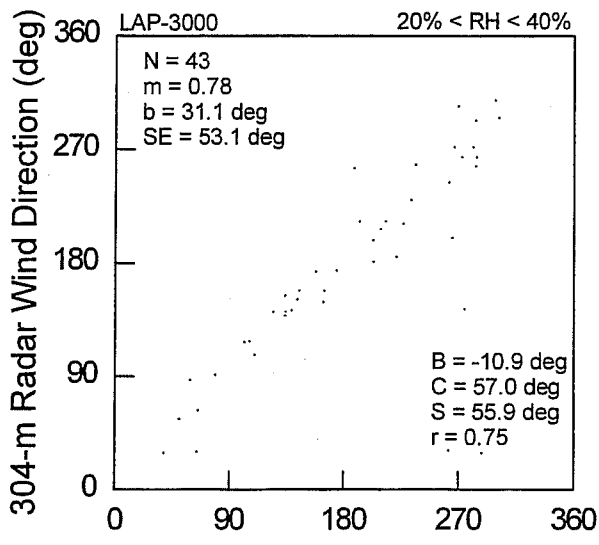
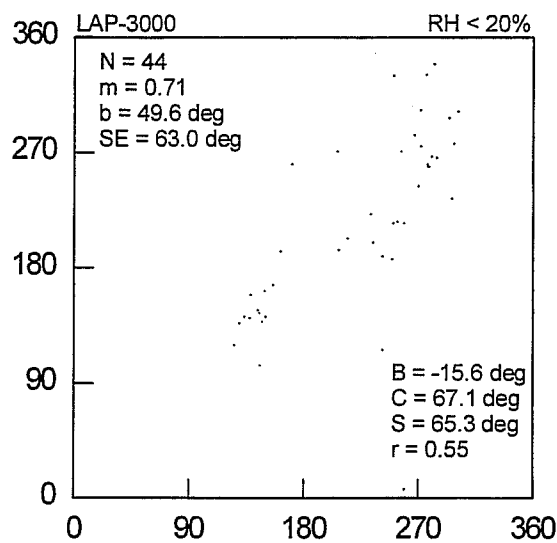
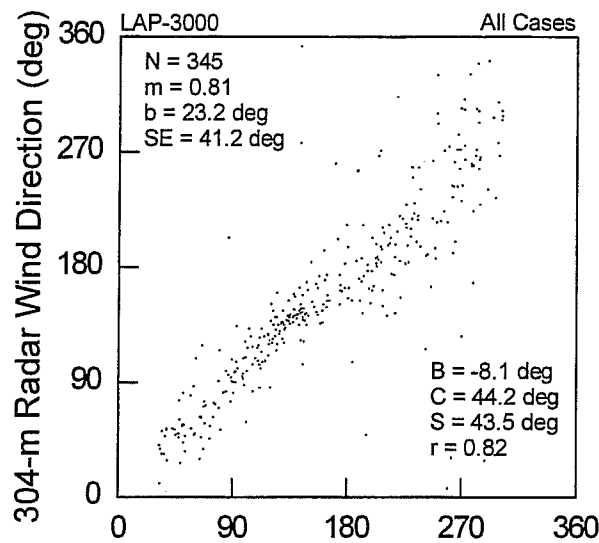


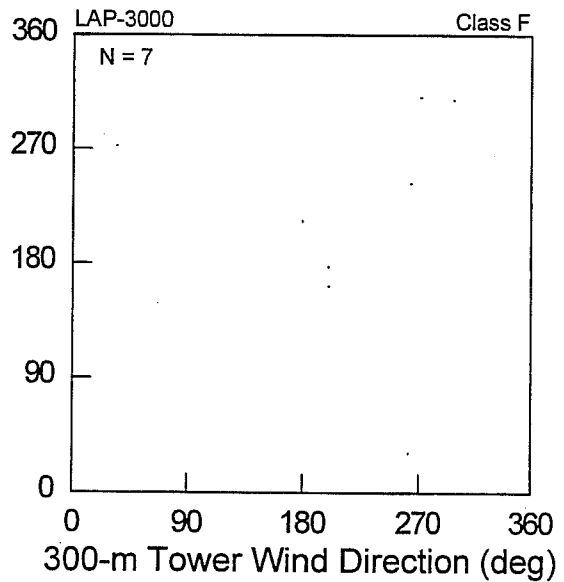
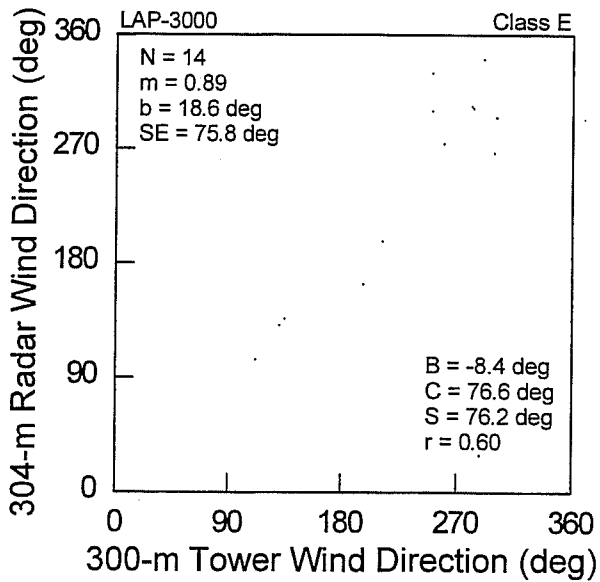
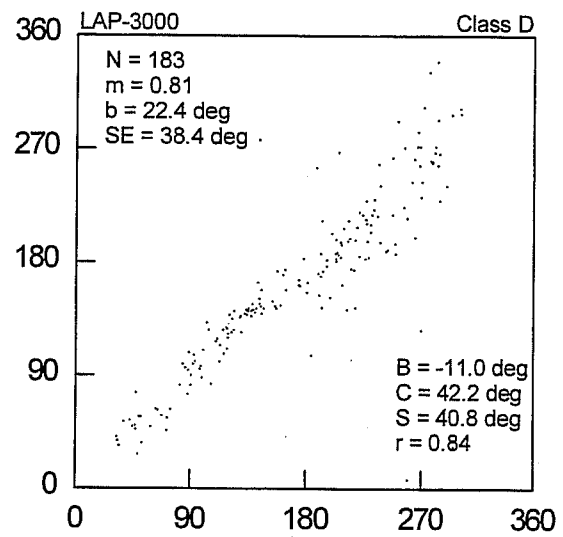
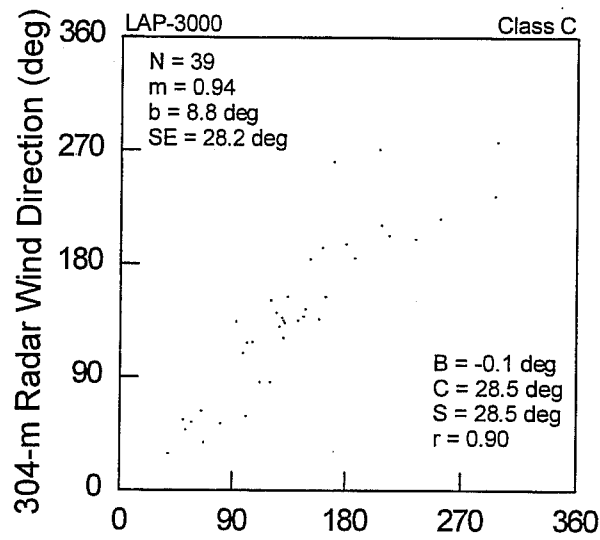
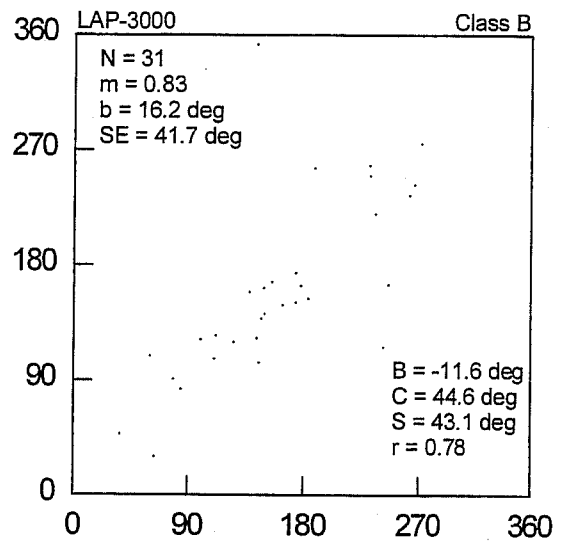
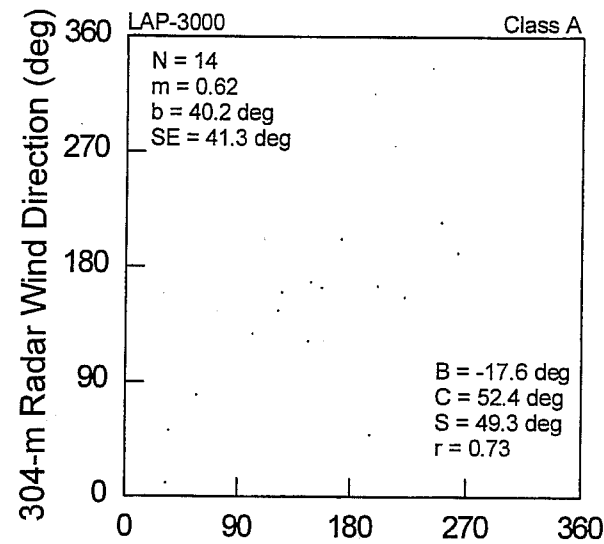


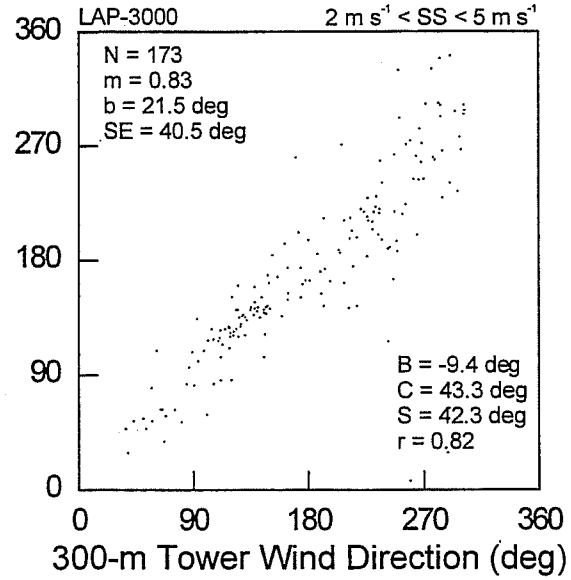
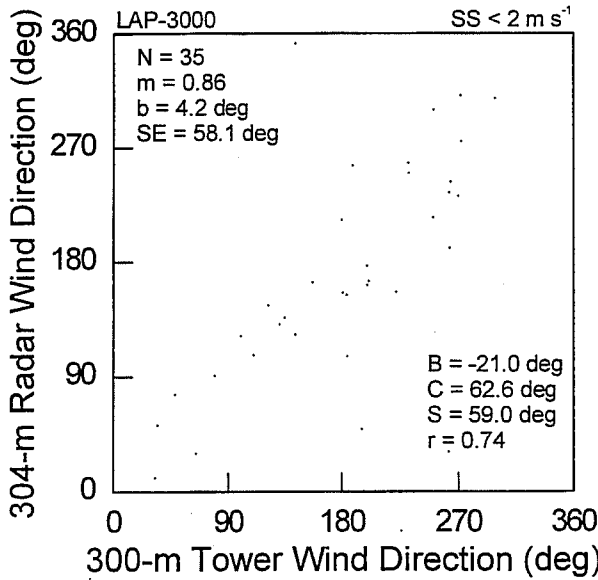
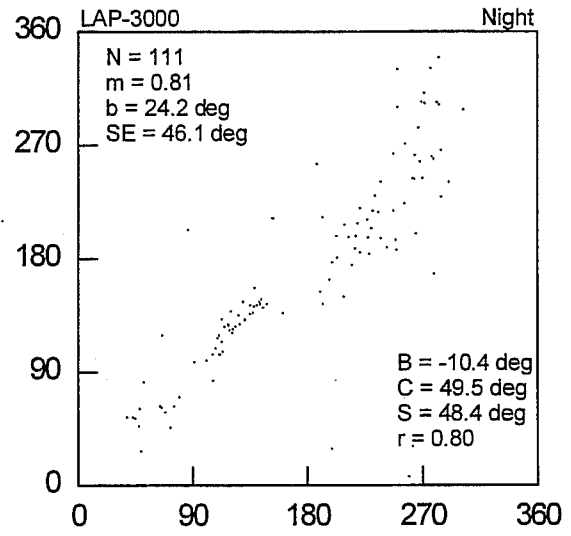
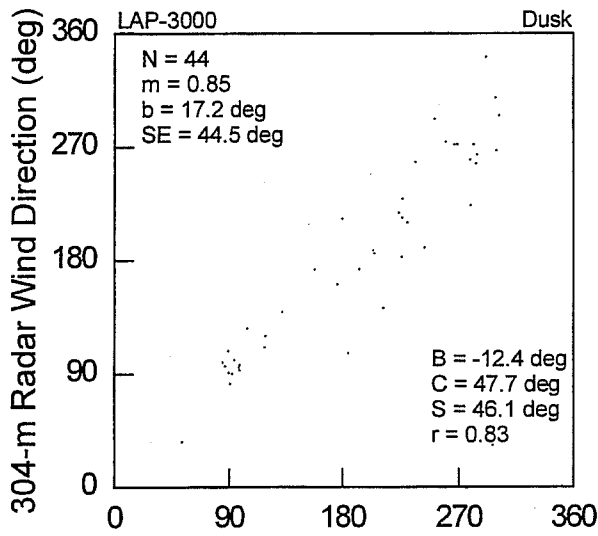
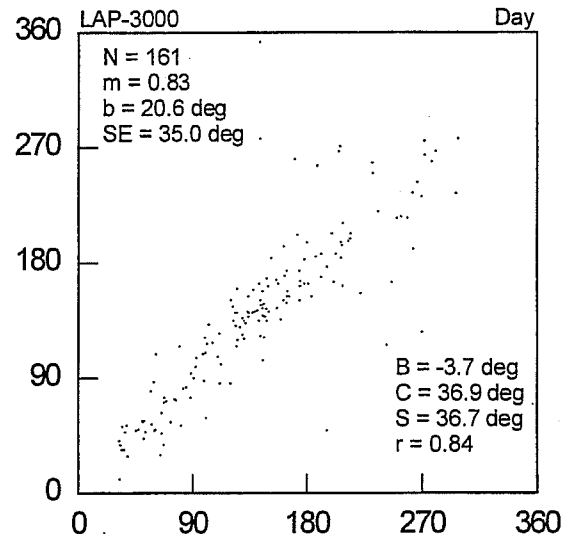
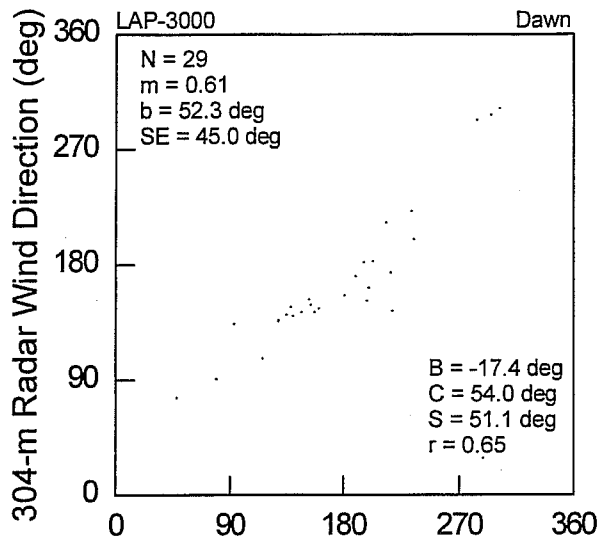


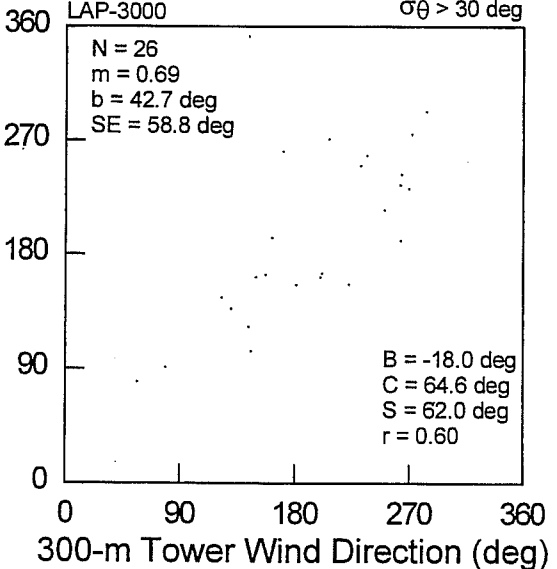
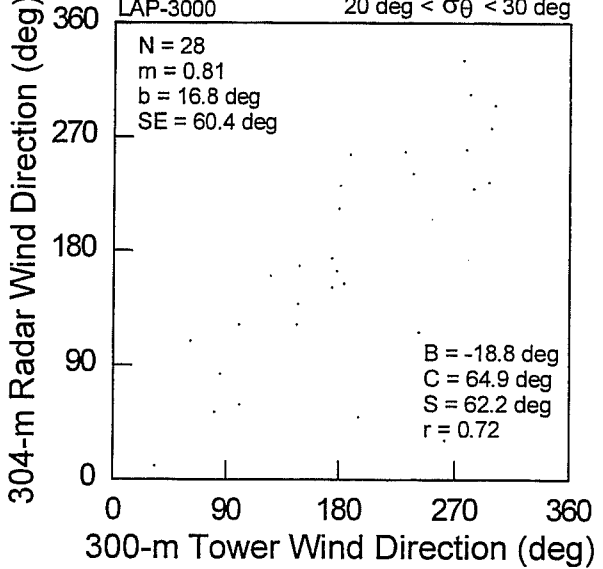
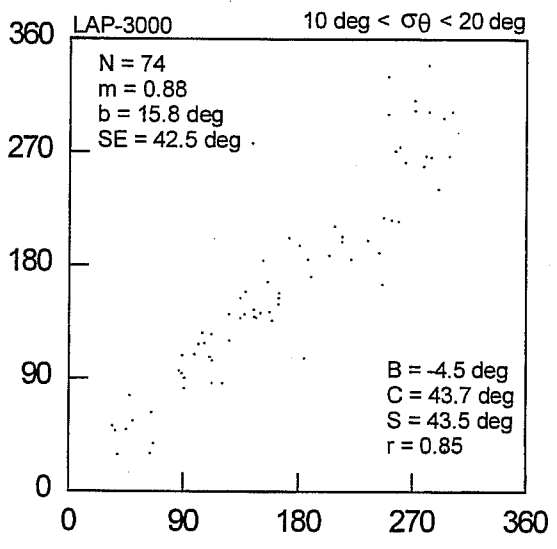
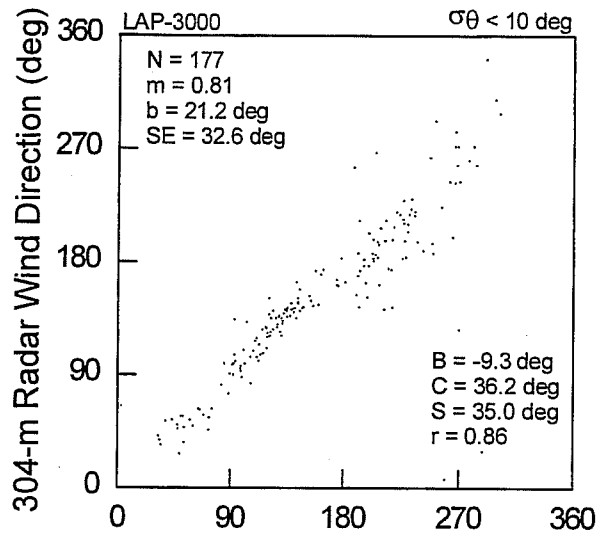
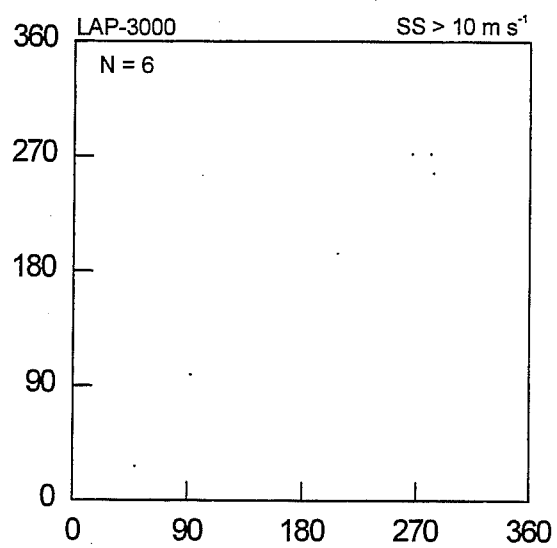
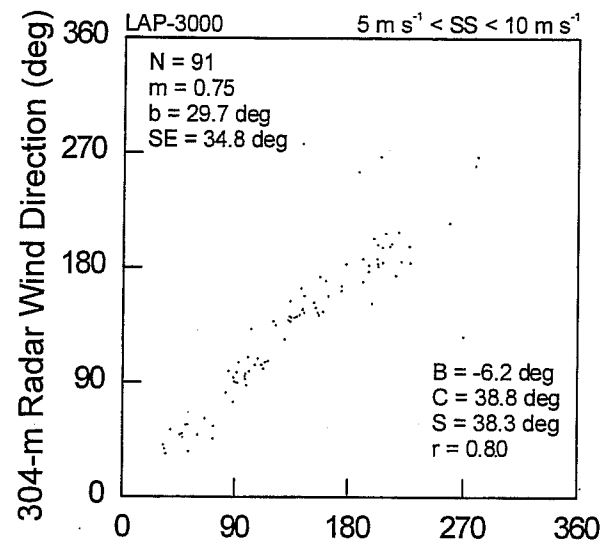


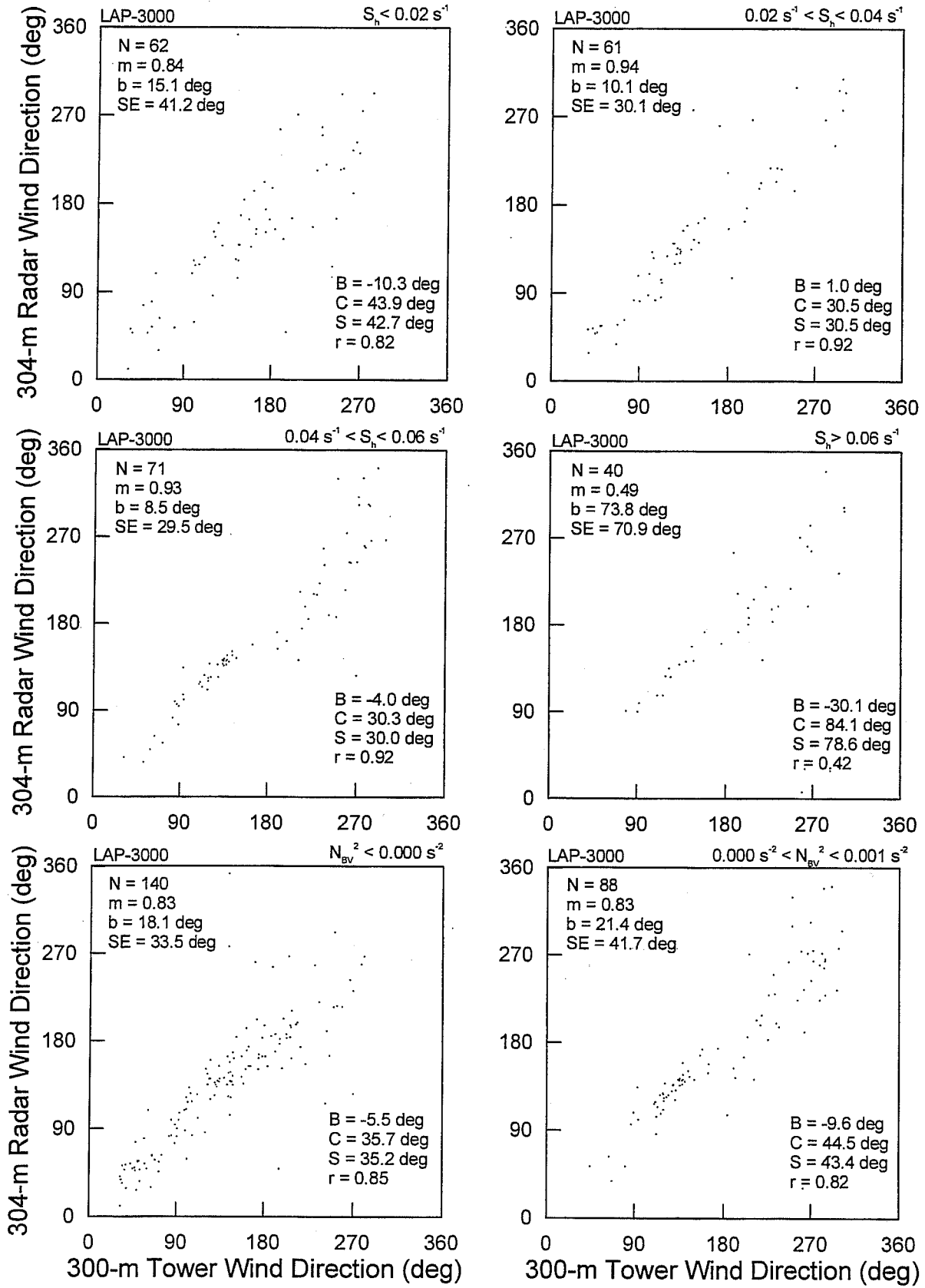


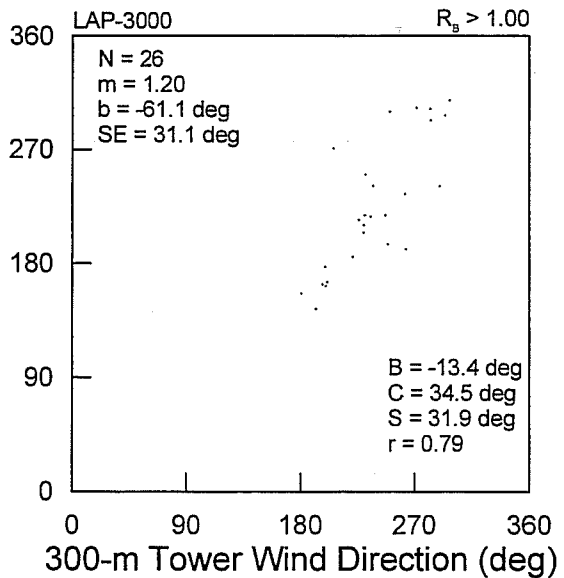
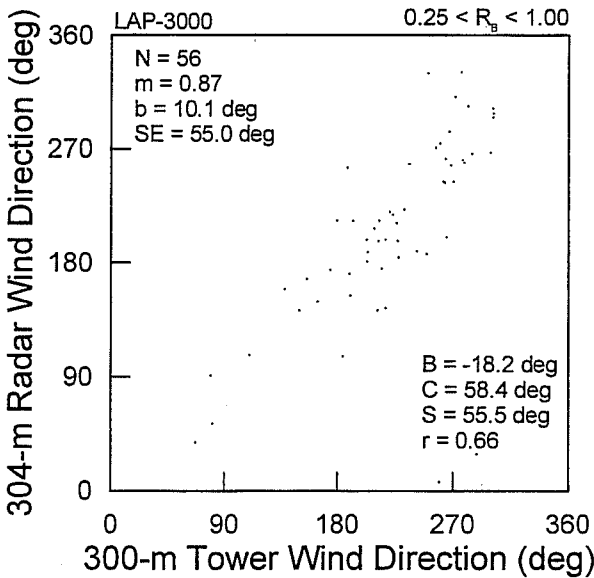
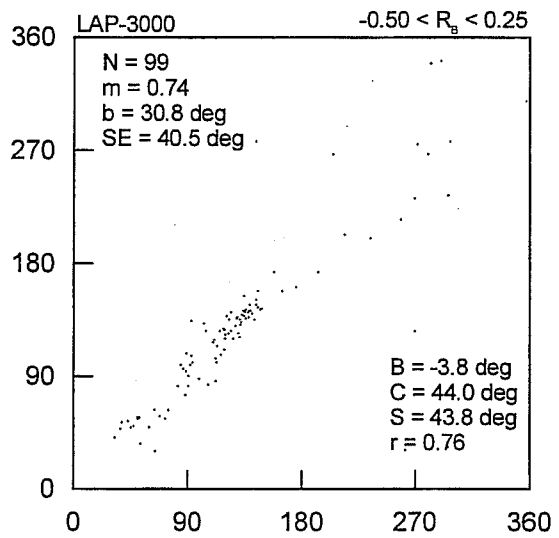
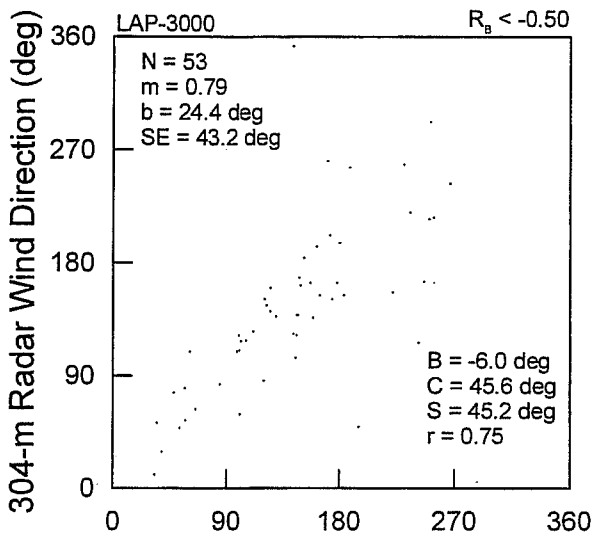
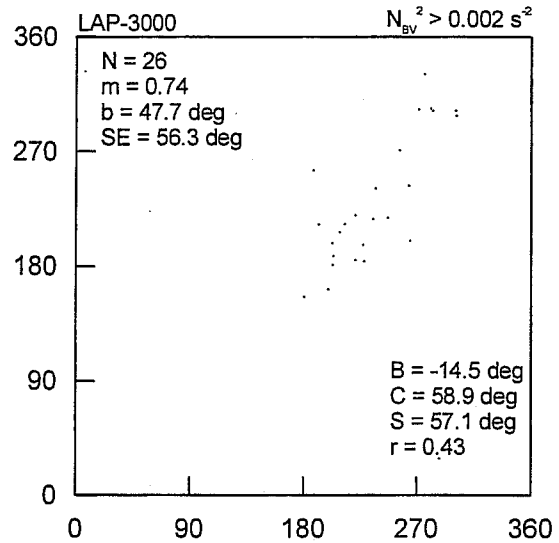
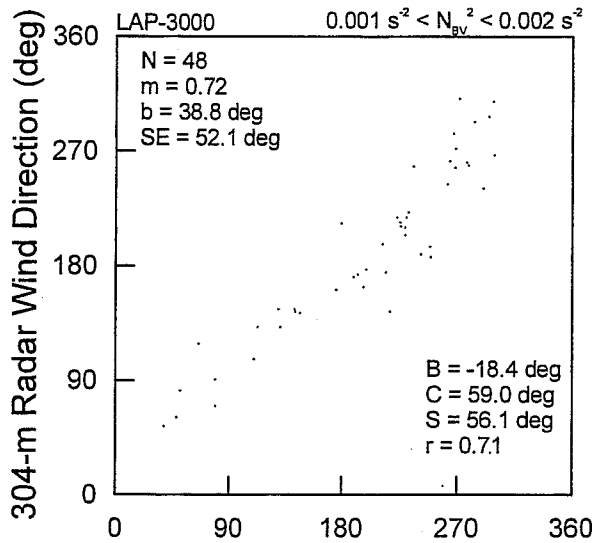












Appendix C: Virtual Air Temperature Scatter Plots with Statistics

The next 18 pages are scatter plots of virtual air temperature of the Radian RASS plotted against tower-based virtual air temperature. The scatter plots are organized in groups of six pages each. Each group consists of a variable (e.g., wind speed) for a particular measurement height (e.g., 100 m) for the following atmospheric conditions or stabilities: all cases, relative humidity (RH), Pasquill-Gifford stability class (A, B, C, D, E, and F), time of day (dawn, day, dusk, and night), scalar wind speed (SS), standard deviation of the horizontal wind direction (σ_θ), wind shear (S_h), Brunt-Vaisala frequency squared (N^2_{BV}), and the bulk Richardson number (R_B).

Each individual scatter plot contains the following statistical information:

N	number of reported data points
m	slope of linear regression
b	y-intercept of linear regression
SE	standard error (rms difference) about the linear regression
B	bias
C	comparability
S	precision
r	correlation coefficient

